



Università degli Studi di Cagliari
Dipartimento di Scienze della Vita e dell'Ambiente

PhD Degree
Life and Environmental Sciences-Drug Sciences Curriculum
XXXII Cycle

Natural and Synthetic Derivatives Targeting Microbial and Cancer-Related Key Enzymes

Scientific Disciplinary Sector
CHIM-08 (Medicinal Chemistry)

PhD Student	Benedetta Fois
Coordinator of the PhD Programme	Prof. Simona Distinto
Supervisor	Prof. Filippo Cottiglia

Final exam. Academic Year 2018 – 2019
Thesis defence: January-February 2020 Session

Table of Contents

ACKNOWLEDGEMENTS.....	I
ABBREVIATIONS.....	II
INTRODUCTION.....	1
REFERENCES.....	8
1. NATURAL AND HYDROLYZED COMPOUNDS FROM <i>TEUCRIUM FLAVUM</i> SUBSP. <i>GLAUCUM</i> AS INHIBITORS OF HIV-1 RT RNASE H FUNCTION.....	9
1.1 HUMAN IMMUNODEFICIENCY VIRUS (HIV)	9
1.1.1 Short history of the discovery of HIV	9
1.1.2 HIV Morphology	10
1.1.3 Replication of HIV	11
1.2 REVERSE TRANSCRIPTASE (RT).....	12
1.3 ANTI-HIV DRUGS	14
1.3.1 Reverse transcription Inhibitors (NRTIs and NNRTIs).....	15
1.3.2 Inhibitors of RNase H function.....	19
1.3.3 Synthetic Allosteric Inhibitors (RNHIs).....	22
1.4 ANTI RNASE H NATURAL AND NATURAL-DERIVED COMPOUNDS	25
1.5 ADVANCED-STAGE ANTI-HIV NATURAL PRODUCTS.....	27
1.6 <i>TEUCRIUM FLAVUM</i> SUBSP. <i>GLAUCUM</i>	30
1.6.1 Aim and Objectives	32
1.6.2 Results and Discussion	33
1.6.3 Structure elucidation of compounds 1-6 isolated from <i>Teucrium flavum</i> subsp. <i>glaucum</i>	38
1.6.4 Structure elucidation of compounds 7-10 obtained from the hydrolysis of teuflavoside.....	48
1.6.5 Inhibitory effects on HIV-1 RT-associated functions and structure-activity relationships.....	62
1.6.6 Site-Directed Mutagenesis.....	66
1.6.7 Docking experiment	68
1.6.8 Conclusion.....	70
1.7 EXPERIMENTAL PART	71
1.7.1 Materials and methods.....	72
1.7.1.1 General procedures.....	72
1.7.1.2 Plant material	72
1.7.1.3 Extraction and isolation of natural compounds	72
1.7.1.4 Hydrolysis of Teuflavoside (6)	75
1.7.1.5 Inhibition test of the RT RNase H function	76
1.7.2 Experimental data of the known compounds isolated from <i>Teucrium flavum</i> subsp <i>glaucum</i>	77
1.7.3 Molecular modelling.....	83
1.8 REFERENCES.....	84
2. HUMAN RHINOVIRUS	89
2.1 STRUCTURE OF HRV.....	89

2.1.1	Replication.....	90
2.2	RHINOVIRUS CELLULAR RECEPTORS.....	91
2.3	CLINICAL SYNDROMES OF RV INFECTION.....	93
2.4	ANTIVIRAL AGENTS FOR TREATMENT OF HRV INFECTION.....	95
2.4.1	Capsid Inhibitors.....	95
2.4.2	3C protease inhibitors.....	97
2.5	AIM AND OBJECTIVES.....	99
2.5.1	Results And Discussion.....	103
2.5.1.1	Synthesis of 2-(3,4-dimethoxyphenoxy)ethyl esters of aliphatic and aromatic acids (14a-e).....	103
2.5.1.2	Synthesis of heterocyclic amides 15a-d,f,n, 16a,b,e and 17a-d.....	104
2.5.2	Anti-Rhinovirus activity of compounds 14 a-e, 15ad,f,n, 16 a,b,e and 17 a-d.....	106
2.5.3	Conclusion.....	111
2.6	EXPERIMENTAL PART.....	112
2.6.1	Materials and Methods.....	113
2.6.1.1	General procedures.....	113
2.6.1.2	Synthesis of compound 11-17.....	113
2.6.2	Citotoxic effect on HeLa cells.....	133
2.6.2.1	Method of reducing the cytopathic effect.....	133
2.7	REFERENCES.....	134
3	ANTIBIOTICS.....	136
3.1	MECHANISM OF ANTIBIOTIC RESISTANCE.....	143
3.2	TARGETS OF ANTIBACTERIAL DRUGS.....	144
3.3	DNA GYRASE.....	145
3.3.1	Mechanism of DNA supercoiling by DNA gyrase.....	146
3.4	DNA GYRASE INHIBITORS.....	147
3.4.1	Quinolones.....	147
3.4.2	Aminocoumarins.....	148
3.4.3	Simocyclinones.....	148
3.4.4	Use of Quinolones.....	149
3.4.5	Novel DNA GyrB inhibitors.....	150
3.5	AIM AND OBJECTIVES.....	156
3.5.1	Results and discussion.....	159
3.5.2	Biological results.....	161
3.5.2.1	Enzymatic Inhibition Results.....	161
3.5.2.2	Antibacterial Results.....	163
3.5.3	Molecular modelling study.....	166
3.5.3.1	Docking of compounds 5b and 10b in <i>E. coli</i> DNA GyrB ATP-binding site (PDB: 4DUH).....	166
3.5.3.2	Crystal structure of moxifloxacin.....	168
3.5.3.3	Docking of compounds 5b and 10b in <i>S.aureus</i> DNA GyrA (PDB: 5CDQ).....	169
3.5.4	Conclusion.....	171
3.6	EXPERIMENTAL PART.....	172
3.6.1	General information.....	173
3.6.2	Synthesis procedures and analytical data of compounds.....	173
3.6.3	¹ H and ¹³ C NMR spectra, IR spectra and HPLC chromatograms.....	182
3.6.4	<i>Escherichia coli</i> DNA gyrase inhibition assay.....	210
3.6.4.1	<i>Escherichia coli</i> DNA gyrase ATP-ase assay.....	210
3.6.4.2	Minimum inhibitory concentration measurements.....	210

3.6.4.3	Frequency of resistance measurements	210
3.7	REFERENCES	212
4	MAGYDARIS PASTINACEA	218
4.1	PHYTOCHEMICAL AND BIOLOGICAL STUDIES OF <i>M. PASTINACEA</i>	219
4.2	CARBONIC ANHYDRASE	220
4.2.1	Inhibition Mechanisms of CAs	221
4.3	CARBONIC ANHYDRASE INHIBITORS	223
4.3.1	The zinc binders as CAIs	224
4.3.2	CAIs anchoring to the zinc-coordinated water/hydroxide ion	227
4.3.3	CA inhibition which bind out of the active site	228
4.3.4	CA inhibition by occlusion of the active site entrance	229
4.4	COUMARINS	230
4.4.1	Anti-tumour properties of coumarins	231
4.5	AIM AND OBJECTIVES	234
4.5.1	Isolation and characterization of compounds 1-15	234
4.5.2	Structure elucidation of compounds 1-15	238
4.5.3	Inhibitory effects of compounds 1-15 toward human carbonic anhydrase	252
4.5.4	In silico modelling of the interaction of compounds 9, 11, 15 with CAs	256
4.5.5	Cytotoxicity of compounds 1-15 toward cancer cells	259
4.5.6	Conclusion	260
4.6	EXPERIMENTAL PART	261
4.6.1	Materials and Methods	262
4.6.1.1	General procedures	262
4.6.1.2	Plant material	262
4.6.1.3	Petroleum ether extract	263
4.6.1.4	Ethyl acetate extract	263
4.6.1.5	Semi-Synthesis of (+)-heraclenol acetate (10)	264
4.6.2	Structural Elucidation of the known compounds	265
4.6.3	Molecular modelling	297
4.6.3.1	Ligand preparation	297
4.6.3.2	Protein preparation	297
4.6.3.3	Docking protocol	297
4.6.3.4	Post docking protocol	297
4.6.4	Biological evaluation	298
4.6.4.1	Carbonic anhydrase inhibition assay	298
4.6.4.2	Cytotoxic activity	298
4.6.4.2.1	Cell culture	298
4.6.4.2.2	MTT assay	299
4.7	REFERENCES	300
	LIST OF PUBLICATIONS	305

ACKNOWLEDGEMENTS

I would like to express my sincere gratitude to my supervisor Prof. Filippo Cottiglia for general help and many fruitful discussions about every aspect of my Ph.D. work, for his continuous support, interest and patience.

My sincere thanks also go to the coordinator of the Ph.D. School, Prof. Simona Distinto for performing most of the molecular modeling studies.

I would especially like to thank Prof. Danijel Kikelj (University of Ljubljana, Slovenia) for giving me the opportunity to carry out my project and to join his group. Thanks to Dr. Janes Ilaš, Tihomir Tomašič, Nace Zidar who taught me so many things, and Davide Benedetto Tiz, Ž. Skok, Martina Durcik and Andraz Lamut for fruitful discussions about my work.

Also I wish to thank Dr. Dirk D. Jochmans and Prof. Johan Neyts of the Department of Microbiology and Immunology, University of Leuven, Belgium, for performing the anti-HRV assays.

Many thanks to Dr. Angela Corona and Prof. Enzo Tramontano (Dept. of Life and Environmental Sciences) for the inhibition assays of HIV-1 reverse transcriptase.

Thanks are also due to Prof. Claudiu Trandafir Supuran (University of Florence, Dept. of Neurofarba) for carbonic anhydrase inhibition assays.

Thanks are also due to Prof. Elias Maccioni and Dr. Rita Meleddu of the Department of Life and Environmental Sciences, University of Cagliari for their support during this work.

Benedetta Fois gratefully acknowledges Sardinian Regional Government for the financial support of her/his PhD scholarship (P.O.R. Sardegna F.S.E. - Operational Programme of the Autonomous Region of Sardinia, European Social Fund 2014-2020 - Axis III Education and training, Thematic goal 10, Investment Priority 10ii), Specific goal 10.5.

I thank all fellow labmates for the stimulating discussions and for all the fun we have had in the last three years. Last but not least I would like to thank my family and friends for supporting me spiritually throughout writing this thesis and my life in general.

ABBREVIATIONS

AAZ Acetazolamide
ABC Abacavir
ACN acetonitrile
ADP Adenosine diphosphate
AG anchoring group
AIDS Acquired Immuno Deficiency Syndrome
AMR Antimicrobial resistance
ATP Adenosine triphosphate
AZT Azidothymidine
BBNH N-(4-tert-butylbenzoyl)-2-hydroxy-1 naphthaldehyde hydrazone
BC Before Christ
BRZ Brinzolamide
CA Carbonic anhydrase
CAI Carbonic anhydrase inhibitors
CC Coloumn Chromatography
CDHR3 Cadherin-related family member 3
CLX Celecoxib
COPD Chronic obstructive pulmonary disease
CP Ciprofloxacin
CV-N Cyanovirin-N
DAP Dapivirine
DAPY Diarylpyrimidine
DCM Dichloromethane
DCP Dichlorophenamide
DDDP DNA-dependent DNA polymerase
DMAP Dimethyl Amino pyridine
DMF Dimethylformamide
DMSO Dimethyl sulfoxide
DNA Deoxyribose Nucleic Acid
DQF-COSY Double Quantum Filtered-CORrelation Spectroscopy
DKAs Diketo Acids
DTT Dithiothreitol
DZA Dorzolamide
EARS-Net European Antimicrobial Resistance Surveillance Network
EFV Efavirens
ESI MS Electron Spray Ionization mass spectrometry
EtOAc Ethyl acetate
ETV Etravirine
EZA Ethoxzolamide
FDA Federal Drug Administration
FQs Fluoroquinolones
GABA γ -Amino Butyric Acid
GLASS Global Antimicrobial Surveillance System

GyrA Gyrase A
GyrB Gyrase B
HAART Highly active antiretroviral therapy
hCA human Carbonic anhydrase
HIV Human immune deficiency virus
HMBC Heteronuclear Multiple Bond Correlation
HPLC High Performance Liquid Chromatography
HR-ESIMS High resolution electron Spray Ionization mass spectrometry
HR-MS High resolution mass spectrometry
HRV Human Rhinovirus
HSQC Heteronuclear Single Quantum Coherence spectroscopy
HTLV Human T Leukemia virus
ICAM-1 Intercellular Adhesion Molecule-1
IMI Innovative Medicines Initiative
IN Integrase
LDLR Low Density Lipoprotein Receptor
LTR Long terminal repeat
MDR Multidrug resistance
MeOH Methanol
MHz megahertz
MRSA Methicillin-resistant *Staphylococcus aureus*
MZA Methazolamide
NMR Nuclear Magnetic Resonance
NNRTI Non-Nucleoside Reverse Transcriptase Inhibitor
NRTI Nucleoside/ Nucleotide reverse transcriptase inhibitor
NSAIDs Non-steroidal anti-inflammatory drugs
NVP Nevirapine
PaβN Phenylalanine-Arginine Beta-Naphthylamide
PCA Pyrimidinol carboxylic acids
PLRP-S Polymeric Reversed-Phase column
PrEP Pre-exposure prophylaxis
PT Prothrombin Time
QMPL QM-Polarized Ligand
RDDP RNA-dependent DNA polymerase
RNA Ribonucleic acid
RNase H Ribonuclease H
RNHI N-hydroxyimides
ROESY Rotating-frame Overhauser Spectroscopy
RP Reversed phase
RPV Rilpivirine
RT Reverse Transcriptase
SAC Saccharin
SAR Structure–activity relationship
SG Sticky group

SI Selectivity index
SLP Sulpiride
SPE Solid Phase Extraction
SPR Surface Plasmon Resonance
ssRNA Single-stranded-RNA
TAMs Thymidine analogue resistance mutations
TEA Triethylamine
TLC Thin Layer Chromatography
TPM Topiramate
tRNA Transfer ribonucleic acid
VLC Vacuum Liquid Chromatography
VLDLR Very low-density lipoprotein receptor
WHO World Health Organization
WT Wild Type
ZNS Zonisamide
7-ACA 7-aminocephalosporanic acid

SUMMARY

The present study is focused on the isolation and structure elucidation of bioactive natural compounds as well as on the semi-synthesis and synthesis of new derivatives as inhibitors of HIV-1 Reverse Transcriptase, Carbonic Anhydrase, DNA Gyrase, and human Rinoviruses replication.

As regards the first target, we found that the EtOAc extract of the Sardinian plant *Teucrium flavum* subsp. *glaucum* was able to inhibit the HIV-1 RT associated RNase H function. A bioassay-guided fractionation of the extract yielded six secondary metabolites and, among all, the flavone Cirsiolol was the most potent inhibitor of RNase H function with an IC_{50} of 8.2 μ M. Furthermore, the hydrolysis of the inactive Teuflavoside led to one known and three new neo-clerodanes. Among all, Flavuglaucin B was the most potent inhibitor with an IC_{50} of 9.1 μ M. Site-directed mutagenesis and docking studies indicated that Flavuglaucin B bind to the RT allosteric pocket close to RNase H site.

Concerning carbonic anhydrases (CAs), the phytochemical investigation of two extracts of the plant *Magdalis pastinacea*, endowed with inhibitory activity toward this enzyme, resulted in the isolation of one new and fourteen known coumarins. All compounds were selective toward the tumor-associated CA IX and CA XII since none was active against the off target CA I and CA II up the concentration of 100 μ M. Some coumarins revealed a strong inhibitory effect toward CA IX and CA XII with K_i s in the range of 74.5-5.7 nM. Molecular docking experiments revealed that the most potent coumarin could be hydrolyzed by the Zn^{2+} activated water molecule of the enzyme cavity and the open compound is stabilized by several hydrogen bonds and π - π interactions in the catalytic site of CA XII.

Based on the evidence that the phenylpropanoid (E)-3-(3,4-dimethoxyphenyl)-2-propen-1-yl(Z)-2-[(Z)-2-methyl-2-butenoyloxymethyl]butenoate isolated from *Bupleurum fruticosum*, behaved as a potent capsid binder, three series of derivatives were synthesized modifying both the phenylpropyl group and the aliphatic ester chain. Interestingly, biological tests revealed that the most part of the synthesized compounds exhibited no cellular toxicity up to 100 μ M and showed a reversal of selectivity towards the viral species B, HRV-14. Among all, some of the phenylpiperazine or piperidinylpyridine derivative amides, inhibited the replication of HRV-14 with EC_{50} values in the low micromolar range.

Bacterial DNA gyrase is an interesting target for the discovery of new antibacterial compounds, overcoming bacterial resistance, insufficient penetration and effluxing and boosting antibacterial activity. Based on this evidence, Ciprofloxacin, a well known Gyrase A inhibitor, was combined with benzothiazole-based gyrase B inhibitors. All dual compounds displayed potent antibacterial activity against *E.coli* due to the interaction of the hybrids with the GyrA and/or topoisomerase IV

ParC subunits, while inhibition of GyrB was not strong enough to provide a substantial contribution to the observed antibacterial activity.

Introduction

Natural products from plants and microorganisms have been the basis for treating human diseases,¹ either in the form of extracts or as single compounds. Awareness and application of plants to prepare food and medicine have been realized through trial and error and gradually human became conscious of their properties. Since ancient times in several countries such as China, Greece, Egypt and India, medicinal plants were used as a resource for the treatment of diseases.² As a matter of fact, the term *medicinal plant* refers to a variety of plants that have medicinal properties. The earliest written evidence of the use of medicinal plants for preparation of drugs has been found on a Sumerian clay slab from Nagpur dating back to nearly 5000 years ago. Moreover, according to some inscriptions, Egyptians and Chinese, who used plants as medicine since more than 27 centuries BC, were among the earliest human beings who did so.³ Ancient Greek people were also familiar with the medicinal properties of some medicinal plants, and Hippocrates, the founder of Greek medicine and Aristotle, pupil of Hippocrates, used medicinal plants for the treatment of diseases. After that, Theophrastus, a Greek scientist, founded the School of Medicinal Plants. Then, Pedanius Dioscorides, a physician and surgeon in the years 75-45 BC, wrote an encyclopedia, called *De Materia Medica*, to describe 600 therapeutic medicinal plants.^{4,5}

Phytotherapy is widely being used across the world on a constantly growing basis. The global trend of synthetic compounds has turned to herbal drugs, which can be referred as a return to nature. In recent years, according to the WHO, more than 80% of inhabitants of the world used traditional medicines for their primary health care needs.⁶ This figure included not only a large population of China, India, which are the countries with great varieties of medicinal plant, but also many advanced Countries.⁷ Traditional Chinese medicine uses over 5000 plant species, while Indian system of traditional medicine uses about 7000 plant species.⁸ From 1959 to 1980, in USA 25% of all prescriptions contained plant extracts or active principles prepared from higher plants and only in 1980 costumers paid more than \$ 8000 million for prescriptions containing plants derivatives^{6,9} and between 1990 and 2000, an increase of over 380 % in sales in the United States was recorded.¹⁰

In the past the method of using herbal drug was the employment of crude plant or parts of plant. In 1829 from the bark of the willow tree (*Salix* spp.), the French pharmacist H. Leroux isolated for the first time a non-steroidal anti-inflammatory drugs (NSAIDs) salicin. Salicin was shown to be a prodrug that was converted to salicylic acid in the intestinal tract and liver after oral administration. Salicylic acid, when taken orally, possesses excellent anti-inflammatory, analgesic, and antipyretic properties; however, even its sodium salt is difficult to tolerate for lengthy periods because of the irritation and damage it produces in the mouth, esophagus, and, particularly, the stomach. Aspirin

was introduced into medicine in 1899 and found to be equally effective and better tolerated (Figure 1).¹¹

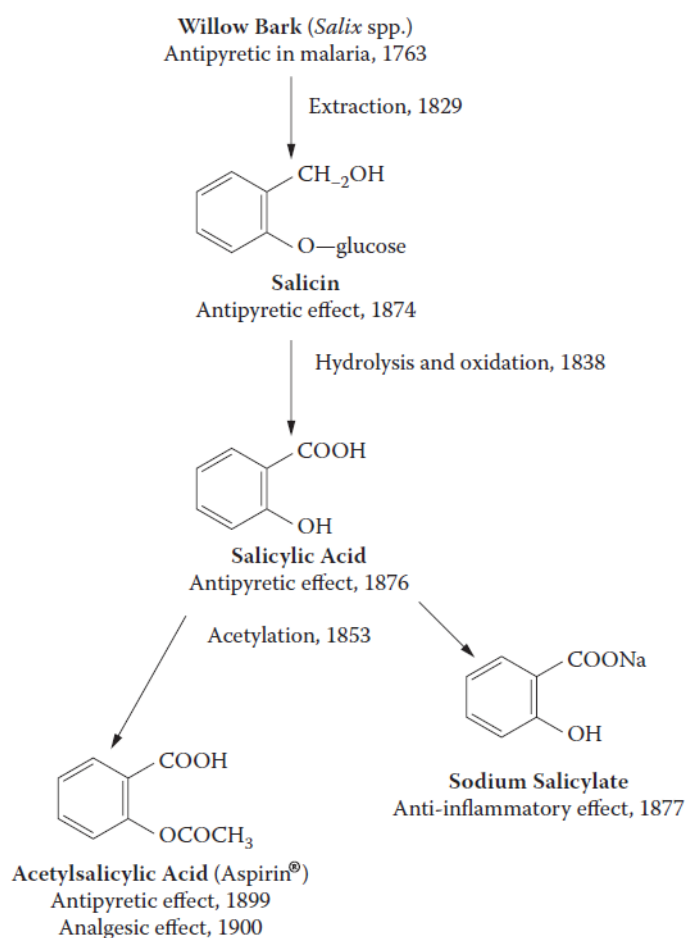


Figure 1. Chronology of drug development from willow bark.

Currently, it is estimated that over 50% of the available drugs are derived from medicinal plants;¹² indeed, a lot of plant-originated drugs have been discovered and various secondary metabolites are actually in use as for example, morphine identified from *Opium*, digoxin from *Foxglove*, quinine from *Cinchona* bark, pilocarpine from *Maranham* Jaborandi, taxol from *Taxus brevifolia*.

It is reported that 11% of the 252 drugs considered as basic and essential by the WHO were exclusively of flowering plant origin.¹³ 49% of the total anti-cancer drugs approved between years 1940-2014 were natural products or directly derived therefrom. 64% of the newly synthesized anti-hypertensive drugs during the period of 1981-2014 have origin in natural products.¹⁴

Drug development has followed a progression from a natural product, to a synthetic modification of that natural compound (e.g. Aspirin) to a synthetic one apparently showing little relationship to its natural forebears. An example is the drug ibuprofen, which was introduced in American market in 1974 as one of the first of a new generation of NSAIDs, developed in order to reduce side effects

associated with prolonged use of aspirin such as increased bleeding tendencies and gastrointestinal irritation.

Thus, although natural products continue to play a highly significant role in the drug discovery, they suffer from several limitations that require chemical modifications leading to semi-synthetic derivatives or totally synthetic analogues with better characteristics.

The most widespread limitations facing the development of drugs from natural compounds are the following:

- Toxicity
- Low potency
- Low selectivity
- Low bioavailability and/or poor solubility
- Natural products are often present in plants in small quantities or as mixtures in extracts, which require labor-intensive and time-consuming purification procedures. Obtaining further quantities for preclinical studies requires long time that would have a substantial impact on the development time line.

Focusing on the anticancer and antimicrobials drugs, below some examples of semi-synthetic and totally synthetic drugs obtained from natural scaffolds.

Podophyllotoxin was isolated for the first time in 1880 by Podwysstzki from the roots and rhizomes of the North American plant *Podophyllum peltatum* L., commonly known as the American mandrake or May apple and recognized as a potent antitumor factor.

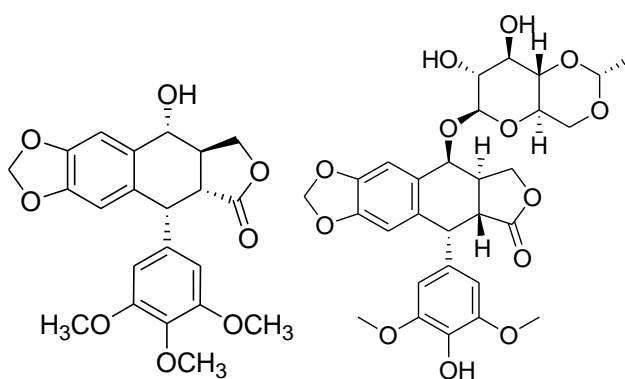


Figure 2. Chemical structure of podophyllotoxin (left) and etoposide (right)

It has been shown that podophyllotoxin has anti-neoplastic properties that prevent the polymerization of tubulin which thereby induce cell cycle arrest at mitosis and impede the formation of the mitotic-spindles microtubules, preventing cancer cells development.¹⁵ Unfortunately, podophyllotoxin is too

toxic for clinical application but podophyllotoxin analogues such as etoposide (Figure 2) and teniposide, possessing higher therapeutic indices, have been approved for the treatment of various solid tumors.¹⁶

Paclitaxel is an antitumor compound isolated from *Taxus brevifolia* and it is classified as microtubule-stabilizing agent.¹⁷ The limited natural availability of this drug made it the focus of many synthetic investigations and extensive SAR studies.

Paclitaxel, along with several key precursors (the baccatins), occurs in the leaves of various *Taxus* species, and the ready semi-synthetic conversion of the baccatins to paclitaxel has provided a major natural source of this important class of drugs.

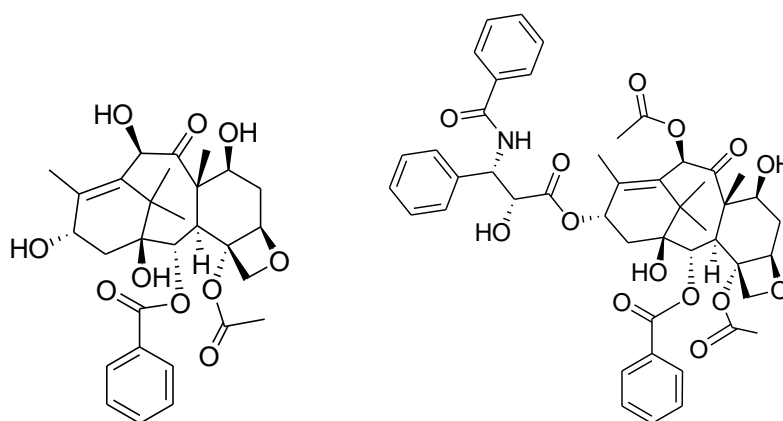


Figure 3. Structure of 10-deacetylbaccatin (left) and paclitaxel (right)

Despite the potent antitumor activity, paclitaxel caused undesirable side effects due to its extremely low solubility and to the associated formulation. Thus, it was apparent in the early 1990s that it would be essential to develop new taxane anticancer agents with fewer side effects, and superior pharmacological properties.

Later, it was discovered that the european yew *Taxus baccata* was a source of 10-deacetylbaccatin III, lacking the side chain at C13 and the acetyl group at C10, a precursor that could provide paclitaxel through a relatively simple route. The semi-synthetic analog docetaxel is more potent and soluble than paclitaxel and is used against many tumors instead of paclitaxel.¹⁷ More recently, by means of other synthetic or semi-synthetic methodologies, such as the β -lactam synthon method,¹⁸ new taxanes with improved water solubility and potency against MDR-expressing cells and tumors (cabazitaxel, Figure 4) or with oral bioavailability (ortataxel, Figure 4) are in clinical trials or approved in cancer therapy.¹⁹

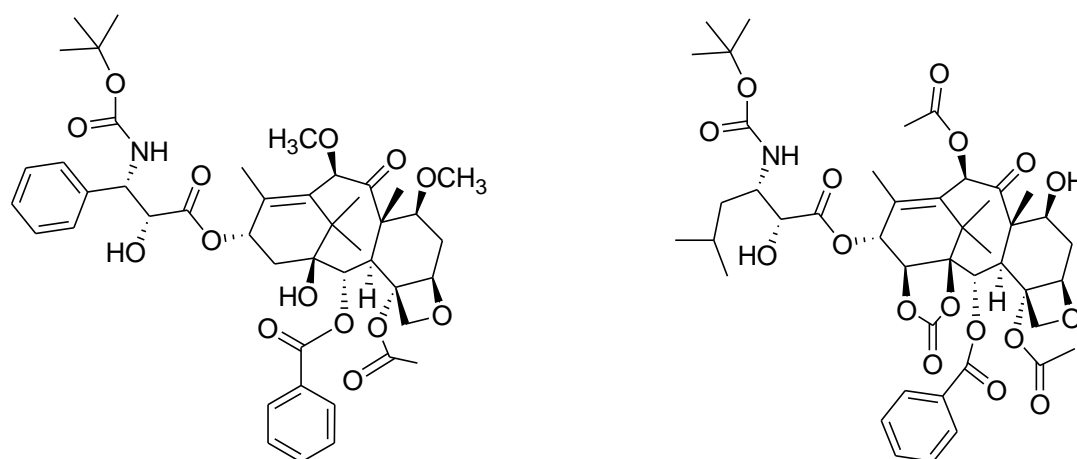


Figure 4. Structure of cabazitaxel (left) and ortataxel (right)

Another interesting plant drug prototype is represented by camptothecin. It is a cytotoxic quinoline alkaloid isolated from the bark and stems of *Camptotheca acuminata* and represents a unique mode of anticancer activity targeting human topoisomerase I.²⁰ Unfortunately, due to a poor solubility and some severe side-effects observed in clinical studies including hemorrhagic cystitis, the clinical trials were abandoned in 1974.

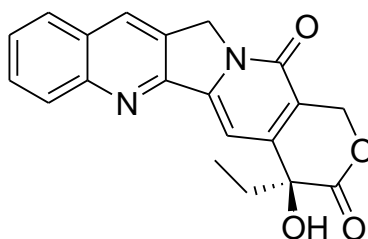


Figure 5. Structure of camptothecin

In order to improve the solubility, pharmacokinetics and toxicity, several camptothecin semi-synthetic derivatives were synthesized and among all, irinotecan and topotecan (Figure 6) reached the market.²¹

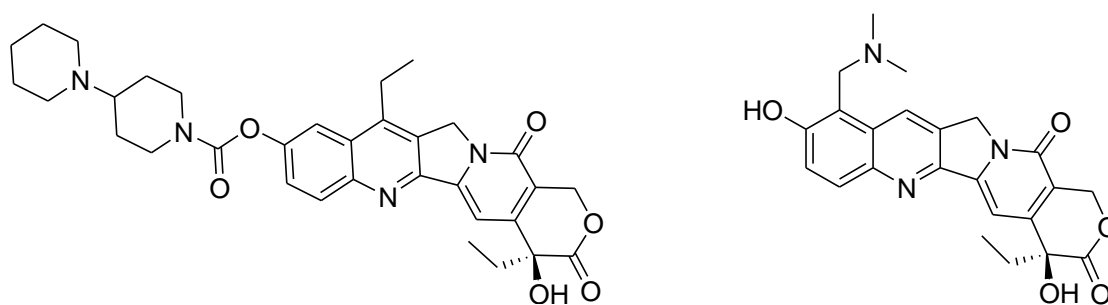


Figure 6. Structure of irinotecan (left) and topotecan (right)

Most antibiotic classes in use were discovered from *Actynomices*, *Penicillum* and *Cephalosporium* genera and, as in the case of anticancer drugs, many natural antibiotics could not be used as they were because of low potency/low bioavailability/pharmacokinetics problems or toxicity.

Probably, the best known case regards the antibiotic Cephalosporin C (Figure 7) discovered by Abraham and his colleagues in Oxford as a minor component of the antibiotic complex produced by *Cephalosporium acremonium*, a mold cultivated from a Sardinian sewage outfall by Prof. Giuseppe Brotzu in 1948 (Figure 7).²² In vitro and in vivo antibacterial screening of Cephalosporin C showed a very low potency against Gram negative bacteria and also a low chemical stability that precluded a therapeutic use. Cefalotin (Figure 7), the first semi-synthetic cephalosporin, was obtained by 7-aminocephalosporanic acid (7-ACA), which is derived from chemical deacylation of Cephalosporin C. With respect to Cephalosporin C, Cefalotin showed much more potency, chemical stability and a larger antibacterial spectrum. Nowadays 7-ACA is the key intermediate for producing about two thirds of cephalosporins in clinical use.²³

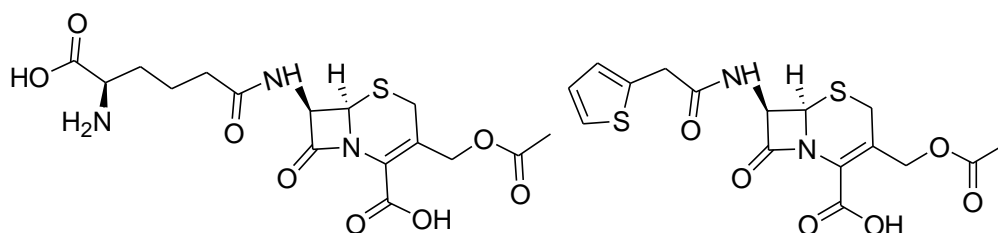


Figure 7. Structure of Cephalosporin C (left) and Cefalotin (right)

Plants furnished the first drug (Quinine, Figure 8) effective against malaria that has been used as one of the most effective treatments for malaria to date.²⁴ However, the low therapeutic index of quinine together with the widespread *P. falciparum* strains resistant to this drug, led to quinine synthetic analogs with few side effects.

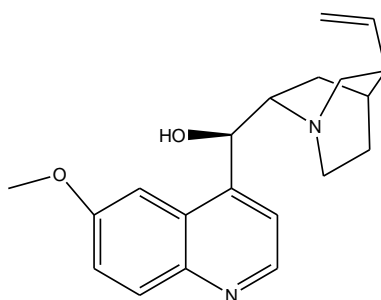


Figure 8. Structure of Quinine

Another plant-derived anti-malarian drug is represented by artemisinin (Figure 9), isolated in 1971 by Tu You You from the plant *Artemisia annua*.²⁴ Due to the importance of artemisinin in combating malaria, You You was awarded the joint Nobel Prize in Physiology or Medicine in 2015.²⁵ The discover that artemisinin metabolite, dihydroartemisinin (Figure 9), was the active compound, led to substitute in the antimalarian therapy artemisinin with the reduced product dihydroartemisinin or with the semi-synthetic prodrug derivatives artemether, artesunate and arteether.²⁴

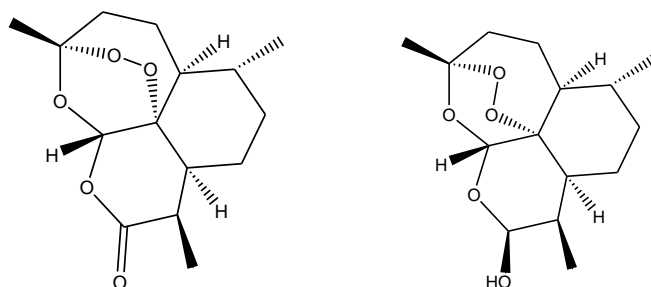


Figure 9. Structure of Artemisinin (left) and Dihydroartemisinin (right)

Natural compounds are still proving to be an invaluable source of medicines for humans. The success stories discussed here indicate that optimization of pharmacokinetics, stability, potency, and/or selectivity of natural products by targeted chemical modifications enables the development of natural products-based drugs.

Plant-derived and other natural product secondary metabolites have provided many novel prototype bioactive molecules, some of which have led to important drugs that are available on the market today.

REFERENCES

1. Firenzuoli, F.; Gori, L., Herbal medicine today: clinical and research issues. *Evidence-based complementary and alternative medicine : eCAM* **2007**, *4* (Suppl 1), 37-40.
2. Qiu, J., Traditional medicine: a culture in the balance. *Nature* **2007**, *448* (7150), 126-128.
3. Schippmann, U. W. L., D.; Cunningham, A.B.;, A comparison of cultivation and wild collection of medicinal and aromatic plants under sustainability aspects. *Frontis* **2006**, *17*, 75-95.
4. Lindberg, M. H. B. G., Spices as antioxidants. *Trends Food Sci Technol.* **1995**, *6* (8), 271-277.
5. Rios, J. L. R., M.C.;, Medicinal plants and antimicrobial activity. *Ethnopharmacol.* **2005**, *100* (1-2), 80-84.
6. Farnsworth, N. R. A., O.; Bingel, A.S.; Soejarto, D.D.; Guo, Z.;, Medicinal plants in therapy. *Bulletin of the World Health Organization* **1985**, *63* (6), 965-981.
7. Ganesan, A., The impact of natural products upon modern drug discovery. *Current opinion in chemical biology* **2008**, *12* (3), 306-317.
8. Folashade, O. O., H.; Ochogu, P.;, Standardization of herbal medicines-A review. *International Journal of Biodiversity and Conservation* **2012**, *4* (3), 101-112.
9. Farnsworth, N. R. S., D. D.;, Potential consequence of plant extinction in the United States on the current and future availability of prescription drugs. *Economic botany* **1985**, *39*, 231-240.
10. Ekka, N. R. N., K.P.; Samal P.K.;, Standardization strategies for herbal drugs-an overview. *Research Journal of Pharmacy and Technology* **2008**, *1* (4), 310-312.
11. Visalyaputra, S.; Petchpaisit, N.; Somcharoen, K.; Choavaratana, R., The efficacy of ginger root in the prevention of postoperative nausea and vomiting after outpatient gynaecological laparoscopy. *Anaesthesia* **1998**, *53* (5), 506-510.
12. Harvey, A. L., Natural products in drug discovery. *Drug Discov Today* **2008**, *13* (19-20), 894-901.
13. Veeresham, C., Natural products derived from plants as a source of drugs. *Journal of advanced pharmaceutical technology & research* **2012**, *3* (4), 200-201.
14. Newman, D. J.; Cragg, G. M.; Snader, K. M., Natural products as sources of new drugs over the period 1981-2002. *J Nat Prod* **2003**, *66* (7), 1022-1037.
15. Passarella, D.; Peretto, B.; Blasco y Yepes, R.; Cappelletti, G.; Cartelli, D.; Ronchi, C.; Snaith, J.; Fontana, G.; Danieli, B.; Borlak, J., Synthesis and biological evaluation of novel thiocolchicine-podophyllotoxin conjugates. *European journal of medicinal chemistry* **2010**, *45* (1), 219-226.
16. Lee, K.-H., Xiao, Z.;, Podophyllotoxins and analogs. In *Anticancer Agents from Natural Products*, Gordon M. Cragg, D. G. I. K., David J. Newman, Ed. Taylor and Francis: Boca Raton, 2005; pp 71-88.
17. Altmann, K. H.; Gertsch, J., Anticancer drugs from nature--natural products as a unique source of new microtubule-stabilizing agents. *Natural product reports* **2007**, *24* (2), 327-357.
18. Ojima, I., Kuduk, S.D., Chakravarty, S., Recent advances in the medicinal chemistry of taxoid anticancer agents. In *Advances in Medicinal Chemistry*, Maryanoff, B. E. R., A. B., Ed. JAI Press: Greenwich, CT, 1999; Vol. 4, pp 69-124.
19. La Regina, G.; Coluccia, A.; Naccarato, V.; Silvestri, R., Towards modern anticancer agents that interact with tubulin. *European journal of pharmaceutical sciences : official journal of the European Federation for Pharmaceutical Sciences* **2019**, *131*, 58-68.
20. Hsiang, Y. H.; Hertzberg, R.; Hecht, S.; Liu, L. F., Camptothecin induces protein-linked DNA breaks via mammalian DNA topoisomerase I. *The Journal of biological chemistry* **1985**, *260* (27), 14873-14878.
21. Bailly, C., Irinotecan: 25 years of cancer treatment. *Pharmacological research* **2019**, *148*, 104398.
22. Greenwood, D., *Antibiotic and Chemotherapy*. Ninth Edition ed.; 2010.
23. Barber, M. S.; Giesecke, U.; Reichert, A.; Minas, W., Industrial enzymatic production of cephalosporin-based beta-lactams. *Advances in biochemical engineering/biotechnology* **2004**, *88*, 179-215.
24. Tse, E. G.; Korsik, M.; Todd, M. H., The past, present and future of anti-malarial medicines. *Malaria journal* **2019**, *18* (1), 93.
25. The Nobel Prize in Physiology or Medicine 2015. (Accessed 24 Mar 2018).

1. Natural and hydrolyzed compounds from *Teucrium flavum* subsp. *glaucum* as inhibitors of HIV-1 RT RNase H function

1.1 Human Immunodeficiency Virus (HIV)

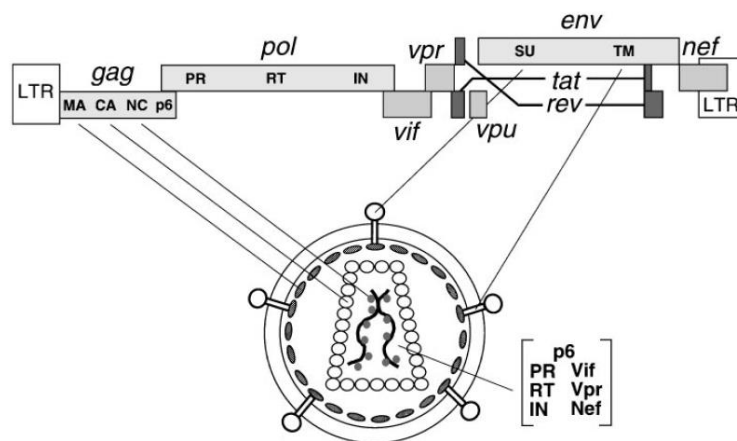
1.6.3 Short history of the discovery of HIV

Human Immunodeficiency virus known by the acronym HIV is the cause of the Acquired Immune Deficiency Syndrome (AIDS). HIV is characterised at the biological level by a profound depression of cellular immunity and clinically by infections in immunodepressed patients. Person afflicted with AIDS do not die because of AIDS itself but they die because of other opportunistic diseases for the reason that HIV weakens the immunity and reduces ability to fight. The World Health Organization (WHO) report indicated that the high increase in financing for HIV programs in low- and middle-income countries is beginning to reach results. As a matter of fact, many countries are making progress in lowering AIDS deaths and preventing new infections; however, in 2017, there were 36.9 million [31.1 million–43.9 million] people living with HIV, whose 35.1 million [29.6 million–41.7 million] are adults and 1.8 million [1.3 million–2.4 million] are children (<15 years).¹ The US Federal Drug Administration (FDA) has already approved 25 drugs for the treatment of AIDS.

In 1983 Luc Montagnier and his colleagues from the Pasteur Institute, claimed to have discovered the virus HIV. HIV was firstly considered similar to Human T Leukemia virus (HTLV) because of these various manifestations: the decrease in the levels of a CD4+ T cells and HTLV was one of those responsible agents. Moreover, there were animal models in which retroviruses caused not only leukemias or lymphomas, but also an AIDS-like syndrome. Furthermore, HTLV was transmitted through blood and sexual activity.^{2,3} Therefore, all these evidences lead to the start a search for the new virus. In 1984 biological and molecular characterization⁴⁻⁶ on HIV, so renamed by an International Nomenclature Committee, confirmed its relationship with AIDS. The identification had been a real challenge because this pathology is characterised by clinical signs that appeared years after the infection had occurred, and by then, patients usually had numerous other infections. It was finally accepted by the scientific and medical community and it was further supported by the isolation of a second virus (HIV-2), from West African patients in 1986.⁷

1.1.2 HIV Morphology

HIV is grouped to the genus *Lentivirus* within the family of *Retroviridae*, subfamily *Orthoretrovirinae*.⁸ The virus particle is spherical in shape with about 145 nm (95-166 nm range) in diameter with an outer lipid membrane as its envelope.⁹ The HIV genome is made of two identical single-stranded RNA molecules that are enclosed within the core of the virus, with several molecules like RT/RNase H and integrase (IN) that bound to the nucleic acid.⁸ The proviral DNA is generated by reverse transcriptase that converts the viral RNA genome into DNA, it degrades RNA and integrates double-stranded into the human genome. The DNA genome contains at both ends long terminal repeat (LTR) sequences. The 5' LTR region codes for the promotor for transcription of the viral genes. The genome is composed of 9 open reading frames encoding 15 viral proteins.¹⁰ From 5' to 3' the reading frame encode, respectively, the *Gag*, *Pol*, and *Env* polyproteins, which are cleaved into individual proteins, during the maturation, the budding process and release of virions from the cell. The four *Gag* proteins and the two *Env* structural components involved in making up the core and outer membrane envelope, while the three *Pol* proteins, encapsulated within the particle, have enzymatic functions. There are, also, two regulatory proteins, *Tat* and *Rev*, and four accessory proteins (*Vif*, *Vpr*, *Vpu*, *Nef*) one of these, *Vpu*, is important in assembly of the virion. HIV-2 codes for *Vpx* instead of *Vpu*, which is partially responsible for the reduced pathogenicity.¹¹



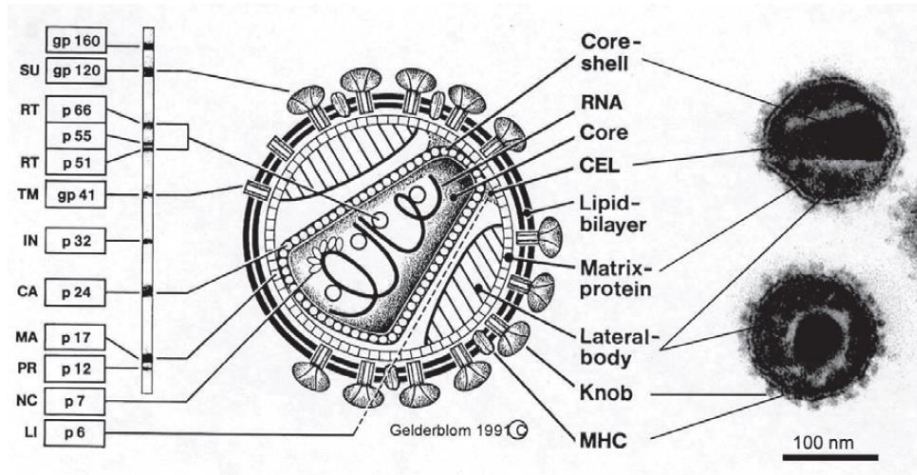


Figure 1. Structure of HIV

1.1.3 Replication of HIV

HIV-1 replication cycle could be divided into 15 steps, as depicted in Figure 2. Entry of HIV into the host cell requires the binding of one or more gp120 molecules on the virus to CD4 molecules on the host cell's surface. Interaction of the gp120 subunit of the HIV-1 envelope with CD4 is followed by binding to an additional coreceptor, either the CC chemokine receptor CCR5 or the CXC chemokine receptor CXCR4.¹²⁻¹⁵ The replication begins with the interaction of the viral genome into a host chromosome.

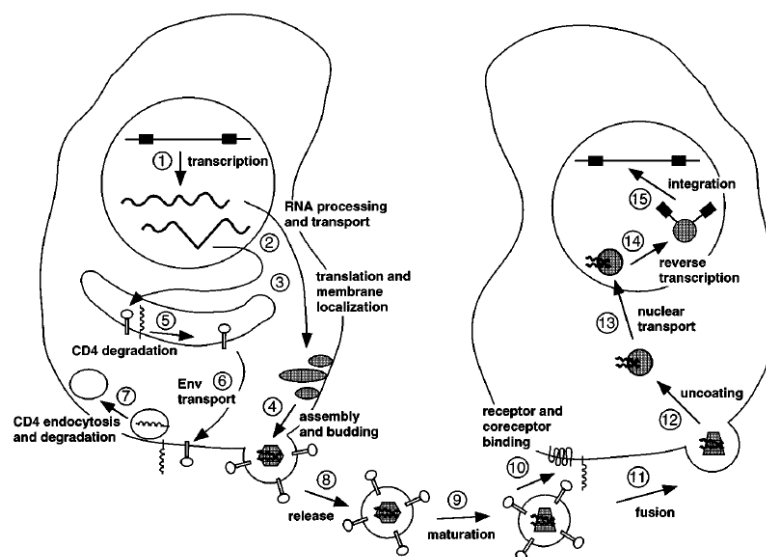


Figure 2. Replication cycle of HIV

1.2 Reverse Transcriptase (RT)

The HIV-1 reverse transcriptase (RT) is a multifunctional enzyme that shows all these activities:

- RNA-dependent DNA polymerase (RDDP)
- DNA-dependent DNA polymerase (DDDP)
- Ribonuclease H (RNase H)

This enzyme is a heterodimer composed of 2 subunits with 560 and 440 residues, p66 (66kDa) and p51 (51kDa). Both subunits share the same amino acid sequence, but p66 contains polymerase and RNase H domain, while p51 plays a more structural role.¹⁶

RT catalyzes the conversion of a single-stranded viral RNA to a DNA, mediated by RDDP, which uses RNA, as a reference, to synthesize a single-stranded of DNA. RNase H plays a central role in the replication cycle because it splits the hybrid RNA/DNA during transcription; afterward DDDP uses DNA to complete the double helix. Finally, IN integrates it into the host DNA.¹⁷

RNase H active site is located in p66 near the carboxyl terminus starting from Tyr₄₂₇¹⁸ and it has been revealed to be a sequence-nonspecific endonuclease, belonging to the nucleotidyl-transferase superfamily.¹⁹ X-ray diffraction proved the structure of RNAase H: a central 5-stranded mixed β -sheet flanked by four α -helices in an asymmetric distribution.²⁰ The active center of the RNase H domain is characterized by a highly conserved DEDD domain, containing D549, E478, D443 and D498, which coordinates two divalent cations (Mn^{2+} or Mg^{2+}) required to hydrolyze the RNA substrate. Mutations in any of these four residues inhibit its activity.²¹ The most recent studies have demonstrated the presence of two-metal ions in the active city as a critical role in the catalysis.^{19,22}

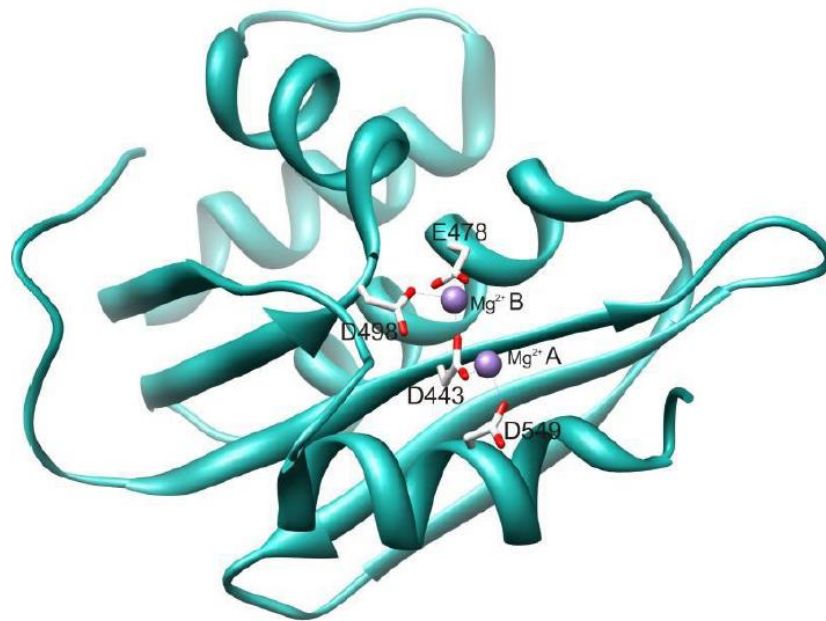


Figure 3. Structure of the RNase H domain of HIV-1 RT

Mechanism of action

The reverse transcription starts with the connection of tRNA^{Lys3} to the primer binding site (PBS) near the 5'-end of the genome. RT elongates the tRNA primer to the 5' end of the viral genome, forming the (-)-strand stop DNA. During the (-)-strand synthesis, RNase H degrades the RNA of the RNA/DNA hybrid intermediate. The new-strand is transferred to the 3' end of the template RNA. Then, while the (-)-strand continues its elongating, RNase H degrades the entire template RNA almost only leaving the polypurine tract (PPT) as primer for the (+)-strand DNA synthesis; afterward, the RNase H removes the PPT and tRNA and the second strand transfer takes place. The synthesis continues until the double stranded DNA molecule is completed.^{23,24}

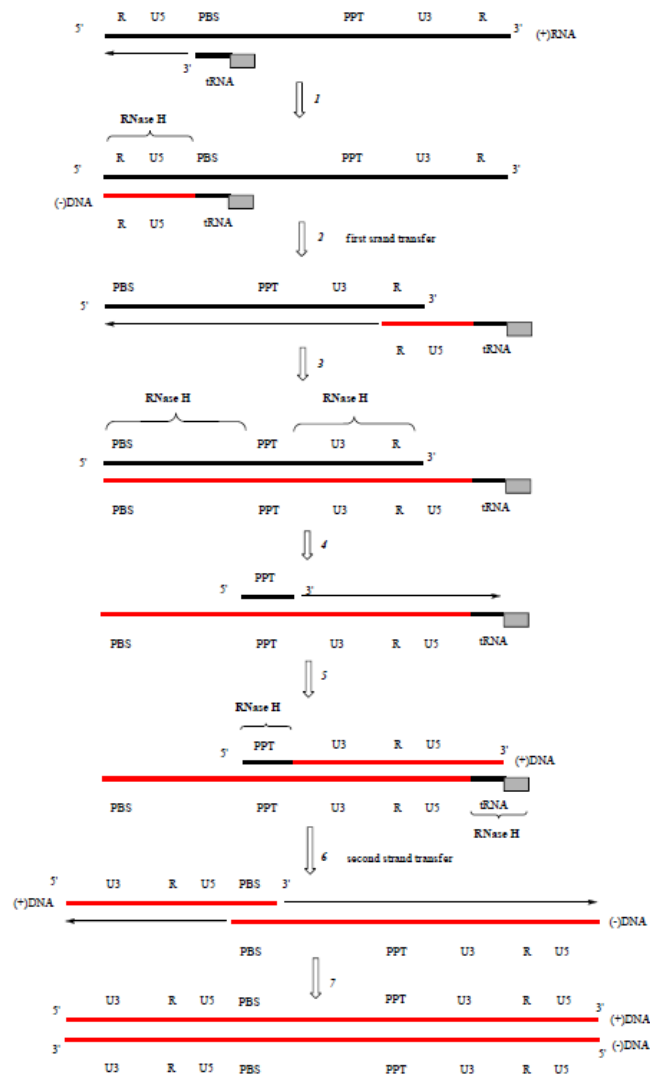


Figure 4. RT-mediated reverse transcription process of HIV-1

1.3 Anti-HIV Drugs

The first drug approved for the treatment of the AIDS was an HIV reverse transcriptase inhibitor, azidothymidine also known as Zidovudine. Therefore, reverse transcriptase has been the first target in the treatment of HIV and it led to the development of antiretroviral therapy. In the fight against AIDS, highly active antiretroviral therapy (HAART) proposed by Dr. David Ho in 1996 has achieved great success in controlling AIDS epidemic. HAART transforms HIV infection from an inevitably fatal disease into a manageable chronic ailment and drastically reduced the morbidity and mortality of HIV-infected patients.²⁵

Despite HAART has great contribution in HIV treatment, associated undesirable side effects of RT inhibitors and development of drug resistance strains limits the use of this therapy. Therefore,

medicinal chemists are still exploring continuously new anti-HIV drug candidates with increased potency, novel targets, improved pharmacokinetic properties, and reduced side effects.

Nowadays, there are 26 drugs licensed for treatment of HIV infection,²⁶ classified into four categories based on the mode of action:

- Reverse transcription Inhibitors (NRTIs and NNRTIs).
- Drugs that block the viral entry into the host cell with entry inhibitors, including fusion inhibitor
- Drug inhibiting integration of viral DNA with host genetic material (Integrase Inhibitors)
- Protease inhibitors that block the viral maturation

In this PhD thesis we focused the attention on the NRTIs and NNRTIs.

1.3.1 Reverse transcription Inhibitors (NRTIs and NNRTIs)

RT inhibitors can be classified as Nucleoside Reverse Transcriptase Inhibitors (NRTIs) and Non-Nucleoside Reverse Transcriptase Inhibitors (NNRTIs).

NRTIs

NRTIs are nucleoside or nucleotide analogues that are converted into triphosphate derivatives that act as competitive inhibitors with natural dNTPs for incorporation in the nascent DNA chain,²⁷ thus DNA elongation is blocked due to the lack of a 3'-OH in the ribose ring. The first drug approved was AZT. However, its use in AIDS patients was soon recognized useless, indeed it induced mutation of the virus.²⁸ After the discovery of AZT, six other drugs were approved in treatment of HIV and HBV:

- Didanosine (ddI [2',3'-dideoxyinosine])
- Zalcitabine (ddC [2',3'-dideoxycytidine])
- Stavudine (d4T [2',3'-didehydro-3'-deoxythymidine])
- Lamivudine (3TC [2',3'-dideoxy-3'-thiacytidine])
- Abacavir (ABC) [(1S, 4R)-4-(2-amino-6-(cyclopropylamino)- 9H-purin-9-yl)-2-cyclopentene-1-methanol]
- Emtricitabine [(-) FTC (2',3'-dideoxy-5-fluoro-3'-thiacytidine).

There are two mechanism of resistance developed against NRTIs. The first includes resistant species that could be able to recognise the triphosphate derivatives of NRTIs. The second involves the

acquisition of mutations known as ‘thymidine analogue resistance mutations’ (TAMs) because they appear after treatment with AZT or d4T; the mutated virus are able to phosphorolysed 30-terminal chain-terminators from blocked DNA primers.²⁹

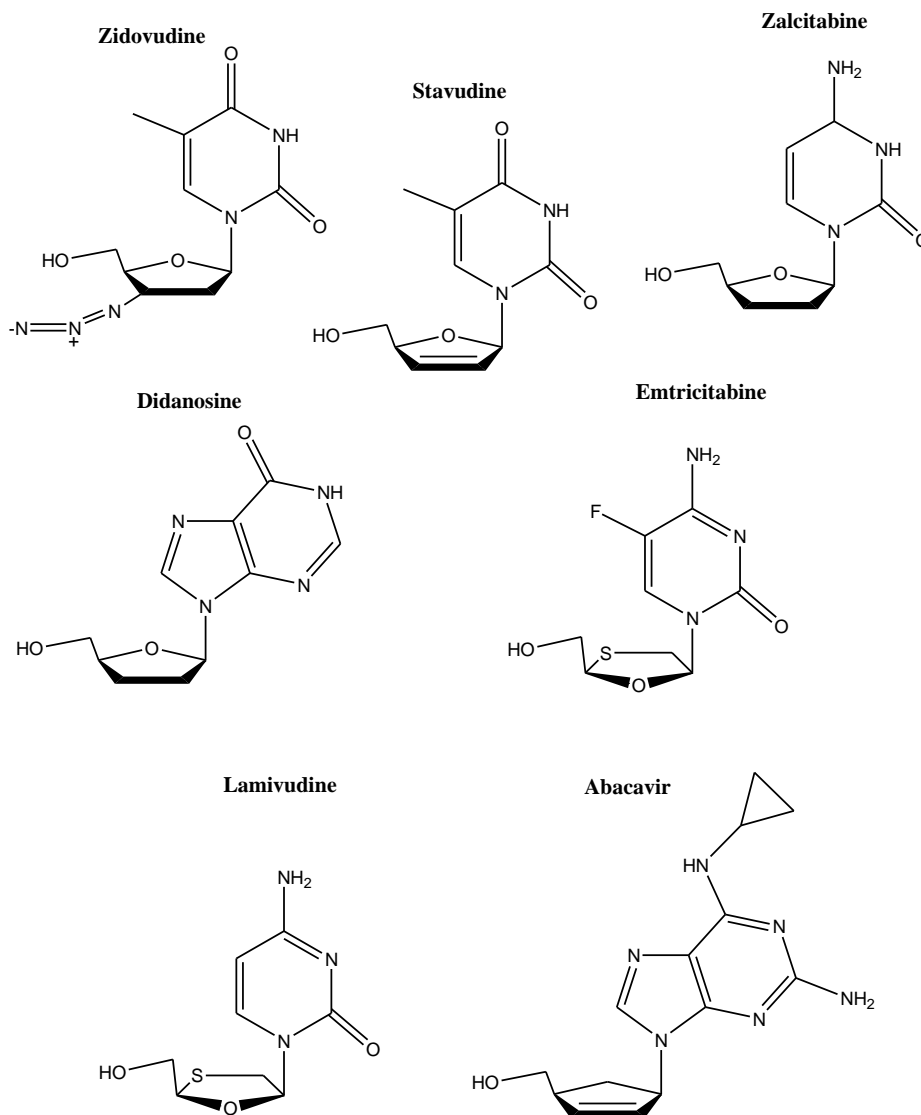


Figure 5. Nucleoside/Nucleotide reverse transcriptase inhibitors (NRTIs)

NNRTIs drugs

Instead of NRTIs, NNRTIs are small hydrophobic compounds that bind at a hydrophobic pocket that is situated approximately 10 Å from the RT DNA polymerase active site,³⁰ serving as non-competitive inhibitors^{31,32} in HIV-1, but not in HIV-2. FDA-approved NNRTIs include nevirapine (NVP), delavirdine, efavirenz (EFV), MIV-150 and three diarylpyrimidine (DAPY) derivatives including

etravirine (ETV) rilpivirine (RPV) and dapivirine (DAP). It has been suggested at least three mechanisms of action, that are not mutually exclusive:

- 1) the first theory suggests that the drug binding distorts the geometry of tyrosine-methionine-aspartic acid-aspartic acid moiety (YMDD) in the DNA polymerase catalytic site locking the enzyme in an inactive conformation;³³
- 2) Hsiou et al. reported a deformation of ‘primer grip’, a region involved in the precise positioning of the primer DNA strand in the polymerase active site, preventing the establishment of a ternary complex.³⁴
- 3) Since the mobility of the thumb might be important for the translocation of template and primer, Kohlstaedt *et al* T/P translocation, NNRTIs could reduce this mobility blocking the translocation and elongation of the nascent DNA moiety.³⁰

NNRTIs drugs have been included in first-line antiretroviral therapy (ART), typically composed by NVP, EFV or RPV in combination with two NRTIs; moreover, in 2008 ETR has been included in this treatment. NVP is used to prevent mother-to-child transmission; an analog of DAP is under study to test if a vaginal ring can prevent HIV-1 infection in women; a microbicide gel formulation containing the urea-PETT derivative MIV-150 is in a phase I study to evaluate safety, pharmacokinetics, pharmacodynamics and acceptability; a long acting RPV formulation is under-development for pre-exposure prophylaxis (PrEP).³⁵

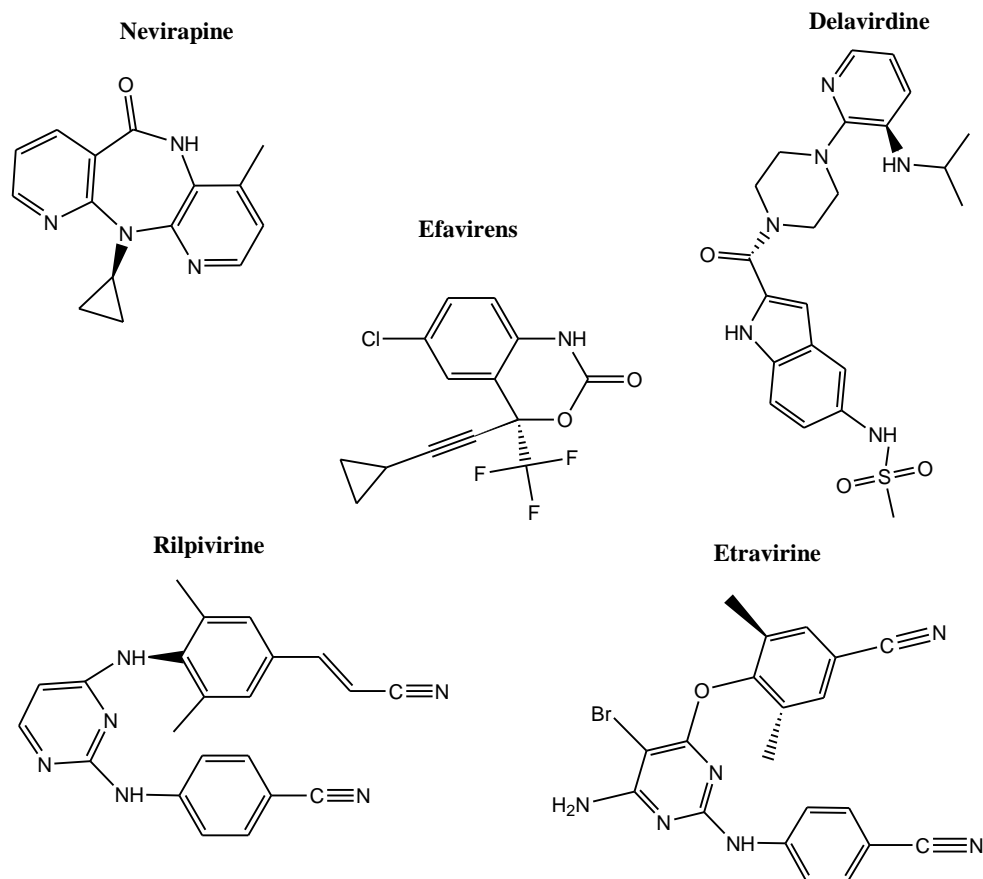


Figure 6. Non-Nucleoside Reverse Transcriptase Inhibitor (NNRTI)

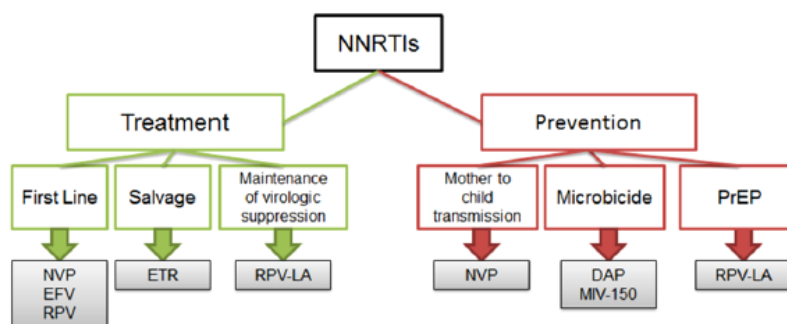


Figure 7. Use of NNRTIs in HIV-1 prevention and treatment strategies

There are two possible mechanisms of resistance developed against NNRTIs. One is that NNRTI resistance mutations are within or adjacent to the NNRTI-binding pocket, reducing susceptibility to two or more bindings. The second mechanism concerns a single mutation that could reduce clinical efficacy, as observed in EFV, NVP and RPV, while ETR requires two mutations. It is also known

that the cross-resistance could be possible in case of HIV-infection during NNRTI-containing PrEP or microbicide therapy, especially with DAPY analogs (DAP, RPV and ETR).³⁵

1.3.2 Inhibitors of RNase H function

Even though RNase H inhibitors have been described as early as 1990,³⁶ none of these have been approved for clinical purpose so far. Nevertheless, RNase H remains an attractive target for HIV therapy. Nowadays several promising compounds have been reported to inhibit HIV-1 replication at low concentration targeting RNase H function. RNase H inhibitors can be divided in two groups according to their mechanism of action: active site directed inhibitors and allosteric inhibitors.¹⁷

Active Site-Directed Inhibitors

The active site-directed inhibitors bind to the RNase H catalytic center by interacting with two metal cations; this interaction blocks the access of the metals to the phosphodiester bond in the RNA strand, thereby preventing the metal catalyzed hydrolysis reaction.³⁷ This subgroup contains several compounds such as: diketo acids, N-hydroxyimides, hydroxylated tropolones, pyrimidinol carboxylic acids, naphthyridinones and nitrofuranyl-2-carboxylic acid carbamoylmethyl esters (NACMEs).

Diketo Acids (DKAs). DKAs were initially developed as integrase inhibitors. Due to similarities between HIV IN and RT RNase H domain, DKAs were evaluated for potential inhibition of HIV-1 RNase H activity.³⁸ 4-[5-(benzoylamino)thien-2-yl]-2,4-dioxobutanoic acid (BTDBA) is one of the most active compounds. In order to be active the presence of metal cations seems to be essential. Thus it is probably that BTDBA binds directly the active site metal ions, confirmed by a moderate activity against HIV IN.³⁹ However, BTDBA did not show viral replication inhibition in cell culture.

Tramontano *et coll.*⁴⁰ reported that the DKA 6-[1-(4-fluorophenyl)methyl-1H-pyrrol-2-yl]-2,4-dioxo-5-hexenoic acid ethyl ester (RDS-1643) inhibited RNase H activity with an IC₅₀ value of 13 μM, selectively, but also inhibits the replication in MT-4 cell culture (EC₅₀ = 14 μM, CC₅₀ = 63 μM) either of wild either of resistant HIV-1 NNRTI strains. Therefore, RDS 1643 could be considered a promising compound.

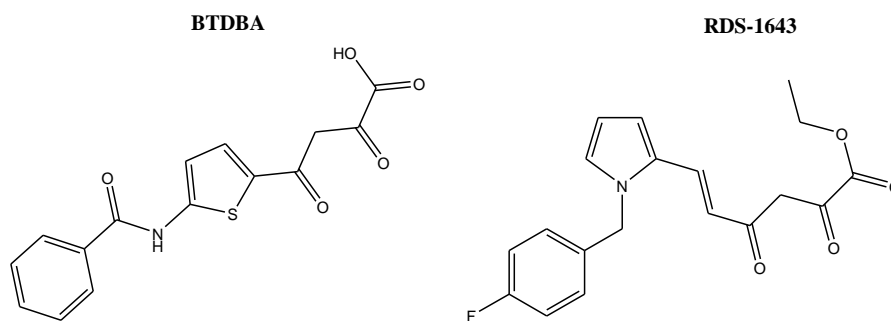


Figure 8. structure of BTDBA (left) and of RDS-1643 (right)

N-hydroxyimides (RNHI) were originally developed against influenza virus endonuclease because they are able to bind the metal ions in the active site. The pharmacophore is characterized by three oxygen atoms that mimic the enzyme active site metal ion interaction with the substrate during catalysis. Thus it would be expected to be competitive inhibitors of RNase H catalysis, confirmed by the crystal structures of the RNase H domain in complex with N-hydroxyimide inhibitors.^{41,42} Unfortunately, none of the compounds was able to inhibit HIV replication. Among all, 2-hydroxy-4H-isoquinoline-1,3-dione showed potent inhibition of HIV-1 RNase H activity with IC_{50} values in the range of 0.6-1 μ M, but inactive against RT polymerase activity. The structure-activity relationship studies showed that the N-hydroxy group is essential for the activity as well as the enol and substitutions on the phenyl moiety.⁴² 2-hydroxy-4-methoxycarbonylisoquinoline-1, 3(2H, 4H)-dione inhibits RT RNase H in vitro with IC_{50} of 61 nM and also HIV IN with less potency ($IC_{50} \sim 5 \mu$ M). Therefore the weak antiviral activity, ($EC_{50} \sim 13 \mu$ M), is mainly due to IN inhibition.⁴³

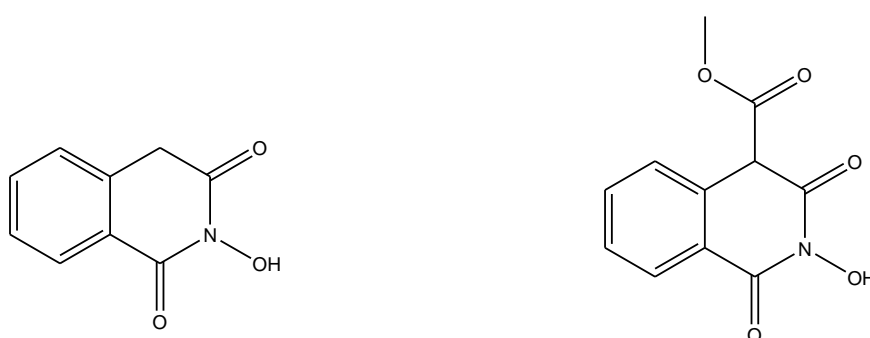


Figure 9. Chemical structures of 2-hydroxy-4H-isoquinoline-1,3-dione (left) and 2-hydroxy-4-methoxycarbonylisoquinoline-1, 3(2H, 4H)-dione (right)

The **pyrimidinol carboxylic acids (PCA)** have been designed by Kirschberg *et coll.*⁴⁴ based on structural analysis of DKAs, N-hydroxyimides and tropolones. These compounds coordinate with the two metal ions in the active site and selectively target the viral RNase H. The SAR studies showed that the carboxylate and phenolic hydroxyl groups are essential for dual metal chelation. Several compounds have been synthesised with modification on 2-position of pyrimidinol ring and some showed a methylene linker introduced between the pyrimidinol ring and phenyl ring (Figure 10); further optimisation on the benzyl moiety of **A** led to compound **B** as the most active PCA, inhibiting HIV-1 RNase H and human RNase H with IC₅₀ values of 0.17 μM and 70 μM, respectively. However, none of these compounds were reported to have antiviral activity.

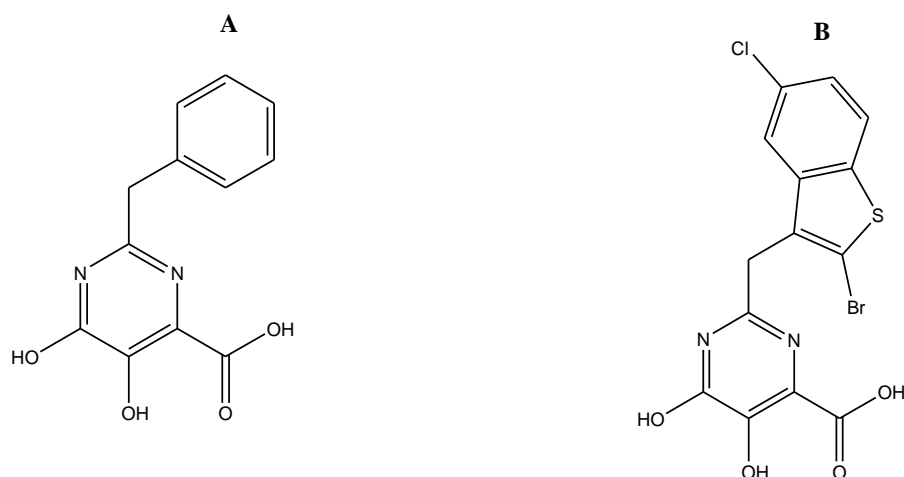


Figure 10. Chemical structure of the most active pyrimidinol carboxylic acids **A** (left) and **B** (right)

In 2010, Williams *et coll.*, with the purpose to obtain potent and selective RNase H inhibitors, designed **naphthyridinones** as new class of RNase H active site inhibitors.⁴⁵ The former compound in this series was MK1 that inhibited RT RNase H *in vitro* with IC₅₀ of 0.11 μM, the HIV IN (IC₅₀ = 0.9 μM), but had no effect on the polymerase activity of RT (IC₅₀ > 50 μM). MK1 showed good antiviral activity (EC₅₀ = 2.5 μM). An analog of MK1, substituted at the 4-position, demonstrated the best potency to inhibit RNase H with IC₅₀ of 45 nM, with 290- and 530-fold more selectivity for the RT polymerase and IN. This compound reported antiviral activity in the range of sub-micromolar (EC₅₀ < 0.2 μM); however, it is quite cytotoxic so that the *in vitro* specificity is insufficient to enable estimation of antiviral activity.³⁷

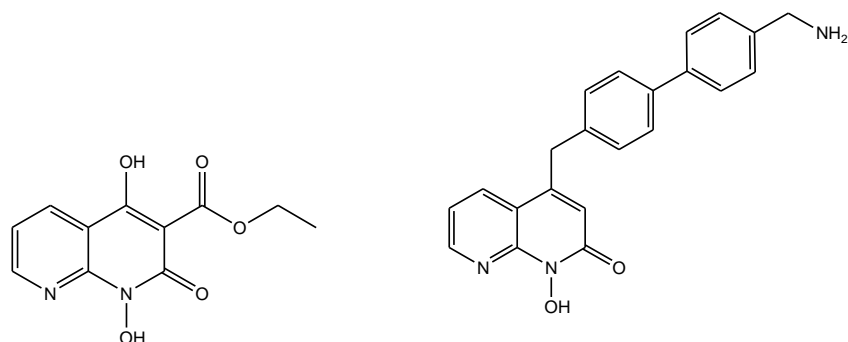


Figure 11. Chemical structure of the most active naphthyridinones

NACMEs have been discovered by Fuji *et coll.*⁴⁶. Among all derivatives, 5-nitro-furan-2-carboxylic acid adamantan-1-carbamoylmethyl ester (**c**) and 5-nitro-furan-2-carboxylic acid [[4-(4-bromophenyl)-thiazol-2-yl]-(tetrahydrofuran-2-ylmethyl)-carbamoyl]-methyl ester (**d**) were the most interesting compounds, which selectively inhibited RNase H activity in μM range, while did not have activity against HIV-1 IN or RT RDDP. Moreover, compound **d** was able to inhibit HIV-1 replication at a concentration of 20-25 μM . The SAR studies demonstrated that 5-nitro-furan moiety is essential for the activity. As a matter of fact, the substitution with other groups caused a drastic decrease in potency. Hiroshi *et al.*⁴⁷ designed new derivatives of 5-nitro-furan-2-carboxylic acid and one of these (**e**) improved by 18-fold the inhibition of RNase H.

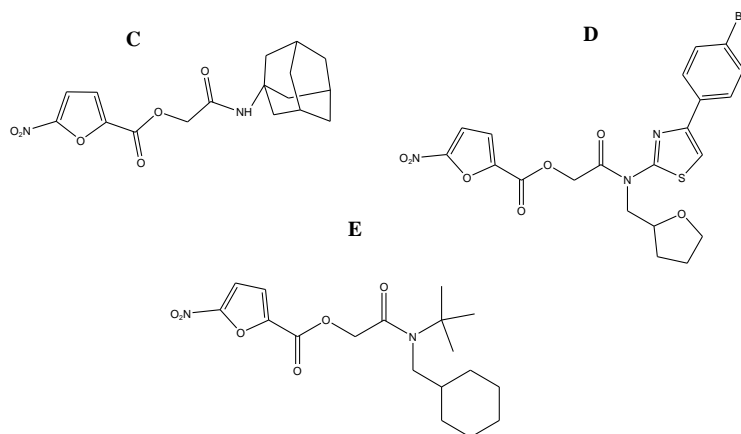


Figure 12. Chemical structure of the most active NACMEs

1.3.3 Synthetic Allosteric Inhibitors (RNHIs)

Synthetic RNHIs target a region outside the RNase H domain, an allosteric site. Up to now, only two class of compounds have been identified: N-acyl hydrazones and thiophene-3-carboxamides and thienopyrimidinones. Interestingly, both categories contain similar fragments in their structures and probably possess a common pharmacophore model.¹⁷

There is evidence that binding of NNRTIs as well as mutations in the allosteric pocket in the RT DNA polymerase domain have an impact on the activity RT RNase H, probably due to a change in the positioning of the RNA/DNA duplex nucleic acid after protein conformation changes in the polymerase domain, following NNRTI binding.⁴⁸⁻⁵⁰

N-acyl hydrazones

Ilina *et coll.*³⁷ have been the first group that reported **N-(4-tert-Butylbenzoyl)-2-hydroxy-1 naphthaldehyde hydrazone (BBNH)** as a good HIV RT RNase H inhibitor at low micromolar concentration, inhibiting both the RNase H and DNA polymerase activities of HIV RT.

Afterwards, some antiviral analogues of BBNH have been designed; these compounds, such as DHBNH, showed reduced metal binding and increased cytotoxicity. **DHBNH** is a potent HIV-1 RNase H inhibitor with an IC₅₀ value of 0.5 μM, but it did not have an effect on the RT RDDP enzyme.⁵¹ It has been confirmed by crystal structure of HIV-1 RT complexed with DHBNH, which also indicates the interaction with a new site, located between the polymerase active site and the non-nucleoside RT inhibitor (NNRTI) allosteric binding pocket (NNIBP). Modifications at *para*-position of the benzoyl ring of DHBNH could increase the inhibition of the RT polymerase activity by interacting with NNIBP.

Recently, new RNase H inhibitor, **BHMP07** has been synthesized; it binds to a pocket in the interface between the p51 subunit and the RNase H domain of the RT p66 subunit, probably recognising the region in the RNase H fragment.⁵²

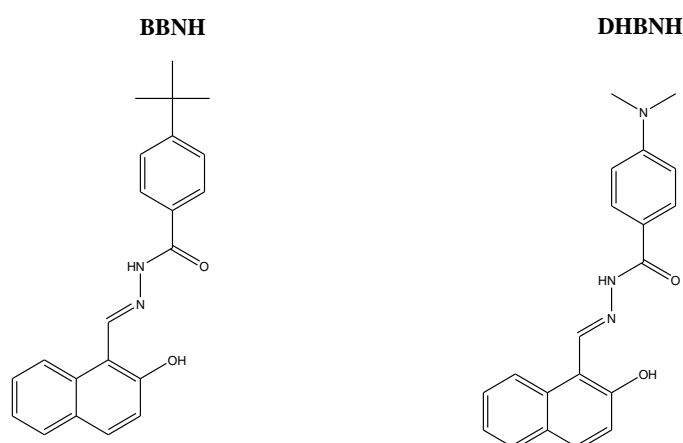


Figure 13. Structure of BBNH (left) and DHBNH (right)

Thiophene-3-carboxamides

Two thiophene-3-carboxamides, **NSC727447** and **NSC727448**, were identified as inhibitors of RNase H activity of HIV-1 and HIV-2 RT, with IC_{50} values of 2.0 and 3.2 μ M, respectively.⁵³ Moreover, NSC727447 is a selective RNase H inhibitor, indeed it did not show activity against DNA polymerase or pyrophosphorolysis up to the concentration of 50 μ M.

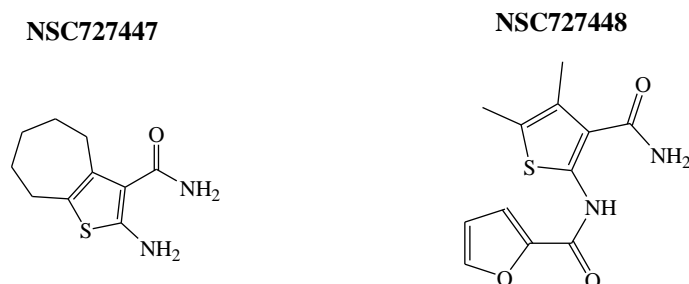


Figure 14. Chemical structure of thiophene-3-carboxamides derivatives.

Thienopyrimidinones

Based on the previous cyclized thiophene-3-carboxamides, Masaoka *et al.*⁵⁴ reported a series of novel thienopyrimidinones with substitutions on the thiophene or the C₂ position of the pyrimidinone ring. Among all, the most active derivatives were those with 3,4'-dihydroxyphenyl ring binding the allosteric site of RNase H function. It provides a new starting point for future optimisation.

Thiocarbamates and 1,2,4-triazoles were identified as inhibitors of HIV RT RNase H at Wyeth company.⁵⁵ However, there are no structural data supporting this theory of interaction with RT RNase H domain, while studies and crystallography show the binding in the NNRTI pocket in the RT DNA polymerase domain.^{56,57} Ilina *et al.* designed some triazole-derivatives,³⁷ but results suggest that these compounds bind RT polymerase NNRTI binding site and it is not ideal, because they would antagonize an entire class of active drugs. Nevertheless, other information about the binding on NNRTI-site, could be useful in the synthesis of dual inhibitors (RT polymerase, RT RNH)

1.4 Anti Rnase H Natural And Natural-Derived Compounds

Tropolones are terpenoids isolated from cupressaceae plants that contain a metal ion-chelating pharmacophore moiety. These compounds show several biological effects such as antitumor, antifungal, insecticidal and antimicrobial effects.

In National Cancer Institute library of pure natural products were identified two hydroxylated tropolones as effective and selective inhibitors of HIV-1 RNase H: β -thujaplicinol (2,7-dihydroxy-4-(1-methylethyl) 2,4,6-cycloheptatrien-1-one) and manicol (1,2,3,4-tetrahydro-5,7-dihydroxy-9-methyl-2-(1-methylethenyl)-6Hbenzocyclohepten-6-one) (Figure 15); the former was the most potent with IC_{50} values of 0.2 μ M for the inhibition of HIV-1 RNase H and 50 μ M for *E.coli* RNase H,⁵⁸ while the second one had inhibitory activity against the human HIV-1 RNase H and *E.coli* RNase H with IC_{50} values of 1.5 and 40 μ M, respectively. Interestingly, it was also observed that β -thujaplicinol, when used in combination with an NNRTI, calanolide A, showed activity due to the synergistic effect on HIV-1 RT polymerase function and RNase H.¹⁷ Another tropolone analog, β -thujaplicin (2-hydroxy-4-(methylethyl)-2,4,6-cycloheptatrien-1-one), lacking the OH group in position 7 of the heptatriene ring, was completely inactive, supporting the importance of 2,7-dihydroxy moiety of the activity.

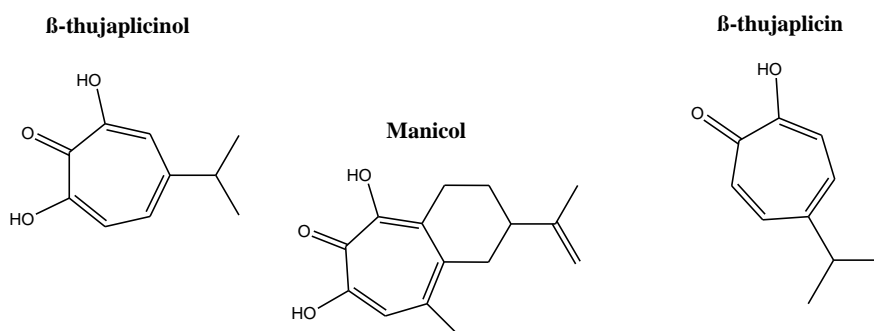


Figure 15. Structure of β -thujaplicinol, manicol and β -thujaplicin

Besides troponole derivatives, which are active Site-Directed Inhibitors on RNase H, natural products were discovered and screened for inhibitory activities against HIV-1 RNase H.

Among all, a secondary metabolite isolated from sponge *Smenospongia*, **illimaquinone**, inhibited the RNase H activity with an IC_{50} value of 15 μ M and low activity against RDDP. In the same study it had been reported that a replacement of 6'-hydroxyl group on the quinone ring with a methyl or acetate

group reduces the activity, which indicates that hydroxyl in ortho position to the carbonyl group is essential.³⁶

Ardimerin digallate, isolated from the plant of *Ardisia japonica*, showed IC₅₀ values of 1.5 and 1.1 μM for HIV-1 and HIV-2 RNase H in vitro, respectively, indicating a galloyl group as an important for anti-HIV activity.⁵⁹ **1,3,4,5-Tetragalloylapiitol**, extracted from *Hylodendron gabunensis*, inhibits HIV-1 and HIV-2 RNase H with IC₅₀ of 0.24 and 0.13 μM and human RNase H at low value (IC₅₀ = 1.5 μM).⁶⁰ Three new galloyl arbutins, obtained from *Eugenia hyemalis*, showed a good activity HIV-1 RNase H in vitro.⁶¹ 6''-O-galloylsalidroside, one of the eight compounds isolated from *Distylium racemosum* with the best IC₅₀ values against HIV-2 and human RNase H of 3.51 and 1.71 μM, respectively.⁶²

Esposito et al. reported a novel series of anthraquinone and alizarine analogs, showing interesting IC₅₀ values for both RT-associated functions.⁶³

During our ongoing search for bioactive secondary metabolites from plants, we discovered several RNase H inhibitors from the ayurvedic plant *Ocimum sanctum*.⁶⁴ Among the identified triterpenes, ursolic acid was the most potent inhibitor with a IC₅₀ value of 5.5 μM but also oleanolic acid and pomolic acid showed high potency with IC₅₀ values of 7.5 and 9.3 μM, respectively. The cyclohexane ring seems to be essential for the activity, indeed, the substitution with a cyclopentane, as reported in betulinic acid, reduced the potency. Although these compounds have already showed to possess anti HIV-1 RT effect,^{65,66} their anti-RNase H activity has been reported for the first time. Besides triterpenes, tetradecyl ferulate demonstrated an interesting anti-RNase H effect with a IC₅₀ of 12.1 μM. Due to the synthetic accessibility of ferulic acid derivatives, a structure-activity relationship study was carried out. For this reason, a series of esters and amides of ferulic and caffeic acids were synthesized and, among all, the most active was N-oleylcaffeamide, which displayed a strong inhibitory activity towards both RT-associated functions, ribonuclease H (IC₅₀ = 0.68 μM) and DNA polymerase (IC₅₀ = 2.3 μM). Indeed, it was observed that a short chain allowed a dual activity against RT functions, while the introduction of double bonds in long alkyl chain ferulates regains the anti RDDP activity and increases potency towards RNase H function. Moreover, caffeic acid derivatives are more active than ferulic acid derivatives, which indicates the importance of free hydroxyl groups of catechol ring to enhance potency towards both RNase H and RDDP. Finally, it was also observed that the substitution of ester moiety with an amide function increases the activity of caffeic acid derivatives; on the contrary, it results in lose of potency toward RNase H enzyme in ferulic acid derivatives, while the RDDP inhibition was increased of 2-fold.

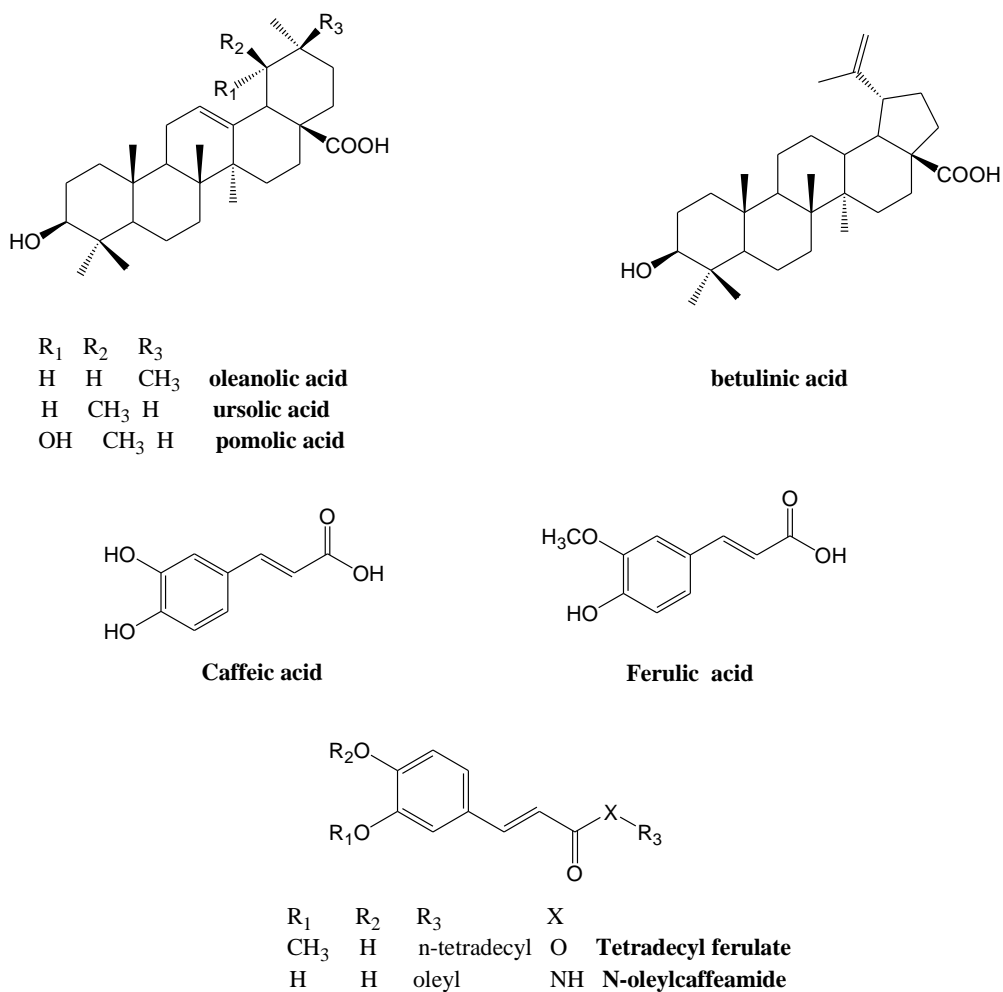


Figure 16. Structure of natural and synthetic compounds from *O.sanctum*

1.5 Advanced-Stage Anti-HIV Natural Products

Several natural products are in an advanced-stage of development in HIV therapy.

Calanolides A, a coumarin isolated from the tropical rainforest Tree, *Calophyllum lanigerum*, was identified as inhibitor of HIV-1 replication and cytopathicity with EC_{50} values of 0.02 μ M and 0.5 μ M, respectively. It inhibited HIV-1 RT interacting near the active site of the enzyme and interfering with dNTP binding. When combined to nevirapine an increase of the activity was observed.⁶⁷ In addition, calanolide A is active against the AZT-resistant G-9106 strain and also against the pyridinone-resistant A17 strain, which are resistant to non-nucleoside RT inhibitors.⁶⁸ Nevertheless, they were inactive against DNA polymerases and HIV-2 RT. The latest information insert Calanolide A in phase IB trials for evaluation of the safety, pharmacokinetics, and effects in HIV-positive patients.⁶⁹

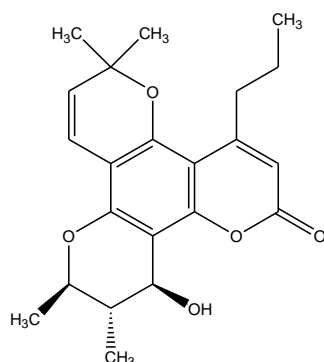


Figure 17. Structure of Calanolide A

Bevirimat [3-*O*-(30,30-dimethylsuccinyl)betulinic acid or PA-457] is a semi-synthetic derivative of betulinic acid.⁷⁰ Li *et coll.*,⁷⁰ demonstrated that PA-457 inhibits replication of WT and drug-resistant HIV-1 isolates, also it does not block virus attachment, entry or inhibit RT/PR activity *in vitro*. Bevirimat, as indinavir, blocks virus replication at a time point after the completion of viral DNA integration and Tat expression. Therefore, it inhibits virion maturation, blocking a late step in Gag processing involved in the conversion of the capsid precursor (p25) to mature capsid protein (p24). This inhibition led to the production of non-infectious and immature viral particle, with virions that display spherical, acentric cores and with an additional electron-dense layer inside the viral membrane. They also found that a single mutation, which confers resistance to PA-457, maps to the p25 to p24 cleavage site. Based on the potent *in vitro* and *in vivo* antiviral activity, PA-457 was granted ‘Fast-Track’ New Drug Development status by the US FDA in December 2004.⁷¹ Since 2008, it is under phase IIb clinical trial.⁷² So far, it has been observed that Bevirimat has a favorable pharmacokinetic profile in healthy humans and HIV-infected patients after a single oral administration.^{73,74} Indeed it is well oral absorbed, it has long half-life, which could support once-daily dosing;⁷³ it is not oxidatively metabolized and it is eliminated by hepatic glucuronidation.⁷⁵

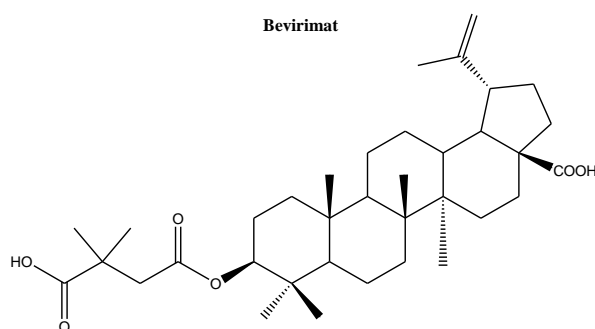


Figure 18. Structure of Bevirimat

PA1050040, an analog of bevirimat, is a maturation inhibitor, as well. It seems to be active against bevirimat-resistant strains and resistant to approved ARVs. Now it is in phase I of clinical trials for single-dose testing.

DCK, 30R,40R-di-*O*-(-)-camphanoyl-(+)-cis-khellactone, is suksdorfin derivative, more potent against HIV-1 with an EC₅₀ 0.049 μM.⁷⁶ Preliminary studies on the mechanism of action indicated that it inhibits replication in infected cells, after viral entry, but before integration and it did not block HIV-RT, PR, and IN activity. 4-Methyl-DCK was 10 times more active than DCK with an EC₅₀ of 0.0059 μM.⁷⁷ Currently it is under preclinical trial.

Cyanovirin-N (CV-N) is a 11-kDa virucidal protein, isolated from cultures of the cyanobacterium (blue-green alga) *Nostoc ellipsosporum*. Boyd *et coll.*⁷⁸ reported that CV-N irreversibly inactivates diverse laboratory strains and primary isolates of HIV-1 and HIV-2 and simian immunodeficiency virus at low nanomolar concentrations. In addition, it interferes with cell-to-cell fusion and transmission of HIV-1 infection. Therefore, the activity is due, at least in part, to the interaction with glycoprotein gp120. Moreover, CV-N is resistant to physicochemical denaturation, increasing its use in anti-HIV therapy. Indeed, cyanovirin-N binds high-mannose oligosaccharides on the viral envelope, which are cell receptors essential for viral entry and cell-to-cell fusion.⁷⁹ It could be used as a systemic compound to control viral load or in the development of microbiocides to prevent primary viral infection. It was showed that PEGylated cyanovirin-N would be helpful to overcome problems associated with the use of proteins.⁸⁰ Now it is under preclinical phase of clinical trial.

1.6 *Teucrium flavum* subsp. *glaucum*

The genus *Teucrium* (Lamiaceae) comprises more than 300 species, and is widely distributed in Europe (50 species), especially in the Mediterranean area. *Teucrium* species are generally aromatic and ornamental plants as well as are valued as pollen sources. The name *Teucrium* derives from Teucer, a son of Talomon, king of Salamis. Teucer was the first to use in ancient Greek age the *Teucrium* species for their curative properties such as diuretic, antiseptic, antipyretic, antispasmodic agents and for the treatment of digestive and pulmonary diseases (coughs and asthma).⁸¹ The activities are mainly due to the presence of flavonoids, phenolic acids, diterpenoids.⁸²⁻⁸⁴ The genus *Teucrium* is one of the richest sources of clerodane diterpenes that have been recognised as insect antifeedants⁸⁵ and potent hepatotoxics.⁸⁶ *Teucrium* species were also used as alimentary plants and some of them are currently employed for flavouring beer and wine, herbal teas, bitters and liqueurs.⁸⁷



Figure 19. *Teucrium flavum* subsp. *glaucum*

Teucrium flavum subsp. *glaucum* is an evergreen perennial shrub with pubescent stems up to 60 cm, triangular-ovate leaves and yellow flowers, which appears from May to August, collected in terminal spikes; it grows up in the calcareous areas of “Supramonte di Orgosolo” and “Monte Marganai” (Iglesias) up to 1000 m above sea level. This species is represented in the Mediterranean flora by four subspecies: *flavum*, *glaucum*, *gymnocalyx* and *hellenicum*.⁸⁸ Relatively to Italy, which displays *glaucum* and *flavum* subspecies as islander and continental species respectively, Sardinia and Corsica islands are the only one that display the *glaucum* subsp. The *glaucum* subsp. exhibited some particularities compared to the other subspecies: plant size is around 25–50 cm, the leaf length is

1.5–2 cm and the leaf and stem are partially covered by peltate hair.⁸⁹ Moreover, *T. flavum* oils are dominated by hydrocarbons (60.5–83.7%) and all compounds have been identified in both subspecies, *glaucum* and *flavum*.⁹⁰

In literature there are few works concerning the chemical composition of the genus *Teucrium flavum*; Harborne *et coll.*⁸² identified the widespread presence of flavonoids like cirsiolol, cirsimaritin, cirsilinol, salvigenin and 5-hydroxy-6,7,3',4'-tetramethoxyflavone. Two studies^{83,91} reported the isolation of the diterpenoids teuflidin and teuflin, while there is only one study about *T. flavum* subsp. *glaucum* describing the identification of a neo-clerodane diterpenoid (teuflavin), a 19-nor-neo-clerodane glucoside (teuflavoside), the neo-clerodane diterpene teuflin and the flavone salvigenin.⁸⁴

1.6.1 Aim and Objectives

As described in the previous chapter, various plant secondary metabolites have been identified as HIV-1 RT-associated RNase function inhibitors and some were also able to block the HIV replication.^{40,45,70, 76} During the continuous search of secondary plant metabolites with inhibitory action of the HIV-1 RT RNase function, we found that the ethyl acetate (EtOAc) extract from the leaves of *Teucrium flavum* subsp. *glaucum* showed a significant inhibitory activity of this enzyme function with an IC₅₀ of 28.6 µg/ml. In order to identify the molecules responsible of this activity, we decided to carry out a bioguided fractionation of the extract.

The secondary metabolites were identified mainly by 1D and 2D NMR techniques as well as HR-MS and tested toward RNase H and RDDP activities of HIV-1 RT. In order to justify the interaction of the most active compound(s) against RT, site-directed mutagenesis was performed.

Finally, with the aim to gain a deeper understanding of the RT–ligand interactions docking experiments were carried out.

1.6.2 Results and Discussion

The active extract was subjected to vacuum liquid chromatography (VLC) with solvent mixtures of increasing polarity. Therefore, 45 fractions were obtained that, on the basis of their similarity in TLC, were combined into seven main fractions (F1-F7). Six fractions were further tested in the RT RNase H inhibition assay. The screening showed that the anti-RNase activity was concentrated in three fractions (F2-F4) and in particular on the fourth one which was able to inhibit this function with an IC₅₀ of 9.9 µg/ml (Table 1). Due to the low yield of F1 fraction (42.4 mg), it was purified without testing. The F5-F7 fractions had no effect on the RT up to the concentration of 100 µg/ml (Table 1).

Table 1. Results of RT RNase H function inhibition by *T. flavum* subsp. *glaucum* fractions

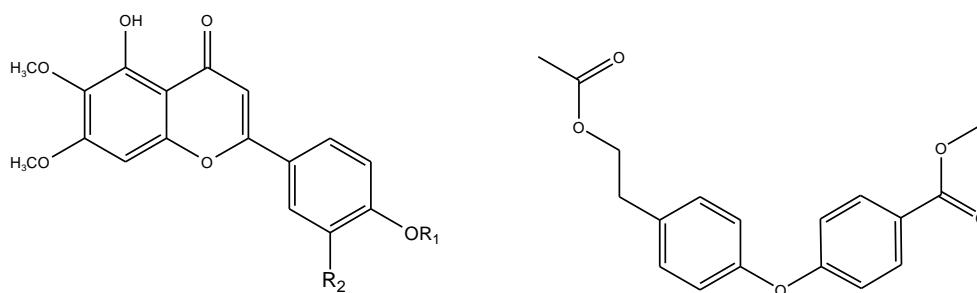
Extract/Fractions	HIV-1 RT RNase H IC ₅₀ (µg/ml) ^a
EtOAc extract	28.6 ± 3.0
F1	ND
F2	25.6 ± 7.4
F3	20.3 ± 4.0
F4	9.9 ± 2.5
F5	>100 (100%) ^b
F6	>100 (100%) ^b
F7	>100 (100%) ^b

^aConcentration capable of inhibiting 50% of enzyme activity

^bPercentage of residual enzyme activity in the presence of 100 µg/ml extract

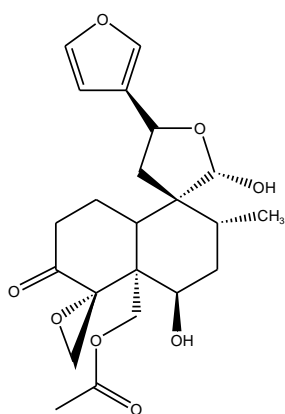
Therefore, we decided to purify the three most active fractions using chromatographic techniques such as column chromatography, solid phase extraction (SPE), VLC and semi-preparative HPLC. These techniques have allowed to isolate three flavones (**1-3**), a diphenyl ether (**4**) and a neo-clerodane, teuflavin (**5**) (Figure 20), whose structures have been elucidated mainly by mono and two-dimensional Nuclear Magnetic Resonance and Mass Spectrometry (ESI MS) techniques. With the aim to find a structure-activity relationship, we also decided to purify the two inactive fractions F5 and F6 resulting in the isolation of a further neo-clerodane, teuflavoside (**6**).

In particular, from F1 fraction a new natural molecule, the methyl ester of 3-[4-(2-acethoxyethyl)-phenoxy]-benzoic acid (**4**), was isolated. Salvigenin (**3**) was isolated from fractions 2-4, while cirsimaritin (**2**) and cirsiolol (**1**) from F3 and F4, respectively. Teuflavin (**5**) was purified from F3 while teuflavoside (**6**) from F5 and F6 (Figure 20).

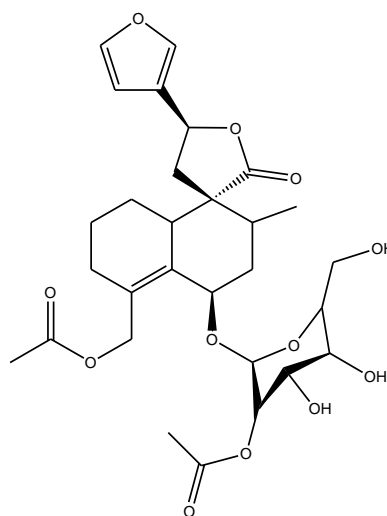


Salvigenin (**1**) $R_1 = \text{CH}_3$ $R_2 = \text{H}$
 Cirsimaritin (**2**) $R_1 = \text{H}$ $R_2 = \text{H}$
 Cirsiolol (**3**) $R_1 = \text{H}$ $R_2 = \text{OH}$

4

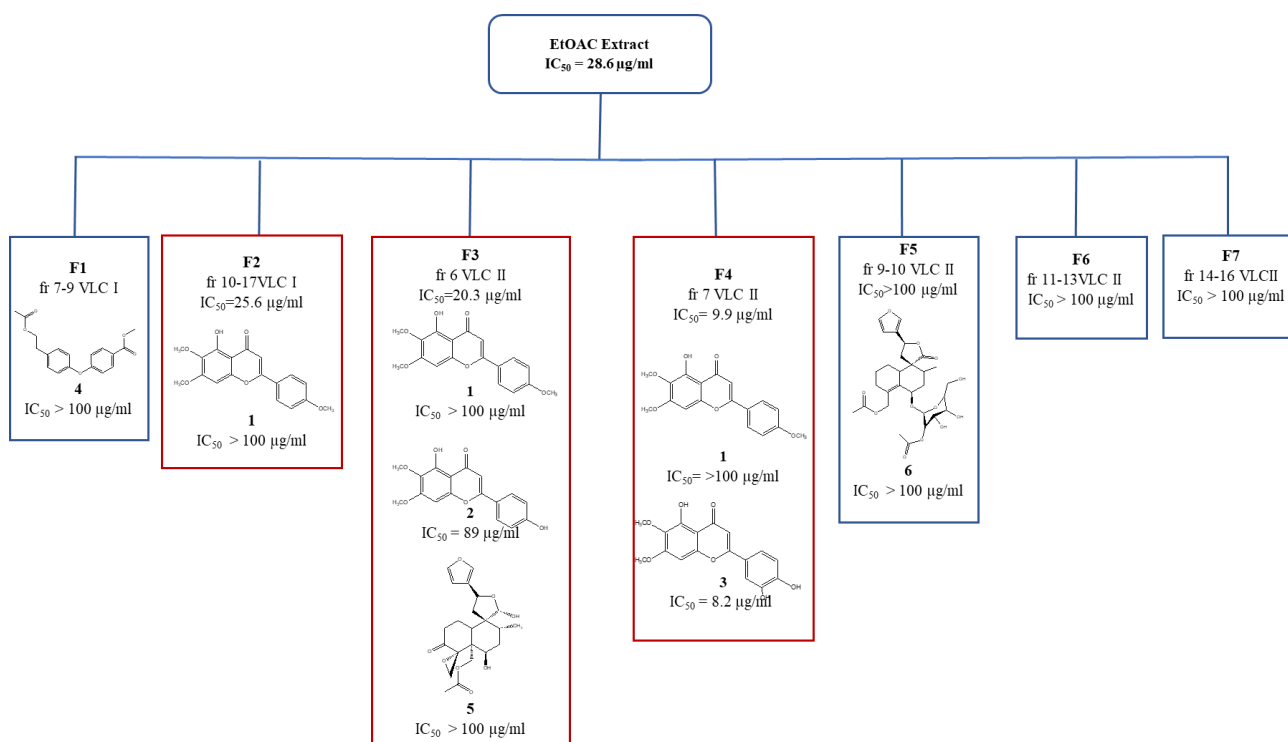


Teuflavin (**5**)



Teuflavoside (**6**)

Figure 20. Structure of the compounds isolated from *T. flavum* subsp. *glaucum*



Since in a previous PhD work,⁹² we identified another clerodane diterpene, columbine, with a moderate anti-RNase H action (IC₅₀ = 46.5 µM) (Figure 21), while its glucosidic derivative (columbine β-glucoside) was inactive (IC₅₀ > 100 µM), we decided to verify whether the hydrolysis of teuflavoside would lead to an aglycone with inhibitory activity on the RT RNase H function.

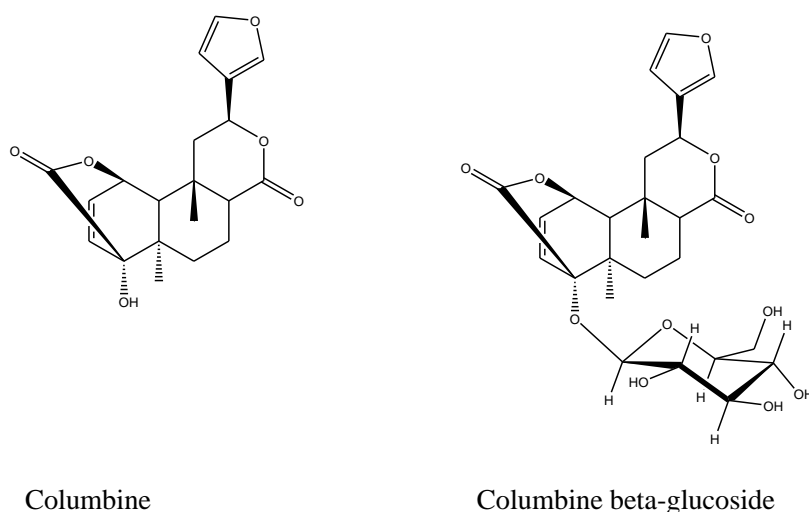
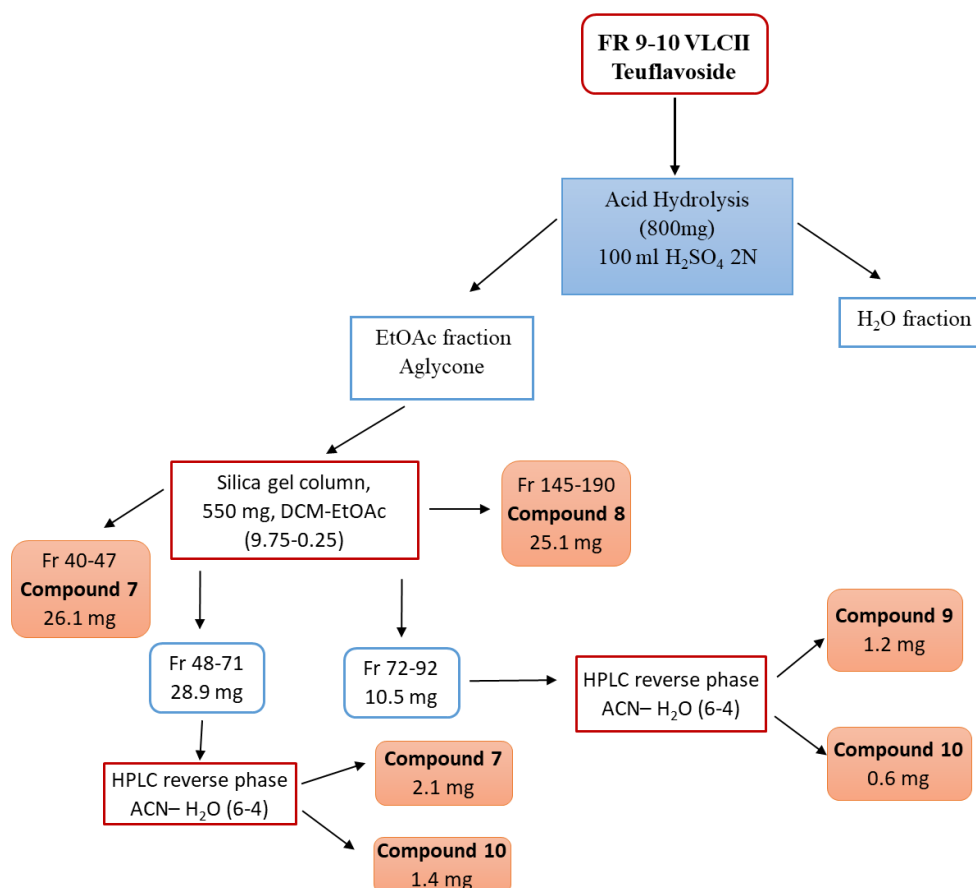


Figure 21. Structures of columbine and columbine β-glucoside

Therefore, due to the high percentage of teuflavoside in the extract (13% of the extract), we decided to subject this compound to acid hydrolysis with 2N H₂SO₄ at reflux for 20 minutes. After cooling to

room temperature, EtOAc was added and the organic phase separated by separatory funnel. The organic layer was evaporated under reduced pressure to afford the crude product. TLC analysis revealed different spots and as consequence, the mixture was separated by column chromatography and semi-preparative HPLC (RP HPLC) to give one known (**10**) and three new (**7-9**) clerodane diterpenes (Figure 22). The structures of the compounds were elucidated by 1D and 2D NMR experiments as well as HR-ESI MS.



Scheme 1. Isolation procedure for compounds **7-10**

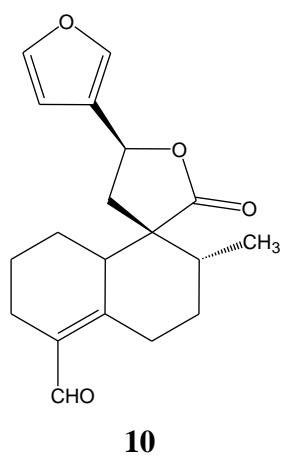
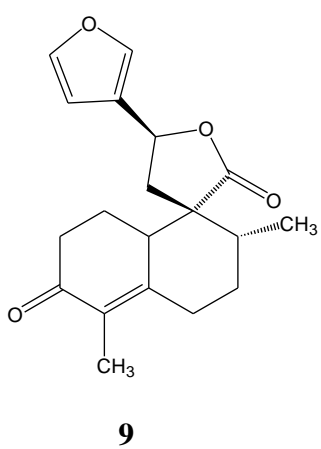
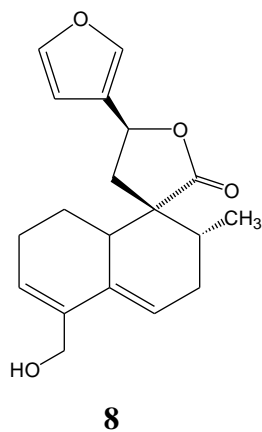
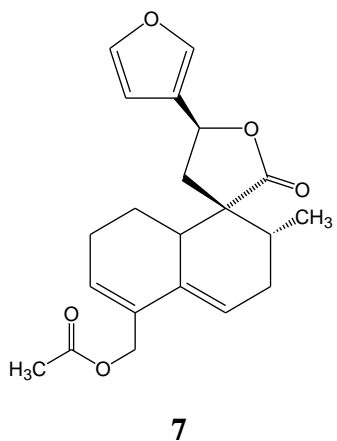


Figure 22. Hydrolyzed compounds obtained from teuflavoside

1.6.3 Structure elucidation of compounds 1-6 isolated from *Teucrium flavum* subsp. *glaucum*

Compound 4

The ^1H NMR spectrum (CDCl_3 , 500 MHz) of compound **4** showed a cluster of four doublets at low fields at 7.95 (d, $J = 9$ Hz), 7.08 (d, $J = 8.5$ Hz), 6.85 (d, $J = 8.5$ Hz), 6.77 (d, $J = 8.5$ Hz) ppm, each integrating for two protons, characteristic of 1,4-disubstituted phenyl rings (Figure 23). Furthermore, two methylene groups at 4.24 (2H, t, $J = 7$ Hz) and 2.86 (2H, t, $J = 7$ Hz) ppm, one methyl singlet at 2.04 (s) and one methoxyl at 3.95 (s) could be detected in the same spectrum.

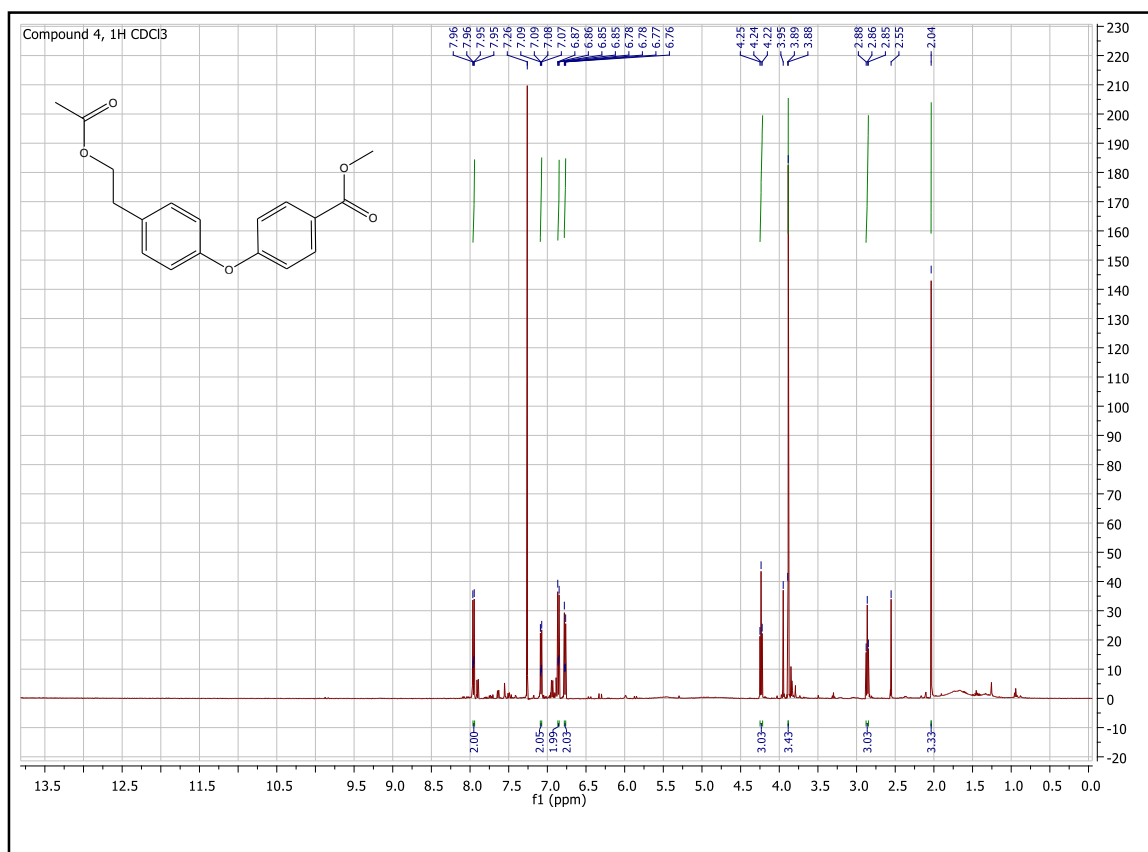


Figure 23. ^1H NMR Spectrum of compound **4** measured in CDCl_3 , 500 MHz.

The ^{13}C NMR spectrum showed fourteen signals which were sorted into six quaternary carbons (124.4, 130.9, 154.2, 159.8, 166.8, 171.1 ppm), two methyl groups (21 and 51.9 ppm), two methylenes (34.2, 65.2 ppm) and four aromatic methines (115.2, 115.3, 130, 131.9 ppm), each of these latter corresponding to two carbons (Figure 24).

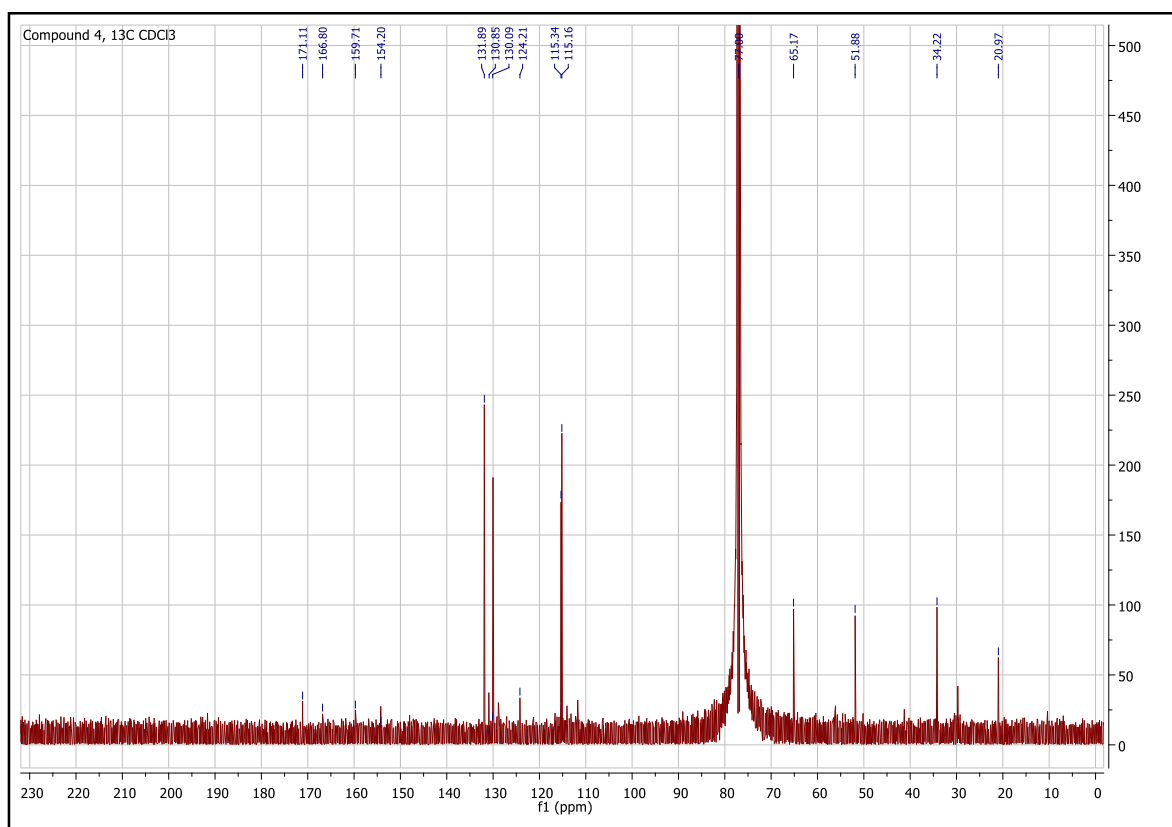


Figure 24. ^{13}C NMR Spectrum of compound **4** measured in CDCl_3 , 100 MHz.

The COSY spectrum (Figure 25) revealed a correlation between the aromatic protons at 7.95 and those at 6.77 ppm as well as between the protons at 7.08 with those at 6.77 ppm. In the same spectrum, the cross-peaks between the two methylene groups at 4.24 and 2.86 ppm suggested they were directly connected.

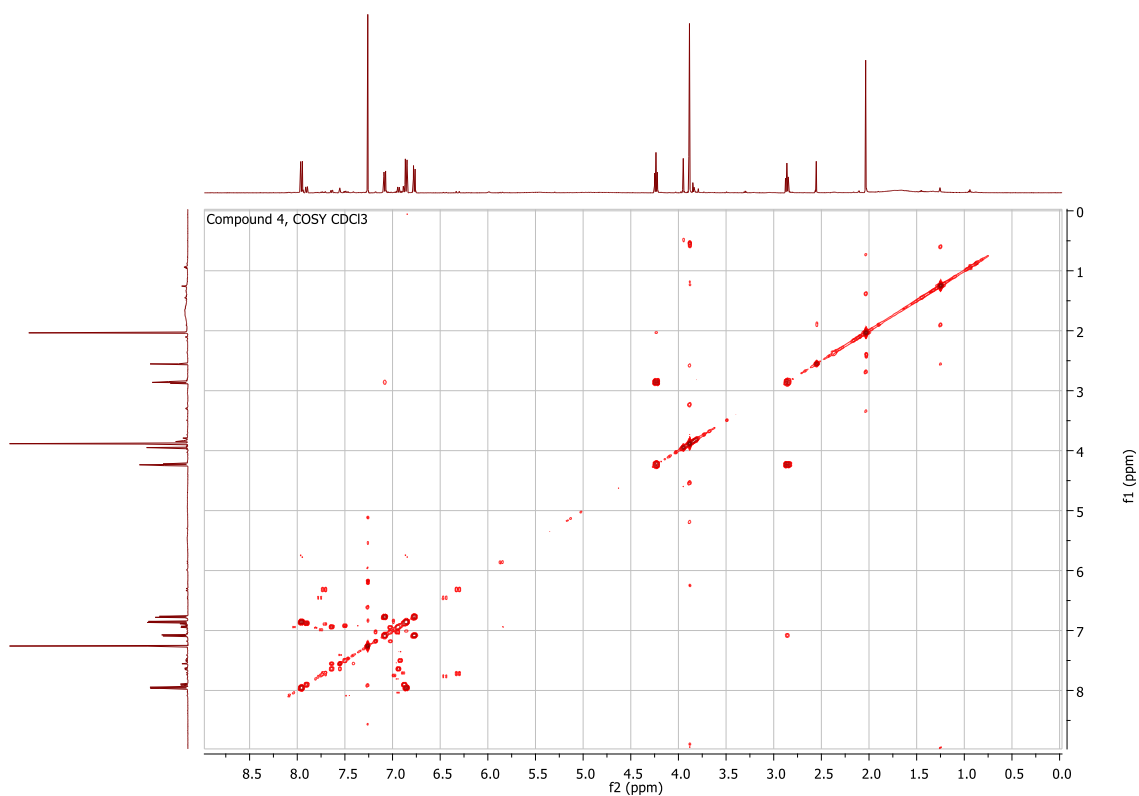


Figure 25. COSY spectrum of compound **4** measured in CDCl_3 , 500 MHz

The HSQC experiments permitted the assignment of each proton to the corresponding carbon (Figure 26).

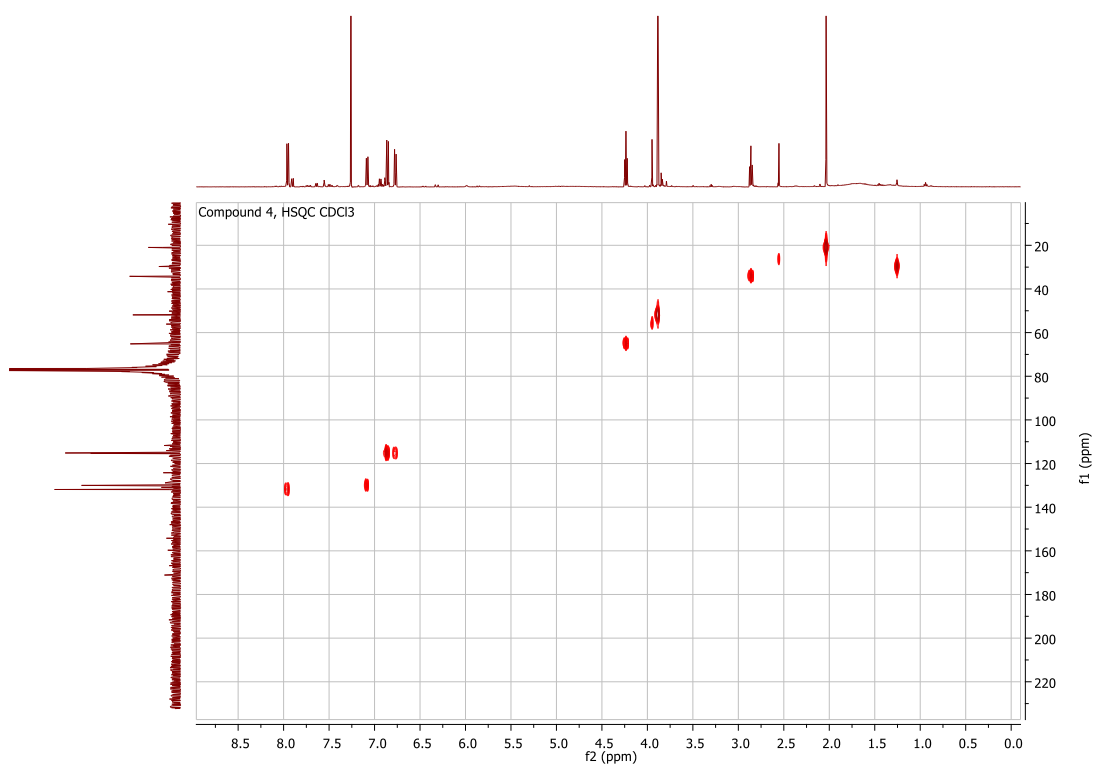


Figure 26. HSQC spectrum of compound **4** measured in CDCl_3 , 500 MHz.

HMBC experiments exhibited correlations from the methylene group at 4.24 ppm to the carbonyl at 171.1 ppm, from the other methylene at 2.86 to the carbons at 65.2, 130.1 and 130.9 ppm, and from the aromatic protons at δ 6.77 to the carbons at 130.9 and 154.2 ppm, allowed to identify a 4-oxyphenethyl acetate moiety (Figure 26). In the HMBC spectrum, further cross-peaks between the proton at δ 7.95 with the carbons at 131.9, 159.8 and 166.8 ppm allowed to identify compound **4** as 3-[4-(2-acethoxyethyl)-phenoxy]-benzoic acid methyl ester (Figure 27). Compound **4** is a new natural product.

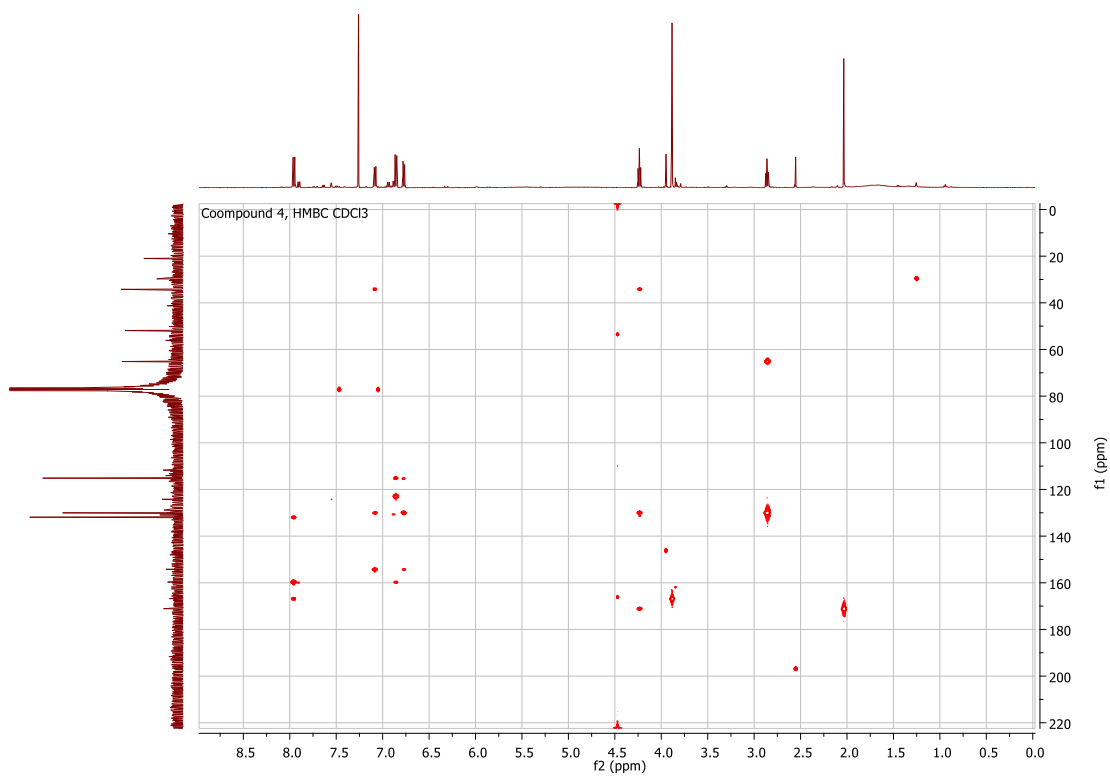


Figure 27. HMBC spectrum of compound **4** measured in CDCl₃, 500 MHz.

Compound 1

Compound 1 was identified as *salvigenin* (5-hydroxy-4',6,7-trimethoxyflavone), based on 1D (^1H e ^{13}C NMR) and 2D NMR (DQF-COSY, HSQC, HMBC) spectra and by comparison with literature data.⁹³

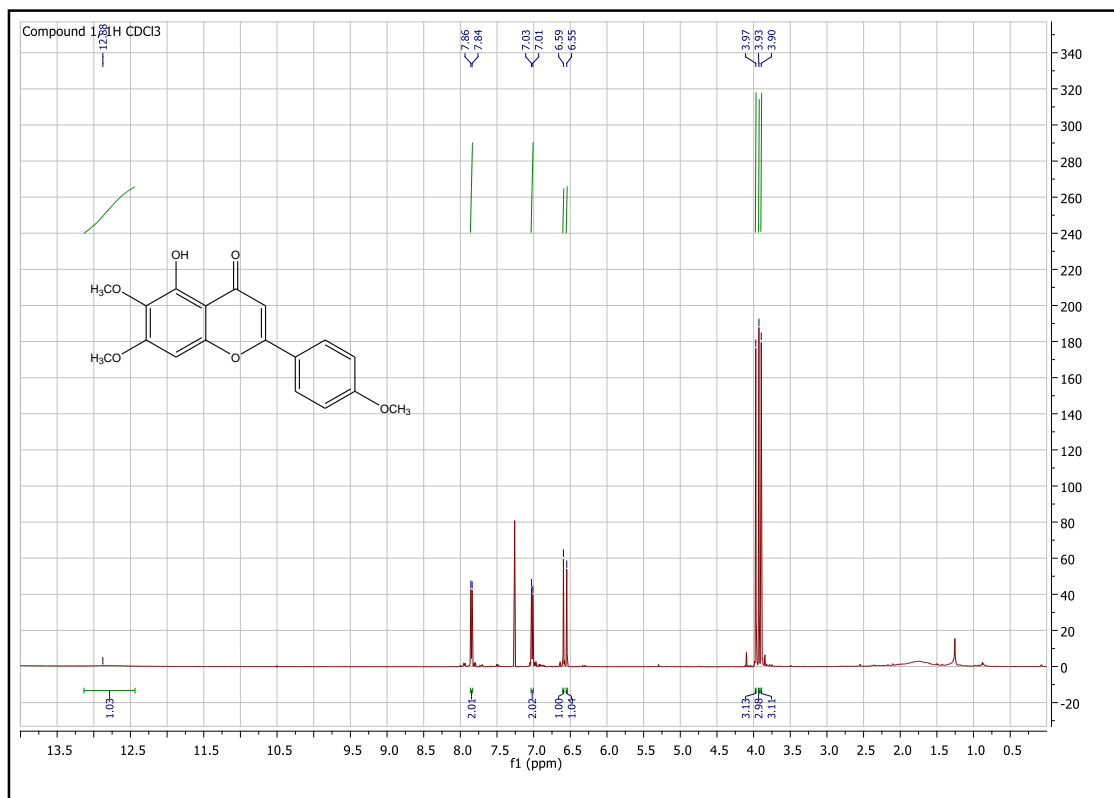


Figure 28. ^1H NMR Spectrum of compound 1 measured in CDCl_3 , 500 MHz.

Compound 2

Compound 2 has been identified as *cirsimarin* (4',5-dihydroxy-6,7-dimethoxyflavone)

through 1D (^1H e ^{13}C NMR) and 2D NMR (DQF-COSY, HSQC, HMBC) spectra and by comparison with literature data .^{94,95}

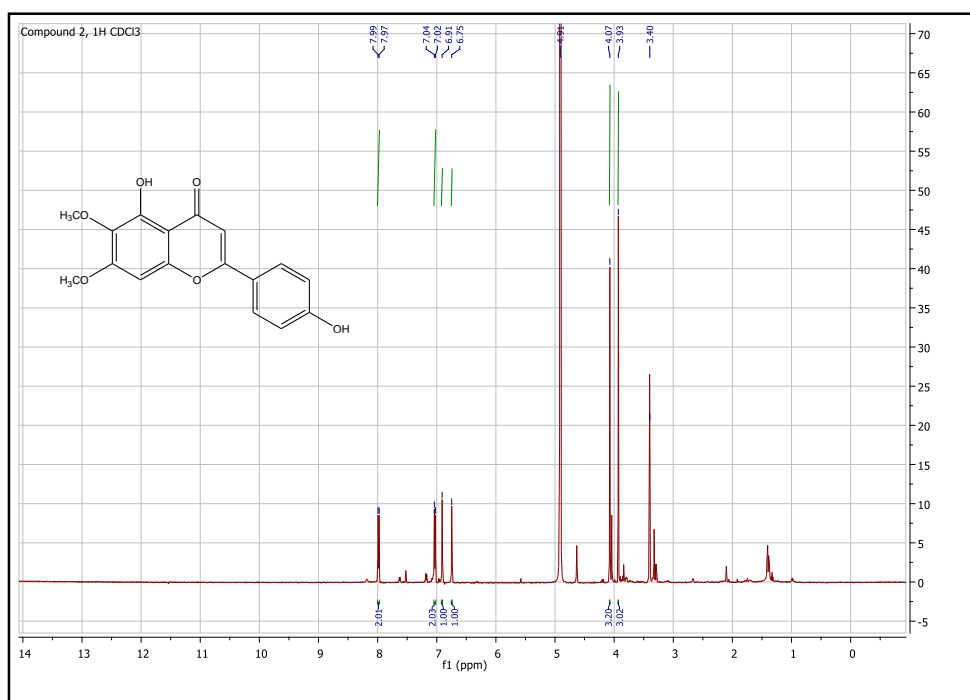


Figure 29. ^1H NMR spectrum of compound 2 measured in CDCl_3 , 500 MHz.

Compound 3

Compound **3** has been identified as *Cirsiliol* (3',4',5-trihydroxy-6,7-dimethoxyflavone) by 1D (^1H e ^{13}C NMR) and 2D NMR (DQF-COSY, HSQC, HMBC) spectra and its structure confirmed by comparison with data literature data.⁹⁴

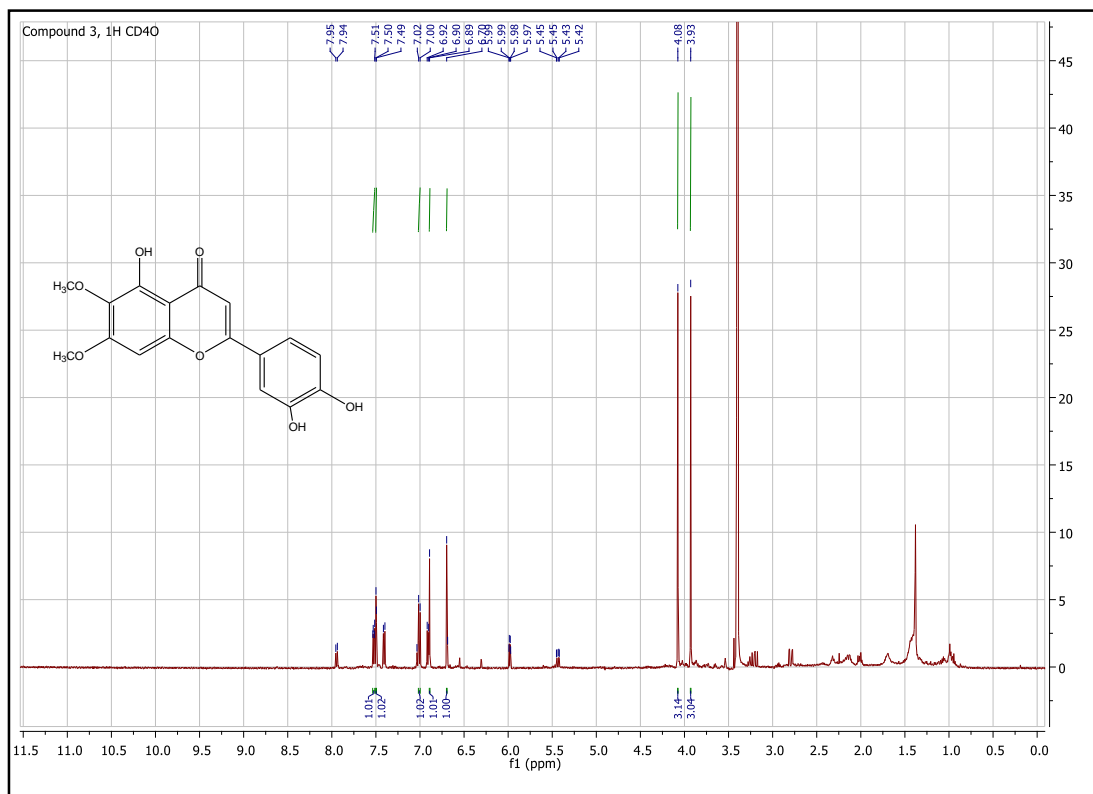


Figure 30. ^1H NMR Spectrum of compound **3** measured in CD₄O, 500 MHz

Compound 5

Compound **5** was identified as *teuflavin* by 1D (^1H and ^{13}C NMR), and 2D NMR spectra, and by comparison with the literature data.⁸⁴

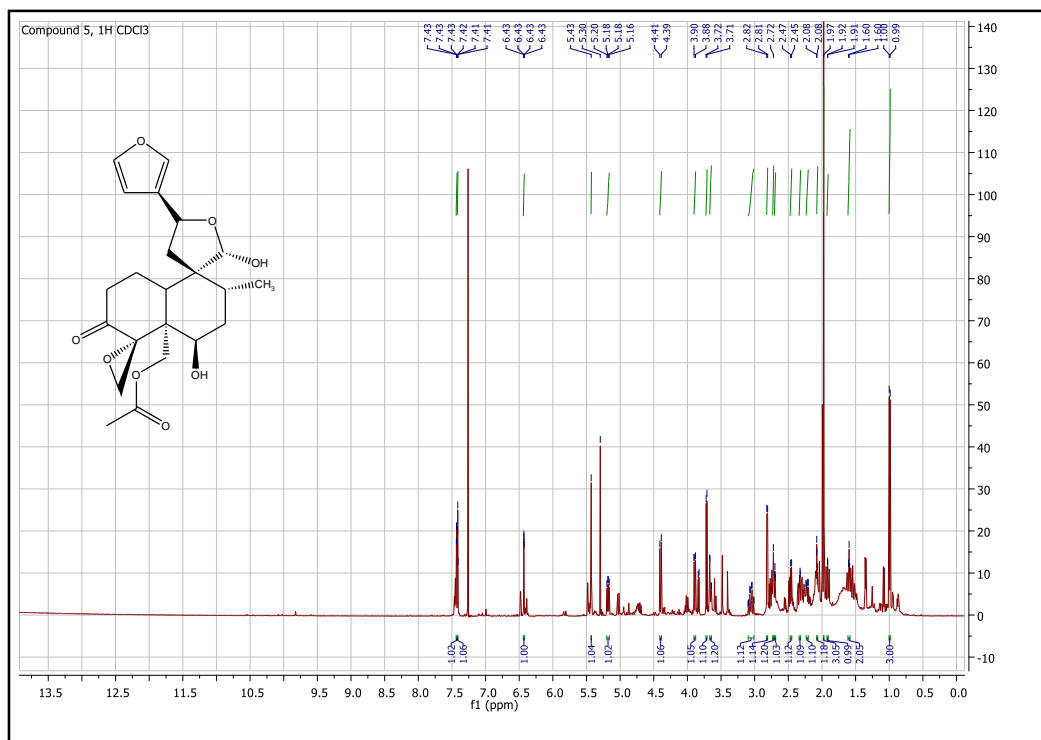


Figure 31. ^1H NMR Spectrum of compound **5** measured in CDCl_3 , 500 MHz

Compound 6

Compound 6 was identified as *tinoporaside* by 1D (^1H and ^{13}C NMR), and 2D NMR spectra (see experimental part), and by comparison with the literature data.⁸⁴

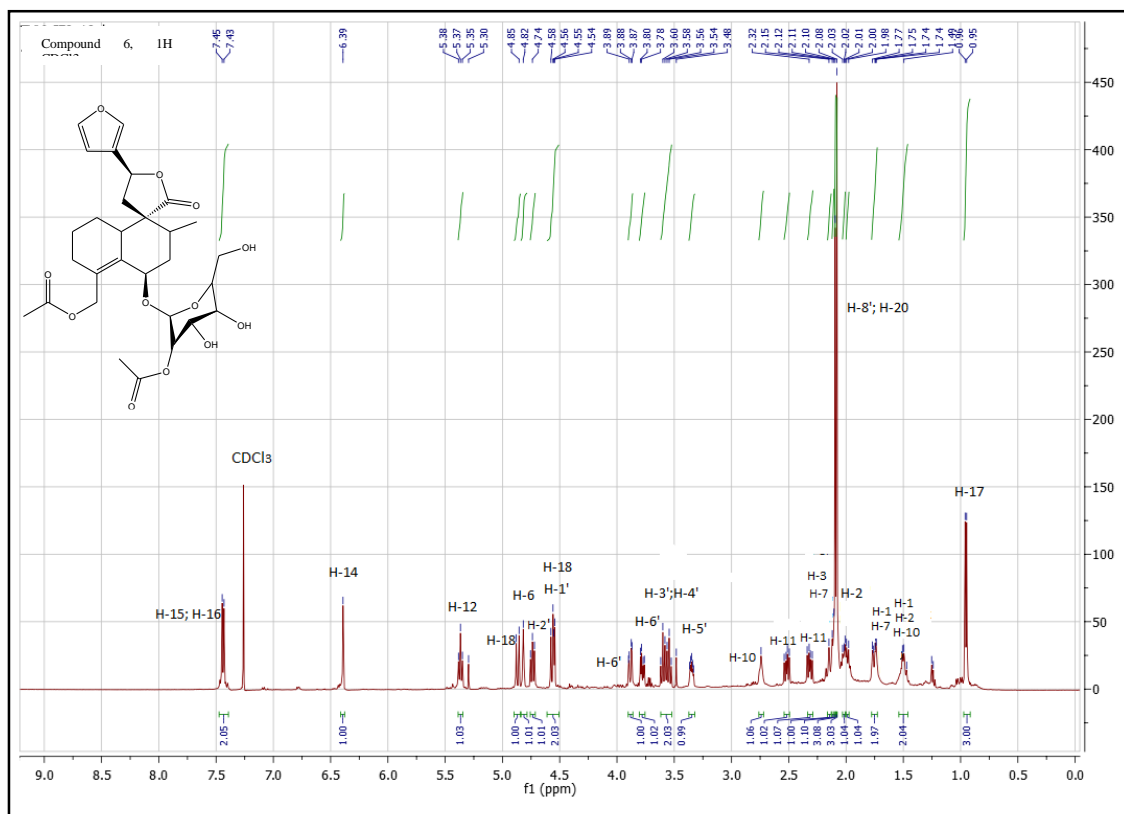


Figure 32. ^1H NMR Spectrum of compound 6 measured in CDCl_3 , 500 MHz

1.6.4 Structure elucidation of compounds 7-10 obtained from the hydrolysis of teuflavoside

Compound 7

Compound 7 showed an ion peak at m/z 379.1519 ($M + Na$) (calcd 379.1515) in the HR-ESIMS (positive mode), accounting for an elemental composition of $C_{21}H_{24}O_5$.

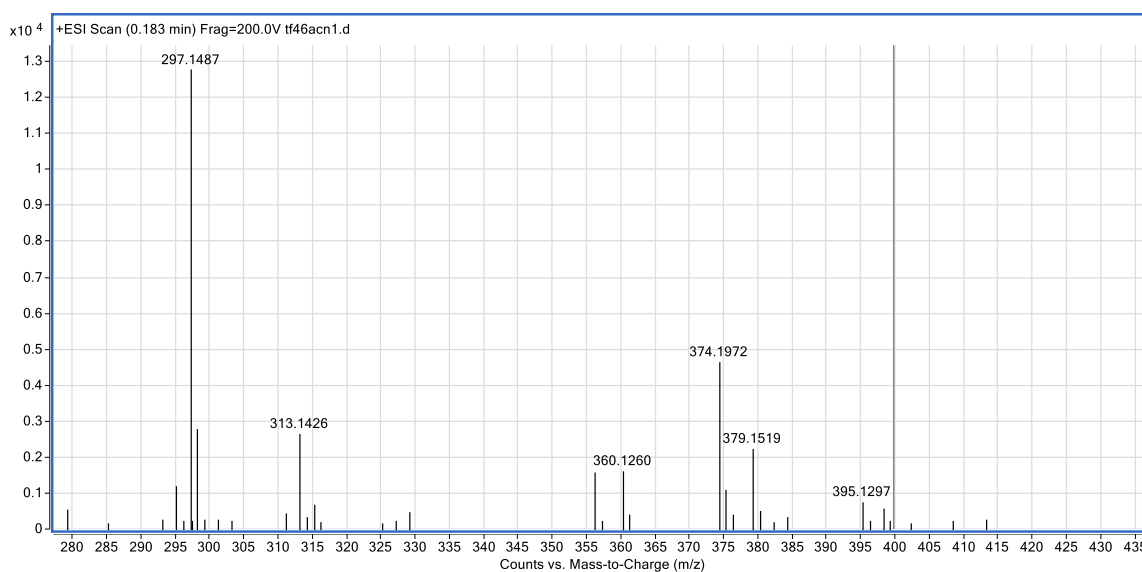


Figure 33. HR-ESIMS spectrum of compound 7

The comparison of the 1H and ^{13}C NMR spectra of compound 7 (Figures 34-35) with those of teuflavoside (6) (Figure 32) showed the lack of the 2'-O-acetyl- β -D-glucopyranoside moiety (Figures 32-34).

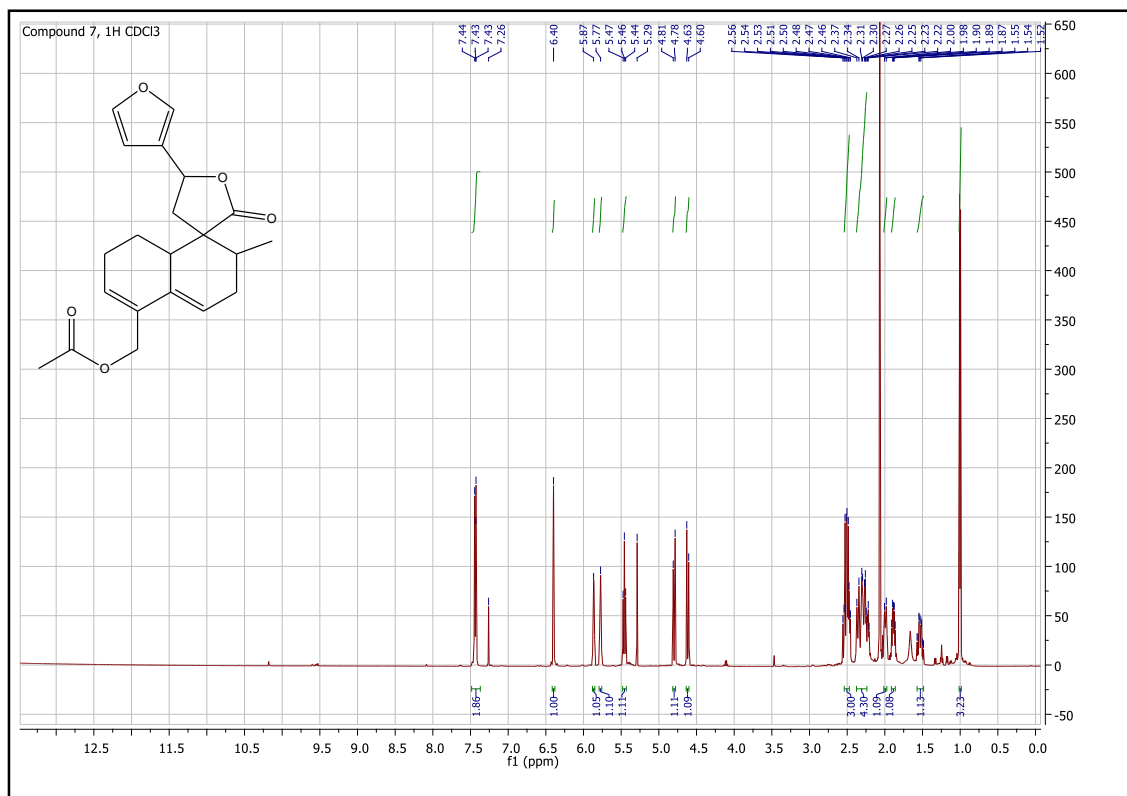


Figure 34. ^1H NMR spectrum of compound **7** measured in CDCl_3 , 500 MHz.

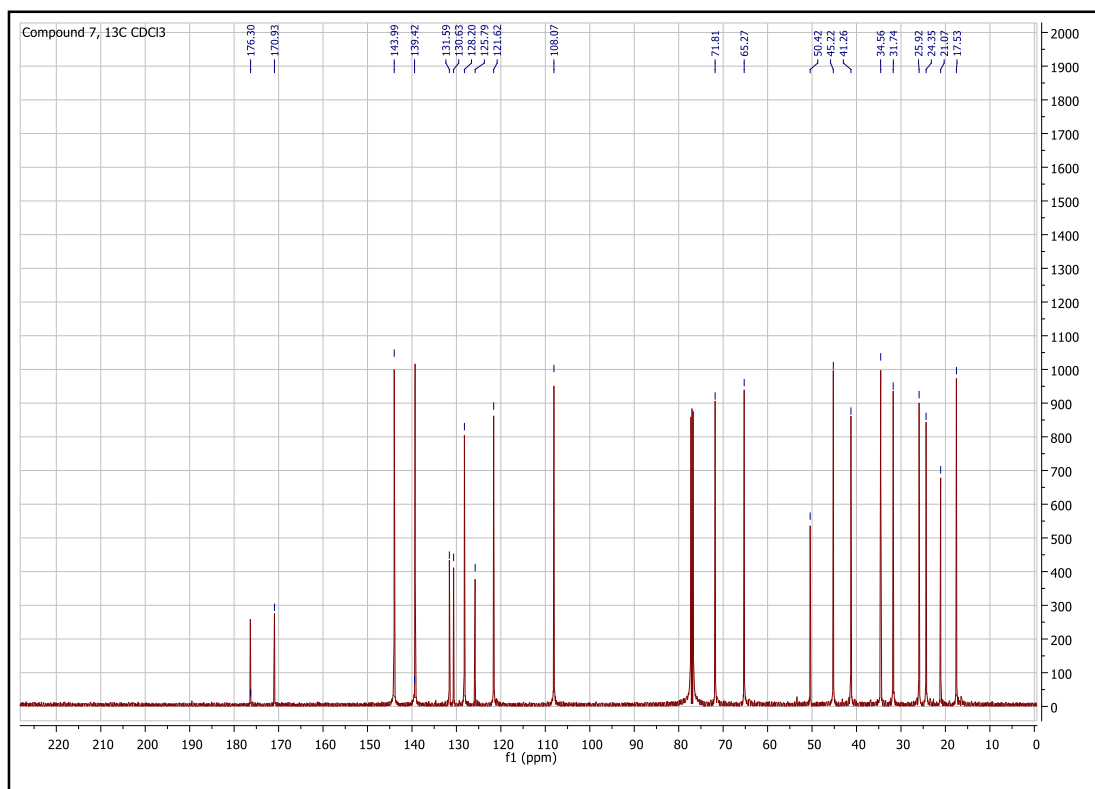


Figure 35. ^{13}C NMR spectrum of compound **7** measured in CDCl_3 , 100 MHz.

In the ^1H NMR spectrum of **7** two olefinic protons at 5.86 (1H, s, br) and 5.77 (1H, s, br) ppm, not present in the spectrum of teuflavoside, could be detected, while the signal at δ 4.82 (1H, m) relative to the oxymethinic proton at position 6 of teuflavoside was missing in the spectrum of compound **7**. These changes suggested that hydrolysis of the glycosidic moiety was accompanied by others structural modifications.

From the HSQC spectrum of compound **7** it was possible to assign the respective carbons to each proton. In particular, the two olefinic protons at 5.86 and 5.77 ppm were assigned to the carbons at 128.2 and 121.6 ppm, respectively (Figure 36).

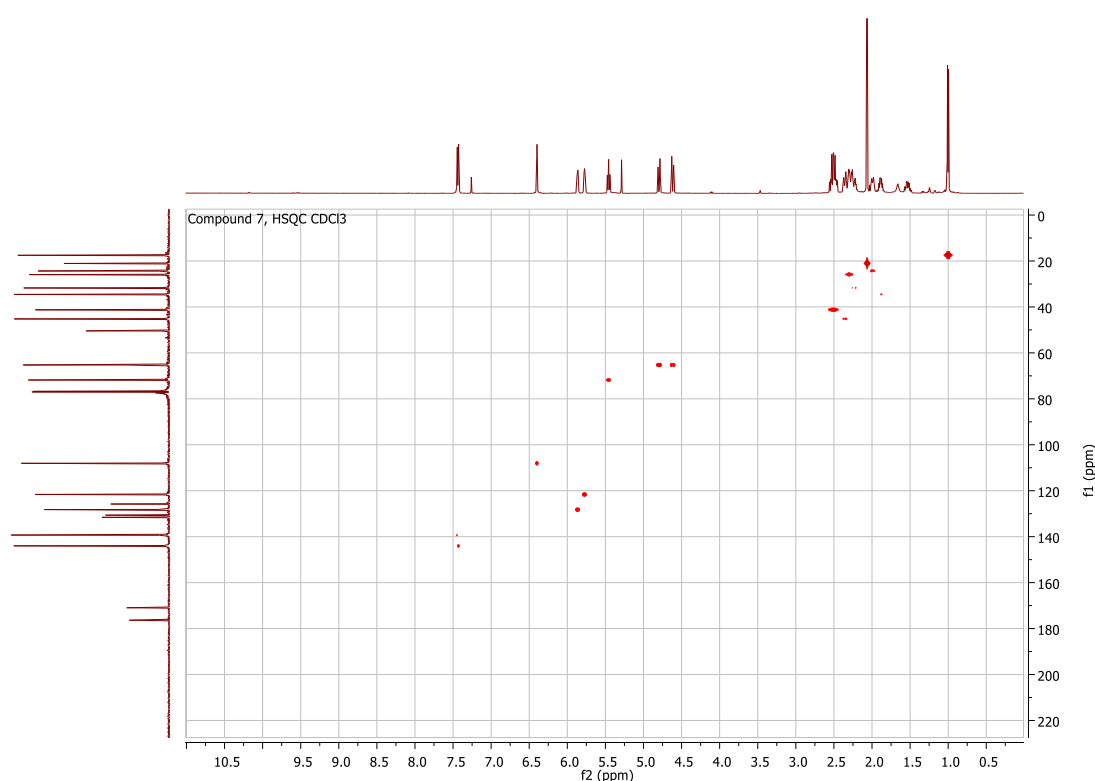


Figure 36. HSQC spectrum of compound **7** measured in CDCl_3 , 500 MHz.

The long-range correlations observed in the HMBC spectrum of **7** between the methylene protons at 4.79 (1Ha, d, $J = 12.5$ Hz) and 4.61 (1Hb, d, $J = 12.5$ Hz) ppm with the carbons at δ 170.9 (COCH₃), 131.6 (C-4), 130.6 (C-5) and 128.2 (C-3), and the olefinic proton at 5.86 with the carbons at 130.6 (C-5), 65.3 (C-1') and 24.2 (C-1) ppm, and the olefinic proton at 5.77 with the carbons at 131.6 (C-4), 45.2 (C-10) 34.6 (C-7) ppm (Figure 37), clearly indicate the presence of two double bonds at position C-3/C-4 and C-5/C-6. ROESY experiments and analysis of scalar ($^3J_{\text{H-H}}$) coupling of H-8, H-12 and H-17 confirmed the same stereochemistry of teuflavoside (Figure 38). DQF-COSY, HSQC,

HMBC, and ROESY experiments allowed the complete assignment of all signals and the identification of the structure as reported in Figure 39. Compound **7** is new to the literature and was trivially named Flavuglaucin A.

As shown in Scheme 2, the acid hydrolysis of teuflavoside involved the loss of the sugar, dehydration, and subsequent rearrangement of the double bonds (Scheme 2).

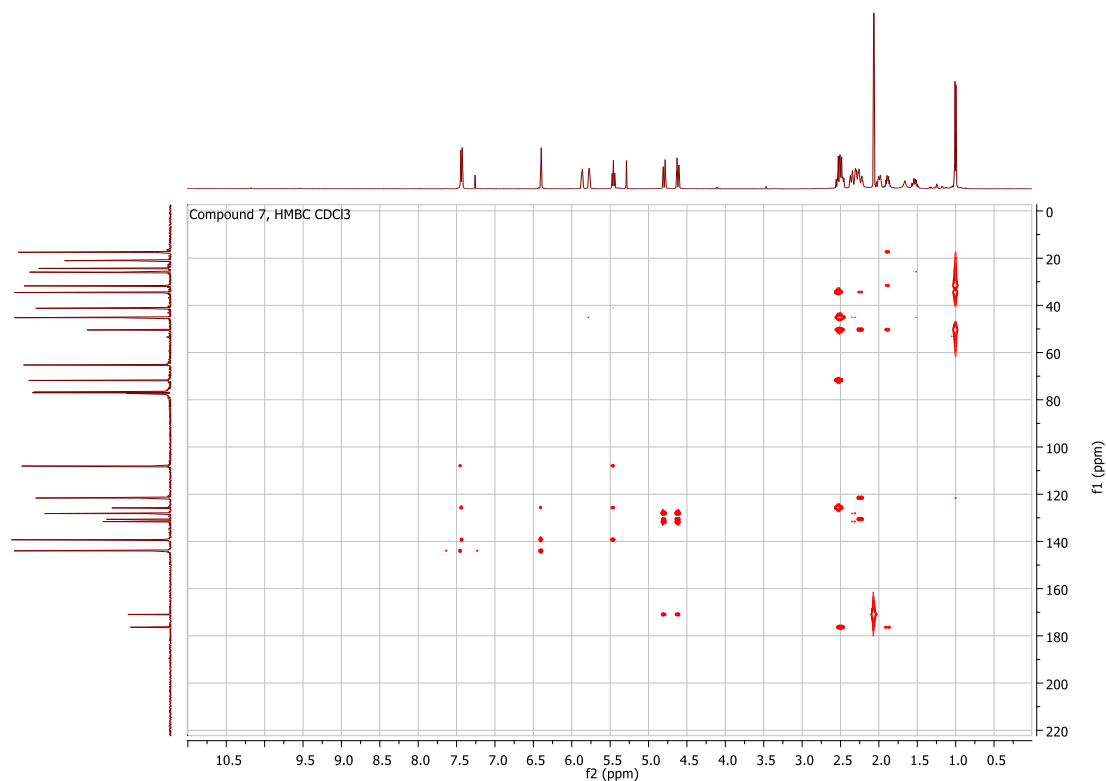


Figure 37. HMBC spectrum of compound **7** measured in CDCl_3 , 500 MHz.

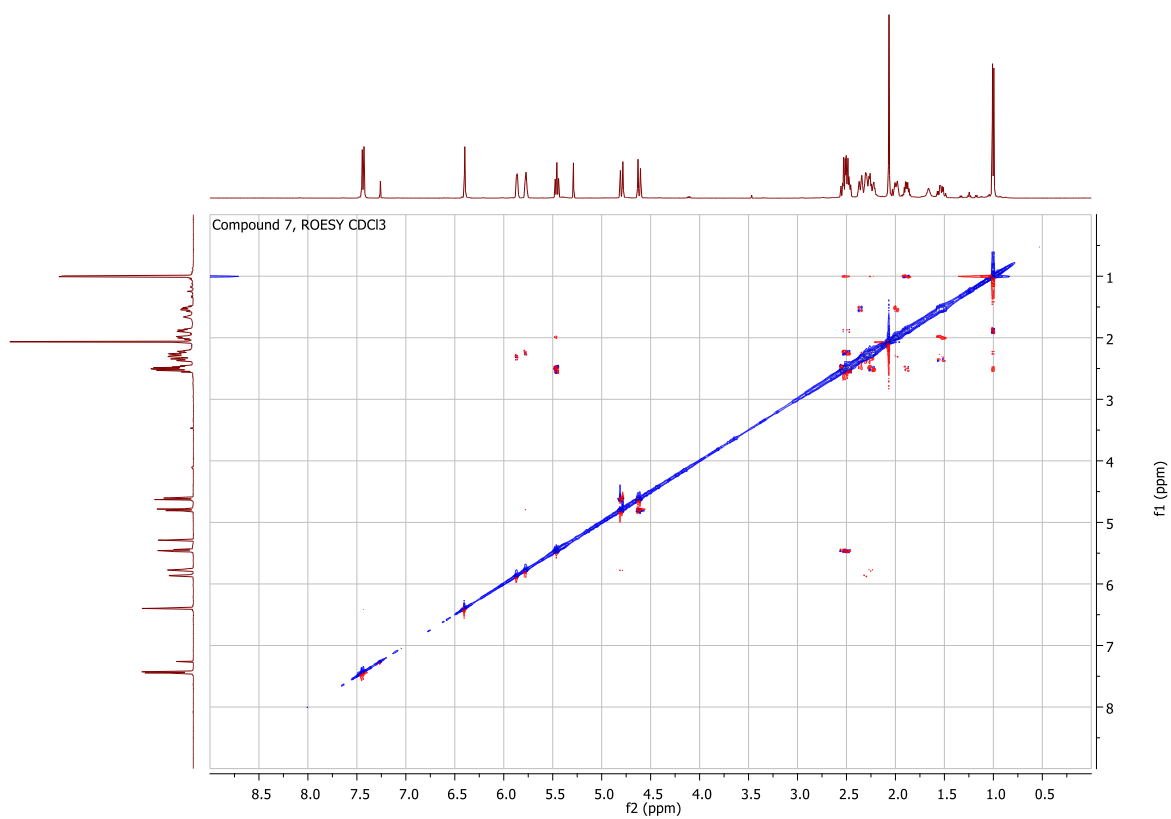


Figure 38. ROESY spectrum of compound **7** measured in CDCl_3 , 500 MHz.

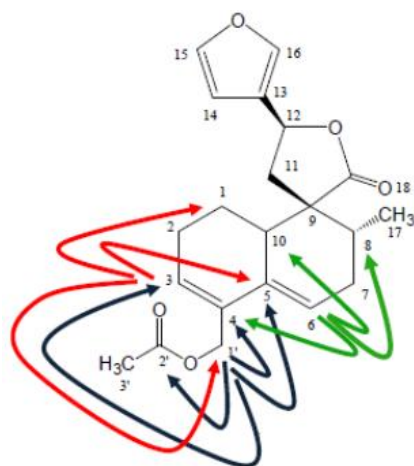
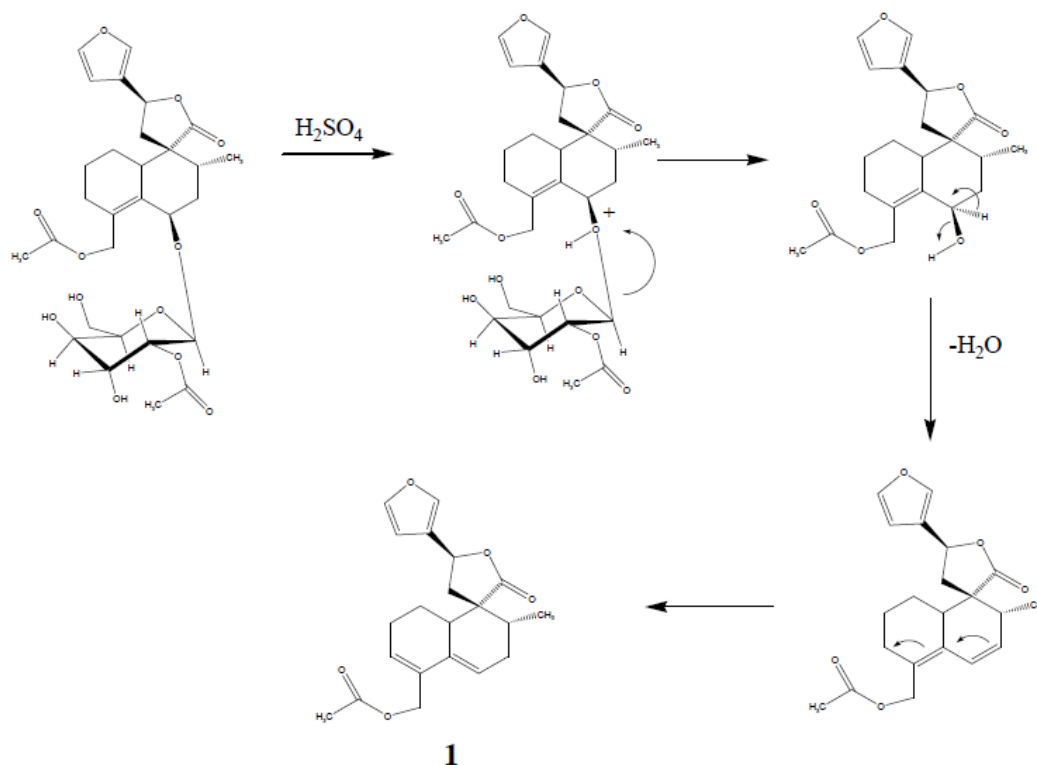


Figure 39. Crucial correlations observed in the HMBC spectrum of compound **7**



Scheme 2. Mechanism of hydrolysis for compound **7**

Compound 7. Yellow oil, $^1\text{H NMR}$ (500 MHz, CDCl_3) δ_{H} 1.00 (d, 3H, $J = 6.5$ Hz, H-17), 1.53 (ddd/m, 1H, $J = 12.0$ Hz, $J = 5.5$ Hz, H-1), 1.89 (m, 1H, H-8), 1.99 (d, 1H, $J = 12.0$ Hz, H-1), 2.07 (s, 3H, COCH_3), 2.29 (m, 4H, H-2, H-7-H-10), 2.51 (m, 3H, H-7, H-11), 4.62 (d, 1H, $J = 12.5$ Hz, H-1'), 4.80 (d, 1H, $J = 12.5$ Hz, H-1'), 5.46 (t, 1H, H-12), 5.77 (s br, 1H, H-6), 5.87 (s br, 1H, H-3), 6.40 (s, 1H, H-14), 7.43 (t, 1H, H-15), 7.45 (s, 1H, H-16) ppm; $^{13}\text{C NMR}$ (100 MHz, CDCl_3) δ_{C} 17.53 (C-17), 21.07 (C-3'), 24.35 (C-1), 25.92 (C-2), 31.74 (C-7), 34.56 (C-8), 41.26 (C-11), 45.22 (C-10), 50.42 (C-9), 65.27 (C-1'), 71.81 (C-12), 108.07 (C-14), 121.62 (C-6), 125.79 (C-13), 128.2 (C-3), 130.63 (C-5), 131.59 (C-4), 139.29 (C-16), 143.99 (C-15), 170.93 (C-2'), 176.35 (C-18) ppm.

Compound 8

Compound **8** showed an ion peak at m/z 337.1399 ($M + Na$) (calcd 337.1392) in the HR- ESIMS (positive mode), accounting for an elemental composition of $C_{19}H_{22}O_4$.

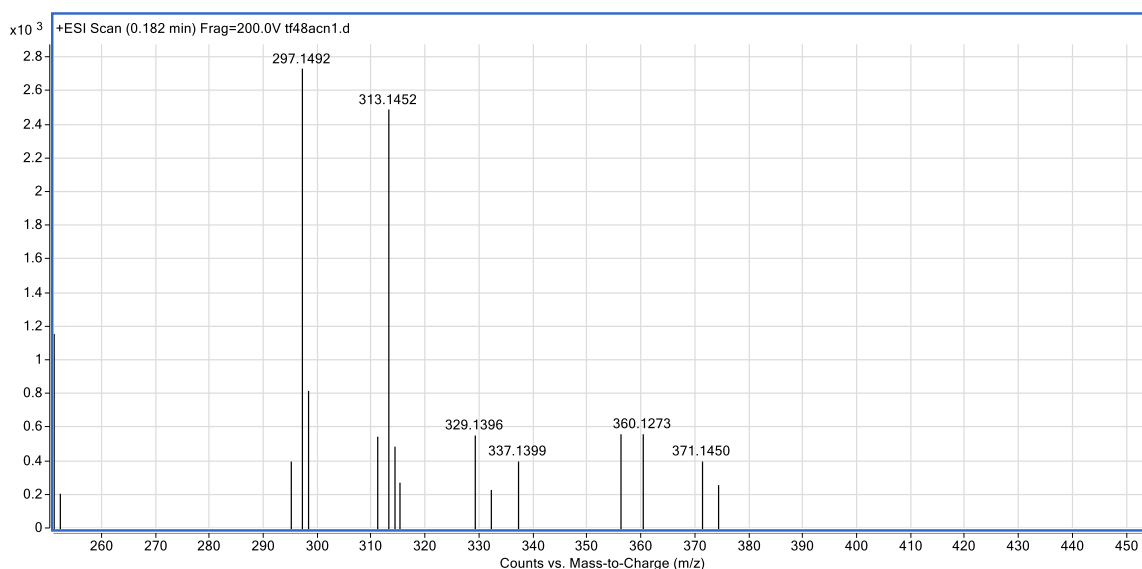


Figure 40. HR ESI MS of compound **8**

The 1H NMR spectrum of compound **8** (Figure 41) was almost superimposable to that of compound **7**, except for the absence of the acetyl group (δ 2.07, s), and the shift of 0.5 ppm to high fields of the oxymethylene protons located at C-1'.

The absence of the acetyl group in **8** was confirmed in the HMBC spectrum (Figure 42) by the absence of cross-peaks between the oxymethylene protons at C-1' (H-1'a: 4.24 (d, 1H, $J = 12.5$ Hz); H-1'b: 4.33 (d, 1H, $J = 12.5$ Hz) with carbonyl groups.

As far as we know, compound **8** is new to the literature and was trivially named Flavuglaucin B.

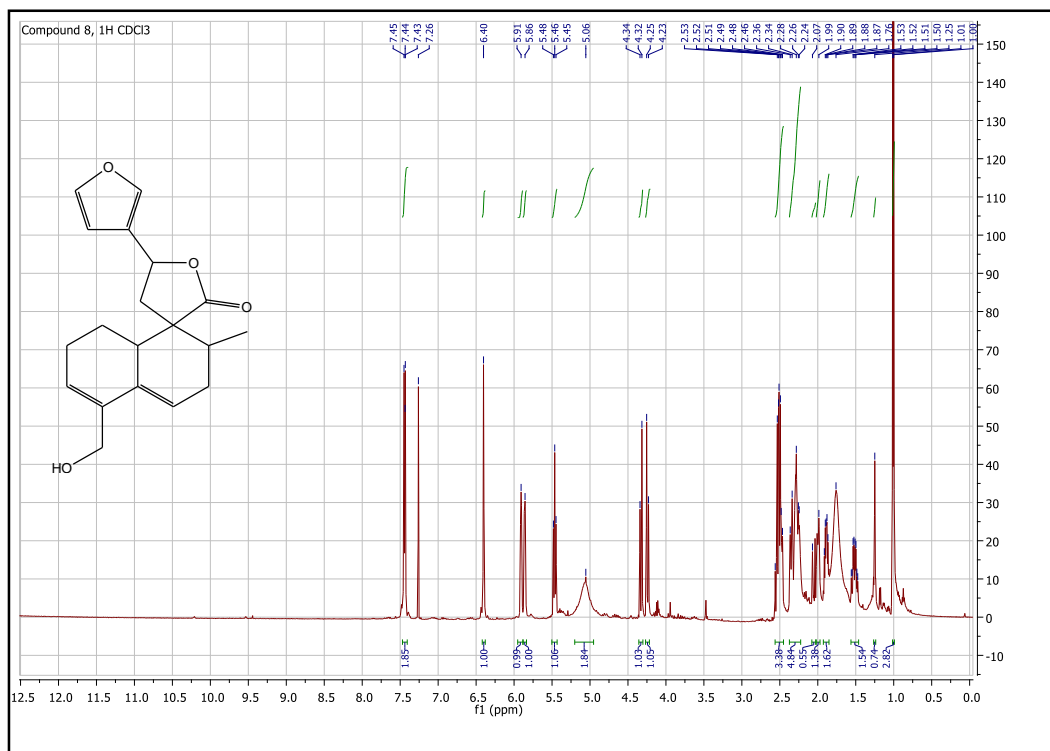


Figure 41. ¹H NMR Spectrum of compound 8 measured in CDCl₃, 500 MHz

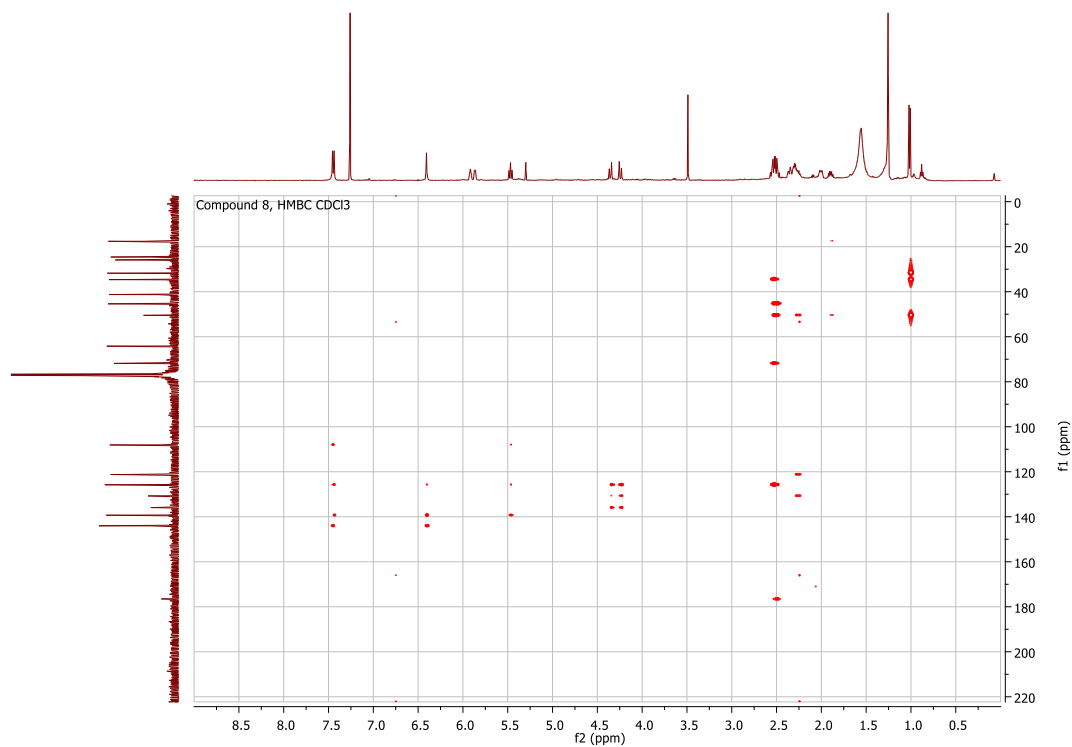


Figure 42. HMBC Spectrum of compound 8 measured in CDCl₃, 500 MHz.

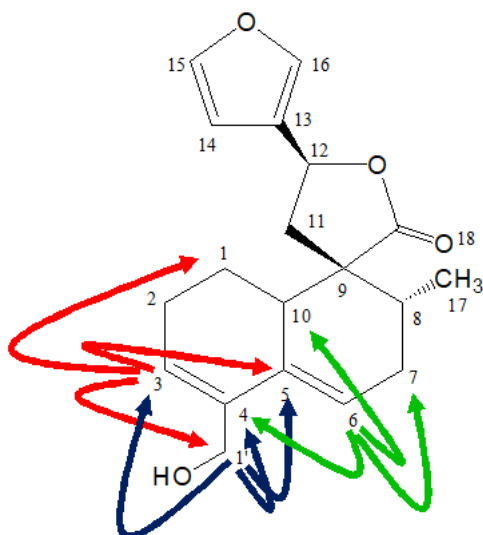


Figure 43. Some important correlations observed in the HMBC spectrum of compound **8**

Compound 8. yellow oil, ^1H NMR (500 MHz, CDCl_3) δ_{H} 1.01 (d, 3H, $J = 6.5$, H-17), 1.52 (ddd/m, 1H, $J = 12$ Hz, $J = 5.5$ Hz, H-1), 1.89 (m, 1H, H-8), 2.0 (m, 1H, H-1), 2.30 (m, 4H, H-2, H-7, H-10), 2.51 (m, 3H, H-7, H-11), 4.24 (d, 1H, $J = 12.5$ Hz, H-1'), 4.33 (d, 1H, $J = 12.5$ Hz, H-1'), 5.05 (s br, H, OH), 5.46 (t, 1H, H-12), 5.86 (s br, 1H, H-3), 5.91 (s br, 1H, H-6), 6.40 (s, 1H, H-14), 7.43 (t, 1H, H-15), 7.45 (s, 1H, H-16) ppm; ^{13}C NMR (100 MHz, CDCl_3) δ_{C} 17.63 (C-17), 24.58 (C-1), 25.81 (C-2), 31.64 (C-7), 34.60 (C-8), 41.20 (C-11), 45.30 (C-10), 50.55 (C-9), 64.10 (C-1'), 71.85 (C-12), 108.09 (C-14), 121.27 (C-6), 125.79 (C-3), 125.82 (C-13), 130.74 (C-5), 135.93 (C-4), 139.42 (C-16), 144.04 (C-15), 176.50 (C-18) ppm.

Compound 9

The HR-ESIMS (Figure 44) showed a molecular ion at m/z 315.1593 ($M + 1$)⁺ (calcd 315.1596). This molecular mass in combination with ¹H and ¹³C NMR data allowed the molecular formula to be established as C₁₉H₂₂O₄.

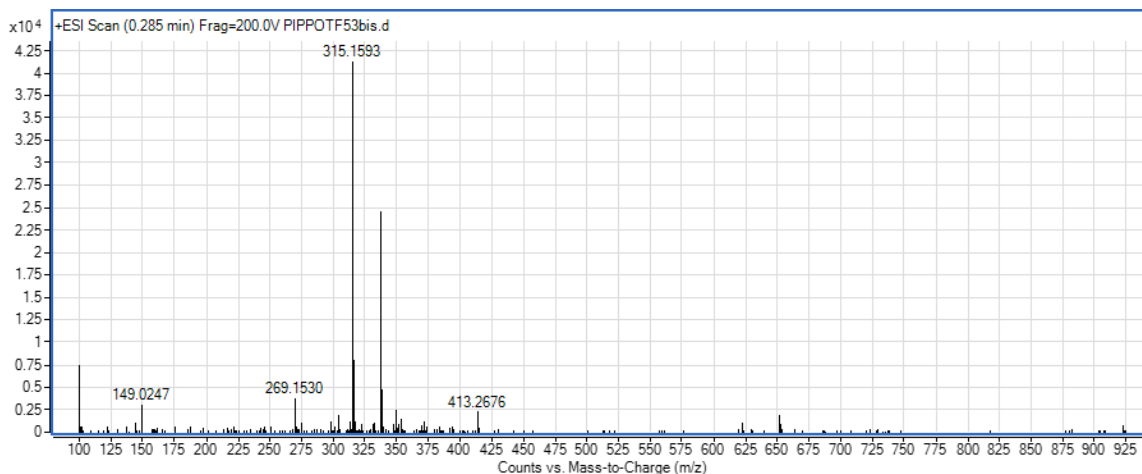


Figure 44. HR-ESIMS spectrum of compound **9**

The analysis of the ¹H NMR spectrum of compound **9** (Figure 45) showed that the low field region is similar to that of teuflavoside but the olefinic protons at C-3/C-4 and C-5/C-6 of compounds **7** and **8**, are absent in **9**. Moreover, a methyl group at 1.85 ppm (3H, s) appeared in the spectrum of **9**.

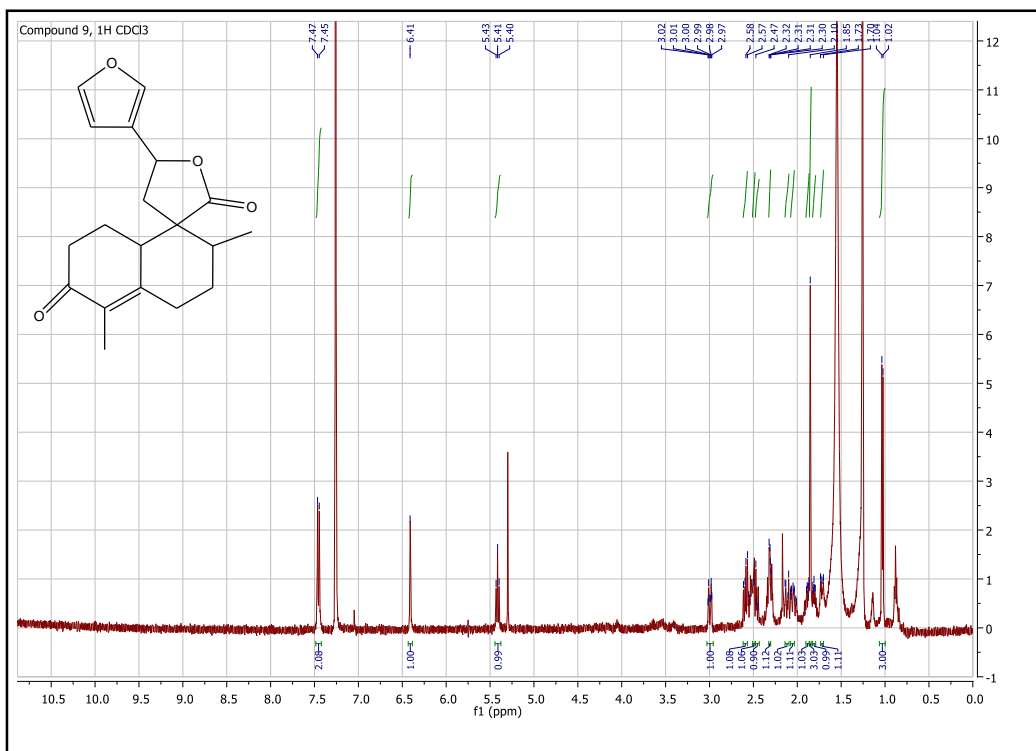


Figure 45. ^1H NMR spectrum of compound **9** measured in CDCl_3 , 500 MHz

The HMBC spectrum of **9** revealed that the above mentioned methyl group was correlated with a carbonyl at 197.6 ppm and two unsaturated quaternary carbons at 131.0 and 154.2 ppm (Figure 46). In the same spectrum, the carbonyl group at 197.6 was correlated to the methylene at 1.88 (1H-a, m) and 2.30 (1H-b, m).

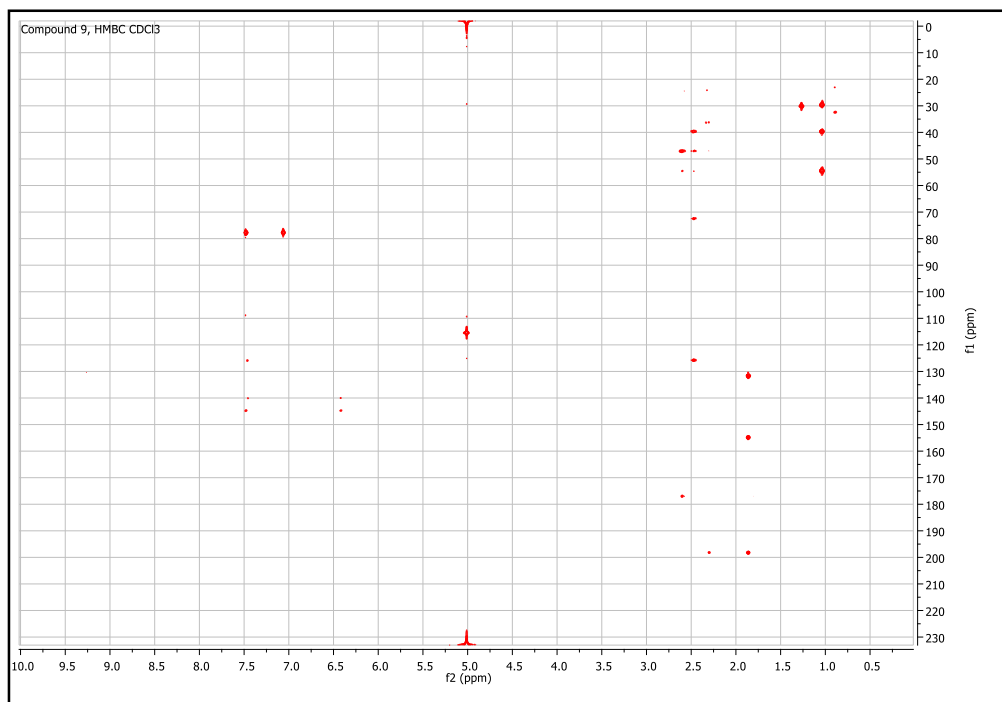


Figure 46. HMBC Spectrum of compound **9** measured in CDCl_3 , 500 MHz.

These two methylenes are directly connected, as demonstrated by their cross-peaks in the COSY spectrum (Figure 47).

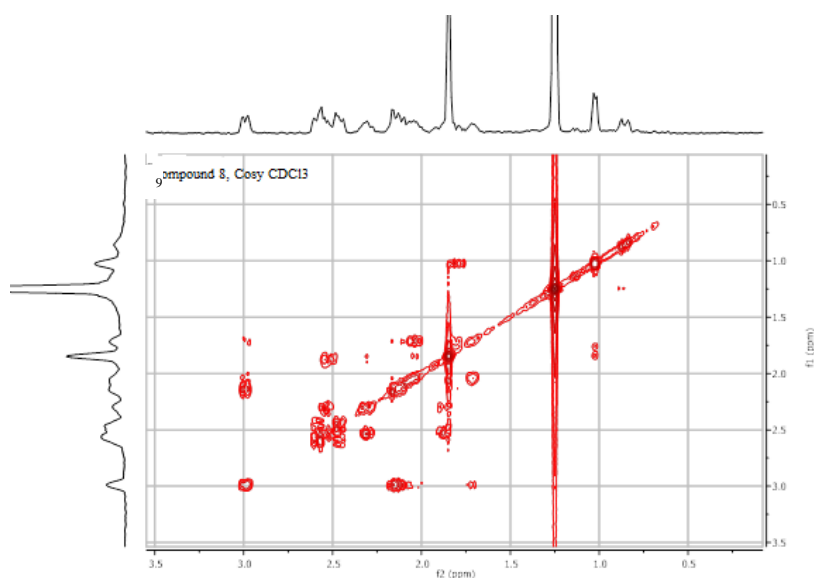


Figure 47. COSY spectrum of compound **9** measured in CDCl_3 , 500 MHz

In the HMBC spectrum of **9**, further correlations of methyl group at 1.02 (1H, d, $J = 7$ Hz) ppm with carbons at 39.0, 54.9 and 29.1 ppm together with those of the methylene proton at 1.73 (1H, m) with

the methylene at 2.05 (1H, m) ppm observed in the COSY spectrum, allowed to identify the decalinic nucleus shown in figure 48.

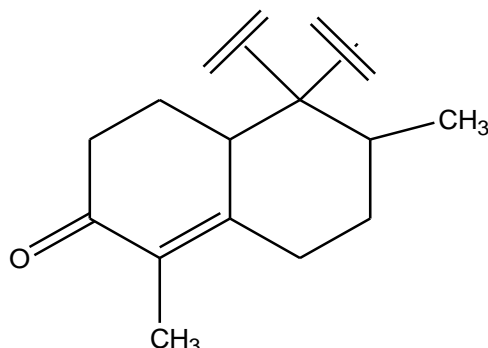


Figure 48. Partial structure of compound **9**

DQF-COSY, HSQC, HMBC, and ROESY experiments allowed the complete assignment of all signals and the identification of the structure as reported in Figure 49. Compound **9** is a previously undescribed molecule and was trivially named Flavuglaucin C.

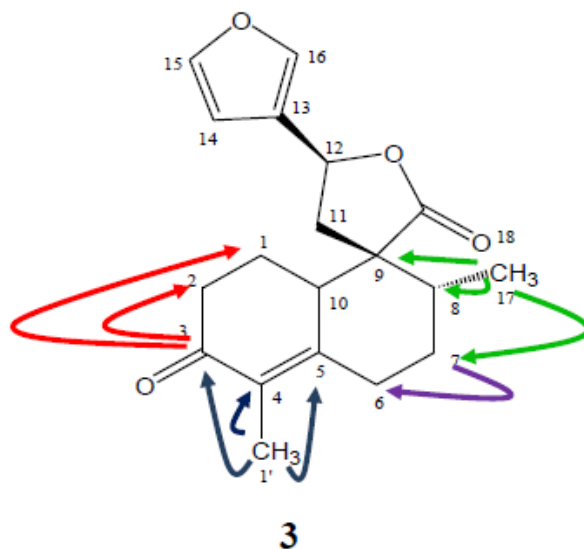


Figure 49. Some important correlations observed in the HMBC spectrum of compound **9**

Compound 9. Transparent solid, ^1H NMR (500 MHz, CDCl_3) δ_{H} 1.03 (d, 3H, $J = 6.5$, H-17), 1.72 (dd, 1H, $J = 14.0$, $J = 3.5$, H-7), 1.80 (m br, 1H, H-8), 1.85 (s, 3H, H-18), 1.88 (m br, 1H, H-1'), 2.06 (dd, 1H, $J = 13.5$, $J = 4.5$, H-6), 2.13 (m, 1H, H-7), 2.31 (m, 1H, H-1), 2.33 (m, 1H, H-2), 2.46 (t, 1H, H-11), 2.49 (s br, 1H, H-10), 2.54 (m, 1H, H-2), 2.59 (m, 1H, H-11), 2.99 (dt, 1H, H-6), 5.41 (t, 1H, H-12), 6.41 (s, 1H, H-14), 7.45 (t br, 1H, H-15), 7.47 (s br, 1H, H-16) ppm; ^{13}C NMR (100 MHz,

CDCl₃) δ_C 10.81 (C-18), 17.04 (C-17), 23.33 (C-1), 29.10 (C-7), 30.50 (C-6), 35.54 (C-2), 38.88 (C-8), 40.68 (C-11), 47.06 (C-10), 54.54 (C-9), 71.82 (C-12), 107.83 (C-14), 125.86 (C-13), 131.68 (C-4), 139.25 (C-16), 143.97 (C-15), 154.99 (C-5), 176.98 (C-20), 198.29 (C-3) ppm.

Compound 10

The structure of compound 10 (figure 49) was deduced from the study of 1D and 2D NMR spectra and MS (Figures 49-56) and confirmed by comparison with the spectral data reported in the literature.⁸⁴

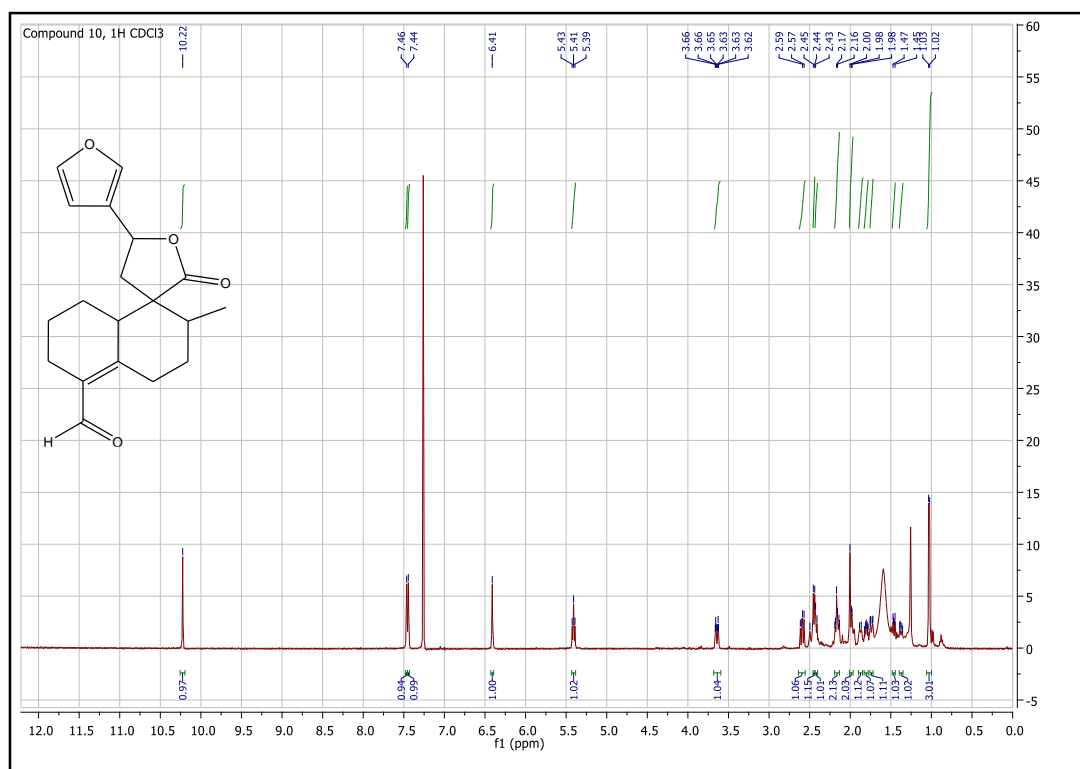


Figure 50. ¹H NMR spectrum of compound 10 measured in CDCl₃, 500 MHz

1.6.5 Inhibitory effects on HIV-1 RT-associated functions and structure-activity relationships

All compounds were tested against RNase H and polymerase function (RDDP) of the HIV-1 RT by the research group of Prof. Enzo Tramontano (Department of Life and Environmental Sciences, University of Cagliari).

The assays revealed that the anti-RNase H activity of the extract was mainly due to the flavone cirsiolol (**3**) with an IC_{50} of 8.2 μM and to a much lower extent ($IC_{50} = 89 \mu M$) to the flavone cirsimaritin (**2**), while the flavone salvigenin was completely inactive up to the concentration of 100 μM .

The SAR analysis of the three flavones pointed out the importance of the catechol group to inhibit the RNase H function. Indeed, removing the hydroxyl group from C-3' position of cirsiolol (**3**) lead to cirsimaritin (**2**) with a decrease in the activity of 10 folds. In addition, methoxylation of hydroxy group at C-4' of cirsimaritin lead to salvigenin (**1**) that was completely inactive ($IC_{50} > 100 \mu M$). Therefore, the maximum activity occurred when both hydroxyl groups are present at C-3' and C-4' of the B ring. The importance of the catechol group to inhibit the RNase H function was already observed in our previous work, comparing a series of caffeic and ferulic acid derivatives (Figure 51).⁶⁴

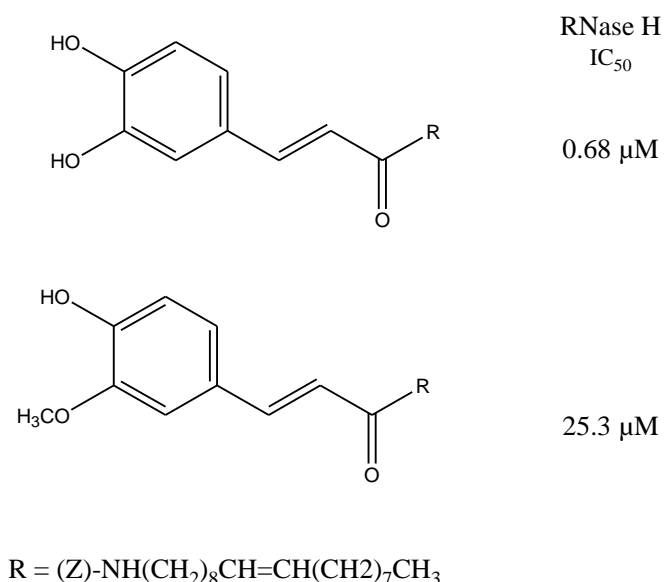


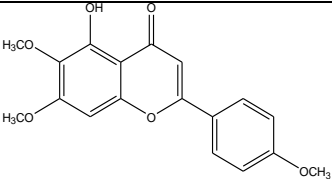
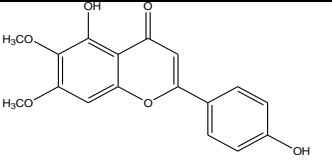
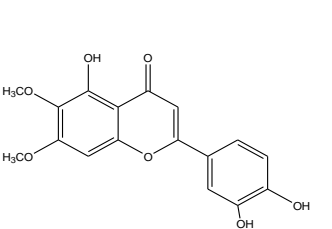
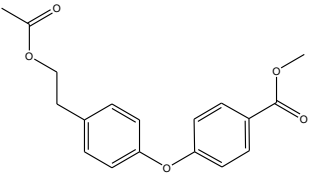
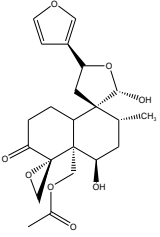
Figure 51. RNase H function inhibition values (IC_{50}) of the caffeic and ferulic acid derivatives

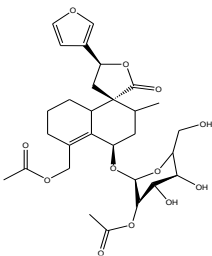
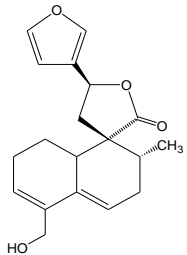
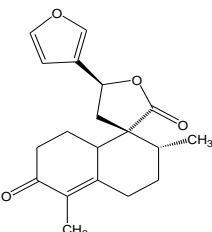
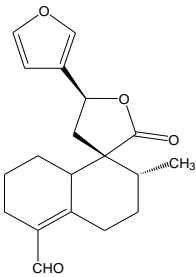
The new natural molecule **4** as well as the neo-clerodanes teuflavin (**5**) and teuflavoside (**6**) resulted inactive up to the concentration of 100 μM ; the lack of activity of teuflavoside was not surprising because it was purified from an inactive fraction.

Among the semi-synthetic neo-clerodanes, Flavuglaucin B (**8**) showed the greatest inhibitory activity on RNase H function with an IC_{50} of 9.1 μM . Flavuglaucin A (**7**) was 3 folds less active when compared with **8**. This data seemed to indicate that the alcohol function was important for interaction with the binding site of the RT. Flavuglaucin C (**9**) and compound **10** were 3 to 5 folds less active than Flavuglaucin B. With respect to Flavuglaucin B, in compounds **9** and **10** the hydroxymethyl moiety has been replaced by a methyl or aldehyde group, respectively, confirming the importance of the alcoholic function. However, the presence of only one double bond in the decalinic nucleus of compounds **9** and **10** change the molecular planarity and thus could influence the interaction with RT.

The neo-clerodanes **7-10** were also evaluated against the RT polymerase function (RDDP) but none inhibitory activity was observed up the concentration of 100 μM (Table 2).

Table 2. Effect of the isolated and hydrolized compounds on the HIV-1 RT-associated RNase H and RDDP functions

Compounds	HIV-1 RT RNase H IC ₅₀ (μM) ^a	HIV-1 RT RDDP IC ₅₀ (μM) ^a
 <p style="text-align: center;">1</p>	>100 (80%) ^b	ND
 <p style="text-align: center;">2</p>	89 ± 7	ND
 <p style="text-align: center;">3</p>	8.2 ± 0.6	ND
 <p style="text-align: center;">4</p>	>100 (80%) ^b	ND
 <p style="text-align: center;">5</p>	>100	ND

 <p style="text-align: center;">6</p>	>100 (74%) ^b	ND ^c
 <p style="text-align: center;">8</p>	9.1 ± 0.2	>100 (80%) ^b
 <p style="text-align: center;">9</p>	52.4 ± 0.4	>100 (80%) ^b
 <p style="text-align: center;">10</p>	36.4 ± 0.4	>100 (80%) ^b

^aConcentration with inhibit 50% of enzyme activity; ^bPercentage of residual enzyme activity in the presence of 100 μ M of the compound; ^cND: Not Done

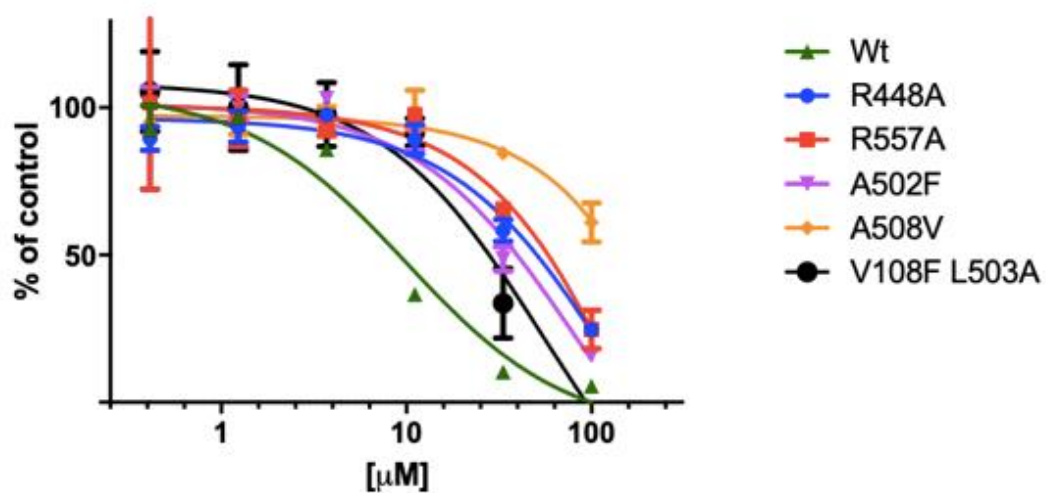
1.6.6 Site-Directed Mutagenesis

Since the neo-clerodane Flavuglaucin B was not able to inhibit the RDDP function and it does not contain any functionality able to bind to the RNase H active site, we supposed that compound Flavuglaucin B might bind to an allosteric RT site. In order to verify this hypothesis, this compound was chosen to perform site-directed mutagenesis, determining the independent impact of several amino acid substitutions on the potency of the compound to inhibit the RNase H function. All the choosed aminoacids are localized in the RNase H domain and are crucial for the binding with the RNase H function inhibitors.

With the aim of verifying a possible interaction for Flavuglaucin B in the allosteric site described by Himmel *et al.*,⁵¹ residue V108 was replaced by a phenylalanine in such a way that it reduced the space at disposal of the compound for the binding in this site. Results showed a slight increase in IC₅₀ when compound **8** Flavuglaucin B was assessed against V108F, compared with the wild type enzyme (Figure 52).

The next mutation involved the residue A502 located in the alpha helix close to the second allosteric binding pocket. This pocket is in the RNase H domain, between the RNase H active site and the primer grip region, close to the interface of subunits p66 and p51. A 502 residue was replaced by a phenylalanine with the aim to cause a movement of alpha helix that reduces the space between the two subunits p51 and p66, thus hindering the entrance of the compound in the pocket. Also in this case, Flavuglaucin B showed a moderate loss in potency (3.5-fold).

Conversely, Flavuglaucin B showed a significant loss in potency in the case of R448A (5.5-fold), R557A (6.5-fold) and, especially, A508V that totally impaired the RNase H inhibition by Flavuglaucin B (IC₅₀>100 μM), suggesting that it had strong interactions within the allosteric pocket located between the RNase H active site and the primer grip region, close to the interface of subunits p66 and p51.



	IC50 (uM)	SD
wt	9,1	0,0
R448A	49,7	5,9
R557A	59,2	4,3
A502F	32,8	2,2
A508V	>100	
L503F	27,3	3,8

Figure 52. Effect of Flavuglaucin B (8) on the HIV-1 RT associated RNase H function of mutated RTs

1.6.7 Docking experiment

To further investigate the mechanism of action of Flavuglaucin B, we carried out QM polarized (QMPL) docking experiments. QMPL docking workflow combines docking with ab initio methods for ligand charges calculation within the protein environment. Subsequently, the best poses were subjected to molecular energy minimization to consider induced-fit protein conformation change (that takes place after ligand binding) and implicit water solvation.

These studies suggested that Flavuglaucin B could be able to bind into an allosteric pocket close to RNase H catalytic site interacting with several residues through hydrogen bonds: Gln428, Gln509, Lys431, a cation- π with Lys424 and several hydrophobic interactions (e.g Leu425, Leu429, Tyr532, Ala508) (Figure 53 a and b).

Hence, when bound to this site, Flavuglaucin B might induce the RNase H domain to a position in which the active site might no longer be able to catalyze hydrolysis cleavage of the RNA strand in the of RNA:DNA duplex. The single point mutation of residue Ala508 to Val in an attempt to reduce the space available for Flavuglaucin B accommodation seems to confirm this mechanism of action.

The docking results into the mutated enzyme show that the compound is not able to be accommodated in the same position and it loses several important interactions (Figure 53, c and d)

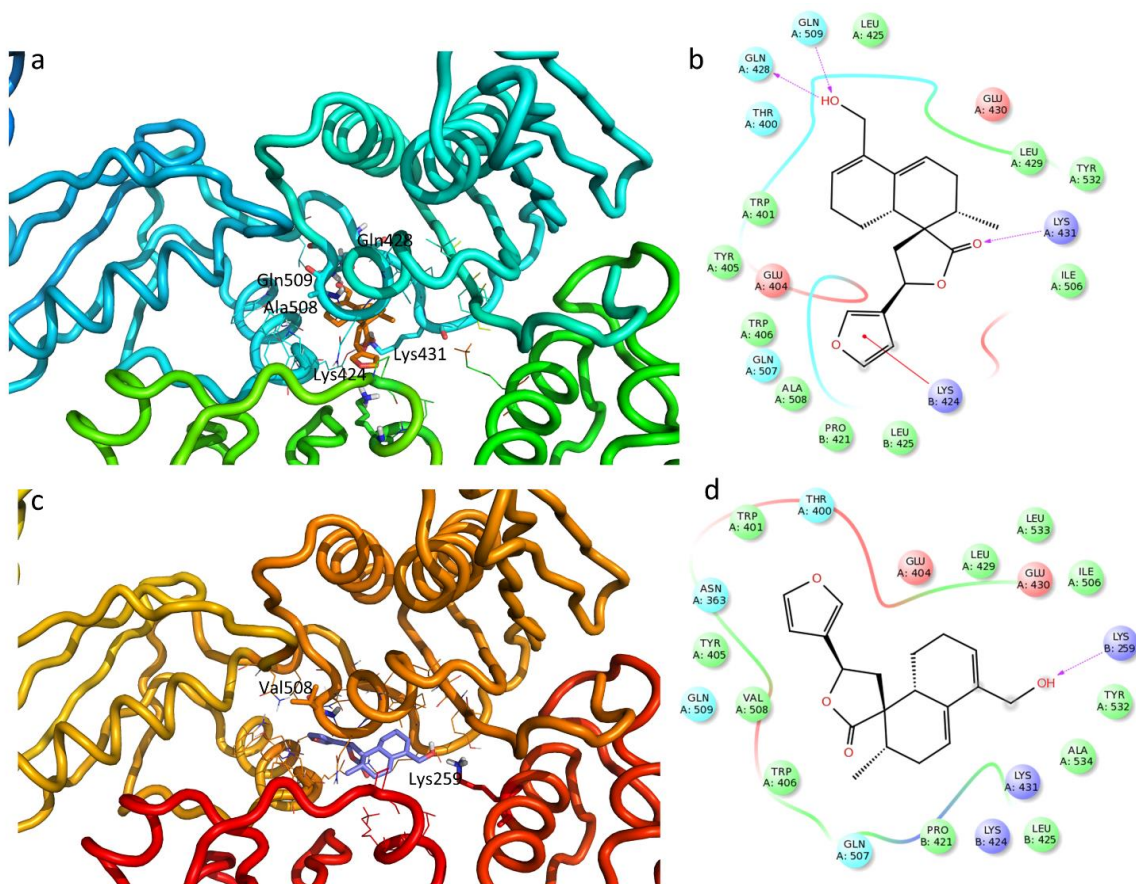


Figure 53. 3D representation of the putative binding mode obtained by docking experiments. a) RTwt- Flavuglaucin B c) A508V-RT- Flavuglaucin B complex and the relative 2D representation of the complexes stabilizing interactions with the binding site residues

1.6.8 Conclusion

From the ethyl acetate extract of the leaves of *Teucrium flavum* subsp. *glaucum* three flavonoids (**1-3**), two clerodanes (**5-6**) and a new diphenyl ether (**4**) were isolated. Moreover, the acid hydrolysis of teuflavoside (**6**) lead to the identification of one known (**10**) and three new neo-clerodanes, Flavuglaucin A-C (**7-9**).⁸⁴

A bioguided fractionation of the extract permitted to identify the flavone cirsiolol as the principal responsible of the inhibitory activity of the RT-associated RNase H function of the extract. The diterpene clerodanes (**5-6**) were completely inactive up to a concentration of 100 μM . As far as we know, the inhibition of the RNase H function of the RT of HIV-1 by cirsiolol has not been reported in the literature. In a previous work, cisiliol was able to inhibit, at very high concentrations, the RT of the avian myeloblastosis virus, the agent responsible for acute myeloblastic leukaemia.⁹⁶ It is interesting to note that cirsiolol was also able to inhibit the HIV-1 integrase at a concentration of 12 μM ,⁹⁷ suggesting cirsiolol as a dual inhibitor of HIV-1.

As regards the products obtained from the hydrolysis of teuflavoside, detailed NMR studies showed that the acid environment did not lead to the expected aglycone, but to a series of clerodanes resulting from dehydration from position 6 and subsequent molecular rearrangement. The results seem to be in agreement with those of Savona *et al.*⁸⁴ reporting that acid hydrolysis of the 18,2'-bis-deacetylteufavoside did not lead to the corresponding aglycone. With the aim to assay the anti-RNase H function of the aglycone of teuflavoside (montanin B), an enzymatic hydrolysis of teuflavoside with β -glucosidase is currently in course.

All semi-synthetic compounds (**7-10**) showed inhibitory activity on the RNase H activity and, in particular, the neo-clerodane Flavuglaucin B (**8**) was the most potent, with an IC_{50} of 9.1 μM . None molecule was able to inhibit the RDDP function of reverse transcriptase up to a concentration of 100 μM . As far as we know, this is the first time that clerodane diterpenes have been identified as inhibitors of HIV-1 RT-associated RNase H activity.

Site-directed mutagenesis studies suggested that Flavuglaucin B bind to the RT allosteric pocket located between the RNase H active site and the primer grip region, close to the interface of subunits p66 and p51

These results prompt us to undergo further studies to verify if the semi-synthetic neo-clerodanes are able to inhibit the HIV-1 replication.

1.7 EXPERIMENTAL PART

1.7.1 Materials and methods

1.7.1.1 General procedures

Optical rotations were measured in CHCl₃ at 25 °C using a PerkinElmer 241 polarimeter. UV spectra were recorded on a GBC Cintra 5 spectrophotometer. NMR spectra of all isolated compounds were recorded at 25 °C on a Unity Inova 500NB high-resolution spectrometer (Agilent Technologies) operating at 500 MHz for ¹H and 100 MHz for ¹³C, respectively or on a VARIAN UNITY INOVA 400 MHz instrument. All spectra were measured at 25°C in CDCl₃ or CD₄O and using the undeuterated residue of CHCl₃ in CDCl₃ (¹H 7.23 ppm and ¹³C 77.0 ppm) or CH₃OH in CD₄O (¹H 3.34 ppm and ¹³C 49.0 ppm) as a reference. HRESIMS were measured on an Agilent 6520 Time of Flight (TOF) MS instrument (Agilent Technologies). Analytical data of the isolated compounds were in agreement within ± 0.4% of the theoretical values. Column chromatography was carried out under TLC monitoring using silica gel (40–63 μm, Merck) and Sephadex LH-20 (25–100 μm, Pharmacia). For VLC, silica gel (40–63 μm) (Merck) was used. TLC was performed on silica gel 60 F₂₅₄ or RP-18 F₂₅₄ (Merck). LiChrolut RP-18 (40–63 μm) 500 mg, 3 mL (Merck) solid phase extraction (SPE) cartridges were also used. Semipreparative HPLC was conducted by means of a Varian 920 LH instrument fitted with an autosampler module with a 1000 μL loop. The peak purities were monitored using a dual-wavelength UV detector settled at 254 and 360 nm. The column was a 250 x 10 mm HyperClone C-18-ODS, particle size 5 μm (Phenomenex).

1.7.1.2 Plant material

Teucrium flavum subsp. *glaucum* was collected in July 2003 at Orgosolo Supramonte. The plant was identified by Professor Bruno De Martis of the Department of Botanical Sciences (2003) of the University of Cagliari.

1.7.1.3 Extraction and isolation of natural compounds

The air-dried and powdered leaves of *Teucrium flavum* were ground and extracted firstly with *n*-hexane, then with ethyl acetate (EtOAc) and finally with methanol.

From the percolation with EtOAc at room temperature, 117 g of green extract were obtained. An aliquot of 18.19 g of the extract was subjected to VLC (silica gel, 150 g, 40–63 μm) using a step gradient of *n*-hexane–EtOAc–MeOH to yield four main fractions.

Solvents	Fr of VLC
<i>n</i> -hexane-EtOAc (75%-25%)	Fr 1-8
<i>n</i> -hexane-EtOAc (50%-50%)	Fr 9-13
<i>n</i> -hexane-EtOAc (25%-75%)	Fr 14-17
EtOAc (100%)	Fr 18-21
EtOAc-MeOH (75%-25%)	Fr 22-26
EtOAc-MeOH (50%-50%)	Fr 27-31
MeOH (100%)	Fr 32-34

After combining fractions 7-9 (42.4 mg), 10-17 (310 mg), 18-31 (13.5 g), 32-34 (170 mg) of the ethyl acetate extract VLC I, the 18-31 fraction of the VLC I was further purified with a VLC II using a step gradient of dichloromethane (CH₂Cl₂) and methanol (MeOH).

Solvents	Fr of VLC
CH ₂ Cl ₂ - MeOH (95%-5%)	Fr 1-9
CH ₂ Cl ₂ - MeOH (90%-10%)	Fr 10-15
CH ₂ Cl ₂ - MeOH (80%-20%)	Fr 16-20

The following fractions have been tested on the RT RNase H function, in order to bioguide the isolation of potentially active compounds:

- F1 = fr 10-17 VLC I
- F2 = fr 6 VLC II
- F3 = fr 7 VLC II
- F4 = fr 9-10 VLC II
- F5 = fr 11-13 VLC II
- F6 = fr 14-16 VLC II

Fraction 7-9 (42.4 mg) VLC I was not tested in advance due to its small quantity and was directly chromatographed by CC over Sephadex LH-20 using MeOH as eluent, yielding fraction 25-35. This fraction was further chromatographed over Sephadex LH-20 (MeOH) by to give an impure compound

that was purified by RP-18 SPE using acetonitrile–H₂O (7:3) as eluent, to give compound **4** (1.8 mg). 86.8 mg of F1, was purified by RP-18 SPE using ACN: H₂O (7:3) as eluents, to remove chlorophyll, obtaining a yellow white solid, which was finally purified by CC over Sephadex LH-20 (MeOH) to give compound **1** (salvigenin, 3.5 mg)

A portion of fraction F2 (900 mg) was subjected to CC over silica gel (90g) using DCM-MeOH (9.75:0.25) as eluent, to furnish fractions 115-122, 161-240 and 241-341. Fraction 115-122 was purified twice using Sephadex LH-20 (MeOH) to give compound **1**, (salvigenin, 2.4 mg). Fraction 161-240 (150 mg), was purified using Sephadex LH-20 (MeOH), to give fraction 27-43, followed by RP-HPLC, using acetonitrile–H₂O (7:3, flow 2.5 mL/min) as eluent, to provide a white solid (cirsimaritin, **2**), (1.9 mg *t_R* = 8.82 min,) and compound **1** (salvigenin, 1 mg, *t_R*=12.1 min). Finally, fraction 241-341 (120 mg) was purified using Sephadex LH-20 (MeOH) to give compound **2** (cirsimaritin, 4.4 mg), and fraction 17-26 which was further chromatographed by RP-18 SPE using MeOH-H₂O (7:3) as mobile phase, to give 86.8 mg of an impure compound. This fraction was further subjected to CC over silica gel (5g), using CH₂Cl₂-MeOH (9.75:0.25) as eluent, to give a white solid (teuflavin, **5**, 11.3 mg).

An aliquot of fraction F3 (590 mg) was chromatographed by CC over Sephadex LH-20 using MeOH as eluent, to give the subfraction 49-55, which was further purified by Sephadex (MeOH), to produce a further subfraction (35-60).

This fraction was further purified by RP-18 SPE using ACN-H₂O (5:5) as eluent, to give compound **3** (Cirsiliol, 1.4 mg).

Based on TLC analysis, fraction 8 of VLC II was found to be very similar to F3. Therefore, it was subjected to VLC III (silica gel 40–63 μm) using a step gradient of CH₂Cl₂ and MeOH.

Solvents	Fr of VLCIII
CH ₂ Cl ₂ - MeOH (97.5%-2.5%)	Fr 1-11
CH ₂ Cl ₂ -MeOH (90%-10%)	Fr 12-13

According to TLC, fraction 7-8 and 9-11 of VLC III were combined and investigated. Fraction 7-8 of VLC III (75.5 mg), was chromatographed using Sephadex LH-20 (MeOH), to give compound **3**, (Cirsiliol, 1.3 mg), already isolated from F3.

From fraction 9-11 (50 mg) of VLC III a CC over Sephadex LH-20 (MeOH) permitted to isolate further 0.6 mg of Cirsiliol (**3**).

Finally, a NMR analysis of fraction 9-10 (VLC II, 2.3 g) revealed that it was Tinosporaside (**6**).

1.7.1.4 Hydrolysis of Teuflavoside (**6**)

The hydrolysis was performed by reacting 800 mg of teuflavoside (**6**) with 5.6 ml of 2N H₂SO₄ in 95 ml of distilled water.

Procedure:

The aqueous solution of H₂SO₄ 2N was raised to 95°C. Subsequently, 800 mg of teuflavoside, dissolved in 3 ml of methanol, were added to the acid solution and reacted for 20 minutes. After cooling, the solution was first diluted in water and then extracted with ethyl acetate in a separatory funnel.

The solvent was removed by vacuum and the residue (550 mg) was chromatographed over silica gel (25g), using CH₂Cl₂-EtOAc (9.75:0.25) as eluent. After TLC comparison similar fractions were combined and four fractions were obtained:

- 40-47 (26.1 mg),
- 48-71 (28.9 mg),
- 72-92 (10.5 mg),
- 145-190 (25.1 mg).

Fractions 40-47 and 145-190 were represented by compound **7** (26.1 mg) and **8** (25.1 mg), respectively.

Fraction 48-71 (28.9 mg) was chromatographed by RP-HPLC, using acetonitrile:H₂O (flow rate 2.5 ml/min), to give a transparent semi-solid compound (**10**) (1.4 mg, t_R= 10 min), and compound **7** (2.1 t_R= 13 min). Fraction 72-92 (10.5 mg) was chromatographed by RP-HPLC, using acetonitrile:H₂O(6:4, flow 2.5 mL/min) giving a transparent solid, compound **9** (1.2 mg, t_R=9.5 minutes), and compound **10** (0.6 mg, t_R= 10 min).

1.7.1.5 Inhibition test of the RT RNase H function

RNase H activity was evaluated in 100 μ L of a mixture containing 50 mM Tris-HCl (pH 7.8, 1mM dithiothreitol (DTT), 80 mM KCl, 6 mM MgCl₂, RNA/DNA hybrid (5'-GTTCTTTTTCCTGCCTGAC-3'-fluorescein, 5'-CAAAGAAAAGGGGGGACUG-3'-Dabcyl) and 3.8 nM RT). The reaction mixture was incubated for 1 h at 37 °C after which the reaction was stopped by addition of EDTA and the products were measured with a Victor 3 (Perkin) instrument at 490/528 nm.

1.7.2 Experimental data of the known compounds isolated from *Teucrium flavum* subsp *glaucum*

Compound 1

Salvigenin (**1**) data (^1H and ^{13}C NMR) are in agreement with those reported in the literature⁹³ (For the ^1H NMR spectrum see the Results and Discussion section).

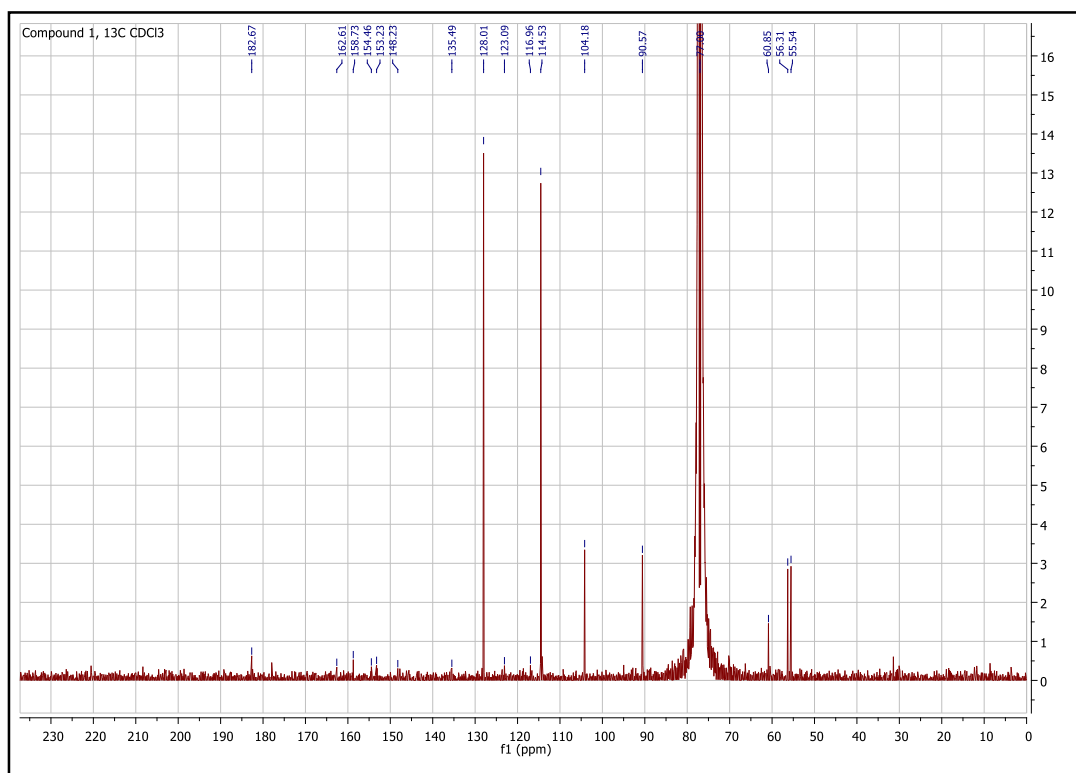


Figure 54. ^{13}C NMR Spectrum of compound **1** measured in CDCl_3 , 100 MHz.

Salvigenin: yellow solid; ^1H NMR (500 MHz, CDCl_3) δ_{H} 3.90 (s, 3H, 4'- OCH_3) 3.93 (s, 3H, 6- OCH_3), 3.97 (s, 3H, 7- OCH_3), 6.55 (s, 1H, H-3), 6.59 (s, 1H, H-8), 7.02 (d, 2H, $J = 9.0$ Hz, H-3', H-5'), 7.85 (d, 2H, $J = 9.0$ Hz, H-2', H-6'), 12.87 (s br, 1H, H-5) ppm ; ^{13}C NMR (100 MHz, CD_3OD) δ_{C} 55.54 (4'- OCH_3), 56.31 (6- OCH_3), 60.85 (7- OCH_3), 90.57 (C-8), 104.18 (C-3), 114.53 (C-3', C-5'), 116.96 (C-10), 123.09 (C-1'), 128.01 (C-2', C-6'), 135.49 (C-6), 148.23 (C-9), 153.23 (C-5), 154.468 (C-4'), 158.72 (C-7), 162.62 (C-2), 183.67 (C-4) ppm.

Compound 2

Cirsimaritin (**2**) data (^1H and ^{13}C NMR) are in agreement with those reported in the literature⁹⁴ (For the ^1H NMR spectrum see the Results and Discussion section).

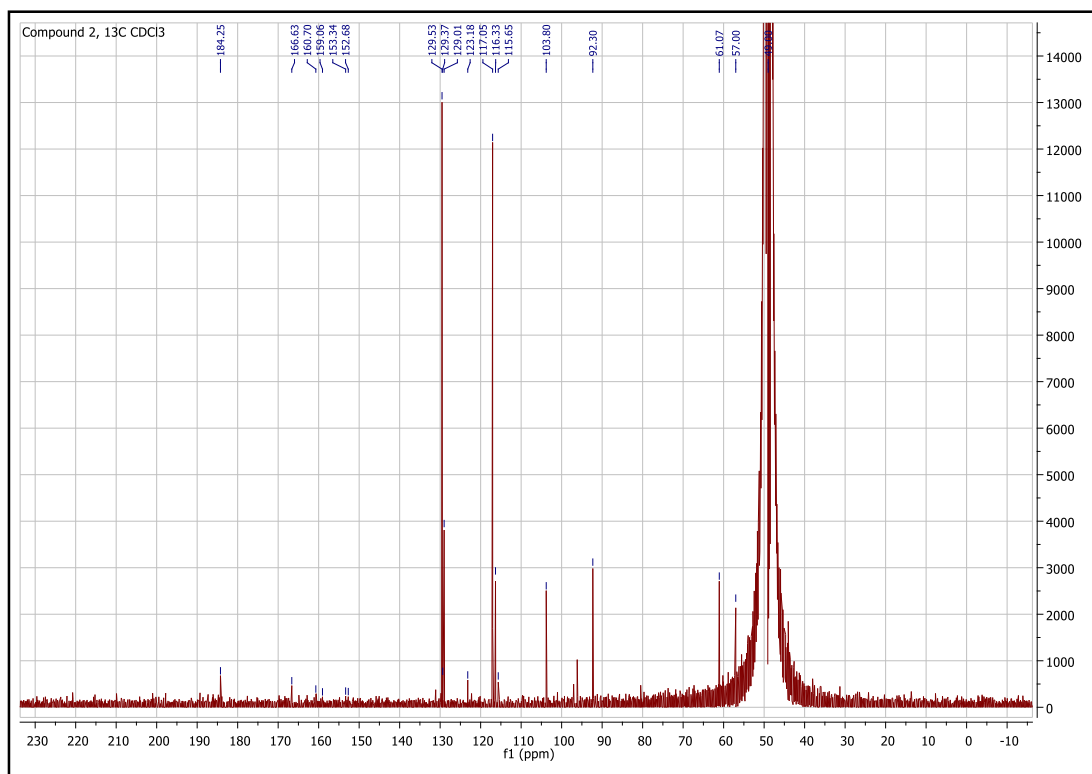


Figure 55. ^{13}C NMR spectrum of compound **2** measured in CDCl_3 , 100 MHz

Cirsimaritin: yellow solid; ^1H NMR (500 MHz, CD_3OD) δ_{H} 3.93 (s, 3H, 6- OCH_3), 4.07 (s, 3H, 7- OCH_3), 6.75 (s, 1H, H-3), 6.91 (s, 1H, H-8), 7.03 (d, 2H, $J = 8.5$ Hz, H-3', H-5'), 7.98 (s, 2H, $J = 8.5$ Hz, H-2', H-6') ppm; ^{13}C NMR (100 MHz, CD_3OD) δ_{C} 57.00 (6- OCH_3), 61.07 (7- OCH_3), 92.30 (C-8), 103.80 (C-3), 115.65 (C-10), 116.33 (C-5'), 117.05 (C-3'), 123.18 (C-1'), 129.01 (C-6'), 129.38 (C-6), 129.53 (C-2'), 152.69 (C-9), 153.34 (C-5), 159.06 (C-7), 160.70 (C-4'), 166.63 (C-2), 184.25 (C-4) ppm.

Compound 3

Cirsiliol (**3**) data (^1H and ^{13}C NMR) are in agreement with those reported in the literature⁹⁵ (For the ^1H NMR spectrum see the Results and Discussion section).

Cirsiliol: yellow solid; ^1H NMR (500 MHz, CD_3OD) δ_{H} 3.93 (s, 3H, 6- OCH_3), 4.08 (s, 3H, 7- OCH_3), 6.70 (s, 1H, H-3), 6.89 (s, 1H, H-8), 7.01 (d, 1H, $J = 8.5$ Hz, H-5'), 7.50 (d, 1H, $J = 8.5$ Hz, H-2'), 7.52 (dd, 1H, $J = 8.5$ Hz, $J = 2.5$ Hz, H-6') ppm; ^{13}C NMR (100 MHz, CD_3OD) δ_{C} 56.85 (7- OCH_3), 60.91 (6- OCH_3), 92.16 (C-8), 103.73 (C-3), 106.50 (C-10), 114.05 (C-2'), 116.68 (C-5'), 120.25 (C-

6'), 123.30 (C-1'), 133.50 (C-6), 147.10 (C-3'), 150.90 (C-4'), 153.34 (C-5), 155.60 (C-9), 160.40 (C-7), 166.70 (C-2), 184.25 (C-4) ppm.

Compound 5

Compound **5** was identified as Teuflavin through the study of the 1D (^1H and ^{13}C NMR), and 2D NMR spectra (DQF-COSY, HSQC, HMBC), mass spectrometry (ESI MS), specific optical rotation and by comparison with data reported in literature.⁸⁴ (For the ^1H NMR spectrum see the Results and Discussion section).

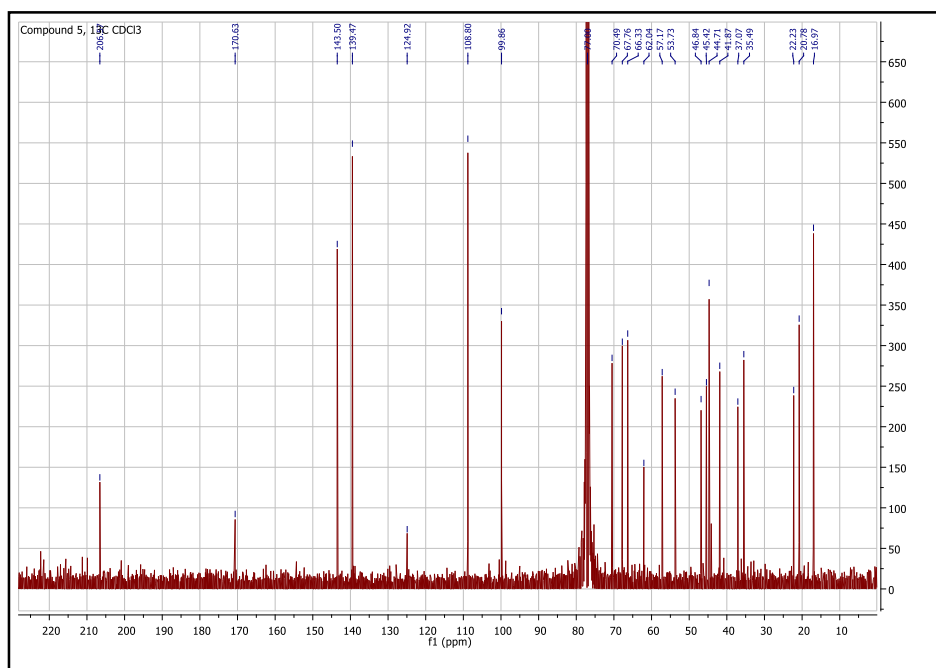


Figure 56. ^{13}C NMR Spectrum of compound **5** measured in CDCl_3 , 100 MHz.

Teuflavin: colorless solid; ^1H NMR (500 MHz, CDCl_3) δ_{H} 0.99 (d, 3H, $J = 7.0$ Hz, H-17), 1.60 (t, 2H, H-7), 1.92 (d, 1H, $J = 2.5$ Hz, H-11), 1.97 (s, 3H, COCH_3), 2.07 (m, 1H, H-8), 2.23 (m, 1H, H-1), 2.33 (m, 1H, H-2), 2.46 (d, 1H, $J = 6.5$, H-11), 2.70 (m, 1H, H-2), 2.73 (m, 1H, H-10), 2.81 (d, 1H, $J = 6.0$, H-18), 3.10 (m, 1H, H-1), 3.66 (dd, 1H, $J = 10.0$ Hz, $J = 1.5$ Hz, H-6), 3.72 (d, 1H, $J = 6.5$, H-18), 3.89 (dd, 1H, $J = 10.5$, Hz, $J = 0.5$ Hz, H-19), 4.40 (d, 1H, $J = 10.5$, H-19) 5.18 (q, 1H, $J = 6.5$, Hz, $J = 3.5$ Hz, H-12), 5.43 (s, 1H, H-20) 6.43 (dd, 1H, $^3J = 1.5$, Hz, $J = 0.5$ Hz, H-14), 7.41 (t, 1H, H-15), 7.43 (m, 1H, H-16) ppm; ^{13}C NMR (100 MHz, CDCl_3) δ_{C} 16.97 (C-17), 20.78 (COCH_3^*), 22.23 (C-1), 35.49 (C-8), 37.07 (C-7), 41.87 (C-2), 44.71 (C-10), 45.42 (C-11), 46.84 (C-5), 53.73 (C-9), 57.17 (C-18), 62.04 (C-4), 66.33 (C-6), 67.76 (C-19), 70.49 (C-12), 99.86 (C-20), 108.80 (C-14), 124.92 (C-13), 139.47 (C-16), 143.50 (C-15), 170.63 (CO^*CH_3), 206.57 (C-3) ppm.

Compound 6

Compound 6 was identified as Teuflavoside through the study of the 1D (^1H and ^{13}C NMR), and 2D NMR (DQF-COSY, HSQC, HMBC) spectra, specific optical rotation and by comparison with the data reported in the literature⁸⁴ (For the ^1H NMR spectrum see the Results and Discussion section).

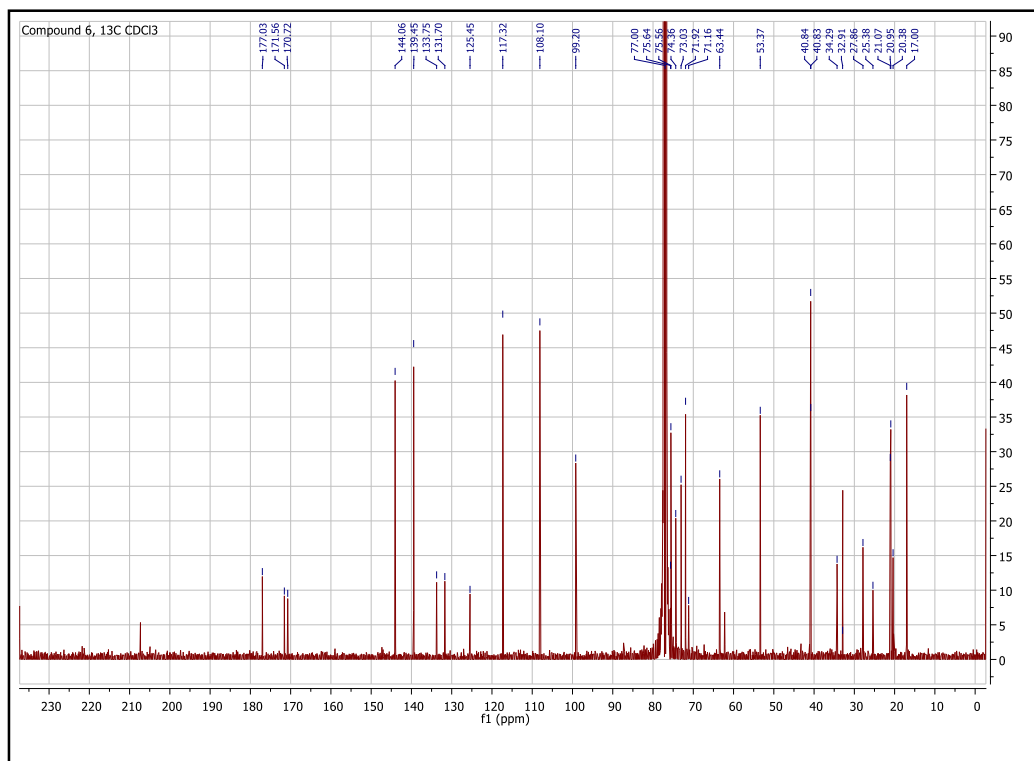


Figure 57. ^{13}C NMR Spectrum of compound 6 measured in CDCl_3 , 100 MHz

Teuflavoside: solid colorless; ^1H NMR (500 MHz, CDCl_3) δ_{H} 0.95 (d, 3H, $J = 6.5$ Hz, H-17), 1.49 (m, 2H, , H-1, H-2), 1.76 (m, 2H, H-1, H-7), 1.97 (m, 1H, H-8), 2.01 (m, 2H, H-2), 2.08 (s, 3H, H-8'), 2.09 (s, 3H, H-20), 2.11 (s, 1H, H-3), 2.13 (m, 1H, H-7), 2.32 (dd, 1H, $J = 14.0$ Hz, $J = 8.5$ Hz, H-11), 2.52 (dd, 1H, $J = 14.0$ Hz, $J = 8.5$ Hz H-11), 2.74 (s br, 1H, H-10), 3.35 (m. 1H, H-5'), 3.54 (t, 1H, H-4'), 3.60 (t, 1H, H-3'), 3.78 (dd, 1H, $J = 12.0$ Hz, $J = 5.0$ Hz, H-6'), 3.88 (dd, 1H, $J = 12.0$ Hz, $J = 3.0$ Hz, H-6') 4.56 (m, 2H, H-7, H-18), 4.74 (t, 1H, H-2'), 4.82 (t, 1H, H-6), 4.87 (d, $J = 12.0$ Hz, H-18), 5.37 (t, 1H, H-12), 6.39 (s, 1H, H-14), 7.43 (m, 1H, H-15), 7.45 (s, 1H, H-16) ppm; ^{13}C NMR (100 MHz, CDCl_3) δ_{C} 17.00 (C-17), 20.38 (C-1), 20.95 (C-8'), 21.07 (C-20), 25.40 (C-2), 27.86 (C-3), 32.88 (C-8), 34.29 (C-7), 40.83 (C-11), 40.84 (C-10), 53.38 (C-9), 62.22 (C-6'), 63.44 (C-18), 71.16 (C-4'), 71.92 (C-12), 73.04 (C-6), 74.37 (C-2'), 75.56 (C-5'), 75.64 (C-3'), 99.20 (C-1'), 108.10 (C-14), 125.45 (C-13), 131.70 (C-4), 133.75 (C-5), 139.45 (C-16), 144.06 (C-15), 170.72 (C-7'), 171.56 (C-19), 177.03 (C-21) ppm.

Compound 10

The analytical and spectroscopic (^1H and ^{13}C NMR) data of compound **10** are in agreement with those reported in the literature.⁸⁴ (For the ^1H NMR spectrum see the Results and Discussion section).

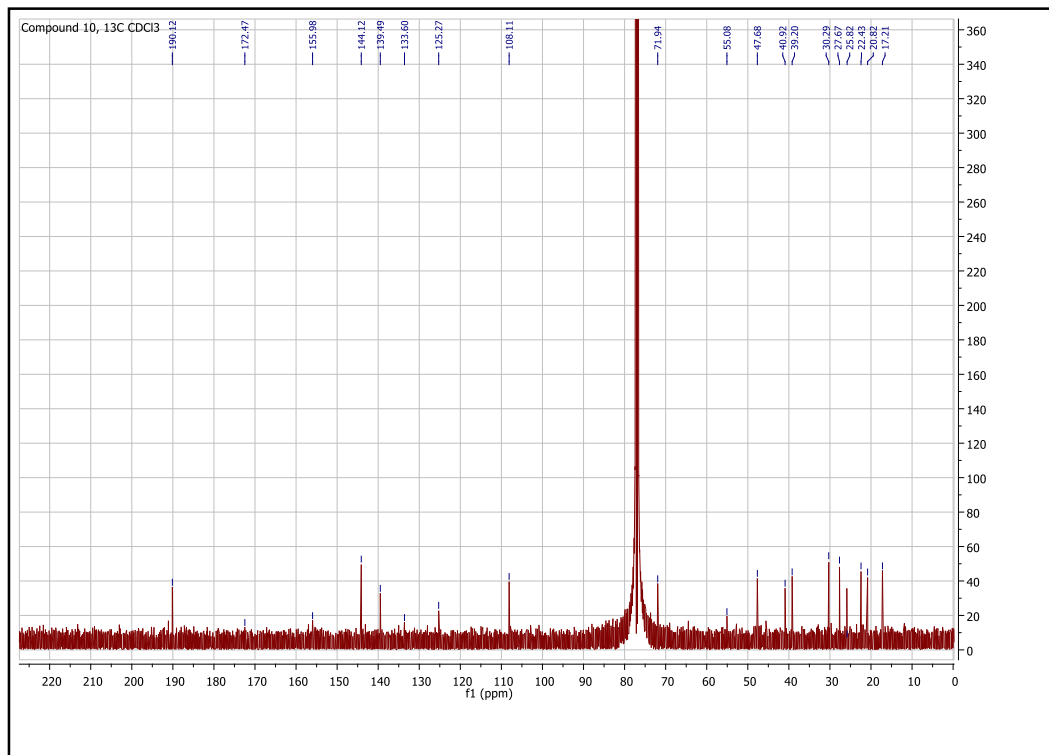


Figure 58. ^{13}C NMR Spectrum of compound **10** measured in CDCl_3 , 100 MHz

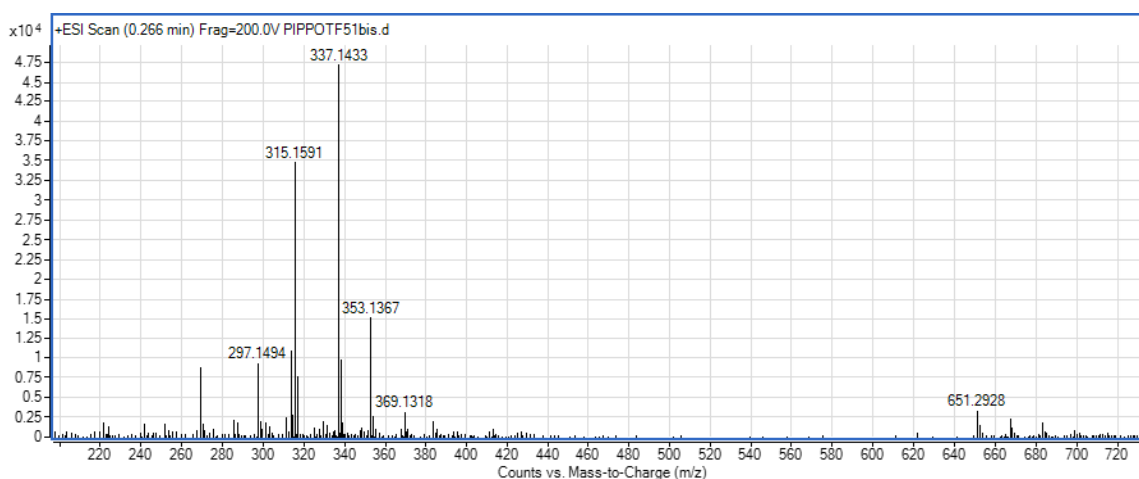


Figure 59. HR ESI MS spectrum of compound **10**

^1H NMR (500 MHz, CDCl_3) δ_{H} 1.03 (d, 3H, $J = 6.5$, H-17), 1.37 (dd br, 1H, $J = 14.0$, $J = 4.5$, H-2), 1.46 (dd, 1H, $J = 10.0$, $J = 3.0$, H-1), 1.74 (dd, 1H, $J = 13.5$, $J = 2.0$, H-7), 1.80 (m, 1H, H-8), 1.88 (d br, 1H, $J = 10.0$, H-2), 1.99 (d, 2H, $J = 13.0$, H-6, H-3), 2.16 (m, 2H, H-7, H-1), 2.42 (d, 1H, $J =$

9.0, H-11), 2.45 (d, 1H, $J = 9.0$, H-10), 2.50 (s br, H-3), 2.60 (dd, 1H, $J = 9.0$, $J = 5.0$, H-11), 3.85 (dt, 1H, H-6), 5.41 (t, 1H, H-12), 6.41(s, 1H, H-14), 7.45 (t br, 1H, H-15), 7.47 (s br, 1H, H-16) ppm; ^{13}C NMR (100 MHz, CDCl_3) δ_{C} 17.21 (C-17), 20.82 (C-2), 22.43 (C-3), 25.88 (C-1), 27.67 (C-6), 30.29 (C-7), 39.20 (C-8), 40.92 (C-11), 47.68 (C-10), 55.08 (C-9), 71.94 (C-12), 108.11 (C-14), 125.27 (C-13), 133.60 (C-4), 139.49 (C-16), 144.12 (C-15), 155.97 (C-5), 172.47 (C-20), 190.12(C-18) ppm.

1.7.3 Molecular modelling

Ligand preparation

The ligand was built within the Maestro platform. The most stable conformation has been determined by molecular mechanics conformational analysis performed with Macromodel software version 9.2.⁹⁸ using the Merck Molecular Force Fields (MMFFs)⁹⁹ and GB/SA water implicit solvation model,¹⁰⁰ Polak-Ribière Conjugate Gradient (PRCG) method, 5000 iterations and a convergence criterion of 0.05 kcal/(mol Å). All the other parameters were left as default.

Protein preparation

The coordinates for reverse transcriptase enzyme was taken from the RCSB Protein Data Bank¹⁰¹ (PDB codes 1rti).¹⁰² The protein was prepared by using the Maestro Protein Preparation Wizard. Original water molecules were removed.

Starting from wt protein the mutated enzymes A508V-RT was generated. Mutated RT was minimized considering OPLS force field in GB/SA implicit water, setting 10000 steps interactions analysis with Polak-Ribier Coniugate Gradient (PRCG) method and a convergence criterion of 0.05 kcal/mol.

Docking protocol

Molecular docking studies were performed using QMPL workflow protocol.¹⁰³ Grids were defined around the refined structure by centering on the residue Q500 (located in the RNaseH domain) and fixing the box volume (46x46x46 Å). The other settings were left as default.

Post docking protocol

In order to better take into account, the induced fit phenomena, the most energy favored generated complexes were fully optimized with the OPLS2005 force field in GB/SA implicit water. The optimization process was performed setting 10000 steps interactions up to the derivative convergence criterion equal to 0.05 kJ/(mol*Å). The resulting complexes were considered for the binding modes graphical analysis with Pymol and Maestro.

1.8 REFERENCES

1. Global HIV & AIDS statistics — 2018 fact sheet.
2. Gallo, R. C. M. D., Montagnier, L.: The Discovery of HIV as the Cause of AIDS. *New England Journal of Medicine* **2003**, 349, 2283-2285.
3. Montagnier, L. 25 years after HIV discovery: prospects for cure and vaccine. *Virology* **2010**, 397, 248-254.
4. Alizon, M.; Sonigo, P.; Barre-Sinoussi, F.; Chermann, J. C.; Tiollais, P.; Montagnier, L.; Wain-Hobson, S. Molecular cloning of lymphadenopathy-associated virus. *Nature* **1984**, 312, 757-760.
5. Ratner, L.; Haseltine, W.; Patarca, R.; Livak, K. J.; Starcich, B.; Josephs, S. F.; Doran, E. R.; Rafalski, J. A.; Whitehorn, E. A.; Baumeister, K.; et al. Complete nucleotide sequence of the AIDS virus, HTLV-III. *Nature* **1985**, 313, 277-284.
6. Wain-Hobson, S.; Sonigo, P.; Danos, O.; Cole, S.; Alizon, M. Nucleotide sequence of the AIDS virus, LAV. *Cell* **1985**, 40, 9-17.
7. F Clavel, D. G., F Brun-Vezinet, S Chamaret, MA Rey, MO Santos-Ferreira, AG Laurent, C Dauguet, C Katlama, C Rouzioux and et al. Isolation of a New Human Retrovirus from West African Patients with AIDS. *Science* **1986**, 233, 343-346.
8. PA, L. Human immunodeficiency viruses and their replication. In *Virology*, Ed. Lippincott-Raven: Philadelphia, 1996; pp 881–1952.
9. Muller, B.; Heilemann, M. Shedding new light on viruses: super-resolution microscopy for studying human immunodeficiency virus. *Trends in microbiology* **2013**, 21, 522-533.
10. Gürtler, L.; Aepfelbacher, M.; Bauerfeind, U.; Blümel, J.; Burger, R.; Gärtner, B.; Gröner, A.; Heiden, M.; Hildebrandt, M.; Jansen, B.; Offergeld, R.; Pauli, G.; Schlenkrich, U.; Schottstedt, V.; Seitz, R.; Strobel, J.; Willkommen., H. Human Immunodeficiency Virus (HIV). *Transfusion medicine and hemotherapy : offizielles Organ der Deutschen Gesellschaft für Transfusionsmedizin und Immunhamatologie* **2016**, 43, 203-222.
11. Vicenzi, E.; Poli, G. Novel factors interfering with human immunodeficiency virus-type 1 replication in vivo and in vitro. *Tissue antigens* **2013**, 81, 61-71.
12. Alkhatib, G.; Combadiere, C.; Broder, C. C.; Feng, Y.; Kennedy, P. E.; Murphy, P. M.; Berger, E. A. CC CKR5: a RANTES, MIP-1alpha, MIP-1beta receptor as a fusion cofactor for macrophage-tropic HIV-1. *Science* **1996**, 272, 1955-1958.
13. Deng, H.; Liu, R.; Ellmeier, W.; Choe, S.; Unutmaz, D.; Burkhardt, M.; Di Marzio, P.; Marmon, S.; Sutton, R. E.; Hill, C. M.; Davis, C. B.; Peiper, S. C.; Schall, T. J.; Littman, D. R.; Landau, N. R. Identification of a major co-receptor for primary isolates of HIV-1. *Nature* **1996**, 381, 661-666.
14. Doranz, B. J.; Rucker, J.; Yi, Y.; Smyth, R. J.; Samson, M.; Peiper, S. C.; Parmentier, M.; Collman, R. G.; Doms, R. W. A dual-tropic primary HIV-1 isolate that uses fusin and the beta-chemokine receptors CKR-5, CKR-3, and CKR-2b as fusion cofactors. *Cell* **1996**, 85, 1149-1158.
15. Feng, Y.; Broder, C. C.; Kennedy, P. E.; Berger, E. A. HIV-1 entry cofactor: functional cDNA cloning of a seven-transmembrane, G protein-coupled receptor. *Science* **1996**, 272, 872-877.
16. Menendez-Arias, L. Molecular basis of human immunodeficiency virus type 1 drug resistance: overview and recent developments. *Antiviral Res* **2013**, 98, 93-120.
17. Lili Cao, W. S., Erik De Clercq, Peng Zhan and Xinyong Liu. Recent Progress in the Research of Small Molecule HIV-1 RNase H Inhibitors. *Current Medicinal Chemistry* **2014**, 21, 1956-1967.
18. Yu, F.; Liu, X.; Zhan, P.; De Clercq, E. Recent advances in the research of HIV-1 RNase H inhibitors. *Mini reviews in medicinal chemistry* **2008**, 8, 1243-1251.
19. Nowotny, M.; Gaidamakov, S. A.; Crouch, R. J.; Yang, W. Crystal structures of RNase H bound to an RNA/DNA hybrid: substrate specificity and metal-dependent catalysis. *Cell* **2005**, 121, 1005-1016.
20. Pari, K.; Mueller, G. A.; DeRose, E. F.; Kirby, T. W.; London, R. E. Solution structure of the RNase H domain of the HIV-1 reverse transcriptase in the presence of magnesium. *Biochemistry* **2003**, 42, 639-650.
21. Klumpp, K.; Mirzadegan, T. Recent progress in the design of small molecule inhibitors of HIV RNase H. *Current pharmaceutical design* **2006**, 12, 1909-1922.
22. Nowotny, M.; Gaidamakov, S. A.; Ghirlando, R.; Cerritelli, S. M.; Crouch, R. J.; Yang, W. Structure of human RNase H1 complexed with an RNA/DNA hybrid: insight into HIV reverse transcription. *Molecular cell* **2007**, 28, 264-276.
23. Arts, E. J.; Le Grice, S. F. Interaction of retroviral reverse transcriptase with template-primer duplexes during replication. *Progress in nucleic acid research and molecular biology* **1998**, 58, 339-393.
24. Rausch, J. W. L. G., S.F. 'Binding, bending and bonding': polypurinetriact-primed initiation of plus-strand DNA synthesis in human immunodeficiency virus. *Int. J. Biochem. Cell. Biol* **2004**, 36, 1752-1766.
25. Zuniga, M., Whiteside, A., Ghaziani, A., Bartlett, J.G., A Decade of HAART. *The Development and Global Impact of Highly Active Antiretroviral Therapy*. 2008.
26. De Clercq, E. Anti-HIV drugs: 25 compounds approved within 25 years after the discovery of HIV. *International journal of antimicrobial agents* **2009**, 33, 307-320.

27. Menendez-Arias, L. Mechanisms of resistance to nucleoside analogue inhibitors of HIV-1 reverse transcriptase. *Virus research* **2008**, 134, 124-146.
28. Seligmann, M., Warrel, D.A., Aboulker, J.P., Carbon, C., Darbyshire, J.H., Dormont, J., Eschwege, E., Girling, D.J., James, D.R., Levy, J.P., Peto, P.T.A., Schwarz, D., Stone, A.B., Weller, I.V.D., Withnall, R., Gelmon, K., Lafon, E., Swart, A.M., Aber, V.R., Babiker, A.G., Lhoro, S., Nunn, A.J., Vray, M., Concorde: MRC/ANRS randomised double-blind controlled trial of immediate and deferred zidovudine in symptom-free HIV infection. Concorde Coordinating Committee. *Lancet (London, England)* **1994**, 343, 871-881.
29. Meyer, P. R.; Matsuura, S. E.; Mian, A. M.; So, A. G.; Scott, W. A. A mechanism of AZT resistance: an increase in nucleotide-dependent primer unblocking by mutant HIV-1 reverse transcriptase. *Molecular cell* **1999**, 4, 35-43.
30. Kohlstaedt, L. A.; Wang, J.; Friedman, J. M.; Rice, P. A.; Steitz, T. A. Crystal structure at 3.5 Å resolution of HIV-1 reverse transcriptase complexed with an inhibitor. *Science* **1992**, 256, 1783-1790.
31. Ren, J.; Stammers, D. K. Structural basis for drug resistance mechanisms for non-nucleoside inhibitors of HIV reverse transcriptase. *Virus research* **2008**, 134, 157-170.
32. Menendez-Arias, L.; Betancor, G.; Matamoros, T. HIV-1 reverse transcriptase connection subdomain mutations involved in resistance to approved non-nucleoside inhibitors. *Antiviral Res* **2011**, 92, 139-149.
33. Esnouf, R.; Ren, J.; Ross, C.; Jones, Y.; Stammers, D.; Stuart, D. Mechanism of inhibition of HIV-1 reverse transcriptase by non-nucleoside inhibitors. *Nature structural biology* **1995**, 2, 303-308.
34. Hsiou, Y.; Ding, J.; Das, K.; Clark, A. D., Jr.; Hughes, S. H.; Arnold, E. Structure of unliganded HIV-1 reverse transcriptase at 2.7 Å resolution: implications of conformational changes for polymerization and inhibition mechanisms. *Structure (London, England : 1993)* **1996**, 4, 853-860.
35. Sluis-Cremer, N. The emerging profile of cross-resistance among the nonnucleoside HIV-1 reverse transcriptase inhibitors. *Viruses* **2014**, 6, 2960-2973.
36. Loya, S.; Tal, R.; Kashman, Y.; Hizi, A. Illimaquinone, a selective inhibitor of the RNase H activity of human immunodeficiency virus type 1 reverse transcriptase. *Antimicrob Agents Chemother* **1990**, 34, 2009-2012.
37. Ilina, T.; Labarge, K.; Sarafianos, S. G.; Ishima, R.; Parniak, M. A. Inhibitors of HIV-1 Reverse Transcriptase-Associated Ribonuclease H Activity. *Biology* **2012**, 1, 521-541.
38. Fletcher, R. S.; Syed, K.; Mithani, S.; Dmitrienko, G. I.; Parniak, M. A. Carboxanilide derivative non-nucleoside inhibitors of HIV-1 reverse transcriptase interact with different mechanistic forms of the enzyme. *Biochemistry* **1995**, 34, 4346-4353.
39. Shaw-Reid, C. A.; Munshi, V.; Graham, P.; Wolfe, A.; Witmer, M.; Danzeisen, R.; Olsen, D. B.; Carroll, S. S.; Embrey, M.; Wai, J. S.; Miller, M. D.; Cole, J. L.; Hazuda, D. J. Inhibition of HIV-1 ribonuclease H by a novel diketo acid, 4-[5-(benzoylamino)thien-2-yl]-2,4-dioxobutanoic acid. *The Journal of biological chemistry* **2003**, 278, 2777-2780.
40. Tramontano, E.; Esposito, F.; Badas, R.; Di Santo, R.; Costi, R.; La Colla, P. 6-[1-(4-Fluorophenyl)methyl-1H-pyrrol-2-yl]-2,4-dioxo-5-hexenoic acid ethyl ester a novel diketo acid derivative which selectively inhibits the HIV-1 viral replication in cell culture and the ribonuclease H activity in vitro. *Antiviral Res* **2005**, 65, 117-124.
41. Hang, J. Q.; Rajendran, S.; Yang, Y.; Li, Y.; In, P. W.; Overton, H.; Parkes, K. E.; Cammack, N.; Martin, J. A.; Klumpp, K. Activity of the isolated HIV RNase H domain and specific inhibition by N-hydroxyimides. *Biochemical and biophysical research communications* **2004**, 317, 321-329.
42. Klumpp, K.; Hang, J. Q.; Rajendran, S.; Yang, Y.; Derosier, A.; Wong Kai In, P.; Overton, H.; Parkes, K. E.; Cammack, N.; Martin, J. A. Two-metal ion mechanism of RNA cleavage by HIV RNase H and mechanism-based design of selective HIV RNase H inhibitors. *Nucleic acids research* **2003**, 31, 6852-6859.
43. Billamboz, M.; Bailly, F.; Lion, C.; Touati, N.; Vezin, H.; Calmels, C.; Andreola, M. L.; Christ, F.; Debyser, Z.; Cotellet, P. Magnesium chelating 2-hydroxyisoquinoline-1,3(2H,4H)-diones, as inhibitors of HIV-1 integrase and/or the HIV-1 reverse transcriptase ribonuclease H domain: discovery of a novel selective inhibitor of the ribonuclease H function. *Journal of medicinal chemistry* **2011**, 54, 1812-1824.
44. Kirschberg, T. A.; Balakrishnan, M.; Squires, N. H.; Barnes, T.; Brendza, K. M.; Chen, X.; Eisenberg, E. J.; Jin, W.; Kutty, N.; Leavitt, S.; Licican, A.; Liu, Q.; Liu, X.; Mak, J.; Perry, J. K.; Wang, M.; Watkins, W. J.; Lansdon, E. B. RNase H active site inhibitors of human immunodeficiency virus type 1 reverse transcriptase: design, biochemical activity, and structural information. *Journal of medicinal chemistry* **2009**, 52, 5781-5784.
45. Williams, P. D.; Staas, D. D.; Venkatraman, S.; Loughran, H. M.; Ruzek, R. D.; Booth, T. M.; Lyle, T. A.; Wai, J. S.; Vacca, J. P.; Feuston, B. P.; Ecto, L. T.; Flynn, J. A.; DiStefano, D. J.; Hazuda, D. J.; Bahnck, C. M.; Himmelberger, A. L.; Dornadula, G.; Hrin, R. C.; Stillmock, K. A.; Witmer, M. V.; Miller, M. D.; Grobler, J. A. Potent and selective HIV-1 ribonuclease H inhibitors based on a 1-hydroxy-1,8-naphthyridin-2(1H)-one scaffold. *Bioorganic & medicinal chemistry letters* **2010**, 20, 6754-6757.
46. Fuji, H.; Urano, E.; Futahashi, Y.; Hamatake, M.; Tatsumi, J.; Hoshino, T.; Morikawa, Y.; Yamamoto, N.; Komano, J. Derivatives of 5-nitro-furan-2-carboxylic acid carbamoylmethyl ester inhibit RNase H activity associated with HIV-1 reverse transcriptase. *Journal of medicinal chemistry* **2009**, 52, 1380-1387.
47. Yanagita, H.; Urano, E.; Matsumoto, K.; Ichikawa, R.; Takaesu, Y.; Ogata, M.; Murakami, T.; Wu, H.; Chiba, J.; Komano, J.; Hoshino, T. Structural and biochemical study on the inhibitory activity of derivatives of 5-nitro-furan-2-carboxylic acid for RNase H function of HIV-1 reverse transcriptase. *Bioorganic & medicinal chemistry* **2011**, 19, 816-825.

48. Archer, R. H.; Dykes, C.; Gerondelis, P.; Lloyd, A.; Fay, P.; Reichman, R. C.; Bambara, R. A.; Demeter, L. M. Mutants of human immunodeficiency virus type 1 (HIV-1) reverse transcriptase resistant to nonnucleoside reverse transcriptase inhibitors demonstrate altered rates of RNase H cleavage that correlate with HIV-1 replication fitness in cell culture. *Journal of virology* **2000**, *74*, 8390-8401.
49. Archer, R. H.; Wisniewski, M.; Bambara, R. A.; Demeter, L. M. The Y181C mutant of HIV-1 reverse transcriptase resistant to nonnucleoside reverse transcriptase inhibitors alters the size distribution of RNase H cleavages. *Biochemistry* **2001**, *40*, 4087-4095.
50. Hang, J. Q.; Li, Y.; Yang, Y.; Cammack, N.; Mirzadegan, T.; Klumpp, K. Substrate-dependent inhibition or stimulation of HIV RNase H activity by non-nucleoside reverse transcriptase inhibitors (NNRTIs). *Biochemical and biophysical research communications* **2007**, *352*, 341-350.
51. Himmel, D. M.; Sarafianos, S. G.; Dharmasena, S.; Hossain, M. M.; McCoy-Simandle, K.; Iliina, T.; Clark, A. D., Jr.; Knight, J. L.; Julias, J. G.; Clark, P. K.; Krogh-Jespersen, K.; Levy, R. M.; Hughes, S. H.; Parniak, M. A.; Arnold, E. HIV-1 reverse transcriptase structure with RNase H inhibitor dihydroxy benzoyl naphthyl hydrazone bound at a novel site. *ACS chemical biology* **2006**, *1*, 702-712.
52. Gong, Q.; Menon, L.; Iliina, T.; Miller, L. G.; Ahn, J.; Parniak, M. A.; Ishima, R. Interaction of HIV-1 reverse transcriptase ribonuclease H with an acylhydrazone inhibitor. *Chemical biology & drug design* **2011**, *77*, 39-47.
53. Wendeler, M.; Lee, H. F.; Bermingham, A.; Miller, J. T.; Chertov, O.; Bona, M. K.; Baichoo, N. S.; Ehteshami, M.; Beutler, J.; O'Keefe, B. R.; Gotte, M.; Kvaratskhelia, M.; Le Grice, S. Vinylogous ureas as a novel class of inhibitors of reverse transcriptase-associated ribonuclease H activity. *ACS chemical biology* **2008**, *3*, 635-644.
54. Masaoka, T.; Chung, S.; Caboni, P.; Rausch, J. W.; Wilson, J. A.; Taskent-Sezgin, H.; Beutler, J. A.; Tocco, G.; Le Grice, S. F. Exploiting drug-resistant enzymes as tools to identify thienopyrimidinone inhibitors of human immunodeficiency virus reverse transcriptase-associated ribonuclease H. *Journal of medicinal chemistry* **2013**, *56*, 5436-5445.
55. Di Grandi, M.; Olson, M.; Prashad, A. S.; Bebernitz, G.; Luckay, A.; Mullen, S.; Hu, Y.; Krishnamurthy, G.; Pitts, K.; O'Connell, J. Small molecule inhibitors of HIV RT Ribonuclease H. *Bioorganic & medicinal chemistry letters* **2010**, *20*, 398-402.
56. Kirschberg, T. A.; Balakrishnan, M.; Huang, W.; Hluhanich, R.; Kutty, N.; Liclican, A. C.; McColl, D. J.; Squires, N. H.; Lansdon, E. B. Triazole derivatives as non-nucleoside inhibitors of HIV-1 reverse transcriptase--structure-activity relationships and crystallographic analysis. *Bioorganic & medicinal chemistry letters* **2008**, *18*, 1131-1134.
57. Cichero, E.; Buffa, L.; Fossa, P. 3,4,5-Trisubstituted-1,2,4-4H-triazoles as WT and Y188L mutant HIV-1 non-nucleoside reverse transcriptase inhibitors: docking-based CoMFA and CoMSIA analyses. *Journal of molecular modeling* **2011**, *17*, 1537-1550.
58. Budihas, S. R.; Gorshkova, I.; Gaidamakov, S.; Wamiru, A.; Bona, M. K.; Parniak, M. A.; Crouch, R. J.; McMahan, J. B.; Beutler, J. A.; Le Grice, S. F. Selective inhibition of HIV-1 reverse transcriptase-associated ribonuclease H activity by hydroxylated tropolones. *Nucleic acids research* **2005**, *33*, 1249-1256.
59. Dat, N. T.; Bae, K.; Wamiru, A.; McMahan, J. B.; Le Grice, S. F.; Bona, M.; Beutler, J. A.; Kim, Y. H. A dimeric lactone from *Ardisia japonica* with inhibitory activity for HIV-1 and HIV-2 ribonuclease H. *J Nat Prod* **2007**, *70*, 839-841.
60. Takada, K.; Bermingham, A.; O'Keefe, B. R.; Wamiru, A.; Beutler, J. A.; Le Grice, S. F.; Lloyd, J.; Gustafson, K. R.; McMahan, J. B. An HIV RNase H inhibitory 1,3,4,5-tetragalloylapiitol from the African plant *Hydodendron gabunensis*. *J Nat Prod* **2007**, *70*, 1647-1649.
61. Bokesch, H. R.; Wamiru, A.; Le Grice, S. F.; Beutler, J. A.; McKee, T. C.; McMahan, J. B. HIV-1 ribonuclease H inhibitory phenolic glycosides from *Eugenia hyemalis*. *J Nat Prod* **2008**, *71*, 1634-1636.
62. Kim, J. A.; Yang, S. Y.; Wamiru, A.; McMahan, J. B.; Le Grice, S. F.; Beutler, J. A.; Kim, Y. H. New monoterpene glycosides and phenolic compounds from *Distylium racemosum* and their inhibitory activity against ribonuclease H. *Bioorganic & medicinal chemistry letters* **2011**, *21*, 2840-2844.
63. Esposito, F.; Corona, A.; Zinzula, L.; Kharlamova, T.; Tramontano, E. New anthraquinone derivatives as inhibitors of the HIV-1 reverse transcriptase-associated ribonuclease H function. *Chemotherapy* **2012**, *58*, 299-307.
64. Sonar, V. P.; Corona, A.; Distinto, S.; Maccioni, E.; Meleddu, R.; Fois, B.; Floris, C.; Malpure, N. V.; Alcaro, S.; Tramontano, E.; Cottiglia, F. Natural product-inspired esters and amides of ferulic and caffeic acid as dual inhibitors of HIV-1 reverse transcriptase. *European journal of medicinal chemistry* **2017**, *130*, 248-260.
65. Akihisa, T.; Ogihara, J.; Kato, J.; Yasukawa, K.; Ukiya, M.; Yamanouchi, S.; Oishi, K. Inhibitory effects of triterpenoids and sterols on human immunodeficiency virus-1 reverse transcriptase. *Lipids* **2001**, *36*, 507-512.
66. Zhang, J.; Liu, X.; De Clercq, E. Capsid (CA) protein as a novel drug target: recent progress in the research of HIV-1 CA inhibitors. *Mini reviews in medicinal chemistry* **2009**, *9*, 510-518.
67. Currens, M. J.; Mariner, J. M.; McMahan, J. B.; Boyd, M. R. Kinetic analysis of inhibition of human immunodeficiency virus type-1 reverse transcriptase by calanolide A. *The Journal of pharmacology and experimental therapeutics* **1996**, *279*, 652-661.
68. Yoel Kashman Kirk R. Gustafson, R. W. F., John H. Cardellina, James B. McMahan, Michael J. Currens, Robert W. Buckheit, Jr. Stephen H. Hughes, Gordon M. Cragg, and Michael R. Boyd. The Calanolides, a Novel HIV-Inhibitory

- Class of Coumarin Derivatives from the Tropical Rainforest Tree, *Calophyllum lanigerum*. *Journal of medicinal chemistry* **1992**, 35, 2735-2743.
69. Singh, I. P.; Bodiwala, H. S. Recent advances in anti-HIV natural products. *Natural product reports* **2010**, 27, 1781-800.
 70. Li, F.; Goila-Gaur, R.; Salzwedel, K.; Kilgore, N. R.; Reddick, M.; Matallana, C.; Castillo, A.; Zoumplis, D.; Martin, D. E.; Orenstein, J. M.; Allaway, G. P.; Freed, E. O.; Wild, C. T. PA-457: a potent HIV inhibitor that disrupts core condensation by targeting a late step in Gag processing. *Proceedings of the National Academy of Sciences of the United States of America* **2003**, 100, 13555-13560.
 71. Yu, D.; Morris-Natschke, S. L.; Lee, K. H. New developments in natural products-based anti-AIDS research. *Medicinal research reviews* **2007**, 27, 108-132.
 72. Kuo, R. Y.; Qian, K.; Morris-Natschke, S. L.; Lee, K. H. Plant-derived triterpenoids and analogues as antitumor and anti-HIV agents. *Natural product reports* **2009**, 26, 1321-1344.
 73. Martin, D. E.; Blum, R.; Wilton, J.; Doto, J.; Galbraith, H.; Burgess, G. L.; Smith, P. C.; Ballow, C. Safety and pharmacokinetics of Bevirimat (PA-457), a novel inhibitor of human immunodeficiency virus maturation, in healthy volunteers. *Antimicrob Agents Chemother* **2007**, 51, 3063-3066.
 74. Smith, P. F.; Ogundele, A.; Forrest, A.; Wilton, J.; Salzwedel, K.; Doto, J.; Allaway, G. P.; Martin, D. E. Phase I and II study of the safety, virologic effect, and pharmacokinetics/pharmacodynamics of single-dose 3-o-(3',3'-dimethylsuccinyl)betulinic acid (bevirimat) against human immunodeficiency virus infection. *Antimicrob Agents Chemother* **2007**, 51, 3574-3581.
 75. Martin, D. E.; Salzwedel, K.; Allaway, G. P. Bevirimat: a novel maturation inhibitor for the treatment of HIV-1 infection. *Antivir Chem Chemother* **2008**, 19, 107-113.
 76. Xie, L.; Takeuchi, Y.; Cosentino, L. M.; Lee, K. H. Anti-AIDS agents. 37. Synthesis and structure-activity relationships of (3'R,4'R)-(+)-cis-khellactone derivatives as novel potent anti-HIV agents. *Journal of medicinal chemistry* **1999**, 42, 2662-2672.
 77. Xie, L.; Takeuchi, Y.; Cosentino, L. M.; Lee, K. H. Anti-AIDS agents. 33. Synthesis and anti-HIV activity of mono-methyl substituted 3',4'-di-O(-)-camphanoyl-(+)-cis-khellactone (DCK) analogues. *Bioorganic & medicinal chemistry letters* **1998**, 8, 2151-2156.
 78. Michael R. Boyd, K. R. G., James B. McMahon, Robert H. Shoemaker, Barry R. O'keefe, Toshiyuki Mori, Robert J. Gulakowski, Lin Wu, Maria I. Rivera, Carolyn M. Laurecot, Michael J. Currens, John H. Cardellina II, Robert W. Buckheit, Jr., Peter L. Nara, Lewis K. Pannell, Raymond C. Sowder II, And Louis E. Henderson. Discovery of Cyanovirin-N, a Novel Human Immunodeficiency Virus-Inactivating Protein That Binds Viral Surface Envelope Glycoprotein gp120: Potential Applications to Microbicide Development. *Antimicrobial agents and chemotherapy* **1991**, 41, 1521-1530.
 79. Anders J. Bolmstedt, B. R. O. k., Shilpa R. Shenoy, James B. McMahon, And Michael R. Boyd. Cyanovirin-N Defines a New Class of Antiviral Agent Targeting N-Linked, High-Mannose Glycans in an Oligosaccharide- Specific Manner. *MOLECULAR PHARMACOLOGY* **2001**, 59, 949-954.
 80. Zappe, H.; Snell, M. E.; Bossard, M. J. PEGylation of cyanovirin-N, an entry inhibitor of HIV. *Advanced drug delivery reviews* **2008**, 60, 79-87.
 81. Fernandez Puntero, B.; Iglesias Peinado, I.; Villar del Fresno, A. M. Anti-inflammatory and antiulcer activity of *Teucrium buxifolium*. *Journal of ethnopharmacology* **1997**, 55, 93-98.
 82. Jeffrey B. Harborne, F. A. T.-B., Christine A. Williams And Maria I. Gil. A Chemotaxonomic Study Of Flavonoids From European *Teucrium* Species. *Phytochemistry* **1986**, 25, 2811-2816.
 83. Savona, G. P., M. P.; Piozzi, F.; Hanson, J. R.; Hitchcock, P. B.; Thomas, S. A.; Teuflidin, A Norclerodane Diterpenoid from *Teucrium flavum*. *J. Chem.Soc.Perkin Trans* **1978**, 1, 1080-1083.
 84. Savona, G. P., F.; Servettaz, O.; Rodriguez, B.; Fernandez-Gadeat, F. F.; Lomas, M. M.; A Neo-Clerodane Glucoside And Neo-Clerodane Diterpenoids From *Teucrium flavum* Subsp. *Glaucum*. *Phytochemistry* **1984**, 23, 843-848.
 85. Bruno, M.; Rosselli, S.; Maggio, A.; Piozzi, F.; Scaglioni, L.; Arnold, N. A.; Simmonds, M. S. Neoclerodanes from *Teucrium orientale*. *Chemical & pharmaceutical bulletin* **2004**, 52, 1497-500.
 86. Piozzi, F.; Bruno, M.; Ciriminna, R.; Fazio, C.; Vassallo, N.; Arnold, N. A.; de la Torre, M. C.; Rodriguez, B. Putative hepatotoxic neoclerodane diterpenoids from *Teucrium* species. *Planta medica* **1997**, 63, 483-484.
 87. Maccioni, S.; Baldini, R.; Tebano, M.; Cioni, P. L.; Flamini, G. Essential oil of *Teucrium scorodonia* L. ssp. *scorodonia* from Italy. *Food Chemistry* **2007**, 104, 1393-1395.
 88. Presti, M. L.; Crupi, M. L.; Costa, R.; Dugo, G.; Mondello, L.; Ragusa, S.; Santi, L. Seasonal Variations of *Teucrium flavum* L. Essential Oil. *Journal of Essential Oil Research* **2010**, 22, 211-216.
 89. Jeanmonod D., G. J. *Flora Corsica* 2007.
 90. Djabou, N.; Battesti, M. J.; Allali, H.; Desjobert, J. M.; Varesi, L.; Costa, J.; Muselli, A. Chemical and genetic differentiation of Corsican subspecies of *Teucrium flavum* L. *Phytochemistry* **2011**, 72, 1390-1399.
 91. Savona, G. P., M. P.; Piozzi, F.; Hanson, J.R.; Hitchcock, P. B.; Thomas, S. A.; The Structure of Teuflin, a Diterpenoid from *Teucrium flavum*; X-Ray Crystallographic and Spectroscopic Determination. *Journal of the Chemical Society, Perkin Transactions 1* **1979**, 1915-1917.

92. Sonar, V. P. Natural and Nature Inspired Compounds Targeting the Replication Cycle of RNA Viruses and GABAA Receptor. Università degli Studi di Cagliari 2017.
93. Ouyang, X.; Wei, L.; Pan, Y.; Huang, S.; Wang, H.; Begonia, G. B.; Ekunwe, S. I. N. Antioxidant properties and chemical constituents of ethanolic extract and its fractions of *Ocimum gratissimum*. *Medicinal Chemistry Research* **2012**, 22, 1124-1130.
94. Awad, B. M.; Habib, E. S.; Ibrahim, A. K.; Wanas, A. S.; Radwan, M. M.; Helal, M. A.; ElSohly, M. A.; Ahmed, S. A. Cytotoxic activity evaluation and molecular docking study of phenolic derivatives from *Achillea fragrantissima* (Forssk.) growing in Egypt. *Medicinal Chemistry Research* **2017**, 26, 2065-2073.
95. Venditti, A.; Frezza, C.; Sciubba, F.; Serafini, M.; Bianco, A.; Cianfaglione, K.; Lupidi, G.; Quassinti, L.; Bramucci, M.; Maggi, F. Volatile components, polar constituents and biological activity of tansy daisy (*Tanacetum macrophyllum* (Waldst. et Kit.) Schultz Bip.). *Industrial Crops and Products* **2018**, 118, 225-235.
96. Beard, J. W. Avian virus growths and their etiologic agents. *Advances in cancer research* **1963**, 7, 1-127.
97. Tewtrakul, S., Miyashiro, H.; Hatrori, M.; Yoshinaga, T.; Fujiwara, T.; Tomimori, T.; Kizu, H.; Miyaichi, Y.;. Inhibitory effects of flavonoids on human immunodeficiency virus type-1 integrase. *Wakan Iyaku-gaku Zasshi* **2001**, 18, 229-238.
98. Mohamadi, F.; Richards, N. G.; Guida, W. C.; Liskamp, R.; Lipton, M.; Caufield, C.; Chang, G.; Hendrickson, T.; Still, W. C. MacroModel—an integrated software system for modeling organic and bioorganic molecules using molecular mechanics. *Journal of Computational Chemistry* **1990**, 11, 440-467.
99. Halgren, T. A. Merck molecular force field. II. MMFF94 van der Waals and electrostatic parameters for intermolecular interactions. *Journal of Computational Chemistry* **1996**, 17, 520-552.
100. Kollman, P. A.; Massova, I.; Reyes, C.; Kuhn, B.; Huo, S.; Chong, L.; Lee, M.; Lee, T.; Duan, Y.; Wang, W.; Donini, O.; Cieplak, P.; Srinivasan, J.; Case, D. A.; Cheatham, T. E. Calculating structures and free energies of complex molecules: combining molecular mechanics and continuum models. *Accounts of Chemical Research* **2000**, 33, 889-897.
101. Berman, H. M.; Westbrook, J.; Feng, Z.; Gilliland, G.; Bhat, T. N.; Weissig, H.; Shindyalov, I. N.; Bourne, P. E. The Protein Data Bank. *Nucleic Acids Research* **2000**, 28, 235-242.
102. Ren, J. S.; Esnouf, R.; Garman, E.; Somers, D.; Ross, C.; Kirby, I.; Keeling, J.; Darby, G.; Jones, Y.; Stuart, D.; Stammers, D. High-resolution structures of HIV-1 rt from 4 RT-inhibitor complexes. *Nature Structural Biology* **1995**, 2, 293-302.
103. Schrödinger LLC. *QMPolarized protocol*, 2012; New York, NY, USA.

2. Human Rhinovirus

Human Rhinoviruses (HRVs) are the most common viral infectious agents. These are members of the family *Picornaviridae* and the genus *Enterovirus*. HRVs are first discovered in 1950s and they are classified in three species (RV-A, -B, and -C) according to phylogenetic sequence criteria and distinct genomic features.¹ Clinical isolates of RV-A and RV-B were in 1987,² while the third species (RV-C) was identified by the International Committee on Taxonomy of Viruses in 2009.³

There are multiple HRVs in each species designated as “serotypes” or “strains”. Hundred different types of strains were collected from sample of patients called prototype or reference set. Partial sequencing of viral capsid-encoding regions, non-coding regions, and a limited number of complete genomes led to a division of the original ninety-nine strains into two species: HRV-A (containing 74 serotypes) and HRV-B (containing 25 serotypes).⁴ To explain how antiviral compounds that belong to HRV-A and B draw a distinction between these two groups of viruses, it is assumed that the hydrophobic pocket of capsid viral protein 1 (VP1), which is the binding site for the capsid inhibitors, is dimorphic in shape and/or composition. As matter of fact, it has been demonstrated that the higher activity of short-chained capsid inhibitors compounds was against group B (serotypes 1A, 2 e 16), while members of group A (es, HRV-3 and -14) were more sensitive to longer chain antiviral compounds; therefore, Andries et al⁵ suggested that group A has longer and narrower hydrophobic pocket than group B.

HRV-C strains have a genomic organisation similar to that of HRV-A and HRV-B; however, there are several distinct characteristics supporting their classification as a new species.

HRVs are the main responsible of the upper respiratory infections such as the common cold. It is known that colds are responsible for millions of work hours lost by sniffing patients, but the public perception is that HRV infections are generally benign. Therefore, the consequences of HRV infections are often overlooked.⁶

2.1 Structure of HRV

HRVs are positive-sense, single-stranded-RNA (ssRNA) viruses of approximately 7.200 bp. The genome is composed of a single gene, the translated protein of which is cleaved by virally encoded proteases to yield 11 proteins. The viral capsid contains four proteins. VP1, VP2, VP3, and VP4, that hold the RNA genome, while the non-structural proteins are involved in viral genome replication and assembly. Three larger proteins (VP1–3, ~30 kDa each) are located on the external surface of the virus, account for the virus antigenic diversity, while smaller protein VP4 (~7 kDa) lines the inner surface, interfacing with VP1–3 and RNA, anchors the RNA core to the capsid. There are 60 copies

each of the four capsid proteins, giving the virion an icosahedral structure, with a canyon in VP1 that is used as a site of attachment to cell surface receptors.

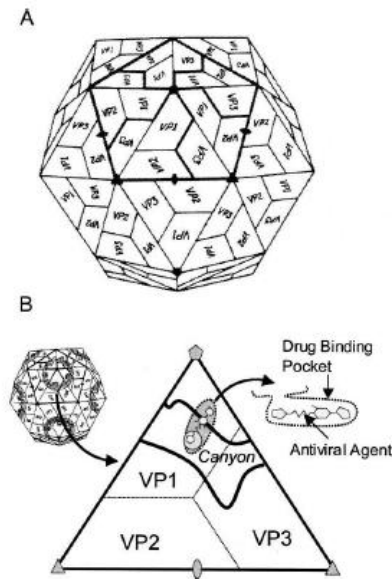


Figure 1. A schematic view of HRV14 icosahedral capsid (A) and partial capsid surface bound with an antiviral drug (B).

2.1.1 Replication

HRVs are generally temperature-restricted in replication, with optimal growth at 33–35 °C, and the temperature observed in the tracheobronchial tree is often lower than body core temperatures and so are permissive for HRV replication.⁷

Virus uptake occurs via clathrin-dependent or -independent endocytosis, or via macropinocytosis. The virions undergo conformational changes that yield hydrophobic subviral particles. This process is initiated by ICAM-1 and/or the low-pH environment in endosomes. It is thought that the RNA genome crosses the endosome membrane into the cytosol through a pore formed by viral proteins or after membrane rupture. After the entry of RNA genome inside the cytosol, the host cell ribosome translates the positive-sense, single-stranded RNA into structural (capsid) and nonstructural proteins. The virion is then assembled and packaged prior to cellular export via cell lysis (Figure 2).⁸

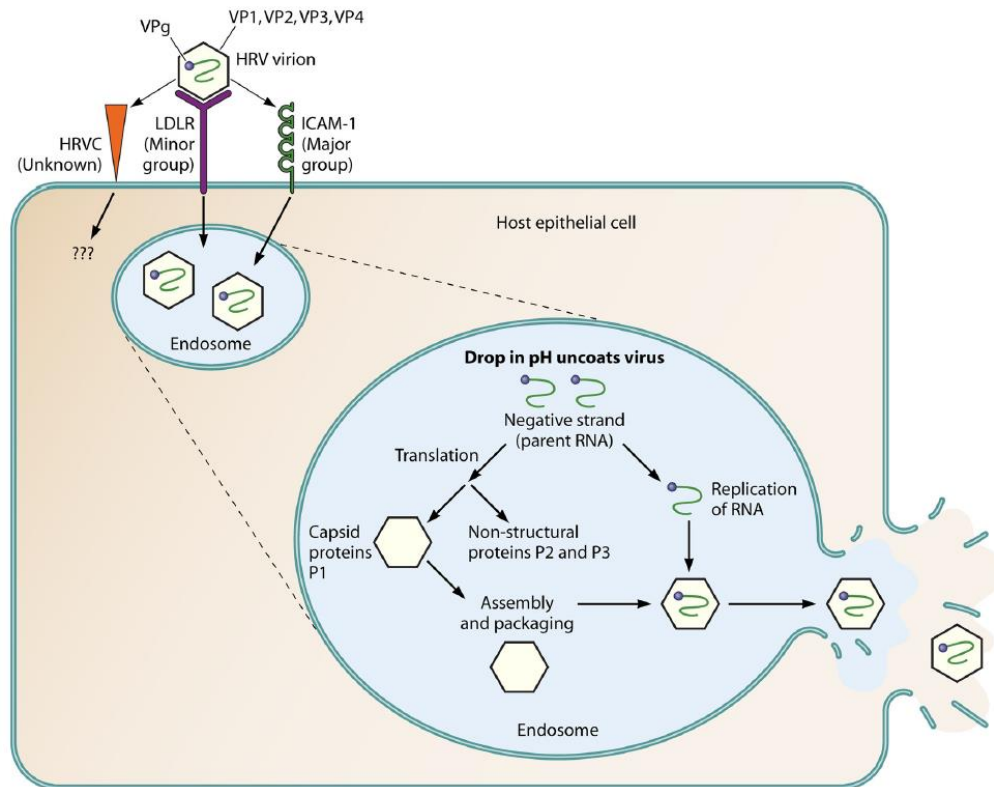


Figure 2. Viral replication in airway epithelial cells

2.2 Rhinovirus cellular receptors

RV-A and RV-B serotypes are also classified into two groups, major and minor. The “major group” utilises, a single receptor, the cell surface receptor intercellular adhesion molecule 1 (ICAM-1); the other one attaches to and enters cells via the low-density lipoprotein receptor (LDLR),⁹ whereas RV-C receptor remained unknown until recently¹⁰ Bochkov *et coll.*¹ have discovered cadherin-related family member 3 (CDHR3), a transmembrane protein with yet unknown biological function that mediates virus binding and replication.

Cell entry and uncoating are initiated when HRVs recognize their respective receptors. By the cryo-EM reconstructions of HRV-ICAM-1 it is observed that: ICAM-1 binds primarily to the floor and south wall of the canyon then, there is a conformational change in the virus surface, visible on the right-hand side of the diagram.

It is reported that the walls and the floor of the canyon probably bind to domain D1 and open the channel. This requires an empty hydrophobic pocket and flexibility of VP1, which is a largest part of the north and south walls of the canyon. The opening of the pentamer vertex, induced by the binding of ICAM-1 molecules, may facilitate externalization of VP4 and other internal viral components, including RNA.

Virus attachment on the receptor is distal from the plasma membrane. This property may be relevant for infection of cells by viruses and may reflect the enhanced ability of the N-terminal Ig domain to penetrate into the HRV canyon.¹¹

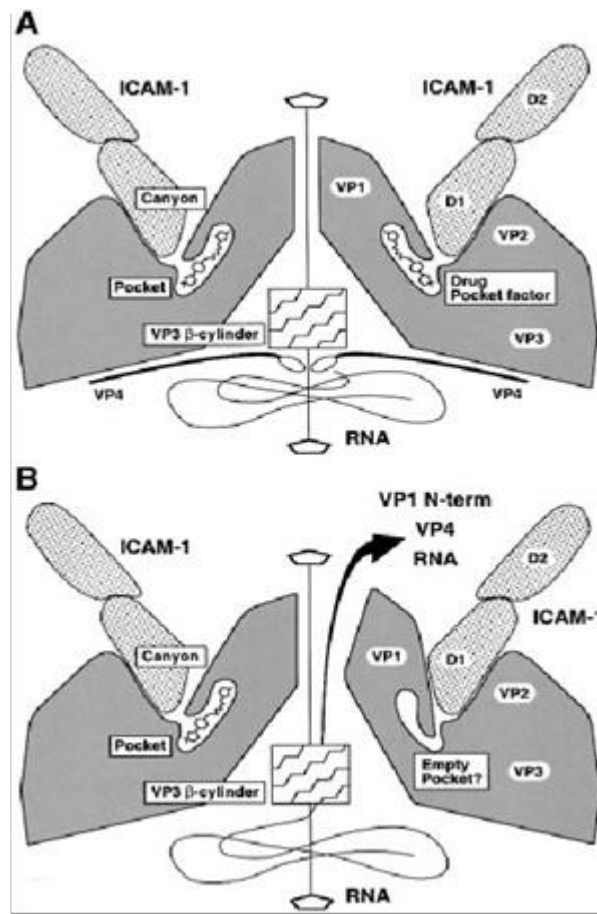


Figure 3. Schematic representation of a proposed two-step binding mechanism between ICAM-1 and major-group HRVs

The low-density lipoprotein receptor (LDLR) is a cell-surface glycoprotein. This family comprises at least three members that can bind and internalize RV including the LDLR, the very low-density lipoprotein receptor (VLDLR), and the LDLR related protein (LRP). These receptors can be recognized by the presence of ligand-binding repeats, epidermal growth factor precursor repeats, YMTD spacer domains (β -propeller modules), a single transmembrane domain and a relatively short cytoplasmic tail. This one contains motifs for interaction with a number of cytoplasmic adaptor and scaffold proteins and mediates signal transduction.^{12,13}

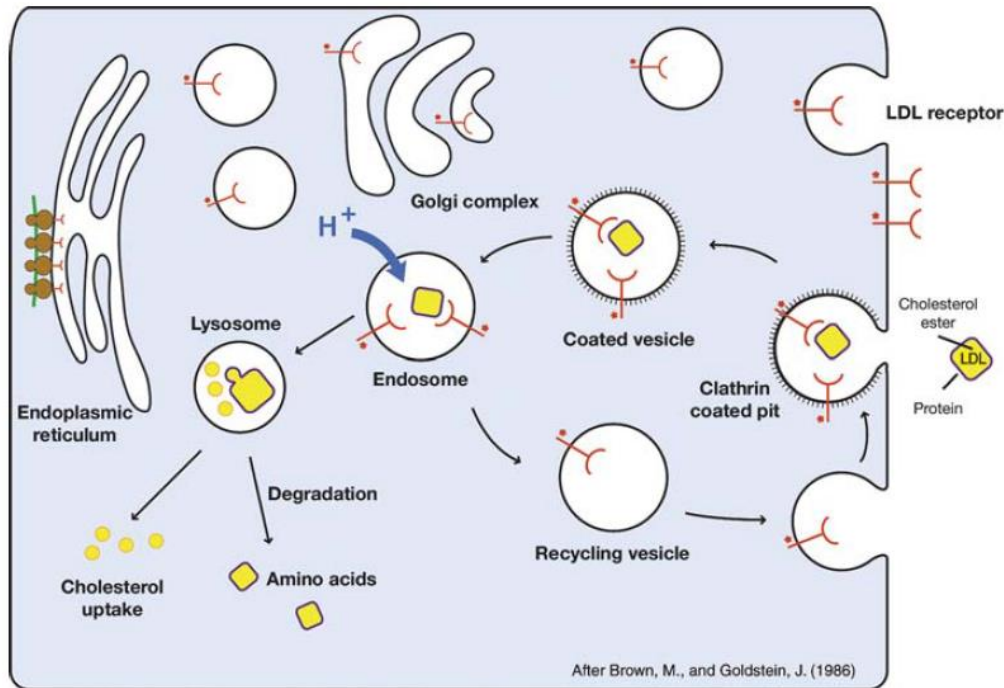


Figure 4. Schematic illustrating the uptake of lipoprotein particles by the LDLR

The entry of a receptor-ligand complex into cells occurs at clathrin-coated pits. The complex is subsequently delivered to the low-pH environment of the endosome, where dissociation of the complex takes place. The receptor is then returned to the cell surface in a process called receptor recycling.¹³ The most important physiologic ligand for the receptor is LDL, which contains a single copy of apolipoprotein B-100 and carries approximately 65% to 70% of plasma cholesterol in humans.^{14,15}

2.3 Clinical syndromes of RV infection

Acute respiratory infections represent a major cause of human disease and the second most important cause of death among children under five years of age.^{16,17}

HRVs are the most frequent cause of respiratory illness including common cold, bronchitis and pneumonia and provoke exacerbations of asthma, cystic fibrosis, and chronic obstructive pulmonary disease (COPD)^{7, 18-20}. Studies on COPD have revealed that higher values of CRP and respiratory viruses, especially rhinovirus (57%), are more frequently detected in exacerbations in hospitalized patients.²⁰ HRVs are typically found in the majority of young children and adults with acute symptoms of asthma^{18,21};

The relationship between HRV infections and asthma reveals that infants who develop virus-induced wheezing episodes are at high risk for asthma, but most acute wheezing illnesses in infancy resolve with no long-term sequelae. Once asthma has been established, HRV infections are the most common cause of acute exacerbations, especially in children. This is plausible because the lungs and the immune system are growing and developing during infancy and might be especially vulnerable during this period of time.²²

As well in adults, there is a correlation with exacerbation of asthma, in fact it is seasonal and in temperate climates there are strong peaks in morbidity in September, shortly after children return to school. It is interesting to notice individuals with asthma do not necessarily have more colds, and neither the severity nor the duration of upper respiratory symptoms is enhanced during experimental HRV infections in adults with asthma. It means the viral infections are specific to the lower airway.²³ Moreover, there is evidence that viral infections exert synergistic effects together with other events to provoke asthma symptoms. For instance, the effects of colds on asthma exacerbations are greatest in allergic individuals²⁴ and are amplified by exposition to allergens²⁵ and air pollutants.²⁶ There is now evidence that the immune response to respiratory viral infections contributes to airway obstruction and respiratory symptoms. The mechanisms are associated with the activation of inflammatory cascade with proinflammatory cytokines and mediators that enhance airway hyper responsiveness and airway obstruction.²¹

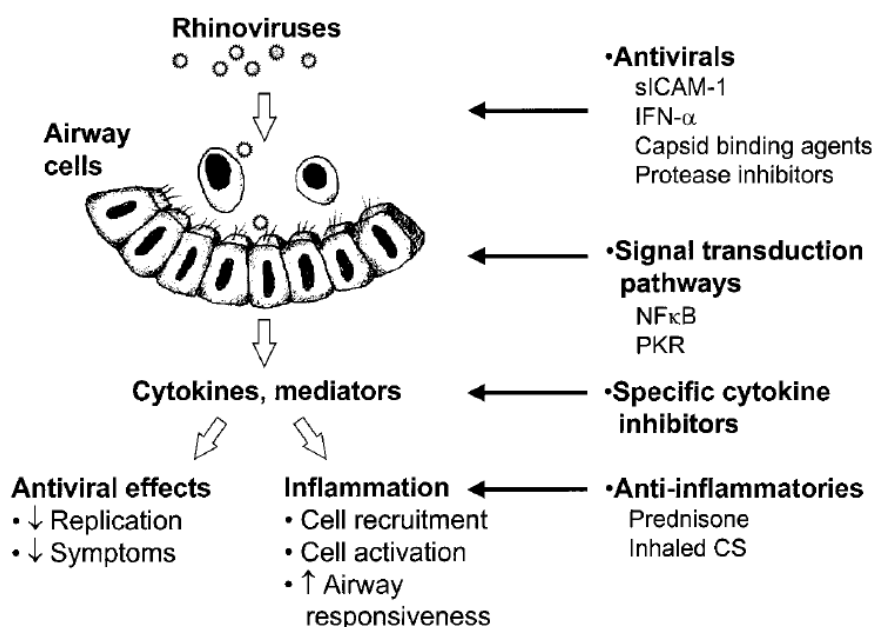


Figure 5. Mechanisms of RV-induced exacerbations of asthma, and therapeutic implications.

2.4 Antiviral agents for treatment of HRV infection

Despite the huge medical and socio-economical relevance of common cold, there are still no approved drugs for the treatment of these infections. However, in recent years several molecules have been reported as promising therapeutic targets.

2.4.1 Capsid Inhibitors

The viral capsid was identified as the first potential target for inhibition of viral replication. During the infection, ICAM-1 binds into the canyon, inducing conformational changes that eventually lead to uncoating of the virus and release of the viral RNA. The capsid binders bind into the hydrophobic pocket, under the canyon floor.²⁷ This event induces conformational changes, thereby increasing the rigidity of the virion and decreasing the ability of the virion to interact with its receptor (Figure 6). For instance, WIN compounds are one of the earliest discovered classes of Enterovirus inhibitors that work in this way and some structural studies demonstrated that, after accidental discovery, these compounds underwent several modifications to improve their antiviral properties.

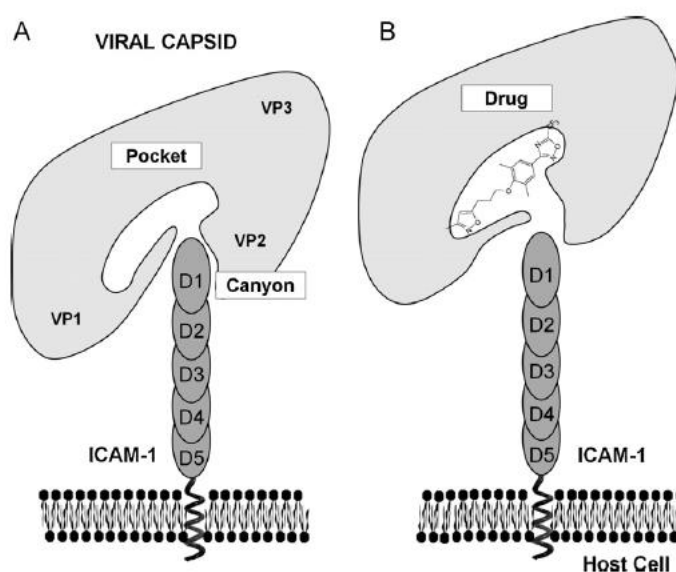


Figure 6. Mechanism of action of capsid binders

Pleconaril

WIN63843 (pleconaril) showed a high oral bioavailability ($\sim 70\%$)^{28,29} and a broad spectrum activity³⁰ against enteroviruses and rhinoviruses. Pleconaril is the first of a new generation capsid inhibitors that binds to hydrophobic sites within the cavities and it has a large volume of distribution with $>99\%$

plasma protein bound. It has good penetration into the central nervous system, and absorption is increased when taken with food, particularly fats.²⁹ The trifluoromethyl substituent on the oxadiazole ring increasing the half-life by reducing degradation in the liver by enzymes involved in oxidative processes.³¹ In previous studies pleconaril was tested for oral activity in animal models infected by coxsackievirus, members of the family *Picornaviridae* and the genus *Enterovirus* as HRVs. The treatment increased the survival rate for prophylactic and therapeutic dosing regimens and dramatically reduced virus levels in target tissues of animals. Therefore, it was considered a promising new drug candidate for potential use in the treatment of human enteroviral infections.³⁰ Pharmacokinetic studies of pleconaril have been taken in adults, children and neonates in 1999.^{28 29} It was demonstrated that the concentrations of pleconaril 12 h after a single oral dose remain 2.5 more than in vitro. In pre-clinical trials, no differences from placebo have been noted like cardiovascular and central nervous system side-effects.

In 2002, after the submission of pleconaril for the treatment of the common cold, the drug was rejected by the FDA mainly due to safety issues.³² Then it has been licensed to Schering-Plough in 2003 to be developed as nasal spray for the treatment of common cold symptoms exacerbations of asthma/COPD in high-risk patients. This study has been completed in 2007, but results of this study have not been revealed yet.³³

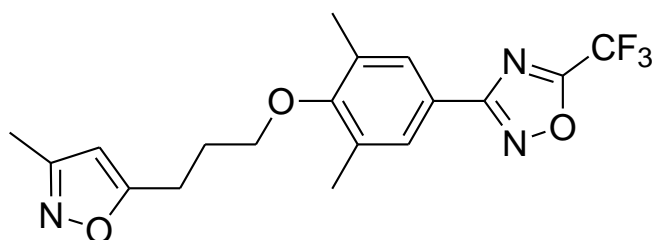


Figure 7. Structure of Pleconaril

Pirodavisir

Pirodavisir (R77975) has been known to have a good level of potency and a broad spectrum of antirhinoviral activity (HRV-A and B), to a lesser extent, that of other enteroviruses.

Previous studies found that pirodavisir:

- is able to inhibit the replication of 80 % of serotypes at concentrations of 1 mg/ml or less.³⁴
- frequent intranasal sprays of pirodavisir (six times daily) provided protection protective against rhinovirus illness, when administration was begun before viral exposure and continued afterward. Three times daily administration provided no protection, and the treatment begun

24 h after rhinovirus challenge. However, the small number of subjects enrolled in that study precluded an assessment of pirodavis's therapeutic use.³⁵

- intranasal sprays of pirodavis (2 mg for six times daily for 5 days) were associated with significant antiviral effects but no clinical benefit.³⁶
- Oral delivery of the ester-derivate pirodavis is not feasible given the fact that it is hydrolysed to an inactive acid and has an unpleasant taste and the more frequent presence of blood in the nasal mucus.³⁷

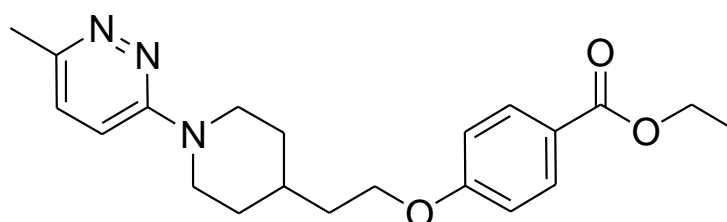


Figure 8. Structure of Pirodavis

Vapendavis

Vapendavis is a more recent capsid inhibitor that shows activity against HRV-A and HRV- B serotypes and some strains of EV.³⁸

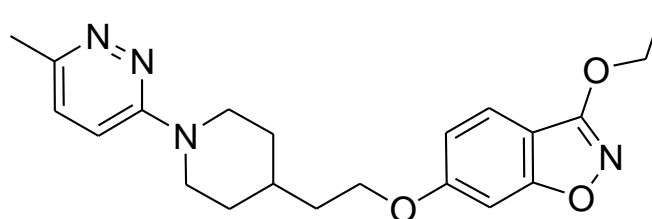


Figure 9. Structure of Vapendavis

2.4.2 3C protease inhibitors

3C protease plays an essential role in viral replication. In fact it is responsible for proteolytic cleavage of polyprotein into proteins that are structurally and enzymatically essential for viral life-cycle.³⁹ Enviroxime and Enveroxime-related compounds are the most promising anti-HRV molecules

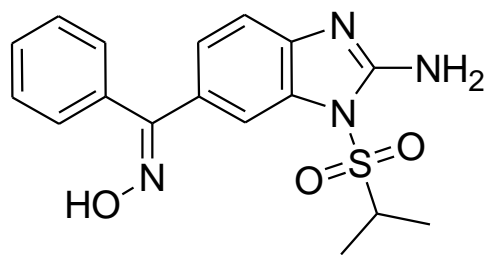


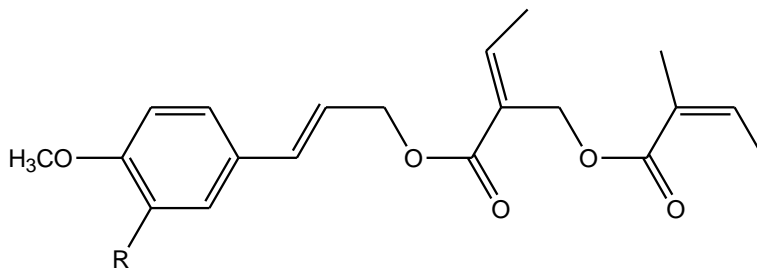
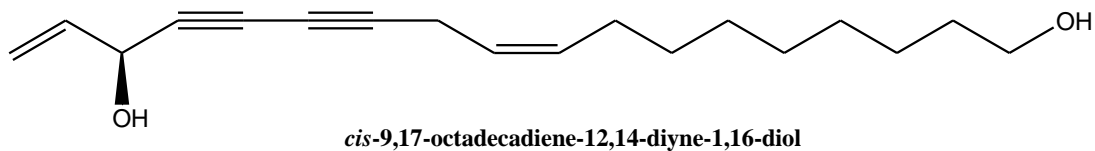
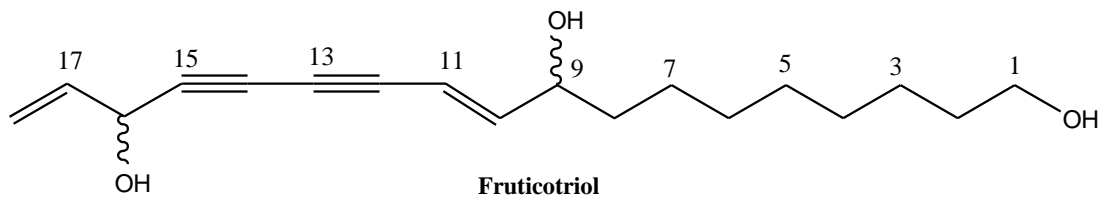
Figure 10. Structure of Enviroxime

2.5 Aim and Objectives

In our recent work,⁴⁰ the phytochemical investigation of the anti-HRV CH₂Cl₂ extract obtained from *Bupleurum fruticosum*, led to the isolation of a series of phenylpropenoids and polyacetylenes (Figure 11). Among all, (*E*)-3-(3,4-dimethoxyphenyl)-2-propen-1-yl(*Z*)-2-[(*Z*)-2-methyl-2-butenoyloxymethyl]butenoate (Figure 11), revealed the most advantageous selectivity index inhibiting HRV-A39 species. This compound showed an IC₅₀ value of $2.4 \pm 0.04 \mu\text{M}$ and a moderate cytotoxicity versus HeLa cells ($7.6 \pm 1.8 \mu\text{M}$).

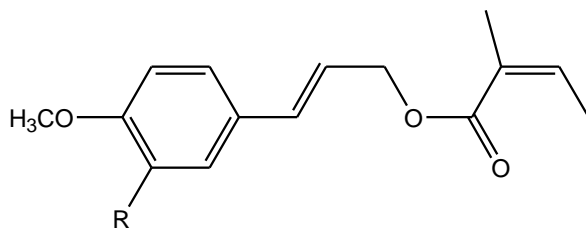
SAR studies allowed us to identify some basic structural requirements for the antiviral action. In particular, the substitution of a methoxy group at C-3 position of the phenyl ring of (*E*)-3-(3,4-dimethoxyphenyl)-2-propen-1-yl(*Z*)-2-[(*Z*)-2-methyl-2-butenoyloxymethyl]butenoate with a hydrogen, as in (*E*)-3-(4-methoxyphenyl)-2-propen-1-yl(*Z*)-2-[(*Z*)-2-methyl-2-butenoyloxymethyl]butenoate, annulled the activity (EC₅₀ >36.3 μM) and increased the cytotoxicity (Figure 11). The replacement at the same time of the angeloyl and 3-methoxy groups with a hydrogen atom, as in 4-*O*-methylcinnamyl angelic acid ester, led to a reduced activity (~10 fold). An ester functionality seems essential for the antiviral activity since 4-methoxycinnamyl alcohol and 3,4-dimethoxycinnamyl alcohol proved to be completely inactive. A 3,4-dimethoxyphenyl ring and an ester function were necessary but not sufficient since 4-*O*-methyl-(*E*)-coniferyl angelic acid ester, containing a shorter alkyl chain with respect to the most active compound, was not able to inhibit the replication of HRVs.

The anti-HRV mechanism of action of the most active phenylpropenoid was evaluated with the aim of the time-of-drug-addition assay, compared to pirodavir, a known capsid inhibitor (Table 1). This assay revealed that the antiviral behaviour of this natural compound is quite similar to that showed by pirodavir, and means that (*E*)-3-(3,4-dimethoxyphenyl)-2-propen-1-yl (*Z*)-2-[(*Z*)-2-methyl-2-butenoyloxymethyl]butenoate is an antiviral molecule which exerts its activity in the early phases of viral replication and behaves as a capsid binder towards HRV 39. In contrast with pirodavir, addition of the natural compound to the infected HeLa cells after 1h post binding still resulted in a strong reduction in virus yield (78%) and after 2-3 h post binding resulted less effective (65% and 50% reduction, respectively) but still significant. The remarkable inhibitory effect when added after virus binding (1-3 h) suggested the ability for the natural compound to enter the host cells and to act with a further mode of action probably based on the uncoating of viral genome or on inhibition of protein synthesis.



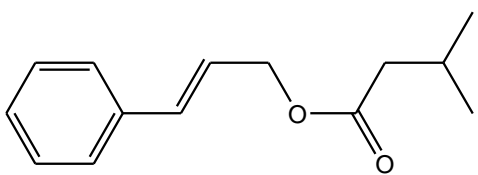
(*E*)-3-(4-methoxyphenyl)-2-propen-1-yl (Z)-2-[(Z)-2-methyl-2-butenoyloxymethyl]butenoate R = H

(*E*)-3-(3,4-dimethoxyphenyl)-2-propen-1-yl (Z)-2-[(Z)-2-methyl-2-butenoyloxymethyl]butenoate R = OCH₃

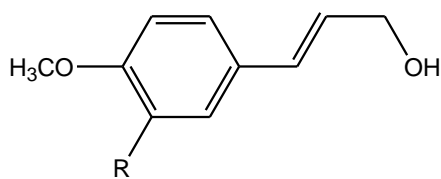


4-O-methylcinnamyl angelic acid ester R = H

4-O-methyl-(*E*)-coniferyl angelic acid ester R = OCH₃



cinnamyl isovalerate



4-methoxycinnamyl alcohol R = H

3,4-dimethoxycinnamyl alcohol R = OCH₃

Figure 11. Structures of the secondary metabolites isolated from *Bupleurum fruticosum*

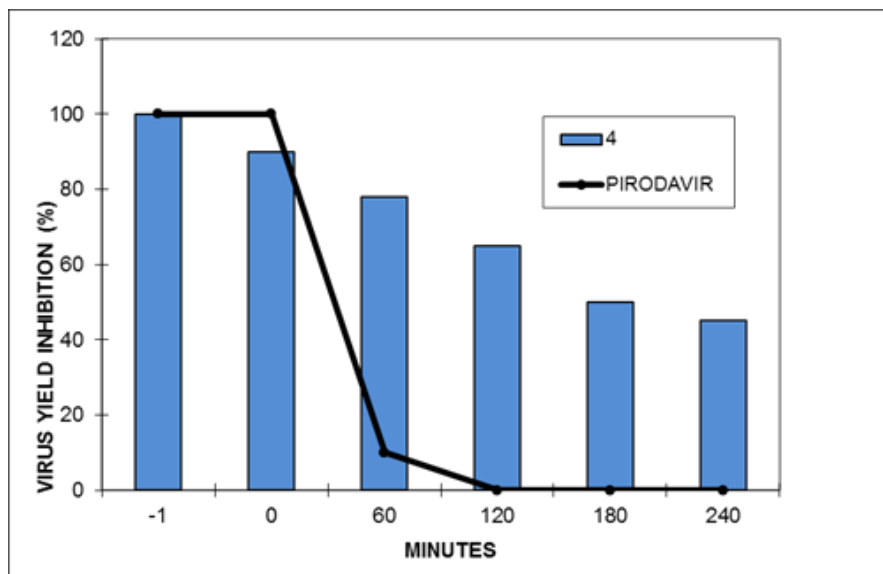


Table 1: Effect of addition of the phenylpropenoid and Pirodavir at different times during HRV growth cycle in HeLa cells. The phenylpropenoid and Pirodavir were used at a concentration of 5 $\mu\text{g/mL}$.

Subsequently, computational studies were carried out in order to identify the key residues involved in the interaction of VP1-HRV39 with the natural compound. The binding pocket of serotype 39 is characterized by the presence of highly hydrophobic residues. These studies indicate that the amino acids concerned in the bonds with the phenylpropenoid are: Tyr144, Leu100, Ile122, Tyr190, Leu184 and Val236. Moreover, complex of the phenylpropenoid was stabilized by hydrogen bonds with Thr100, with the oxygen of the methoxy group of the phenyl ring. It fit nicely the binding pocket and is able to occupy most of it, by establishing a large number of hydrophobic interactions with the aliphatic chain. The selectivity of the most active phenylpropenoid toward HRV39 could be explained by the different interactions of this compound with VP1. Indeed, in VP1-HRV14 the presence of Tyr128 with its steric hindrance does not allow a proper accommodation into the hydrophobic binding pocket. In VP1-HRV39, Tyr128 is replaced by an isoleucine, which is a key residue in protein–compound interactions.⁴⁰

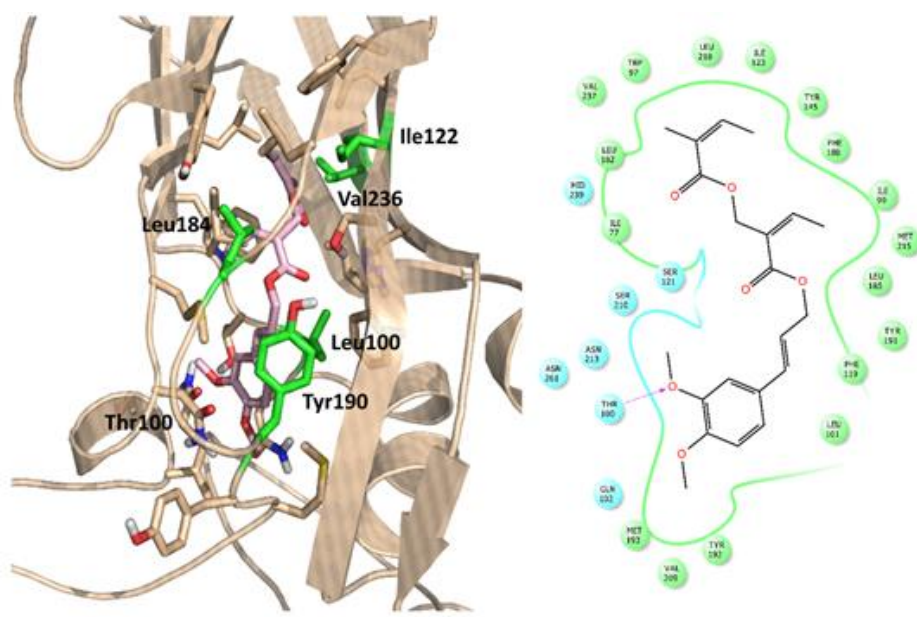


Figure 12. 3D and relative 2D representation of the phenylpropenoid and putative binding mode resulting from the docking experiments into the built model of VP1-HRV39. The key residues are highlighted in green in the 3D depiction.

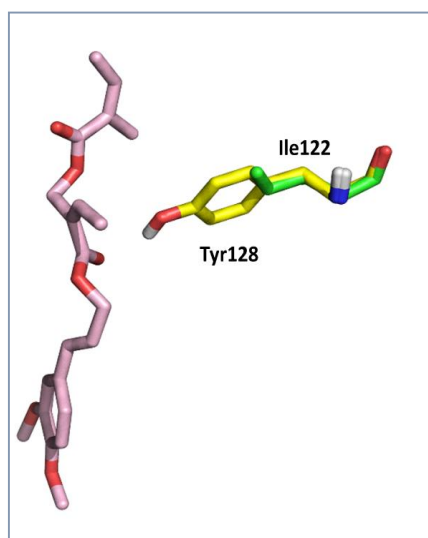


Figure 13. Docking of the phenylpropenoid inside VP1-HRV14 (pdb code 1NCQ) where Tyr128 of VP1-HRV14 and Ile122 of VP1-HRV39 are highlighted in yellow and green respectively.

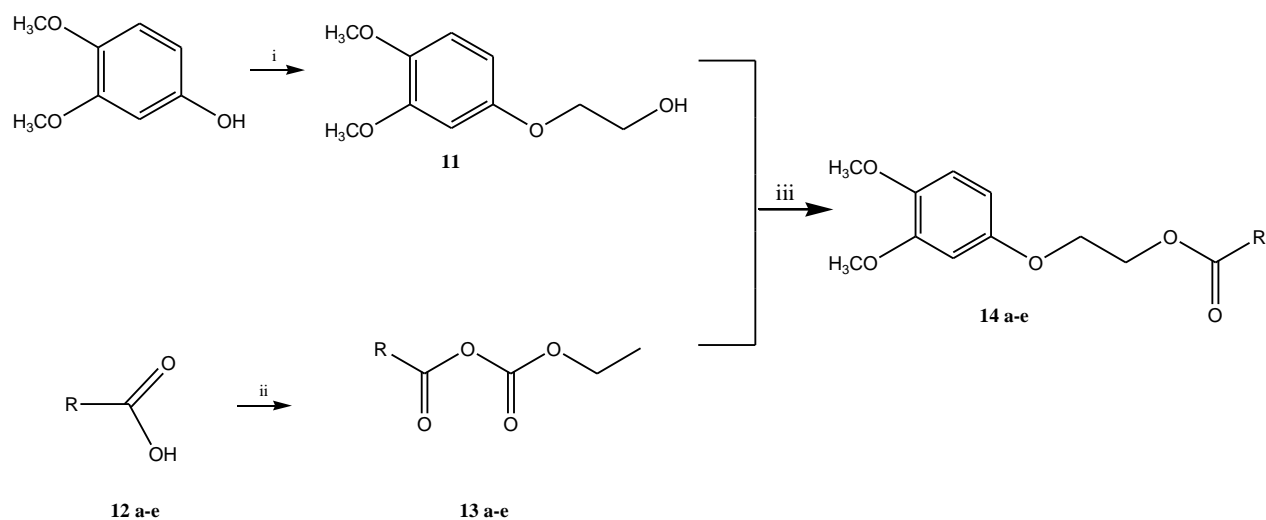
Tacking into account the SAR and docking studies of the natural phenylpropenoid, I decided to synthesize some analogues in order to improve the antiviral potency and/or the selectivity index (SI) of the natural compound.

2.5.1 Results And Discussion

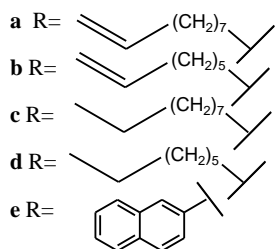
2.5.1.1 Synthesis of 2-(3,4-dimethoxyphenoxy)ethyl esters of aliphatic and aromatic acids (**14a-e**)

The first series of newly synthesized compounds were designed preserving the dimethoxyphenyl group, which proved to be essential for the activity, as reported for the phenylpropenoid and others capsid inhibitors.⁴⁰⁻⁴² The original aliphatic chain of the natural compound was simplified and, since all the most promising capsid-binding inhibitors possess a phenoxyalkyl chain, the propenic moiety linked to the benzene ring of the natural compound was replaced by an oxyethyl group. The aliphatic saturated or unsaturated ester portions have been chosen so that the dimensions of the new synthetic molecules were similar to that of the natural phenylpropenoid.

I first prepared 2-(3,4-dimethoxyphenoxy)ethanol (**11**) by reaction of 3,4-dimethoxyphenol with ethylene carbonate in DMF at reflux (Scheme 1), obtaining the expected product in high yield (84%). The commercial aliphatic carboxylic acids (**12a-e**) were reacted with ethyl chloroformate in the presence of triethylamine (TEA) and dimethylaminopyridine, at -15 °C, via an intermediate, represented by a mixed anhydride (**13a-e**), which was not isolated (Scheme 1). This reaction allowed the activation of the acid function. Then, the addition of alcohol to the reaction mixture led to the ester derivatives **14a-e**.



i: ethylene carbonate, $C_4H_{12}BrN$, DMF, 140 °C, 6 h, ii: **11**, ClCOOEt, TEA, DCM, -15 °C, 5h, iii: **11**, DMAO, r.t.



Scheme 1. General procedure for the synthesis of 2-(3,4-dimethoxyphenoxy)ethanol derivatives (**14a-e**)

2.5.1.2 Synthesis of heterocyclic amides **15a-d,f,n**, **16a,b,e** and **17a-d**

On the basis of the biological results of compounds **14a-e** (see next paragraph), the second series of derivatives were synthesized replacing the 2-(3,4-dimethoxyphenoxy)ethanolic group with heterocyclic systems, such as phenylpiperazine, piperidinylpyridine and morfolinpyperidine, leading to the corresponding amides **15a-d,f,n**, **16a,b,e** and **17a-d** (Figure 14). The new derivatives contain an amide function instead of an ester. Since it is known that an ester moiety is potentially a target of human esterases, this modification could preserve the molecules from the enzymatic hydrolysis.

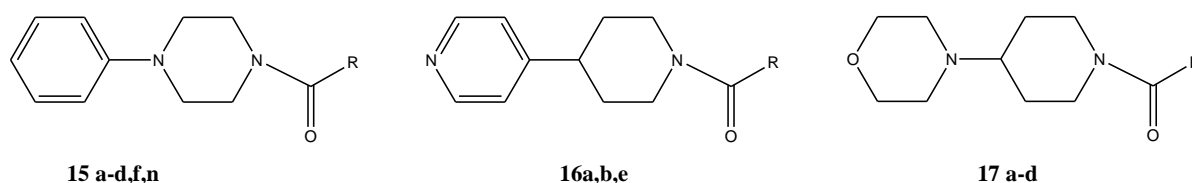
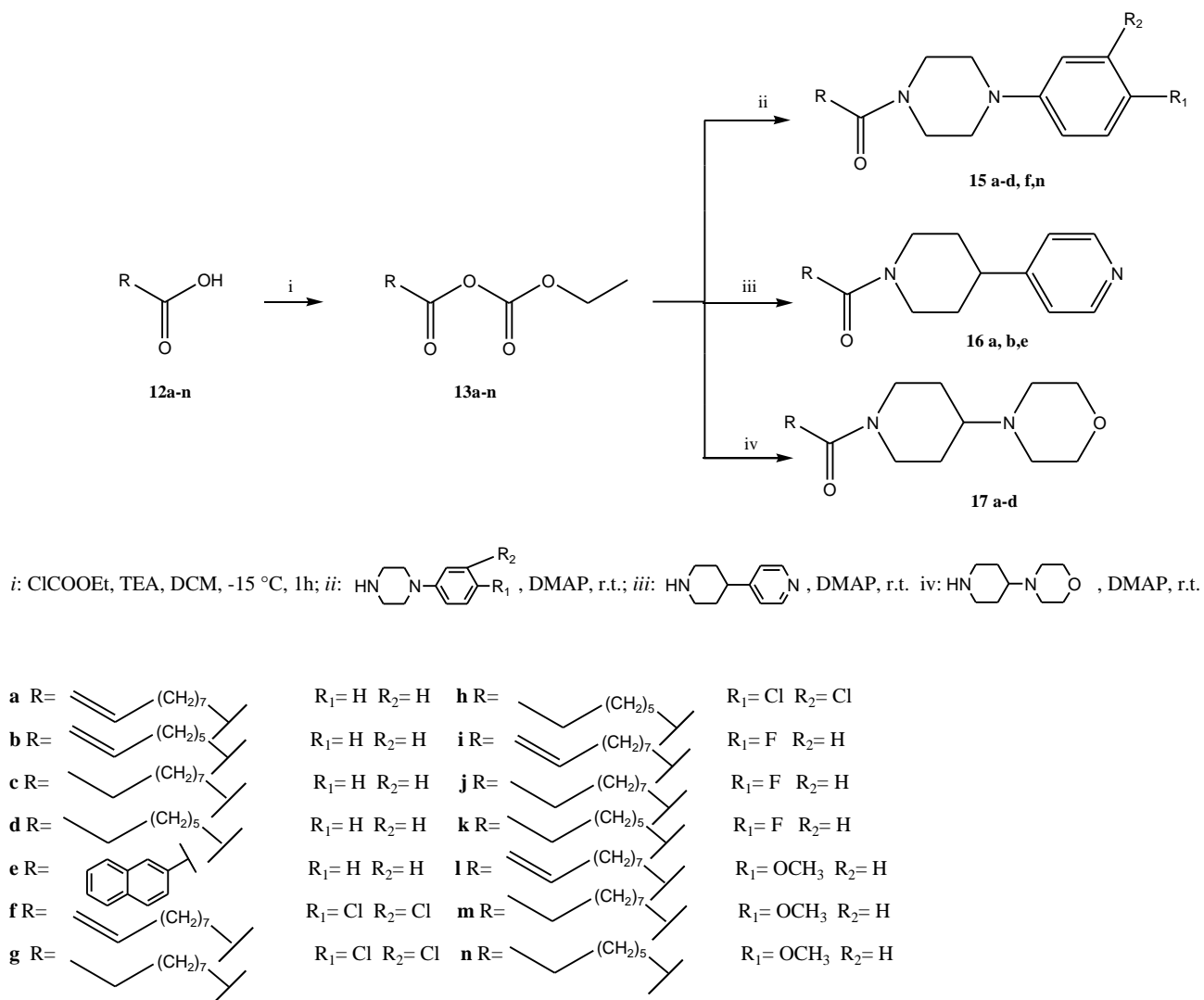


Figure 14. General structure of the heterocyclic amides synthesized **15a-d,f,n**; **16a,b,e**; **17a-d**

In the second series of molecules, the mixed anhydrides (**13a-n**) were prepared according to the procedure reported for compounds **14a-e**. The mixed anhydrides were not isolated and the addition of an excess of a secondary amine to the reaction mixture led to the amides **15a-d,f,n**, **16a,b,e**, and **17a-d**.



Scheme 2. General procedure for the synthesis of heterocyclic amides **15a-d,f,n**, **16a,b,e**, and **17a-d**

2.5.2 Anti-Rhinovirus activity of compounds **14 a-e**, **15ad,f,n**, **16 a,b,e** and **17 a-d**

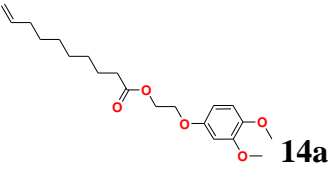
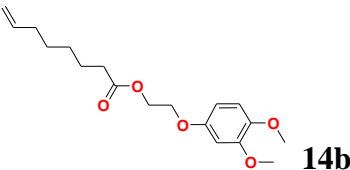
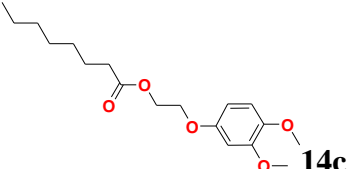
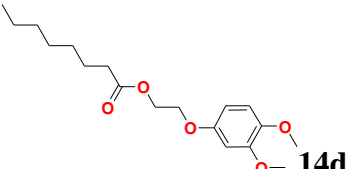
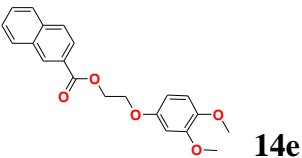
All derivatives (**14a-e**, **15ad,f,n**, **16a,b,e** and **17a-d**) were tested at the Department of Microbiology and Immunology, Rega Institute for Medical Research, Leuven, Belgium by the group of Professor Johan Neyts. The cytotoxicity has been evaluated on HeLa cells and the anti-HRV activity was tested on Rhinovirus 02 (HRV-A02) and Rhinovirus 14 (HRV-B14) belonging to the serotype A and B, respectively (Table 2). The antiviral potency was evaluated by the method of inhibition of the virus-induced cytopathic effect in HeLa cells and expressed as EC₅₀, i.e. as an effective dose to reduce the cytopathic effect by 50%. Pleconaril was used as a reference. Cytotoxicity (CC₅₀) was assessed in parallel in compound-treated, uninfected cells.

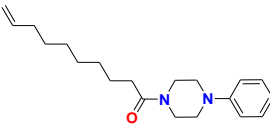
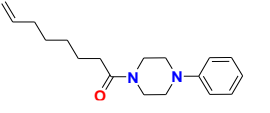
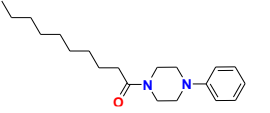
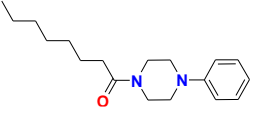
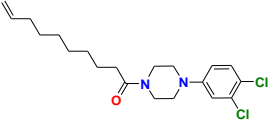
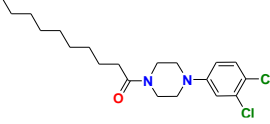
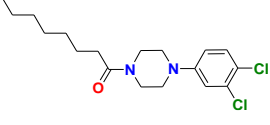
The antiviral screening indicated that all of the 2-(3,4-dimethoxyphenoxy) ethanol derivatives did not show any antiviral effect up to 100 μM, except for the naphthalene-bearing compound **14e** that revealed a moderate activity against HRV-A02 and HRV-B14 with EC₅₀ of 15.3 and 24.6 μM, respectively (Table 2). Interestingly, compounds **14a-e** were not toxic up to 100 μM.

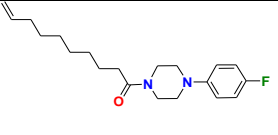
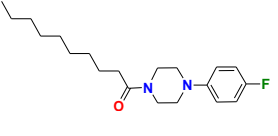
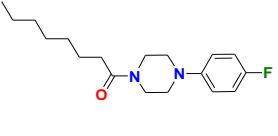
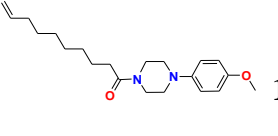
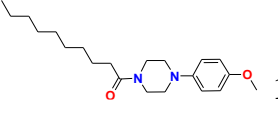
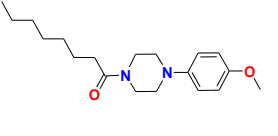
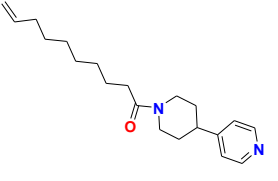
Unlike the 3,4-dimethoxybenzene derivatives, various heterocyclic amides showed strong activity in the low micromolar range and, with respect to the natural compound, a reversal of selectivity towards the viral species B (HRV-14) was observed. In particular, among the phenylpiperazine amides (**15a-d,f,n**), we first assessed their antiviral activity only varying the aliphatic chain. Thus, among compounds **15a-d**, the most active was **15c**, containing a decanoic chain, with an EC₅₀ of 5.7 μM and selectivity index (SI) of 14 (Table 2). The substitution in **15c** of the decanoic moiety with an octanoic, 7-octenoic or 9-decenoic led to complete loss of activity (EC₅₀ >100) as in **15d**, or a decrease in the activity as for **15b** (EC₅₀ = 45 μM) and **15a** (EC₅₀ = 11.9 μM).

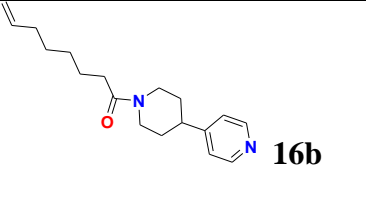
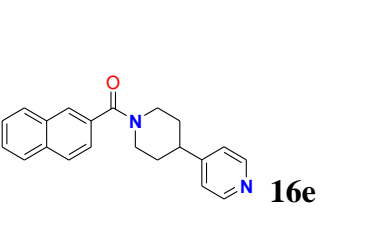
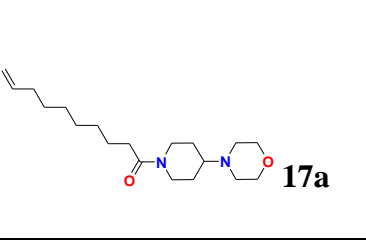
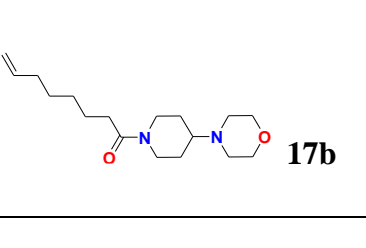
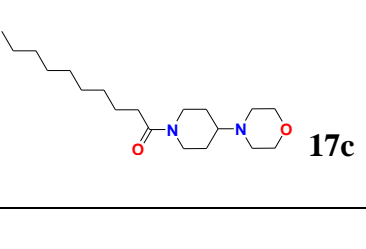
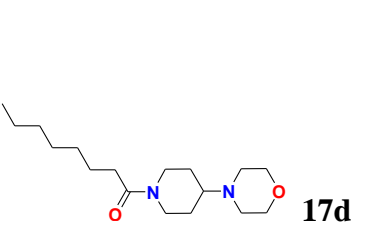
The importance of the decanoic chain was also confirmed introducing electron withdrawing or donor groups in the phenyl ring as reported for compounds **15g**, **15j** and **15m**. Furthermore, when halogen atoms were introduced in the phenyl ring of **15c**, the 3,4-dichloro substitution resulted more favourable respect to the 4-fluorine substitution. The most active compound of the phenylpiperazine amides was the 4-methoxyphenyl derivative **15m** with an EC₅₀ of 1.0 μM, value very close to that of the 3,4-dichlorophenylpiperazine **15g** (EC₅₀ = 1.4 μM). Moreover, **15m** revealed the best SI (>100). In a third series of compounds, we evaluated the influence of the substitution of the phenylpiperazine moiety with a piperidinylpyridine. Also in this case, the piperidinylpyridine amide **16a**, containing a 10 carbon aliphatic chain, yielded the best inhibition of HRV-B14 with a IC₅₀ value of 1.4 μM (Table 2).

Table 2. Inhibition of replication of HRV-A02 and HRV-B14 serotypes by compounds **14 a-e**, **15a-d**, **3f-n**, **16 a, b, e**, and **17 a-d**

Compound	CC ₅₀ ^a	EC ₅₀ ^b	EC ₅₀ ^b
	μM	μM (SI) ^c	μM (SI) ^c
	HeLa	HRV-B14	HRV-A02
 14a	>100	>100	>100
 14b	>100	>100	>100
 14c	>100	>100	>100
 14d	>100	>100	>100
 14e	>100	24.6 ± 1.7 (4.1)	15.3 ± 0.1 (6.5)

 15a	81.8 ± 3.1	11.9 ± 1.1 (6.9)	>100
 15b	>100	45.0 ± 2.4 (2.2)	>100
 15c	79.2 ± 2.2	5.7 ± 0.01 (13.9)	>100
 15d	>100	>100	>100
 15f	98.3 ± 4.8	4.0 ± 0.1 (24.6)	>75
 15g	98.0 ± 3.3	1.4 ± 0.08 (70)	>75
 15h	88.3 ± 3.8	>15	>15

 15i	77 ± 1.7	6.7 ± 0.1 (11.5)	>100
 15j	75.4 ± 5.1	3.1 ± 0.08 (24.3)	>100
 15k	>100	>100	>100
 15l	>100	2.9 ± 0.05 (34.5)	>100
 15m	>100	1.0 ± 0.02 (100)	>100
 15n	>100	>100	>100
 16a	81.1 ± 6.0	1.4 ± 0.07 (57.9)	>75

 16b	>100	>100	>100
 16e	>100	>100	>100
 17a	>100	>100	>100
 17b	>100	>100	>100
 17c	>100	>100	>100
 17d	>100	>100	>100
Pleconaril	>100	0.2 ± 0.01 (500)	0.3 ± 0.02 (333)

^aCC₅₀: cytotoxic concentration for 50% of cell death, measured with MTT assay in HeLa cells.

^bEC₅₀: effective concentration for 50% inhibition of each HRV species measured with MTT assay in HeLa cells. ^cSI: selective index, calculated by CC₅₀/EC₅₀.

2.5.3 Conclusion

In conclusion, I synthesized two series of derivatives, the first (**14a-e**) were analogues of the anti-HRV39 (E)-3-(3,4-dimethoxyphenyl)-2-propen-1-yl (Z)-2-[(Z)-2-methyl-2-butenoyloxymethyl]butenoate, obtained simply by changing the aliphatic chain and replacing the propenic moiety linked to the benzene ring of the natural compound by an oxyethyl group. However, these compounds were completely inactive against both serotypes HRV A and B.

Subsequently, the second series of derivatives was synthesized replacing the 3,4-dimethoxyphenylpropenic group of the natural compound with heterocyclic systems such as phenylpiperazine (**15a-d,f,n**), piperidinyipyridine (**16a,b,e**) or morfolinpyperidine (**17a-d**), linked by an amide group with the same saturated or unsaturated aliphatic chain employed for the series **14a-e**.

Biological tests have shown that all compounds have a low cytotoxicity on HeLa cells and, among all, the p-methoxyphenyl derivatives (**15 l-n**) were not toxic up to 100 μM , while that of the natural compound was 20.3 μM .

Anti-HRV assays revealed that compounds **15m**, **16a**, **15g** were more active than the natural compound to inhibit HRV replication showing an EC_{50} values of 1.0, 1.4, 1.5 μM , respectively, whereas the EC_{50} for the natural phenylpropanoid was 2.4 μM . However, and more interestingly, compounds **15m**, **16a** and **15g** showed a selectivity index that was significantly higher than that of the natural compound. In particular, among all, the most intriguing compound was the 4-methoxyphenyl derivative **15m** showing a $\text{SI} > 100$ whereas the SI of the natural phenylpropenoid was 8.4.

Furthermore, all the synthetic derivatives revealed a high selectivity against the serotype B (HRV-B14) whereas the natural compound was selective towards the serotype A (HRV-A39).

A further benefit of the heterocyclic amides is that they have a potential greater metabolic stability against human esterases, than that of the natural compound.

These new compounds can offer a valid "scaffold" for the development of new drugs against the cold virus, an etiological agent for which, at moment, there is no approved drug.

2.6 EXPERIMENTAL PART

2.6.1 Materials and Methods

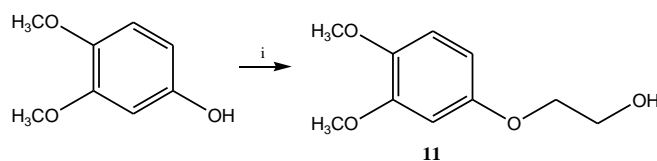
2.6.1.1 General procedures

The NMR spectra were recorded at 25 °C on a high-resolution Unity Inova 500NB spectrometer (Agilent Technologies, CA, USA) operating at 500 MHz for ^1H and 100 MHz for ^{13}C or on a VARIAN UNITY INOVA 400 MHz instrument. All spectra were measured at 25°C in CDCl_3 or CD_4O and using the undeuterated CHCl_3 residue in CDCl_3 (^1H 7.26 ppm and ^{13}C 77.0 ppm) and CH_3OH in CD_4O (^1H 3.34 ppm and ^{13}C 49.0 ppm) as a reference. HRESIMS were measured on an Agilent 6520 time of flight (TOF) MS instrument (Agilent Technologies). Column chromatography was conducted using silica gel (40-63 μm , Merck), aluminium oxide (neutral) and Sephadex LH-20 (25-100 μm , Pharmacy) as stationary phases and monitoring the TLC fractions. TLC was performed on silica gel 60 F₂₅₄ or RP-18 F₂₅₄ (Merck). LiChrolut RP-18 (40–63 μm) 500 mg, 3 ml (Merck) solid phase extraction (SPE) cartridges were also used. Semi-preparative HPLC was conducted using a Varian LH 920 instrument with autosampler. The column was a Varian RP-18 of 250 x 10 mm, particle size 5 μm . The wavelength of UV detection was 254 and 360 nm

2.6.1.2 Synthesis of compound 11-17

Synthesis of 2-(3,4-dimethoxyphenoxy)ethanol derivatives 2-(3,4-dimethoxyphenoxy)ethanol (11)

7.7 g (50 mmol) of 3,4-dimethoxyphenol, dissolved in 3.7 ml of dimethylformamide (DMF), reacted with 5.81 g (66 mmol) of ethylene carbonate and 1.85 g tetraethylammonium bromide (8.8 mmol) for 6 h at 140°C until the TLC analysis revealed total disappearance of starting reagent. The resulting mixture was filtered at room temperature. The liquid part was separated by separating funnel containing DMF, distilled water and ethyl acetate. After this preliminary separation, the organic phase was anhydried with sodium sulfate (Na_2SO_4). After filtration, the solution was evaporated and the resulting solid was purified by liquid chromatography under vacuum (VLC) with silica gel using *n*-hexane/ethyl acetate (6:4) as eluents, to give compound **11** (2-(3,4-dimethoxyphenoxy)ethanol, yield 84%).



i: ethylene carbonate, $\text{C}_4\text{H}_{12}\text{BrN}$, DMF, 140 °C, 6 h,

Figure 15. Scheme of synthesis of 2-(3,4-dimethoxyphenoxy)ethanol **11**.

Synthesis of 14a

0.67 ml of ethyl chloroformate (7.06 mmol) and 0.98 ml of TEA (7.06 mmol) were added to a suspension of 9-decenoic acid (1.0 g, 1.1 ml, 5.88 mmol) (2a) in CH₂Cl₂ and the reaction mixture was left to shake for 5 h at -15 °C until the complete disappearance of the original product. Subsequently, the mixture obtained has been filtered at room temperature.

2-(3,4-dimethoxyphenoxy)ethanol (**11**) (7.06 mmol) and DMAP (0.060 g, 0.49 mmol) were added and left for 15 hours at room temperature. Then, the solvent was evaporated and the product was purified by VLC (silica gel) using *n*-hexane/ethyl acetate (9:1) as eluents, to give 0.190 g of compound **14a**.

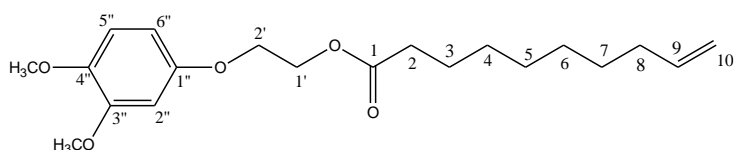


Figure 16. Structure of compound **14a**

Compound 14a. yellow oil, yield: 9%; HR-ESIMS (positive mode) m/z 351.2166 [$M + H$]⁺ (calcd for C₂₀H₃₁O₅, 351.2166); ¹H NMR (500 MHz, CDCl₃): δ 6.748 (d, 1H, J=9 Hz, H-5''), 6.526 (d, 1H, J=3 Hz, H-2''), 6.374 (d,d, 1H, J=0.5 Hz, j= 3, H-6''), 5.770 (m, 1H, H-9), 4.937 (m, 2H, H-10), 4.384 (t, 2H, H-2'), 4.097 (t, 2H, H-1'), 3.826 (s, 3H, OCH₃), 3.804 (s, 3H, OCH₃), 2.32 (m, 2H, H-2), 2.002 (q, 2H, H-3), 1.612 (m, 2H, H-8), 1.324 (m, 8H, H-4, H-7) ppm; ¹³C NMR (100 MHz, CDCl₃): δC 173.660 (C-1), 153.042 (C-3''), 149.841 (C-4''), 143.771 (C-1'') 138.923 (C-9), 114.079 (C-10), 111.762 (C-5''), 103.879 (C-6''), 101.074 (C-2''), 66.506 (C-1'), 62.576 (C-2'), 56.334 (C-3''OCH₃), 55.733 (C-4''OCH₃), 34.055 (C-2), 33.614 (C-3), 28.968 (C-8), 28.923 (C-7), 28.784 (C-6), 28.716 (C-4), 24.774 (C-5) ppm.

Synthesis of ester 14b

0.16 ml of ethyl chloroformate (1.68 mmol) and 0.23 ml of TEA (1.68 mmol) were added to a suspension of 7-octenoic acid (0.2 g, 0.22 ml, 1.4 mmol) in CH₂Cl₂ (2.5 ml) and the reaction mixture was left under agitation for 5 h at -15 °C until the TLC showed the complete disappearance of the original product. The mixture was filtered at room temperature.

2-(3,4-dimethoxyphenoxy)ethanol (**11**) (1.68 mmol) and DMAP (0.01 g, 0.082 mmol) were added for 17 hours at room temperature. Then, the solvent was evaporated under pressure and the product

was purified by VLC (silica gel) using toluene/ethyl acetate as eluents (8:2), to give 95.7 mg of compound **14b**.

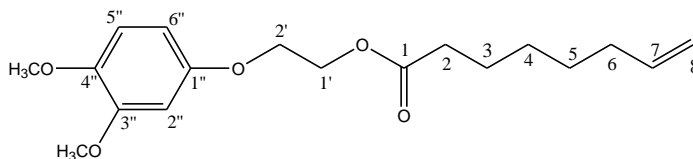


Figure 17. Structure of compound **14b**

Compound 14b transparent oil, yield: 21%; HR-ESIMS (positive mode) m/z 323.1862 $[M + H]^+$ (calcd for $C_{18}H_{27}O_5$, 323.1853); 1H NMR (500 MHz, $CDCl_3$): δ 6.762 (d, 1H, $J=8.5$ Hz, H-5''), 6.537 (d, 1H, $J=2.5$ Hz, H-2''), 6.386 (d,d, 1H, $J=0.5$ Hz, $j=3$, H-6''), 5.772 (m, 1H, H-7), 4.948 (m, 2H, H-8), 4.397 (t, 2H, H-2'), 4.111 (t, 2H, H-1'), 3.839 (s, 3H, OCH_3), 3.819 (s, 3H, OCH_3), 2.343 (t, 2H, $J=8$, H-2), 2.025 (q, 2H, H-3), 1.636 (m, 2H, H-6), 1.366 (m, 4H, H-4, H-5) ppm; ^{13}C NMR (100 MHz, $CDCl_3$): δ 173.614 (C-1), 153.081 (C-3''), 149,892 (C-4''), 143.827 (C-1''), 138.680 (C-7), 114.347 (C-8), 111.788 (C-5''), 103.901 (C-6''), 101.119 (C-2''), 66.551 (C-1'), 62.630 (C-2'), 56.396 (C-3'' OCH_3), 55.796 (C-4'' OCH_3), 34.056 (C-2), 33.449 (C-3), 28.482 (C-6), 28.432 (C-4), 24.685 (C-5) ppm.

Synthesis of the ester **14c**

0.33 ml of ethyl chloroformate (3.49 mmol) and 0.49 ml of TEA (3.49 mmol) were added to a suspension of decanoic acid (0.5 g, 2.91 mmol) in CH_2Cl_2 (5.0 ml) and the reaction mixture was left to shake for 5 h at -15 °C until the complete disappearance of the original product. Subsequently, the mixture has been filtered at room temperature. 2-(3,4-Dimethoxyphenoxy)ethanol (**11**) (3.49 mmol) and DMAP (0.03 g, 0.25 mmol) were added for 17 hours at room temperature. Then, the solvent was then evaporated and the product was purified by a column chromatography with silica gel, using *n*-hexane/ethyl acetate as eluents (8:2), to give 0.245 g of compound **14c**.

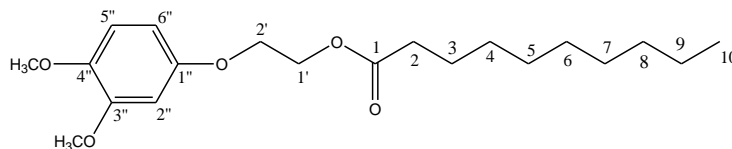


Figure 18. Structure of compound **14c**

Compound 14c. transparent oil, yield: 20%; HR-ESIMS (positive mode) m/z 353.2294 $[M + H]^+$ (calcd for $C_{20}H_{33}O_5$, 353.2323); 1H NMR (500 MHz, $CDCl_3$): δ 6.742 (d, 1H, $J=8.5$ Hz, H-5''), 6.521 (d, 1H, $J=3$ Hz, H-2''), 6.368 (d,d, 1H, $J=0.5$ Hz, $J=3$, H-6''), 4.377 (t, 2H, H-2'), 4.091 (t, 2H, H-

1'), 3.820 (s, 3H, OCH₃), 3.798 (s, 3H, OCH₃), 2.319 (t, 2H, H-2), 1.606 (m, 2H, H-3), 1.226 (s, 11H, H-4/H-9), 0.848 (t, 3H, J=7.5, H-10) ppm; ¹³C NMR (100 MHz, CDCl₃): δ 173.622 (C1), 153.064 (C-3''), 149.857 (C-4''), 143.785 (C-1''), 111.761 (C-5''), 103.876 (C-6''), 101.079 (C-2''), 66.519 (C-1'), 62.546 (C-2'), 56.327 (C-3'' OCH₃), 55.742 (C-4'' OCH₃), 34.086 (C-2), 31.749 (C-3), 29.306 (C-4), 29.160 (C-5), 29.144 (C-6), 29.010 (C-7), 24.824 (C-8), 22.544 (C-9), 13.913 (C-10) ppm.

Synthesis of the ester **14d**

0.40 ml of ethyl chloroformate (4.16 mmol) and 0.58 ml of TEA (4.16 mmol) were added to a suspension of octanoic acid (0.5 g, 0.55 ml, 3.47 mmol) in CH₂Cl₂ (5.0 ml) and the reaction mixture was left to shake for 5 h at -15 °C until the complete disappearance of the original product. Then, the mixture was filtered at room temperature.

2-(3,4-Dimethoxyphenoxy)ethanol (**11**) (4.16 mmol) and DMAP (0.03 g, 0.25 mmol) were added for 16 hours at room temperature. The solvent was evaporated at reduced pressure and the product was subjected to column chromatography (silica gel) by using *n*-hexane/ethyl acetate as eluents in a ratio of 8:2 to give 0.375g of compound **14d**.

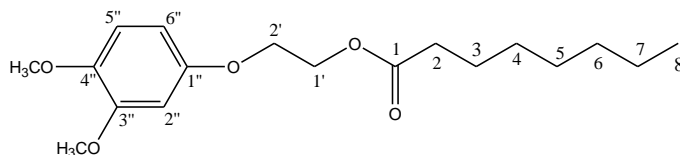


Figure 19. Structure of compound **14d**

Compound 14d. transparent oil, yield: 33%; HR-ESIMS (positive mode) *m/z* 325.1984 [M + H]⁺ (calcd for C₁₈H₂₉O₅, 325.2009); ¹H NMR (500 MHz, CDCl₃): δ 6.762 (d, 1H, J=8.5 Hz, J-5''), 6.540 (d, 1H, J=3 Hz, H-2''), 6.387 (d,d, 1H, J=0.5 Hz, j= 3, H-6''), 4.396 (t, 2H, H-2'), 4.110 (t, 2H, H-1'), 3.839 (s, 3H, OCH₃), 3.817 (s, 3H, OCH₃), 2.339 (t, 2H, H-2), 1.627 (m, 2H, H-3), 1.276 (m, 8H, H-4/H-7), 0.862 (t, 3H, H-8) ppm; ¹³C NMR (100 MHz, CDCl₃): δC 173.587 (C1), 153.029 (C-3''), 149.821 (C-4''), 143.745 (C-1''), 111.733 (C-5''), 103.838 (C-6''), 101.042 (C-2''), 66.480 (C-1'), 62.512 (C-2'), 56.297 (C-3'' OCH₃), 55.693 (C-4'' OCH₃), 34.045 (C-2), 31.506 (C-3), 28.919 (C-4), 28.771 (C-5), 24.785 (C-6), 22.437 (C-7), 13.889 (C-8) ppm.

Synthesis of the ester **14e**

0.33 ml of ethyl chloroformate (3.49 mmol) and 0.49 ml of TEA (3.49 mmol) were added to a suspension of 2-naphthoic acid (0.5 g, 2.91 mmol) (**2a**) in CH₂Cl₂ (5.0 ml) and the reaction mixture was left to shake for 5 h at -15 °C until the TLC showed the complete disappearance of the original product. The resulting mixture was filtered at room temperature.

2-(3,4-Dimethoxyphenoxy)ethanol (**11**) (3.49 mmol) and DMAP (0.03 g, 0.25 mmol) were added for 15 hours at room temperature. Then, the solvent was then evaporated and the product was purified by VLC (silica gel) using *n*-hexane/ethyl acetate as eluents (7:3) to give an impure product, which was further purified by RP- HPLC using acetonitrile/H₂O (7:3, flow 2.5 ml/min) to give 0.100 g of compound **14e**.

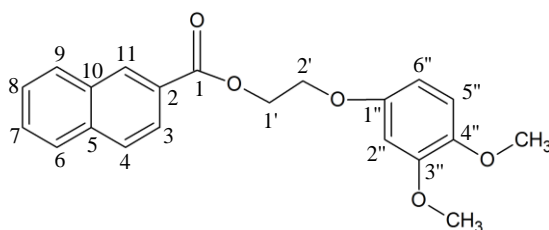


Figure 20. Structure of compound **14e**

Compound 14e. white solid, yield: 20%; HR-ESIMS (positive mode) m/z 353.1381 [M + H]⁺ (calcd for C₂₁H₂₁O₅, 353.1383); ¹H NMR (500 MHz, CDCl₃): δ 8.615 (s, 1H, H-3), 8.076 (d,d, 1H, J=0.5 Hz, j=2, H-4), 7.941 (d, 1H, J=8 Hz, H-11), 7.873 (d, 2H, J=8.5 Hz, H-9, H-10), 7.562 (m, 2H, H-7, H-8), 6.789 (d, 1H, J=9 Hz, H-5''), 6.607 (d, 1H, J=3 Hz, H-2''), 6.473 (d,d, 1H, J=0.5 Hz, j= 3, H-6''), 4.716 (t, 2H, H-2'), 4.323 (t, 2H, H-1'), 3.846 (s, 3H, OCH₃), 3.832 (s, 3H, OCH₃) ppm; ¹³C NMR (100 MHz, CDCl₃): δ 166.636 (C1), 153.197 (C-3''), 149,925 (C-4''), 143.880 (C-1''), 135.550 (C-2), 132.408 (C-5), 131.226 (C-3), 129.309 (C-11), 128.277 (C-4), 128.105 (C-6), 127.707 (C-9), 127.086 (C-10), 126.620 (C-7), 125.219 (C-8), 111.819(C-5''), 104.145 (C-6''), 101.260 (C-2''), 66.715 (C-1'), 63.598 (C-2'), 56.404 (C-3'' OCH₃), 55.818 (C-4'' OCH₃) ppm.

Synthesis of the amide **15a**

0.67 ml of ethyl chloroformate (7.06 mmol) and 0.98 ml of TEA (7.06 mmol) were added to a suspension of 9-decenoic acid (1.0 g, 1.1 ml, 5.88 mmol) in CH₂Cl₂ (13 ml) and the reaction mixture was left to shake for 5 h at -15 °C until the complete disappearance of the starting reagent. The resulting mixture was filtered at room temperature.

Phenylpiperazine amine (1.912 g, 1.80 mL) and DMAP (0.060 g, 0.49 mmol) were added to anhydride **13a** for 15 hours at room temperature. Then, the solvent was then evaporated and the product was washed with acetone and filtered to give a crystalline powder and a solution. The solution

was evaporated (2.59 g) and chromatographed with alumina column, using *n*-hexan and EtOAc (8:2) as solvents, to give 0.314 g of the final compound **15a**.

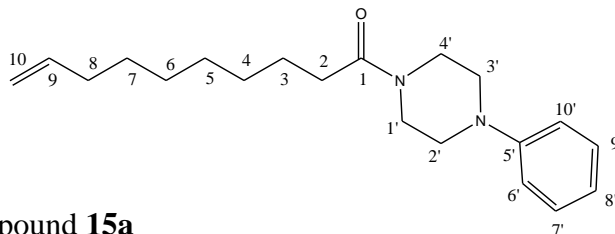


Figure 21. Structure of compound **15a**

Compound 15a. orange solid, yield: 68%; HR-ESIMS (positive mode) m/z 315.2430 $[M + H]^+$ (calcd for $C_{20}H_{31}N_2O$, 315.2430); 1H NMR (500 MHz, $CDCl_3$): δ 7.28 (m, 2H, H-6', H-10'), 6.94 (d, 2H, $^3J=8.0$, H-7', H-9'), 6.90 (d, 1H, $^3J=7.0$, H-8') 5.80 (m, 1H, H-7), 4.99 (dq, 1H, H-8), 4.93 (dq, 1H, H-8), 3.78 (s, 2H, H-2', H-3'), 3.63 (s, 2H, H-2', H-3'), 3.16 (m, 4H, H-1'-H-4'), 2.36 (t, 1H, H-2), 2.04 (q, 2H, H-3), 1.65 (m, 2H, H-8), 1.37 (m, 8H, H-4, H-7) ppm; ^{13}C NMR (100 MHz, $CDCl_3$): δ 171.65 (C-1), 150.85, 139.05, 129.20, 120.54, 116.62, 1114.14, 49.85, 49.47, 45.50, 41.37, 33.71, 33.26, 29.39, 29.22, 28.92, 28.81, 25.29 ppm.

Synthesis of the amide **15b**

0.16 ml of ethyl chloroformate (1.68 mmol) and 0.23 ml of TEA (1.68 mmol) were added to a suspension of 7-octenoic acid (0.2 g, 0.22 ml, 1.4 mmol) in CH_2Cl_2 (4 ml) and the reaction mixture was left to shake for 5 h at -15 °C until the complete disappearance of the starting compound. The resulting mixture was filtered at room temperature.

Phenylpiperazine amine (0.453 g, 0.43 ml) and DMAP (10 mg, 0.082 mmol) were added to anhydride **13b**, for 15 hours at room temperature. Subsequently, the solvent was evaporated and the product washed with acetone and filtered to give a crystalline powder and a solution. The solution was evaporated (0.77 g) and chromatographed with alumina column, using *n*-hexan and EtOAc (8:2) as solvents, to give 0.241. g of the final compound **15b**.

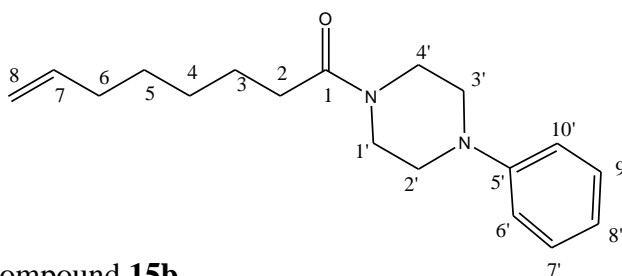


Figure 22. Structure of compound **15b**

Compound 15b. orange solid, yield: 60%; HR-ESIMS (positive mode) m/z 287.2107 $[M + H]^+$ (calcd for $C_{18}H_{27}N_2O$, 287.2118); 1H NMR (500 MHz, $CDCl_3$): δ 7.48 (t, 2H, H-6', H-10'), 6.94 (d, 2H, $^3J=8.5$, H-7', H-9'), 6.90 (d, 1H, $^3J=7.0$, H-8') 5.80 (m, 1H, H-7), 5.0 (dq, 1H, H-8), 4.94 (dq, 1H, H-8), 3.78 (s, 2H, H-2', H-3'), 3.62 (s, 2H, H-2', H-3'), 3.16 (m, 4H, H-1'-H-4'), 2.36 (t, 1H, H-2), 2.07 (q, 2H, H-3), 1.67 (m, 2H, H-6), 1.41 (m, 4H, H-4, H-5) ppm; ^{13}C NMR (100 MHz, $CDCl_3$): δ 171.55 (C-1), 150.87, 138.80, 129.20, 120.53, 116.61, 114.35, 49.83, 49.44, 45.48, 41.37, 33.56, 33.19, 28.90, 28.65, 25.13 ppm.

Synthesis of the amide 15c

0.33 ml ethyl chloroformate (3.49 mmol) and 0.50 ml TEA (3.49 mmol) were added to a suspension of decanoic acid (0.5 g, 2.91 mmol) in CH_2Cl_2 and the reaction mixture was left to shake for 5 h at $-15\text{ }^\circ C$ until the complete disappearance of the starting compound. The resulting mixture was filtered at room temperature.

Phenylpiperazine amine (0.943g, 0.89mL) DMAP (30mg, 0.25 mmol) were added to anhydride **13c**, which had not been isolated, for 15 hours at room temperature. When the reaction was over, the solvent was evaporated and the crude product was washed with acetone and filtered, leaving a white crystalline solid and a solution. The solution was evaporated to give 1.55 g of a white solid, which was purified by VLC (alumina) using *n*-hexane/ethyl acetate (8:2) as eluent, to give 0.300 g of amide **15c**.

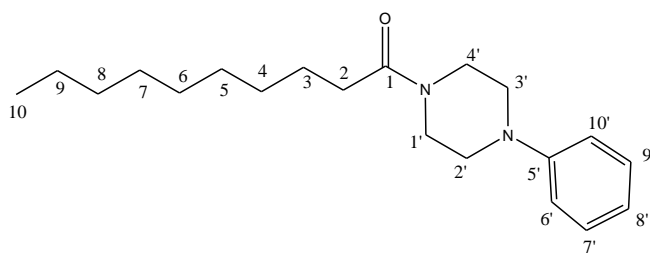


Figure 23. Structure of compound **15c**

Compound 15c. white crystal, yield: 33%; HR-ESIMS (positive mode) m/z 317.2537 $[M + H]^+$ (calcd for $C_{20}H_{33}N_2O$, 317.2587); 1H NMR (500 MHz, $CDCl_3$): δ 7.29 (t, 2H, H-6', H-10'), 6.92 (d, 2H, $^3J=8.5$, H-7', H-9'), 6.88 (d, 1H, $^3J=7.0$, H-8'), 3.76 (t, 2H, H-1', H-4'), 3.61 (t br, 2H, H-1', H-4'), 3.15 (t, 4H, H-2', H-3'), 2.35 (t, 2H, H-2), 1.64 (m, 2H, H-3), 1.29 (m, 12H, H-4/H-9), 0.87 (t, 3H, H-10) ppm; ^{13}C NMR (100 MHz, $CDCl_3$): δ 171.65 (C-1), 150.91 (C-5'), 129.13 (C-6'-C-10'), 120.39 (C-8'), 116.52 (C-7', C-9'), 49.73 (C-1'), 49.36 (C-4'), 45.49 (C-2'), 41.36 (C-3'), 33.25 (C-2), 31.78 (C-3), 29.46, 29.42, 29.39, 29.22, 25.30, 22.57 (C-9), 14.01 (C-10) ppm.

Synthesis of the amide 15d

0.40 ml ethyl chloroformate (4.16 mmol) and 0.58 ml TEA (4.16 mmol) were added to a suspension of octanoic acid (0.5 g, 0.55 mL, 3.47 mmol) in CH₂Cl₂ and the reaction mixture was left to shake for 5 h at -15 °C until the complete disappearance of the original product. The resulting mixture was filtered at room temperature.

Phenylpiperazine amine (1.06 mL, 6.94 mmol) and DMAP (30mg, 0.25 mmol) were added to anhydride **13d**, which had not been isolated, for 15 hours at room temperature. When the reaction was over, the solvent was evaporated and the crude product was washed with acetone and filtered, leaving a white crystalline solid and a solution. The solution was evaporated to give 1.78 g of a white solid, which was purified through VLC (alumina) using *n*-hexane/ethyl acetate (8:2) as eluent, giving 0.150 g of impure product. It was washed with acetone and filtered. The resulting solution was evaporated to give 89.6 mg of the pure product **15d**.

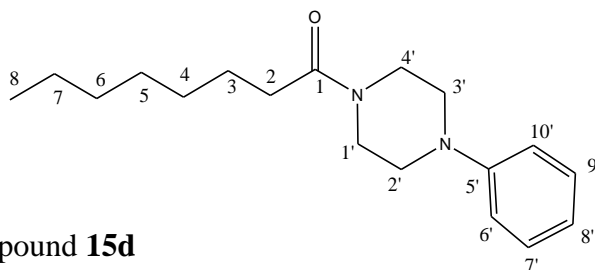


Figure 24. Structure of compound **15d**

Compound 15d. white crystal, yield: 9%; HR-ESIMS (positive mode) m/z 289.2270 [M + H]⁺ (calcd for C₁₈H₂₉N₂O, 289.2274); ¹H NMR (500 MHz, CDCl₃): δ 7.27 (t, 2H, H-6', H-10'), 6.94 (d, 2H, ³J = 8.0, H-7', H-9'), 6.90 (d, 1H, ³J = 7.0, H-8'), 3.78 (t br, 2H, H-1', H-4'), 3.63 (t br, 2H, H-1', H-4'), 3.17 (m, 4H, H-2', H-3'), 2.36 (t, 2H, H-2), 1.65 (m, 2H, H-3), 1.32 (m, 8H, H-4/H-7), 0.88 (t, 3H, H-8) ppm; ¹³C NMR (100 MHz, CDCl₃): δ 171.75 (C-1), 129.26 (C-5'), 117.31 (C-8'), 116.73 (C-6'-C-10'), 112.88 (C-7', C-9'), 50.02 (C-1'), 49.56 (C-4'), 45.50 (C-2'), 41.86 (C-3'), 33.33 (C-2), 31.70 (C-3), 29.45, 29.08, 25.37, 22.60 (C-7), 14.05 (C-8) ppm.

Synthesis of the amide 15f

0.33 ml ethyl chloroformate (3.49 mmol) and 0.50 ml TEA (3.49 mmol) were added to a suspension of 9-decenoic acid (0.495 g, 0.54 ml, 2.91 mmol) in CH₂Cl₂ and the reaction mixture was left to shake for 5 h at -15 °C until the complete disappearance of the original product. The resulting mixture was filtered at room temperature.

Phenylpiperazine amine with Cl₂ (0.806 g, 3.49 mmol) and DMAP (0.305g, 2.49 mmol) were added to anhydride **13f**, which had not been isolated, for 15 hours at room temperature. The, the solvent was evaporated and an aliquot (1/3) of the impure product was purified in Sephadex using MeOH as

eluent. The crude product was washed with acetone to give a white crystalline solid and a solution. After solvent evaporation, 24.5 mg of compound **15f** were obtained.

The remaining aliquot (2/3) was purified by VLC using *n*-hexane/ethyl acetate (7.5:2.5) as eluent, to give 220 mg of compound **15f**.

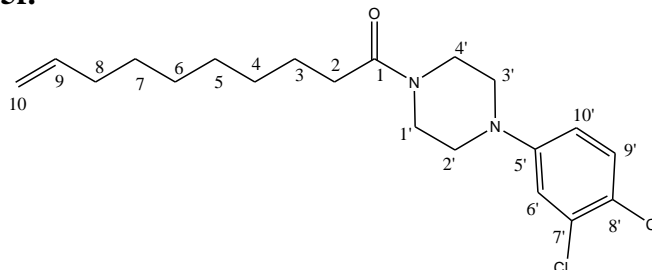


Figure 25. Structure of compound **15f**

Compound 15f. yellow oil, yield: 22%; HR-ESIMS (positive mode) m/z 383.1654 $[M + H]^+$ (calcd for $C_{20}H_{29}Cl_2N_2O$, 383.1651); 1H NMR (500 MHz, $CDCl_3$): δ 7.25 (d, 1H, $^3J = 9.0$, H-6'), 6.95 (d, 1H, $^4J = 2.5$, H-9'), 6.73 (dd, 1H, $^3J = 9.0$, $^4J = 2.5$, H-10'), 5.79 (m, 1H, H-9), 4.98 (dq, 1H, H-10), 4.92 (dq, 1H, H-10), 3.75 (t, 2H, H-1', H-4'), 3.61 (t, 2H, H-1', H-4'), 3.13 (m, 4H, H-2', H-3'), 2.34 (t, 2H, H-2), 2.03 (q, 2H, H-8), 1.64 (m, 2H, H-3), 1.36 (m, 8H, H-4/H-7)ppm; ^{13}C NMR (100 MHz, $CDCl_3$): δ 171.84 (C-1), 150.26 (C-5'), 139.03 (C-7'), 130.55 (C-6'), 117.76 (C-8'), 115.73 (C-9'), 114.11 (C-10'), 49.17 (C-1'), 48.88 (C-4'), 45.73 (C-2'), 41.14 (C-3'), 33.70 (C-2), 33.22 (C-3), 29.36, 29.20, 29.05, 28.88, 28.80, 25.25, 24.85 ppm.

Synthesis of the amide **15g**

0.33 ml ethyl chloroformate (3.49 mmol) and 0.50 ml TEA (3.49 mmol) were added to a suspension of decanoic acid (0.5 g, 2.91 mmol) in CH_2Cl_2 and the reaction mixture was left to shake for 5 h at -15 °C until the complete disappearance of the starting compound. The resulting mixture was filtered at room temperature.

Phenylpiperazine amine (0.806g, 3.49 mmol) and DMAP (30.5mg, 0.25 mmol) were added to anhydride **13g**, which had not been isolated, for 15 hours at room temperature. Then, the solvent evaporated and the crude product (1.82 g), purified by gel chromatography on Sephadex using MeOH as eluent to give 1.06 of compound **15g**.

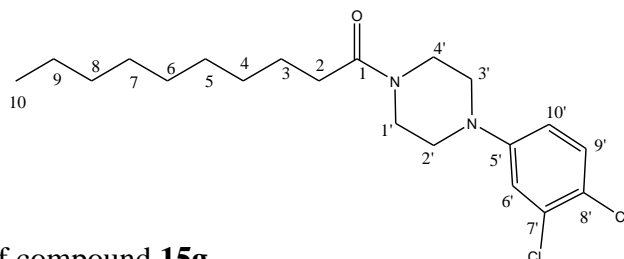


Figure 26. Structure of compound **15g**

Compound 15g. white solid, yield: 95%; HR-ESIMS (positive mode) m/z 385.1820 $[M + H]^+$ (calcd for $C_{20}H_{31}Cl_2N_2O$, 385.1807); 1H NMR (500 MHz, $CDCl_3$): δ 7.29 (d, 1H, $^3J = 9.0$, H-6'), 6.96 (d, 1H, $^4J = 2.5$, H-9'), 6.74 (dd, 1H, $^3J = 9.0$, $^4J = 3.0$, H-10'), 3.76 (t, 2H, H-1', H-4'), 3.61 (t, 2H, H-1', H-4'), 3.14 (m, 4H, H-2', H-3'), 2.35 (t, 2H, H-2), 1.64 (m, 2H, H-3), 1.29 (m, 12H, H-4/H-9), 0.87 (t, 3H, H-10)ppm; ^{13}C NMR (100 MHz, $CDCl_3$): δ 171.79 (C-1), 150.22 (C-5'), 132.96 (C-7'), 130.59 (C-6'), 123.19 (C-8'), 117.84 (C-9'), 115.84 (C-10'), 49.73 (C-1'), 48.98 (C-4'), 45.20 (C-2'), 41.10 (C-3'), 33.28 (C-2), 31.85 (C-3), 29.46, 29.45, 29.41, 29.25, 25.32, 22.64 (C-9), 14.07 (C-10) ppm.

Synthesis of the amide 15h

0.33 ml ethyl chloroformate (3.49 mmol) and 0.50 ml TEA (3.49 mmol) were added to a suspension of octanoic acid (0.42 g, 0.46mL, 2.91 mmol) in CH_2Cl_2 and the reaction mixture was left to shake for 5 h at $-15^\circ C$ until the complete disappearance of the starting compound. The resulting mixture was filtered at room temperature.

Phenylpiperazine amine (0.806g, 3.49 mmol) and DMAP (30.5mg, 0.25 mmol) were added to anhydride **13h**, which had not been isolated, for 15h at room temperature. When the reaction was over, the solvent was evaporated and the crude product was washed with acetone and filtered, leaving a white crystalline solid and a solution. The solution was dried and the residue purified with gel chromatography on Sephadex using MeOH as solvent, to give 0.275 g of compound **15h**.

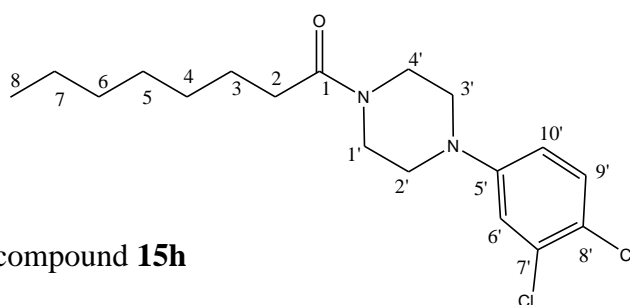


Figure 27. Structure of compound **15h**

Compound 15h. yellow solid, yield: 26%; HR-ESIMS (positive mode) m/z 357.1506 $[M + H]^+$ (calcd for $C_{18}H_{27}Cl_2N_2O$, 357.1495); 1H NMR (500 MHz, $CDCl_3$): δ 7.28 (d, 1H, $^3J = 9.0$, H-6'), 6.94 (d, 1H, $^4J = 3.0$, H-7', H-9'), 6.74 (dd, 1H, $^3J = 9.0$, $^3J = 3.0$ H-8'), 3.75 (t, 2H, H-1', H-4'), 3.63 (t, 2H, H-1', H-4'), 3.14 (m, 4H, H-2', H-3'), 2.35 (t, 2H, H-2), 1.64 (m, 2H, H-3), 1.30 (m, 8H, H-4/H-7), 0.87 (t, 3H, H-8)ppm; ^{13}C NMR (100 MHz, $CDCl_3$): δ 171.80 (C-1), 150.04 (C-5'), 132.95 (C-7'), 130.98 (C-6'), 123.21 (C-8'), 117.85 (C-9'), 115.86 (C-10'), 49.28 (C-1'), 48.99 (C-4'), 45.78 (C-2'), 41.09 (C-3'), 33.33 (C-2), 31.68 (C-3), 29.41, 29.06, 25.41, 22.98 (C-7), 14.04 (C-8) ppm.

Synthesis of the amide **15i**

0.33 ml ethyl chloroformate (3.49 mmol) and 0.50 ml TEA (3.49 mmol) were added to a suspension of 9-decenoic acid (0.54 ml, 2.91 mmol) in CH₂Cl₂ and the reaction mixture was left to shake for 5 h at -15 °C until the complete disappearance of the starting compound. The resulting mixture was filtered at room temperature.

Penylpiperazine amine (0.629 g, 3.49 mmol) and DMAP (30.5 mg, 0.25 mmol) were added to anhydride **13i**, which had not been isolated, for 15 hours at room temperature. When the reaction was over, the solvent was evaporated and the crude product was washed with acetone and filtered, leaving a white crystalline solid and a solution. The solution was dried and the residue chromatographed by VLC (silica gel) using *n*-hexane/ethyl acetate (7.5:2.5) as eluent, to give 0.300 g of the compound **15i**.

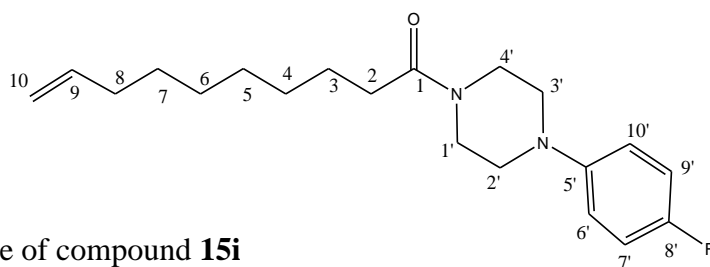


Figure 28. Structure of compound **15i**

Compound 15i. yellow oil, yield: 31%; HR-ESIMS (positive mode) m/z 333.2282 [M + H]⁺ (calcd for C₂₀H₃₀FN₂O, 333.2337); ¹H NMR (500 MHz, CDCl₃): δ 6.96 (t, 2H, H-7', H-9'), 6.87 (m, 2H, H-6', H-10') 5.79 (m, 1H, H-9), 4.97 (dq, 1H, H-10), 4.91 (dq, 1H, H-10), 3.76 (t, 2H, H-1', H-4'), 3.61 (t, 2H, H-1', H-4'), 3.06 (m, 4H, H-2', H-3'), 2.34 (t, 2H, H-2), 2.03 (q, 2H, H-8), 1.65 (m, 2H, H-3), 1.35 (m, 8H, H-4/H-7) ppm; ¹³C NMR (100 MHz, CDCl₃): δ 171.84 (C-1), 161.09, 158.51, 147.59, 139.02, 118.45, 115.70, 114.12, 50.82 (C-1'), 50.41 (C-4'), 45.54 (C-2'), 41.42 (C-3'), 33.68 (C-2), 33.23 (C-3) 29.36, 29.20, 28.89, 28.79, 25.27 ppm.

Synthesis of the amide **15j**

0.33 ml ethyl chloroformate (3.49 mmol) and 0.50 ml TEA (3.49 mmol) were added to a suspension of decanoic acid (0.5g, 2.91 mmol) in CH₂Cl₂ and the reaction mixture was left to shake for 5 h at -15 °C until the complete disappearance of the starting compound. The resulting mixture was filtered at room temperature.

Phenylpiperazine amine (0.629g, 3.49 mmol) and DMAP (30.5mg, 0.25 mmol) were added to anhydride **13j**, which is not isolated, for 15 hours at room temperature. When the reaction was over, the solvent was evaporated and the crude product was washed with acetone and filtered, leaving a white crystalline solid and a solution. The solution was purified through VLC (silica gel) using *n*-hexane/ethyl acetate (7.5:2.5) as eluent, to give amide **15j**.

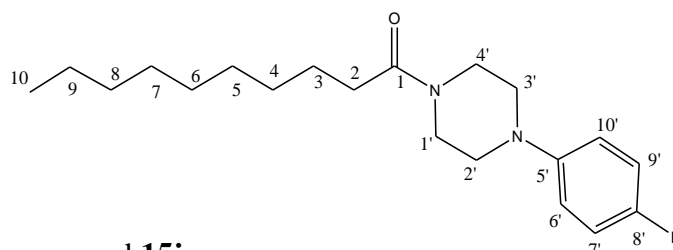


Figure 29. Structure of compound **15j**

Compound 15j. white crystal, yield: 29%; HR-ESIMS (positive mode) m/z 335.2464 $[M + H]^+$ (calcd for $C_{20}H_{32}FN_2O$, 335.2493); 1H NMR (500 MHz, $CDCl_3$): δ 6.97 (t, 2H, H-7', H-9'), 6.88 (m, 2H, H-6', H-10'), 3.77 (t br, 2H, H-1', H-4'), 3.62 (t, 2H, H-1', H-4'), 3.06 (m, 4H, H-2', H-3'), 2.35 (t, 2H, H-2), 1.64 (m, 2H, H-3), 1.29 (m, 12H, H-4/H-9), 0.87 (t, 3H, H-8) ppm; ^{13}C NMR (100 MHz, $CDCl_3$): δ 171.73 (C-1), 158.60 (C-8'), 147.60 (C-5'), 118.98 (C-7'), 118.51 (C-9'), 115.75 (C-6'), 115.57 (C-10'), 50.88 (C-1'), 50.47 (C-4'), 45.99 (C-2'), 41.45 (C-3'), 33.31 (C-2), 31.84 (C-3), 29.48, 29.44, 29.41, 29.24, 25.36, 22.63 (C-9), 13.97 (C-10) ppm.

Synthesis of the amide **15k**

0.33 ml of ethyl chloroformate (3.49 mmol) and 0.50 ml of TEA (3.49 mmol) were added to a suspension of octanoic acid (0.46g, 2.91 mmol) in CH_2Cl_2 and the reaction mixture was left to shake for 5 h at -15 °C until the complete disappearance of the starting compound. The resulting mixture was filtered at room temperature.

Phenylpiperazine amine (0.629 g, 3.49 mmol) and DMAP (30.5mg, 0.25 mmol) were added to anhydride **13k**, which is not isolated, for 15 hours at room temperature. When the reaction was over, the solvent was evaporated and the crude product was washed with acetone and filtered, leaving a white crystalline solid and a solution. The solution was dried and purified through VLC (silica gel) using *n*-hexane/ethyl acetate (7.5:2.5) as eluent, to give 0.390 g of amide **15k**.

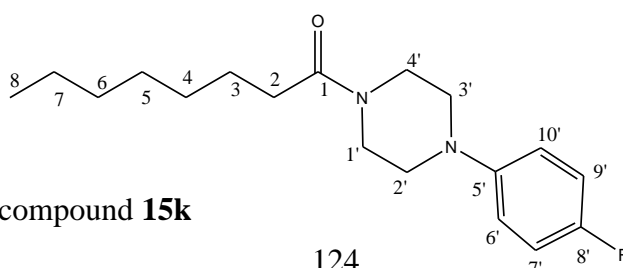


Figure 30. Structure of compound **15k**

Compound 15k. white solid, yield: 44%; HR-ESIMS (positive mode) m/z 307.2202 $[M + H]^+$ (calcd for $C_{18}H_{28}FN_2O$, 307.2180); 1H NMR (500 MHz, $CDCl_3$): δ 6.98 (t, 2H, H-7', H-9'), 6.89 (q, 2H, H-6', H-10'), 3.77 (t, 2H, H-1', H-4'), 3.62 (t, 2H, H-1', H-4'), 3.07 (m, 4H, H-2', H-3'), 2.35 (t, 2H, H-2), 1.65 (m, 2H, H-3), 1.28 (m, 8H, H-4/H-7), 0.88 (t, 3H, H-8) ppm; ^{13}C NMR (100 MHz, $CDCl_3$): δ 171.72 (C-1), 158.62 (C-8'), 147.59 (C-5'), 118.61 (C-7'), 118.55 (C-9'), 115.78 (C-6'), 115.60 (C-10'), 50.93 (C-1'), 50.52 (C-4'), 45.58 (C-2'), 41.44 (C-3'), 33.31 (C-2), 31.70 (C-3), 29.44, 29.07, 25.36, 22.99 (C-7), 14.04 (C-8) ppm.

Synthesis of the amide 15l

0.33 ml ethyl chloroformate (3.49 mmol) and 0.50 ml TEA (3.49 mmol) were added to a suspension of 9-decenoic acid (0.54g, 2.91 mmol) in CH_2Cl_2 and the reaction mixture was left to shake for 5 h at -15 °C until the complete disappearance of the starting compound. The resulting mixture was filtered at room temperature.

Phenylpiperazine amine (0.671 g, 3.49 mmol) and DMAP (30.5mg, 0.25 mmol) were added to anhydride **13l**, which is not isolated, for 15 hours at room temperature. When the reaction was over, the solvent was evaporated and the crude product was washed with acetone and filtered, leaving a white crystalline solid and a solution. The solution was dried and the residue purified through VLC (silica gel) using *n*-hexane/ethyl acetate (7:3) as eluent to give 0.340 g of compound **15l**.

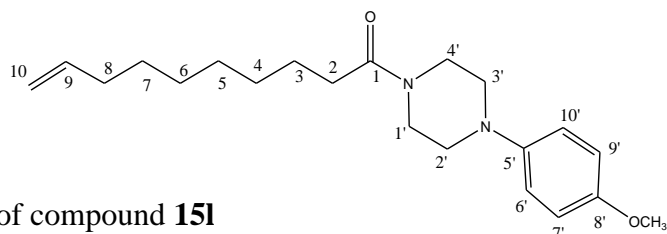


Figure 31. Structure of compound **15l**

Compound 15l. beige solid, yield: 34%; HR-ESIMS (positive mode) m/z 345.2523 $[M + H]^+$ (calcd for $C_{21}H_{33}N_2O_2$, 345.2537); 1H NMR (500 MHz, $CDCl_3$): δ 6.91 (d, 2H, $^3J = 7.0$, H-7', H-9'), 6.84 (d, 2H, $^3J = 9.0$, H-6', H-10'), 5.80 (m, 1H, H-9), 4.98 (dq, 1H, H-10), 4.92 (dq, 1H, H-10), 3.76 (s, 5H, H-1', H-4', H-8'), 3.62 (t br, 2H, H-1', H-4'), 3.03 (m, 4H, H-2', H-3'), 2.35 (t, 2H, H-2), 2.03 (q, 2H, H-8), 1.64 (m, 2H, H-3), 1.36 (m, 8H, H-4/H-7) ppm; ^{13}C NMR (100 MHz, $CDCl_3$): δ 171.62 (C-1), 154.42, 145.39, 139.05, 118.88, 114.51, 114.13 (C-5'), 55.51 (OCH₃), 51.39 (C-1'), 50.96 (C-4'), 45.66 (C-2'), 41.52 (C-3'), 33.71 (C-2), 33.26 (C-3), 29.39, 29.72, 28.92, 28.82, 25.40 ppm.

Synthesis of the amide 15m

0.33 ml ethyl chloroformate (3.49 mmol) and 0.50 ml TEA (3.49 mmol) were added to a suspension of decanoic acid (0.5g, 2.91 mmol) in CH₂Cl₂ and the reaction mixture was left to shake for 5 h at -15 °C until the complete disappearance of the starting compound. The resulting mixture was filtered at room temperature.

Phenylpiperazine amine (0.671g, 3.49 mmol) DMAP (30.5mg, 0.25 mmol) were added to anhydride **13m**, which had not been isolated, for 15 hours at room temperature. When the reaction was over, the solvent was evaporated and the crude product was washed with acetone and filtered, leaving a white crystalline solid and a solution. The solution was dried and the residue purified through VLC (silica gel) using *n*-hexane/ethyl acetate (7:3) as eluent, to give 0.310 g of compound **15m**.

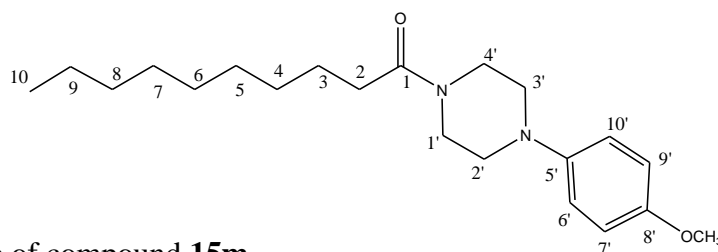


Figure 32. Structure of compound **15m**

Compound 15m. white solid, yield: 31%; HR-ESIMS (positive mode) m/z 347.2688 [M + H]⁺ (calcd for C₂₁H₃₅N₂O₂, 347.2993); ¹H NMR (500 MHz, CDCl₃): δ 6.91 (d, 2H, ³J = 9.0, H-7', H-9'), 6.85 (d, 2H, ³J = 9.0, H-6', H-10'), 3.77 (s, 5H, H-1', H-4', H-8'), 3.62 (t br, 2H, H-1', H-4'), 3.04 (m, 4H, H-2', H-3'), 2.35 (t, 2H, H-2), 1.65 (m, 2H, H-3), 1.35 (m, 12H, H-4/H-9), 0.88 (t, 3H, H-10) ppm; ¹³C NMR (100 MHz, CDCl₃): δ 171.72 (C-1), 159.22, 139.14, 118.91 (C-7'-C-9'), 114.55 (C-6', C-10'), 55.56 (OCH₃), 51.43 (C-1'), 50.98 (C-4'), 45.72 (C-2'), 41.57 (C-3'), 33.34 (C-2), 31.86 (C-3), 29.5, 29.46, 29.43, 29.26, 25.39, 22.66 (C-9), 14.08 (C-10) ppm

Synthesis of the amide 15n

0.33 ml of ethyl chloroformate (3.49 mmol) and 0.50 ml of TEA (3.49 mmol) were added to a suspension of octanoic acid (0.46g, 2.91 mmol) in CH₂Cl₂ and the reaction mixture was left to shake for 5 h at -15 °C until the complete disappearance of the starting compound. The resulting mixture was filtered at room temperature.

Phenylpiperazine amine (0.671g, 3.49 mmol) DMAP (30.5mg, 0.25 mmol) were added to anhydride **13n**, which had not been isolated, for 15 hours at room temperature. When the reaction was over, the solvent was evaporated and the crude product was washed with acetone and filtered, leaving a white

crystalline solid and a solution. The solution was dried and the residue purified through VLC (silica gel) using *n*-hexane/ethyl acetate (7:3) as eluent to give 0.410 g of compound **15n**.

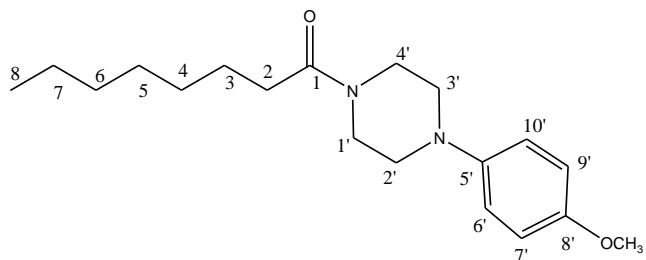


Figure 33. Structure of compound **15n**

Compound 15n. beige solid, yield: 44%; HR-ESIMS (positive mode) m/z 319.2346 $[M + H]^+$ (calcd for $C_{19}H_{31}N_2O_2$, 319.2380); 1H NMR (500 MHz, $CDCl_3$): δ 6.91 (d, 2H, $^3J = 9.0$, H-7', H-9'), 6.85 (d, 2H, $^3J = 9.0$, H-6', H-10'), 3.77 (s, 5H, H-1', H-4', H-8'), 3.62 (t br, 2H, H-1', H-4'), 3.05 (m, 4H, H-2', H-3'), 2.35 (t, 2H, H-2), 1.64 (m, 2H, H-3), 1.31 (m, 8H, H-4/H-7), 0.88 (t, 3H, H-10) ppm; ^{13}C NMR (100 MHz, $CDCl_3$): δ 171.67 (C-1), 154.49, 135.47, 118.91 (C-7'-C-9'), 114.52 (C-6', C-10'), 55.52 (OCH₃), 51.42 (C-1'), 50.89 (C-4'), 45.66 (C-2'), 41.51 (C-3'), 33.29 (C-2), 31.67 (C-3), 29.42, , 29.05, 25.35, 22.57 (C-7), 14.02 (C-8) ppm.

Synthesis of the amide **16a**

0.05 ml ethyl chloroformate (0.564 mmol) and 0.08 ml TEA (0.564 mmol) were added to a suspension of 9-decenoic acid (0.09g, 0.47 mmol) in CH_2Cl_2 and the reaction mixture was left to shake for 5 h at -15 °C until the complete disappearance of the original product. The resulting mixture was filtered at room temperature.

Piperidinyropyridine amine (90 mg) and DMAP (2.4 mg, 0.019 mmol) were added to anhydride **13a**, which had not been isolated, for 15 hours at room temperature. When the reaction was over, the solvent was evaporated and the crude product was washed with ethyl ether and filtered, leaving a white crystalline solid and a solution. The solution was evaporated and the solid (0.222 mg) was chromatographed with an alumina column using *n*-hexane/ethyl ether/ (3:7) as eluent, to give 10.3 mg of amide **16a**.

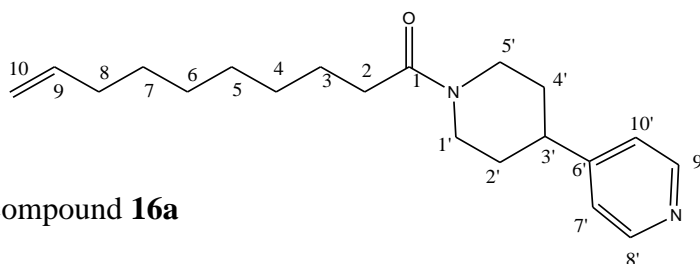
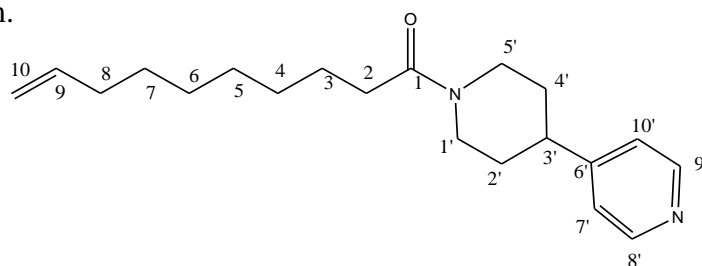


Figure 34. Structure of compound **16a**

Compound 16a. beige solid, yield: 7%; $^1\text{H NMR}$ (500 MHz, CDCl_3): δ 8.53 (d, 2H, $J=3.5$ H-8', H-9'), 7.12 (d, 2H, $J=6.0$, H-7', H-10') 5.80 (m, 1H, H-9), 4.98 (dq, 1H, H-10), 4.92 (dq, 1H, H-10), 4.82 (d, 1H, $J=12.5$, H-5'), 4.00 (d, 1H, $J=14.0$, H-1'), 3.13 (t, 1H, H-5'), 2.74 (m, 1H, H-1'), 2.62 (t, 1H, H-6'), 2.35 (t, 2H, H-2), 2.31 (t, 1H, H-3'), 2.04 (q, 2H, H-2', H-4'), 1.91 (t, 2H, H-2', H-4'), 1.61 (m, 4H, H-3, H-8), 1.33 (m, 6H, H-4/H-7) ppm; $^{13}\text{C NMR}$ (100 MHz, CDCl_3): δ 171.60 (C-1), 153.82, 149.99, 139.10, 122.15, 114.17, 45.95, 42.08, 41.92, 33.75, 33.45, 33.10, 31.96, 29.46, 29.27, 28.97, 28.86, 25.39 ppm.



Synthesis of the amide 16b

0.06 ml of ethyl chloroformate (0.672 mmol) and 0.09 ml of TEA (0.672 mmol) were added to a suspension of 7-octenoic acid (0.08 g, 0.09ml, 0.56 mmol) in CH_2Cl_2 and the reaction mixture was left under agitation for 5 h at $-15\text{ }^\circ\text{C}$ until the complete disappearance of the starting compound. The resulting mixture was filtered at room temperature.

Piperidinyropyridine amine (0.109g, 0.672 mmol) and DMAP (2.4mg, 0.019 mmol) were added to anhydride **13b**, which had not been isolated, for 15 hours at room temperature. When the reaction was over, the solvent was evaporated and the crude product (0.222 g) was chromatographed with alumina column using phase *n*-hexane/ethyl acetate (5:5) as eluent, to give 0.120 g of compound **16b**.

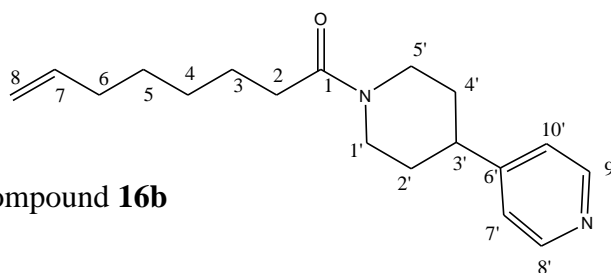


Figure 35. Structure of compound **16b**

Compound 16b. white solid, yield: 75%; HR-ESIMS (positive mode) m/z 287.2116 $[\text{M} + \text{H}]^+$ (calcd for $\text{C}_{18}\text{H}_{27}\text{N}_2\text{O}$, 287.2118); $^1\text{H NMR}$ (500 MHz, CDCl_3): δ 8.49 (s, 2H, H-8', H-9'), 7.09 (d, 2H, $^3J=5.5$, H-7', H-10') 5.77 (m, 1H, H-7), 4.96 (dq, 1H, H-8), 4.90 (dq, 1H, H-8), 4.78 (d, 1H, $^3J=13.0$, H-5'), 3.96 (d, 1H, $^3J=13.5$, H-1'), 3.10 (t, 1H, H-5'), 2.71 (m, 1H, H-1'), 2.59 (t, 1H, H-6'), 2.52 (s br, 1H, H-3'), 2.33 (t, 2H, H-2), 2.03 (q, 2H, H-2', H-4'), 1.87 (t, 2H, H-2', H-4'), 1.59 (m, 4H, H-5, H-6), 1.37 (m, 4H, H-3, H-4) ppm; $^{13}\text{C NMR}$ (100 MHz, CDCl_3): δ 171.42 (C-1), 153.78,

149.80, 138.75, 122.08, 114.27, 45.82, 41.94, 41.81, 33.50, 33.26, 32.96, 31.84, 28.85, 28.58, 25.13 ppm.

Synthesis of the amide 16e

0.053 ml ethyl chloroformate (0.558 mmol) and 0.08 ml TEA (0.558 mmol) were added to a suspension of 2-naphthoic acid (0.08g, 0.465 mmol) in CH₂Cl₂ and the reaction mixture was left to shake for 5 h at -15 °C until the complete disappearance of the starting compound. The resulting mixture was filtered at room temperature.

Piperidinylnicotinamide (0.09 g, 0.558 mmol) and DMAP (2.5mg, 0.019 mmol) were added to anhydride **13e**, which had not been isolated, for 15 hours at room temperature. When the reaction was over, the solvent was evaporated and the crude product was purified by alumina column chromatography using *n*-hexane/ethyl acetate (5:5) as eluent, providing 15 mg of impure compound, which was further purified in Sephadex using MeOH as eluent, to give 10.5 mg of compound **16e**.

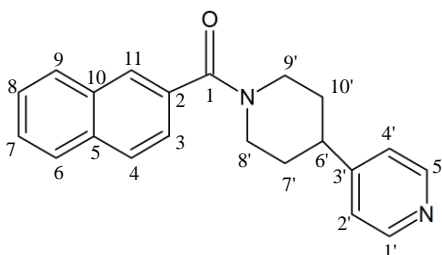


Figure 36. Structure of compound **16e**

Compound 16e. white solid, yield: 7%; HR-ESIMS (positive mode) m/z 317.1648 [$M + H$]⁺ (calcd for C₂₁H₂₁N₂O, 317.1648); ¹H NMR (500 MHz, C₆D₆): δ 8.55 (d, 2H, ³J = 5.5, H-1', H-5'), 7.93 (s, 1H, H-3), 7.60 (m, 4H, H-6, H-7, H-8, H-9), 7.25 (m, 2H, H-4, H-11), 6.55 (d, 2H, ³J = 6.0, H-2', H-4'), 2.45 (m, 2H, H-8', H-9'), 2.03 (m, 1H, H-6'), 1.25 (s br, 6H, H-7', H-8', H-9', H-10') ppm; ¹³C NMR (100 MHz, CDCl₃): δ 170.49 (C-1), 154.02 (C-3'), 149.71* (C-1', C-5'), 133.68 (C-2), 133.24 (C-5), 132.73 (C-10), 128.37 (C-11), 128.34 (C-9), 127.79* (C-6), 127.08* (C-3), 126.73* (C-4), 124.16* (C-7, C-8), 122.23 (C-2', C-4'), 42.06* (C-6'), 32.13* (C-7', C-8', C-9', C-10') ppm.

Synthesis of the amide 17a

0.34 ml of ethyl chloroformate (3.53 mmol) and 0.50 ml of TEA (3.53 mmol) were added to a suspension of 9-decenoic acid (0.5 g, 0.55 ml, 2.94 mmol) in CH₂Cl₂ and the reaction mixture was

left under agitation for 5 h at -15 °C until the complete disappearance of the starting compound. The resulting mixture was filtered at room temperature.

Morfolinpyperidine amine (0.99g, 5.88 mmol) and DMAP (30 mg, 0.25 mmol) were added to anhydride **13a**, which had not been isolated, for 15 hours at room temperature. When the reaction was over, the solvent was evaporated and the crude product (221.8 mg) was chromatographed with SEPHADEX using MeOH as eluent, providing an impure product (1.55 g), which was purified with alumina column chromatography using *n*-hexane/ethyl acetate (5:5) as eluents to give 0.490 g of compound **17a**.

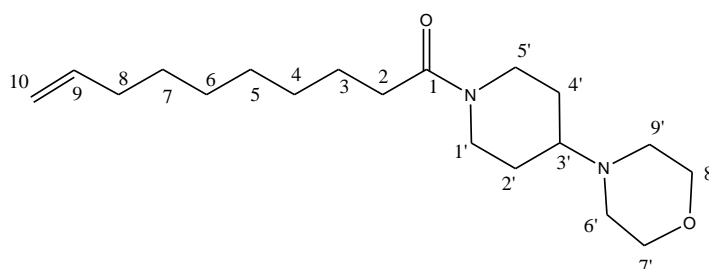


Figure 37. Structure of compound **17a**

Compound 17a orange oil, yield: 52% ; HR-ESIMS (positive mode) m/z 323.2693 [$M + H$]⁺ (calcd for C₁₉H₃₅N₂O₂, 323.2693); ¹H NMR (500 MHz, CDCl₃): δ 5.79 (m, 1H, H-9), 4.97 (dq, 1H, H-10), 4.91 (dq, 1H, H-10), 4.62 (d, 1H, ³*J* = 13.0, H-5'), 3.88 (d, ³*J* = 13.0, H-1'), 3.71 (t, 4H, H-7', H-8'), 3.0 (t, 1H, H-5'), 2.54 (t, 4H, H-6', H-9'), 2.35 (t, 1H, H-3'), 2.30 (t, 2H, H-2), 2.02 (q, 2H, H-8), 1.87 (t, 1H, H-2', H-4'), 1.60 (m, 2H, H-3), 1.38 (m, 2H, H-2'-H-4'), 1.30 (s, 8H, H-4/H-7) ppm; ¹³C NMR (100 MHz, CDCl₃): δ 171.41 (C-1), 139.13, 114.13, 67.14, 61.98, 49.74, 44.79, 40.82, 33.72, 33.35, 29.42, 29.23, 28.93, 28.83, 25.38 ppm.

Synthesis of the amide **17b**

0.33 ml of ethyl chloroformate (3.49 mmol) and 0.50 ml of TEA (3.49 mmol) were added to a suspension of 7-octenoic acid (0.2 g, 1.4 mmol) in CH₂Cl₂ and the reaction mixture was left under agitation for 5 h at -15 °C until the complete disappearance of the original product. The resulting mixture was filtered at room temperature.

Morfolinpyperidine amine (0.476 g, 2.8 mmol) and DMAP (30 mg, 0.082 mmol) were added to anhydride (**13b**), which had not been isolated, for 15 hours at room temperature. When the reaction was over, the solvent was removed in a vacuum and the crude product (1.02 g) was chromatographed with alumina column chromatography using *n*-hexane/ethyl acetate (5:5) as solvents to give 372.2 of compound **17b**.

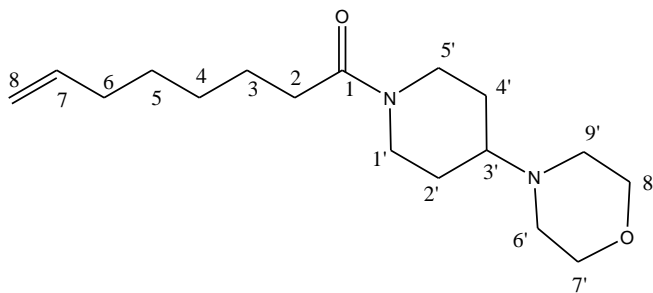


Figure 38. Structure of compound **17b**

Compound 17b. orange oil, yield: 90%; HR-ESIMS (positive mode) m/z 295.2381 $[M + H]^+$ (calcd for $C_{17}H_{31}N_2O_2$, 295.2380); 1H NMR (500 MHz, $CDCl_3$): δ 5.80 (m, 1H, H-7), 4.99 (dq, 1H, H-8), 4.93 (dq, 1H, H-8), 4.64 (d, 1H, $^3J = 14.5$, H-5'), 3.90 (d, 1H, $^3J = 14.5$, H-1'), 3.74 (s, 4H, H-7', H-8'), 3.01 (t, 1H, H-5'), 2.57 (t, 5H, H-1', H-6', H-9'), 2.44 (s br, 1H, H-3'), 2.32 (t, 2H, H-2), 2.05 (q, 2H, H-6), 1.89 (t, 1H, H-2', H-4'), 1.63 (m, 2H, H-3), 1.42 (m, 2H, H-2'-H-4'), 1.35 (m, 4H, H-4/H-6) ppm; ^{13}C NMR (100 MHz, $CDCl_3$): δ 171.32 (C-1), 138.78, 114.27, 67.14, 61.85, 49.74, 44.73, 40.78, 33.52, 33.22, 28.90, 28.87, 28.61, 27.92, 25.17 ppm.

Synthesis of the amide **17c**

0.16 ml of ethyl chloroformate (1.7 mmol) and 0.22 ml of TEA (1.7 mmol) were added to a suspension of decanoic acid (0.5 g, 2.91 mmol) in CH_2Cl_2 and the reaction mixture was left under agitation for 5 h at -15 °C until the complete disappearance of the starting compound. The resulting mixture was filtered at room temperature.

Morfolinpyperidine amine (0.99 g, 5.82 mmol) and DMAP (30 mg, 0.25 mmol) were added to anhydride (**13c**), which had not been isolated, for 15 hours at room temperature. When the reaction was over, the solvent was evaporated and the crude product (1.44 g) was chromatographed with alumina column chromatography using *n*-hexane/ethyl acetate (5:5) as solvents, to give 0.170 g of compound **17c**.

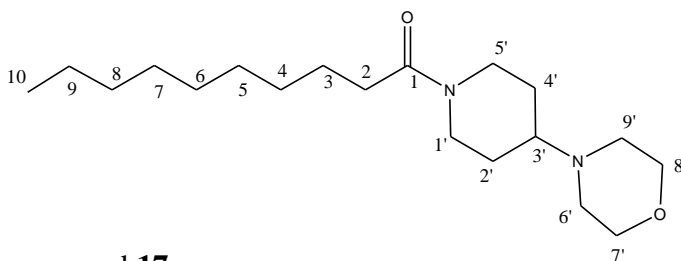


Figure 39. Structure of compound **17c**

Compound 17c. orange solid, yield: 18%; HR-ESIMS (positive mode) m/z 325.2854 $[M + H]^+$ (calcd for $C_{19}H_{37}N_2O_2$, 325.2850); 1H NMR (500 MHz, $CDCl_3$): 4.62 (d, 1H, $^3J = 13.5$, H-5'), 3.87 (d, $^3J = 12.0$, H-1'), 3.71 (t, 4H, H-7', H-8'), 3.0 (t, 1H, H-5'), 2.56 (t, 4H, H-6', H-9'), 2.42 (t, 1H, H-3'), 2.33 (t, 2H, H-2), 1.90 (t, 1H, H-2', H-4'), 1.62 (m, 2H, H-3), 1.41 (m, 2H, H-2'-H-4'), 1.27 (s, 12H,

H-4/H-9), 0.89 (t, 3H, H-10) ppm; ^{13}C NMR (100 MHz, CDCl_3): δ 171.47 (C-1), 117.31, 67.15, 62.00, 49.75, 44.80, 33.40, 31.84, 29.50, 29.44, 29.41, 29.24, 25.44, 22.63, 14.06 ppm.

Synthesis of the amide **17d**

0.140 ml of ethyl chloroformate (4.16 mmol) and 0.58 ml of TEA (4.16 mmol) were added to a suspension of octanoic acid (0.5 g, 0.55 ml, 3.47 mmol) in CH_2Cl_2 and the reaction mixture was left under agitation for 5 h at $-15\text{ }^\circ\text{C}$ until the complete disappearance of the starting compound. The resulting mixture was filtered at room temperature.

Morfolinpyperidine amine (1.2 g, 6.94 mmol) and DMAP (20 mg, 0.16 mmol) were added to anhydride (**13d**), which had not been isolated, for 15 hours at room temperature. When the reaction was over, the solvent was evaporated and the crude product (1.67 g) was chromatographed with alumina column chromatography using *n*-hexane/ethyl acetate (5:5) as solvents, to give 0.420 g of compound **17d**.

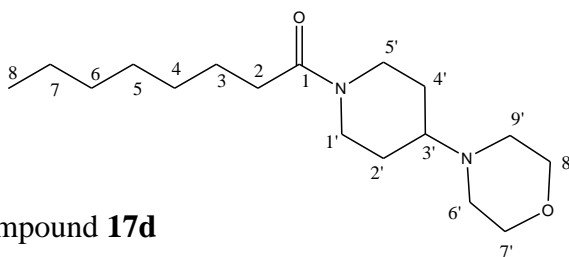


Figure 40. Structure of compound **17d**

Compounds 17d. yellow solid, yield: 41%; HR-ESIMS (positive mode) m/z 297.2531 $[\text{M} + \text{H}]^+$ (calcd for $\text{C}_{17}\text{H}_{33}\text{N}_2\text{O}_2$, 297.2537); ^1H NMR (500 MHz, CDCl_3): δ 4.65 (d, 1H, $^3J = 16.0$, H-5'), 3.91 (d, 1H, $^3J = 17.0$, H-1'), 3.75 (s, 4H, H-7', H-8'), 3.01 (t, 1H, H-5'), 2.57 (t, 5H, H-1', H-6', H-9'), 2.44 (s br, 1H, H-3'), 2.31 (t, 2H, H-2), 1.89 (m, 1H, H-2', H-4'), 1.61 (m, 2H, H-3), 1.42 (t br, 2H, H-2'-H-4') 1.28 (m, 8H, H-4/H-7), 0.88 (t, 3H, H-8) ppm; ^{13}C NMR (100 MHz, CDCl_3): δ 171.32 (C-1), 67.15, 61.97, 49.74, 44.79, 40.80, 33.73, 31.67, 29.44, 29.05, 28.93, 27.93, 25.42, 22.57, 14.02 ppm.

2.6.2 Citotoxic effect on HeLa cells

The cytotoxicity of the test compounds was evaluated by measuring the effect produced on cell morphology and cell growth in vitro. Cell monolayers were prepared in 24-well tissue culture plates and exposed to various concentrations of the compounds. Plates were checked by light microscopy after 24, 48 and 72 h. Cytotoxicity was scored as morphological alterations (e.g., rounding up, shrinking, detachment). The viability of the cells was determined by a tetrazolium-based colorimetric method using 3-(4,5-dimethylthiazol-2-yl)-2,5-diphenyltetrazolium bromide (MTT), as previously described.^{24,26} The 50% cytotoxic dose (CC₅₀) is the concentration of the compound that reduced the absorbance of the control sample by 50%.

2.6.2.1 Method of reducing the cytopathic effect

HeLa cells were seeded at a density of 1.8×10^4 cells per well (100 μ L) in 96-well culture plates. Studies on rhinoviruses were performed using the MEM Rega 3 medium associated with 2% FBS, 2 mM L-glutamine, 0.075% NaHCO₃ and 30 mM MgCl₂. The cells had the ability to adhere throughout the night, after which a series of dilutions of the compound and the viral inoculum were added. The cultures were then incubated for 3 days at 35° until a complete cytopathic effect (virus-induced CPE) was observed, in the untreated and in the control status of the infected viruses. After removal of the medium, 100 μ L of red-free MEM phenol containing 5% MTS-phenazine was added. After an incubation of 1h at 35°, the optical density of each well at 496 nm was determined with a microplate reader. The optical density values were converted to control percentage, the EC₅₀ was calculated by logarithmic interpolation as the concentration of compound that was effective against virus-induced CPE. In addition, the cell and morphology of the monolayer after the addition of each compound was evaluated microscopically for minor signs of CPE or adverse effects caused by the compound.

2.7 REFERENCES

1. Bochkov, Y. A.; Gern, J. E. Rhinoviruses and Their Receptors: Implications for Allergic Disease. *Current allergy and asthma reports* **2016**, 16, 30.
2. A Collaborative Report: Rhinoviruses- Extension of the Numbering System from 89 to 100. *Virology* **1987**, 159, 191-192.
3. Daryl Lamson, N. R., Vishal Kapoor, Zhiqiang Liu, Gustavo Palacios, Jingyue Ju, Amy Dean, Kirsten St. George, Thomas Briese, and W. Ian Lipkin. MassTag Polymerase-Chain-Reaction Detection of Respiratory Pathogens, Including a New Rhinovirus Genotype, That Caused Influenza-Like Illness in New York State during 2004–2005. *The Journal of Infectious Diseases* **2006**, 194, 1398-1402.
4. Palmenberg, A. C.; Rathe, J. A.; Liggett, S. B. Analysis of the complete genome sequences of human rhinovirus. *The Journal of allergy and clinical immunology* **2010**, 125, 1190-9; quiz 1200-1.
5. K. Andries, B. D., J. Snoeks, R. Willebrords, R. Stokbrockx and P.J. Lcwi A comparative test of fifteen compounds against all known human rhinovirus serotypes as a basis for a more rational screening program *Antiviral Research* **1991**, 16, 213-225.
6. Bochkov, Y. A.; Gern, J. E. Clinical and molecular features of human rhinovirus C. *Microbes and infection* **2012**, 14, 485-94.
7. Hayden, F. G. Rhinovirus and the lower respiratory tract. *Reviews in medical virology* **2004**, 14, 17-31.
8. Fuchs, R.; Blaas, D. Uncoating of human rhinoviruses. *Reviews in medical virology* **2010**, 20, 281-97.
9. Jacobs, S. E.; Lamson, D. M.; St George, K.; Walsh, T. J. Human rhinoviruses. *Clinical microbiology reviews* **2013**, 26, 135-62.
10. Bochkov, Y. A.; Watters, K.; Ashraf, S.; Griggs, T. F.; Devries, M. K.; Jackson, D. J.; Palmenberg, A. C.; Gern, J. E. Cadherin-related family member 3, a childhood asthma susceptibility gene product, mediates rhinovirus C binding and replication. *Proceedings of the National Academy of Sciences of the United States of America* **2015**, 112, 5485-90.
11. Rossmann, M. G.; Bella, J.; Kolatkar, P. R.; He, Y.; Wimmer, E.; Kuhn, R. J.; Baker, T. S. Cell recognition and entry by rhino- and enteroviruses. *Virology* **2000**, 269, 239-47.
12. Li, Y.; Cam, J.; Bu, G. Low-density lipoprotein receptor family: endocytosis and signal transduction. *Molecular neurobiology* **2001**, 23, 53-67.
13. Jeon, H.; Blacklow, S. C. Structure and physiologic function of the low-density lipoprotein receptor. *Annual review of biochemistry* **2005**, 74, 535-62.
14. Brown, M. S.; Goldstein, J. L. Familial hypercholesterolemia: defective binding of lipoproteins to cultured fibroblasts associated with impaired regulation of 3-hydroxy-3-methylglutaryl coenzyme A reductase activity. *Proceedings of the National Academy of Sciences of the United States of America* **1974**, 71, 788-92.
15. Goldstein, J. L.; Brown, M. S. Binding and degradation of low density lipoproteins by cultured human fibroblasts. Comparison of cells from a normal subject and from a patient with homozygous familial hypercholesterolemia. *The Journal of biological chemistry* **1974**, 249, 5153-62.
16. Kahn, J. S. Newly discovered respiratory viruses: significance and implications. *Current opinion in pharmacology* **2007**, 7, 478-83.
17. Sloots, T. P.; Whiley, D. M.; Lambert, S. B.; Nissen, M. D. Emerging respiratory agents: new viruses for old diseases? *Journal of clinical virology : the official publication of the Pan American Society for Clinical Virology* **2008**, 42, 233-43.
18. Gern, J. E. The ABCs of rhinoviruses, wheezing, and asthma. *Journal of virology* **2010**, 84, 7418-26.
19. James E. Gern, A. W. W. B. Association of Rhinovirus Infections with Asthma. *Clinical microbiology reviews* **1999**, 12, 9-18.
20. McManus, T. E.; Marley, A. M.; Baxter, N.; Christie, S. N.; O'Neill, H. J.; Elborn, J. S.; Coyle, P. V.; Kidney, J. C. Respiratory viral infection in exacerbations of COPD. *Respiratory medicine* **2008**, 102, 1575-80.
21. Gern, J. E.; Busse, W. W. Association of rhinovirus infections with asthma. *Clinical microbiology reviews* **1999**, 12, 9-18.
22. Gern, J. E.; Rosenthal, L. A.; Sorkness, R. L.; Lemanske, R. F., Jr. Effects of viral respiratory infections on lung development and childhood asthma. *The Journal of allergy and clinical immunology* **2005**, 115, 668-74; quiz 675.
23. Corne, J. M.; Marshall, C.; Smith, S.; Schreiber, J.; Sanderson, G.; Holgate, S. T.; Johnston, S. L. Frequency, severity, and duration of rhinovirus infections in asthmatic and non-asthmatic individuals: a longitudinal cohort study. *Lancet (London, England)* **2002**, 359, 831-4.
24. Rakes, G. P.; Arruda, E.; Ingram, J. M.; Hoover, G. E.; Zambrano, J. C.; Hayden, F. G.; Platts-Mills, T. A.; Heymann, P. W. Rhinovirus and respiratory syncytial virus in wheezing children requiring emergency care. IgE and eosinophil analyses. *American journal of respiratory and critical care medicine* **1999**, 159, 785-90.
25. Green, R. M.; Custovic, A.; Sanderson, G.; Hunter, J.; Johnston, S. L.; Woodcock, A. Synergism between allergens and viruses and risk of hospital admission with asthma: case-control study. *BMJ (Clinical research ed.)* **2002**, 324, 763.

26. Tarlo, S. M.; Broder, I.; Corey, P.; Chan-Yeung, M.; Ferguson, A.; Becker, A.; Rogers, C.; Okada, M.; Manfreda, J. The role of symptomatic colds in asthma exacerbations: Influence of outdoor allergens and air pollutants. *The Journal of allergy and clinical immunology* **2001**, 108, 52-8.
27. Rossmann, M. G. The structure of antiviral agents that inhibit uncoating when complexed with viral capsids. *Antiviral Res* **1989**, 11, 3-13.
28. Kearns, G. L.; Abdel-Rahman, S. M.; James, L. P.; Blowey, D. L.; Marshall, J. D.; Wells, T. G.; Jacobs, R. F. Single-dose pharmacokinetics of a pleconaril (VP63843) oral solution in children and adolescents. Pediatric Pharmacology Research Unit Network. *Antimicrob Agents Chemother* **1999**, 43, 634-8.
29. Abdel-Rahman, S. M.; Kearns, G. L. Single oral dose escalation pharmacokinetics of pleconaril (VP 63843) capsules in adults. *Journal of clinical pharmacology* **1999**, 39, 613-8.
30. Daniel C. Pevear, T. M. T., Martin E. Seipel, And James M. Groarke. Activity of Pleconaril against Enteroviruses. *Antimicrobial Agents And Chemotherapy* **1999**, 43, 2109-2115.
31. Diana, G. D.; Rudewicz, P.; Pevear, D. C.; Nitz, T. J.; Aldous, S. C.; Aldous, D. J.; Robinson, D. T.; Draper, T.; Dutko, F. J.; Aldi, C.; et al. Picornavirus inhibitors: trifluoromethyl substitution provides a global protective effect against hepatic metabolism. *Journal of medicinal chemistry* **1995**, 38, 1355-71.
32. Senior, K. FDA panel rejects common cold treatment. *The Lancet. Infectious diseases* **2002**, 2, 264.
33. A Placebo-Controlled Study of the Effects of Pleconaril Nasal Spray on Common Cold Symptoms and Asthma Exacerbations Following Rhinovirus Exposure. <http://www.clinicaltrials.gov>. NCT00394914
34. Andries, K.; Dewindt, B.; Snoeks, J.; Willebrords, R.; van Eemeren, K.; Stokbroekx, R.; Janssen, P. A. In vitro activity of pirodavir (R 77975), a substituted phenoxy-pyridazinamine with broad-spectrum antipicornaviral activity. *Antimicrob Agents Chemother* **1992**, 36, 100-7.
35. Frederick G. Hayden, K. A., And Paul A. J. Janssen. Safety and Efficacy of Intranasal Pirodavir (R77975) in Experimental Rhinovirus Infection. *Antimicrobial Agents And Chemotherapy* **1992**, 36, 727-732.
36. Frederick G. Hayden, G. J. H., Diane H. Woerner, Gerald F. Eisen, Monique Janssens, Paul A. J. Janssen, And Koen Andries. Intranasal Pirodavir (R77,975) Treatment of Rhinovirus Colds. *Antimicrobial Agents And Chemotherapy* **1995**, 39, 290-294.
37. Lacroix, C.; Laconi, S.; Angius, F.; Coluccia, A.; Silvestri, R.; Pompei, R.; Neyts, J.; Leyssen, P. In vitro characterisation of a pleconaril/pirodavir-like compound with potent activity against rhinoviruses. *Virology journal* **2015**, 12, 106.
38. Tijmsma, A. F., D.; Tucker, S.; Hilgenfeld, R.; Froeyen, M.; Leyssen, P.; Neyts, J.; The Capsid Binder Vapendavir and the Novel Protease Inhibitor SG85 Inhibit Enterovirus 71 Replication. *Antimicrobial Agents and Chemotherapy* **2014**, 58, 6990 – 6992.
39. Rotbart, H. A. Antiviral therapy for enteroviruses and rhinoviruses. *Antiviral Chemistry & Chemotherapy* **2000**, 11, 261-271.
40. Fois, B.; Bianco, G.; Sonar, V. P.; Distinto, S.; Maccioni, E.; Meleddu, R.; Melis, C.; Marras, L.; Pompei, R.; Floris, C.; Caboni, P.; Cottiglia, F. Phenylpropenoids from *Bupleurum fruticosum* as Anti-Human Rhinovirus Species A Selective Capsid Binders. *J Nat Prod* **2017**, 80, 2799-2806.
41. Da Costa, L.; Roche, M.; Scheers, E.; Coluccia, A.; Neyts, J.; Terme, T.; Leyssen, P.; Silvestri, R.; Vanelle, P. VP1 crystal structure-guided exploration and optimization of 4,5-dimethoxybenzene-based inhibitors of rhinovirus 14 infection. *European journal of medicinal chemistry* **2016**, 115, 453-462.
42. Roche, M.; Lacroix, C.; Khoumeri, O.; Franco, D.; Neyts, J.; Terme, T.; Leyssen, P.; Vanelle, P. Synthesis, biological activity and structure-activity relationship of 4,5-dimethoxybenzene derivatives inhibitor of rhinovirus 14 infection. *European journal of medicinal chemistry* **2014**, 76, 445-459.

3 Antibiotics

The discovery of antibiotics is rightly considered one of the most significant health-related events of modern times. As a matter of fact, these natural products, biosynthesized by microorganisms, are able to prevent the growth of bacteria and, thus, cure infectious diseases. The definition of “antibiotic,” as first proposed by Selman Waksman, the discoverer of streptomycin, is a generic term used to describe any class of organic molecule that inhibits or kills microbes by specific interactions with bacterial targets, without any specific classification.¹

Paul Ehrlich, since he promoted the use of salvarsan, as a new scientific approach to the treatment of infectious diseases of humans, can be considered the father of chemotherapy era. Afterwards, in 1928, Alexander Fleming discovered the antibiotic penicillin and only in 1940, a bacterial penicillinase was identified by two members of the penicillin discovery team.² The history of antibiotics discovery and resistance can be divided in four phases: the dark ages, the golden ages, the lean years and the disenchantment period.³ The first period was also called pre-antibiotic era. It included Semmelweis’s advice of hand washing as a way of avoiding infection; it ended with the discovery of the first effective antibiotic sulphonamides and it is directly connected to the development of specific mechanisms of resistance which has restricted their therapeutic use. During the golden ages, most of the antibiotics, such as tetracycline, rifamycin, quinolone and aminoglycoside families, used today, were discovered, to name just a few. In contrast, the lean years were characterised by a low rate of new antibiotic discovery and the attention was focused on pharmacologic, biochemical, target, mode-of-action and genetic studies, in order to understand and improve the use of antibiotics. Furthermore, in the middle of 1960’s the foundation of the FDA Office of New Drugs, after the thalidomide disaster, established stricter requirements for novel compounds, which slowed the registration of new drugs, including antibiotics. In addition, the discovery of new drugs is often more problematic than for other therapeutic areas. It is due to the limited antibiotic penetration into bacterial cells, resistance mechanisms, such as efflux pumps, and drug-inactivating enzymes, and to the required high concentrations that sometimes provokes side effects. These are some of the biggest complications in antibiotic development.^{4,5} In 2000 started the disenchantment period. This era was characterised by the failure of the investment in genome-based methods and lead many companies to discontinue their antibacterial discovery programs.³

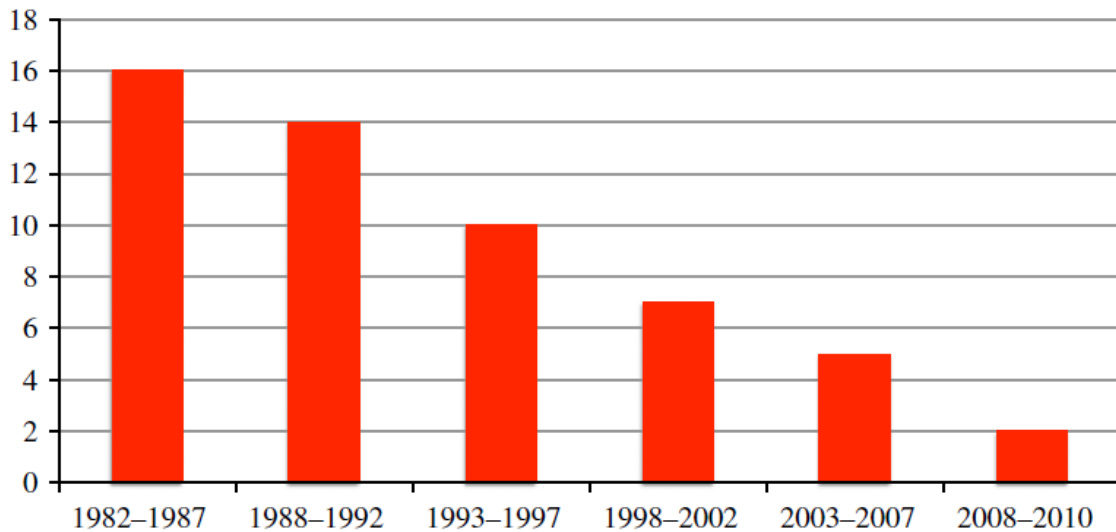


Figure 1. New antibiotics approved for human use in the last 30 years⁶

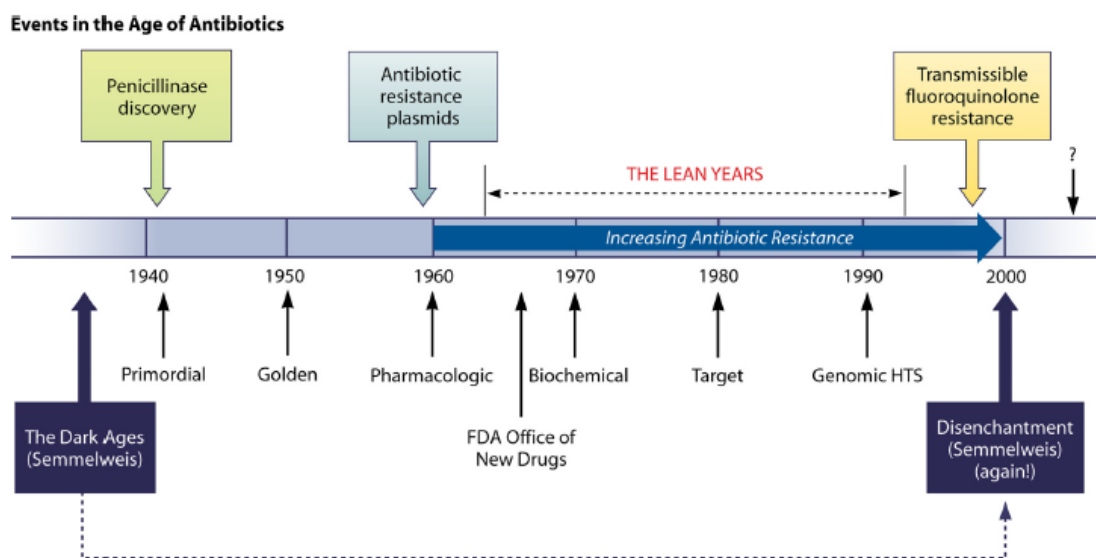


Figure 2. History of antibiotic discovery and concomitant development of antibiotic resistance³

In the last 60s, an enormous amount of antibiotics has been produced and employed for the treatment of numerous infectious diseases. They have provided better costs and encouraged inappropriate use in medical practice, such as underdosing, prescriptions to treat minor bacterial infections or viral infections⁷ and uncontrolled use in animals to increase meat production.⁸ Moreover, outer membrane of some Gram-negative bacteria, blocks antibiotics access to their targets inside the cell and leads to the development of resistant strains.⁹ Another important aspect of bacteria-resistance is that the

antibacterials research is still focused on improved versions of existing molecules and not on novel targets. These events led to the development of antibiotic-resistance and economic burdens in term of period and cost of hospital care. The term “superbugs” is used to describe microbes with high morbidity and mortality due to multiple mutations, which increased resistance to the antibiotic classes recommended for their treatment; sometimes, super resistant strains have acquired increased virulence and transmissibility.³ Antibiotic resistance is a huge problem over the world. For this reason, in 2014, WHO (World Health Organization) understood the urgent need for a global surveillance system, which was activated in 2015 and was called Global Antimicrobial Surveillance System (GLASS). It works together with WHO Collaborating Centres and existing antimicrobial resistance surveillance networks and it based its studies on the experience of other WHO surveillance programmes in order to monitor antimicrobial resistance (AMR) at a global level.

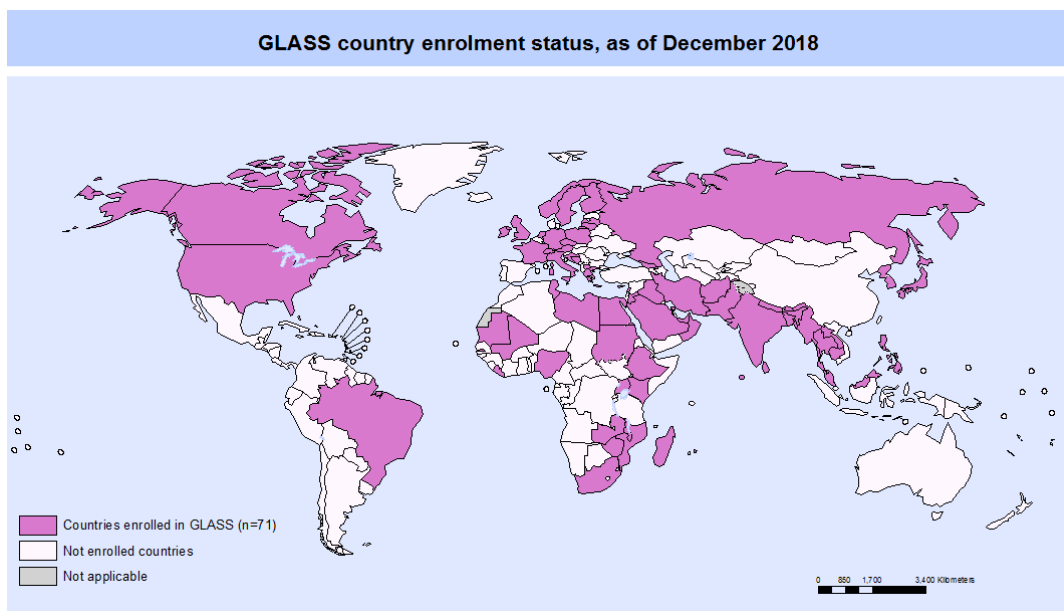


Figure 3. Global distribution of Antimicrobial Surveillance System (GLASS)

Compared to 2017, GLASS has revealed a 64% increase in country enrolment and more than twice the number of countries submitting AMR data in 2018, indicating a collective understanding and engagement toward AMR.^{10, 11} A report of 2017 indicated that at least 700,000 people die of resistant bacterial infections globally every year and it is estimated that in 2050 the value would rise up to 10 million. WHO analysed many potential solutions to combat AMR, which included investment in research and development of new antibiotics, reduction of antibiotic use in rearing of livestock and vaccination.¹² It has been observed that the prophylactic use of bacterial vaccines prevents bacterial

infections, thus antibiotic prescriptions, whereas viral vaccines could reduce inappropriate antibiotic prescriptions for a viral disease and limit superinfections that require antibacterial therapy.¹³ There are several benefits from the vaccination. First of all, vaccines work by training the immune system to recognize and respond to a pathogen, avoiding infection or decreasing disease severity.¹⁴ Secondly, immunization could prevent millions of deaths every year, a number that could grow if people continue to be vaccinated.¹⁵ For instance, if a population is not immunized against bacteria, most members of the population are susceptible to the pathogen. The infection of a susceptible individual can be rapidly spread to other susceptible individuals and require antibiotic therapy, which, sometimes lead to antibiotic resistance bacteria, over the world. On the contrary, if a large number of population have been vaccinated, there will be lower antibiotic use, preventing and reducing the development of AMR. Besides, many vaccines also protect unvaccinated individuals through a process called herd immunity; in this way transmission of the infection is interrupted and limited to a small number of susceptible people who had not been immunized or immunocompromised.¹⁶

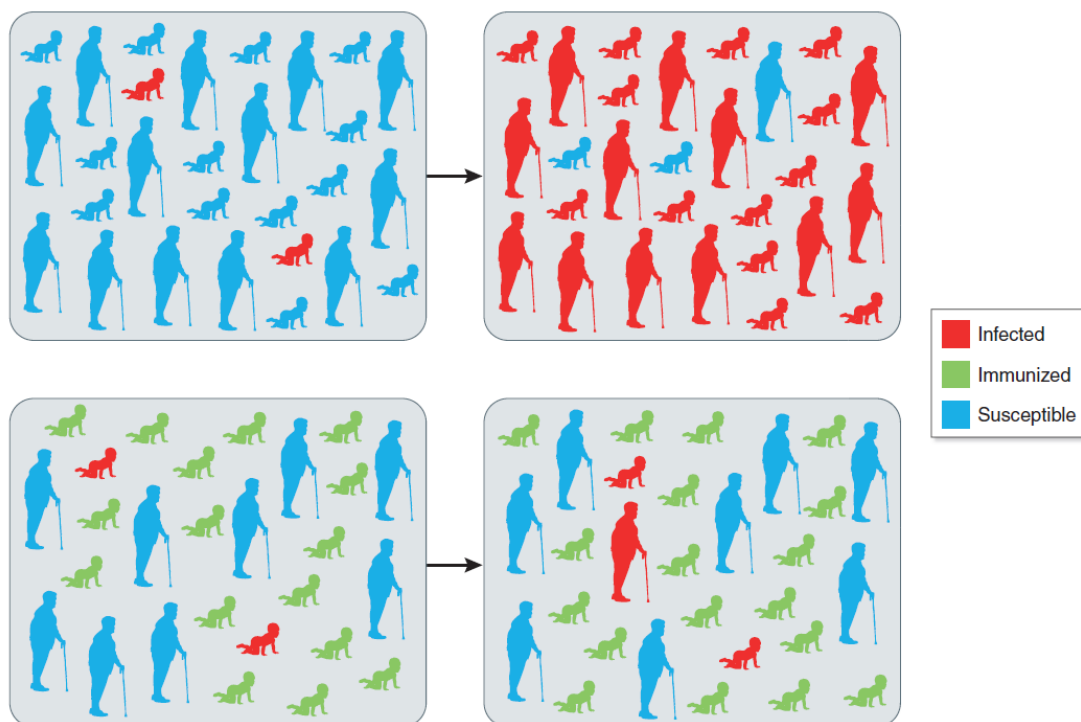


Figure 4. Susceptibility to the bacteria of immunized and not immunized population.

Viral vaccines, such as influenza vaccines, are able to decrease secondary bacterial infection, like pneumonia and otitis media¹⁷ and thus prevent antibiotic use, sometimes inappropriately prescribed.

The table below presents global antibiotic resistance data associated with major bacterial pathogens, from 2000 to 2014, and shows that Gram-negative Enterobacteriaceae, such as *Escherichia coli*, *Klebsiella pneumoniae*, *Enterobacter* spp., are the greatest threat to human health with the highest levels of resistance.^{18, 19}

Table 1. Global antibiotic resistance data associated with major bacterial pathogens (2000-2014)

Pathogen	Resistance rate				
	United States	S. Africa	UK	India	Australia
<i>S. pneumoniae</i>	17–34	ND	7–8	ND	ND
<i>S. aureus</i>	0–45	0–29	0–11	2–94	0–18
<i>E. coli</i>	1–55	0–84	0–66	11–92	0–55
<i>Enterobacter</i> spp.	5–88	3–100	ND	ND	3–30
<i>K. pneumoniae</i>	8–22	2–68	0–14	2–80	0–9
<i>P. aeruginosa</i>	5–26	1–35	3–14	0–69	ND
<i>A. baumannii</i>	6–49	2–41	2–9	3–90	ND
<i>M. tuberculosis</i>	0–2.9	3–5.9	0–2.9	ND	0–2.9
<i>N. gonorrhoeae</i>	0.1–3	0.1–70	0–70	0.1–70	0.1–70

The European Antimicrobial Resistance Surveillance Network (EARS-Net) is the main EU surveillance system for AMR. A group of 30 countries, composed of all EU Member States and two EEA countries (Iceland and Norway) reported AMR data for 2017 to EARS-Net before the end of August 2018.²⁰ These data serve as important indicators on the occurrence and spread of AMR in Europe. Among all, *E. coli*-AMR is one of the most spread *E. coli* is a Gram-negative bacterium usually present on the intestinal microbiota of humans, but it is also a common cause of severe infections. EARS-Net reported that in 2017, the highest resistance percentage toward *E. coli* was for aminopenicillins (58.7%), followed by fluoroquinolones (25.7%), third-generation cephalosporins (14.9%) and aminoglycosides (11.4%).

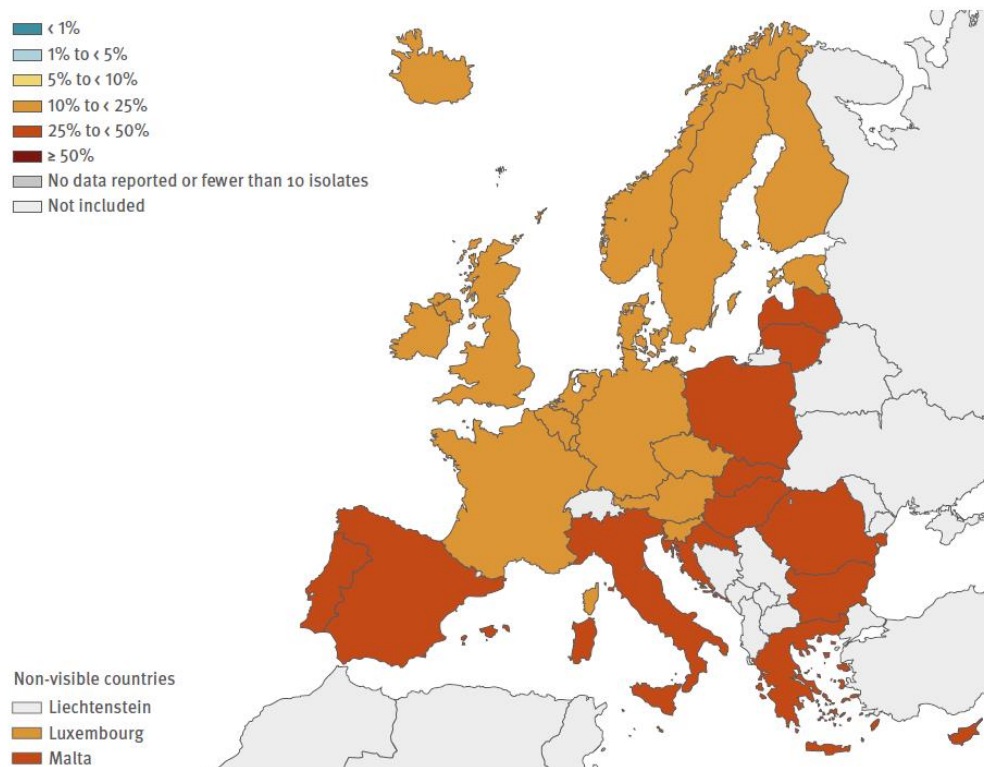


Figure 5. Percentage of *E. coli* resistance to fluoroquinolones, by country, EU/EEA countries in 2017

The graphic above shows that the states at the Mediterranean area, such as Italy, Spain, Portugal, Malta, Greece, and the Eastern Europe countries have the highest value of resistance to fluoroquinolones, between 25 to 50%.

A similar distribution has been perceived in *S. aureus* resistance (MRSA). *S. aureus* is a Gram-positive bacterium that frequently colonises the skin; however, it is also an opportunistic microorganism, leading cause of skin, soft tissue, bone and bloodstream infections. In 2017, the percentage of MRSA was around 16.9%, significantly lower than 2014. As observed among the states of Mediterranean area.

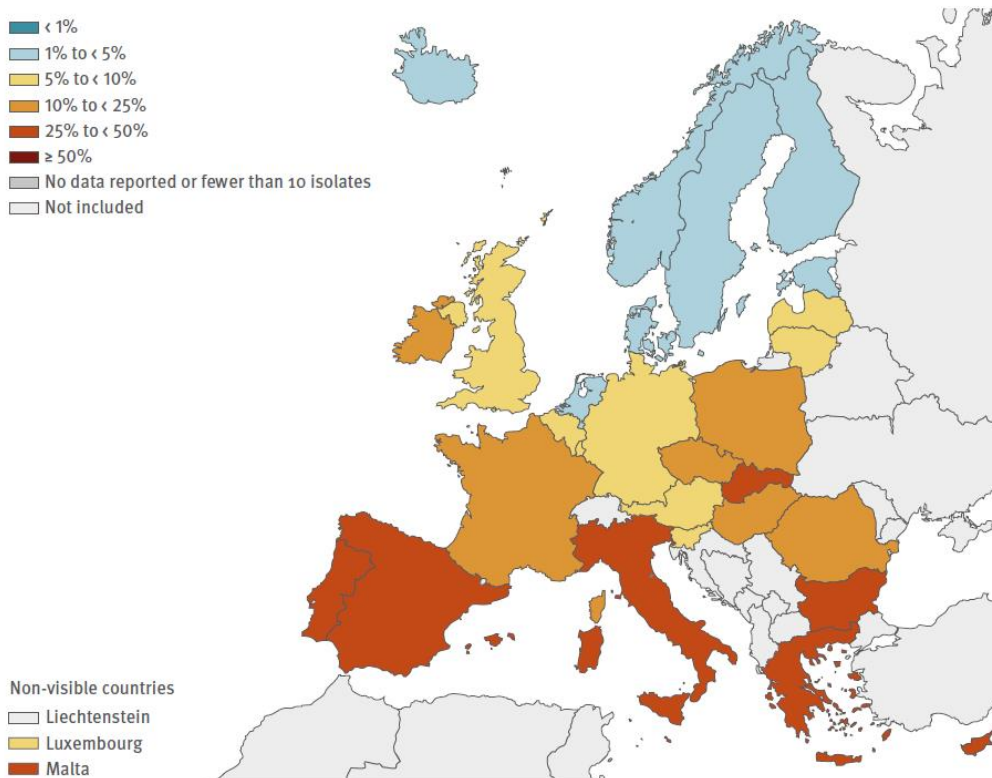


Figure 6. Percentage of *S. aureus* resistance to to meticillin (MRSA), by country, EU/EEA countries in 2017

Italy showed one of the highest percentage of antibacterial resistance against Gram + and Gram- bacteria. For instance, percentage of MRSA, in Italy, is about twice compared to the other EU countries, with around 40% versus 22%, *E. coli* resistance to the third-generation cephalosporins presents values of 21% for Italy against 11% of EU states.²⁰

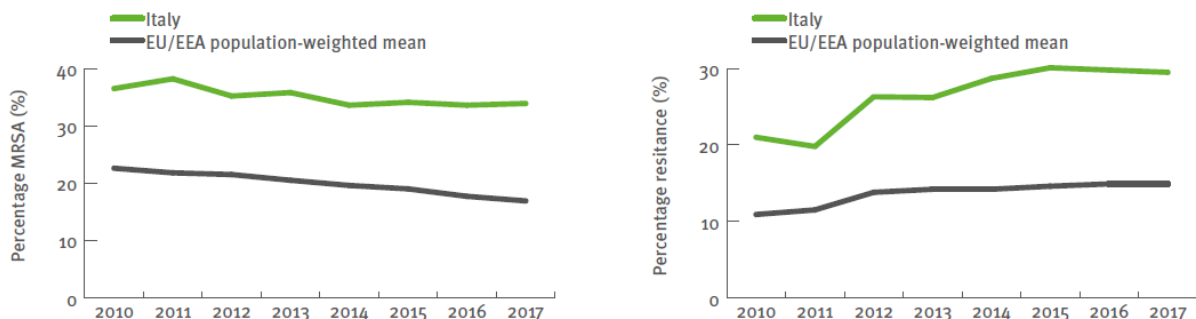


Figure 7: MRSA resistance, on the left, and *E. coli* resistance to third-generation cephalosporins, on the right

This problem is intensified by a poor global initiative to develop new antibacterial agents. However, some industrialised countries, such as the UK, have raised political awareness of the grave risk to national and international health and most governments dedicate approximately 1% of their GDP to research and development new antibacterial drug.⁶ Publically funded patents for new NCEs often remain unexploited because of insufficient funding available to support the development phase. Nevertheless, some public-private partnerships, such as Europe's Innovative Medicines Initiative (IMI), may remove this obstacle supporting the research. Moreover, the emerging economies of Brazil, Russia, India, China and South Africa (the BRICS), which are all home to excellent pharmaceutical companies that produce generic medicines, could encourage and finance drug development. It is central to reduce the costs and encourage companies to invest in new drugs.⁶ As a matter of fact, it is reported that it takes more than 10 years to bring a new drug to market and the costs incurred are well in excess of one billion dollars.²¹ Additionally, phase III clinical trials, which is crucial to ensure patient safety, account for over half the cost of drug development.²² Therefore, various forms of incentives could be provided, including interest-free credits, tax reductions from national governments, cash rewards from international funds and extended patent life for products deemed essential in healthcare sector.²³

Consequently, developing new drugs to solve antibacterial infections have global importance and need to be supported with the knowledge that microbial evolution will constantly continue and drug resistance will always emerge as a result of natural selection. These opportunities could ensure that future generations benefit from antibiotics as our has done.⁶

3.1 Mechanism of antibiotic resistance

The evolution of resistant strains is a natural phenomenon by which microorganisms respond towards antibiotics. Indeed, during DNA replication several mutation are likely and casual, at a frequency of $\sim 10^{-9}$ to 10^{-10} per gene and copying errors may lead to the partial or complete deletion of individual genes.²⁴ As a result, some proteins that are targets of antibacterials can be modified, drug-inactivation or efflux systems may be up- or down-regulated, and uptake pathways (porins and active transporters) can be modified. In addition, DNA transfer, via plasmids, play an important role on the dissemination of resistance.²⁵ Within plasmids, resistance genes are often carried by transposons. Some transposons are directly transferred between bacteria, especially among Gram + ones, whereas MRSA staphylococci use lysogenic bacteriophages as a vehicle.²⁶ Gram – bacteria use integrons, which are natural recombination systems that facilitate the acquisition and expression of resistance determinants

behind a single promoter, as observed in sulfonamides (sul1), and streptomycin (aadA3).²⁷ The dissemination of plasmids, transposons, and integrons among bacteria and species give rise to so-called gene epidemics. Many of the resistance determinants discovered on plasmids originated in the chromosomes of other species, for instance the plasmid-mediated SHV β -lactamases are derived from the chromosomal β -lactamases of *Klebsiella pneumonia* and several CTX-M cefotaximases are chromosomal escapes from *Kluyvera* spp.²⁸ Many plasmids and transposons transmit multiple resistance genes conferring resistance to different antibacterials.

3.2 Targets of antibacterial drugs

Antibiotic are divided according to the step of cell life inhibited; indeed, they can interfere with cell-wall biosynthesis, protein biosynthesis, RNA polymerase, inhibition of replication systems, the folic acid metabolism or they could modify the membrane structure.

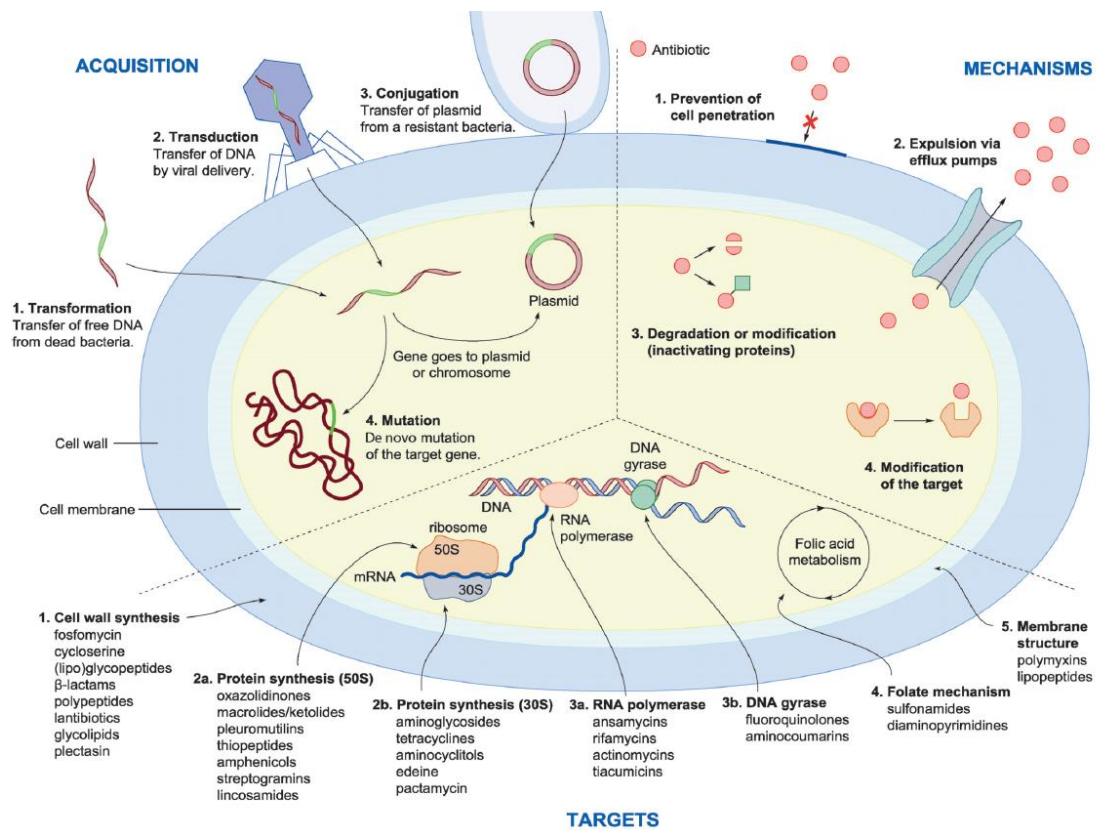


Figure 8. The four resistance acquisition pathways, the four main mechanisms of resistance, and the five main targets for antibiotics²⁹

3.3 DNA gyrase

Among all antibiotic targets, I focused my studies on DNA gyrase, which has attracted attention since its discovery in 1976, when it was first isolated from *E. coli*³⁰ and identified as a target of the aminocoumarin class of antibacterial compounds, e.g. novobiocin.

DNA gyrase belongs to the family of topoisomerases. DNA topoisomerases are enzymes that catalyse changes in the topology of DNA,^{31,32} indeed they can interconvert relaxed and supercoiled forms or introduce and remove chains and knots.³³ DNA topoisomerases are classified in two types, type I which catalyse the transient breakage of one strand, while type II breaks both strains of DNA.³⁴ All enzymes relax supercoiled DNA, but only DNA gyrase (a type II enzyme) can also introduce negative supercoils, after ATP hydrolysis.^{35,36} Eukaryotic type II topoisomerases such as human or yeast topo II, are large single-subunit enzymes (~170 kDa) and are active as homodimers, while prokaryotic enzymes, like gyrase and topoisomerase IV, are heterotetrameric proteins composed of two subunits: A and B in the case of gyrase, which associate to form an A₂B₂ complex in the active enzyme.³⁷ This difference in structure is necessary for the selectivity toward prokaryotic enzymes. Prokaryotic DNA gyrase is composed of two A subunits (GyrA) and two B subunits (GyrB), whereas topoisomerase IV consists of two C subunits (ParC) and two E subunits (ParE), which are homologous to GyrA and GyrB, respectively.³⁸ The GyrA and ParC subunits are involved in DNA transit, while the GyrB and ParE subunits contain an ATP-binding domain.³⁷

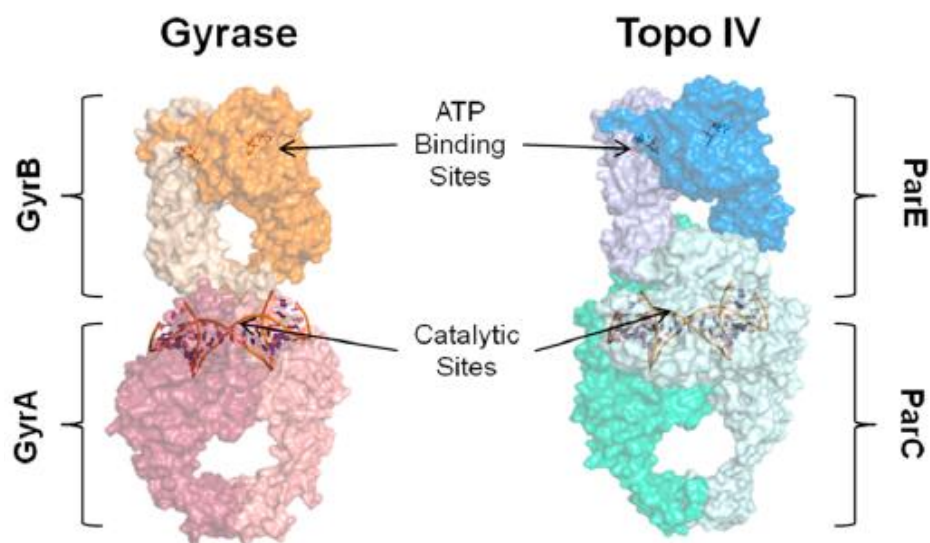


Figure 9. Models for bacteria topoisomerase II tetramers: DNA gyrase (left) and topoisomerase IV (right)³⁹

3.3.1 Mechanism of DNA supercoiling by DNA gyrase

The mechanism of action of DNA gyrase is known as the “two-gate mechanism”.^{40,41} DNA gyrase possesses three interfaces: the N-terminal domain of GyrB (N-gate), the GyrA–GyrB–DNA interface, where the DNA is cleaved (DNA gate), and the C-terminal area of coiled coils called exit gate (E).

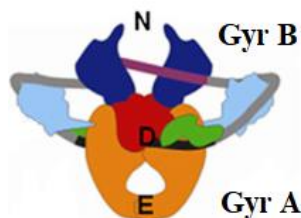


Figure 10. Structure of DNA gyrase

The mechanism of cleavage could be summarised in the following steps:

1. the DNA G (or gate) segment associates with the enzyme and DNA is wrapped around the enzyme in a right-handed supercoil of ~ 130 base pairs.⁴²
2. Wrapping of DNA on the gyrase C terminal domains facilitates a T segment, belonging to the same DNA molecule, to reach the N over the G segment, in preparation for strand passage.⁴³
3. After ATP binding, GyrB dimerises and traps the T segment. The G segment is transiently cleaved forming DNA–phosphorus tyrosyl bonds 4 bp apart, resulting in the covalent attachment of GyrA to the DNA.^{44,45}
4. Hydrolysis of one ATP is essential for GyrB rotation and for the passage of the T segment through the cleaved G segment.
5. The last step consists in release of the T segment and in relegation of the G segment, introducing two negative supercoils into the DNA molecule. Hydrolysis of the second ATP produces ADP, which opens the N gate and resets the enzyme for the next supercoiling cycle.

The gyrase supercoiling reaction is a complex process, which has become an attractive target for discovery of antibacterial agents.

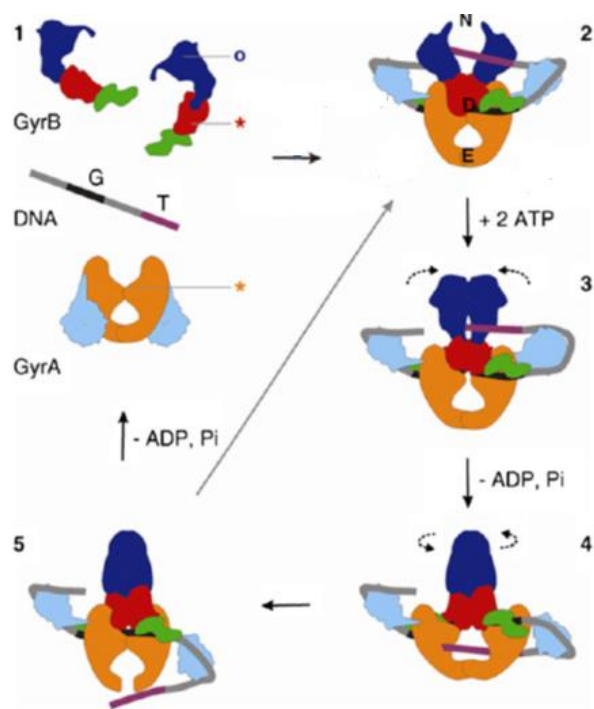


Figure 11. DNA gyrase mechanism of action³⁸

3.4 DNA gyrase inhibitors

There are two main mechanisms which are responsible of antibacterial activity of DNA gyrase inhibitors. The first consists in the stabilisation of the covalent enzyme–DNA complex, blocking GyrA subunit; quinolones, which interrupts DNA cleavage-relegation, are an example. The second mechanism which is present in compounds such as novobiocin, involves the inhibition of enzymatic activity by targeting ATP-binding sites at the GyrB. In addition, other compounds, like simocyclinones, could prevent DNA binding.

3.4.1 Quinolones

Fluoroquinolones (FQs), are so far the most interesting antibacterials targeting DNA gyrase. One of the most known FQ is ciprofloxacin. They originated from nalidixic acid, by-product discovered during the synthesis of chloroquine.⁴⁶ The first-generation quinolones, nalidixic acid and oxolinic acid, displayed weak activity, while fluoroquinolones, such as norfloxacin and ciprofloxacin (second generation), levofloxacin (third generation), moxifloxacin and gemifloxacin (fourth generation) showed clinical and commercial success, due to its high potency against bacteria.^{47,48,49} Quinolones inhibit the DNA supercoiling and relaxation stabilising a covalent complex with GyrA and 5' ends of

the broken DNA.^{50,51} The aromatic rings are found to be stacked against the DNA bases at the site of DNA cleavage, while Ser and Asp (or Glu) residues in GyrA and Mg²⁺ ion⁵² are involved in the binding. Furthermore, it has been demonstrated that 3-oxo-4-carboxylic acid moiety binds the active site, and replacement of the carboxylic acid group results in reduction of the potency.^{53,54} However, the exact interactions of the drugs with the proteins are not completely clear.³⁸

3.4.2 Aminocoumarins

Aminocoumarins are well-known as the ‘Cinderellas’ of the gyrase inhibitors, compared to fluoroquinolones.³⁸ Although they bind to gyrase, they did not show significant clinical success. For instance, aminocoumarins, novobiocin, clorobiocin and coumermycin A1, are natural products isolated from *Streptomyces* species, which contain a 3-amino-4,7-dihydroxycoumarin ring with some substitution in position 8’ and 3’. These antibacterial compounds have been known since the 1950s for their inhibitory activity on DNA synthesis in bacteria. Only later was discovered the enzymatic inhibition of ATPase by competing with ATP in GyrB subunit,⁵⁵⁻⁵⁷ in a domain that does not bind ATP by itself, but overlap the site and prevent the ATP-binding,⁵⁸ despite aminocoumarins have limited structural resemblance to ATP. It is noteworthy that mutations conferring resistance to aminocoumarins tend to inactivate the enzyme due to their proximity to the ATPase active site.³⁸ Nevertheless coumarins were not considered promising drugs due to their poor activity against Gram-negative bacteria, high cytotoxicity and low solubility. For instance, novobiocin was the only GyrB inhibitor to be used in clinical practice, which has progressed beyond phase I clinical trials.³⁹ Unfortunately, it was rapidly withdrawn from the market due to its toxicity and to the high rate of resistance development. Several studies focused on the development of novobiocin analogues were unsuccessful due to their adverse pharmacokinetic profile and lack of activity.⁵⁹

3.4.3 Simocyclinones

Simocyclinones are classified as hybrid antibiotics containing both aminocoumarin and polyketide elements. SD8 is known as ‘two headed’ antibiotic because, through its elements, it targets two separate binding pockets in the N-terminal domain of GyrA, avoiding DNA binding.⁶⁰ Moreover, Sissi *et al.*⁶¹ have found a second binding site in the C-terminal domain of GyrB. Although simocyclinones possess modest antibacterial activity against Gram-positive and are ineffective against Gram-negative,^{62,63} they appear to have higher potency in clinical settings.⁶² Indeed, they showed inhibitory activity toward bacterial gyrase^{64,60} of *E. coli* and *S. aureus*.⁶⁵

3.4.4 Use of Quinolones

Since the discovery of nalidixic acid, in 1962, FQs have been introduced in clinical for the treatment of urinary infections.⁶⁶ Nowadays, FQs, are among the most common drugs approved for the treatment of upper and lower respiratory infections, and some skin, bone, soft tissue infections and community acquired pneumonia.^{67,68} In addition, 4-quinolones displayed also antitumor, antitubercular, anti-HIV and antimalarial activities.^{69,70} However, in the last five decades, antibiotic resistance develops rapidly and spreads widely throughout the world, creating urgent needs to develop new antibacterial agents. The main strategy was to synthesize new analogues or modify existing FQs with lower or without cross-resistance to the existing antibiotics. Therefore, many ciprofloxacin-based derivatives have been synthesized and some of them exhibited promising potency. It has been demonstrated that carboxylic acid plays a key role, indeed modification at C-3 position resulted in loss of the activity,^{71,72} whereas when carboxylic acid was replaced by an aromatic amide group, significant enhancements of potency are observed.⁷³ Furthermore, the derivatives with an ester group exhibited greater dermal penetration and higher efficacy in the treatment of methicillin susceptible *S. aureus* (MSSA) and MRSA.⁷⁴

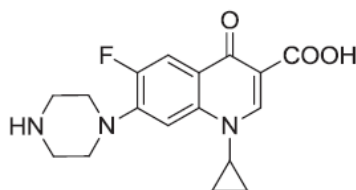


Figure 12. Structure of ciprofloxacin

Several FQs substituted at N-1 position of core structure and at N⁴-position of piperazinyl exhibited considerable activity.^{75,76} For instance, the introduction of N⁴-carboxymethyl increases the antibacterial activity slightly,⁷⁷ while N⁴-formyl reduces the potency.⁷⁸ Moreover, acylation of the piperazinyl nitrogen showed highly effect against Gram-positive and Gram-negative bacteria and several derivatives possess good activity against MRSA and *Bartonella* species.⁷⁹ The arene sulfonyl moiety linked in N⁴-position presented comparable activity to ciprofloxacin, having the same binding mode with additional classical and non-classical hydrogen bonds,⁸⁰ while carboxamide derivatives seem to be less potent than ciprofloxacin.⁸¹ In addition, it was observed that chloro-substituted phenethyl group attached to a piperazine ring displayed excellent in vitro activity against Gram-positive and Gram-negative, which was sometimes superior to the others,⁸² indicating that piperazine NH substitution with moieties of different size is tolerated without loss of gyrase A inhibition.

3.4.5 Novel DNA GyrB inhibitors

Despite new GyrB and dual targeting GyrB/ParE inhibitors have been already identified, none have advanced into the clinic. Several of these compounds, such as 5-(3-pyrazolyl)-thiazoles,⁸³ azaindoles,⁸⁴ pyrrolo[2,3-d]pyrimidines,^{85,86} imidazo[1,2-a]pyridine ureas,⁸⁷ benzimidazole ureas⁸⁸ and pyrrolamides^{89,90} target the ATP-binding site of GyrB and/or ParE. Most of the dual inhibitors displayed potent MICs values against Gram positive, but only few showed activity against Gram negative bacteria.

Based on previous work, the research group of the Faculty of Pharmacy of the University of Ljubljana has been investigating some novel DNA Gyrase B inhibitors. For instance, Tomašič *et al.*,⁹¹ starting from a library of marine alkaloid oroidin analogues, identified low micromolar inhibitors of *E. coli* DNA gyrase based on the 5,6,7,8-tetrahydroquinazoline and 4,5,6,7-tetrahydrobenzo[1,2-*d*]thiazole scaffolds. Structure-based optimization of these compounds led to inhibitors with improved activity in the nanomolar range, in which tetrahydrobenzothiazole derivatives result more potent than tetrahydroquinazoline ones. Supercoiling assay, in agreement with ATPase assay, SPR experiment and SAR, suggested that these inhibitors bind to the ATP-binding site of the *E. coli* enzyme, while they display a weaker inhibition of *S. aureus* DNA gyrase. Subsequently, 2-(2-aminothiazol-4-yl)acetic acids designed as ring-opened analogues of the 4,5,6,7-tetrahydrobenzo[1,2-*d*]thiazoles, displayed lower DNA gyrase inhibition with IC₅₀ values between 15.9 and 169 μM against Gram-positive and Gram-negative bacteria. However, docking studies suggested similar binding modes for benzothiazoles and thiazoles, with two hydrogen bonds with Asp73 and Arg136.⁹²

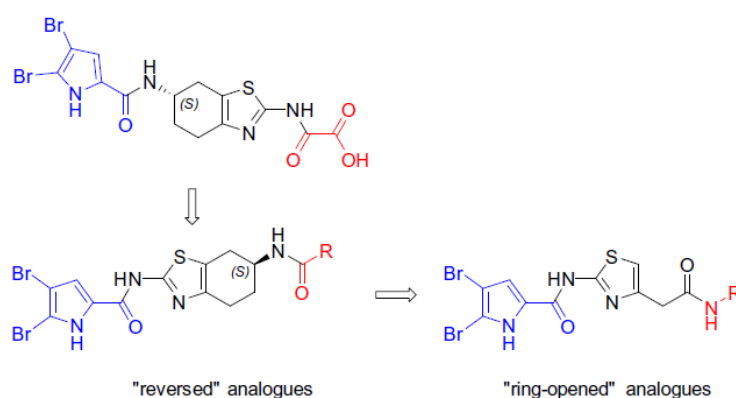


Figure 13. Analogues of the alkaloid oroidin

Then, based on the knowledge that Asp73 sidechain carboxylate of DNA gyrase forms two hydrogen bonds with the two NH groups of the ethylurea moiety,⁹³ while the nitrogen atom of the central scaffold forms an additional hydrogen bond with a conserved water molecule, some ethylurea derivatives of 4,5,6,7-tetrahydrobenzo[1,2-d]thiazole-2,6-diamine, 2-(2-aminothiazol-4-yl)acetic acid, and benzo[1,2-d]thiazole-2,6-diamine were synthesized. The results of the *in vitro* *E. coli* DNA gyrase supercoiling assay showed that the most potent were benzo[1,2-d]thiazoles-based ethylurea derivatives with an IC₅₀ values in the low micromolar range, while other series of compounds were only weakly active or inactive, probably due to the lack of cation- π interaction between the Arg76 side-chain and the ring of these inhibitors. Antibacterial activity showed weak inhibition of bacterial growth at 50 μ M against Gram-positives like *S. aureus*, *E. faecalis*, and Gram-negatives like *E. coli*, and *P. aeruginosa*. It could be due to the efflux pump action, micromolar enzyme inhibition or poor penetration through the bacterial cell wall.⁹⁴

To optimize π -stacking with Glu50-Arg76 salt bridge and hydrogen bond interactions with Arg136, the thiazole-carboxylic acid moiety was replaced by an oxadiazole-carboxylic acid (Figure 14). The first generation inhibitors present the 1,3,4-oxadiazole moiety directly linked to the phenyl ring, while the second generation show a methylene/imine linker connecting the phenyl and oxadiazole moieties.⁹⁵

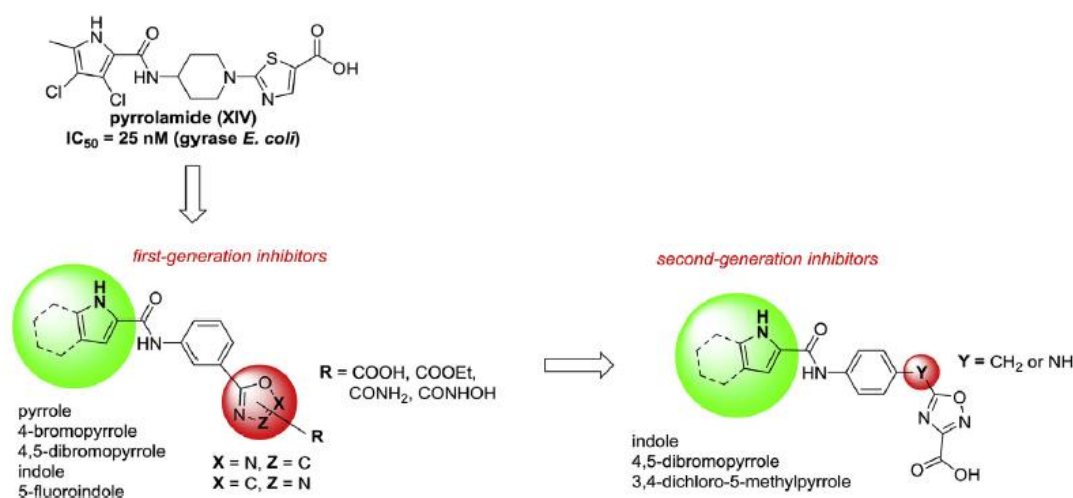


Figure 14. Substituted oxadiazoles as novel scaffold of DNA gyrase

Among all, the most active compound was 5-((4-(3,4-dichloro-5-methyl-1*H*-pyrrole-2-carboxamido)phenyl)amino)-1,2,4-oxadiazole-3-carboxylic acid which displayed an IC₅₀ of 1.2 μ M against *E. coli* DNA gyrase and micromolar inhibition of *E. coli* topoisomerase IV. Furthermore, it

also exhibited a modest inhibition against *E. faecalis* ($MIC_{90} = 75 \mu M$), but no activity against the tested Gram-negative bacteria. As predicted by docking, this compound was active thanks to the flexible linker, which directs the carboxylic acid function toward Arg136 and to 5-methyl-3,4-dichloropyrrole moiety, which increase the potency compared to 4,5-dibromopyrrole. The reason probably lies in the smaller size of the binding pockets of *S. aureus* DNA gyrase that results from differences in certain amino acid residues in the ATP binding site.^{91,96} 3,4-Dichloro-5-methylpyrrole with smaller groups on the pyrrole ring bind more effectively to the enzyme.

Cotman *et al.*⁹⁷ synthesized some 1*H*-pyrrole-2-carboxamido-tyrosine derivatives; overall, the most promising compounds inhibited the ATPase activity of DNA-gyrase B of Gram-positive and Gram-negative bacteria with IC_{50} values in the low micromolar range and had a good antibacterial activity against *S. aureus* and *E. faecalis* with minimal inhibitory concentrations (MIC_{90}) between 14 and 28 $\mu g/mL$.

Zidar *et al.* designed, synthesized and tested different series of *N*-phenyl-4,5-dibromopyrrolamides and *N*-phenylindolamides against *E. coli* and *S. aureus*.^{96,98} Among all, the most potent compound was 2-((4-(4,5-dibromo-1*H*-pyrrole-2-carboxamido) phenyl)amino)-2-oxoacetic acid (**N° 9a**) with an IC_{50} of 0.18 μM against *E. coli* gyrase and weaker activity against *S. aureus*. It has been confirmed by docking experiment, which showed the interaction of the carbonyl amide with Arg136 instead of Arg76 and hydrogen bonds between carboxylate group and Arg76 and Arg136. However, it did not display any considerable antibacterial effect, which can be attributed to the poor penetration into the cell and/or the activity of efflux pumps.⁹⁸

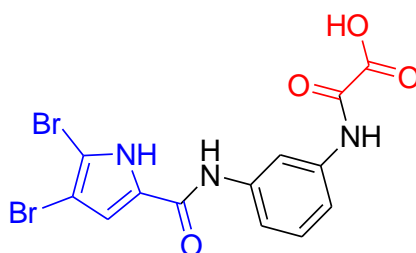


Figure 15. Structure of compound N° 9a

Based on an ongoing research aimed to improve GyrB inhibitory potency and antibacterial activity, some novel *N*-phenylpyrrolamides have been synthesized.^{99,100} Several compounds showed low nanomolar IC_{50} values against DNA gyrase, and low micromolar MIC values against *E. faecalis* and *S. aureus*.

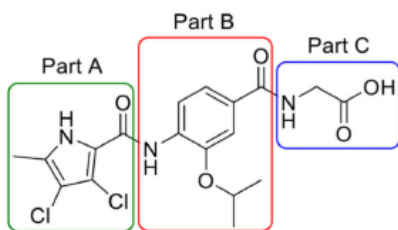


Figure 16. General structure of *N*-phenylpyrrolamides derivatives.

These results indicated that 4-dichloro-5-methyl-pyrrolamides in Part A create more favourable interactions than 4,5-dibromopyrrolamides. Furthermore, lipophilic substituents at the 3-position of the Part B benzene ring (e.g. methoxy, isopropoxy and benzyloxy substituents) interact with the hydrophobic floor of the enzyme.¹⁰⁰ As predicted with docking experiments, 2-aminoethoxy substituents were generally more potent; indeed, the amino group of the 2-aminoethoxy substituent could form an H-bond with Ala100 that is part of the flexible loop formed by Gly97-Ser108. Moreover, free carboxylic acids in the part C are essential for the activity since they are able to establish ionic interactions and/or hydrogen bonds with the Arg136 side chain in the binding site of the enzyme, while esters can only interact with weaker hydrogen bonds. In addition, compounds with alanine side chains in Part C displayed the strongest inhibitory activity. As a result, the most active compound in enzymatic assays was (*S*)-4-(5-((1-carboxyethyl)carbamoyl)-2-(3,4-dichloro-5-methyl-1*H*-pyrrole-2-carboxamido) 3-isopropoxybenzoyl)-*L*-valine with an IC_{50} value of 38 nM against *E. coli* gyrase and 93 nM against *S. aureus* gyrase, and was also active against *E. coli* topoisomerase IV (IC_{50} = 0.45 μ M) and *S. aureus* topoisomerase IV (IC_{50} = 0.28 μ M). However, it showed no antibacterial activity against *S. aureus* and around 3 μ M toward *E. faecalis*, comparable to ciprofloxacin. On the other hand, the analogue oxadiazolone, (*S*)-3,4-dichloro-*N*-(2-isopropoxy-4-((1-(5-oxo-4,5-dihydro-1,3,4-oxadiazol-2-yl)ethyl)carbamoyl)phenyl)-5-methyl-1*H*-pyrrole-2-carboxamide, which displayed only an IC_{50} value of 85 nM against *E. coli* DNA gyrase, possessed the strongest antibacterial activity, with MIC values of 1.56 μ M against *E. faecalis*, and 3.13 μ M against wild type *S. aureus*, methicillin-resistant *S. aureus* (MRSA) and vancomycin-resistant *Enterococcus* (VRE). It was active against *E. coli* strains only in the presence of efflux inhibitor PA β N, suggesting that it is sensible to the efflux mechanism.¹⁰⁰

Subsequently, the optimisation of these derivatives led to more potent *N*-phenylpyrrolamides, substituted with piperidin-4-yloxy in benzyl ring, such as (*S*)-4-(5-((1-carboxyethyl)carbamoyl)-2-(3,4-dichloro-5-methyl-1*H*-pyrrole-2-carboxamido)phenoxy)piperidin-1-ium chloride. It displayed excellent IC_{50} values of 6.9 nM against *E. coli* DNA gyrase and 0.96 μ M against *S. aureus*

topoisomerase IV. Several compounds displayed antibacterial activity against Gram-positive strains. The most potent was a quinolone derivative, 7-(3,4-dichloro-5-methyl-1*H*-pyrrole-2-carboxamido)-1-ethyl-4-oxo-1,4-dihydroquinoline-3-carboxylic acid, that inhibited the growth of several bacteria with excellent MIC values: *E. faecalis* (MIC = 1.56 μ M), *S. aureus* (MIC = 0.78 μ M), *S. pyogenes* (MIC = 0.72 μ M), MRSA (MIC = 2.5 μ M) and MRSA VISA - extremely drug resistant strain of *S. aureus* (MIC = 2.5 μ M).¹⁰¹

Afterwards, in several reviews it has been described that benzothiazole is a common scaffold in many therapeutically useful compounds.¹⁰² For instance, it shows promising activities against several Gram-positive and Gram-negative bacteria, and also against *Mycobacterium tuberculosis*. They block proteins involved in either cell division or in biosynthesis of the bacterial cell wall,¹⁰³ such as type II Topoisomerases (DNA gyrase and topoisomerase IV). Studies have defined that some benzothiazole compounds are selective inhibitors of the DNA gyrase and topoisomerase IV, with no inhibition of human type II topoisomerases, and with potent antibacterial activities against several Gram-positive bacterial strains, such as *Streptococcus pneumoniae*, *E. faecalis*, *S. aureus*, *S. epidermidis*, and *Propionibacterium acnes*, with MICs from 0.008 μ g/mL to 0.12 μ g/mL,^{104,105} but not active against most of the tested Gram-negative.¹⁰⁴

Thus, Giorgjieva *et al.*⁵⁹ replaced the central tetrahydrobenzothiazole core with a planar aromatic benzothiazole scaffold, in order to enable additional cation- π interaction of the benzene ring with Arg76 within the Glu50-Arg76 salt bridge, which was shown to be important for the inhibition of DNA gyrase B.³⁹ Then dibromopyrrole moiety was replaced by a smaller dichloropyrrole moiety to improve activity against *S. aureus* DNA gyrase and *E. coli* and *S. aureus* topoisomerase IV, which possess a smaller hydrophobic pocket compared to that of *E. coli* DNA gyrase.⁹¹ Moreover, docking experiments suggested similar binding modes of compounds incorporating the pyrrole-2-carboxamido moiety at positions 6 and 2 of the central heterocyclic core, therefore two series of compounds which bind to the position 2 or 6 of the benzothiazole were synthesized. These compounds were nearly equipotent with the 4,5,6,7-tetrahydrobenzo[1,2-*d*]thiazole compounds as inhibitors of *E. coli* DNA gyrase but displayed improved inhibition of *S. aureus* DNA gyrase and topoisomerase IV from both bacteria. For instance, the crystal structure of 2-((2-(4,5-dibromo-1*H*-pyrrole-2-carboxamido)benzothiazol-6-yl)amino)-2-oxoacetic acid, one of the most active compound, in complex with *E. coli* DNA gyrase B, revealed that the pyrrole nitrogen forms a hydrogen bond with the side chain of Asp73. The 4,5-dibromopyrrole moiety forms additional hydrophobic contacts with Val43, Asn46, Val71, Val120, Thr165, and Val167, while the benzothiazole scaffold forms hydrophobic interactions with the Glu50, Gly77, Ile78, and Pro79 amino-acid residues. Moreover,

docking studies showed that the acyl moiety is important for interactions with the Arg136 residue. However, no significant antibacterial activity against both Gram-negative and Gram-positive bacteria was observed, most likely due to efflux of inhibitors. Indeed, some of the compounds possessed only weak antibacterial activity against *E. faecalis*. These results provide a good starting point to design improved DNA gyrase inhibitors with antibacterial activity.

3.5 Aim and Objectives

As a part of an ongoing research program focused on the design of new GyrB inhibitors, some compounds have been synthesized.

We recently reported several structural types of low-nanomolar pyrrole-2-carboxamide GyrB inhibitors^{59,91,96} and established the binding mode of 2-((2-(4,5-dibromo-1H-pyrrole-2-carboxamido)benzo[d]thiazol-6-yl)amino)-2-oxoacetic acid (**1a**; IC₅₀ *E. coli* = 58 nM),⁵⁹ and 4,5-dibromo-pyrrole analog of **1b** (IC₅₀ *E. coli* = 43 nM),¹⁰⁶ to GyrB from *E. coli* with X-ray crystallography. However, most of these inhibitors were devoid of in vitro antibacterial activity because of insufficient permeation and/or extrusion by bacterial efflux pumps.^{59,106}

Dual targeting of GyrB and structurally similar topoisomerase IV ParE subunits has been suggested to prolong the onset of resistance in bacteria because mutations at both essential sites are less probable than single mutations at GyrB or ParE ATP-binding sites.^{107,108}

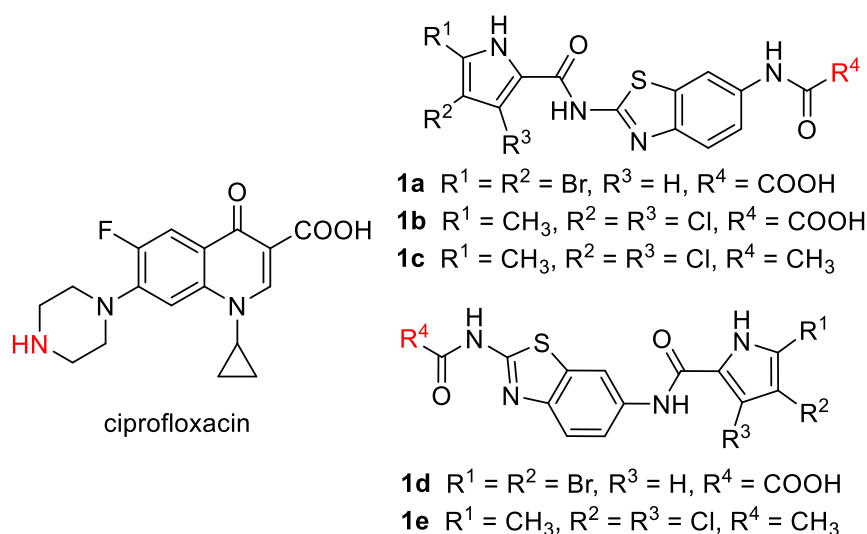
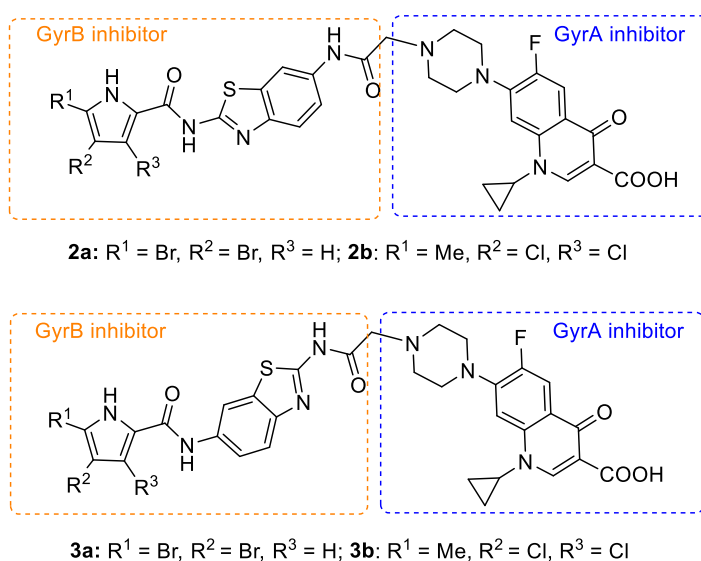


Figure 17. Ciprofloxacin and GyrB inhibitors **1a-e**.

This observation evoked our interest in the design and preparation of the first dual inhibitors of Gyr A and Gyr B that could open new avenues for DNA gyrase inhibition and fighting bacterial resistance.²⁹

Designed multiple ligands can be obtained by linking, merging or fusing individual pharmacophores in a way tolerated by respective targets.¹⁰⁹⁻¹¹² Several 4-quinolone hybrids with trimethoprim,¹¹³ linezolid,¹¹⁴ and tobramycin¹¹⁵ were obtained, and these as well as other studies^{81,116} demonstrated that moieties of different sizes attached to the piperazine NH group of ciprofloxacin are well tolerated, with retention of DNA gyrase inhibition and antibacterial activity. Furthermore, exposure of the terminal carboxylate group of our GyrB inhibitors to bulk water observed in the crystal structure of the 4,5-dibromo-1*H*-pyrrole-2-carboxamide inhibitor **1a** bound to *E. coli* GyrB and simulated by docking for a reversed inhibitor **1d** (IC₅₀ *E. coli* = 38 nM)⁵⁹ should allow functionalization in this region without losing DNA gyrase B inhibitory activity (positions in ciprofloxacin and in **1a-e** which should tolerate substitution without loss of DNA gyrase inhibition are colored red; Figure 1).

Figure 18. GyrA/GyrB inhibitor hybrids **2a-b** and **3a-b**.



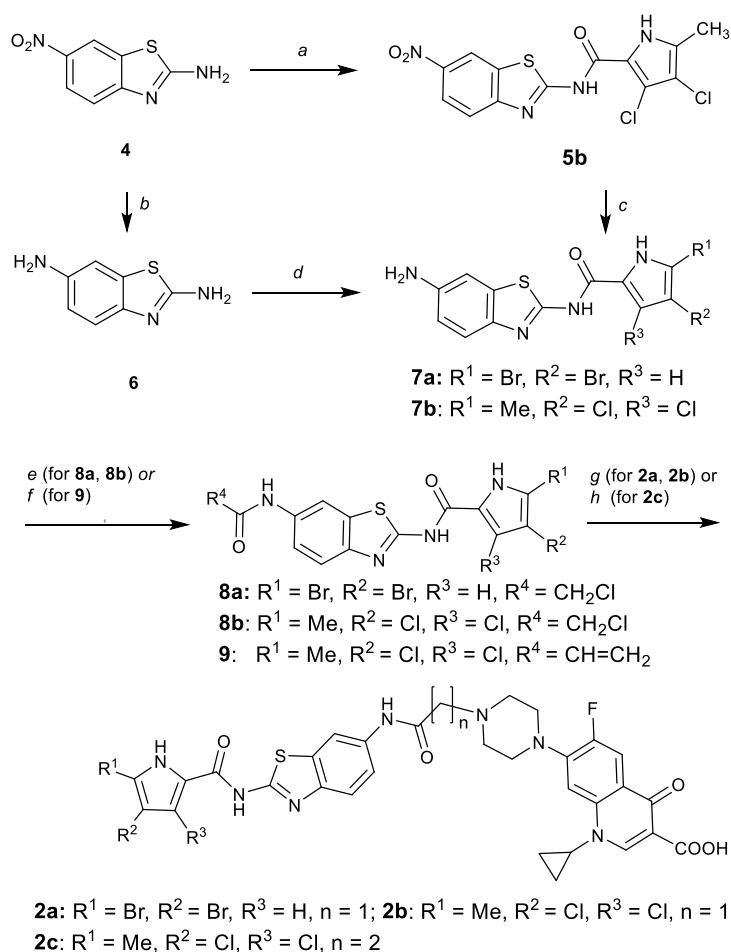
The presence of carboxylate groups in **1a**, **1b** and **1d** did not seem critical for GyrB inhibition since the N-acetyl analog of **1b** (**1c**; IC₅₀ *E. coli* = 9 nM) and its reversed analog N-(2-acetamido-benzo[*d*]thiazol-6-yl)-3,4-dichloro-5-methyl-1*H*-pyrrole-2-carbox-amide (**1e**; IC₅₀ *E. coli* = 66 nM) also showed good inhibition of DNA gyrase. Because DNA gyrase A-inhibiting fluoroquinolones and our pyrrole-2-carboxamide GyrB inhibitors **1a-e** do not share common structural features that would allow fusion of both pharmacophores, we decided to use a merging strategy to combine the GyrA inhibitor ciprofloxacin and our GyrB inhibitors in the same molecule and obtain hybrid compounds **2** and **3** containing both GyrA and GyrB-inhibiting pharmacophores (Figure 2). Docking of

compounds **2b** and **3b** to *E. coli* GyrB (PDB: 4DUH)¹¹⁷ and to *S. aureus* GyrA (PDB: 5CDQ)¹¹⁸ suggested that they could bind to both subunits since there was no steric clash with GyrA or GyrB binding site residues. (the reason for using *S. aureus* DNA gyrase A structure and not the one from *E. coli* is a simple fact that there is no experimental *E. coli* GyrA structure available in PDB). We further anticipated that merging our GyrB inhibitors with highly permeable ciprofloxacin would facilitate entry of the hybrid GyrA/GyrB inhibitors and make them active against bacteria.

3.5.1 Results and discussion

The hybrids **2a** and **2b** were prepared (Scheme 1) by acylation of the amines **7a** and **7b** with chloroacetyl chloride and subsequent substitution of chlorine in **8a** and **8b** with ciprofloxacin. Amine **7a** was obtained by selective N₂ acylation of the diamine **6** with 4,5-dibromopyrrole-2-yl trichloromethyl ketone, whereas the amine **7b** was prepared by acylation of 6-nitrobenzo[*d*]thiazol-2-amine (**4**) with 3,4-dichloro-5-methyl-pyrrole-2-carboxylic acid chloride and subsequent reduction of the nitro group in the obtained **5b**.

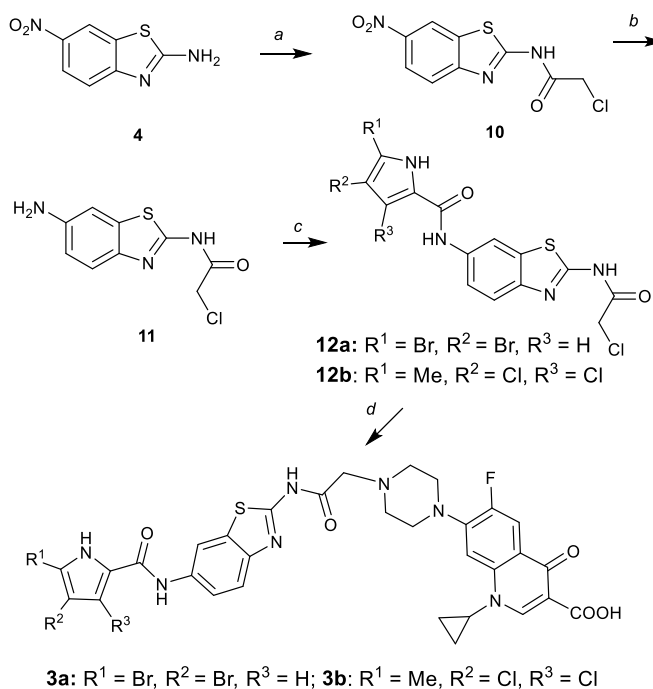
Scheme 1. (a) 3,4-dichloro-5-methyl-1*H*-pyrrole-2-carbonyl chloride, toluene, reflux, 18 h; (b) H₂, Pd/C (10%), 1.5 bar,



EtOH, rt, 18 h; (c) SnCl₂ × 2 H₂O, EtOH, reflux, 24 h; (d) 4,5-dibromopyrrole-2-yl-trichloromethyl ketone, K₂CO₃, DMF, 80 °C, 20 h; (e) ClCH₂COCl, Et₃N, dichloromethane, rt, 24 h; (f) acryloyl chloride, K₂CO₃, THF, ice bath, 0.5 h; (g) ciprofloxacin, KI, Na₂CO₃, CH₃CN, reflux, 4 h; (h) ciprofloxacin, CH₃CN/AcOH, reflux, 72 h

For the synthesis of the isomeric hybrids **3a** and **3b** (Scheme 2) bearing a *1H*-pyrrole-2-carboxamido moiety at position 6, **4** was acylated with chloroacetyl chloride¹¹⁹, and the obtained nitro derivative **10** was reduced to the 6-aminobenzothiazole derivative **11** by catalytic hydrogenation over 10% Pd on charcoal in ethyl acetate. Attempts to reduce the nitro group of **10** with tin(II) chloride in ethanol or with sodium sulfide nonahydrate were not successful since, in both cases, reduction of the nitro group was accompanied by amide bond cleavage, and benzo[*d*]thiazole-2,6-diamine was isolated as the main product. The amine **11** was coupled with 4,5-dibromo-pyrrole-2-carboxylic acid chloride or 3,4-dichloro-5-methyl-pyrrole-2-carboxylic acid chloride in the presence of triethylamine in dioxane, and the resulting intermediates **12** underwent nucleophilic substitution with unprotected ciprofloxacin to produce the target inhibitors **3a** and **3b**. The final compounds **2a-b** and **3a-b** were purified on Sephadex LH-20 to remove traces of ciprofloxacin.

Scheme 2. (a) ClCH₂COCl, Et₃N, dichloromethane, rt, 12 h; (b) H₂, Pd/C (10%), EtOAc, rt, 24 h; (c) 4,5-dibromo-*1H*-pyrrole-2-carboxylic acid chloride or 3,4-dichloro-5-methyl-*1H*-pyrrole-2-carboxylic acid chloride, Et₃N, dioxane, rt, 18 h; (d) ciprofloxacin, KI, Na₂CO₃, CH₃CN, reflux, 12 h.



3.5.2 Biological results

3.5.2.1 Enzymatic Inhibition Results

A DNA gyrase supercoiling assay^{59,91,96} demonstrated weaker inhibition of *E. coli* DNA gyrase by the hybrids **2a-b** and **3a-b** (IC₅₀ values from 0.17 to 6.2 μM) than by the GyrB inhibitors **1a-e** (IC₅₀ values from 9 to 66 nM) and slightly weaker inhibition than by the GyrA inhibitor ciprofloxacin (Table 1). The hybrids **2a** and **2b** with ciprofloxacin bound to position 6 of a benzothiazole core were better (submicromolar) inhibitors than **3a** and **3b** that possessed low micromolar *E. coli* gyrase IC₅₀ values. Whereas increasing the size of the 6-(N-acetylamino) substituent of **1c**, producing **8b** (N-chloroacetyl), and **2b** in each case resulted in a ca. 20-fold increase in IC₅₀ irrespective of the size of the N-substituent, increasing the size of the 2-(N-acylamino) substituent in the series **1e** (N-acetyl) → **12b** (N-chloroacetyl) → **3b** clearly increased the IC₅₀ values at each step, increasing in total 78-fold from **1e** to **3b**. This observation indicated that appending the ciprofloxacin moiety to position 6, resulting in the compounds **2a** and **2b**, is better tolerated than its attachment to position 2, producing the compounds **3a** and **3b**. Because the observed inhibition of *E. coli* DNA gyrase in the supercoiling assay could not be undoubtedly attributed to inhibition of the GyrA or GyrB subunit, a DNA gyrase ATPase assay (Table 1) was performed to detect binding of the hybrid compounds to *E. coli* GyrB. Further, MIC assays in the *E. coli* wild-type strain and in two strains with a mutated GyrB or mutated fluoroquinolone-binding sites were performed to assess the effect of the hybrids on *E. coli* (Table 2).

Table 2. Inhibition of *E. coli* DNA gyrase supercoiling and ATPase activities

Compound	MW	Supercoiling <i>IC</i>₅₀ (μM)	ATPase <i>IC</i>₅₀ (μM)
1a	485.85	0.058±0.03	n.d.
1b	413.23	0.043±0.03	n.d.
1c	383.25	0.0095±0.002	n.d.
1e	383.25	0.066±0.008	n.d.
2a	787.45	0.91±0.37	0.27±0.01
2b	712.58	0.17±0.03	0.055±0.005
2c	726.61	0.16±0.01	0.054±0.025
3a	787.45	6.2±1.7	0.35±0.18
3b	712.58	5.2±2.0	0.32±0.19
8a	492.57	2.3±0.2	n.d.
8b	417.70	0.18±0.02	n.d.
12a	492.57	0.43±0.02	0.38±0.09
12b	417.70	0.33±0.02	n.d.
novobiocin	612.62	0.17±0.01	0.16±0.05
ciprofloxacin	313.35	0.12±0.02	n.d.

n.d.: not determined

3.5.2.2 Antibacterial Results

All four hybrid compounds (**2a-b** and **3a-b**) displayed potent activity against the *E. coli* strains ATCC 25922 and K-12 MG1655 in the presence of the efflux pump inhibitor Pa β N (MIC values between 130 and 439 ng/mL). MIC values in the absence of Pa β N were in the range 1481-3333 ng/mL in the strains ATCC 25922 and K-12 MG1655, which indicates that the hybrids **2a-b** and **3a-b** are not intensively effluxed in *E. coli*. The antibacterial activity of the hybrids in the absence of an efflux pump inhibitor was confirmed also against gram-negative *Shigella flexneri* HNCMB 20018 and *Shigella sonnei* HNCMB 25021 (MICs between 1481 and 3333 ng/mL) as well as against *Klebsiella pneumoniae* ATCC 10031 (MICs between 293 and 658 ng/mL). These results indicate good penetration of the studied GyrA/GyrB-inhibiting hybrids through the bacterial cell wall and provide evidence that their efflux in *E. coli* and in other tested bacteria is not intensive and not detrimental for their anti-bacterial activity. However, the hybrid molecules **2a-b** and **3a-b** did not show any reduction in antibacterial activity in the *E. coli* K-12 MG1655 GyrB R136C mutant and suffered a substantial loss of antibacterial activity toward the *E. coli* mutant in which the fluoroquinolone-binding site was abolished by four mutations (*E. coli* K-12 MG1655 GyrA S83L, D87N; ParC S80I, E84G). This finding indicates that the observed antibacterial activity of the hybrid molecules **2a-b** and **3a-b** is mainly due to interaction with GyrA and/or ParC and not with the GyrB subunit. Although the ATPase assay demonstrated that the hybrids **2a-b** and **3a-b** inhibit the GyrB subunit, the inhibition is obviously too weak (IC₅₀ values between 0.055 and 0.35 μ M) to result in antibacterial activity. Assuming that increasing the flexibility of the linker between the GyrB and GyrA inhibitor moieties could increase GyrB inhibition, we synthesized the hybrid **2c**, a homolog of the hybrid **2b** that was most potent in the supercoiling and ATPase assays, possessing an additional methylene group between the ciprofloxacin and GyrB inhibitor moieties (Scheme 1). To this end, the amine **7b** was acylated with acryloyl chloride in the presence of potassium carbonate in tetrahydrofuran, and the obtained acrylamide **9** was reacted with ciprofloxacin to produce the compound **2c** with an elongated linker. However, the hybrid **2c** displayed behavior similar to that of **2b** in the supercoiling assay (IC₅₀ = 0.16 μ M), ATPase assay (IC₅₀ = 0.054 μ M) and MIC assays in *E. coli*, demonstrating that elongating the linker by one C-atom did not increase GyrB inhibition and antibacterial activity against the wild-type and mutated *E. coli* strains.

Table 3. MIC values (ng/mL) of the hybrids **2a**, **2b**, **2c**, **3a** and **3b**.

Bacterium	2a	2b	2c	3a	3b	CCP ^[a]
<i>E. coli</i> ATCC 25922 + PaβN	130	130	500	130	130	4.4
<i>E. coli</i> K-12 MG1655 + PaβN	439	439	250	293	293	6.6
<i>E. coli</i> ATCC 25922	2222	1481	439	1481	1481	9
<i>E. coli</i> K-12 MG1655	3333	1481	658	1481	2222	12
<i>S. flexneri</i> HNCMB 20018	3333	1481	658	1481	2222	12
<i>S. sonnei</i> HNCMB 25021	3333	1481	658	1481	2222	12
<i>K. pneumoniae</i> ATCC 10031	658	293	195	293	293	4
<i>E. cloacae</i> ATCC 13047	5000	2222	1481	2222	3333	26
<i>E. coli</i> GyrB R136C + PaβN	439	439	250	293	293	6.6
<i>E. coli</i> K-12 MG1655 GyrA S83L, D87N; ParC S80I, E84G + PaβN	5000	5000	16000	5000	20000	33000

^[a] CP = ciprofloxacin

To investigate bacterial evolvability toward the dual inhibitors, as many as 10^{10} wild-type *E. coli* cells were exposed to a 4×MIC concentration of the tested compounds in a standard frequency of resistance assay.¹²⁰ The two tested *E. coli* strains showed similar potential to develop spontaneous resistance

against the hybrid molecules as they did against ciprofloxacin (Table 3). This result supports other aforementioned results indicating that the observed antimicrobial activity of the tested hybrid molecules is due mainly to their interaction with GyrA and/or ParC, whereas GyrB inhibition by the hybrid molecules is limited. Therefore, resistance can arise in the form of canonical mutations against ciprofloxacin derivatives on GyrA and/or ParC

Table 4. Frequency of resistance against a 4×MIC concentration of the hybrids **2a-c** and **3a-b** and ciprofloxacin

Bacterium	Frequency of resistance ($\times 10^{-9}$)					
	2a	2b	2c	3a	3b	CP ^[a]
<i>E. coli</i> K-12 MG1655	1.30	2.60	3.13	3.07	4.43	1.56
<i>E. coli</i> ATCC 25922	11.2	4.17	11.9	4.88	13.9	6.31

^[a] CP = ciprofloxacin

3.5.3 Molecular modelling study

3.5.3.1 Docking of compounds 5b and 10b in *E. coli* DNA GyrB ATP-binding site (PDB: 4DUH)

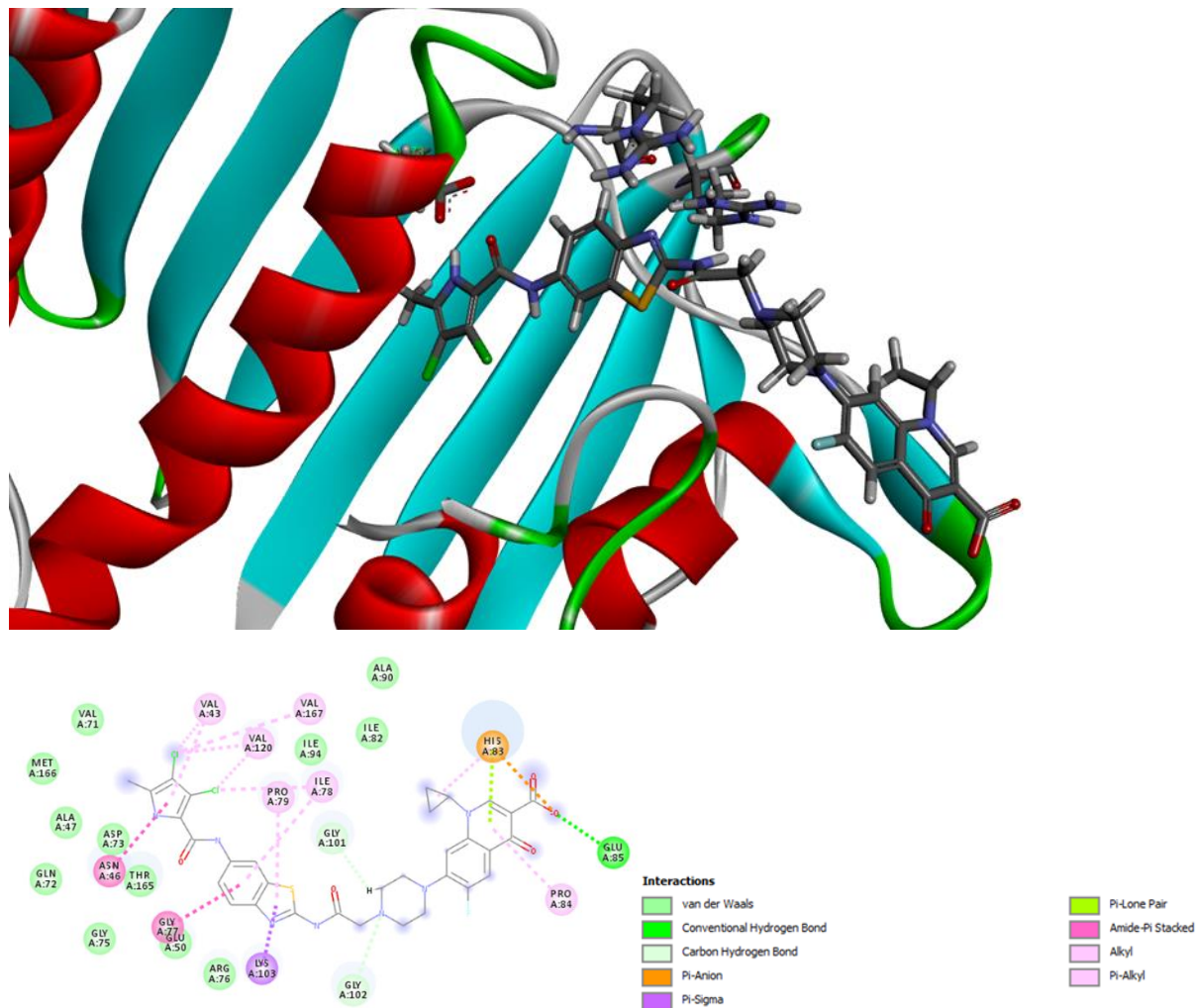


Figure 19. Docking experiment into the *E. coli* DNA gyrase B ATP-binding site of compound **5b**

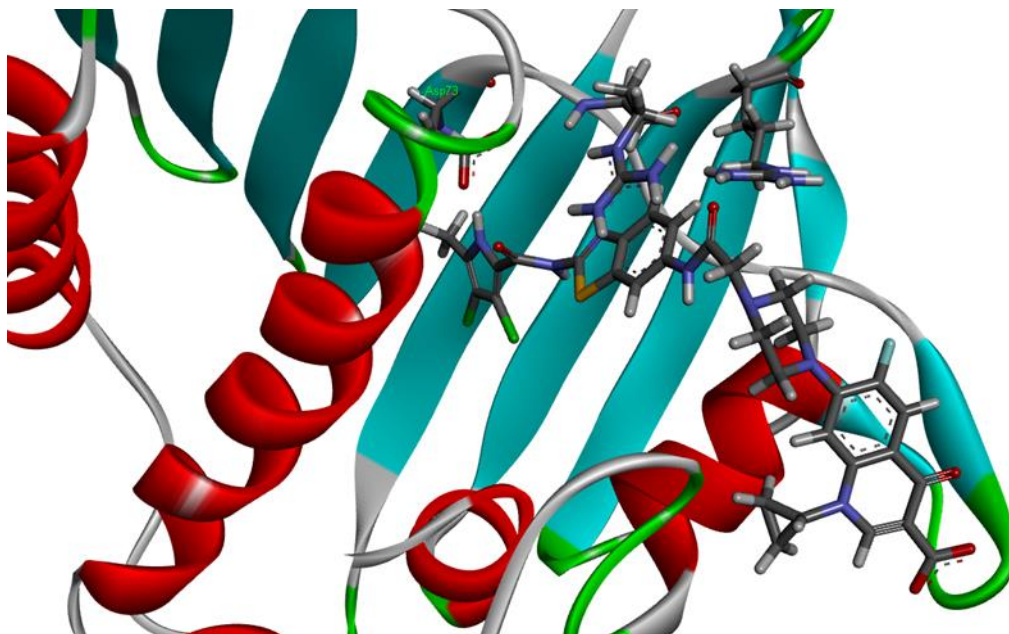


Figure 20. docking experiment into the *E. coli* DNA gyrase B ATP-binding site of compound **10b**

Compounds **5b** and **10b** were docked into the *E. coli* DNA gyrase B ATP-binding site using GOLD (The Cambridge Crystallographic Data Center). Both compounds were drawn in ChemDraw and then minimized using Chem3D and MMFF94 force field. Carboxylic group was drawn in the form of the carboxylate ion. Binding site for docking was prepared in GOLD GUI using crystallized ligand for definition of the binding site. Genetic algorithm was repeated 10 times and 10 docking solutions were checked visually.

These preliminary docking experiments place the benzothiazolpyrrolamide moiety in the GyrB ATP-binding pocket, while the fluoroquinolone part of the hybrid is oriented toward solvent, but docking also predicts some additional interactions. These results confirmed the enzymatic binding of **5b** and **10b** on GyrB, since there is no steric clash with the protein with such a big ligand.

3.5.3.2 Crystal structure of moxifloxacin

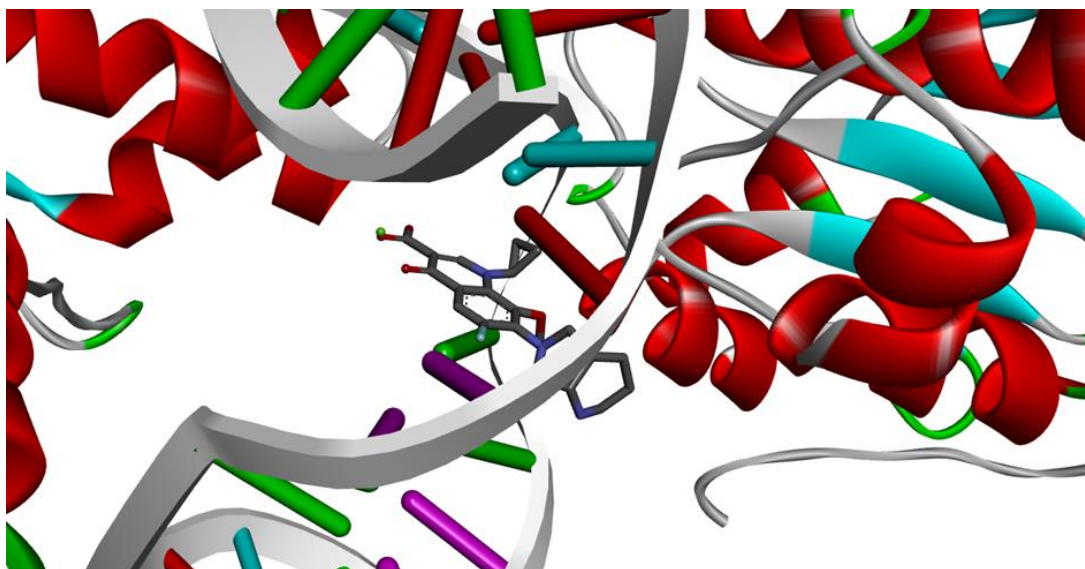


Figure 21. Docking in *S. aureus* DNA Gyrase (PDB: 5CDQ) in the complex with moxifloxacin and DNA

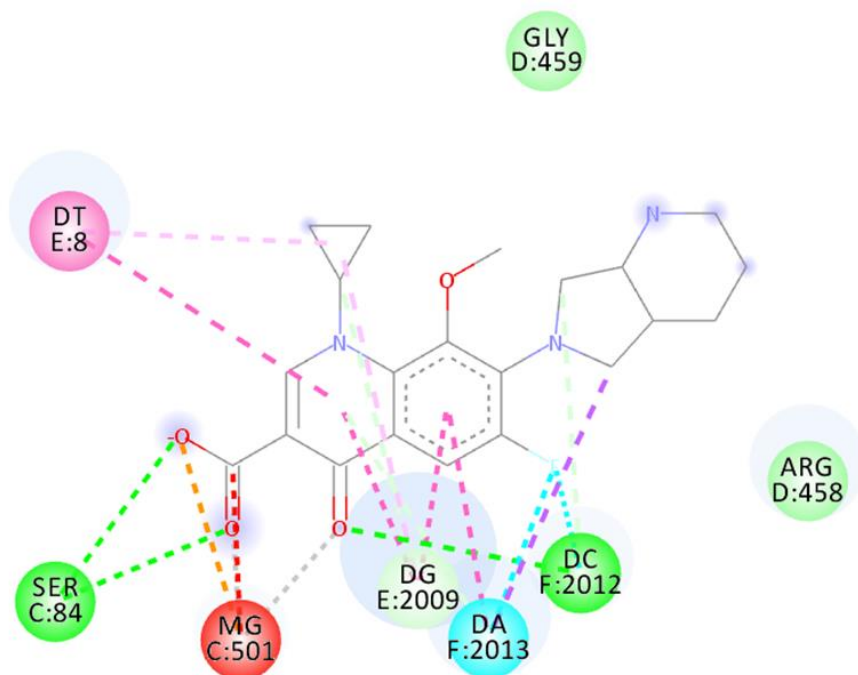


Figure 22. Crystal structure of moxifloxacin

The crystal structure of moxifloxacin, which predicts the interaction of this fluoroquinolone with *S. aureus* DNA Gyrase and DNA, has been already reported. *S. aureus* DNA gyrase structure, and not that from *E. coli*, was used, because there was no crystal structure of *E. coli* DNA gyrase A available in PDB. The binding should be similar because of the high sequence homology in Gram positive and negative bacteria. Moreover, moxifloxacin is very similar to ciprofloxacin and fluoroquinolone core

binds the same way in both cases. As observed in the x-ray structure, moxifloxacin interacts with Mg^{2+} ion, some van der Waals interactions, hydrogen bonds with Ser84 and several stacking interactions with DNA bases.

3.5.3.3 Docking of compounds 5b and 10b in *S.aureus* DNA GyrA (PDB: 5CDQ)

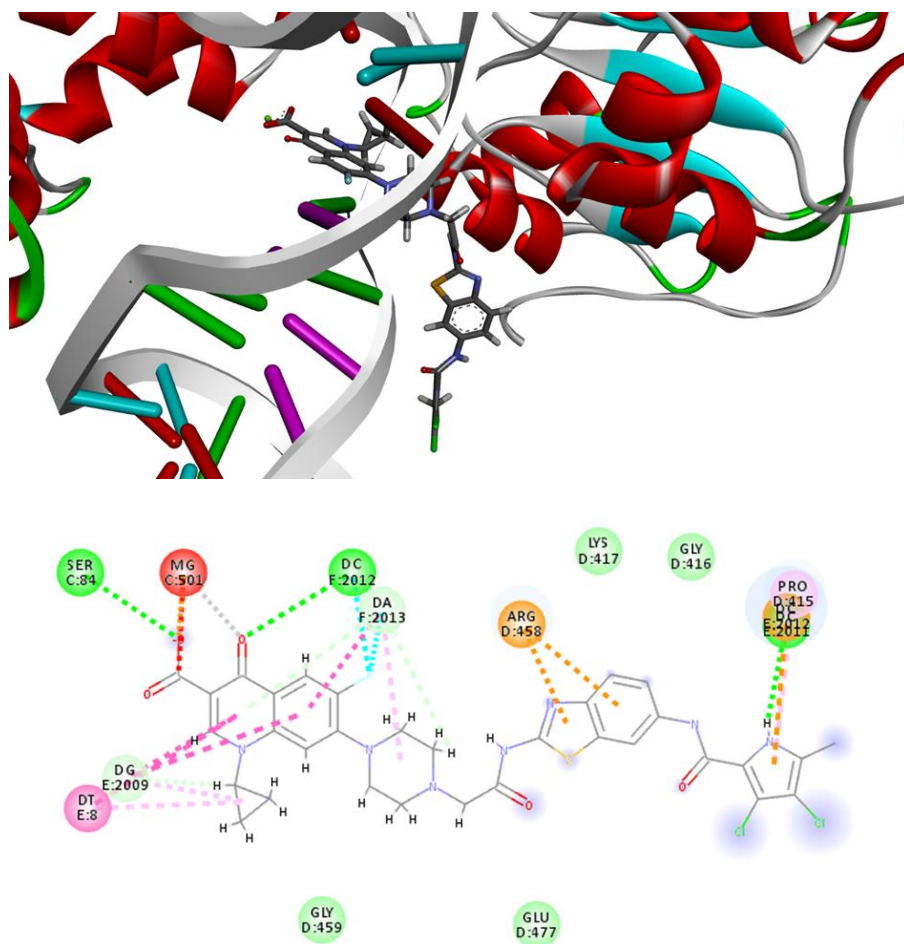


Figure 23. Docking experiment into the *S. aureus* DNA gyrase A binding site of compound **5b**

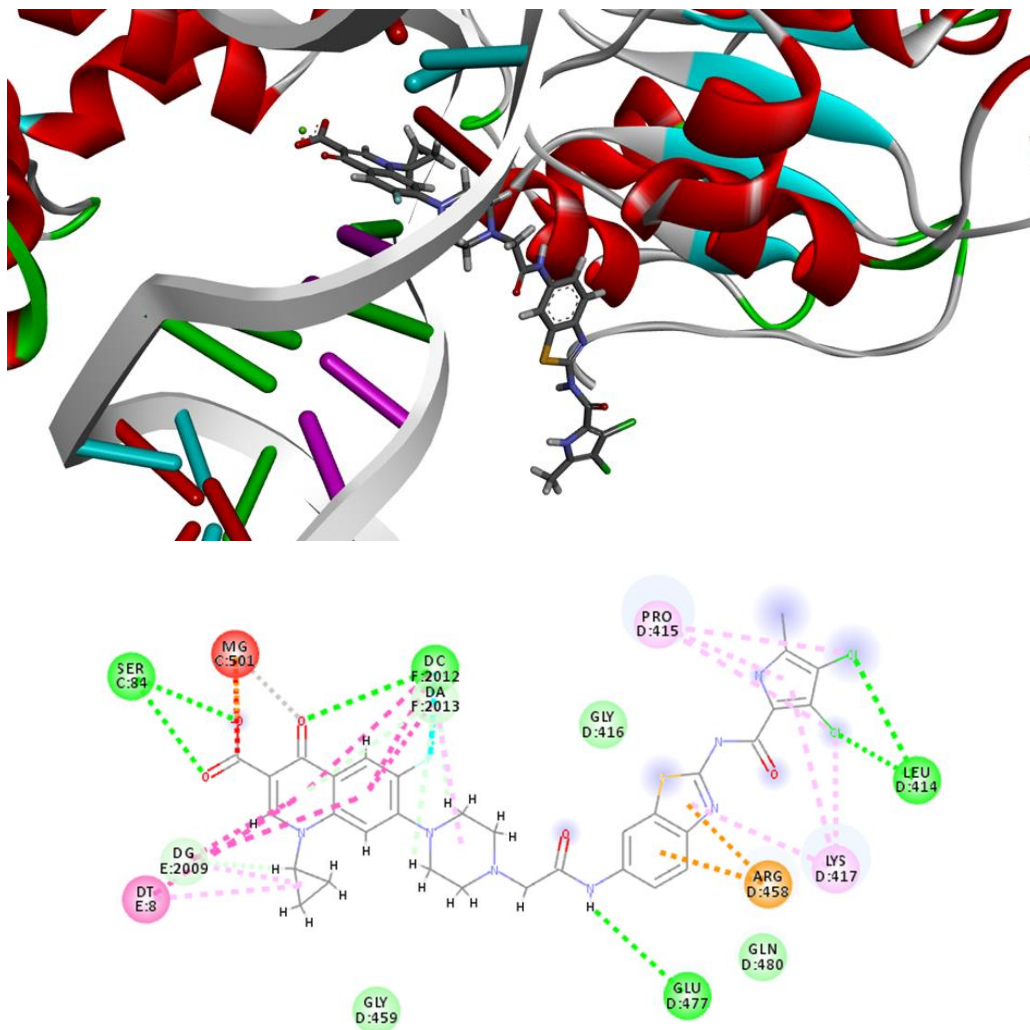


Figure 24. Docking experiment into the *S.aureus* DNA gyrase A binding site of compound **10b**

The fluoroquinolone moiety of both compounds seems to interact to the GyrA binding site in the same way as reported in the crystal structure of moxifloxacin. Conjugation of ciprofloxacin with GyrB inhibitor does not hinder its binding to GyrA. Moreover, additional interactions are predicted between GyrA and GyrB inhibitor. However, to confirm such a binding mode additional studies, especially by X-ray crystallography are needed.

3.5.4 Conclusion

In conclusion, the first dual DNA gyrase A and B inhibitors reported in this paper enter *E. coli*, from which they are not intensively effluxed, and display a strong antibacterial activity due to the interaction of the hybrids with the GyrA and/or topoisomerase IV ParC subunits. As demonstrated by DNA gyrase ATPase and MIC assays, inhibition of GyrB by the presented hybrids, although present, is not strong enough to provide a substantial contribution to the observed antibacterial activity. In perspective, hybrids combining a benzothiazole DNA gyrase B inhibitor and the DNA gyrase A inhibitor ciprofloxacin in the same molecule connected by a cleavable linker, are a logical extension of the presented concept that could result in strong inhibition of both the DNA gyrase A and B subunits in the bacterial cell and in potent antibacterial activity.

3.6 EXPERIMENTAL PART

3.6.1 General information

Chemicals were obtained from Acros Organics (Geel, Belgium), Sigma-Aldrich (St. Louis, MO, USA) and Apollo Scientific (Stockport, UK) and used without further purification. Analytical TLC was performed on silica gel Merck 60 F₂₅₄ plates (0.25 mm), using visualization with UV light and visualization reagents. Column chromatography was carried out on silica gel 60 (particle size 240–400 mesh). HPLC analyses were performed on a Waters 2695 Separations Module with a Waters 2996 Photodiode Array UV-Vis detector or Thermo Scientific UltiMate 3000 HPLC system using a Zorbax Eclipse Plus C18 5- μ m column (4.6 \times 150 mm or 4.6 \times 250 mm, Agilent, USA), a flow rate of 1.0 mL/min and detection at 254 nm. The eluent consisted of 0.1% trifluoroacetic acid in water as solvent A and acetonitrile as solvent B, with gradient: 5 min of 90% A, then gradient to 30% A in 15 min and 5 min of 30% A. Melting points were determined on a Reichert hot stage microscope and are uncorrected. ¹H and ¹³C NMR spectra were recorded at 400 and 100 MHz, respectively, on a Bruker AVANCE III 400 spectrometer (Bruker Corporation, Billerica, MA, USA) in DMSO-*d*₆ solutions, with TMS as the internal standard. IR spectra were recorded on a PerkinElmer Spectrum BX FT-IR spectrometer (PerkinElmer, Inc., Waltham, MA, USA) or Thermo Nicolet Nexus 470 ESP FT-IR spectrometer (Thermo Fisher Scientific, Waltham, MA, USA). Mass spectra were obtained using a Exactive™ Plus Orbitrap Mass Spectrometer (Thermo Fischer Scientific Inc., Waltham, MA 02451 USA). The purity of the tested compounds was established to be \geq 95%. The tested compounds contained less than 0.1% ciprofloxacin impurity.

3.6.2 Synthesis procedures and analytical data of compounds

3,4-Dichloro-5-methyl-*N*-(6-nitrobenzo[*d*]thiazol-2-yl)-1*H*-pyrrole-2-carboxamide (5b): To a solution of compound **4** (1.045 g, 5.35 mmol) in dry toluene (26 mL) 3,4-dichloro-5-methyl-1*H*-pyrrole-2-carbonyl chloride (0.542 g, 2.55 mmol) was added and the mixture was heated under reflux for 4h and followed by TLC (silica gel; CH₂Cl₂/MeOH = 9/1, R_f=0.85). The reaction mixture was evaporated in vacuo, triturated with 1M HCl and filtered off to give 0.870 g of compound **5b** as dark green crystals (yield: 92%). mp >300 °C; ¹H NMR (400 MHz, DMSO-*d*₆) δ 2.29 (s, 3H, CH₃), 7.91 (d br, 1H, ³*J* = 9.2 Hz, Ar-H4), 8.30-8.33 (dd, 1H, ³*J* = 9.2 Hz, ⁴*J* = 2.4 Hz, Hz, Ar-H5), 9.08 (s br, 1H, Ar-H7), 12.17 (s br, 1H, NHCO) 12.39 (s br, 1H, pyrrole-NH) ppm; ¹³C NMR (100 MHz, DMSO-*d*₆) δ 10.99, 110.04, 117.44, 117.67, 119.05, 121.91, 121.95, 125.24, 125.83, 128.14, 128.83, 130.42, 142.95 ppm; IR (ATR) ν 3335, 1632, 1557, 1509, 1424, 1300, 1184, 1046, 829, 736, 735, 554 cm⁻¹; HRMS (ESI) *m/z* for C₁₃H₇Cl₂N₄O₃S [M-H]⁻: calcd. 368.96214, found 368.96215.

Benzothiazole-2,6-diamine (6): A solution of compound **4** (2.45 g, 130 mmol) in EtOH (150 mL) was hydrogenated over 10% Pd/C (0.245 g, 10 wt. percent) in Parr hydrogenator at 1.5 bar pressure at room temperature for 17 h and the reaction followed by TLC (silica gel; CH₂Cl₂/MeOH = 9/1, R_f= 0.40). The reaction mixture was filtered warm through Celite to remove the catalyst and the filtrate was evaporated in vacuo to give 2.135 g (yield: 99%) of a dark brown amorphous powder; mp 156-158 °C (mp Ref.¹²¹ 204 °C); ¹H NMR (400 MHz, DMSO-d₆) δ 4.89 (s br, 2H, 6-NH₂), 6.49-6.52 (dd, 1H, ³J = 8.4 Hz, ⁴J = 2.4 Hz, Ar-H5), 6.82 (d, 1H, ⁴J = 2.4 Hz, Ar-H7), 6.95 (s br, 2-NH₂), 7.04 (d, 1H, ³J = 8.4 Hz, Ar-H4) ppm; IR (ATR) ν 3261, 3095, 1612, 1540, 1463, 1280, 1224, 1118, 809, 575 cm⁻¹; MS (ESI⁺) m/z for C₇H₈N₃S = 165.9 [M+H]⁺.

N-(6-Aminobenzo[d]thiazol-2-yl)-4,5-dibromo-1H-pyrrole-2-carboxamide (7a): To a stirred solution of the amine **6** (0.500 g, 3.03 mmol) in DMF (21 mL) 2,2,2-trichloro-1-(4,5-dibromopyrrolidin-2-yl)-ethanone (1.12 g, 3.03 mmol) and Na₂CO₃ (0.321 g, 3.03 mmol) was added. The mixture was heated at 80 °C under reflux for 22 h (TLC, silica gel; CH₂Cl₂/MeOH = 9/1, R_f= 0.75), evaporated in vacuo and the residue treated with 20 mL of water. The precipitate was filtered off to give pure coupled product **7a** as brown powder (0.477 g, yield: 37%); mp 191-193 °C (mp Ref.⁹¹ 269-271 °C); ¹H NMR (400 MHz, DMSO-d₆) δ 5.21 (s br, 2H, NH₂), 6.73 (dd, 1H, ³J = 8.4 Hz, ⁴J = 2.0 Hz, Ar-H5), 7.03 (d, 1H, ⁴J = 2.0 Hz, Ar-H7), 7.42-7.4 (m, 2H, Ar-H4, pyrrole-H3), 12.31 (s br, 1H, NHCO), 13.18 (s br, 1H, pyrrole-NH) ppm; IR (ATR) ν 2848, 1534, 1400, 1323, 1266, 1158, 976, 813, 738, 661, 550 cm⁻¹; MS (ESI⁺) m/z for C₁₂H₉Br₂N₄OS = 414.8 [M+H]⁺; MS (ESI⁻) m/z for C₁₂H₇Br₂N₄OS = 412.8 [M-H]⁻.

4,5-Dibromo-N-(6-(2-chloroacetamido)benzo[d]thiazol-2-yl)-1H-pyrrole-2-carboxamide (8a): To a stirred mixture of the amine **7a** (0.700 g, 1.7 mmol) and chloroacetyl chloride (0.441 g, 0.31 mL, 3.91 mmol) in dry dichloromethane (140 mL) triethylamine (0.257 g, 0.35 mL, 2.55 mmol) was added dropwise over 5 minutes at room temperature. After 24 h when TLC (silica gel; CH₂Cl₂/MeOH, R_f= 0.80) showed complete conversion of the amine, the solution was evaporated in vacuo and the residue triturated with saturated NaHCO₃ solution (30 mL), 1M hydrochloric acid (30 mL) and water. After filtration the residual water was removed azeotropically with toluene and the product was dried to give 0.672 g of light brown compound **8a** (yield: 80%); mp >300 °C; ¹H NMR (400 MHz, DMSO-d₆) δ 4.30 (s, 2H, CH₂), 7.51 (d, 1H, ⁴J = 2.4 Hz, pyrrole-H3), 7.53-7.58 (dd, 1H, ³J = 8.8 Hz, ⁴J = 1.8 Hz, Ar-H5), 7.74 (d, 1H, ³J = 8.8 Hz, Ar-H4), 8.32 (d, 1H, ⁴J = 1.8 Hz, Ar-7),

10.5 (s, 1H, 6-NHCO), 12.6 (s br, 1H, 2-NHCO), 13.25 (d br, 1H, $^4J = 2.4$ Hz, pyrrole-NH) ppm; ^{13}C NMR (100 MHz, DMSO- d_6) δ 43.56, 99.01, 108.52, 111.86, 115.99, 118.77, 120.42, 125.66, 132.11, 134.45, 145.03, 157.00, 157.58, 164.56 ppm; IR (ATR) ν 3121, 1646, 1536, 1468, 1407, 1380, 1320, 1273, 1174, 978, 816, 739, 553 cm^{-1} ; HRMS (ESI $^+$) m/z for $\text{C}_{14}\text{H}_{10}\text{Br}_2\text{ClN}_4\text{O}_2\text{S}$ $[\text{M}+\text{H}]^+$: calcd. 490.8574, found 490.8575.

1-Cyclopropyl-7-(4-(2-((2-(4,5-dibromo-1H-pyrrole-2-carboxamido)benzo[*d*]thiazol-6-yl)amino)-2-oxoethyl)piperazin-1-yl)-6-fluoro-4-oxo-1,4-dihydroquinoline-3-carboxylic acid hydrochloride (2a): A stirred mixture of compound **8a** (0.200 g, 0.41 mmol), ciprofloxacin (0.272 g, 0.82 mmol) and potassium iodide (0.068 g, 0.41 mmol) in acetonitrile (25 mL) was heated under reflux for 4 h (TLC, silica gel; $\text{CH}_2\text{Cl}_2/\text{MeOH} = 9/1$, $R_f = 0.0-0.20$). The precipitate was filtered off and triturated with 1M hydrochloric acid (10 mL) to remove most of ciprofloxacin. The solid residue (0.205 g, yield: 75%) was purified with column chromatography on Sephadex LH-20 (30 g), eluting first with MeOH and then with DMSO to give 0.089 g of pure **2a** as bright brown crystals (yield: 28%); mp 207-209 $^\circ\text{C}$; ^1H NMR (400 MHz, DMSO- d_6) δ 1.19 (m, 2H, CH_2 – cyclopropyl), 1.33 (m, 2H, CH_2 – cyclopropyl), 2.80 (m br, 4H, $2\times\text{CH}_2$ -piperazine), 3.29 (s, 2H, COCH $_2$), 3.44 (m br, 4H, $2\times\text{CH}_2$ -piperazine), 3.84 (m br, 1H, CH-cyclopropyl), 7.47 (s br, 1H, pyrrole- H3), 7.59 (d, 1H, $^4J_{H,F} = 7.2$ Hz, quinolone-H8), 7.63-7.65 (dd, 1H, $^3J = 8.8$ Hz, $^4J = 1.6$ Hz, Ar-H5), 7.71 (d, 1H, $^3J = 8.8$ Hz, Ar-H4), 7.93 (d, 1H, $^3J_{H,F} = 13.2$ Hz, quinolone-H5), 8.36 (d, 1H, $^4J = 1.6$ Hz, Ar-H7), 8.67 (s, 1H, quinolone-H2), 9.97 (s, 1H, 6-NHCO), 12.54 (s br, 1H, 2-NHCO), 13.13 (s br, 1H, NH-pyrrole), 15.24 (s br, 1H, COOH) ppm; ^{13}C NMR (100 MHz, DMSO- d_6) δ 7.57, 35.90, 42.56, 51.97, 51.99, 66.31, 99.04, 106.56, 106.72, 108.52, 111.07 (d, $^2J_{C,F} = 21$ Hz, quinolone-C5), 111.99, 116.02, 118.87, 118.98, 120.40, 125.68, 132.02, 134.36, 139.13, 144.3, 144.76, 148.14 (d, $^2J_{C,F} = 14$ Hz, quinolone-C7), 152.07, 152.50, 152.93 (d, $^1J_{C,F} = 248$ Hz, quinolone-C6), 165.94, 176.26, 176.37 ppm; IR (ATR) ν 2926, 1832, 1662, 1626, 1509, 1455, 1256, 1136, 1014, 944, 826, 806, 746, 514 cm^{-1} ; HRMS (ESI) m/z $\text{C}_{31}\text{H}_{25}\text{Br}_2\text{FN}_7\text{O}_5\text{S}$ $[\text{M}-\text{H}]^-$: calcd. 783.9994, found 784.0010; HPLC: $t_r = 19.06$ min (95.7% at 280 nm).

***N*-(6-Aminobenzo[*d*]thiazol-2-yl)-3,4-dichloro-5-methyl-1H-pyrrole-2-carboxamide (7b):** A stirred mixture of the compound **5b** (0.570 g, 1.53 mmol) and $\text{SnCl}_2 \times 2\text{H}_2\text{O}$ (1.74 g, 7.7 mmol) in dry EtOH (45 mL) was heated under reflux for 24 h (TLC, silica gel; $\text{CH}_2\text{Cl}_2/\text{MeOH} = 50/1$, $R_f = 0.17$) and evaporated in vacuo. 2M NaOH (5 mL) was added to arrive at pH 8-9. The solution was extracted

with ethyl acetate, the organic phase was washed with 1M HCl and brine, dried over Na₂SO₄, filtered and evaporated under reduced pressure to give 0.343 g (yield: 44%) of **7b** as a mustard colored powder; mp 267-269 °C; ¹H NMR (400 MHz, DMSO-d₆) δ 2.28 (s, 3H, CH₃), 7.34-7.36 (dd, 1H, ³J = 8.4 Hz, ⁴J = 2.4 Hz, Ar-5), 7.79 (d, 1H, ³J = 8.4 Hz, Ar-H4), 7.90 (s, 1H, Ar-H7), 9.84 (s br, 2H, NH₂), 11.88 (s br, 1H, NHCO), 12.55 (s br, 1H, pyrrole-NH) ppm; ¹³C NMR (100 MHz, DMSO-d₆) δ 10.96, 109.80, 115.22, 115.58, 117.14, 120.62, 120.96, 128.82, 129.89, 132.26, 157.23, 157.27, 159.08 ppm; IR (ATR) ν 2904, 2707, 2538, 1638, 1548, 1463, 1406, 1262, 1040, 918, 821, 747, 672, 648 cm⁻¹; HRMS (ESI) m/z for C₁₃H₉Cl₂N₄OS [M-H]⁻: calcd. 338.9880, found 338.9883.

3,4-Dichloro-N-(6-(2-chloroacetamido)benzo[d]thiazol-2-yl)-5-methyl-1H-pyrrole-2-

carboxamide (8b): To a stirred mixture of amine **7b** (0.300 g, 0.88 mmol) and chloroacetyl chloride (0.227 g, 0.16 mL, 2.02 mmol) in dry dichloromethane (60 mL) triethylamine (0.133 g, 0.18 mL, 1.32 mmol) was added dropwise over 5 minutes at room temperature. After 43h when TLC (silica gel; CH₂Cl₂/MeOH, R_f=0.8) showed complete conversion of the amine, the solution was evaporated in vacuo and triturated with satd. NaHCO₃ solution, 1M hydrochloric acid (15 mL) and water. After filtration the residual water was removed azeotropically with toluene and the product was dried to give 0.331 g of compound **8b** as a grey powder (yield: 90 %); mp >300 °C; ¹H NMR (400 MHz, DMSO-d₆) δ 2.27 (s, 3H, CH₃), 4.31 (s, 2H, CH₂), 7.55-7.58 (dd, 1H, ³J = 8.8 Hz, ⁴J = 2.2 Hz, Ar-H5), 7.70 (d, 1H, ³J = 8.8 Hz, Ar-H4), 8.32 (d, 1H, ⁴J = 2.2 Hz, Ar-7), 10.57 (s, 1H, 2-NHCO); 12.44 (s br, 1H, 6-NHCO) ppm, pyrrole-NH not seen; ¹³C NMR (100 MHz, DMSO-d₆) δ 10.95, 43.54, 109.70, 111.89, 114.96, 117.32, 118.79, 119.87, 129.67, 131.68, 134.55, 143.69, 157.29, 157.89, 164.59 ppm; IR (ATR) ν 3085, 1655, 1508, 1403, 1255, 1159, 1023, 819, 741, 667, 555 cm⁻¹; HRMS (ESI) m/z for C₁₅H₁₀Cl₃N₄O₂S [M-H]⁻: calcd. 414.9596, found 414.9599.

1-Cyclopropyl-7-(4-(2-((2-(3,4-dichloro-5-methyl-1H-pyrrole-2-carboxamido)benzo[d]thiazol-6-yl)amino)-2-oxoethyl)piperazin-1-yl)-6-fluoro-4-oxo-1,4-dihydroquinoline-3-carboxylic acid hydrochloride (2b): A stirred mixture of compound **8b** (0.200 g, 0.48 mmol), ciprofloxacin (0.318 g, 0.96 mmol) and potassium iodide (0.08 g, 0.48 mmol) in acetonitrile (25 mL) was heated under reflux for 3 h. (TLC, silica gel; CH₂Cl₂/MeOH = 9/1, R_f = 0.0-0.20). The residue was filtered off and washed with 1M hydrochloric acid (20 mL) to remove ciprofloxacin. The solid residue (0.205 g, yield: 75%) was purified with column chromatography on Sephadex LH-20 (30 g), eluting first with MeOH and then with DMSO to give **2b** as bright beige crystals (0.068 g, yield: 20%); mp 195-197

°C; ¹H NMR (400 MHz, DMSO-d₆) δ 1.19 (m, 2H, CH₂ – cyclopropyl), 1.32 (m, 2H, CH₂ – cyclopropyl), 2.27 (s, 3H, CH₃), 2.79 (m br, 4H, 2×CH₂-piperazine), 3.29 (s, 2H, COCH₂), 3.43 (m br, 4H, 2×CH₂-piperazine), 3.84 (m br, 1H, CH-cyclopropyl), 7.60 (d, 1H, ⁴J_{H,F} = 7.2 Hz, quinolone-H8), 7.63-7.68 (m, 2H, Ar-H5, Ar-H4), 7.93 (d, 1H, ³J_{H,F} = 13.6 Hz, quinolone-H5), 8.35 (s, 1H, Ar-H7), 8.67 (s, 1H, quinolone-H2), 9.98 (s, 1H, 6-NHCO), 11.6 (s br, 1H, 2-NHCO), 12.30 (s br, 1H, NH-pyrrole), 15.24 (s br, 1H, COOH) ppm; ¹³C NMR (100 MHz, DMSO-d₆) δ 7.58, 10.96, 35.92, 42.51, 51.78, 51.81, 66.32, 106.61, 106.74, 109.71, 111.08 ((d, ²J_{C,F} = 23 Hz, quinolone-C5), 112.11, 112.13, 114.91, 118.91, 119.01, 120.01, 129.74, 131.91, 134.26, 139.09, 144.09, 144.51, 148.11 (d, ²J_{C,F} = 10 Hz, quinolone-C7), 152.88 (d, ¹J_{C,F} = 248 Hz, quinolone-C6), 157.02, 157.18, 165.89, 176.32, 176.33 ppm; IR (ATR) ν 2917, 2828, 1659, 1625, 1612, 1503, 1453, 1256, 1013, 949, 745, 544 cm⁻¹; HRMS (ESI) m/z C₃₂H₂₇Cl₂FN₇O₅S [M-H]⁻: calcd. 710.1161, found 710.1178; HPLC: t_r = 20.08 min (99.32% at 280 nm).

***N*-(6-Acrylamidobenzo[*d*]thiazol-2-yl)-3,4-dichloro-5-methyl-1*H*-pyrrole-2-carboxamide (9):**

To a stirred mixture of amine **7b** (0.135 g, 0.40 mmol) and potassium carbonate (0.066 g, 0.48 mmol) in dry THF (20 mL) acryloyl chloride (0.043 g, 0.038 mL, 0.48 mmol) was added dropwise over 5 minutes at room temperature. After 20 min when TLC (silica gel; CH₂Cl₂/MeOH = 9/1, R_f=0.5) showed complete conversion of the amine, the solution was evaporated in vacuo. Dry residue was then dissolved in ethyl acetate and washed with satd. NaHCO₃ solution, 1M hydrochloric acid (15 mL) and brine, and afterwards dried over Na₂SO₄, filtered and evaporated under reduced pressure. Recrystallization from acetonitrile gave 0.096 g of compound **9** as a light brown powder (yield: 62 %); mp 243-247 °C; ¹H NMR (400 MHz, DMSO-d₆) δ 2.27 (s, 3H, CH₃), 5.79 (dd, ³J = 10.1 Hz, ²J = 2.0 Hz, 1H, CH₂), 6.29 (dd, ³J = 17.0 Hz, ²J = 2.0 Hz, 1H, CH₂), 6.48 (dd, ³J = 17.0 Hz, ³J = 10.1 Hz, 1H, CH), 7.61 (dd, ³J = 8.7 Hz, ⁴J = 2.1 Hz, 1H, Ar-H5), 7.71 (d, ³J = 8.3 Hz, 1H, Ar-H4), 8.42 (s, 1H, Ar-H7), 10.34 (s, 1H, 6-NHCO), 11.68 (s br, 1H, 2-NHCO), 12.33 (s br, 1H, NH-pyrrole); IR (ATR) ν 3350, 1646, 1608, 1526, 1463, 1405, 1267, 1229, 1195, 1092, 1063, 1041, 983, 890, 864, 816, 795, 693, 591, 555, 520 cm⁻¹; HRMS (ESI⁺) m/z C₁₆H₁₃Cl₂N₄O₂S [M+H]⁺: calcd. 395.0131, found 395.0132; HPLC: t_r = 8.62 min (96.05% at 254 nm).

1-Cyclopropyl-7-(4-(3-((2-(3,4-dichloro-5-methyl-1*H*-pyrrole-2-carboxamido)benzo[*d*]thiazol-6-yl)amino)-3-oxopropyl)-piperazin-1-yl)-6-fluoro-4-oxo-1,4-dihydroquinoline-3-carboxylic acid (2c):

A stirred mixture of compound **9** (0.038 g, 0.096 mmol) and ciprofloxacin (0.032 g, 0.096

mmol) in acetonitrile (7 mL) and acetic acid (1 mL) was heated under reflux for 72 h. (TLC, silica gel; CH₂Cl₂/MeOH = 9/1, R_f = 0.37). The residue was filtered off and the precipitate was further triturated with 1M hydrochloric acid (30 mL) and methanol (5 mL), filtered and dried to give **2c** as brown powder (0.011 g, yield: 16%); mp 252-255 °C; ¹H NMR (400 MHz, DMSO-d₆) δ 1.14-1.21 (m, 2H, CH₂ – cyclopropyl), 1.27-1.38 (m, 2H, CH₂ – cyclopropyl), 2.27 (s, 3H, CH₃), 2.58 (t, 2H, COCH₂CH₂), 2.65-2.73 (m, 4H, 2×CH₂-piperazine), 2.78 (t, 2H, COCH₂CH₂), 3.79-3.84 (m, 1H, CH-cyclopropyl), 7.54 (dd, ³J = 8.8 Hz, ⁴J = 2.0 Hz, 1H, Ar-H5), 7.58 (d, 1H, ⁴J_{H,F} = 7.6 Hz, quinolone-H8), 7.68 (s br, 1H, Ar-H4), 7.92 (d, 1H, ³J_{H,F} = 13.2 Hz, quinolone-H5), 8.35 (s, 1H, Ar-H7), 8.67 (s, 1H, quinolone-H2), 10.23 (s, 1H, 6-NHCO), 11.67 (s br, 1H, 2-NHCO), 12.32 (s br, 1H, NH-pyrrole), 15.25 (s br, 1H, COOH), 2×CH₂-piperazine covered by water peak; solubility too poor to perform ¹³C experiment; IR (ATR) ν 3365, 2831, 1724, 1673, 1648, 1629, 1549, 1463, 1406, 1379, 1297, 1258, 1139, 1098, 1041, 948, 903, 872, 818, 745, 690, 621, 592, 557, 519 cm⁻¹; HRMS (ESI) m/z C₃₃H₂₉Cl₂FN₇O₅S [M-H]⁻: calcd. 724.1317, found 724.1338; HPLC: t_r = 6.44 min (96.84% at 254 nm).

2-Chloro-N-(6-nitro-benzothiazol-2-yl)-acetamide (10): To a stirred mixture of 6-nitrobenzo[*d*]thiazol-2-amine (**4**) (3.90 g, 20 mmol) and chloroacetyl chloride (2.48 g, 1.76 mL), 22 mmol) in dichloromethane (150 mL) triethylamine (2.22 g, 3.06 mL, 22 mmol) was added dropwise over 5 minutes at room temperature. After 18 h when TLC (silica gel; CH₂Cl₂/MeOH, R_f = 0.60) showed complete conversion of the starting amine, the solution was evaporated in vacuo and triturated with satd. NaHCO₃ solution. The precipitate was filtered off, washed with water and recrystallized from acetone (220 mL) to give 3.69 g (yield: 68%) of compound **10** as pale yellow powder; mp 204-206 °C (mp Ref.¹¹⁹ 190 °C); ¹H NMR (400 MHz, DMSO-d₆) δ 4.54 (s, 2H, CH₂), 7.93 (d, 1H, ³J = 8.8 Hz, Ar-H4), 8.31 (dd, 1H, ³J = 8.8 Hz, ⁴J = 2.4 Hz, Ar-H5), 9.12 (d, 1H, ⁴J = 2.4 Hz, Ar-H7), 13.15 (s br, 1H, NHCO) ppm; ¹³C NMR (100 MHz, DMSO-d₆) δ 42.55, 119.16, 120.83, 121.82, 132.19, 143.12, 153.31, 163.09, 166.64 ppm; IR (ATR) ν 3298, 3090, 2943, 1716, 1510, 1443, 1331, 1275, 1144, 902, 813, 747, 550 cm⁻¹; MS (ESI) m/z for C₉H₅ClN₃O₃S = 269.7 [M-H]⁻.

N-(6-Amino-benzothiazol-2-yl)-2-chloro-acetamide (11): A solution of compound **10** (1 g, 3.68 mmol) in ethyl acetate (300 mL) was hydrogenated over 10% Pd/C (0.200 g, 20 wt. percent) in Parr hydrogenator at 1.5 bar pressure at room temperature for 17 h and followed by TLC (silica gel; CH₂Cl₂/MeOH = 9/1). The reaction mixture was filtered warm through Celite to remove the catalyst

and the filtrate was evaporated in vacuo. The crude residue was triturated with 1M hydrochloric acid (40 mL), filtered and the filtrate was neutralized with solid NaHCO₃ to pH 8. The precipitate was filtered off, washed with water and dried to give 0.520 g (yield: 59 %) of a grey amorphous powder; mp >300 °C; ¹H NMR (100 MHz, DMSO-d₆) δ 4.41 (s, 2H, CH₂), 5.34 (s br, 2H, NH₂), 6.73 (dd, 1H, ³J = 8.4 Hz, ⁴J = 2.0 Hz, Ar-H5), 7.03 (d, 1H, ⁴J = 2.0 Hz, Ar-H7), 7.44 (d, 1H, ³J = 8.4 Hz, Ar-H4), 12.40 (s br, 1H, NHCO) ppm; ¹³C NMR (400 MHz, DMSO-d₆) δ 42.45, 106.76, 116.

4,5-Dibromo-N-(2-(2-chloroacetamido)benzo[d]thiazol-6-yl)-1H-pyrrole-2-carboxamide (12a):

To a stirred solution of the amine **11** (0.242 g, 1 mmol) and 4,5-dibromo-1H-pyrrole-2-carbonyl chloride (0.331 g, 1.15 mmol) in dioxane (11.8 mL) triethylamine (0.116 g, 1.15 mmol, 0.16mL) was added. The mixture was stirred for 22 h at room temperature and followed by TLC (silica gel; CH₂Cl₂/MeOH = 9/1, R_f = 0.55), evaporated in vacuo and the residue triturated with saturated NaHCO₃ solution (10 mL), 1M hydrochloric (10 mL) acid and water. After filtration the residual water was removed azeotropically with toluene and the product was dried to give **12a** as a brown powder (yield: 0.248 g, 50%), mp 188-200 °C; ¹H NMR (100 MHz, DMSO-d₆) δ 4.47 (s, 2H, CH₂), 7.26 (d, 1H, ⁴J = 2.4 Hz, pyrrole-H3), 7.69 (dd, 1H, ³J = 8.8 Hz, ⁴J = 2.0 Hz, Ar-H5), 7.75 (d, 1H, ³J = 8.8 Hz, Ar-H4), 8.41 (d, 1H, ⁴J = 2.0 Hz, Ar-H7), 10.04 (s, 1H, 6-NHCO), 12.70 (s br, 1H, 2-NHCO), 12.95 (d br, 1H, ⁴J = 2.4 Hz, pyrrole-NH) ppm; ¹³C NMR (400 MHz, DMSO-d₆) δ 42.47, 98.16, 105.95, 112.48, 113.82, 119.57, 120.71, 127.84, 131.93, 134.98, 144.65, 156.57, 157.26, 165.74 ppm; IR (ATR) ν 3129, 2954, 1638, 1524, 1410, 1330, 1274, 1182, 975, 806, 644 cm⁻¹; HRMS (ESI⁺) m/z for C₁₄H₁₀Br₂ClN₄O₂S [M+H]⁺: calcd. 490.8574, found 490.8574.

1-Cyclopropyl-7-(4-(2-((6-(4,5-dibromo-1H-pyrrole-2-carboxamido)benzo[d]thiazol-2-yl)amino)-2-oxoethyl)piperazin-1-yl)-6-fluoro-4-oxo-1,4-dihydroquinoline-3-carboxylic acid hydrochloride (3a): A stirred mixture of compound **12a** (0.200 g, 0.41 mmol), ciprofloxacin (0.272 g, 0.82 mmol) and potassium iodide (0.068 g, 0.41 mmol) in acetonitrile (25 mL) was heated under reflux for 3.5 h (TLC silica gel, CH₂Cl₂/MeOH = 9/1, R_f = 0.0-0.20). The precipitate was filtered off and triturated with 1M hydrochloric acid (10 mL) to remove most of ciprofloxacin. The solid residue (0.218 g, yield 68%) was purified with column chromatography on Sephadex LH-20 (30 g), eluting first with MeOH and then with DMSO to give bright brown crystals; (0.147 g, yield: 46 %); mp 201-203 °C; ¹H NMR (400 MHz, DMSO-d₆) δ 1.20 (m, 2H, CH₂ – cyclopropyl), 1.33 (m, 2H, CH₂ – cyclopropyl), 2.82 (m br, 4H, 2×CH₂-piperazine), 3.41 (m br, 4H, 2×CH₂-piperazine), 3.49 (s, 2H,

COCH₂), 3.84 (m br, 1H, CH-cyclopropyl), 7.26 (d, 1H, ⁴J = 2.8, pyrrole-H3), 7.61 (d, 1H, ⁴J_{H,F} = 7.6, quinolone-H8), 7.67- 7.70 (dd, 1H, ³J = 8.8 Hz, ⁴J = 2.0 Hz, Ar-H5), 7.74 (d, 1H, ³J = 8.8 Hz, Ar-H4), 7.93 (d, 1H, ³J_{H,F} = 13.2 Hz, quinolone-H5), 8.40 (d, 1H, ⁴J = 2.0 Hz, Ar-H7), 8.68 (s, 1H, quinolone-H2), 10.02 (s, 1H, 6-NHCO), 12.17 (s br, 1H, 2-NHCO), 12.94 (d br, 1H, ⁴J = 2.8 Hz, pyrrole-NH), 15.25 (s br, 1H, COOH) ppm; ¹³C NMR (100 MHz, DMSO-d₆) δ 7.56, 35.88, 42.52, 49.16, 51.99, 98.17, 105.91, 106.54, 106.71, 110.99 (d, ²J_{C,F} = 22 Hz, quinolone-C5), 112.43, 113.87, 118.74, 119.51, 120.52, 127.85, 131.85, 134.91, 139.15, 144.58 (d, ²J_{C,F} = 6, quinolone-C7), 144.60, 148.06, 152.9 (d, ¹J_{C,F} = 247 Hz, quinolone-C6), 156.54, 157.24, 165.92, 176.33, 176.35 ppm; IR (ATR) ν 2933, 2834, 1717, 1626, 1523, 1461, 1257, 1136, 1016, 944, 825, 748, 551 cm⁻¹; HRMS (ESI) m/z for C₃₁H₂₅Br₂FN₇O₅S [M-H]⁻: calcd. 783.9994, found 784.0004; HPLC: t_r = 19.50 min (97.1% at 280 nm).

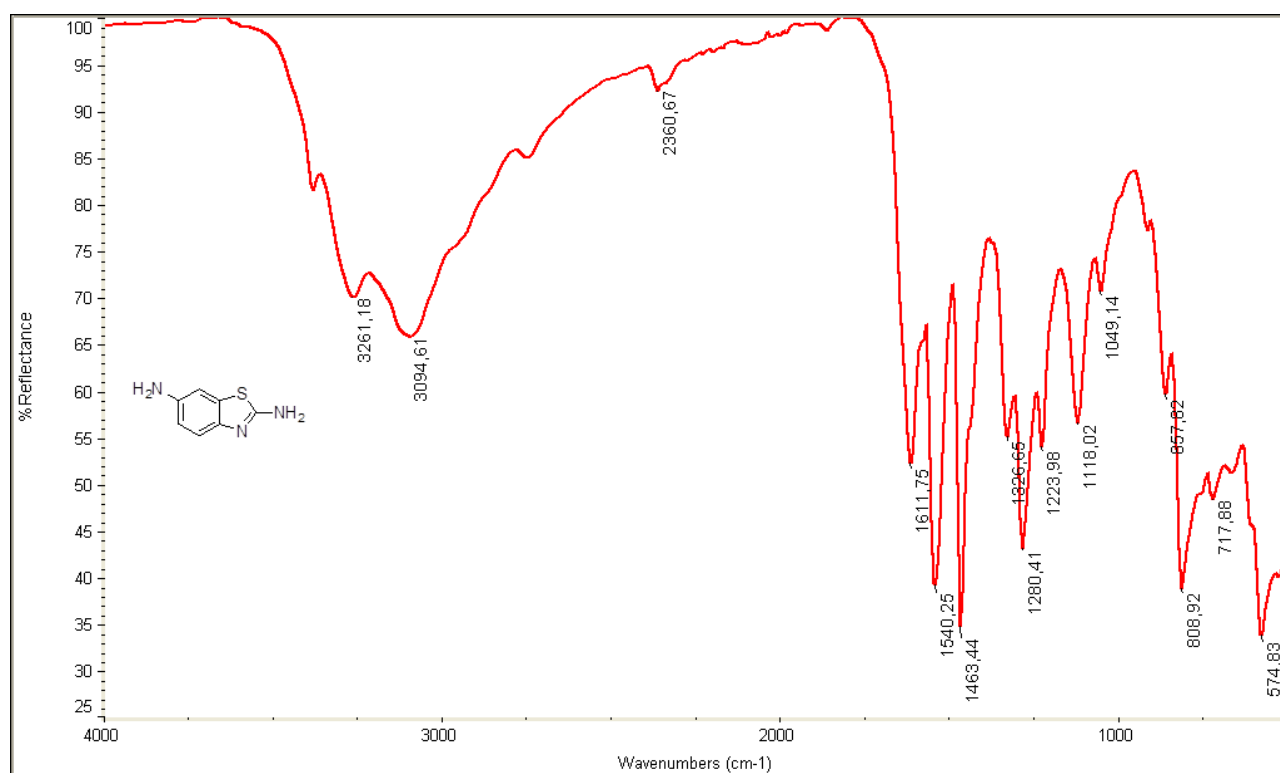
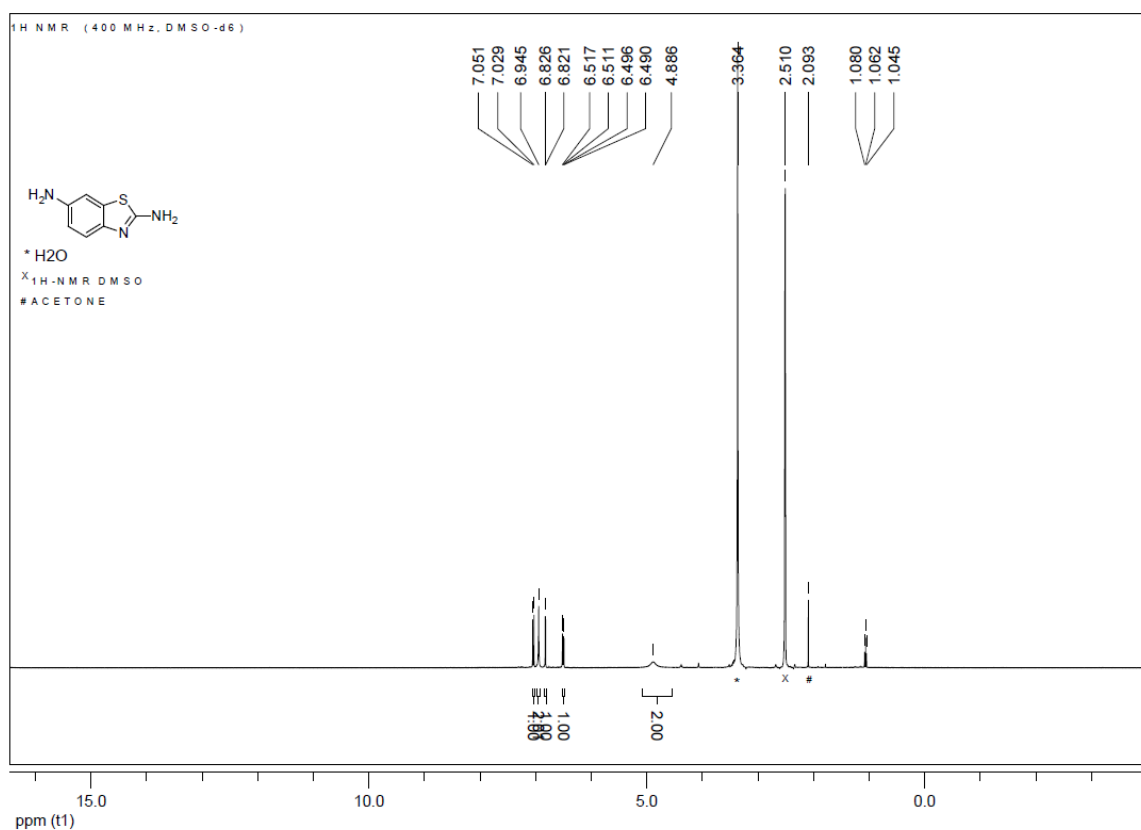
3,4-Dichloro-5-methyl-N-(2-(2-chloroacetamido) benzo[d]thiazol-6-yl)-1H-pyrrole-2-carboxamide (12b): To a stirred solution of the amine **11** (0.302 g, 1.25 mmol) and 3,4-dichloro-5-methyl-1H-pyrrole-2-carbonyl chloride (0.306 g, 1.44 mmol) in dioxane (14.6 mL) triethylamine (0.148 g, 1.44 mmol, 0.20 mL), was added. The mixture was stirred for 22 h at room temperature and controlled by TLC (silica gel; CH₂Cl₂/MeOH = 9/1, R_f = 0.55). The reaction mixture was evaporated in vacuo and the residue triturated with saturated NaHCO₃ solution (10 mL), 1M hydrochloric acid (10 mL) and water and dried by azeotropic distillation with toluene to give 0.195 g of a grey powder (yield: 37%); mp 254-256 °C (from DMF/MeOH = 1:2); ¹H NMR (400 MHz, DMSO-d₆) δ 2.25 (s, 3H, CH₃) 4.47 (s, 2H, CH₂), 7.67 (dd, 1H, ³J = 8.8 Hz, ⁴J = 2.2 Hz, Ar-H5) 7.75 (d, 1H, ³J = 8.8 Hz, Ar-H4), 8.38 (d, 1H, ⁴J = 2.2 Hz, Ar-H7), 9.67 (s, 1H, 6-NHCO), 12.29 (s br, 1H, 2-NHCO), 12.70 (s, 1H, pyrrole-NH) ppm; ¹³C NMR (100 MHz, DMSO-d₆) δ 10.76, 42.47, 108.50, 111.62, 112.40, 119.35, 119.53, 120.68, 127.93, 131.93, 134.81, 144.66, 156.66, 157.12, 165.81 ppm; IR (ATR) ν 3397, 3248, 1648, 1531, 1463, 1328, 1249, 1040, 806, 744, 666, 549 cm⁻¹; HRMS (ESI) m/z for C₁₅H₁₀Cl₃N₄O₂S [M-H]⁻: calcd. 414.9596, found 414.9599.

1-Cyclopropyl-7-(4-(2-(((6-(3,4-dichloro-5-methyl-1H-pyrrole-2-carboxamido)benzo[d]thiazol-2-yl)amino)-2-oxoethyl)piperazin-1-yl)-6-fluoro-4-oxo-1,4-dihydroquinoline-3-carboxylic acid hydrochloride (3b): A stirred mixture of compound **12b** (0.160 g, 0.38 mmol), ciprofloxacin (0.252 g, 0.76 mmol) and potassium iodide (0.063 g, 0.38 mmol) in acetonitrile (20 mL) was heated under reflux for 5 h (TLC, silica gel; CH₂Cl₂/MeOH = 9/1, R_f = 0.0-0.20). The precipitate was filtered off and triturated with 1M hydrochloric acid (10 mL) to remove most of ciprofloxacin. The solid residue

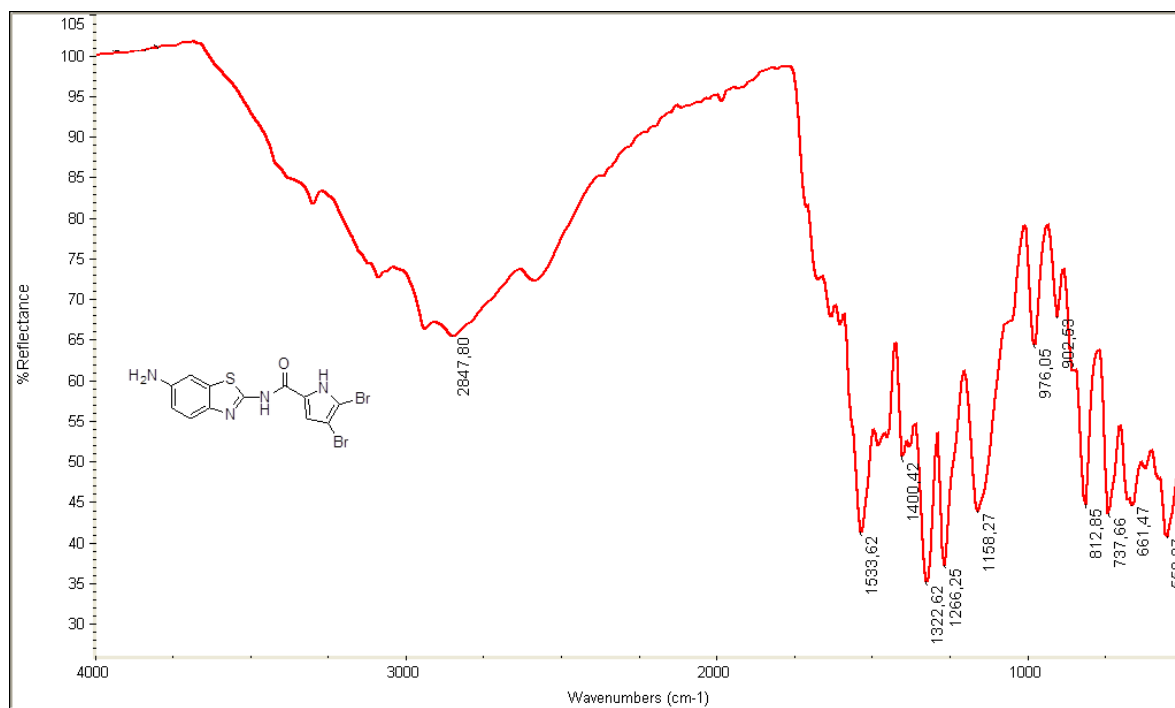
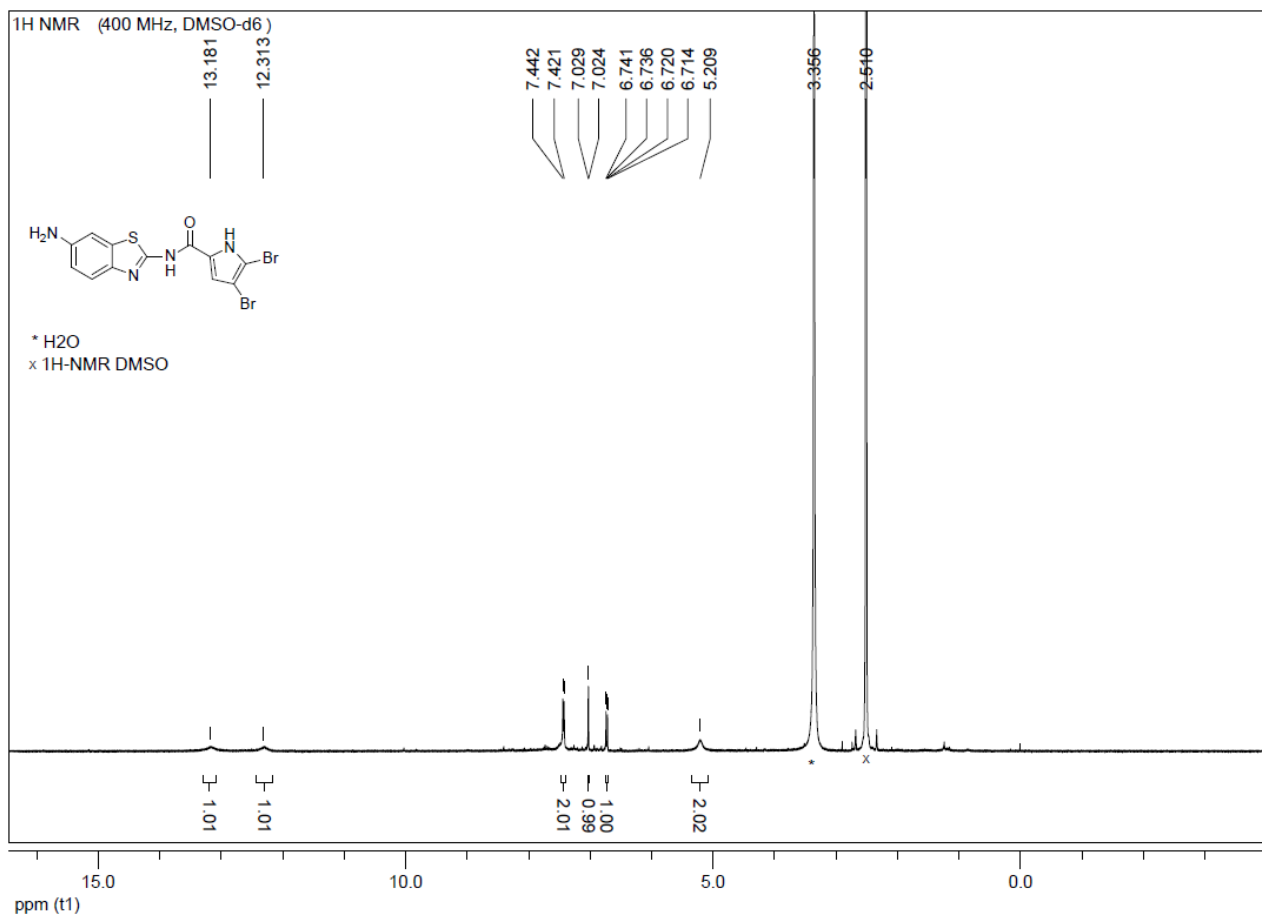
(0.205 g, yield: 75%) was purified with column chromatography on Sephadex LH-20 (30 g), eluting first with MeOH and then with DMSO to give **3b** as bright beige crystals (0.070 g, yield: 26 %); mp 278-280 °C (from DMF/MeOH = 1:2); ¹H NMR (400 MHz, DMSO-d₆) δ 1.20 (m, 2H, CH₂ – cyclopropyl), 1.33 (m, 2H, CH₂ – cyclopropyl), 2.24 (s, 3H, CH₃), 2.83 (m br, 4H, 2×CH₂-piperazine), 3.41 (m br, 4H, 2×CH₂-piperazine), 3.49 (s, 2H, COCH₂), 3.84 (m br, 1H, CH-cyclopropyl), 7.61 (d, 1H, ⁴J_{H,F} = 7.6 Hz, quinolone-H8), 7.64-7.66 (dd, 1H, ³J = 8.8 Hz, ⁴J = 2.0 Hz, Ar-H5), 7.74 (d, 1H, ³J = 8.8 Hz, Ar-H4), 7.93 (d, 1H, ³J_{H,F} = 13.2 Hz, quinolone-H5), 8.36 (d, 1H, ⁴J = 2.0 Hz, Ar-H7), 8.68 (s, 1H, quinolone-H2), 9.59 (s, 1H, 6-NHCO), 12.20 (s br, 2H, 2-NHCO, NH-pyrrole), 15.25 (s br, 1H, COOH) ppm; ¹³C NMR (100 MHz, DMSO-d₆) δ 7.51, 10.68, 35.86, 42.40, 47.06, 51.64, 106.70, 106.85, 108.51, 111.01 (d, ²J_{C,F} = 21 Hz, quinolone-C5), 111.97, 112.20, 118.98, 119.10, 119.43, 120.55, 127.75, 131.75, 134.97, 139.00, 144.04, 144.3 (d, ²J_{C,F} = 7.4 Hz, quinolone-C7), 148.1, 152.8 (d, ¹J_{C,F} = 248 Hz, quinolone-C6), 156.34, 156.99, 165.79, 176.26, 176.28 ppm; IR (ATR) ν 2917, 2828, 1726, 1642, 1624, 1529, 1450, 1251, 1137, 1015, 939, 806, 748, 580 cm⁻¹; HRMS (ESI) m/z for C₃₂H₂₇Cl₂FN₇O₅S [M-H]⁻: calcd. 710.1161, found 710.1167; HPLC: t_r = 20.65 min (98.30 % at 280 nm).

3.6.3 ^1H and ^{13}C NMR spectra, IR spectra and HPLC chromatograms

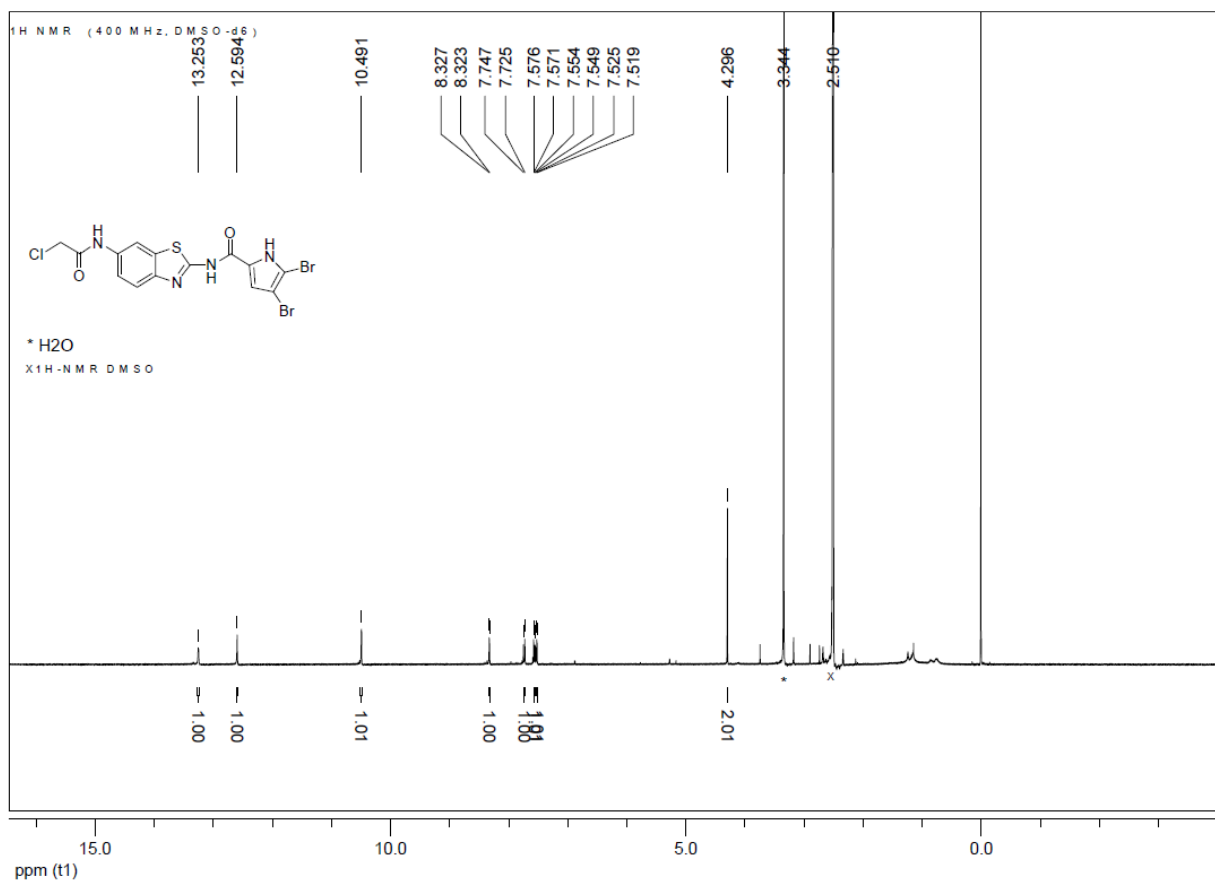
Benzothiazole-2,6-diamine (6)

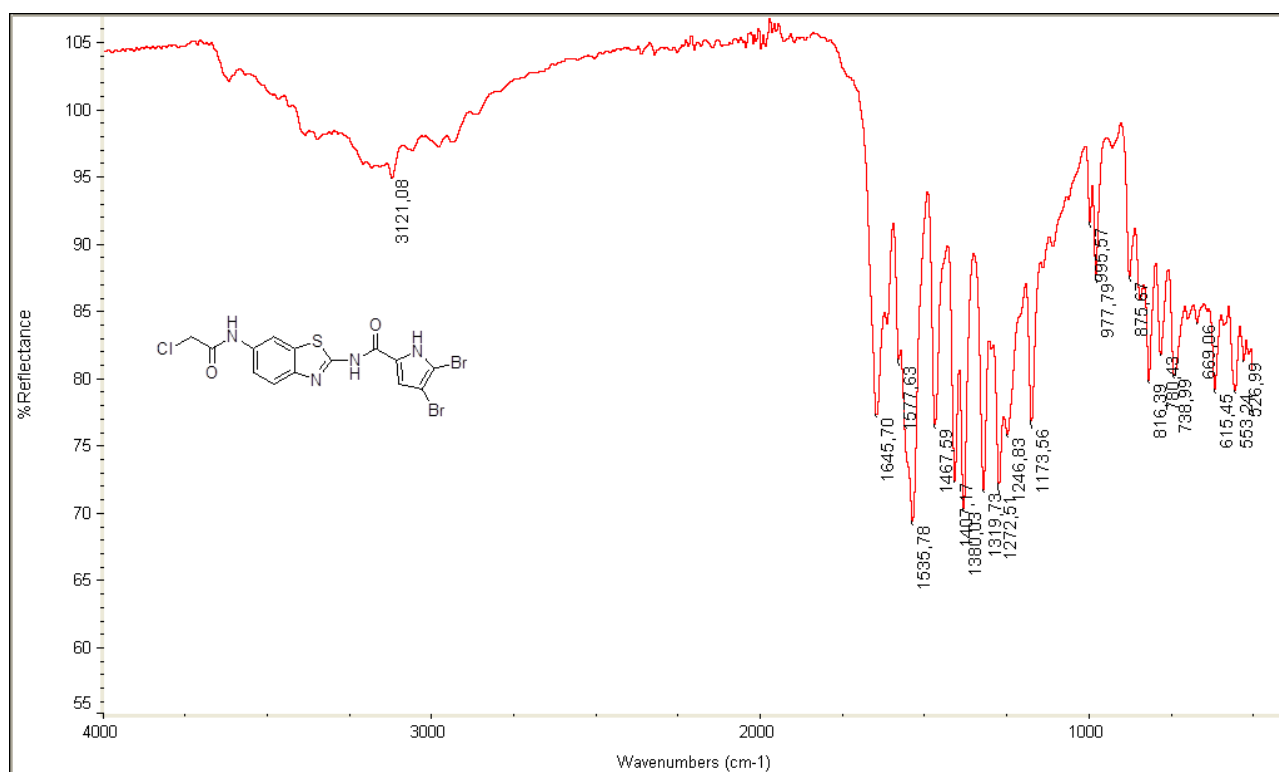
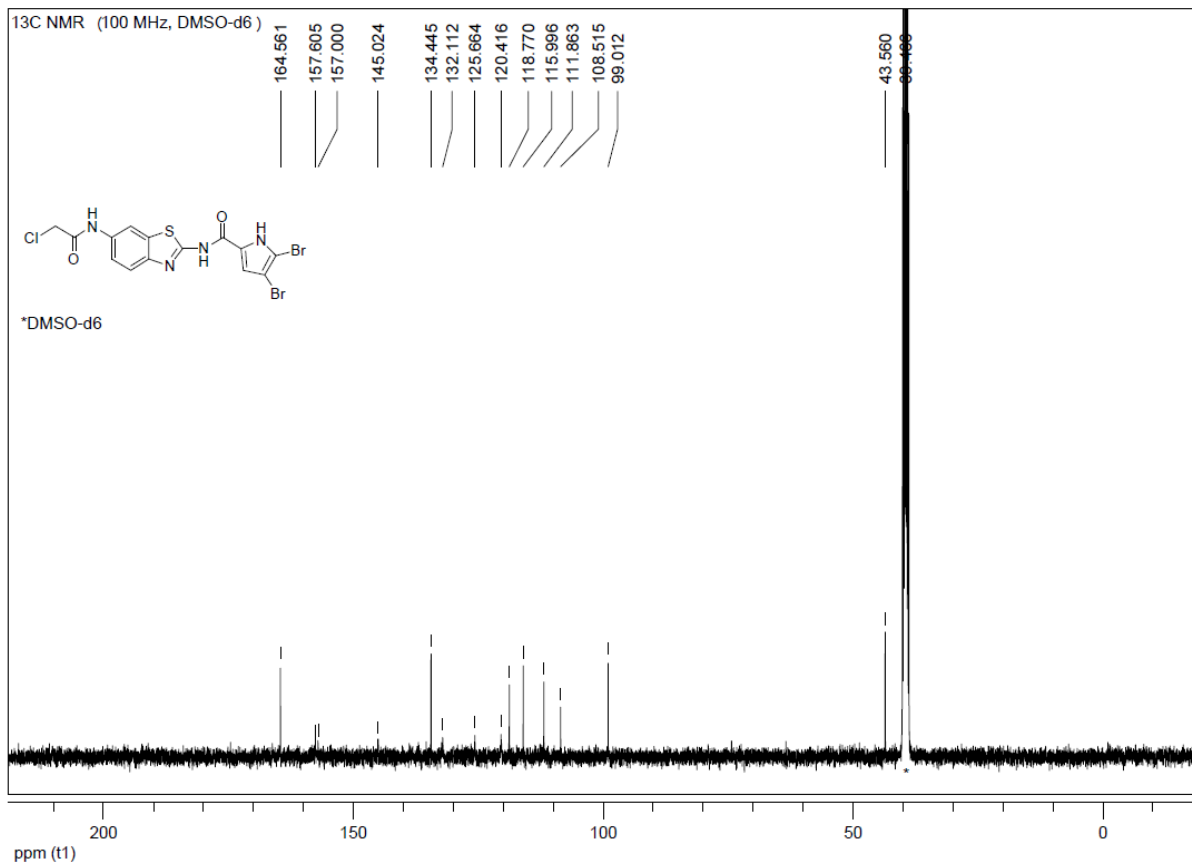


***N*-(6-Aminobenzo[*d*]thiazol-2-yl)-4,5-dibromo-1*H*-pyrrole-2-carboxamide (7a)**

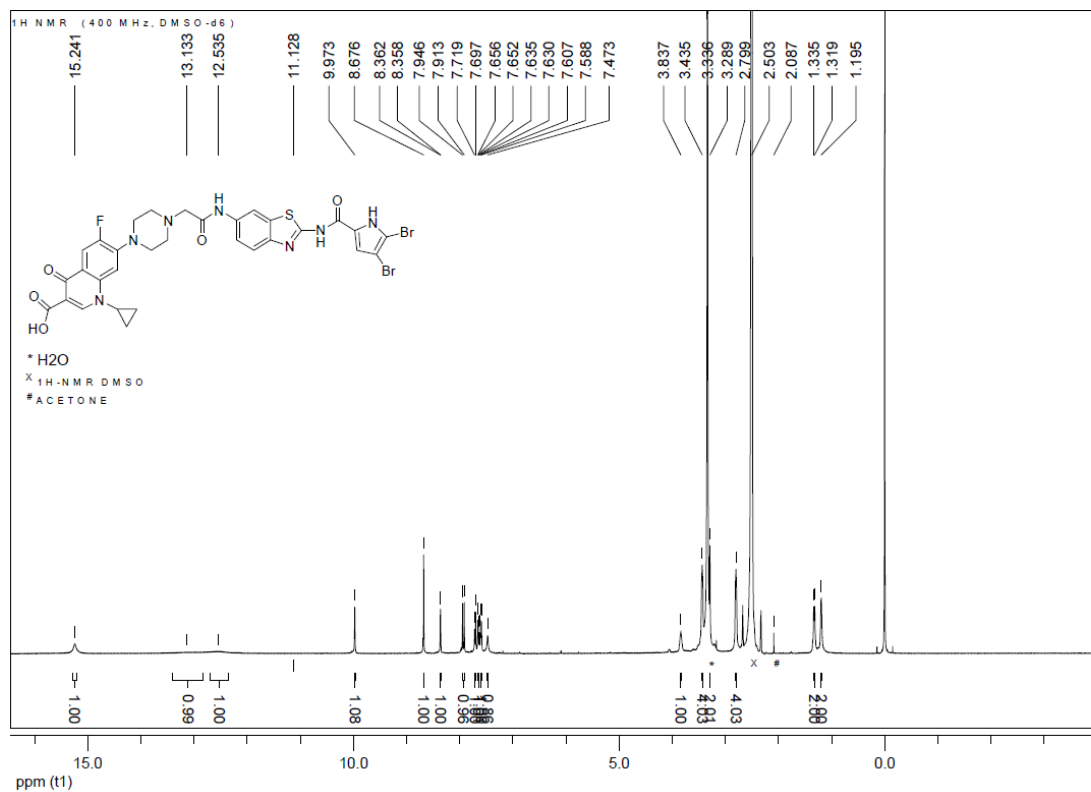


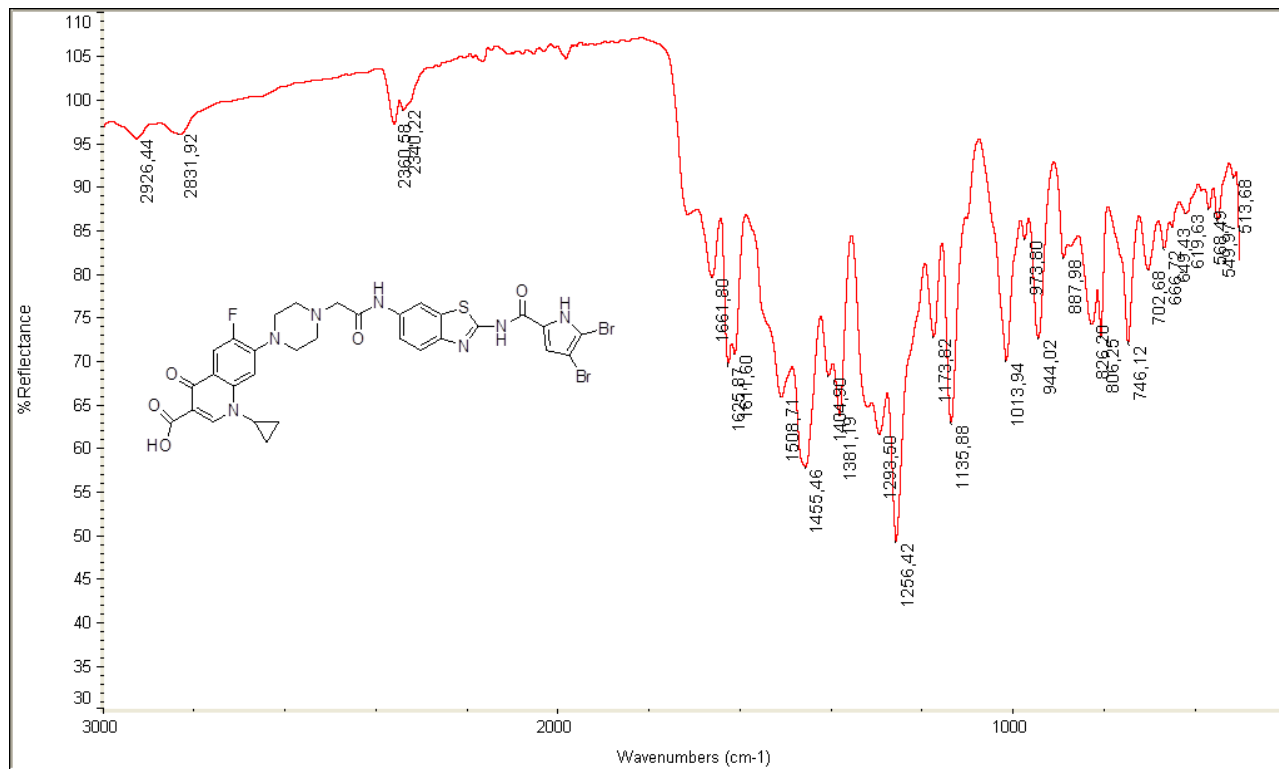
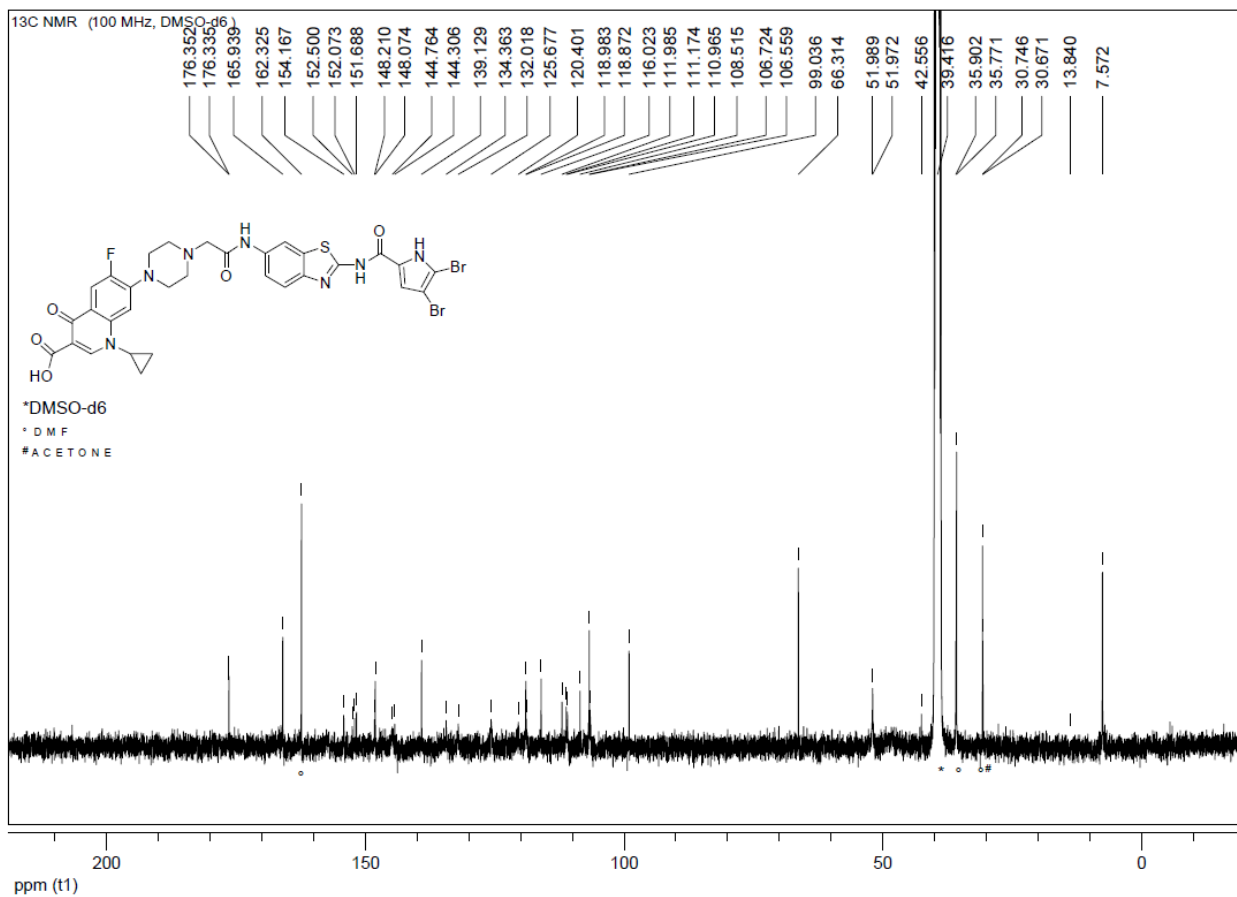
4,5-Dibromo-N-(6-(2-chloroacetamido)benzo[d]thiazol-2-yl)-1H-pyrrole-2-carboxamide (8a)

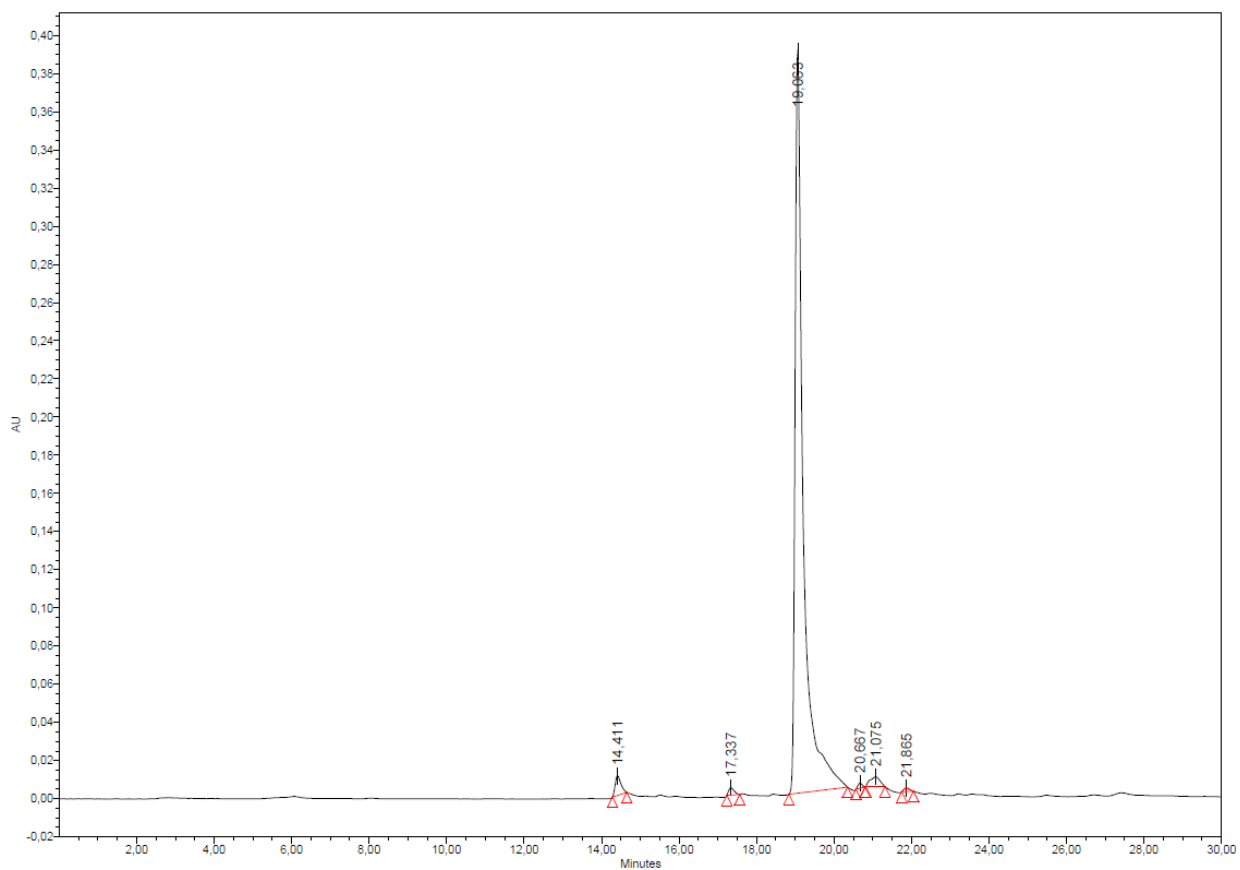




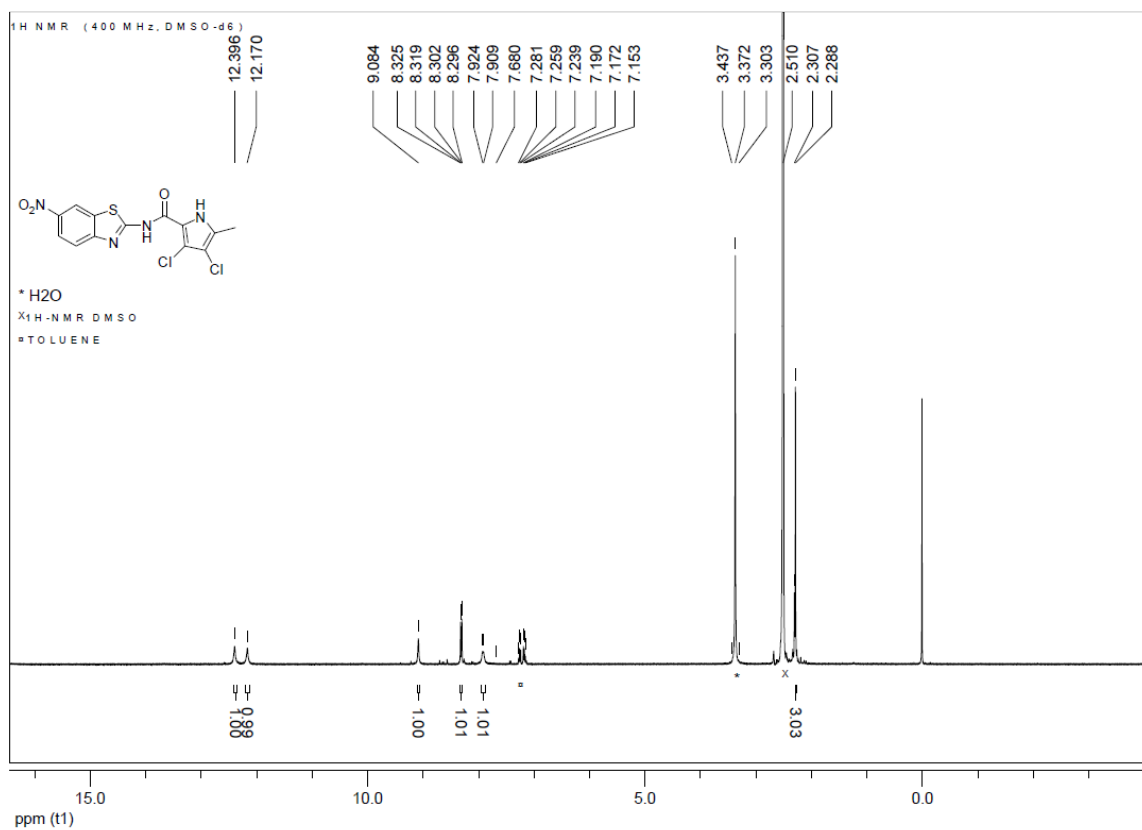
1-Cyclopropyl-7-(4-(2-((2-(4,5-dibromo-1H-pyrrole-2-carboxamido)benzo[d]thiazol-6-yl)amino)-2-oxoethyl)piperazin-1-yl)-6-fluoro-4-oxo-1,4-dihydroquinoline-3-carboxylic acid hydrochloride (2a)

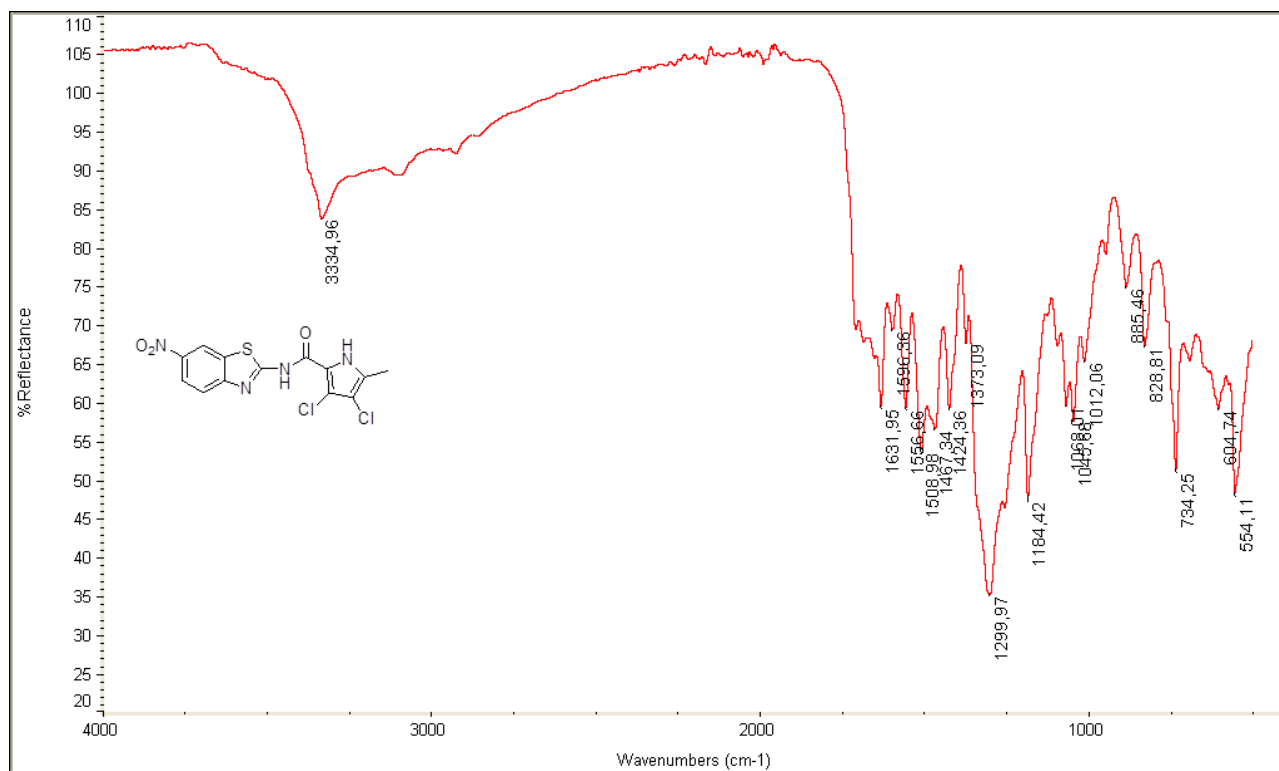
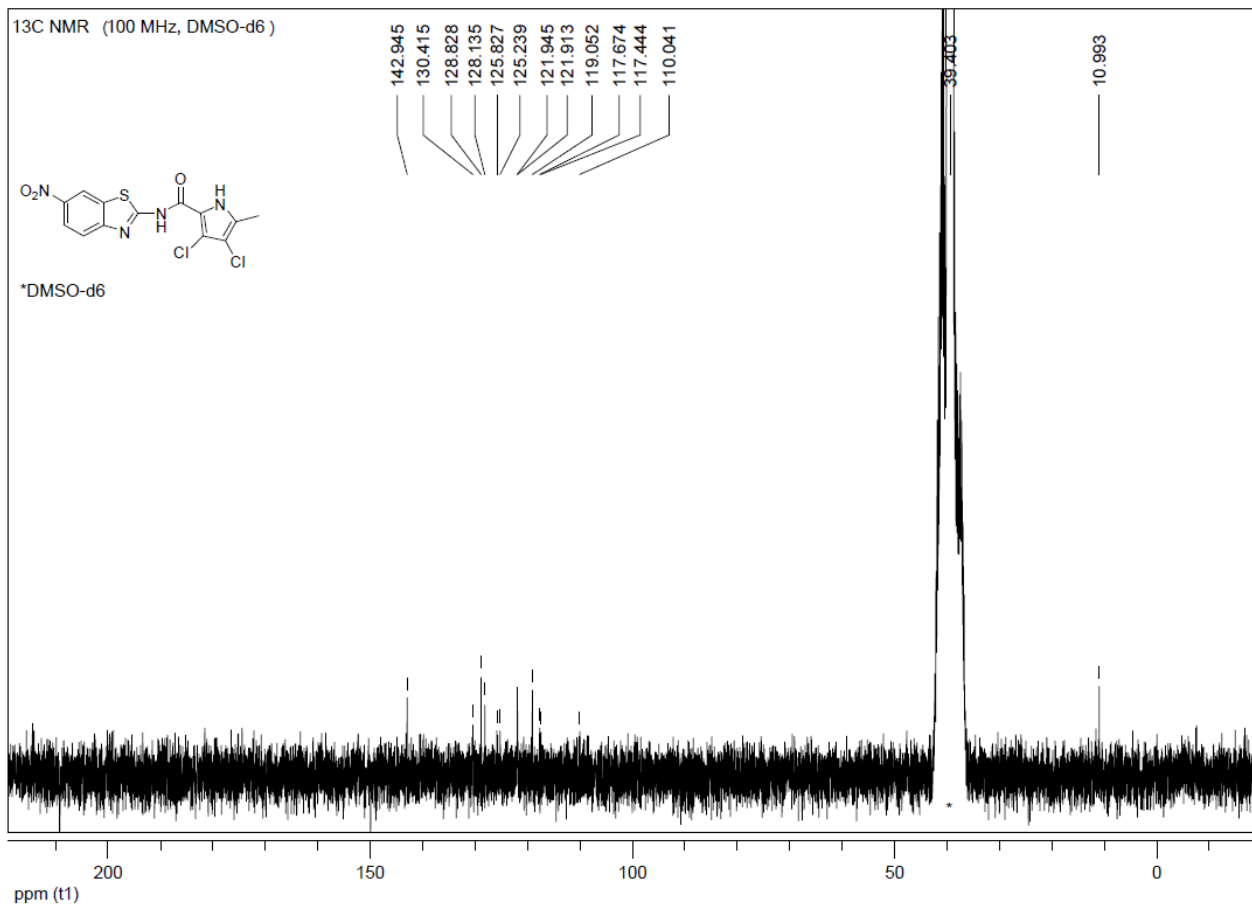




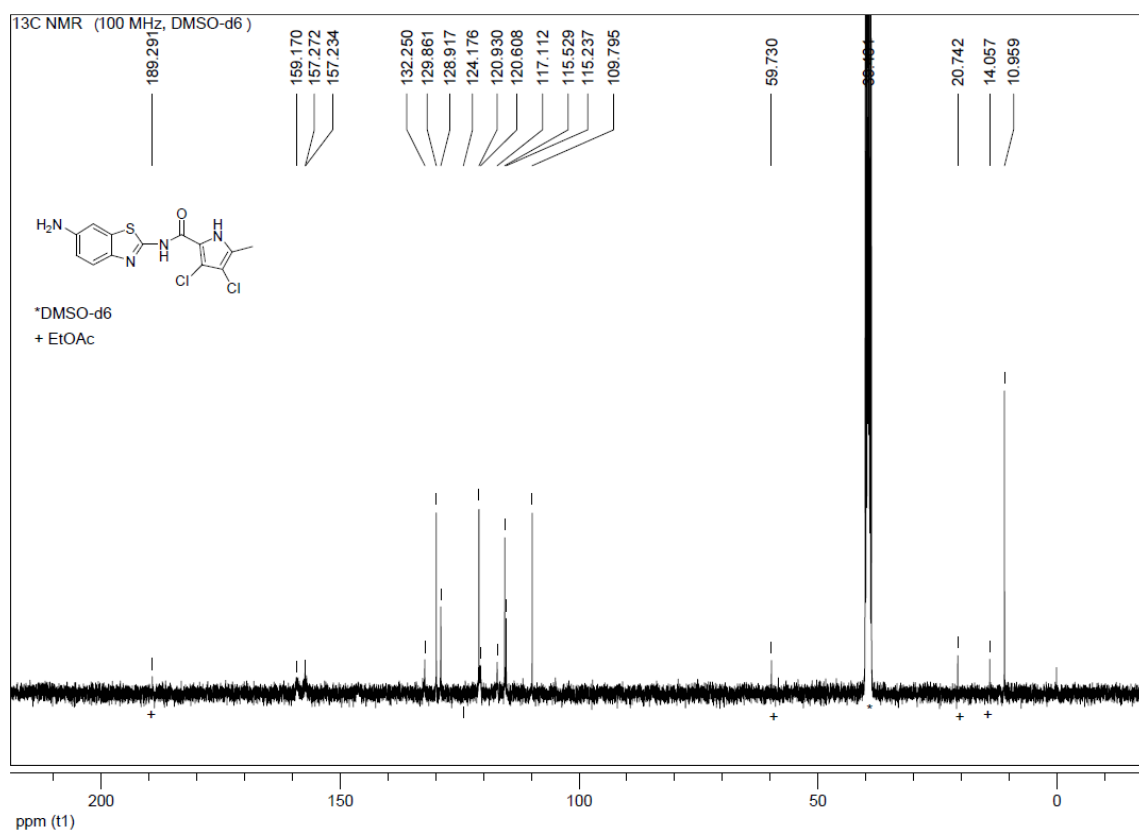
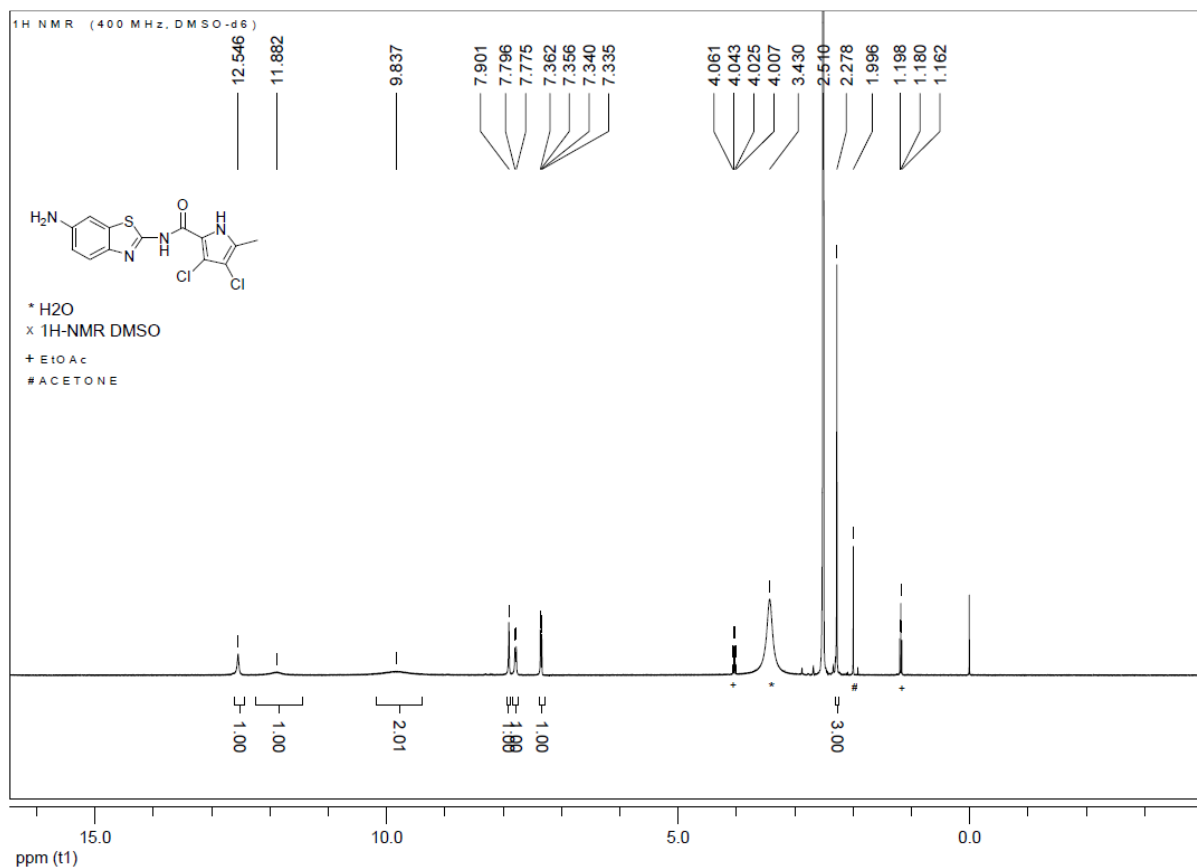


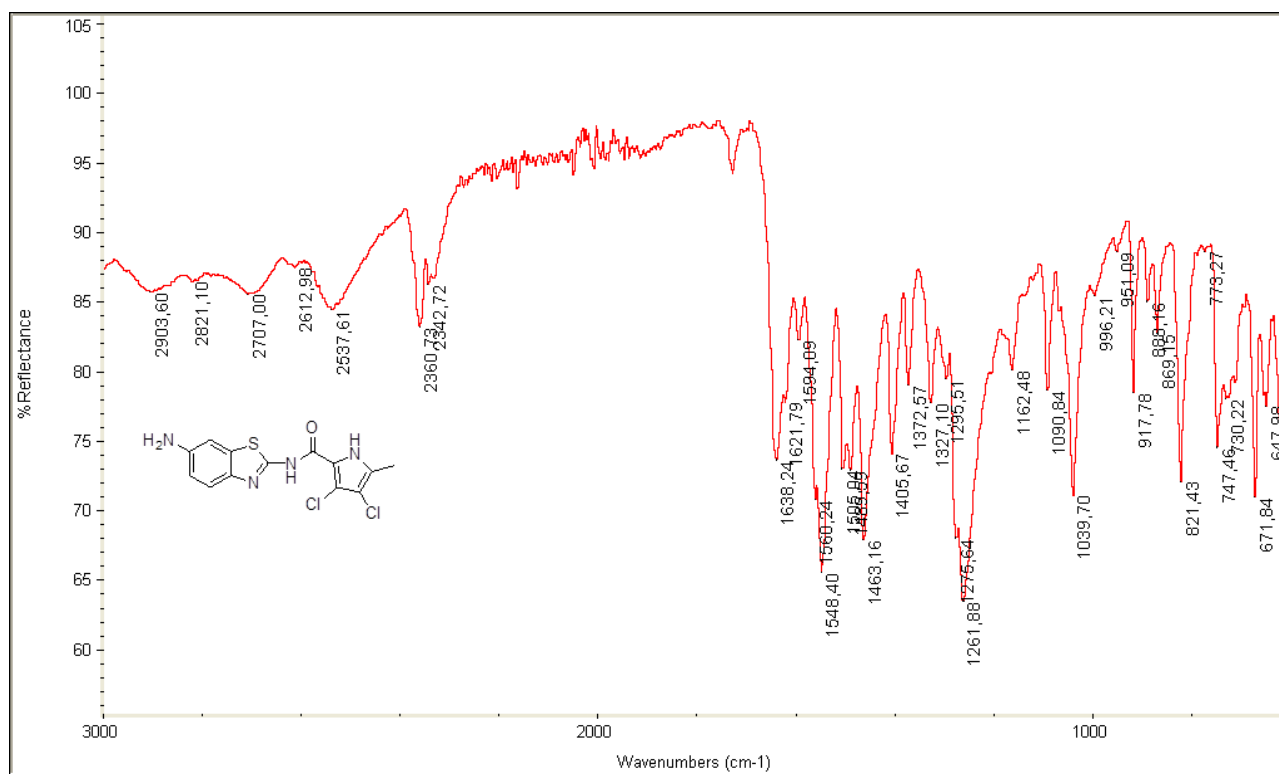
3,4-Dichloro-5-methyl-N-(6-nitrobenzo[d]thiazol-2-yl)-1H-pyrrole-2-carboxamide (5b)



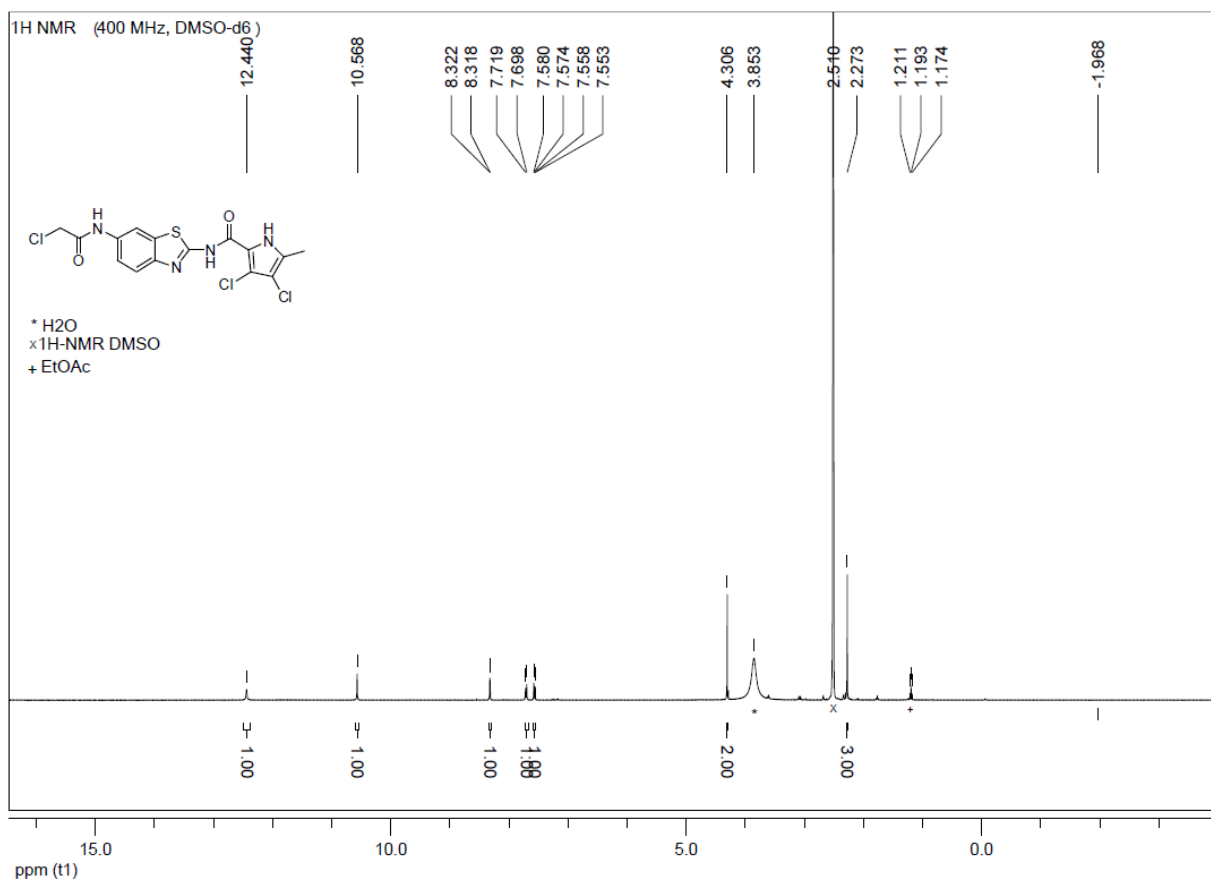


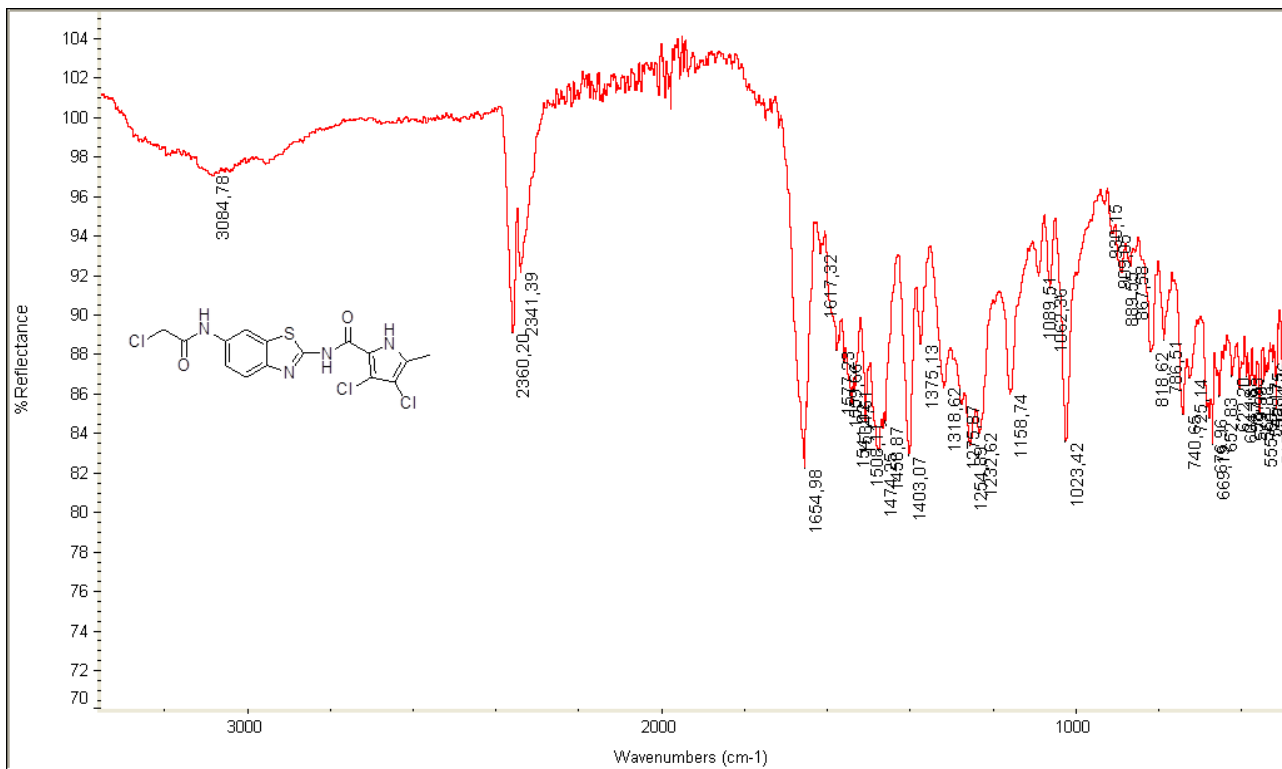
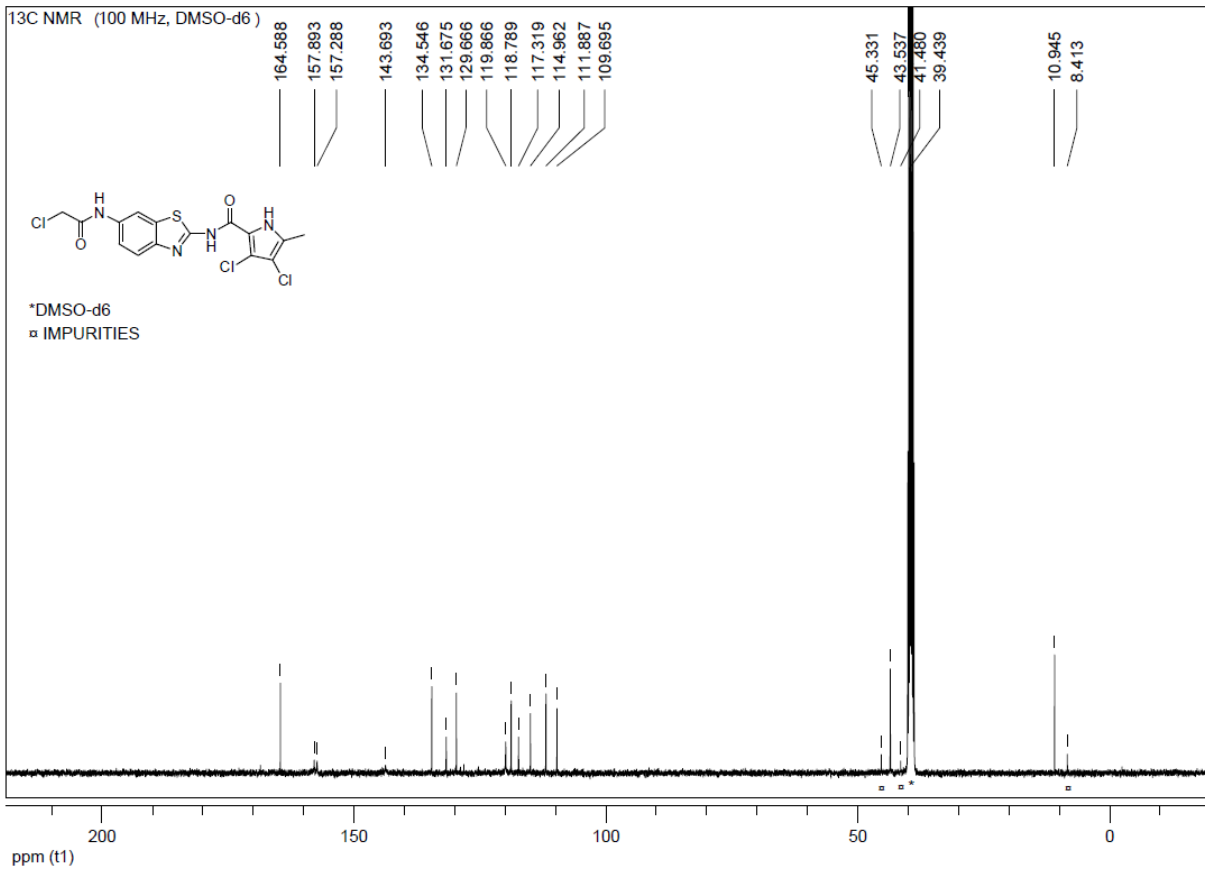
***N*-(6-Aminobenzo[*d*]thiazol-2-yl)-3,4-dichloro-5-methyl-1*H*-pyrrole-2-carboxamide (7b)**



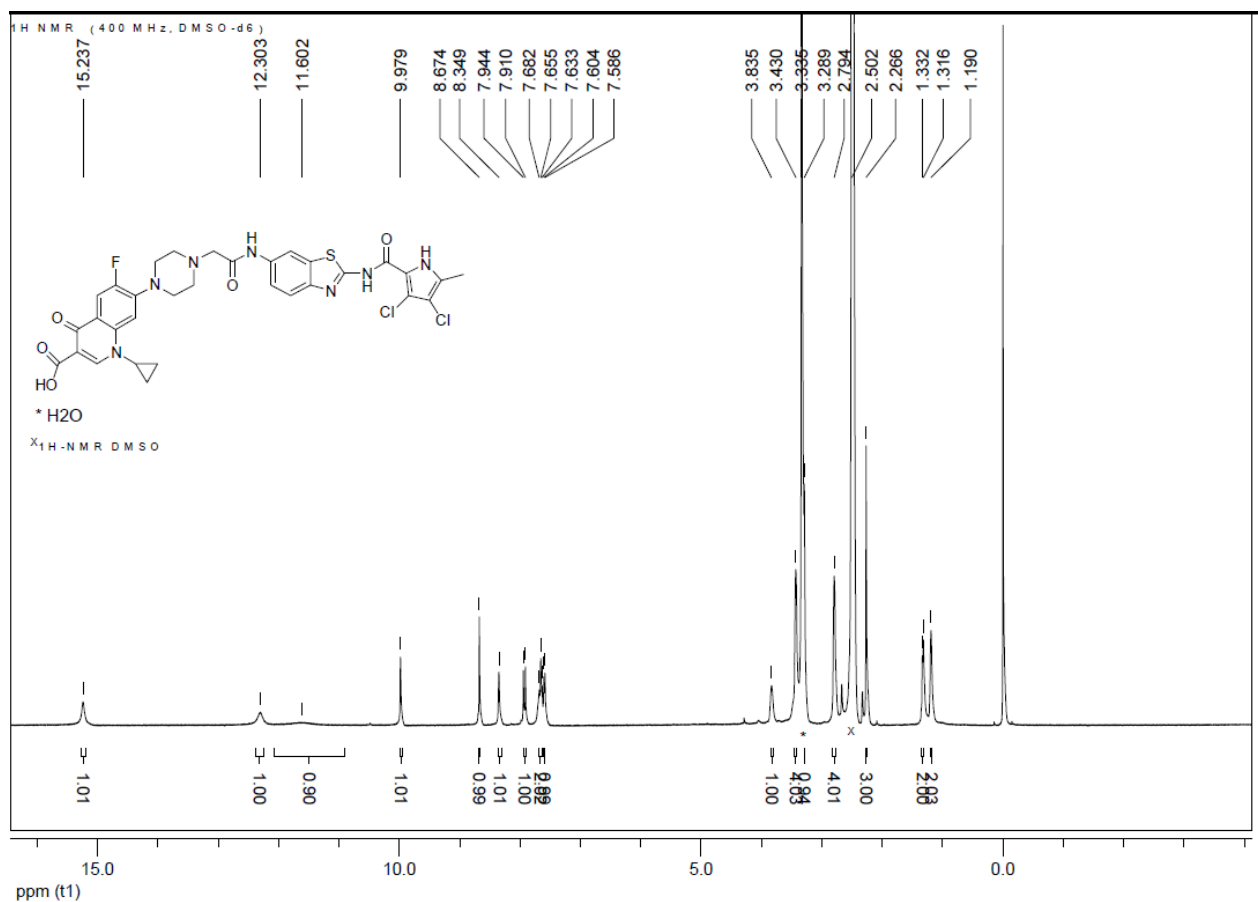


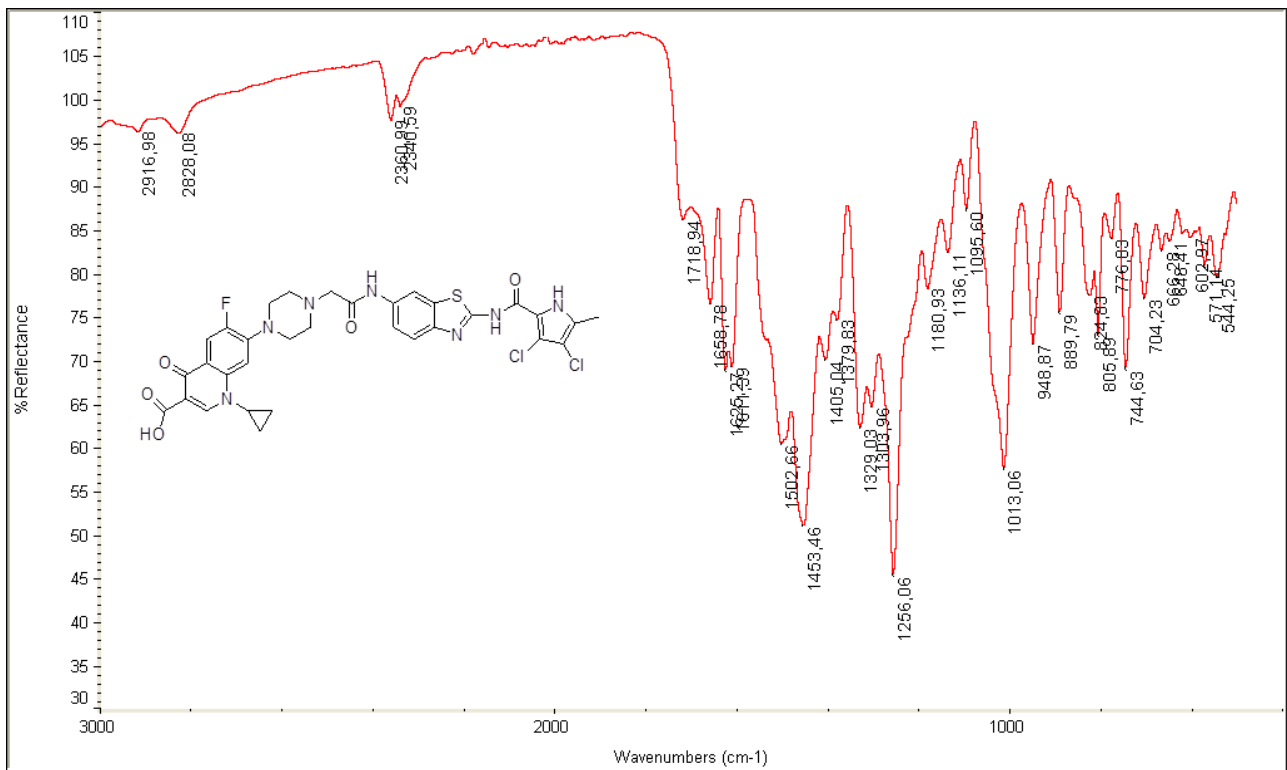
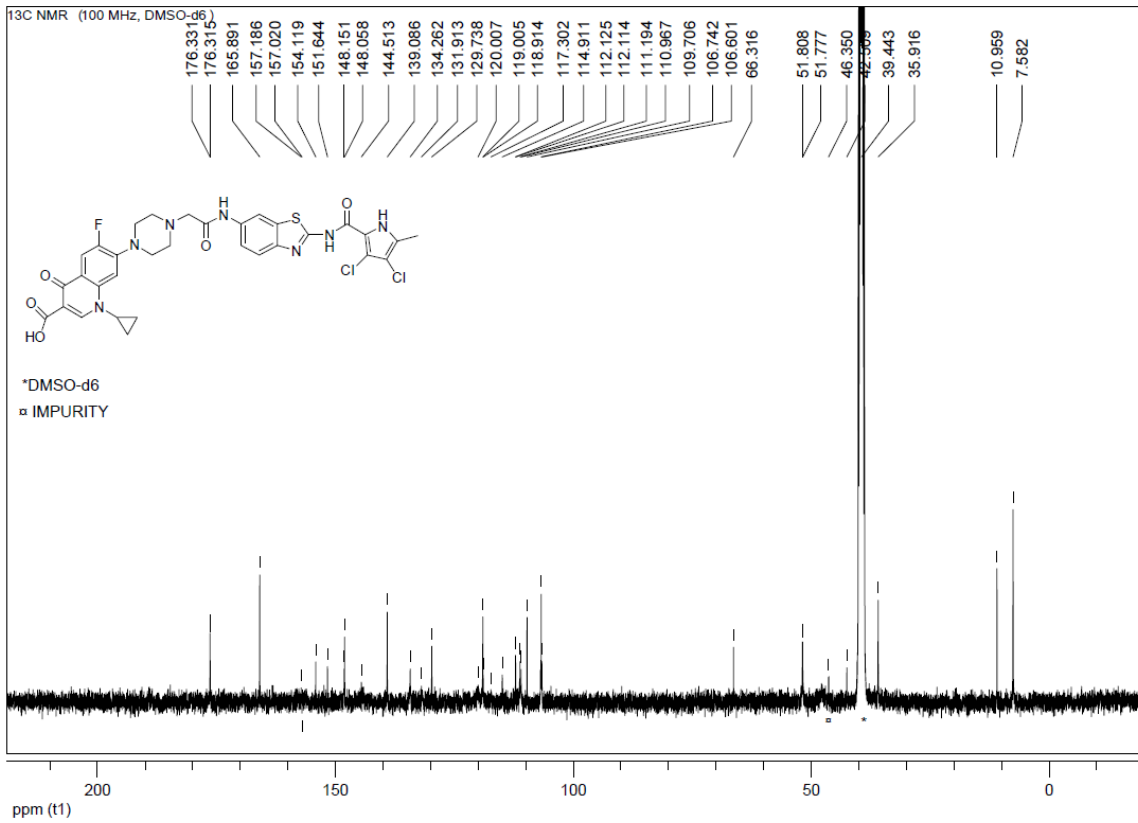
3,4-Dichloro-N-(6-(2-chloroacetamido)benzo[d]thiazol-2-yl)-5-methyl-1H-pyrrole-2-carboxamide (8b)

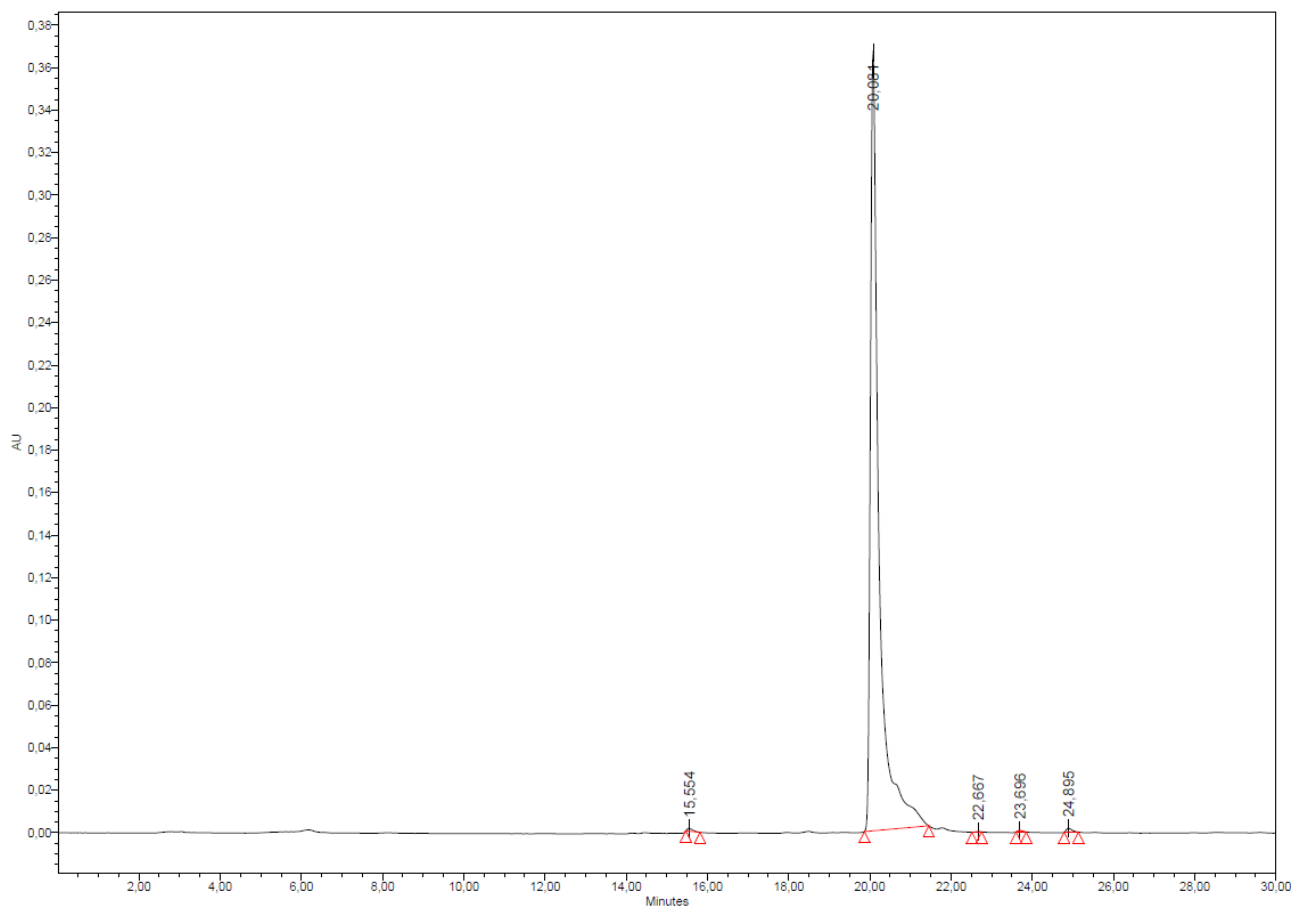




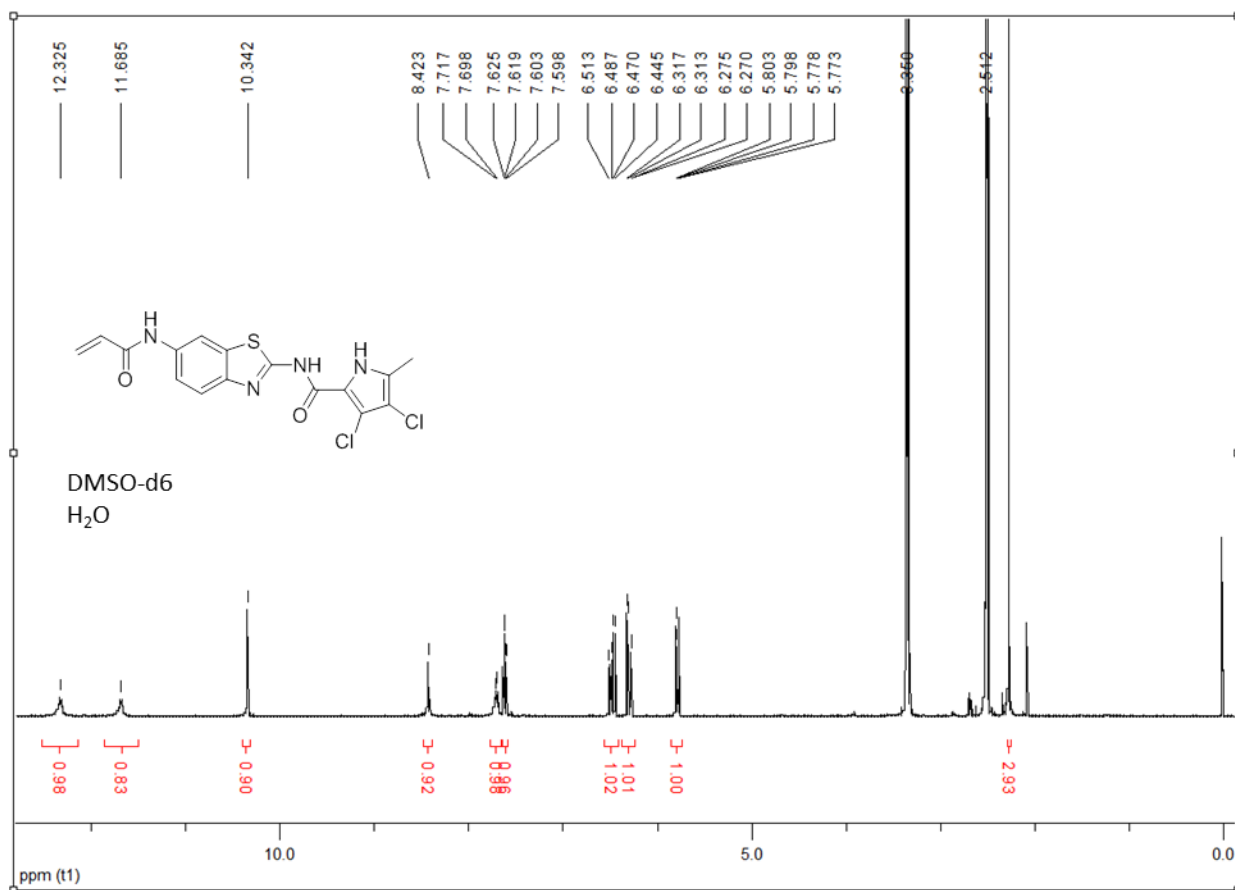
1-Cyclopropyl-7-(4-(2-((2-(3,4-dichloro-5-methyl-1H-pyrrole-2-carboxamido)benzo[d]thiazol-6-yl)amino)-2-oxoethyl)piperazin-1-yl)-6-fluoro-4-oxo-1,4-dihydroquinoline-3-carboxylic acid hydrochloride (2b)

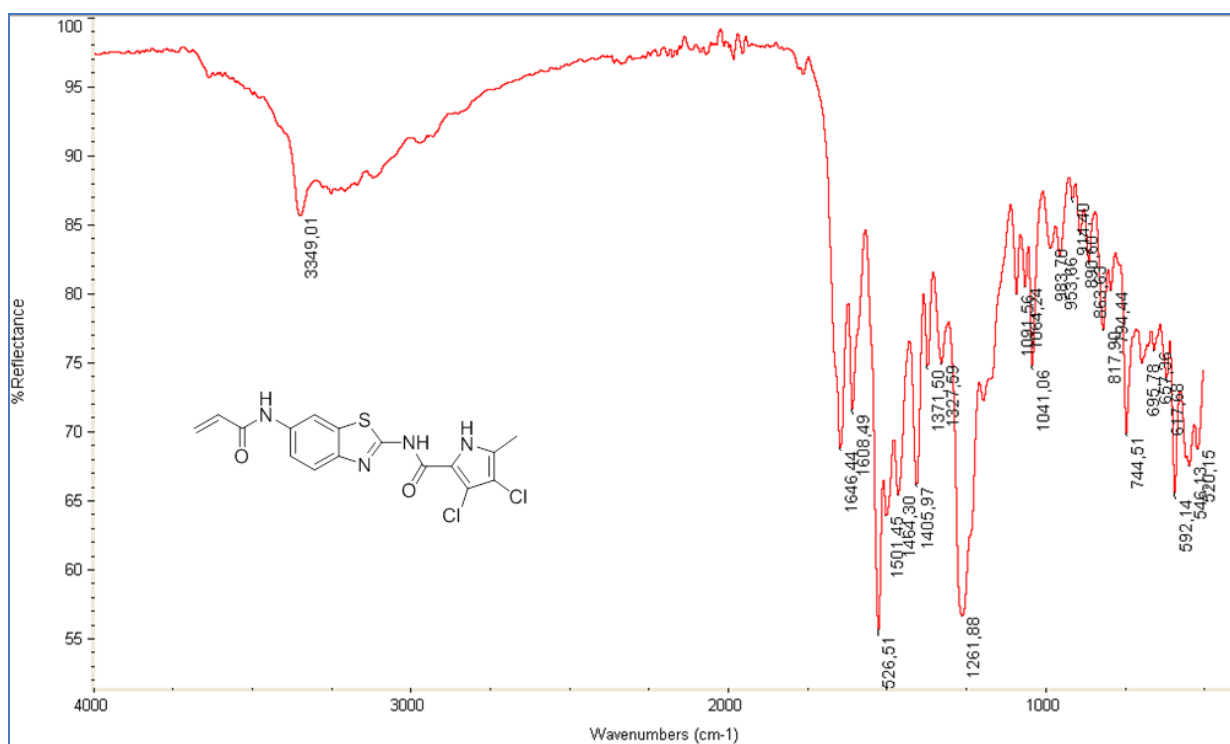




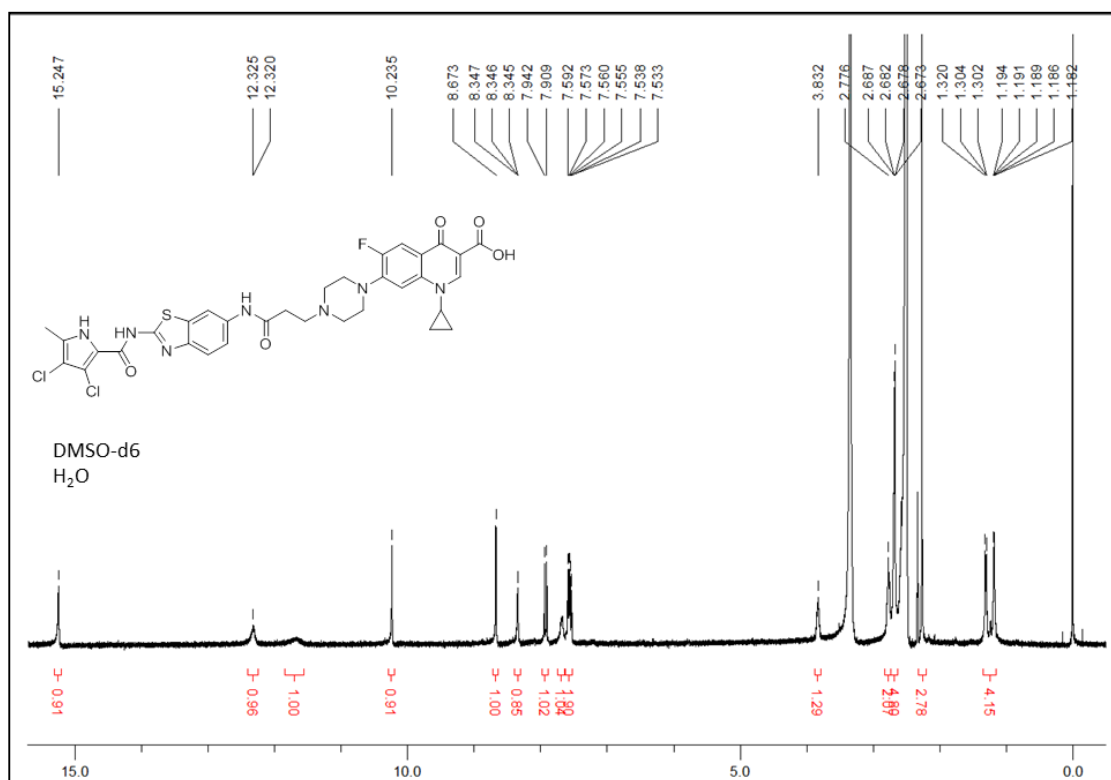


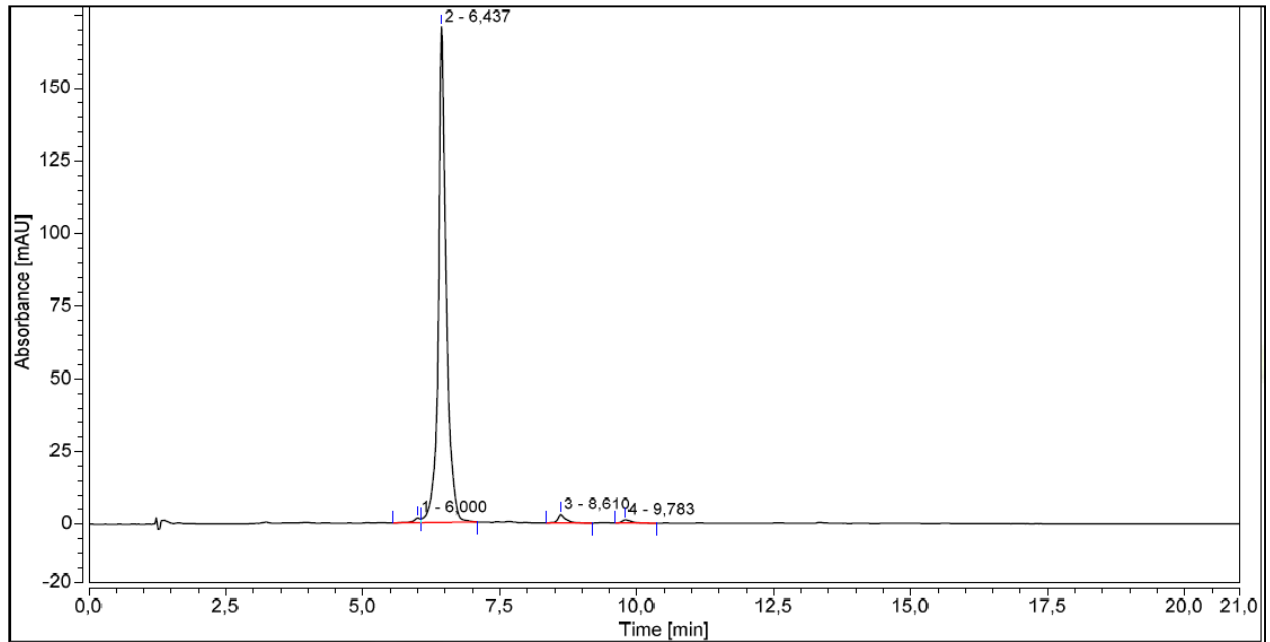
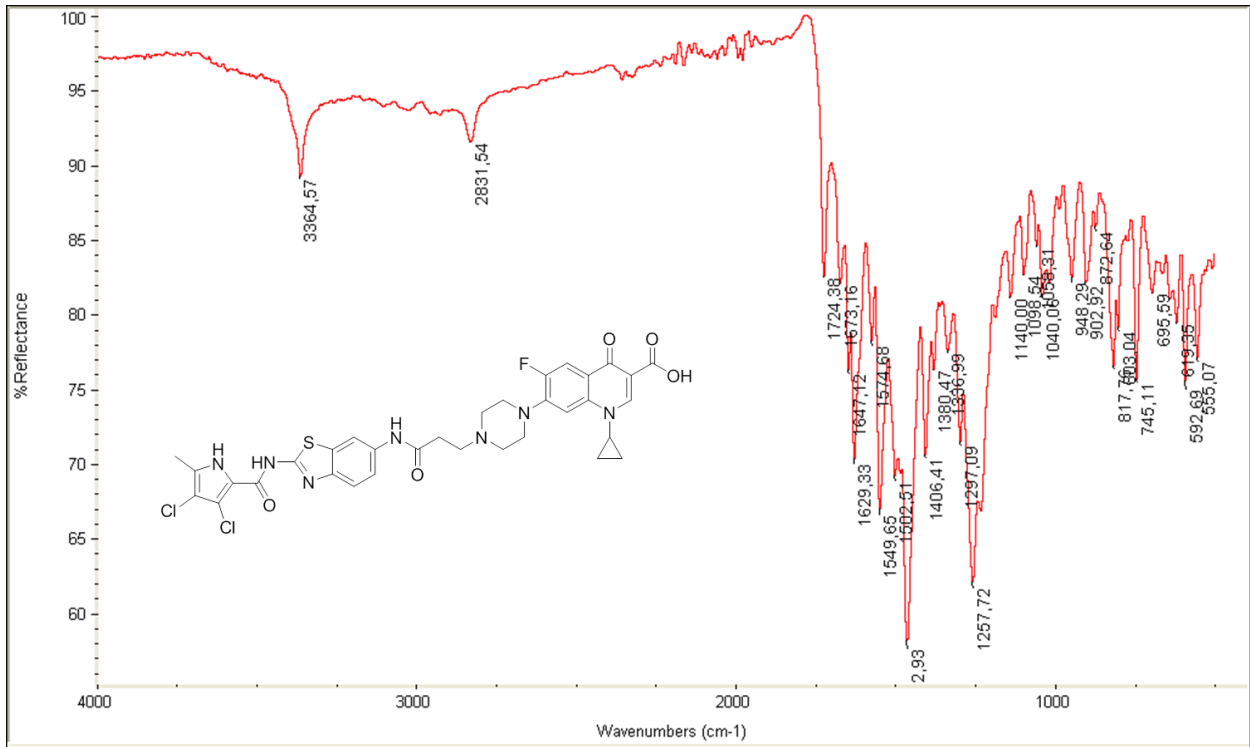
***N*-(6-acrylamidobenzo[*d*]thiazol-2-yl)-3,4-dichloro-5-methyl-1*H*-pyrrole-2-carboxamide (9)**



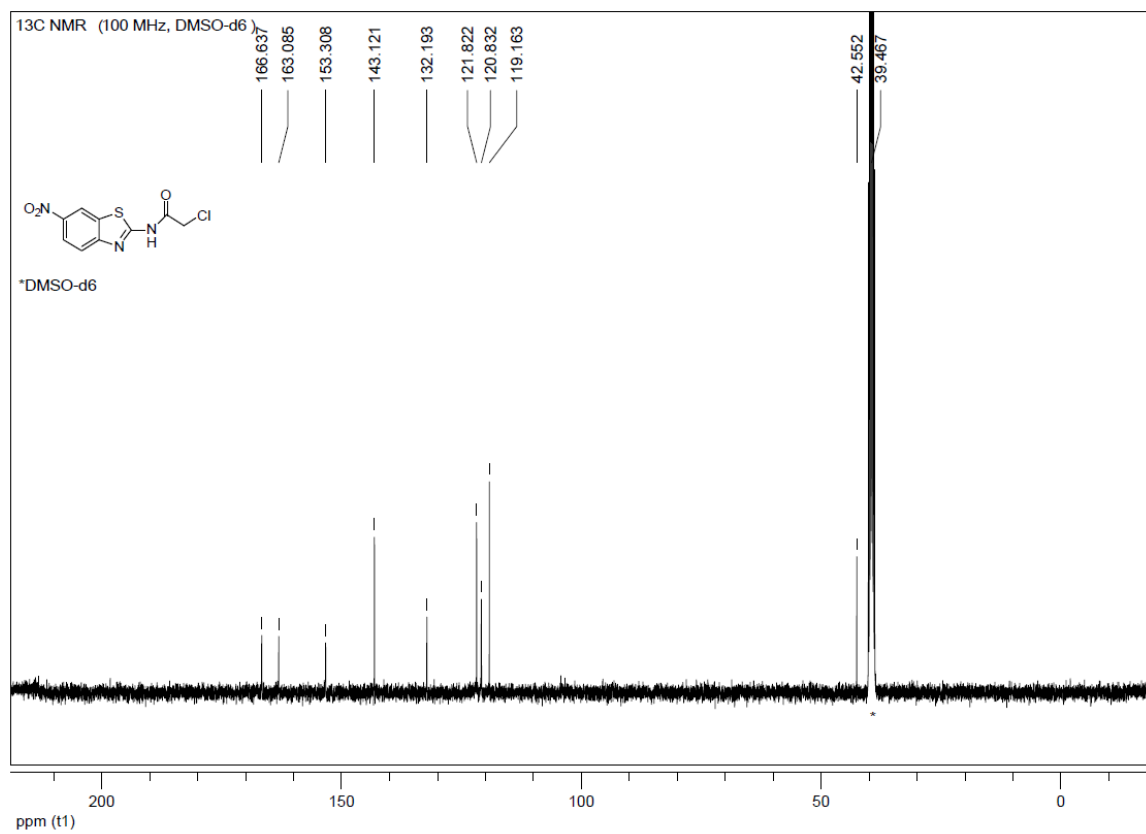
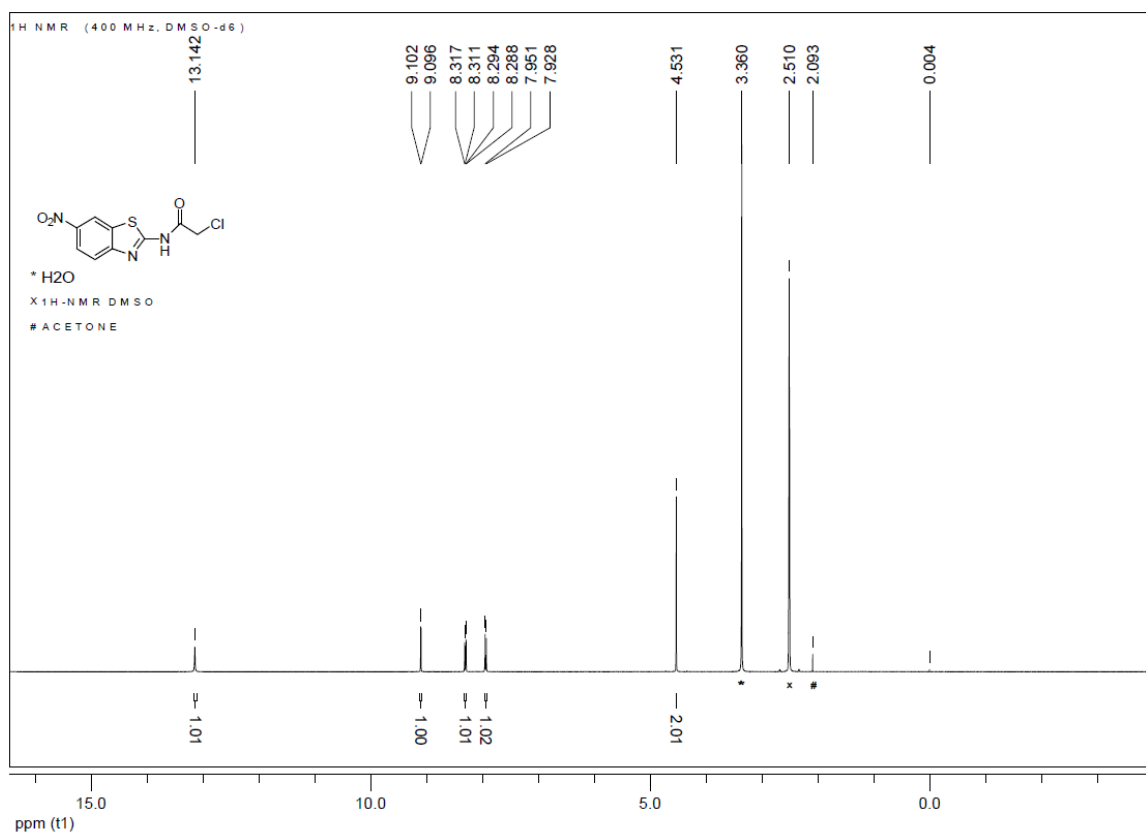


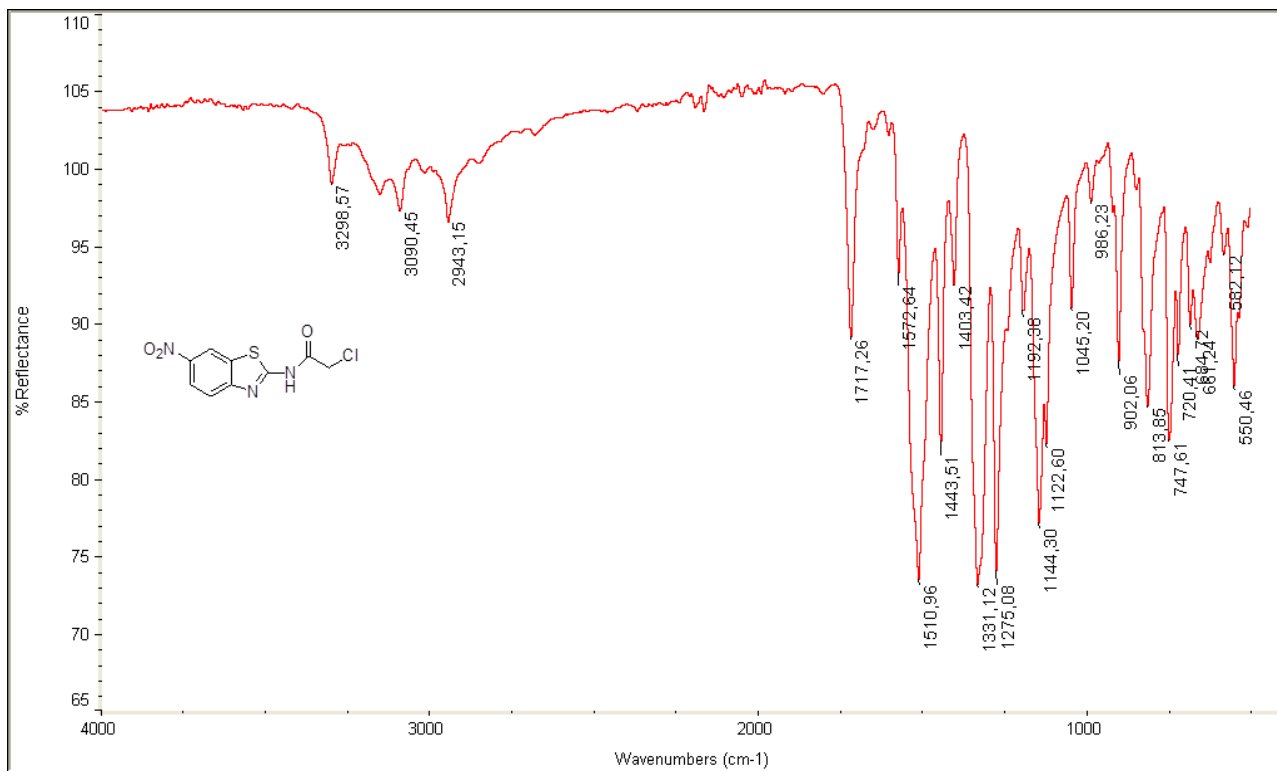
1-Cyclopropyl-7-(4-(3-((2-(3,4-dichloro-5-methyl-1H-pyrrole-2-carboxamido)benzo[d]thiazol-6-yl)amino)-3-oxopropyl)piperazin-1-yl)-6-fluoro-4-oxo-1,4-dihydroquinoline-3-carboxylic acid (2c)



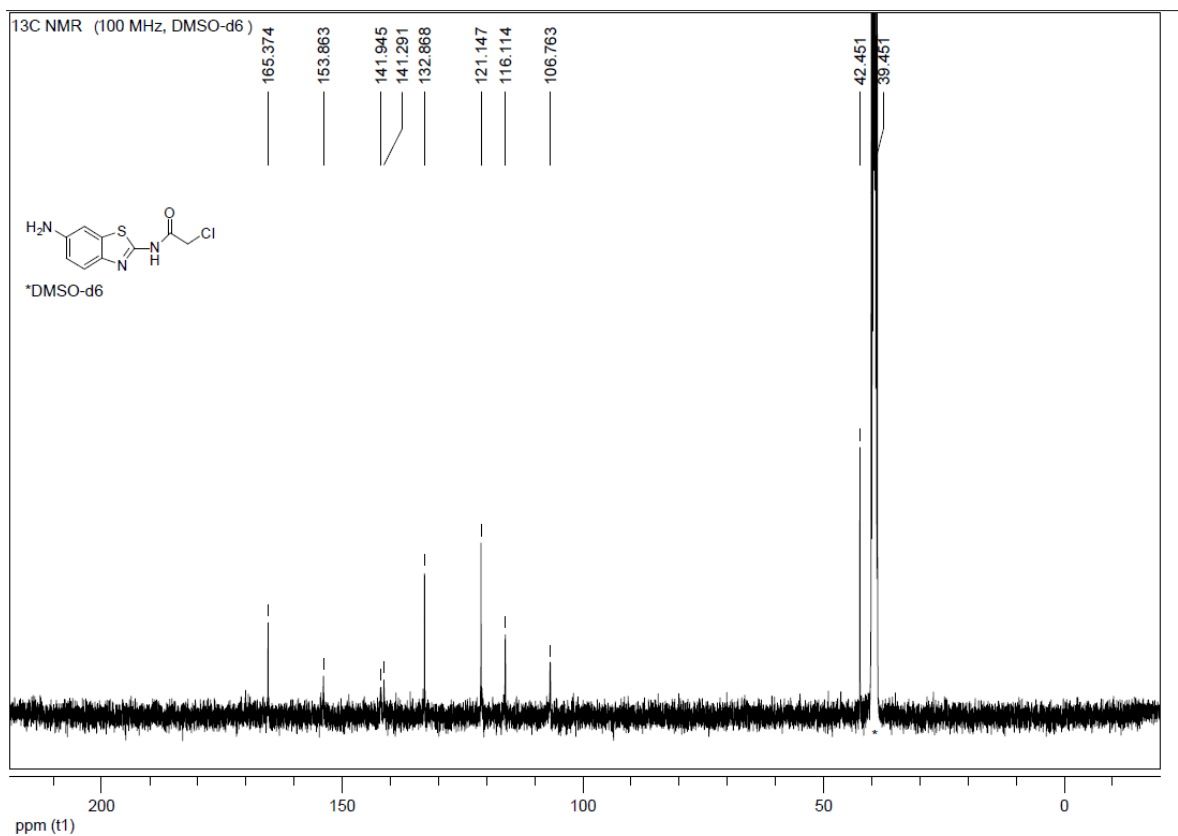
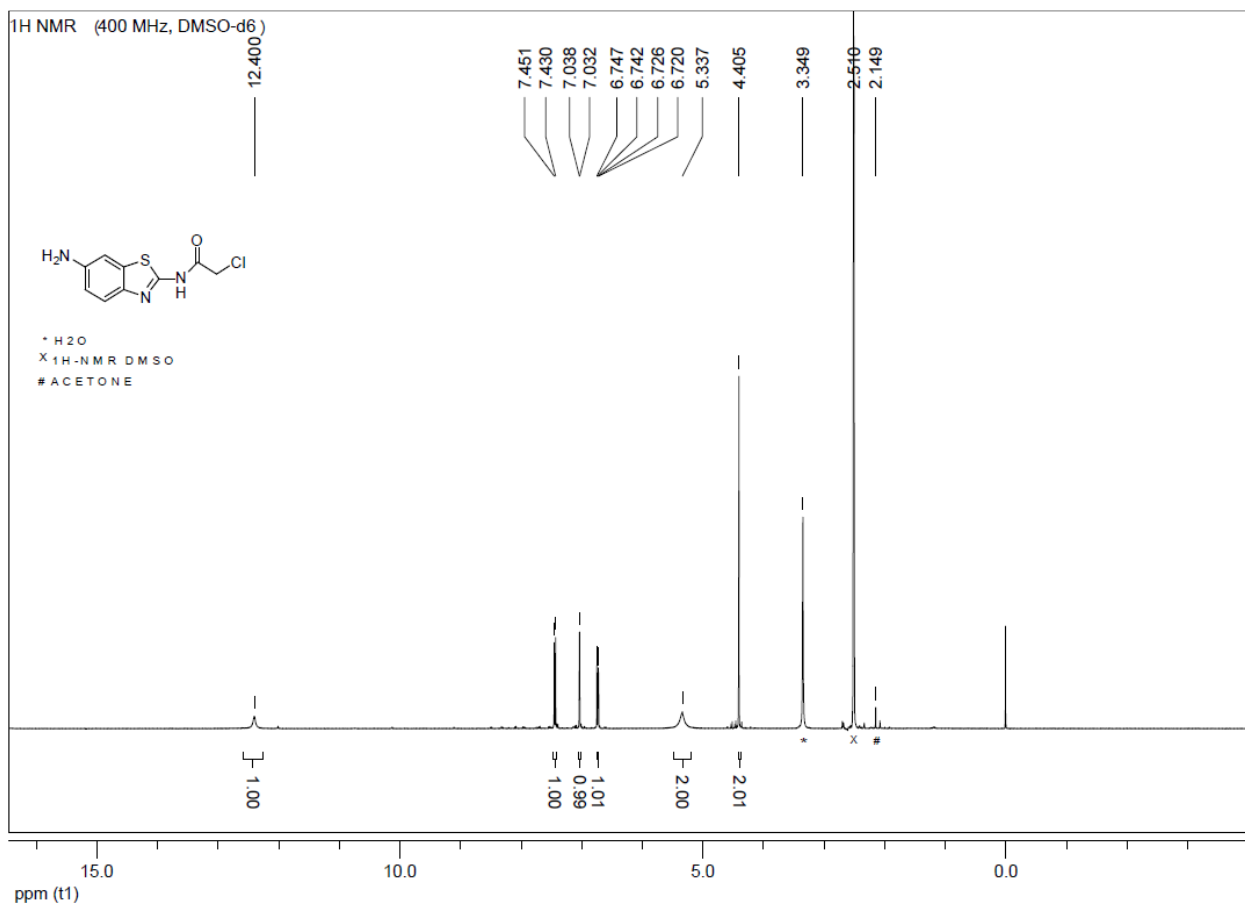


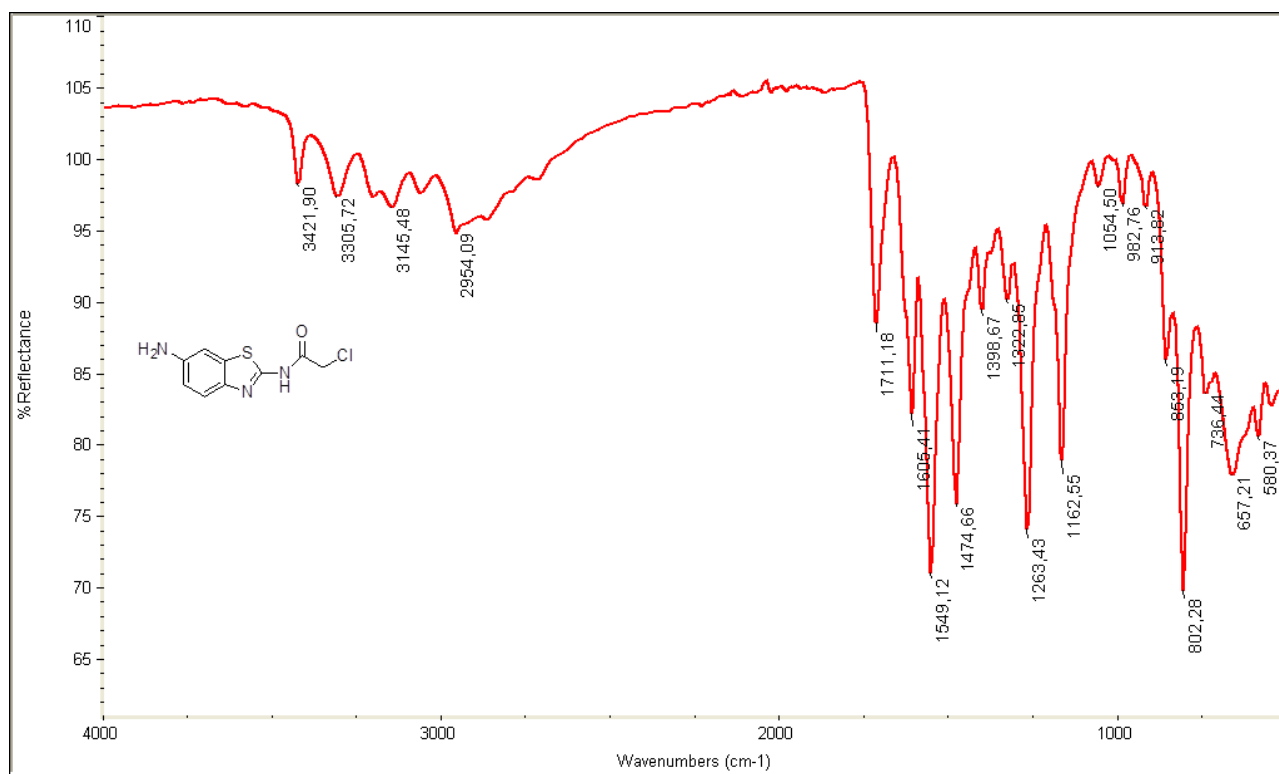
2-Chloro-N-(6-nitro-benzothiazol-2-yl)-acetamide (10)



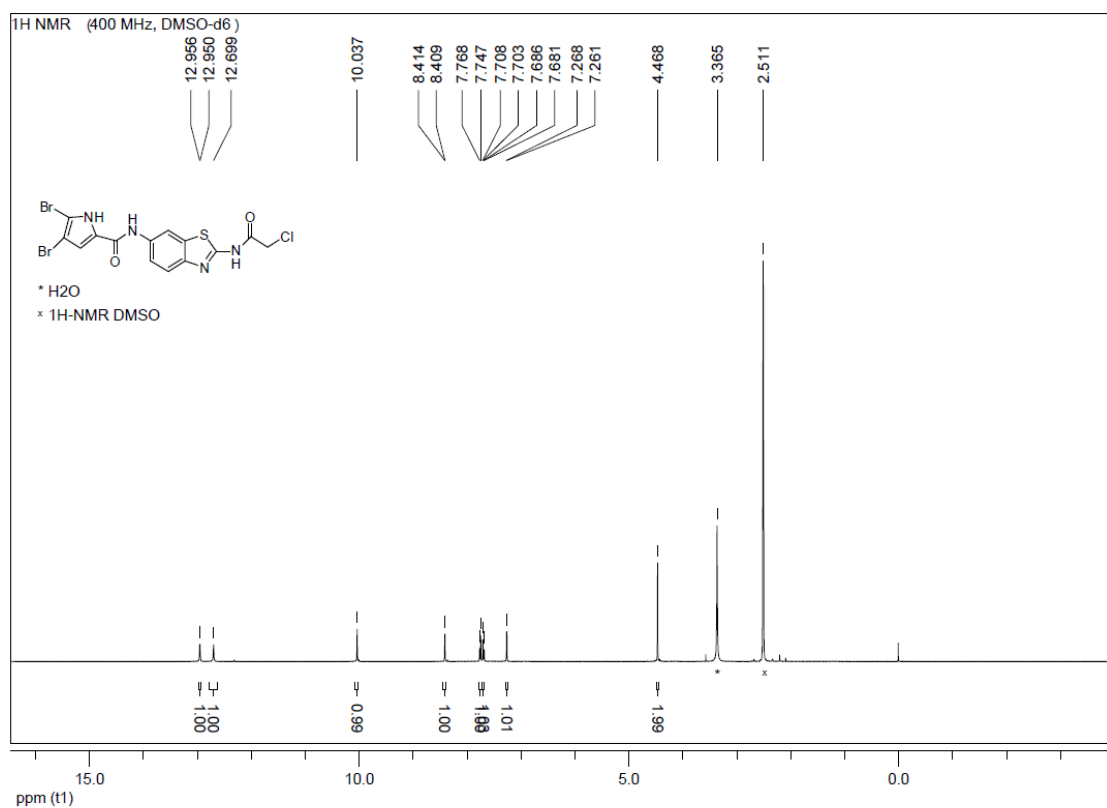


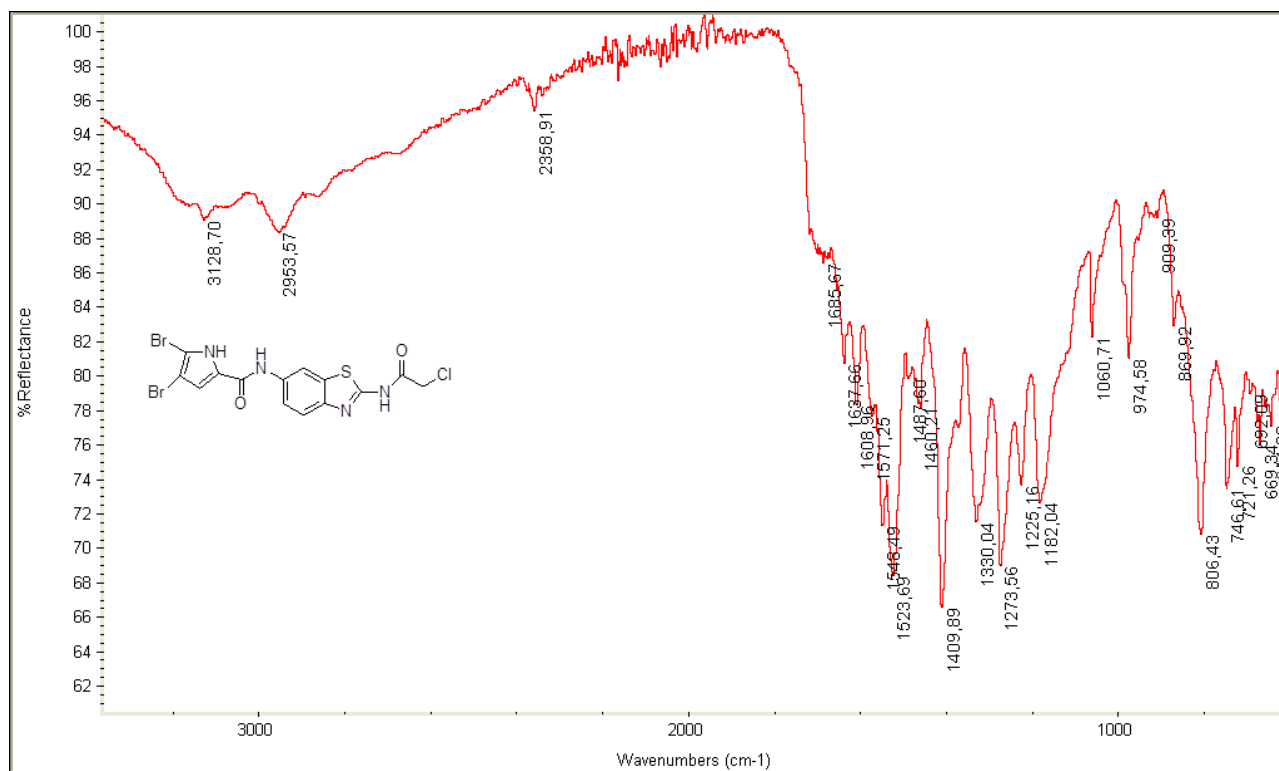
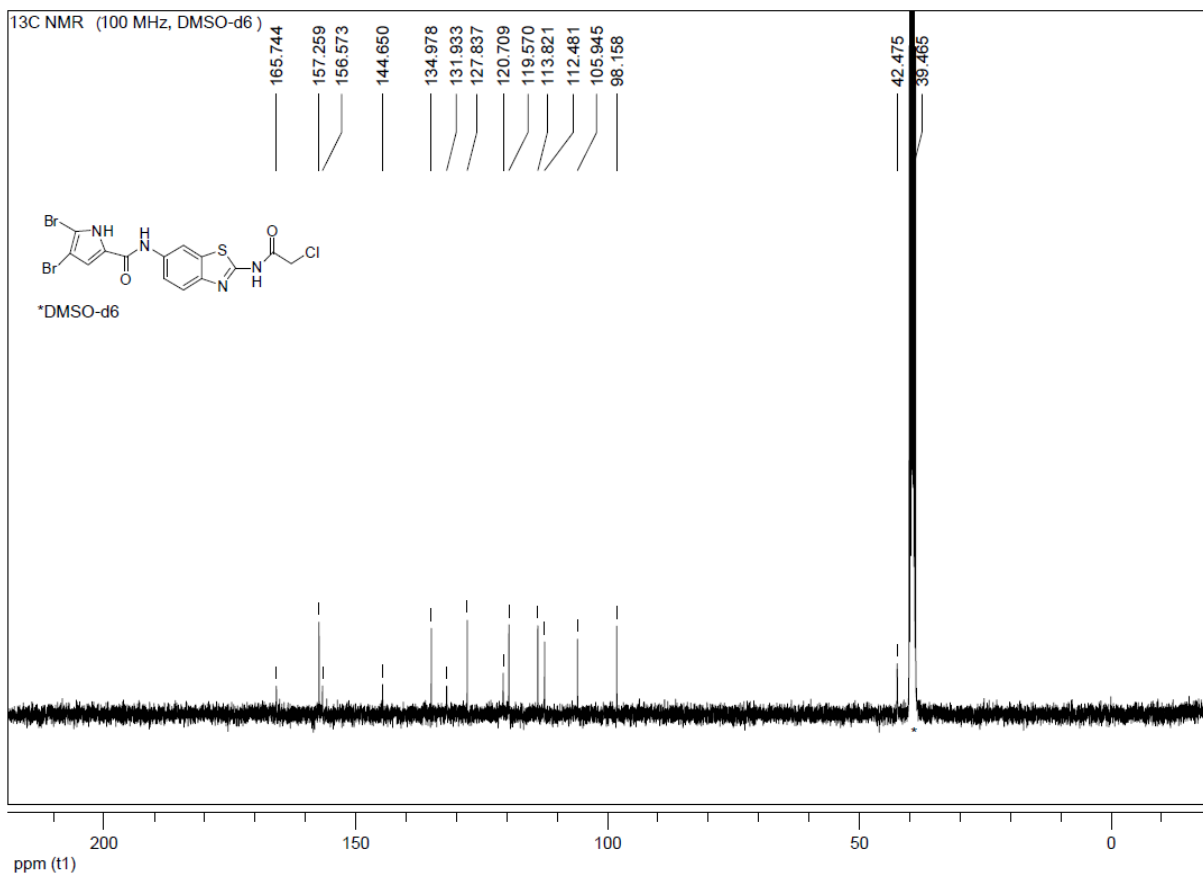
N-(6-Amino-benzothiazol-2-yl)-2-chloro-acetamide (11)



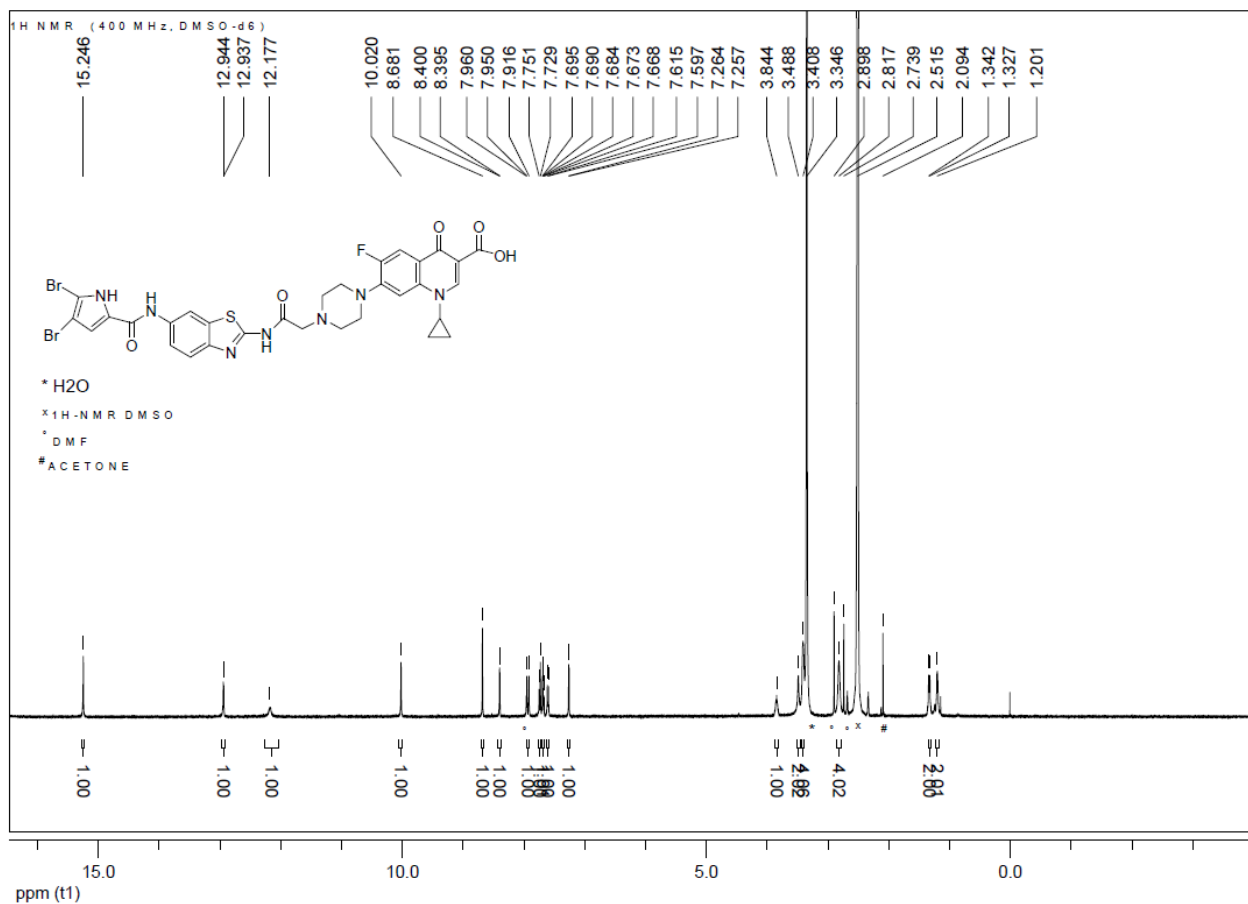


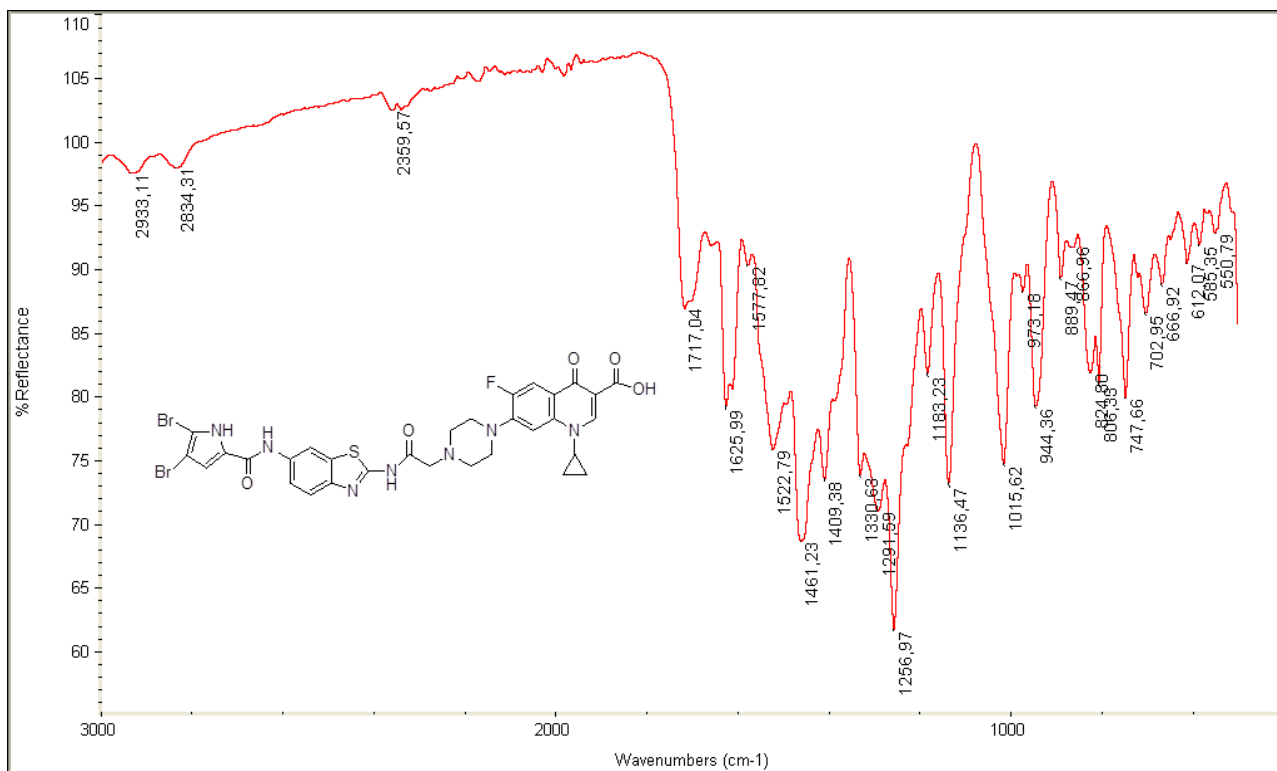
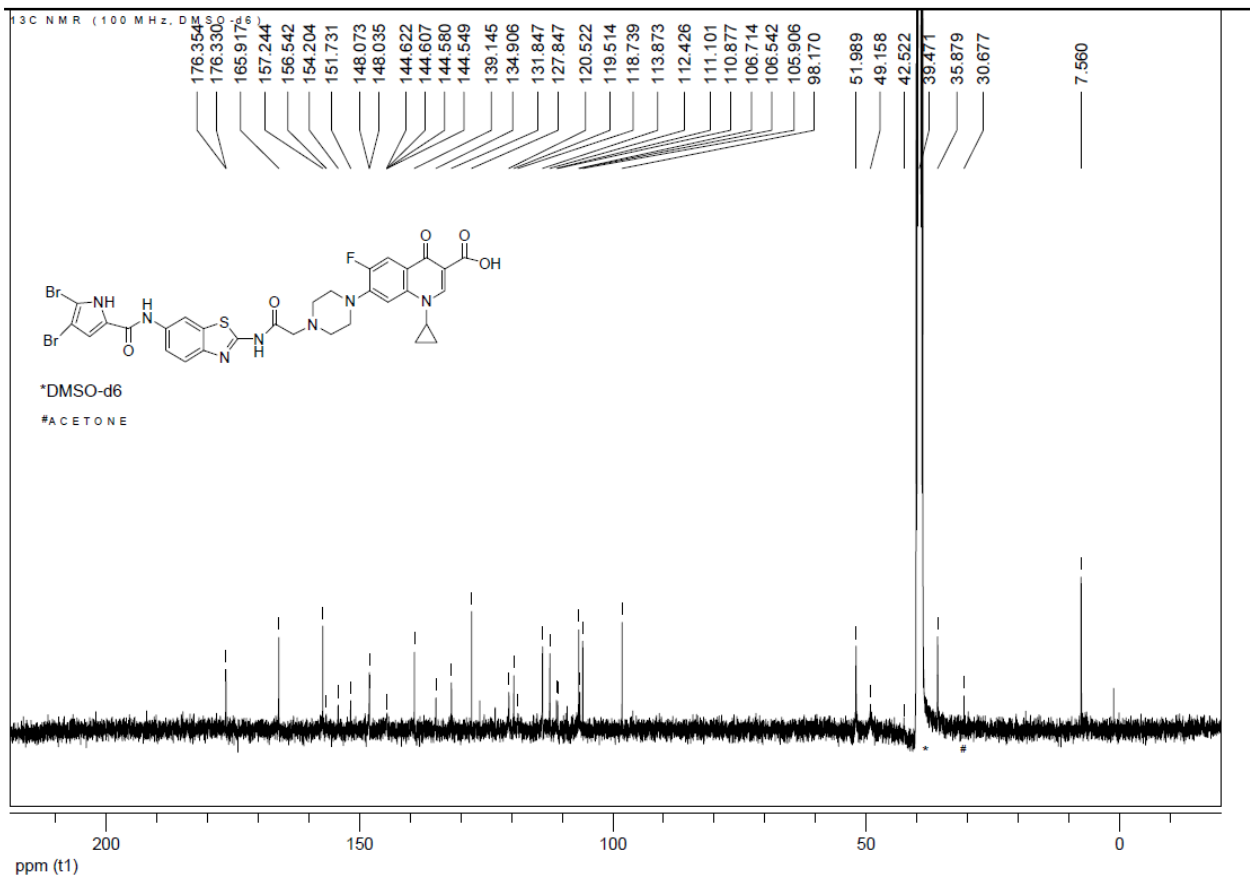
4,5-Dibromo-N-(2-(2-chloroacetamido)benzo[d]thiazol-6-yl)-1H-pyrrole-2-carboxamide (12a)

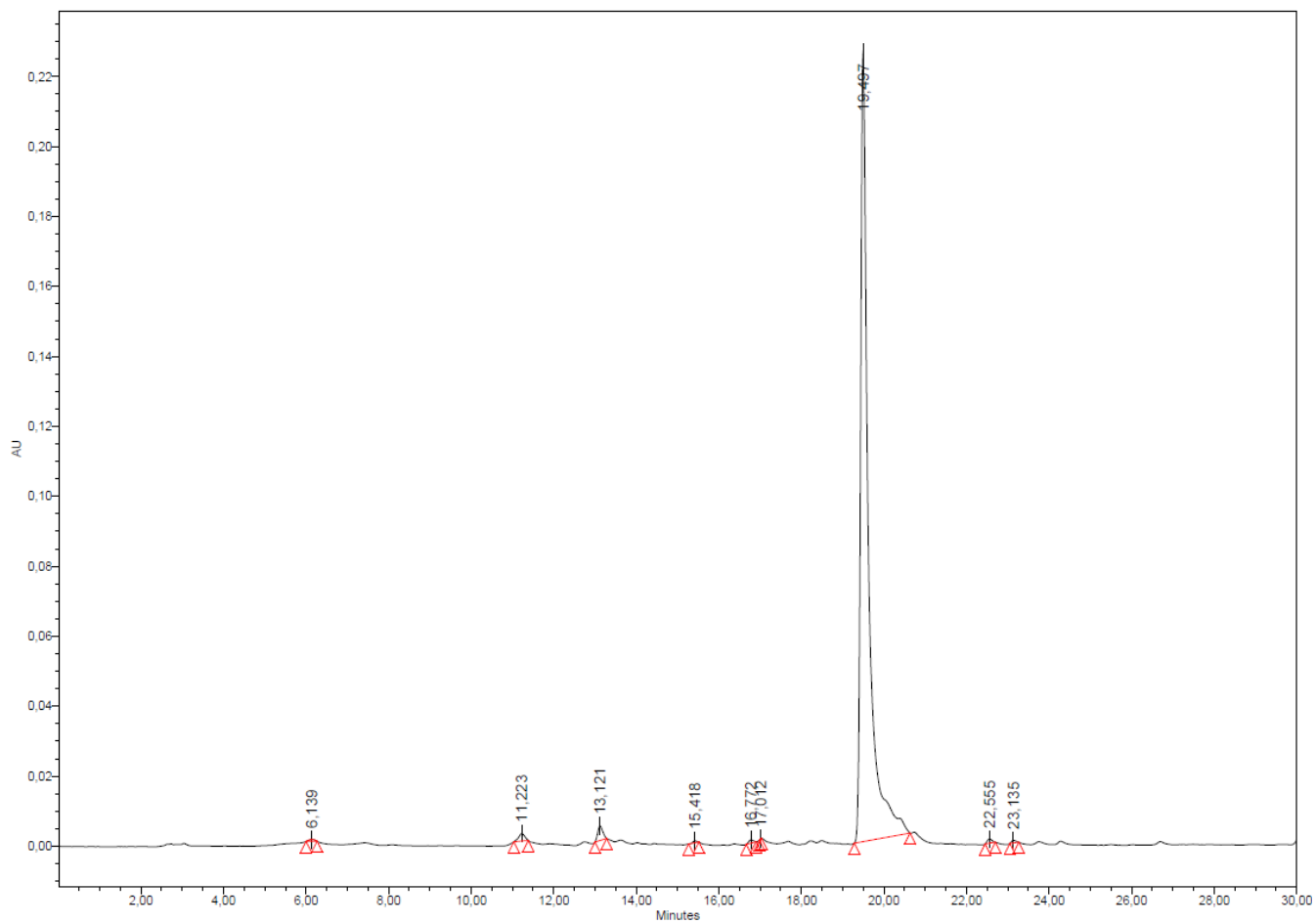




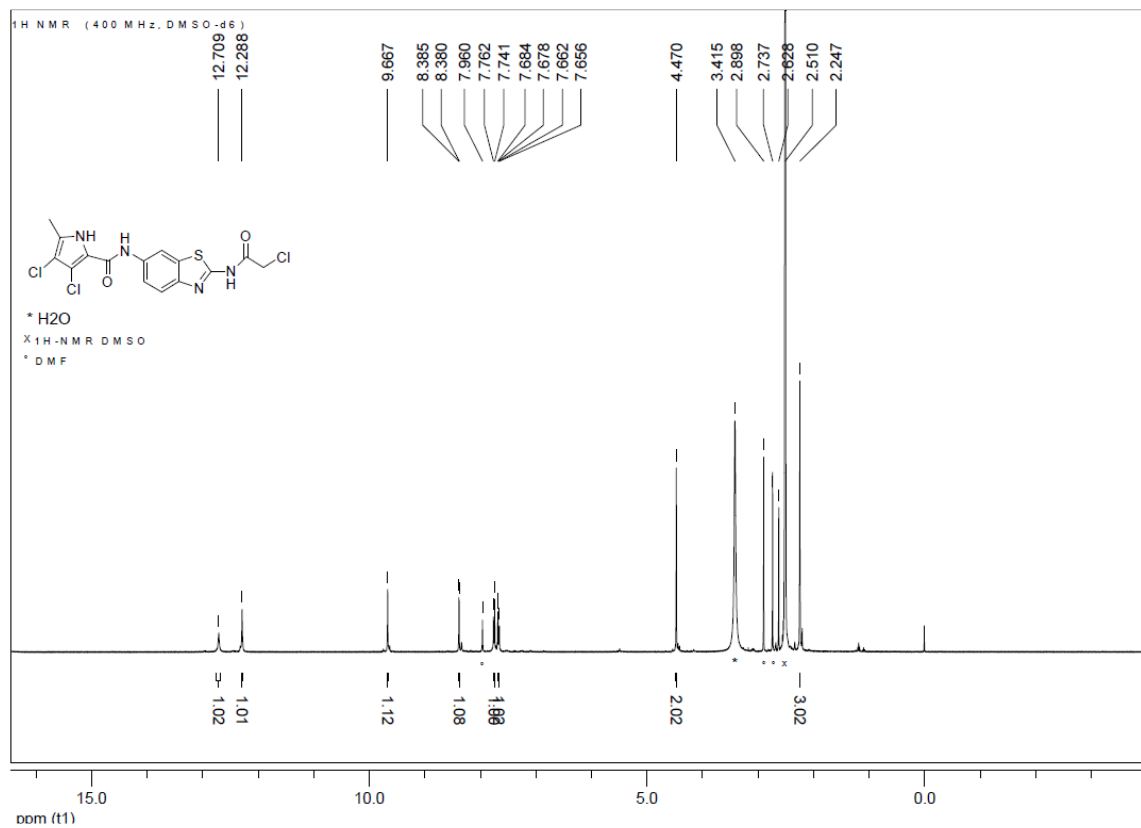
1-Cyclopropyl-7-(4-(2-((6-(4,5-dibromo-1H-pyrrole-2-carboxamido)benzo[d]thiazol-2-yl)amino)-2-oxoethyl)piperazin-1-yl)-6-fluoro-4-oxo-1,4-dihydroquinoline-3-carboxylic acid hydrochloride (3a)

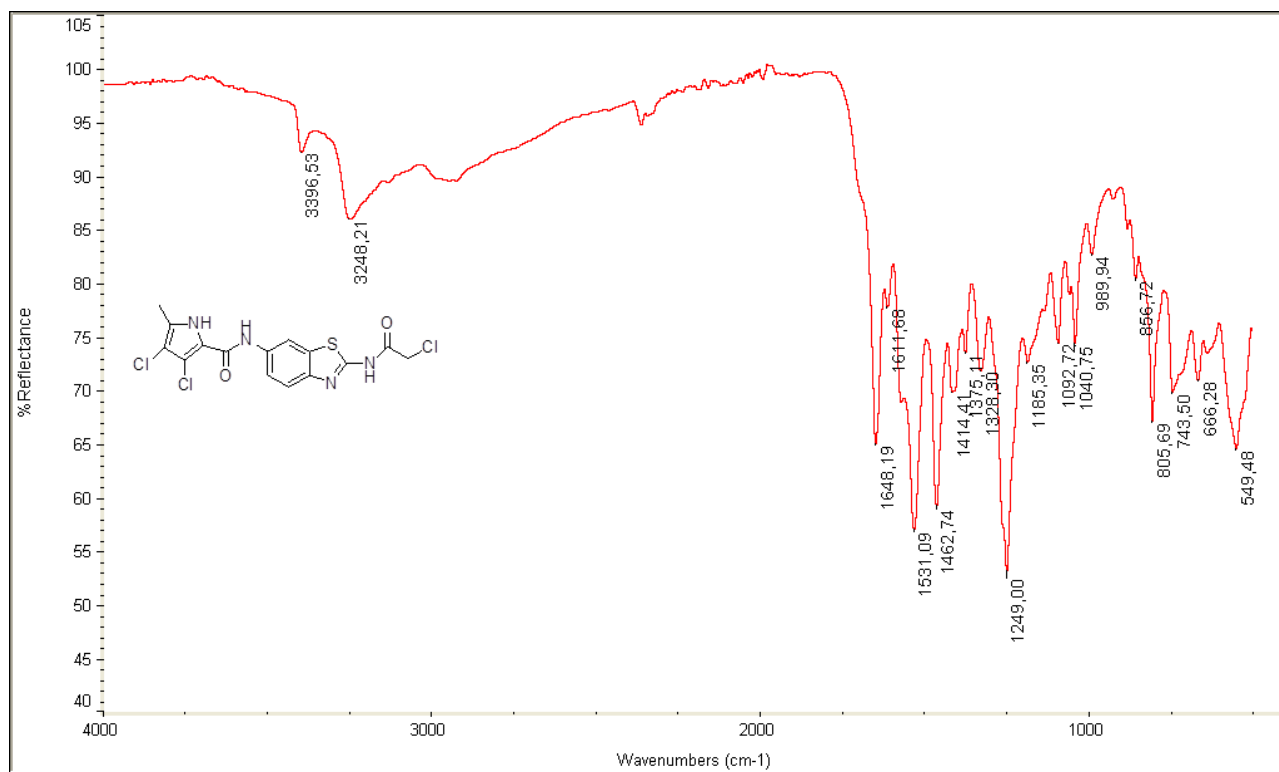
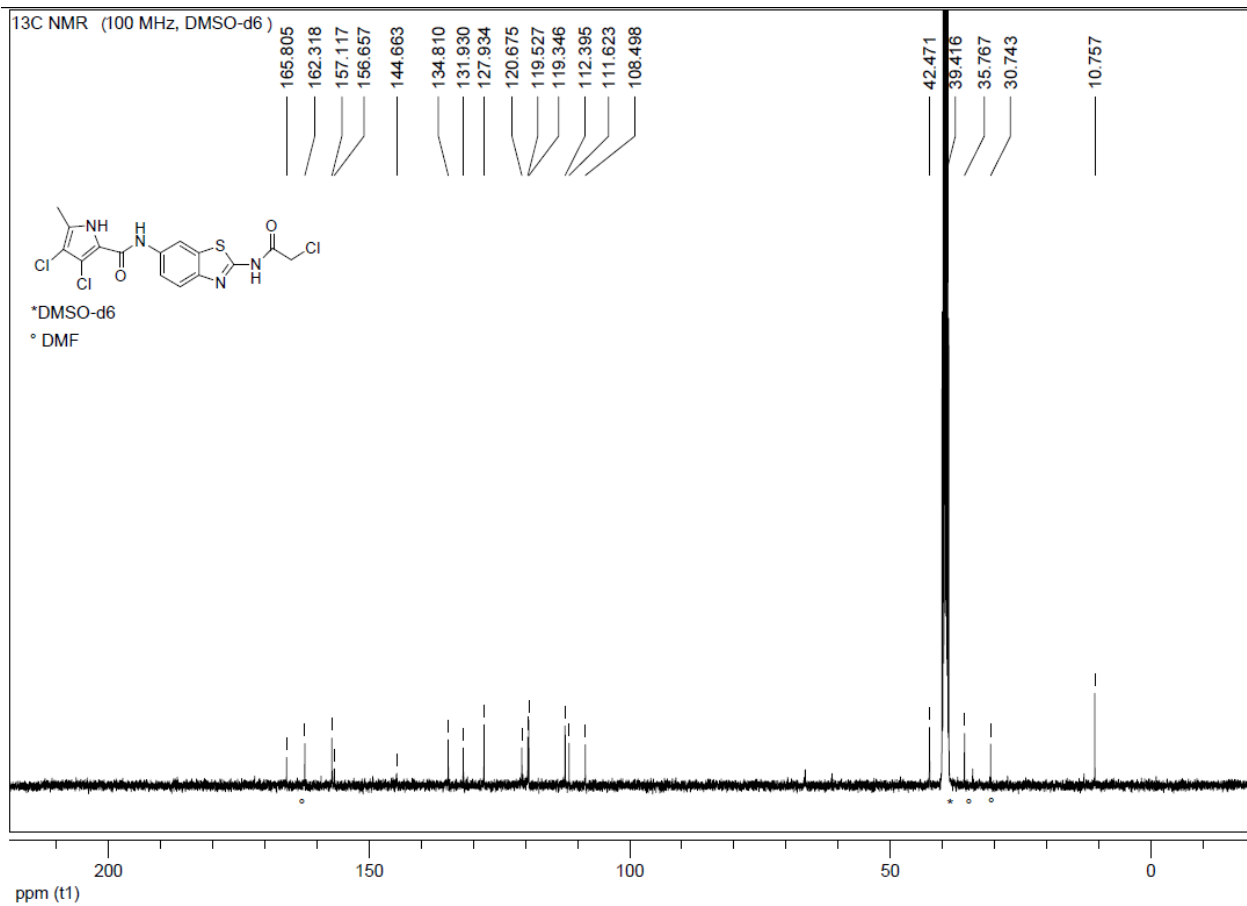




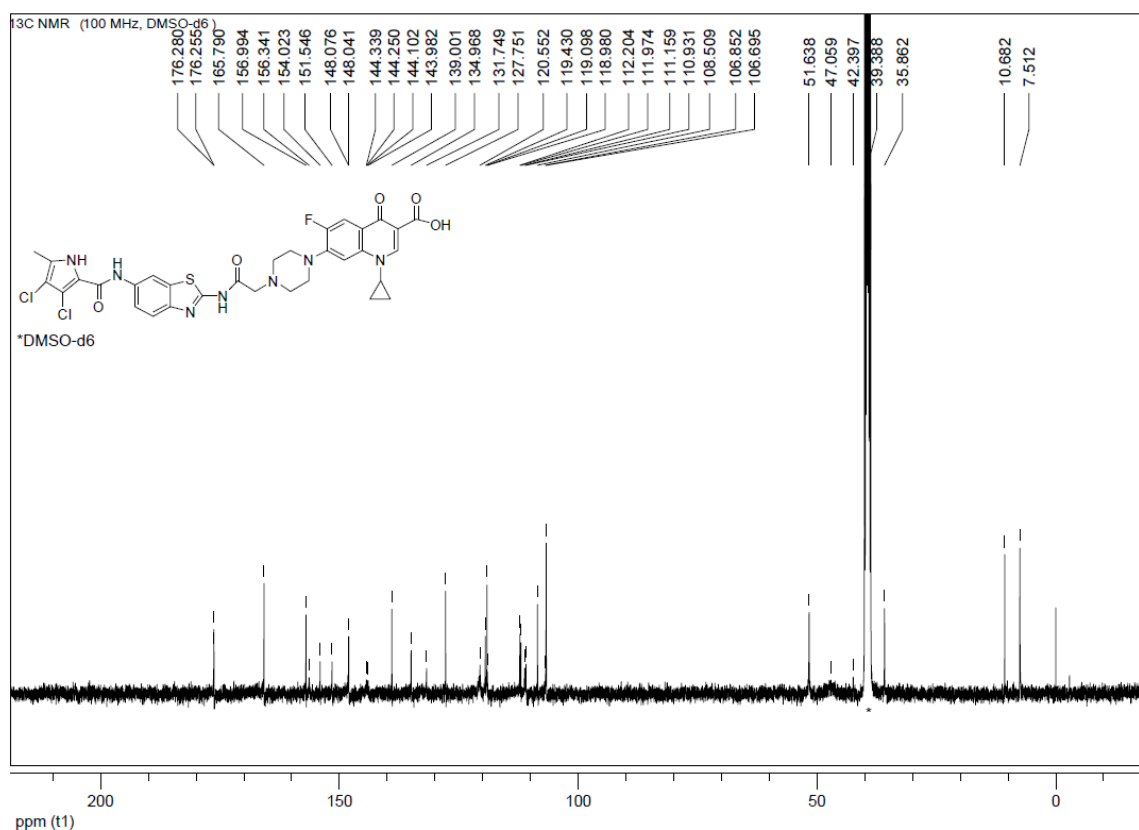
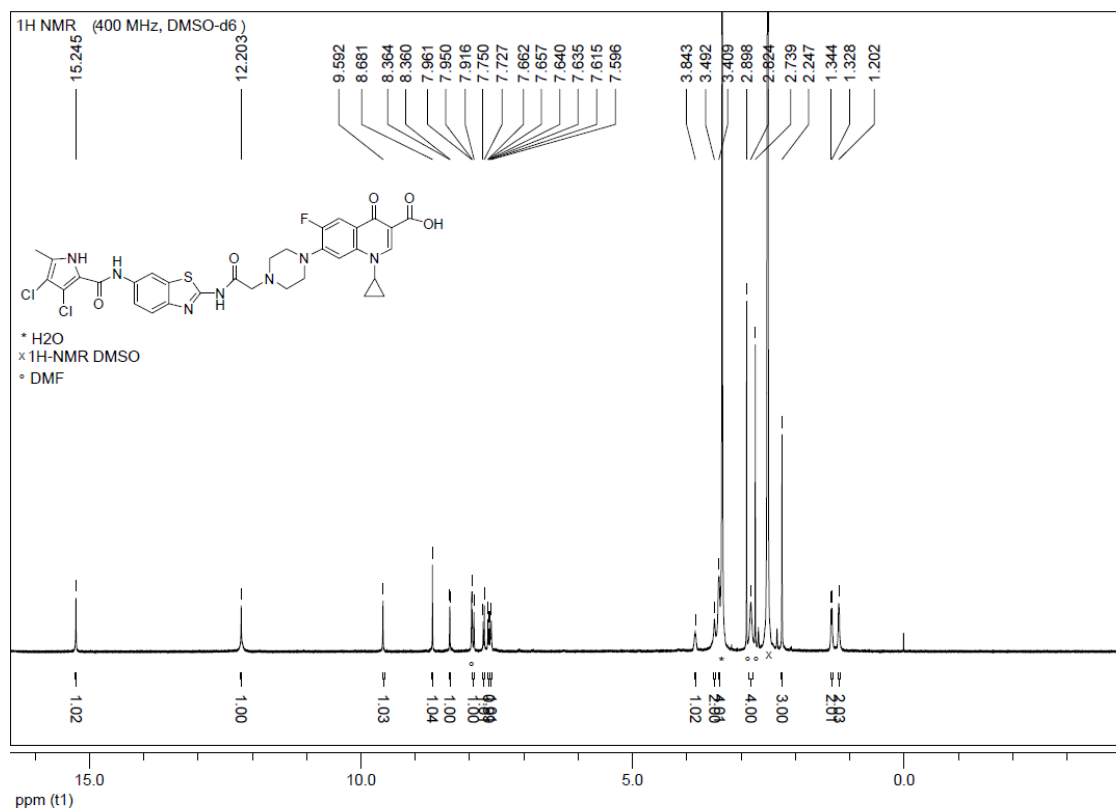


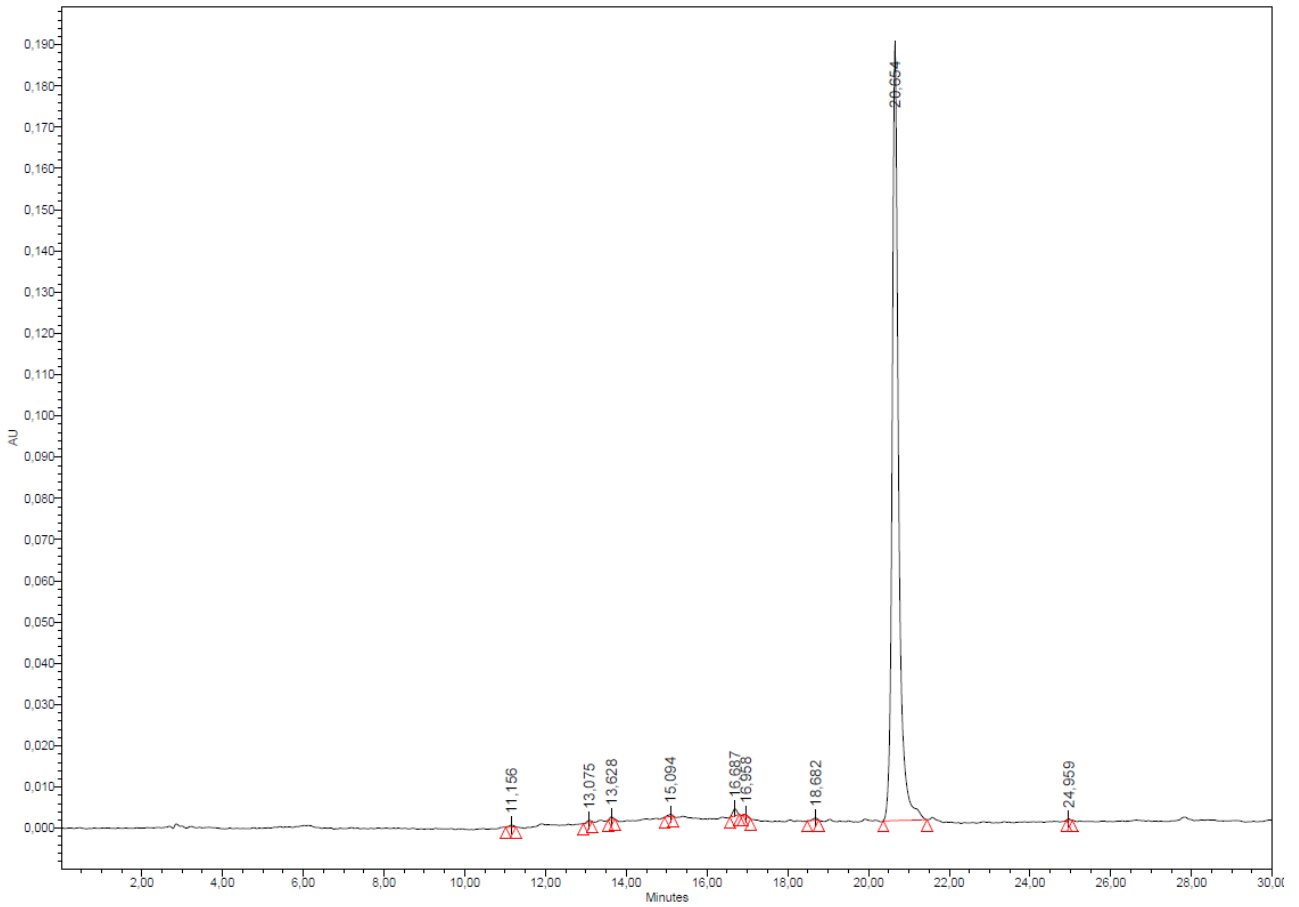
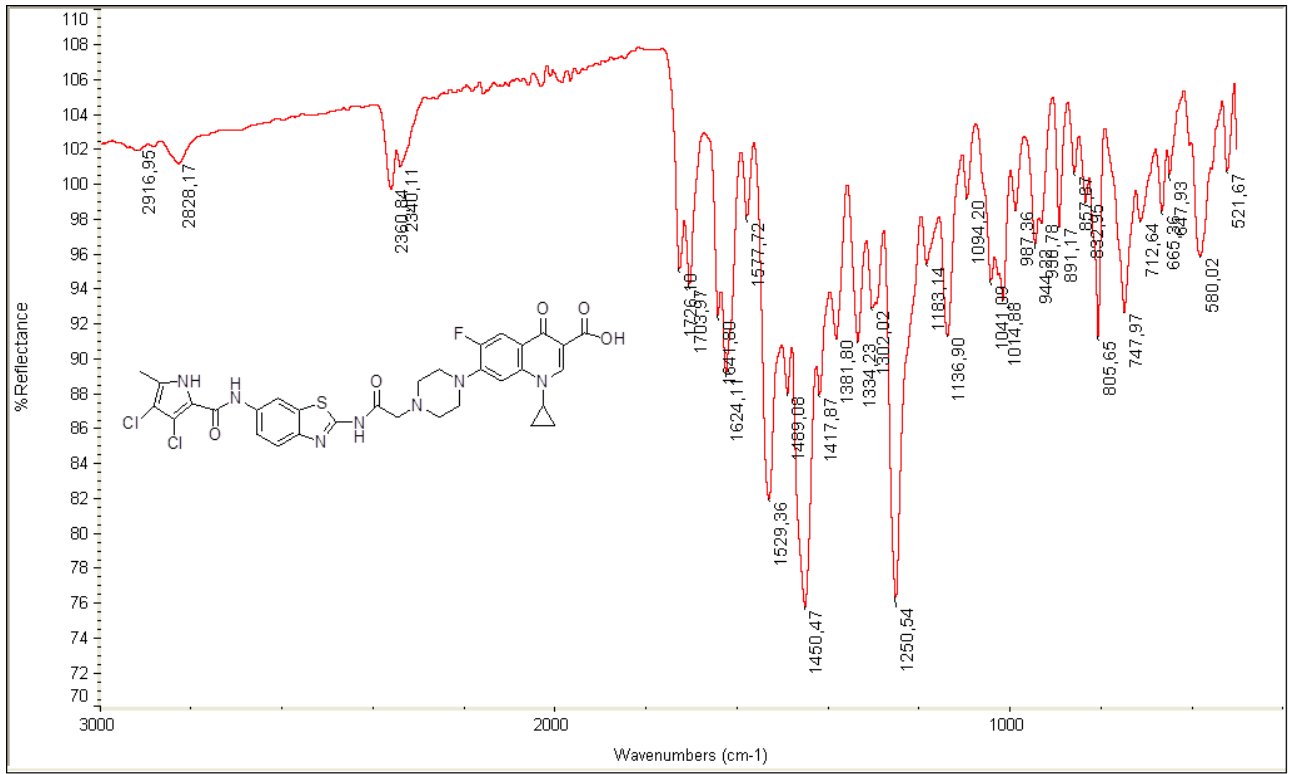
3,4-Dichloro-5-methyl-N-(2-(2-chloroacetamido)benzo[d]thiazol-6-yl)-1H-pyrrole-2-carboxamide (12b)





1-Cyclopropyl-7-(4-(2-((6-(3,4-dichloro-5-methyl-1H-pyrrole-2-carboxamido)benzo[d]thiazol-2-yl)amino)-2-oxoethyl)piperazin-1-yl)-6-fluoro-4-oxo-1,4-dihydroquinoline-3-carboxylic acid hydrochloride (3b)





3.6.4 *Escherichia coli* DNA gyrase inhibition assay

The assays for the determination of IC₅₀ values against *E. coli* and *S. aureus* DNA gyrase were performed according to the previously reported procedures.⁹¹

3.6.4.1 *Escherichia coli* DNA gyrase ATP-ase assay

A commercial Inspiralis *E. coli* DNA gyrase ATP-ase assay was performed as described in Ref.⁹¹

3.6.4.2 Minimum inhibitory concentration measurements

Minimum Inhibitory Concentrations (MICs) were determined using a standard serial broth microdilution technique according to the EUCAST guidelines.¹²² Briefly, bacterial strains were inoculated from frozen cultures onto MHBII agar plates and were grown overnight at 37 °C. Next, independent colonies from each strain were inoculated into 1 ml MHBII medium and were propagated at 37 °C, 250 rpm overnight. To perform MIC assays, 12-step serial dilutions using 1.5-fold dilution-steps of the given antibiotic were generated in 96-well microtiter plates (Sarstedt 96-well microtest plate with lid, flat base). Antibiotics were diluted in 100 µl of MHBII medium. Following dilutions, each well was seeded with an inoculum of 5×10⁴ bacterial cells. Each measurements were performed at least in 4 parallel replicates. Following inoculations, plates were covered with lids and wrapped in polyethylene plastic bags to minimize evaporation but allow for aerobic O₂ transfer. Plates were incubated at 37 °C under continuous shaking at 150 RPM for 18 hours in an INFORS HT shaker. After incubation, OD₆₀₀ of each well on the microwell plate was measured using a Biotek Synergy 2 microplate reader. MIC was defined as the antibiotic concentration which inhibited the growth of the bacterial culture, i.e., the drug concentration where the average OD₆₀₀ increment of the three replicates was below 0.05.

3.6.4.3 Frequency of resistance measurements

The occurrence of spontaneously arising resistant bacteria was quantified using the ‘frequency of resistance’ assay.¹²⁰ Overnight cultures of *E. coli* K-12 MG1655 and *E. coli* ATCC 25922 strains were grown using cation-adjusted Mueller Hinton II Broth (MHBII). Bacterial cultures were washed once in equal volume of fresh MHBII medium. Washed cultures containing approximately 3×10⁹ CFU/mL were plated onto MHBII supplemented with 1% agarose (SeaKem LE, Lonza Bioscience) plates containing 4×MIC of the test agent to allow generation and enumeration of resistant mutants. Ciprofloxacin was used as comparator antibiotic. Cultures were also diluted in MHBII and were plated onto drug-free agar plates for the enumeration of total viable cells. Plates were incubated at

37 °C for 24 hours. The spontaneous frequency of resistance was expressed as a ratio of the number of resistant colonies (CFU/mL) to the total number of viable cells (CFU/mL).

3.7 REFERENCES

1. Waksman, S. A.; Flynn, J. E. History of the word 'antibiotic'. *Journal of the history of medicine and allied sciences* **1973**, 28, 284-286.
2. Abraham, E. P.; Chain, E. An enzyme from bacteria able to destroy penicillin. 1940. *Reviews of infectious diseases* **1988**, 10, 677-678.
3. Davies, J.; Davies, D. Origins and evolution of antibiotic resistance. *Microbiology and molecular biology reviews* : *MMBR* **2010**, 74, 417-433.
4. DA, H. *Streptomyces in nature and medicine: the antibiotic makers*. Oxford, UK, 2007.
5. C., W. *Antibiotics: actions, origins, resistance*. Washington, DC, 2003.
6. Cole, S. T. Who will develop new antibacterial agents? *Philosophical transactions of the Royal Society of London. Series B, Biological sciences* **2014**, 369, 1-7.
7. Fleming-Dutra, K. E.; Hersh, A. L.; Shapiro, D. J.; Bartoces, M.; Enns, E. A.; File, T. M., Jr.; Finkelstein, J. A.; Gerber, J. S.; Hyun, D. Y.; Linder, J. A.; Lynfield, R.; Margolis, D. J.; May, L. S.; Merenstein, D.; Metlay, J. P.; Newland, J. G.; Piccirillo, J. F.; Roberts, R. M.; Sanchez, G. V.; Suda, K. J.; Thomas, A.; Woo, T. M.; Zetts, R. M.; Hicks, L. A. Prevalence of Inappropriate Antibiotic Prescriptions Among US Ambulatory Care Visits, 2010-2011. *Jama* **2016**, 315, 1864-1873.
8. Landers, T. F.; Cohen, B.; Wittum, T. E.; Larson, E. L. A review of antibiotic use in food animals: perspective, policy, and potential. *Public health reports (Washington, D.C. : 1974)* **2012**, 127, 4-22.
9. Savage, P. B. Multidrug-resistant bacteria: overcoming antibiotic permeability barriers of gram-negative bacteria. *Annals of medicine* **2001**, 33, 167-171.
10. <https://www.who.int/gho/glass/en/>
11. Center for Disease Dynamics, E. a. P. <https://resistancemap.cddep.org/>
12. Jansen, K. U.; Knirsch, C.; Anderson, A. S. The role of vaccines in preventing bacterial antimicrobial resistance. *Nature medicine* **2018**, 24, 10-19.
13. Kwong, J. C.; Maaten, S.; Upshur, R. E.; Patrick, D. M.; Marra, F. The effect of universal influenza immunization on antibiotic prescriptions: an ecological study. *Clinical infectious diseases : an official publication of the Infectious Diseases Society of America* **2009**, 49, 750-756.
14. Raviglione, M.; Marais, B.; Floyd, K.; Lonroth, K.; Getahun, H.; Migliori, G. B.; Harries, A. D.; Nunn, P.; Lienhardt, C.; Graham, S.; Chakaya, J.; Weyer, K.; Cole, S.; Kaufmann, S. H.; Zumla, A. Scaling up interventions to achieve global tuberculosis control: progress and new developments. *Lancet (London, England)* **2012**, 379, 1902-1913.
15. Klatt, T. E.; Hopp, E. Effect of a best-practice alert on the rate of influenza vaccination of pregnant women. *Obstetrics and gynecology* **2012**, 119, 301-305.
16. Greenwood, B. The contribution of vaccination to global health: past, present and future. *Philosophical transactions of the Royal Society of London. Series B, Biological sciences* **2014**, 369, 1-9.
17. Kash, J. C.; Taubenberger, J. K. The role of viral, host, and secondary bacterial factors in influenza pathogenesis. *The American journal of pathology* **2015**, 185, 1528-1536.
18. (GASP), W. G. A. S. P. http://www.who.int/reproductivehealth/topics/rtis/gonococcal_resistance/en/
19. *Global tuberculosis report.*; World Health Organization: 2016.
20. *Surveillance of antimicrobial resistance in Europe 2017*; pp 1-97.
21. Life sciences R&D: changing the innovation equation in India 2011. http://www.bcg.com/expertise_impact/biopharma_summit.aspx.
22. Lachmann, P. J. The penumbra of thalidomide, the litigation culture and the licensing of pharmaceuticals. *QJM : monthly journal of the Association of Physicians* **2012**, 105, 1179-1189.
23. *Accelerating innovation and access to medicines for tuberculosis through open collaboration: a push, pull, pool approach.*; Me'decins Sans Frontie`res/Doctors without Borders: 2014.
24. Bridges, B. A. Hypermutation in bacteria and other cellular systems. *Philosophical transactions of the Royal Society of London. Series B, Biological sciences* **2001**, 356, 29-39.
25. Rice, L. B. Bacterial monopolists: the bundling and dissemination of antimicrobial resistance genes in gram-positive bacteria. *Clinical infectious diseases : an official publication of the Infectious Diseases Society of America* **2000**, 31, 762-769.
26. Livermore, D. M. Antibiotic resistance in staphylococci. *International journal of antimicrobial agents* **2000**, 16 Suppl 1, S3-10.
27. Hall, R. M. Mobile gene cassettes and integrons: moving antibiotic resistance genes in gram-negative bacteria. *Ciba Foundation symposium* **1997**, 207, 192-202; discussion 202-205.
28. Oliver, A.; Perez-Diaz, J. C.; Coque, T. M.; Baquero, F.; Canton, R. Nucleotide sequence and characterization of a novel cefotaxime-hydrolyzing beta-lactamase (CTX-M-10) isolated in Spain. *Antimicrob Agents Chemother* **2001**, 45, 616-620.
29. Chellat, M. F. M. R., L.; Riedl, R. Targeting Antibiotic Resistance. *Angew. Chem. Int. Ed.* **2016**, 55, 6600 – 6626.

30. Gellert, M.; Mizuuchi, K.; O'Dea, M. H.; Nash, H. A. DNA gyrase: an enzyme that introduces superhelical turns into DNA. *Proceedings of the National Academy of Sciences of the United States of America* **1976**, *73*, 3872-3876.
31. Bates AD, M. A. *DNA Topology*. Oxford University Press: Oxford, 2005.
32. Wang, J. C. A journey in the world of DNA rings and beyond. *Annual review of biochemistry* **2009**, *78*, 31-54.
33. Schoeffler, A. J.; Berger, J. M. DNA topoisomerases: harnessing and constraining energy to govern chromosome topology. *Quarterly reviews of biophysics* **2008**, *41*, 41-101.
34. Liu, L. F.; Liu, C. C.; Alberts, B. M. Type II DNA topoisomerases: enzymes that can unknot a topologically knotted DNA molecule via a reversible double-strand break. *Cell* **1980**, *19*, 697-707.
35. Nollmann, M.; Crisona, N. J.; Arimondo, P. B. Thirty years of Escherichia coli DNA gyrase: from in vivo function to single-molecule mechanism. *Biochimie* **2007**, *89*, 490-499.
36. Bates, A. D.; Maxwell, A. Energy coupling in type II topoisomerases: why do they hydrolyze ATP? *Biochemistry* **2007**, *46*, 7929-7941.
37. Champoux, J. J. DNA topoisomerases: structure, function and mechanism. *Annu. Rev. Biochem* **2001**, *70*, 369-413.
38. Collin, F.; Karkare, S.; Maxwell, A. Exploiting bacterial DNA gyrase as a drug target: current state and perspectives. *Applied microbiology and biotechnology* **2011**, *92*, 479-497.
39. Bisacchi, G. S.; Manchester, J. I. A New-Class Antibacterial-Almost. Lessons in Drug Discovery and Development: A Critical Analysis of More than 50 Years of Effort toward ATPase Inhibitors of DNA Gyrase and Topoisomerase IV. *ACS infectious diseases* **2015**, *1*, 4-41.
40. Roca, J.; Wang, J. C. The capture of a DNA double helix by an ATP-dependent protein clamp: a key step in DNA transport by type II DNA topoisomerases. *Cell* **1992**, *71*, 833-840.
41. Roca, J.; Wang, J. C. DNA transport by a type II DNA topoisomerase: evidence in favor of a two-gate mechanism. *Cell* **1994**, *77*, 609-616.
42. Orphanides, G.; Maxwell, A. Evidence for a conformational change in the DNA gyrase-DNA complex from hydroxyl radical footprinting. *Nucleic acids research* **1994**, *22*, 1567-1575.
43. Heddle, J. G.; Mitelheiser, S.; Maxwell, A.; Thomson, N. H. Nucleotide binding to DNA gyrase causes loss of DNA wrap. *Journal of molecular biology* **2004**, *337*, 597-610.
44. Brino, L.; Urzhumtsev, A.; Mousli, M.; Bronner, C.; Mitschler, A.; Oudet, P.; Moras, D. Dimerization of Escherichia coli DNA-gyrase B provides a structural mechanism for activating the ATPase catalytic center. *The Journal of biological chemistry* **2000**, *275*, 9468-9475.
45. Wigley, D. B.; Davies, G. J.; Dodson, E. J.; Maxwell, A.; Dodson, G. Crystal structure of an N-terminal fragment of the DNA gyrase B protein. *Nature* **1991**, *351*, 624-629.
46. Leshner, G. Y.; Froelich, E. J.; Gruett, M. D.; Bailey, J. H.; Brundage, R. P. 1,8-Naphthyridine Derivatives. A New Class Of Chemotherapeutic Agents. *Journal of medicinal and pharmaceutical chemistry* **1962**, *91*, 1063-1065.
47. Emmerson, A. M.; Jones, A. M. The quinolones: decades of development and use. *The Journal of antimicrobial chemotherapy* **2003**, *51* Suppl 1, 13-20.
48. King, D. E.; Malone, R.; Lilley, S. H. New classification and update on the quinolone antibiotics. *American family physician* **2000**, *61*, 2741-2748.
49. Oliphant, C. M.; Green, G. M. Quinolones: a comprehensive review. *American family physician* **2002**, *65*, 455-464.
50. Gellert, M.; Mizuuchi, K.; O'Dea, M. H.; Itoh, T.; Tomizawa, J. I. Nalidixic acid resistance: a second genetic character involved in DNA gyrase activity. *Proceedings of the National Academy of Sciences of the United States of America* **1977**, *74*, 4772-4776.
51. Sugino, A.; Peebles, C. L.; Kreuzer, K. N.; Cozzarelli, N. R. Mechanism of action of nalidixic acid: purification of Escherichia coli nalA gene product and its relationship to DNA gyrase and a novel nicking-closing enzyme. *Proceedings of the National Academy of Sciences of the United States of America* **1977**, *74*, 4767-4771.
52. Sissi, C.; Palumbo, M. Effects of magnesium and related divalent metal ions in topoisomerase structure and function. *Nucleic acids research* **2009**, *37*, 702-711.
53. Zhi, C.; Long, Z. Y.; Manikowski, A.; Comstock, J.; Xu, W. C.; Brown, N. C.; Tarantino, P. M., Jr.; Holm, K. A.; Dix, E. J.; Wright, G. E.; Barnes, M. H.; Butler, M. M.; Foster, K. A.; LaMarr, W. A.; Bachand, B.; Bethell, R.; Cadilhac, C.; Charron, S.; Lamothe, S.; Motorina, I.; Storer, R. Hybrid antibacterials. DNA polymerase-topoisomerase inhibitors. *Journal of medicinal chemistry* **2006**, *49*, 1455-1465.
54. Li, X.; Zhang, Y. K.; Plattner, J. J.; Mao, W.; Alley, M. R.; Xia, Y.; Hernandez, V.; Zhou, Y.; Ding, C. Z.; Li, J.; Shao, Z.; Zhang, H.; Xu, M. Synthesis and antibacterial evaluation of a novel tricyclic oxaborole-fused fluoroquinolone. *Bioorganic & medicinal chemistry letters* **2013**, *23*, 963-966.
55. Mizuuchi, K.; O'Dea, M. H.; Gellert, M. DNA gyrase: subunit structure and ATPase activity of the purified enzyme. *Proceedings of the National Academy of Sciences of the United States of America* **1978**, *75*, 5960-5963.
56. Sugino, A.; Cozzarelli, N. R. The intrinsic ATPase of DNA gyrase. *The Journal of biological chemistry* **1980**, *255*, 6299-6306.

57. Sugino, A.; Higgins, N. P.; Brown, P. O.; Peebles, C. L.; Cozzarelli, N. R. Energy coupling in DNA gyrase and the mechanism of action of novobiocin. *Proceedings of the National Academy of Sciences of the United States of America* **1978**, *75*, 4838-4842.
58. Lewis, R. J.; Singh, O. M.; Smith, C. V.; Skarzynski, T.; Maxwell, A.; Wonacott, A. J.; Wigley, D. B. The nature of inhibition of DNA gyrase by the coumarins and the cyclothialidines revealed by X-ray crystallography. *The EMBO journal* **1996**, *15*, 1412-1420.
59. Gjorgjieva, M.; Tomasic, T.; Barancokova, M.; Katsamakos, S.; Ilas, J.; Tammela, P.; Peterlin Masic, L.; Kikelj, D. Discovery of Benzothiazole Scaffold-Based DNA Gyrase B Inhibitors. *Journal of medicinal chemistry* **2016**, *59*, 8941-8954.
60. Edwards, M. J.; Flatman, R. H.; Mitchenall, L. A.; Stevenson, C. E.; Le, T. B.; Clarke, T. A.; McKay, A. R.; Fiedler, H. P.; Buttner, M. J.; Lawson, D. M.; Maxwell, A. A crystal structure of the bifunctional antibiotic simocyclinone D8, bound to DNA gyrase. *Science* **2009**, *326*, 1415-1418.
61. Sissi, C.; Vazquez, E.; Chemello, A.; Mitchenall, L. A.; Maxwell, A.; Palumbo, M. Mapping Simocyclinone D8 Interaction with DNA Gyrase: Evidence for a New Binding Site on GyrB. *Antimicrobial Agents and Chemotherapy* **2010**, *54*, 213-220.
62. Richter, S. N.; Frasson, I.; Palumbo, M.; Sissi, C.; Palu, G. Simocyclinone D8 turns on against Gram-negative bacteria in a clinical setting. *Bioorganic & medicinal chemistry letters* **2010**, *20*, 1202-1204.
63. Schimana, J.; Fiedler, H. P.; Groth, I.; Sussmuth, R.; Beil, W.; Walker, M.; Zeeck, A. Simocyclinones, novel cytostatic angucyclinone antibiotics produced by *Streptomyces antibioticus* Tu 6040. I. Taxonomy, fermentation, isolation and biological activities. *The Journal of antibiotics* **2000**, *53*, 779-787.
64. Flatman, R. H.; Howells, A. J.; Heide, L.; Fiedler, H. P.; Maxwell, A. Simocyclinone D8, an inhibitor of DNA gyrase with a novel mode of action. *Antimicrob Agents Chemother* **2005**, *49*, 1093-1100.
65. Opegard, L. M.; Hamann, B. L.; Streck, K. R.; Ellis, K. C.; Fiedler, H. P.; Khodursky, A. B.; Hiasa, H. In vivo and in vitro patterns of the activity of simocyclinone D8, an angucyclinone antibiotic from *Streptomyces antibioticus*. *Antimicrob Agents Chemother* **2009**, *53*, 2110-2119.
66. Gootz, T. D.; Brighty, K. E. Fluoroquinolone antibacterials: SAR mechanism of action, resistance, and clinical aspects. *Medicinal research reviews* **1996**, *16*, 433-486.
67. Mitscher, L. A. Bacterial topoisomerase inhibitors: quinolone and pyridone antibacterial agents. *Chemical reviews* **2005**, *105*, 559-592.
68. Bisacchi, G. S. Origins of the Quinolone Class of Antibacterials: An Expanded "Discovery Story". *Journal of medicinal chemistry* **2015**, *58*, 4874-4882.
69. Jia, X.-D.; Wang, S.; Wang, M.-H.; Liu, M.-L.; Xia, G.-M.; Liu, X.-J.; Chai, Y.; He, H.-W. Synthesis and in vitro antitumor activity of novel naphthyridinone derivatives. *Chinese Chemical Letters* **2017**, *28*, 235-239.
70. Hu, Y.-Q.; Meng, L.-D.; Qiang, M.; Song, X.-F. Design, Synthesis, and In Vitro Anti-mycobacterial Evaluation 1H-1,2,3-triazole-tethered Ciprofloxacin and Isatin Conjugates. *Journal of Heterocyclic Chemistry* **2017**, *54*, 3725-3729.
71. Patel, N. B., Patel, S.D.; . Synthesis and antimicrobial studies of some 4-Thiazolidinone containing Fluoroquinolones analogous. *Der. Pharma. Chem* **2009**, *1*, 199-209.
72. Patel, N. B., Patel, S.D.;. Synthesis and antimicrobial study of fluoroquinolone based 4-thiazolidinones. *Med. Chem. Res.* **2010**, *19*, 757-770.
73. Sultana, N. A., M.S; Rizvi, S.B.S; Haroon, U;. Synthesis, characterization and biological evaluations of ciprofloxacin carboxamide analogues. *Bull. Kor. Chem. Soc.* **2011**, *32*, 483-488.
74. Bartzatt, R.; Cirillo, S. L.; Cirillo, J. D. Design of ciprofloxacin derivatives that inhibit growth of methicillin resistant *Staphylococcus aureus* (MRSA) and methicillin susceptible *Staphylococcus aureus* (MSSA). *Medicinal chemistry (Shariqah (United Arab Emirates))* **2010**, *6*, 51-56.
75. Asahina, Y.; Araya, I.; Iwase, K.; Inuma, F.; Hosaka, M.; Ishizaki, T. Synthesis and antibacterial activity of the 4-quinolone-3-carboxylic acid derivatives having a trifluoromethyl group as a novel N-1 substituent. *Journal of medicinal chemistry* **2005**, *48*, 3443-3446.
76. Marquez, B.; Pourcelle, V.; Vallet, C. M.; Mingeot-Leclercq, M. P.; Tulkens, P. M.; Marchand-Bruynaert, J.; Van Bambeke, F. Pharmacological characterization of 7-(4-(Piperazin-1-yl)) ciprofloxacin derivatives: antibacterial activity, cellular accumulation, susceptibility to efflux transporters, and intracellular activity. *Pharmaceutical research* **2014**, *31*, 1290-1301.
77. Fardeau, S.; Dassonville-Klimpt, A.; Audic, N.; Sasaki, A.; Pillon, M.; Baudrin, E.; Mullie, C.; Sonnet, P. Synthesis and antibacterial activity of catecholate-ciprofloxacin conjugates. *Bioorganic & medicinal chemistry* **2014**, *22*, 4049-4060.
78. Nguyen, S. T.; Ding, X.; Butler, M. M.; Tashjian, T. F.; Peet, N. P.; Bowlin, T. L. Preparation and antibacterial evaluation of decarboxylated fluoroquinolones. *Bioorganic & medicinal chemistry letters* **2011**, *21*, 5961-5963.
79. Cormier, R.; Burda, W. N.; Harrington, L.; Edlinger, J.; Kodigepalli, K. M.; Thomas, J.; Kapolka, R.; Roma, G.; Anderson, B. E.; Turos, E.; Shaw, L. N. Studies on the antimicrobial properties of N-acylated ciprofloxacin. *Bioorganic & medicinal chemistry letters* **2012**, *22*, 6513-6520.

80. Abdel-Aziz, A. A.; Asiri, Y. A.; Al-Agamy, M. H. Design, synthesis and antibacterial activity of fluoroquinolones containing bulky arenesulfonyl fragment: 2D-QSAR and docking study. *European journal of medicinal chemistry* **2011**, *46*, 5487-5497.
81. Zhang, G. F.; Liu, X.; Zhang, S.; Pan, B.; Liu, M. L. Ciprofloxacin derivatives and their antibacterial activities. *European journal of medicinal chemistry* **2018**, *146*, 599-612.
82. Foroumadi, A.; Ghodsi, S.; Emami, S.; Najjari, S.; Samadi, N.; Faramarzi, M. A.; Beikmohammadi, L.; Shirazi, F. H.; Shafiee, A. Synthesis and antibacterial activity of new fluoroquinolones containing a substituted N-(phenethyl)piperazine moiety. *Bioorganic & medicinal chemistry letters* **2006**, *16*, 3499-3503.
83. Ronkin, S. M.; Badia, M.; Bellon, S.; Grillot, A. L.; Gross, C. H.; Grossman, T. H.; Mani, N.; Parsons, J. D.; Stamos, D.; Trudeau, M.; Wei, Y.; Charifson, P. S. Discovery of pyrazolthiazoles as novel and potent inhibitors of bacterial gyrase. *Bioorganic & medicinal chemistry letters* **2010**, *20*, 2828-2831.
84. Manchester, J. I.; Dussault, D. D.; Rose, J. A.; Boriack-Sjodin, P. A.; Uria-Nickelsen, M.; Ioannidis, G.; Bist, S.; Fleming, P.; Hull, K. G. Discovery of a novel azaindole class of antibacterial agents targeting the ATPase domains of DNA gyrase and Topoisomerase IV. *Bioorganic & medicinal chemistry letters* **2012**, *22*, 5150-5156.
85. Tari, L. W.; Trzoss, M.; Bensen, D. C.; Li, X.; Chen, Z.; Lam, T.; Zhang, J.; Creighton, C. J.; Cunningham, M. L.; Kwan, B.; Stidham, M.; Shaw, K. J.; Lightstone, F. C.; Wong, S. E.; Nguyen, T. B.; Nix, J.; Finn, J. Pyrrolopyrimidine inhibitors of DNA gyrase B (GyrB) and topoisomerase IV (ParE). Part I: Structure guided discovery and optimization of dual targeting agents with potent, broad-spectrum enzymatic activity. *Bioorganic & medicinal chemistry letters* **2013**, *23*, 1529-1536.
86. Trzoss, M.; Bensen, D. C.; Li, X.; Chen, Z.; Lam, T.; Zhang, J.; Creighton, C. J.; Cunningham, M. L.; Kwan, B.; Stidham, M.; Nelson, K.; Brown-Driver, V.; Castellano, A.; Shaw, K. J.; Lightstone, F. C.; Wong, S. E.; Nguyen, T. B.; Finn, J.; Tari, L. W. Pyrrolopyrimidine inhibitors of DNA gyrase B (GyrB) and topoisomerase IV (ParE), Part II: development of inhibitors with broad spectrum, Gram-negative antibacterial activity. *Bioorganic & medicinal chemistry letters* **2013**, *23*, 1537-1543.
87. Starr, J. T.; Sciotti, R. J.; Hanna, D. L.; Huband, M. D.; Mullins, L. M.; Cai, H.; Gage, J. W.; Lockard, M.; Rauckhorst, M. R.; Owen, R. M.; Lall, M. S.; Tomilo, M.; Chen, H.; McCurdy, S. P.; Barbachyn, M. R. 5-(2-Pyrimidinyl)-imidazo[1,2-a]pyridines are antibacterial agents targeting the ATPase domains of DNA gyrase and topoisomerase IV. *Bioorganic & medicinal chemistry letters* **2009**, *19*, 5302-5306.
88. Charifson, P. S.; Grillot, A. L.; Grossman, T. H.; Parsons, J. D.; Badia, M.; Bellon, S.; Deininger, D. D.; Drumm, J. E.; Gross, C. H.; LeTiran, A.; Liao, Y.; Mani, N.; Nicolau, D. P.; Perola, E.; Ronkin, S.; Shannon, D.; Swenson, L. L.; Tang, Q.; Tessier, P. R.; Tian, S. K.; Trudeau, M.; Wang, T.; Wei, Y.; Zhang, H.; Stamos, D. Novel dual-targeting benzimidazole urea inhibitors of DNA gyrase and topoisomerase IV possessing potent antibacterial activity: intelligent design and evolution through the judicious use of structure-guided design and structure-activity relationships. *Journal of medicinal chemistry* **2008**, *51*, 5243-5263.
89. Sherer, B. A.; Hull, K.; Green, O.; Basarab, G.; Hauck, S.; Hill, P.; Loch, J. T., 3rd; Mullen, G.; Bist, S.; Bryant, J.; Boriack-Sjodin, A.; Read, J.; DeGrace, N.; Uria-Nickelsen, M.; Illingworth, R. N.; Eakin, A. E. Pyrrolamide DNA gyrase inhibitors: optimization of antibacterial activity and efficacy. *Bioorganic & medicinal chemistry letters* **2011**, *21*, 7416-7420.
90. Basarab, G. S.; Hill, P. J.; Garner, C. E.; Hull, K.; Green, O.; Sherer, B. A.; Dangel, P. B.; Manchester, J. I.; Bist, S.; Hauck, S.; Zhou, F.; Uria-Nickelsen, M.; Illingworth, R.; Alm, R.; Rooney, M.; Eakin, A. E. Optimization of pyrrolamide topoisomerase II inhibitors toward identification of an antibacterial clinical candidate (AZD5099). *Journal of medicinal chemistry* **2014**, *57*, 6060-6082.
91. Tomasic, T.; Katsamakos, S.; Hodnik, Z.; Ilas, J.; Brvar, M.; Solmajer, T.; Montalvao, S.; Tammela, P.; Banjanac, M.; Ergovic, G.; Anderluh, M.; Peterlin Masic, L.; Kikelj, D. Discovery of 4,5,6,7-Tetrahydrobenzo[1,2-d]thiazoles as Novel DNA Gyrase Inhibitors Targeting the ATP-Binding Site. *Journal of medicinal chemistry* **2015**, *58*, 5501-5521.
92. Tomasic, T.; Mirt, M.; Barancokova, M.; Ilas, J.; Zidar, N.; Tammela, P.; Kikelj, D. Design, synthesis and biological evaluation of 4,5-dibromo-N-(thiazol-2-yl)-1H-pyrrole-2-carboxamide derivatives as novel DNA gyrase inhibitors. *Bioorganic & medicinal chemistry* **2017**, *25*, 338-349.
93. Zhang, J. Y., Q.Y.; Cross, J.B.; Romero, J.A.C.; Poutsiaka, K.M; Epie, F.; Bevan, D.; Wang, B.; Zhang, Y.Z.; Chavan, A.; Zhang, X.; Moy, T.; Daniel, A.; Nguyen, K.; Chamberlain, B.; Carter, N.; Shotwell, J.; Silverman, J.; Metcalf, C.A.; Ryan, D.; Lippa, B.; Dolle, R.E. Discovery of Azaindole Ureas as a Novel Class of Bacterial Gyrase B Inhibitors. **2015**, *58*, 8503-8512.
94. Tomasic, T.; Barancokova, M.; Zidar, N.; Ilas, J.; Tammela, P.; Kikelj, D. Design, synthesis, and biological evaluation of 1-ethyl-3-(thiazol-2-yl)urea derivatives as Escherichia coli DNA gyrase inhibitors. *Archiv der Pharmazie* **2018**, *351*.
95. Jakopin, Z.; Ilas, J.; Barancokova, M.; Brvar, M.; Tammela, P.; Sollner Dolenc, M.; Tomasic, T.; Kikelj, D. Discovery of substituted oxadiazoles as a novel scaffold for DNA gyrase inhibitors. *European journal of medicinal chemistry* **2017**, *130*, 171-184.

96. Zidar, N.; Macut, H.; Tomasic, T.; Brvar, M.; Montalvao, S.; Tammela, P.; Solmajer, T.; Peterlin Masic, L.; Ilas, J.; Kikelj, D. N-Phenyl-4,5-dibromopyrrolamides and N-Phenylindolamides as ATP Competitive DNA Gyrase B Inhibitors: Design, Synthesis, and Evaluation. *Journal of medicinal chemistry* **2015**, *58*, 6179-6194.
97. Cotman, A. E.; Trampuz, M.; Brvar, M.; Kikelj, D.; Ilas, J.; Peterlin-Masic, L.; Montalvao, S.; Tammela, P.; Frlan, R. Design, Synthesis, and Evaluation of Novel Tyrosine-Based DNA Gyrase B Inhibitors. *Archiv der Pharmazie* **2017**, *350*, 1-16.
98. Zidar, N.; Tomasic, T.; Macut, H.; Sirc, A.; Brvar, M.; Montalvao, S.; Tammela, P.; Ilas, J.; Kikelj, D. New N-phenyl-4,5-dibromopyrrolamides and N-Phenylindolamides as ATPase inhibitors of DNA gyrase. *European journal of medicinal chemistry* **2016**, *117*, 197-211.
99. Durcik, M.; Lovison, D.; Skok, Z.; Durante Cruz, C.; Tammela, P.; Tomasic, T.; Benedetto Tiz, D.; Draskovits, G.; Nyerges, A.; Pal, C.; Ilas, J.; Peterlin Masic, L.; Kikelj, D.; Zidar, N. New N-phenylpyrrolamide DNA gyrase B inhibitors: Optimization of efficacy and antibacterial activity. *European journal of medicinal chemistry* **2018**, *154*, 117-132.
100. Durcik, M.; Tammela, P.; Barancokova, M.; Tomasic, T.; Ilas, J.; Kikelj, D.; Zidar, N. Synthesis and Evaluation of N-Phenylpyrrolamides as DNA Gyrase B Inhibitors. *ChemMedChem* **2018**, *13*, 186-198.
101. Tiz, D. B.; Skok, Z.; Durcik, M.; Tomasic, T.; Masic, L. P.; Ilas, J.; Zega, A.; Draskovits, G.; Revesz, T.; Nyerges, A.; Pal, C.; Cruz, C. D.; Tammela, P.; Zigon, D.; Kikelj, D.; Zidar, N. An optimised series of substituted N-phenylpyrrolamides as DNA gyrase B inhibitors. *European journal of medicinal chemistry* **2019**, *167*, 269-290.
102. Keri, R. S.; Patil, M. R.; Patil, S. A.; Budagumpi, S. A comprehensive review in current developments of benzothiazole-based molecules in medicinal chemistry. *European journal of medicinal chemistry* **2015**, *89*, 207-251.
103. Gjorgjieva, M.; Tomasic, T.; Kikelj, D.; Masic, L. P. Benzothiazole-based Compounds in Antibacterial Drug Discovery. *Curr Med Chem* **2018**, *25*, 5218-5236.
104. Stokes, N. R.; Thomaidis-Brears, H. B.; Barker, S.; Bennett, J. M.; Berry, J.; Collins, I.; Czaplewski, L. G.; Gamble, V.; Lancett, P.; Logan, A.; Lunniss, C. J.; Peasley, H.; Pommier, S.; Price, D.; Smee, C.; Haydon, D. J. Biological evaluation of benzothiazole ethyl urea inhibitors of bacterial type II topoisomerases. *Antimicrob Agents Chemother* **2013**, *57*, 5977-5986.
105. Axford, L. C.; Agarwal, P. K.; Anderson, K. H.; Andrau, L. N.; Atherall, J.; Barker, S.; Bennett, J. M.; Blair, M.; Collins, I.; Czaplewski, L. G.; Davies, D. T.; Gannon, C. T.; Kumar, D.; Lancett, P.; Logan, A.; Lunniss, C. J.; Mitchell, D. R.; Offermann, D. A.; Palmer, J. T.; Palmer, N.; Pitt, G. R.; Pommier, S.; Price, D.; Narasinga Rao, B.; Saxena, R.; Shukla, T.; Singh, A. K.; Singh, M.; Srivastava, A.; Steele, C.; Stokes, N. R.; Thomaidis-Brears, H. B.; Tyndall, E. M.; Watson, D.; Haydon, D. J. Design, synthesis and biological evaluation of alpha-substituted isonipecotic acid benzothiazole analogues as potent bacterial type II topoisomerase inhibitors. *Bioorganic & medicinal chemistry letters* **2013**, *23*, 6598-6603.
106. M. Barančokova, D. K., J. Ilaš et al., .
107. Azam, M. A.; Thathan, J.; Jubie, S. Dual targeting DNA gyrase B (GyrB) and topoisomerase IV (ParE) inhibitors: A review. *Bioorganic chemistry* **2015**, *62*, 41-63.
108. Bellon, S.; Parsons, J. D.; Wei, Y.; Hayakawa, K.; Swenson, L. L.; Charifson, P. S.; Lippke, J. A.; Aldape, R.; Gross, C. H. Crystal structures of Escherichia coli topoisomerase IV ParE subunit (24 and 43 kilodaltons): a single residue dictates differences in novobiocin potency against topoisomerase IV and DNA gyrase. *Antimicrob Agents Chemother* **2004**, *48*, 1856-1864.
109. Bolognesi, M. L.; Cavalli, A. Multitarget Drug Discovery and Polypharmacology. *ChemMedChem* **2016**, *11*, 1190-1192.
110. Morphy, R.; Kay, C.; Rankovic, Z. From magic bullets to designed multiple ligands. *Drug Discovery Today* **2004**, *9*, 641-651.
111. Morphy, R.; Rankovic, Z. Designed multiple ligands. An emerging drug discovery paradigm. *Journal of medicinal chemistry* **2005**, *48*, 6523-6543.
112. Morphy, R.; Rankovic, Z. The physicochemical challenges of designing multiple ligands. *Journal of medicinal chemistry* **2006**, *49*, 4961-4970.
113. Huovinen, P.; Wolfson, J. S.; Hooper, D. C. Synergism of trimethoprim and ciprofloxacin in vitro against clinical bacterial isolates. *European journal of clinical microbiology & infectious diseases : official publication of the European Society of Clinical Microbiology* **1992**, *11*, 255-257.
114. Rashid, M. U.; Dalhoff, A.; Backstrom, T.; Bjorkhem-Bergman, L.; Panagiotidis, G.; Weintraub, A.; Nord, C. E. Ecological impact of MCB3837 on the normal human microbiota. *International journal of antimicrobial agents* **2014**, *44*, 125-130.
115. Gorityala, B. K.; Guchhait, G.; Fernando, D. M.; Deo, S.; McKenna, S. A.; Zhanel, G. G.; Kumar, A.; Schweizer, F. Adjuvants Based on Hybrid Antibiotics Overcome Resistance in Pseudomonas aeruginosa and Enhance Fluoroquinolone Efficacy. *Angewandte Chemie (International ed. in English)* **2016**, *55*, 555-559.
116. Hu, Y. Q.; Zhang, S.; Xu, Z.; Lv, Z. S.; Liu, M. L.; Feng, L. S. 4-Quinolone hybrids and their antibacterial activities. *European journal of medicinal chemistry* **2017**, *141*, 335-345.
117. Brvar, M.; Perdih, A.; Renko, M.; Anderluh, G.; Turk, D.; Solmajer, T. Structure-based discovery of substituted 4,5'-bithiazoles as novel DNA gyrase inhibitors. *Journal of medicinal chemistry* **2012**, *55*, 6413-6426.

118. Chan, P. F.; Srikannathasan, V.; Huang, J.; Cui, H.; Fosberry, A. P.; Gu, M.; Hann, M. M.; Hibbs, M.; Homes, P.; Ingraham, K.; Pizzollo, J.; Shen, C.; Shillings, A. J.; Spitzfaden, C. E.; Tanner, R.; Theobald, A. J.; Stavenger, R. A.; Bax, B. D.; Gwynn, M. N. Structural basis of DNA gyrase inhibition by antibacterial QPT-1, anticancer drug etoposide and moxifloxacin. *Nature communications* **2015**, *6*, 10048.
119. Navarrete-Vazquez, G.; Chavez-Silva, F.; Colin-Lozano, B.; Estrada-Soto, S.; Hidalgo-Figueroa, S.; Guerrero-Alvarez, J.; Mendez, S. T.; Reyes-Vivas, H.; Oria-Hernandez, J.; Canul-Canche, J.; Ortiz-Andrade, R.; Moo-Puc, R. Synthesis of nitro(benzo)thiazole acetamides and in vitro antiprotozoal effect against amitochondriate parasites *Giardia intestinalis* and *Trichomonas vaginalis*. *Bioorganic & medicinal chemistry* **2015**, *23*, 2204-2210.
120. Savage, V. J.; Charrier, C.; Salisbury, A. M.; Moyo, E.; Forward, H.; Chaffer-Malam, N.; Metzger, R.; Huxley, A.; Kirk, R.; Uosis-Martin, M.; Noonan, G.; Mohamed, S.; Best, S. A.; Ratcliffe, A. J.; Stokes, N. R. Biological profiling of novel tricyclic inhibitors of bacterial DNA gyrase and topoisomerase IV. *The Journal of antimicrobial chemotherapy* **2016**, *71*, 1905-1913.
121. Sankaranarayanan, A.; Raman, G.; Busch, C.; Schultz, T.; Zimin, P. I.; Hoyer, J.; Kohler, R.; Wulff, H. Naphtho[1,2-d]thiazol-2-ylamine (SKA-31), a new activator of KCa2 and KCa3.1 potassium channels, potentiates the endothelium-derived hyperpolarizing factor response and lowers blood pressure. *Mol Pharmacol* **2009**, *75*, 281-295.
122. ISO 20776-1:2006 - Clinical laboratory testing and in vitro diagnostic test systems - Susceptibility testing of infectious agents and evaluation of performance of antimicrobial susceptibility test devices -- Part 1: Reference method for testing the in vitro activity of antimicrobial agents against rapidly growing aerobic bacteria involved in infectious diseases ISO. . In.

4 *Magydaris pastinacea*

Magydaris pastinacea (Lam.) Paol. (Apiaceae) [syn.: *Magydaris tomentosa*] is a plant that spontaneously grows in few regions of Mediterranean area like Sicily, Sardinia, Corse, Balears and North Africa (Tunisia, Algeria and Morocco).^{1,2} It is characterized by a thick, striated, sulcate stalk, and reaches a height of over two metres. The leaves are large and white, and velvety underneath; the primordia are undivided or have 3-5 lobes and are crenate, while the leaves have three long oval segments. The umbels are large (40-50 pedicels) with white flowers; the fruit is oblong with slightly flattened sides.³



Figure 1. *Magydaris pastinacea*

Like most plants belonging to the family of Apiaceae, its aerial parts are very rich in several coumarins and furanocoumarins, which are the main responsible of skin irritation, with intense redness and streaking for a few weeks, as noted on the arms of people that were picking other plants in its vicinity.⁴ Interestingly, *M. pastinacea* quickly turned the skin of the hands persistently dark when touched. This phenomenon is probably due to low polarity compounds occurring in trichomes of the plant's organs breaking under pressure.

4.1 Phytochemical and biological studies of *M. pastinacea*

In literature there are some studies concerning the chemical composition and biological activity of this plant. Cerri *et al.*^{4,5} isolated several coumarin and furocoumarin glucosides from the fresh rhizomes, which showed inhibitor activity on platelet aggregation, probably acting specifically on the intraplatelet metabolism of arachidonic acid. In 1996 Camarda *et al.*⁶ identified some known coumarins from the fruit. More recently, the antibacterial and anticoagulant activities of the coumarins isolated from the flowers were investigated.⁷ It was observed that some coumarins isolated from the acetone and methanol extracts were active against Gram-positive and Gram-negative bacteria. Among all, imperatorin and ciropten were the most potent. The anticoagulant results indicated that the isolated compounds weakly prolonged the Prothrombin Time (PT) value, while meranzine hydrate exhibited a pro-coagulant activity, as demonstrated by the shortening of the PT value.⁷ Then, one year later, the same research group isolated new irregular acyclic diterpene, magyatomol acetate, from the petroleum ether extract of the flowers,⁸ Thereafter, an analysis on the essential oil of the flowers of *M. pastinacea* collected in Sicily and Algeria was reported.⁹ Some differences between the oil composition of two populations of the *Magydaris* were observed. Moreover, a moderate antimicrobial activity of the essential oil was detected. A further study of the petroleum ether extract of *M. pastinacea* flowers reported the isolation of several furanocoumarins such as xanthotoxin, xanthotoxol, isopimpinellin and bergaptene as well as simple coumarins. The extract has been evaluated in vitro on murine monocyte/macrophages (J774A.1), human melanoma (A375) and human breast cancer (MCF-7) tumor cell lines for its cytotoxic activity, showing a major activity against the latter, with an IC₅₀ of 0.94 µg/ml.¹⁰ These results were better than the single compounds constituting the most part of the extract, such as xanthotoxin for which has been previously reported a significant antiproliferative activity of 10 µg/ml against MCF-7 cell line,¹¹ while xanthotoxol showed a similar IC₅₀ value (11.92 µg/ml).¹² This finding could be explained by some synergic effects arising among the furanocoumarins occurring in the extract.

Furanocoumarins are phototoxic and photogenotoxic natural constituents occurring in a broad variety of plants used in cosmetics, food and drugs but especially known for their photosensitizing UV-induced action and used in many drugs for skin disorders such as psoriasis and vitiligo.¹³

4.2 Carbonic anhydrase

Carbonic anhydrases (CAs, EC 4.2.1.1) are ubiquitous metallo-enzymes, which are widely present in prokaryotes and eukaryotes. These enzymes catalyse a very simple but essential physiological reaction of the life cycle of many organisms, the reversible hydration of carbon dioxide to bicarbonate and protons according to the following reaction:¹⁴



This reaction, which represents the basis for the regulation of acid–base balance in organisms, occurs also without a catalyst but it is too slow. Moreover, CAs participate in a number of physiological processes, such as

- CO₂ and HCO₃[−] transport between metabolizing tissues and lungs,
- pH and CO₂ homeostasis,
- bone resorption, production of body fluids,
- biosynthetic reactions such as gluconeogenesis, lipogenesis, ureagenesis in animals and CO₂ fixation (in plants and algae),
- calcification,
- tumorigenicity and many other physiological or pathological processes.¹⁵⁻¹⁹

These enzymes are encoded by seven distinct gene families known to date, the α -, β -, γ -, δ -, ζ -, η - and θ -CAs.²⁰⁻²³ α -CAs are normally monomers and rarely dimers, which are present in vertebrates, protozoa, algae, and cytoplasm of green plants and in some *Bacteria*.^{24,20} β -CAs are dimers, tetramers, or octamers; they are predominantly found in *Bacteria*, algae and chloroplasts of both mono- as well as dicotyledons, but also in many fungi and some *Archaea*.^{20,24, 25} γ -CAs are trimers, found in *Archaea*, cyanobacteria, and most types of *Bacteria*.^{20,26} δ - the and ζ -CAs are probably monomers present only in marine diatom,²⁷ where it plays a crucial role in carbon dioxide fixation. ζ -CA's family contain three different active sites in the same protein, therefore it can be considered a pseudotrimer.²⁸⁻³¹ η -CAs seems to be present only in protozoa,³² but its role is poorly understood for the moment.²⁷

Nowadays, there are at least 25 CA inhibitors (CAIs) exploited in the therapy of different diseases, such as glaucoma,³³ epilepsy,³⁴ ulcers,³⁵ osteoporosis,³⁶ obesity,³⁷ Alzheimer's disease,²⁴ and cancer.³⁸ For instance, human CA II (hCA II), hCA IV, and hCA XII are usually referred as anti-glaucoma drug targets,^{33,39} hCA IX and hCA XII are well-known tumor-associated isoforms,^{40,41} hCA VA is a promising drug target for the treatment of obesity,⁴² while hCA VII is a drug target for the treatment of neuropathic pain and epilepsy.^{43,44} Moreover, in the last decades, it was demonstrated that these enzymes presented in some organism, such as protozoa, bacteria and fungi, constitute new drug targets with the potential to design anti-infectives and can be used for the structure-based drug design of novel generation, isoform-selective inhibitors.^{25,45} Due to their ubiquitous and their critical role in cell homeostasis, indiscriminate inhibition of many hCA isoforms lead to detrimental side effects.

CAs are classified according to their distribution in human body. For instance, some of them are cytosolic (CA I, CA II, CA III, CA VII, CA XIII), others are membrane-bound (CA IV, CA IX, CA XII, CA XIV and CA XV), CA VA and CA VB are mitochondrial, and CA VI is secreted in saliva and milk. Moreover, three acatalytic forms, CA-related proteins (CARP), CARP VIII, CARP X, and CARP XI, seem to be cytosolic proteins too.^{17,24,37}

4.2.1 Inhibition Mechanisms of CAs

All CAs are metalloenzymes, but whereas α -, β -, and δ -CAs use Zn(II) ions at the active site,^{24,46} the γ -CAs are probably Fe(II) enzymes, but they are active also with bound Zn(II) or Co(II) ions.^{28, 31,30, 47} The ζ -class uses Cd(II) or Zn(II) to perform the physiologic reaction catalysis.^{31, 47}

X-ray crystallographic data show that the metal ion from the CA active site is coordinated by three His residues (His 94, His 96 and His 119), in the α - and γ -classes, while in the β -class two His are replaced by two Cys residues. The fourth ligand is a water molecule/hydroxide ion acting as a nucleophile in the catalytic cycle of the enzyme.^{20, 22, 24} The zinc-bound water is also engaged in hydrogen bond interactions with the hydroxyl moiety of Thr 199, which is bridged to the carboxylate moiety of Glu 106. All these interactions increase the nucleophilicity of the zinc-bound water molecule and orient CO₂ in order to be attacked by Zinc ion.^{14,17}

The main step of the catalytic process is the formation of the active form of the enzyme (**A**), the metal hydroxide species, by the transfer of a proton from the metal-coordinated water molecule to the solvent, possibly via proton-shuttling residues.^{20,48} The active form of the enzyme attacks a CO₂ molecule bound in a hydrophobic pocket nearby located (**B**), leading to the formation of bicarbonate

coordinated to Zn(II), **C**. The bicarbonate ion is then displaced by a water molecule and liberated into solution, forming the inactive, acid form of the enzyme (**D**), with water coordinated to Zn(II). To return to form **A**, a proton transfer reaction from the active site to the environment or by buffers present in the medium occurs.

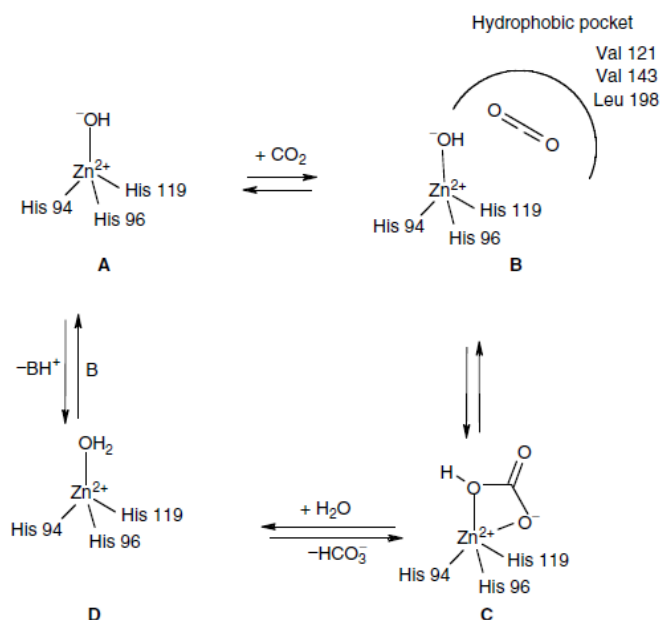
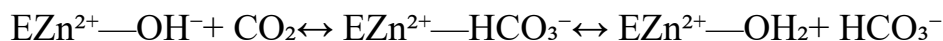


Figure 2. General inhibition mechanisms of CAs

The rate-limiting step in catalysis is the second reaction, i.e., the proton transfer that regenerates the zinc hydroxide species of the enzyme.^{14,17}



In some active isozyme, such as CA IV, CA V, CA VII and CA IX, assisted by a histidine residue (His 64) at the entrance of the active site, as well as by a cluster of histidines that protrudes from the rim of the active site to the surface of the enzyme, assuring a very efficient proton transfer process, for the most active isozyme, CA II.⁴⁹

4.3 Carbonic anhydrase Inhibitors

Inhibition of the CAs has pharmacologic applications in many fields, such as diuretics,⁵⁰ antiglaucoma,³³ anticonvulsant,^{51,52} antiobesity,⁵² and anticancer agents/diagnostic tools,^{22,24} but they are also used as anti-infectives agents (antifungal, antibacterial, and antiprotozoan potential drugs).

CA inhibitors can be divided into different groups:

- 1) The metal ion binders (anion, sulfonamides, and their bioisosteres, dithiocarbamates, xanthates, etc.)
- 2) Compounds which anchor to the zinc-coordinated water molecule/hydroxide ion (phenols, polyamines, thioxocoumarins, sulfocoumarins);
- 3) Compounds binding out of the active site⁵³
- 4) Compounds occluding the active site entrance, such as coumarins and their isosteres

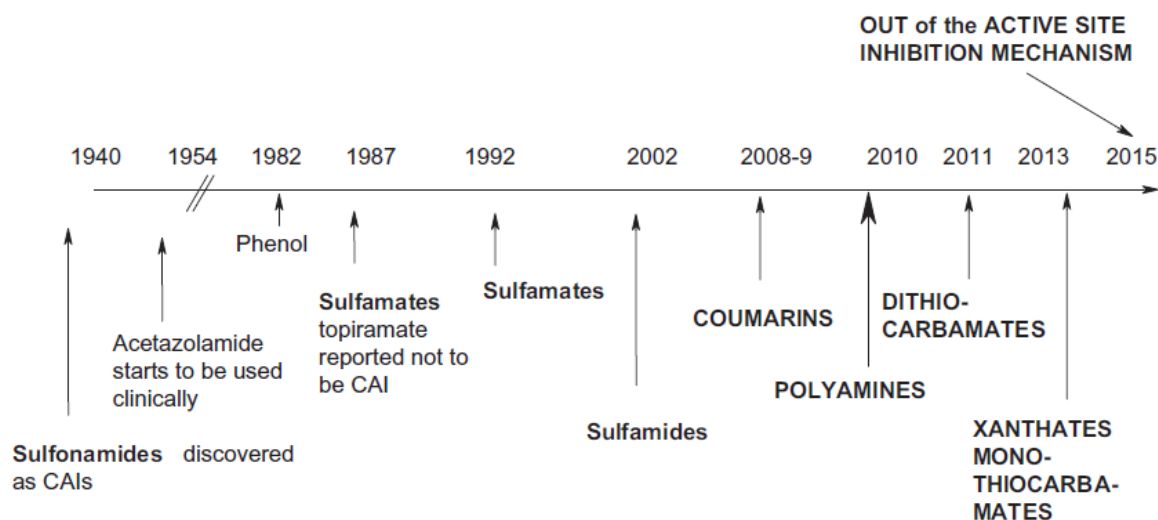


Figure 3. History of CAIs

However, in the last period, the precise mechanism of action of other classes of CAIs is not known due to the fact that they were not yet crystallized in adducts with the enzyme. For example, the secondary sulfonamide moiety is present in a large variety of clinically used drugs, such as the sulfa drugs like sulfadiazine and sulfapyridine.^{54,55} A particular feature of these new classes of CAIs discovered in the last years is that they show a much higher isoform-selectivity profile compared to most sulfonamides and sulfamates. As a matter of fact, they could show less side effects and more

efficacy for the treatment of the classical pathologies associated with these enzymes but also to newer ones such as neuropathic pain,⁵⁶ cerebral ischemia,⁵⁷ and tumors.^{58,59}

4.3.1 The zinc binders as CAIs

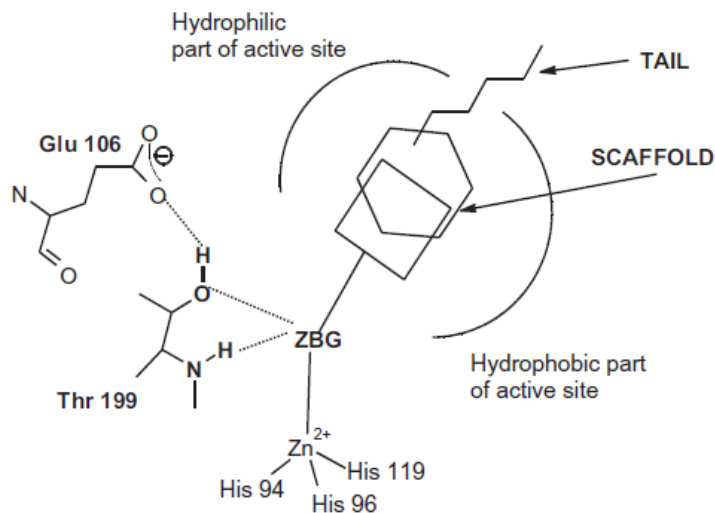


Figure 4. CAIs belonging to the zinc binders.

This group included sulfonamides, sulfamates, and sulfamides (which are in fact sulfonamide isosters). These CAIs bind in deprotonated form (zinc-binding group, ZBG, SO_2NH^-), to the Zn(II) ion of the enzyme active site, which is in a tetrahedral geometry. The ZBG participates in strong interactions with the gate keeper residues Thr199–Glu106. The scaffold may occupy either the hydrophilic or hydrophobic (or both) halves of the active site, whereas the tails generally are orientated toward the exit of the cavity where the most variable amino acid residues are present.²⁴

Sulfonamides are the most important class of CAIs, discovered already in 1940; they are in clinical use for more than 50 years, at the first as antimicrobial drugs and, then, as diuretics and antiglaucoma drugs.^{17,24,60} They include: acetazolamide (AAZ), methazolamide (MZA), ethoxzolamide (EZA), sulthiame, dichlorophenamide (DCP), dorzolamide (DZA), brinzolamide (BRZ), sulpiride (SLP), zonisamide (ZNS), topiramate (TPM), saccharin (SAC), celecoxib (CLX), chlorothiazide/highceiling diuretics of types including hydrochlorothiazide (HCT), furosemide etc. Sulfonamides bind in a tetrahedral geometry to the Zn(II) ion in the deprotonated state, with the nitrogen atom of the moiety coordinated to Zn(II) and a network of hydrogen bonds, involving amino acid residues of the enzyme;^{22,53,61} moreover, the heterocyclic part of the inhibitor interacts with the hydrophilic and hydrophobic residues of the catalytic cavity.^{44,62} Most of sulfonamides act as potent CAIs and are in

clinical use for decades, but the high number of isoforms in humans, their rather diffuse localization in many tissues/organs and the lack of isozyme selectivity toward specific isoforms, led to a wide range of side effect.^{17,24} For instance, acetazolamide, an antiglaucoma agent, has a limited use due to numerous side effects caused by inhibition of CAs other than those present in the eye ciliary processes (i.e., CA II, IV, and XII), leading to fatigue, paresthesias, and kidney stones.²⁴ Moreover, some of the side-effects observed in obese epileptic patients treated with topiramate or zonisamide consisted of a significant weight loss.⁶³ It is due to the lipogenesis inhibition of some CA isozymes involved in the carboxylation of pyruvate to oxaloacetate (mitochondrial isoforms CA VA and VB) and of acetylcoenzyme A to malonylcoenzyme A (cytosolic isoform CA II). Therefore, a combination of topiramate with phentermine, *Qnexa*, is in Phase III clinical trials for the treatment of obesity.⁶⁴

Anions inhibitors are important both for understanding the mechanisms of CAs enzymes and for designing novel types of inhibitors.^{53,61}

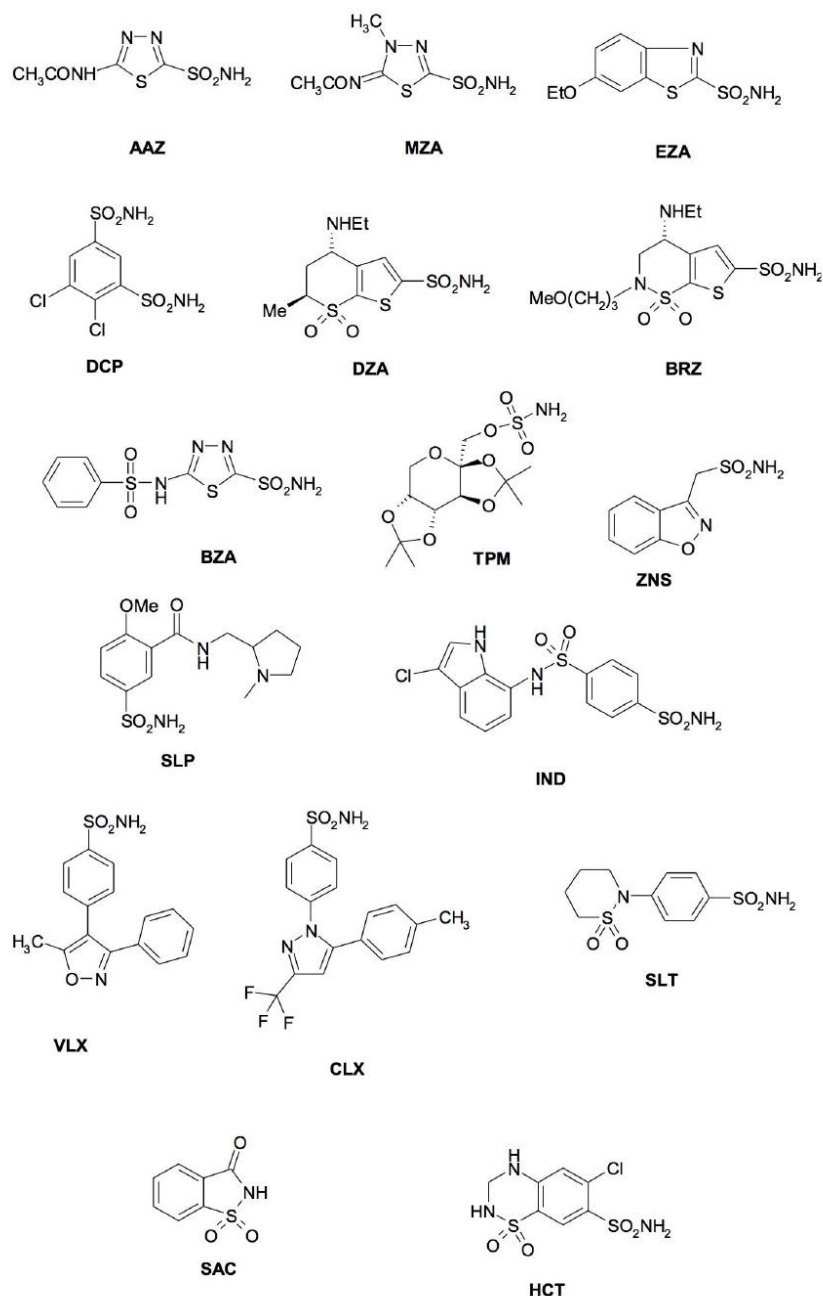


Figure 5. Clinically used sulfonamide and sulfamate CAIs

It is known that some of aromatic/heterocyclic sulfonamides and sulfamates have good affinity for IX isoform and were assessed as potent inhibitors of growth of a multitude of tumor cell lines, but they do not show specificity the remaining CA isozymes (CA I–VII and XII–XV) found in mammals, resulting in many side effects.

Therefore, the main scope of the drug design campaigns in the last years was to obtain isoform-selective CAIs inhibitors for the various isoforms involved in different pathologies. Several approaches were reported for obtaining compounds that specific target the tumor-associated isoforms such as charged compounds or sugar containing sulfonamides/sulfamates/sulfamides, which cannot

cross plasma membranes due to their charged character and their highly hydrophilic character and thus inhibit selectively only extracellular CAs (CA IX and XII),^{24,65} nanoparticles coated with CAIs⁶⁶ and hypoxia-activatable compounds which use hypoxic tumors to convert an inactive prodrug into an active CAI.⁶⁷

4.3.2 CAIs anchoring to the zinc-coordinated water/hydroxide ion

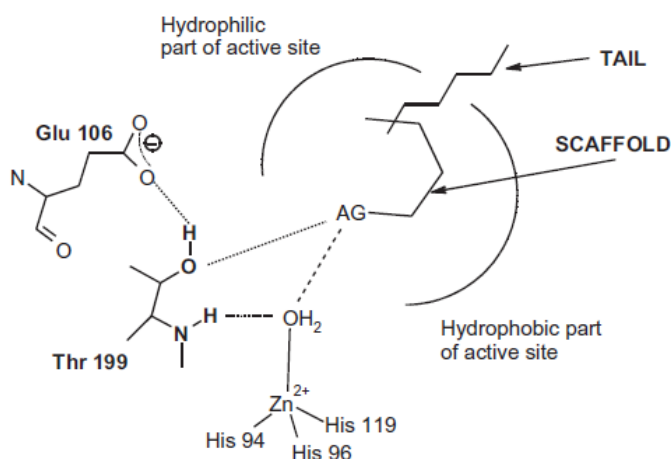


Figure 6. Compounds which anchor to the Zn(II)-coordinated water molecule/hydroxide ion

These inhibitors are characterized by a presence of an anchoring group (AG) which is attached to a scaffold which can interact with the two halves of the active site (as for the zinc binders). The main difference with the zinc binders consists in the fact that the inhibitor is not in a direct contact with the metal ion, but through an AG. The AG might belong to a various chemical functionalities such as phenolic OH (**A**, resorcinol),⁶⁸⁻⁷⁰ primary amine (**B**, spermine),⁶⁹ COOH (**C**, 2,5-dihydroxybenzoic acid),⁷⁰ COOMe (**D**, xylariamide),⁷¹ and SO_3H (**E**, hydrolysed 6-bromo-sulfocoumarin)⁷² moieties.

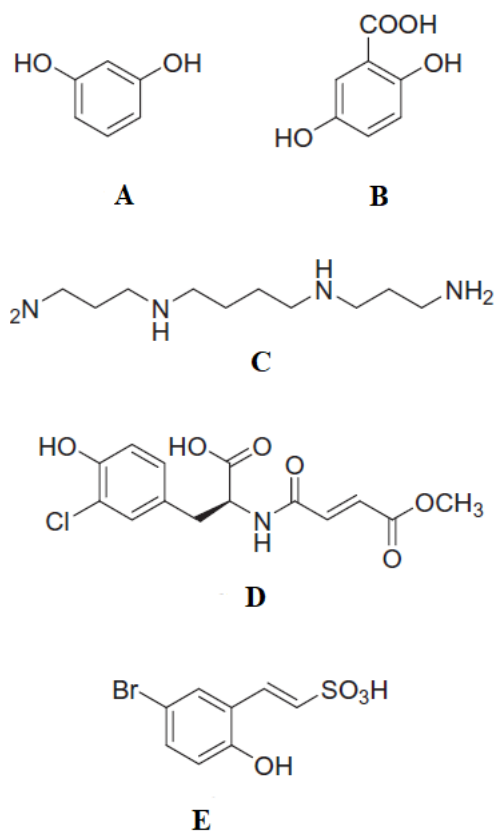


Figure 7. Chemical structures of compounds which anchor to the Zn(II)-coordinated water molecule/hydroxide ion

4.3.3 CA inhibition which bind out of the active site

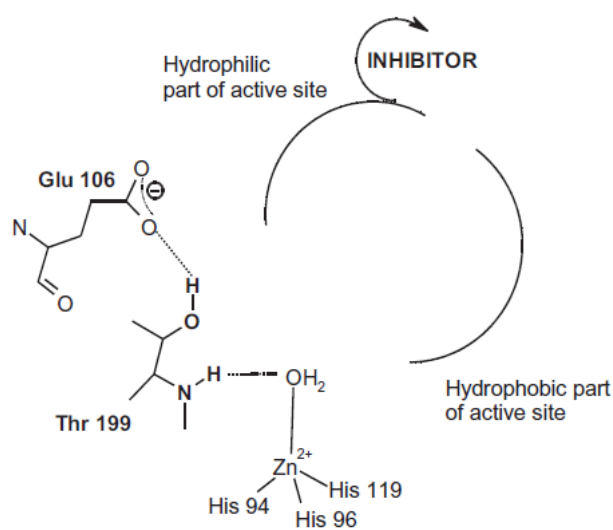


Figure 8. Compounds which inhibit the CAs by binding out of the active site

This mechanism has been discovered quite recently. It was observed that the electronic density of the inhibitor was in an adjacent binding pocket to the active site. CA inhibitor blocks His64, in its *out* conformation, which is the shuttle of a proton from the zinc-coordinated water molecule to the environment, with generation of the zinc hydroxide species of the enzyme.^{17,24,51} Indeed, His64 has a high flexibility with two main conformations, the *in* one (closer to the metal ion) and the *out* one, toward the exit of the active site cavity.⁶¹

4.3.4 CA inhibition by occlusion of the active site entrance

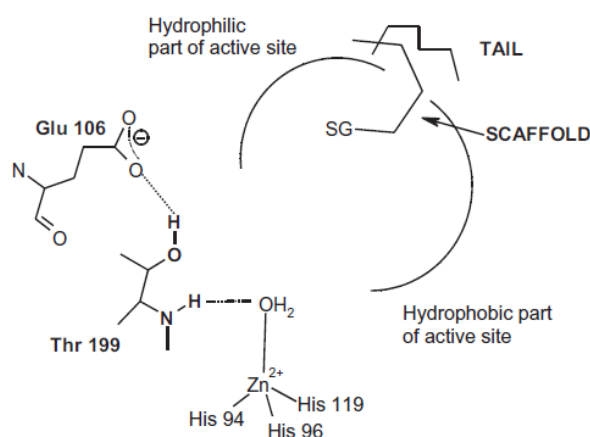


Figure 9. Compounds which inhibit the CAs by occluding the entrance to the active site

These compounds inhibit CAs by occluding the entrance of the active site cavity and binding far away from the metal ion compared to the previous two type of inhibitors. Compounds acting by this mechanism of inhibition possess a sticky group (SG) attached to a scaffold which can be aromatic, heterocyclic, or aliphatic.⁶¹ They may also incorporate a tail, which interact with residues on the surface of the protein.⁷³ This mechanism has been reported for the first time for coumarins.⁷⁴

4.4 Coumarins

Coumarins occur as secondary metabolites in seeds, roots and leaves of many plant species, notably in high concentration in the tonka bean and thus the name comes from a French word, *coumarou*, used for the tonka bean. Plant coumarins are phytoalexins, defense compounds produced when the plant is under threat from other organisms. Their function is not clear, although suggestions include plant growth regulations, fungistasis, bacteriostasis and, even, waste products.⁷⁵ They have attracted interest owing to a range of biological activities including antimicrobial, antiviral, anticancer, antioxidant and antiinflammatory properties.⁷⁶

Coumarins act as prodrugs because α CAs possess esterase activity which is responsible for the hydrolysis of the lactone ring of coumarins (**A-B**); the obtained 2-hydroxycinnamic acids interferes with the binding in the neighbourhood of the metal ion of the enzyme. The product of hydrolysis may bind as *cis* isomers, as observed for bulkier groups **A1**,⁷⁷ or as *trans* isomers, as reported for less bulky groups **B1**.⁷⁴

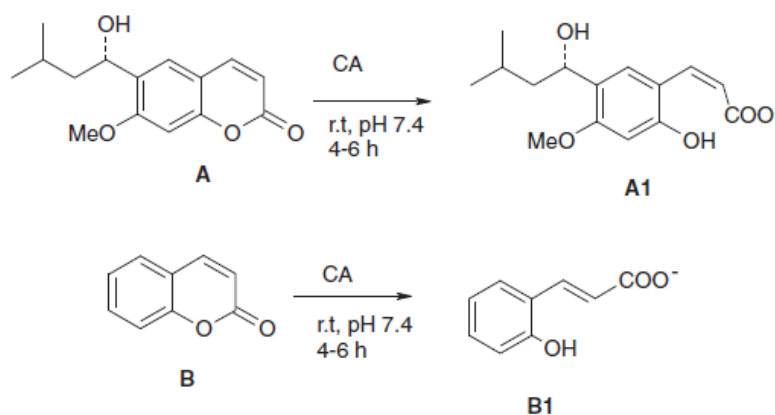


Figure 10. Mechanism of CA inhibition by coumarins

The most relevant aspect of this inhibition is that coumarins bind in the entrance region which is the most variable between the various isoforms. Therefore, it has important consequence for the design of CAIs, since compounds binding in that region should interact differently with the various CAs and thus show isoform selectivity.

4.4.1 Anti-tumour properties of coumarins

As reported above, it is known that isozymes CA IX and XII are overexpressed in many tumors^{24,78} and show a restricted expression in normal tissues. Indeed, solid tumours show an alkaline pH inside the cells and an acid pH in microenvironment, which allows them to survive in hypoxic conditions and to metastasize. CA IX and CA XII, containing extracellular enzyme active sites, appear to participate in this process via their ability to catalyse hydration of CO₂ to bicarbonate and a proton and regulate intratumoral pH. CA IX shows restricted expression in normal tissues but is tightly associated with different types of tumors, because it is induced by tumor hypoxia that involves HIF-1 binding to a hypoxia response element in the CA9 promoter. CA XII is present in many normal tissues and overexpressed in some tumors. It is also induced by hypoxia, but the molecular mechanism remains undetermined. High catalytic activity of these two CA isoforms supports their role in acidification of the tumor. Therefore, modulating extracellular tumor pH by inhibiting CA activity, is a promising approach to anticancer therapy.

In previous works, the anti-tumour properties of coumarins have been reported. Davis *et al.*⁷⁹, for the first time, had used a Nature Bank to provide a diverse collection of coumarins pharmacophore, which have been tested against some CAs isoenzymes (I, II, VII, IX, XII and XIII). For instance, these coumarins revealed CA inhibition profiles consistent with a lot of compounds which inhibited, selectively or at both, CA IX and XII, in submicromolar range.

Winum *et al.*⁸⁰ reported a sweet approach against cancer, incorporating various glycosyl moieties not only into sulfonamides/sulfamates/sulfamides but also in position 7 of the coumarins. The results indicated that they are weak inhibitors of CA I and CA II but very effective against CAIX and CAXII with activity in the nanomolar range.⁸¹ These glycosidic carbonic anhydrase IX inhibitors blocked the growth of primary tumours and metastasis in a human and mouse model of orthotopic, CA IX-positive breast cancer.

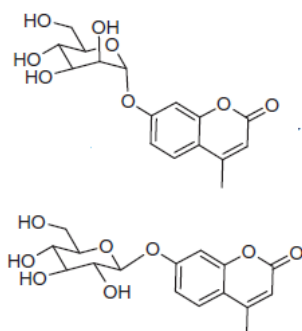


Figure 11. Structures of the synthesized glycosyl coumarins

In 2010, it was investigated the CAIs potency of a series of coumarins incorporating hydroxy-, chloro- and/or chloromethyl- moieties at positions 3-, 4-, 6- and 7- of the heterocyclic ring. All coumarins displayed a weak activity against cytosolic isoforms CA I and II, but some of them presented effective, submicromolar inhibition of the transmembrane, tumor-associated isoforms CA IX and XII, depending to the nature and the position of the groups substituting the coumarin ring. Indeed, the most active coumarin bearing an OH group at position 6, showed $K_{Is} > 100 \mu\text{M}$ against CA I and II, K_{Is} of $0.198 \mu\text{M}$ against CA IX and K_{Is} of $0.683 \mu\text{M}$ against CA XII, being thus a selective CA inhibitor.⁸²

Based on the evidence that 7-hydroxycoumarin (umbelliferone) and some of its derivatives are selective inhibitors of the tumor-associated isoforms CA IX and XII,⁸² several umbelliferone-based compounds were synthesized. They resulted potent inhibitors at low nanomolar concentration against CAIX and CA XII and showed relevant selectivity over ubiquitous hCA I and hCA II isoforms. Moreover, the substitution of the OH with an ester group in position 6 or 7 led to a reduction of the inhibition on CA IX and CA XII, as well as the introduction of an aryl group at C-4 and a methyl in position 8 of the coumarin nucleus.⁸³

Nocentini *et al.*,⁸⁴ synthesized other 7-substituted coumarins incorporating aryl-triazole moieties by using click chemistry. Most of the coumarins were weak inhibitors or did not inhibit significantly hCA I and II, but showed low nanomolar inhibitory action against the transmembrane isoforms, with a K_I of $14.3\text{--}34.4 \text{ nM}$ against hCA IX and of $4.7\text{--}37.8 \text{ nM}$ against hCA XII. A crucial aspect is that all derivatives are hCA IX/XII selective inhibitors over hCA I and II, which constitutes a very important feature for this class of compounds.

In our previous work,⁸⁵ a small library of coumarin and psoralen derivatives together with a series of psoralen-benzenesulfonamide hybrids showing potent and selective inhibition of the tumor associated hCA IX and XII isoforms in the low nanomolar range, were synthesized. A SAR study highlighted different activity profile, according to the substitution of the phenyl ring. Indeed, the introduction of a halogen atom (Cl or F) in position 4 of the phenyl substituent of coumarins derivatives oriented the activity and selectivity toward the IX isozyme, while a methyl substituent increase the activity toward the hCA XII isoform. As regards psoralen derivatives, the biological activity is more influenced by the size of the substituent on the phenyl ring rather than by its nature, indeed unsubstituted phenyl and a fluorophenyl psoralen derivatives resulted the most potent inhibitors. In the case of the psoralen-benzenesulfonamide hybrids, an inhibition toward IX and XII isozymes ranging from nanomolar to low nanomolar, was observed but a lower selectivity is generally measured toward the off-target isozyme hCA II.

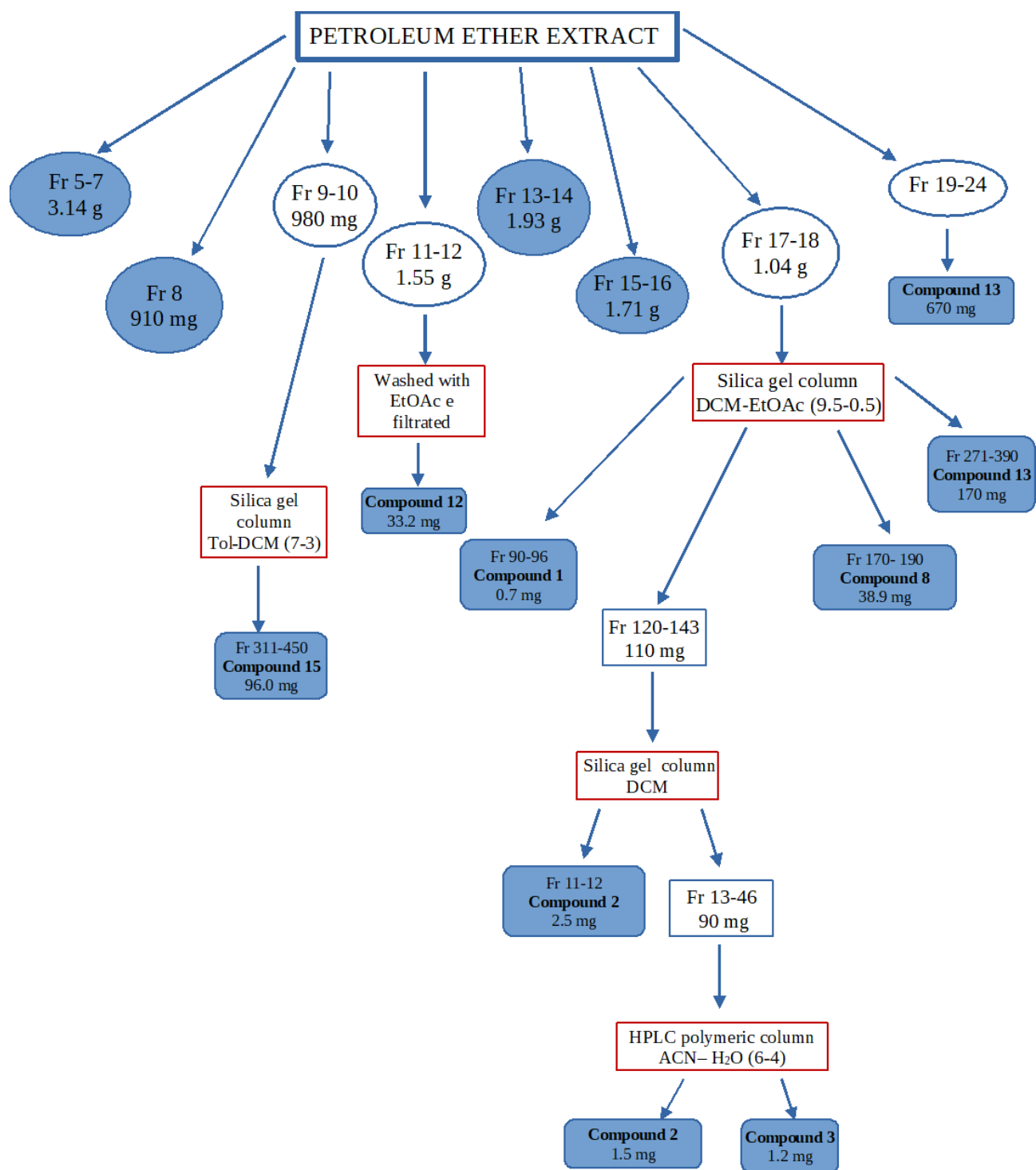
Docking simulations well explain the selectivity of these compounds. In fact, coumarins and psoralen derivatives are not able to enter deeply in the active site of hCA II because of the steric hindrance of Phe 131, but they perfectly fit into the active site of hCA IX and hCA XII, where Phe 131 is substituted by Val 130 and Ala 129, respectively. As a matter of fact, the coumarin moiety could reach the catalytic site and be hydrolysed. In contrast with previous reported binding mode of coumarins,⁷⁷ these derivatives interact as a bidentate chelator with Zn^{2+} . Benzenesulfonamide compounds act interacting with the sulfonamide moiety, while the coumarin portion, oriented outside the pocket, cannot be hydrolysed, indicating that these compounds may act as traditional Zn^{2+} binders, probably due to the strong interaction between SO_2NH_2 and Zn^{2+} , which, on the one hand, may lead to very potent compounds but, on the other, could affect selectivity.⁸⁵

4.5 Aim and Objectives

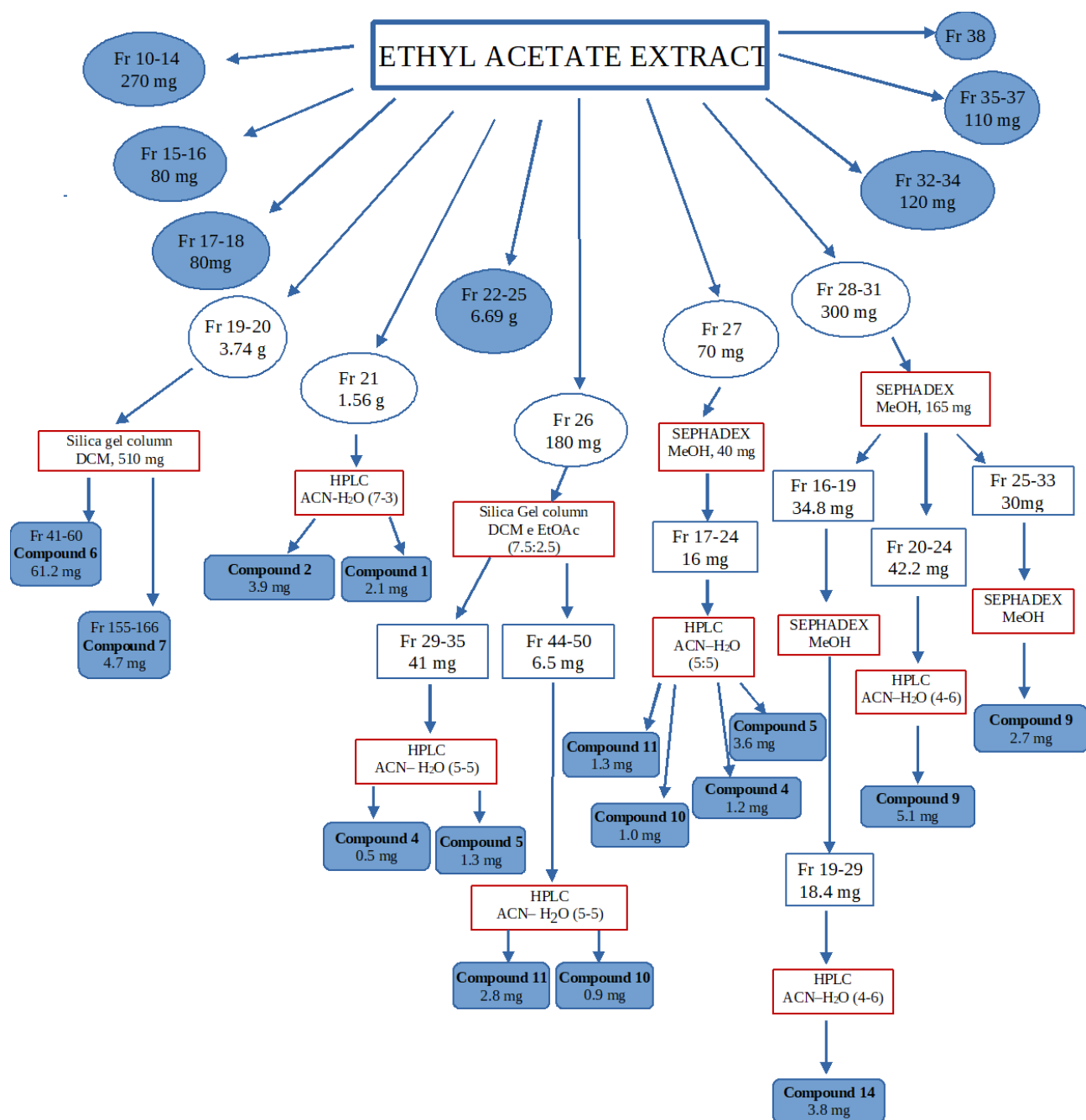
In view of the importance of coumarins as inhibitors of CA and the rich presence of this class of compounds in the seeds of *M. pastinacea*, we first decided to assay, in collaboration with the research group of Prof. Claudiu Supuran of the University of Florence, the inhibitory activity of the petroleum ether and ethyl acetate extracts toward four hCA isoforms. Since both extracts exhibited high activity (Table 2), we proceed to isolate, identify and test against the four CA isoenzymes the coumarins contained therein.

4.5.1 Isolation and characterization of compounds 1-15

The petroleum ether and ethyl acetate extracts of *M. pastinacea* showed high potency to inhibit hCA IX and XII isoforms (Table 2) and were therefore subjected to fractionation by silica gel vacuum-liquid chromatography (VLC), column chromatography (silica gel and Sephadex LH 20) and semi-preparative HPLC (Polymeric RP-HPLC) to give one new angular dihydrofurocoumarin (**11**) along with ten linear furocoumarins (**1-10**) and four simple coumarins (**12-15**) (Figure 12).



Scheme 1. Isolation procedure of coumarins from the petroleum ether extract



Scheme 2. Isolation procedure of coumarins from the ethyl acetate extract

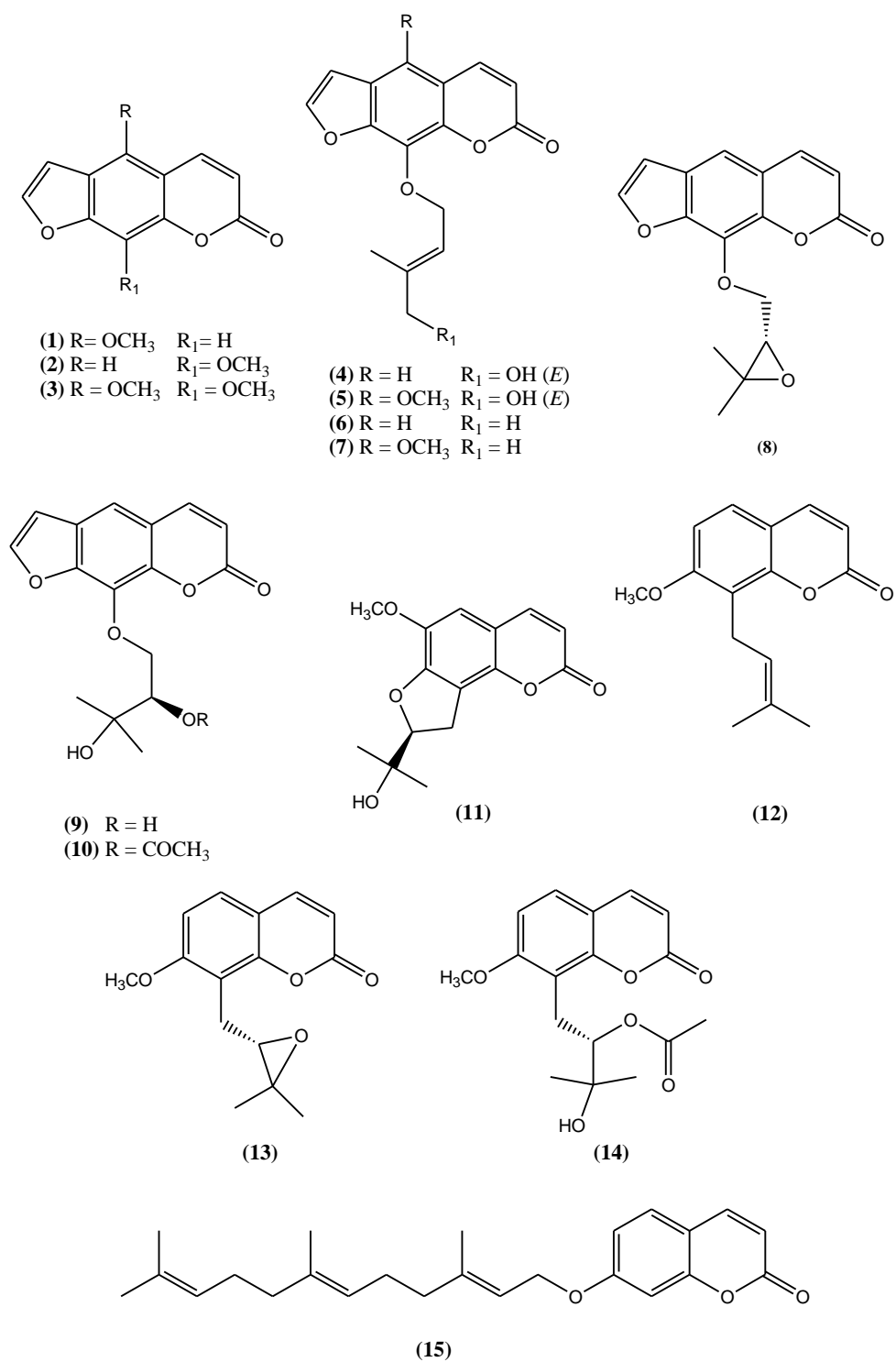


Figure 12. Structures of coumarins and furocoumarins isolated from *M. pastinacea* extracts

4.5.2 Structure elucidation of compounds 1-15

Compound 11

The HR-ESIMS of compound **11** showed a molecular ion at m/z 277.1078 ($M + H$)⁺ which is in accordance with the molecular formula C₁₅H₁₆O₅ (calcd. 277.1076) (Figure 13).

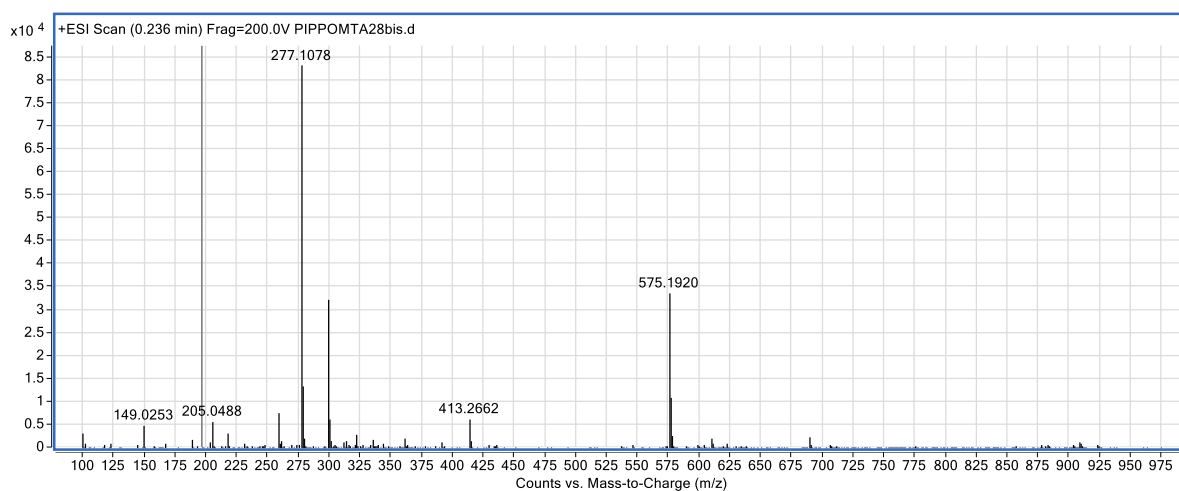


Figure 13. HR-ESIMS spectrum of compound **11** measured in positive mode

The ¹H NMR spectrum of compound **11** showed two doublets at 6.23 (H-3, $J = 9.5$ Hz) and 7.59 (H-4, $J = 9.5$ Hz) ppm and a singlet at 6.77 ppm characteristic of a coumarin nucleus substituted at C-6, C-7 and C-8 (Table 1). In the high field spectrum region a further singlet at δ 3.91 (3H, s) was characteristic of a methoxy group, while two singlets at 1.25 (3H, s) and 1.40 (3H, s) were assigned to two tertiary methyl groups. Finally, the signals at 3.36 (2H, dd, $J = 1.5, 9$ Hz) and 4.86 (1H, t, $J = 9$ Hz) could be ascribed to a methylene and a methine group, respectively (Table 1).

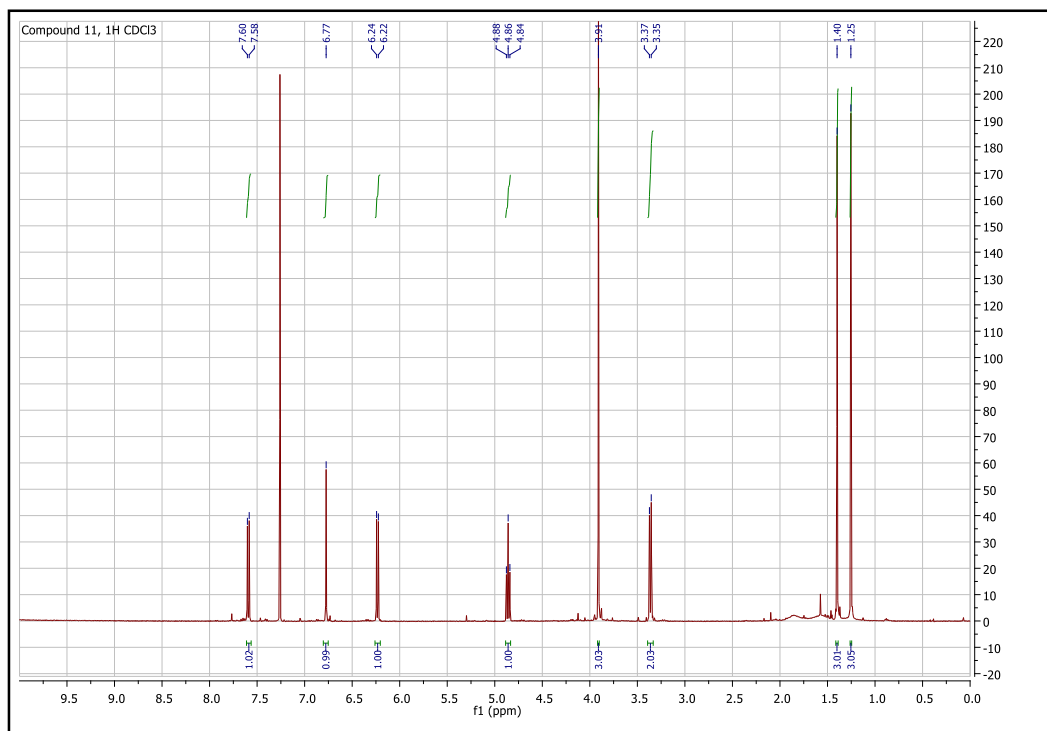


Figure 14. ^1H NMR spectrum (500 MHz, CDCl_3) of magydarin (**11**)

The ^{13}C NMR spectrum highlighted 14 carbons of which those at 161.2, 143.7 and 112.8 ppm were characteristic respectively of C-2, C-3 and C-4 of a coumarin nucleus

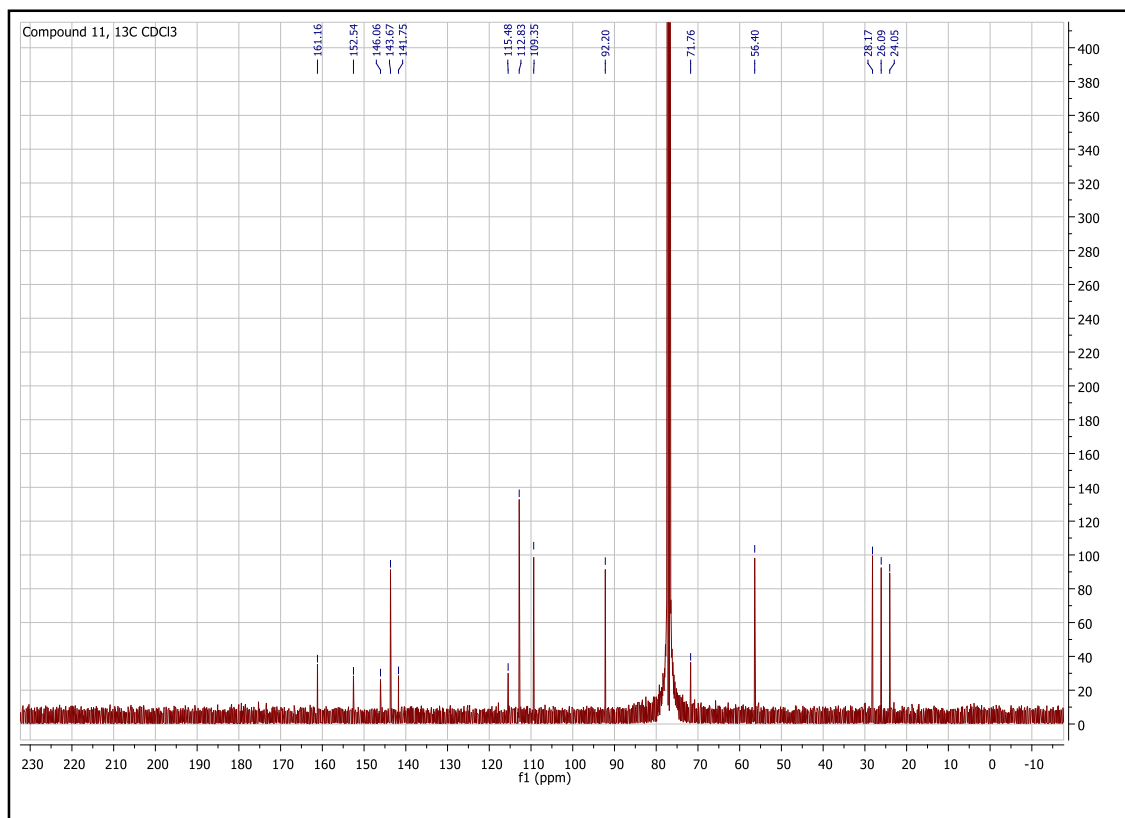


Figure 15. ^{13}C NMR spectrum (100 MHz, CDCl_3) of magydarin (**11**)

The connectivity of each proton with its respective carbon has been identified through HSQC experiment.

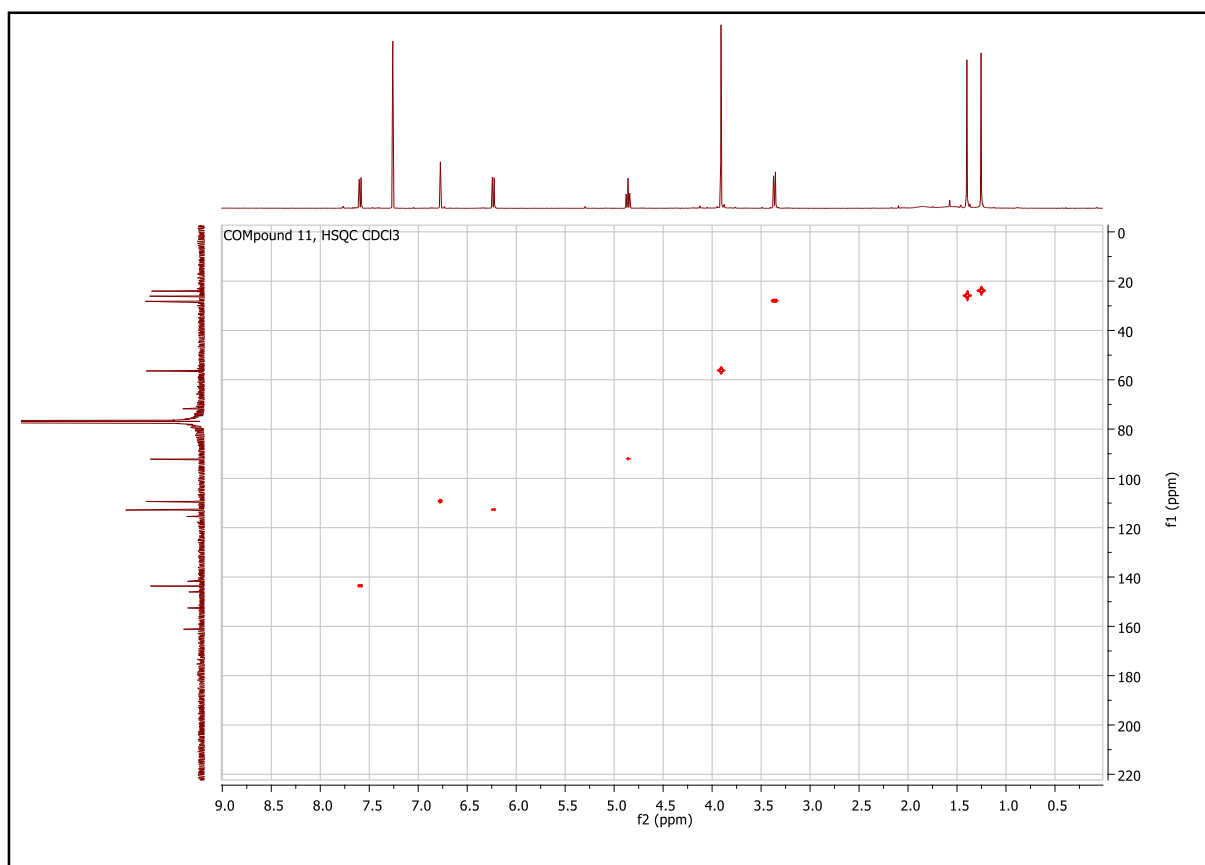


Figure 16. HSQC spectrum (500 MHz CDCl₃) of magydarin (**11**)

In the HMBC spectrum, the correlations between the aromatic proton at δ 6.77 (1H, s) and the carbons at 152.5, 146.1, 143.7 and 141.8 ppm located this proton at position 5 of the coumarin system (Figure 17). This was confirmed by the fact that no cross-peak of this proton with the carbon at 143.7 ppm could be observed if it would be located at C-6, C-7 or C-8. In the same spectrum the cross-peaks between the signal at 1.25 (s) and the carbons at 26.1, 71.8 and 92.2 ppm and between the signal at 1.40 (s) ppm and the carbons at 24.1, 71.8 and 92.2 ppm, confirmed the presence of two geminal methyls.

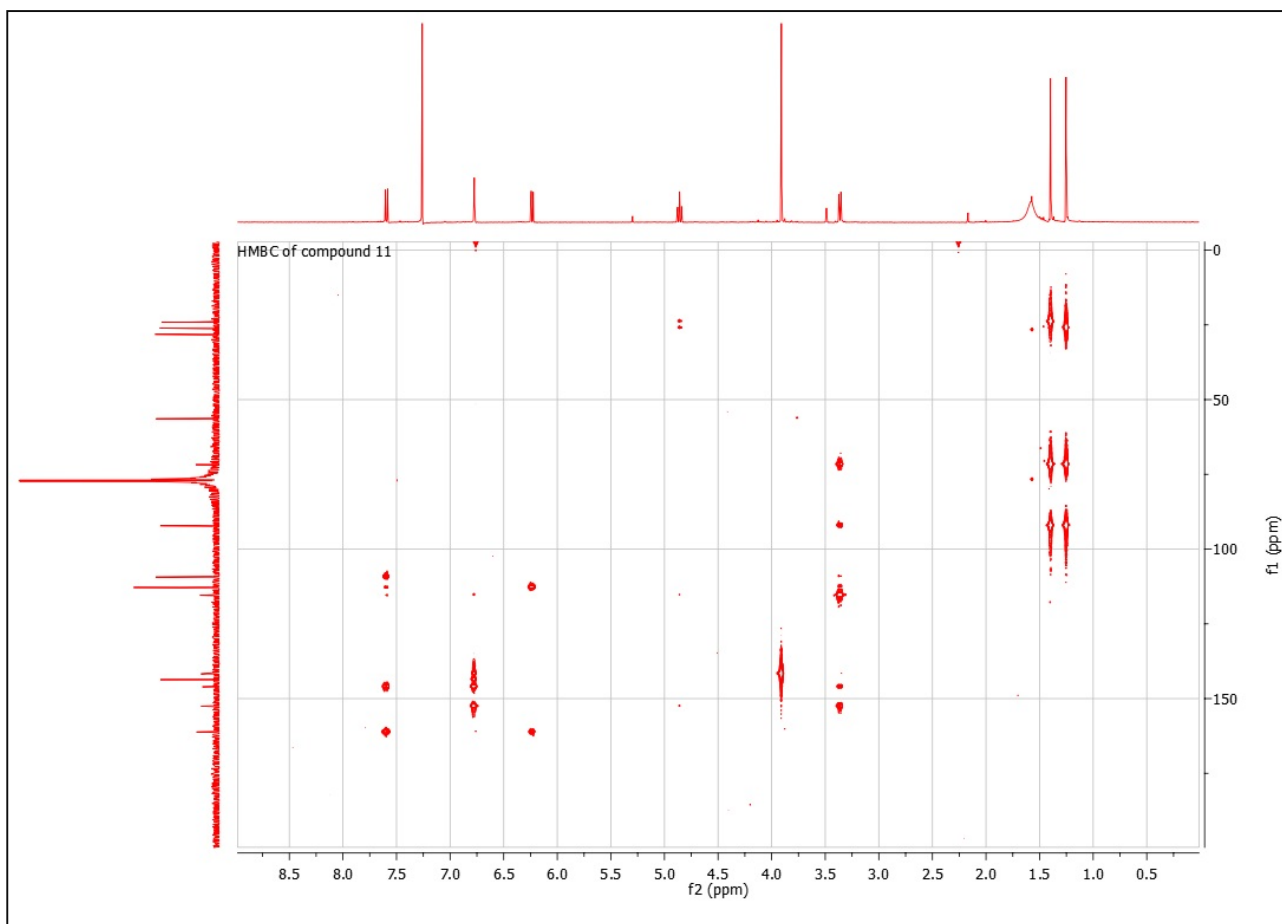


Figure 17. HMBC spectrum (500 MHz CDCl_3) of magydarin (**11**)

Further correlations of the methylene protons at δ 3.36 (2H, dd, $J = 1.5, 9$ Hz) with the carbons at 71.8, 92.2, 115.5, 146.1 and 152.5 ppm fixed the 1,1-dimethyl-2-oxopropanol chain at C-8 of the coumarin nucleus.

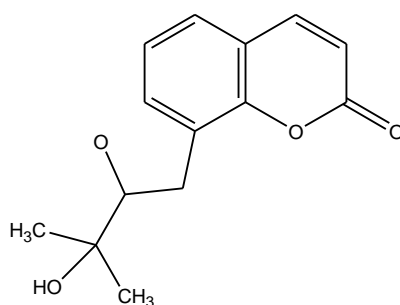


Figure 18. Partial structure of the compound **11**

In the HMBC experiment it could be observed that the methoxyl group at 3.91 ppm was linked to the coumarin nucleus on carbon at 141.8 ppm. This data, together with the correlation between the

aromatic proton at C-5 and carbon at 141.8 ppm, allowed us to place the methoxy group at C-6. (Figure 19).

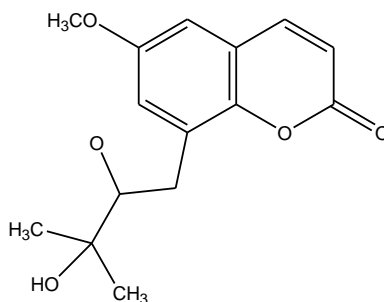


Figure 19. Partial structure of the compound **11**

The absence of further aromatic protons and the presence of only one alcohol group (δ 1.58) in the proton spectrum, suggested the cyclization of the alcohol chain at position 7 of the coumarin ring.

(Figure

20).

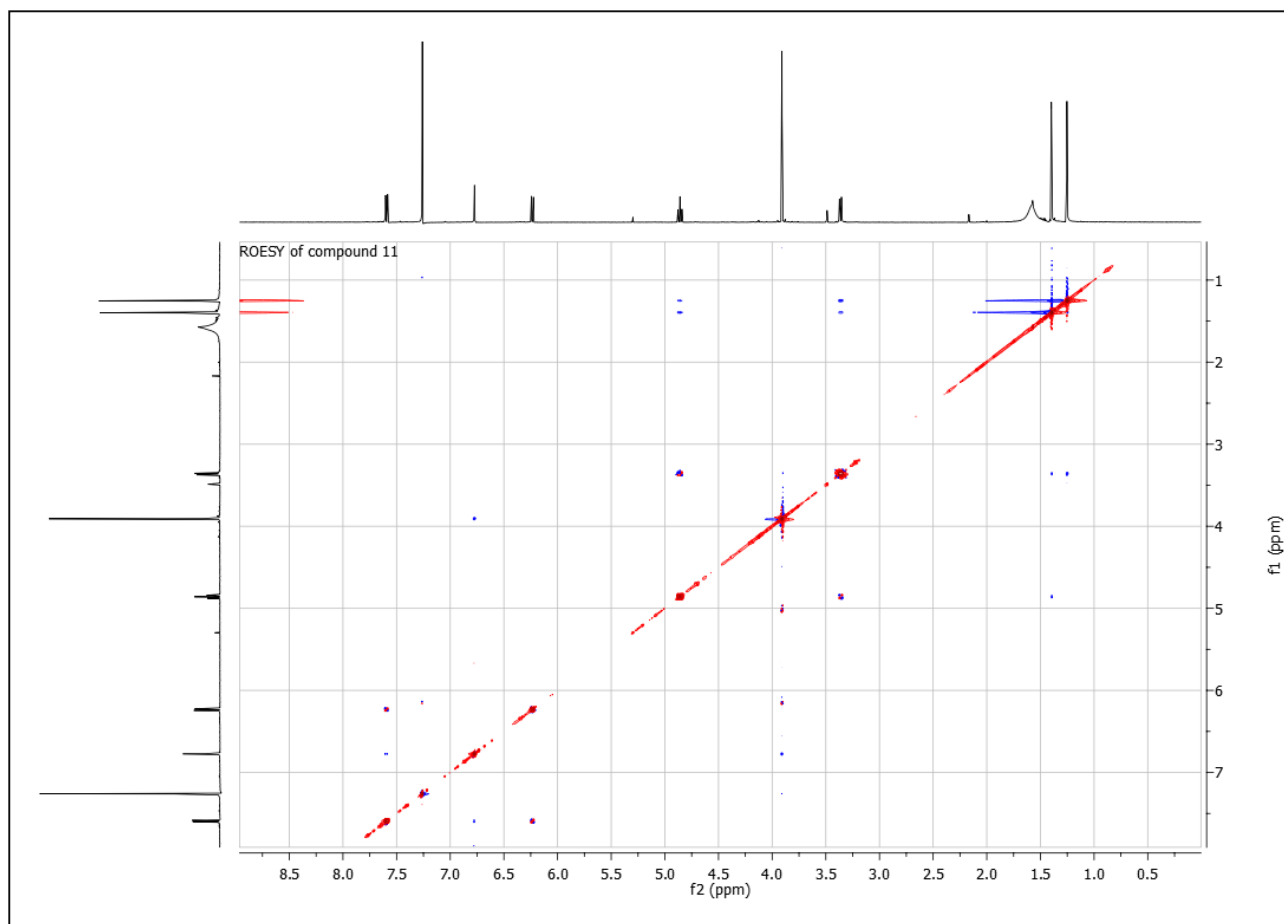


Figure 20. ROESY spectrum (500 MHz CDCl_3) of magydarin (**11**)

HSQC, HMBC, and ROESY experiments allowed the complete assignment of all signals and the identification of the structure as reported in Figure 21.

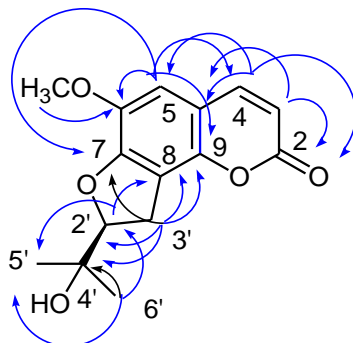


Figure 21. Main HMBC correlations observed for compound **11**

The absolute configuration of the (+)-diidrofurocoumarin **11** has been established studying its Electronic Circular Dicroism (ECD) spectrum. The positive Cotton effect at 348 nm in the ECD spectrum (Figure 23) was ascribed to the $n \rightarrow \pi^*$ electronic transition of the unsaturated lactone ring, which permitted the assignment of the (2'S) absolute configuration (Figure 22) based on the modified octant rule.^{86,87} In fact, the 1-hydroxy-1-methylethyl group was located in the upper left (+) octant. Compound **11** is a previously undescribed diidrofurocoumarin and was named magydarin.

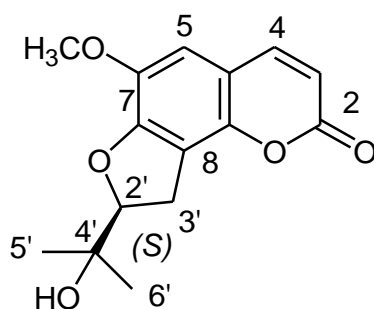


Figure 22. Structure of compound **11**

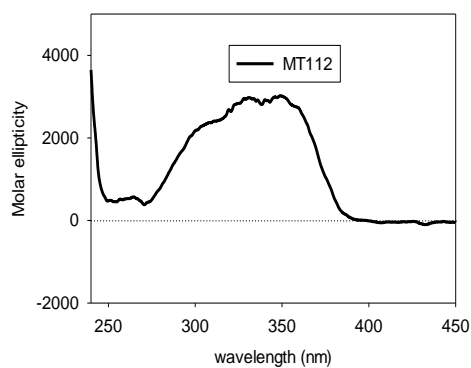


Figure 23. ECD spectrum of compound **11**

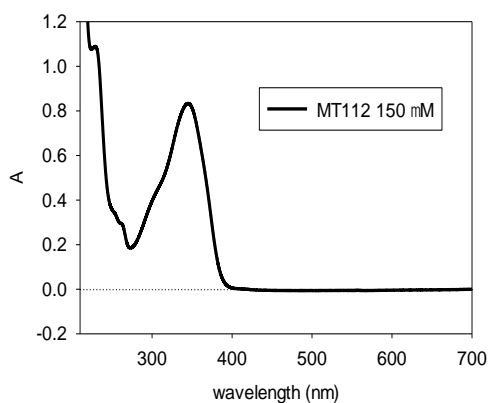


Figure 24. UV spectrum of compound **11**

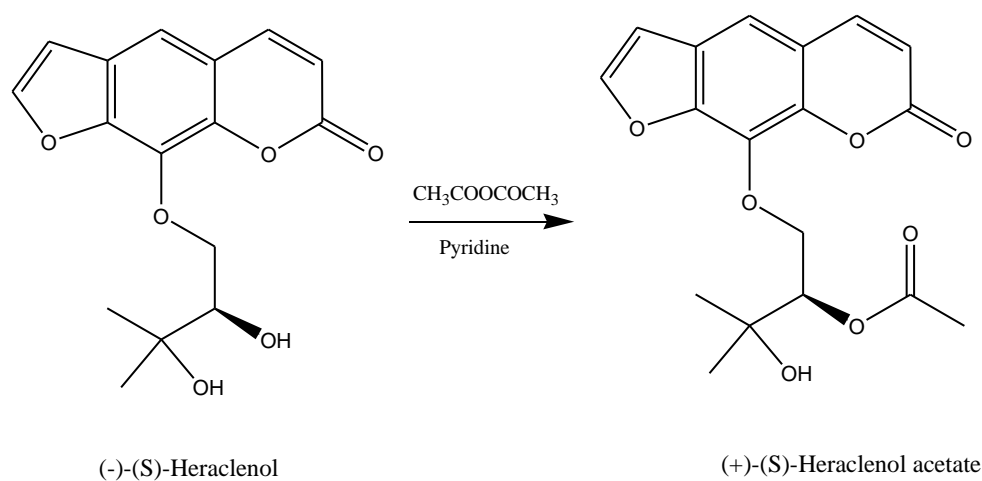
Table 1. ^1H NMR and ^{13}C NMR Spectroscopic Data for Compound **11** (CDCl_3 , δ in ppm)

Compound 11		
position	δ_{C} , type	δ_{H} (J in Hz)
2	161.2, C	
3	112.8, CH	6.23, d (9.5)
4	143.7, CH	7.59, d (9.5)
5	109.4, CH	6.77, s
6	141.8, C	
7	146.1, C	
8	115.5, C	
9	152.5, C	
10	112.8, C	
2'	92.2, CH	4.86, t, (9)
3'	28.2 CH_2	3.36, dd (1.5, 9)
4'	71.8, C	
5'	24.1 CH_3	1.25, s
6'	26.1, CH_3	1.40, s
OCH_3	56.4, CH_3	3.91, s

Compound 10

The absolute configuration of the (+)-heraclenol acetate⁸⁸ **10** is not reported in the literature and therefore it has been established through the acetylation of the isolated (-)-heraclenol **9**, for which the S configuration has been previously assigned.^{89,90}

The specific optical rotation of compound **9** ($[\alpha]_{\text{D}}^{25} = -7.1$) revealed that its absolute configuration is S.⁹¹ Acetylation with acetic anhydride in pyridine of (-)-S-heraclenol yielded S-heraclenol acetate possessing a specific optical rotation $[\alpha]_{\text{D}}^{25} +10$ (Scheme 3). As consequence, the natural (+)-heraclenol acetate (**10**) must have an absolute configuration S.



Scheme 3. Acetylation of (-)-S-heraclenol

Compound 4

Compound **4** has been identified as *trichoclin* by comparison with analytical and spectroscopic data reported in the literature.⁹² However, *trichoclin* contain a double bond whose geometric configuration could not be determined by comparison with the data reported in the literature.

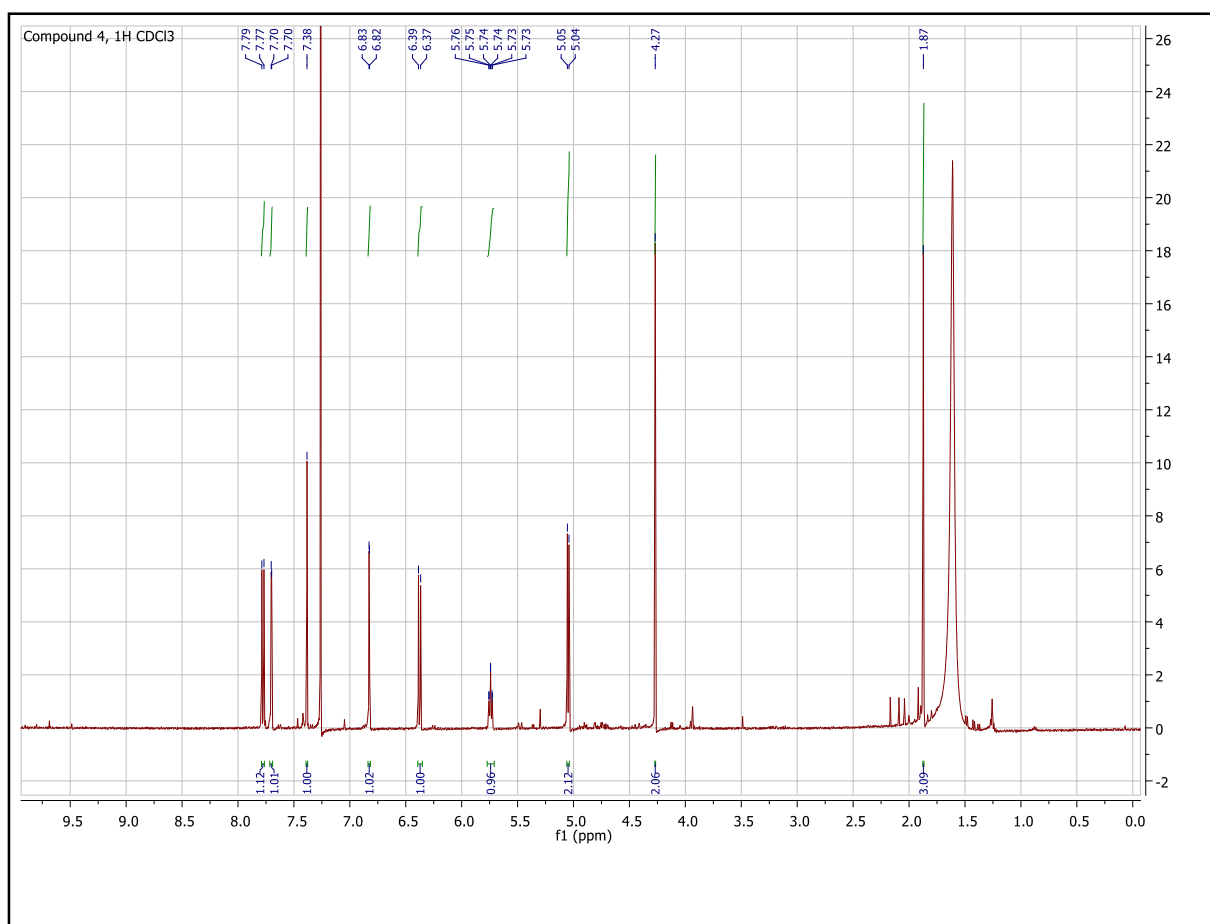


Figure 25. ¹H NMR Spectrum of compound **4** measured in CDCl₃, 500 MHz

In order to assign the *Z* or *E* configuration to the double bond, a ROESY spectrum (Figure 26) of compound **4** was recorded. The ROESY spectrum revealed a cross-peak between the olefinic proton at δ 5.74 (1H, t, $J = 7$ Hz) and the oxymethylene protons at 5.05 (2H, d, $J = 7$ Hz) but the correlation between the proton at δ 5.74 with the methyl group at 1.87 (3H, s) ppm could not be observed. This is well suited to an *E* geometry. In fact, a 3D molecular model of *E*-trichoclin highlight that the distance between the olefinic proton and the oxymethylene protons is 3.2 Å, whereas the distance between the same proton and the methyl group is 4 Å.

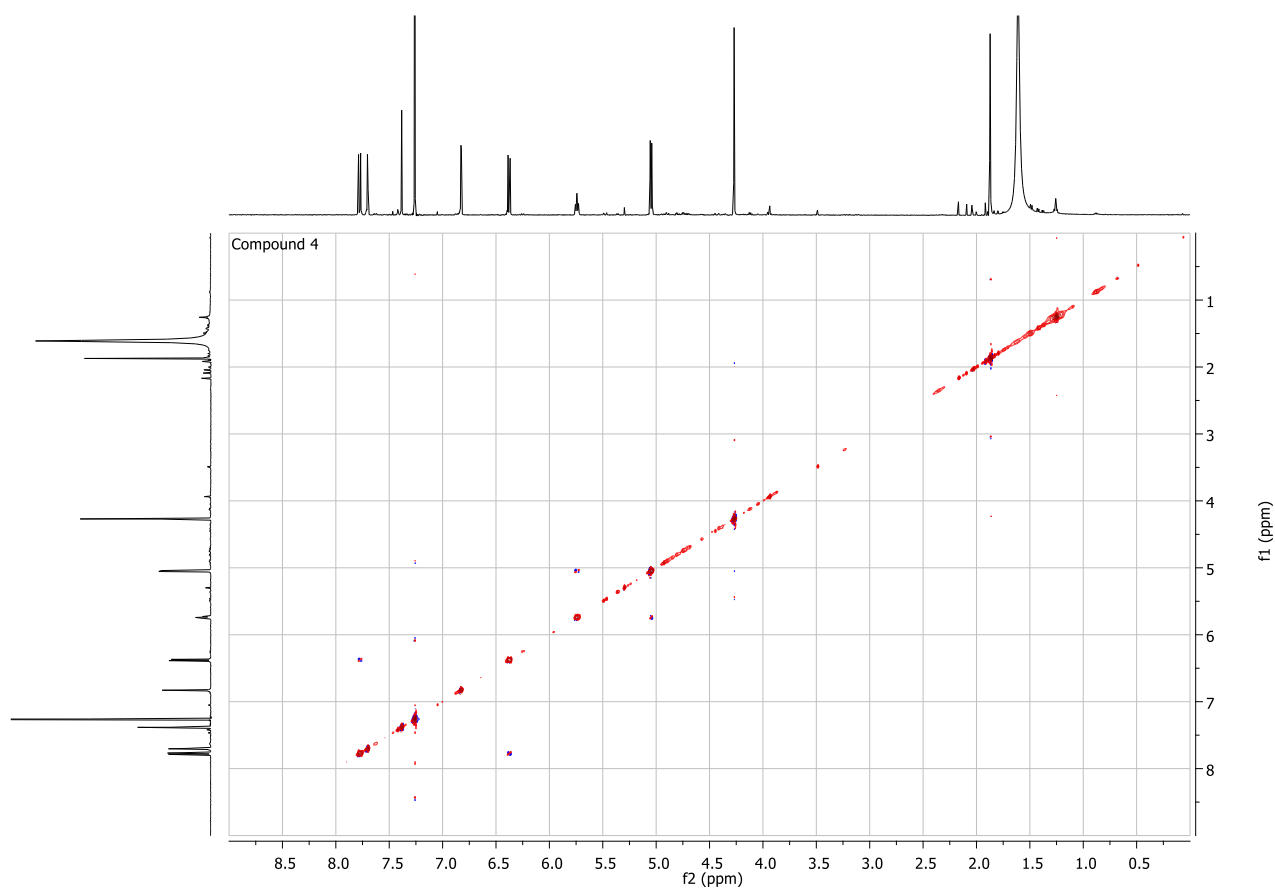


Figure 26. ROESY spectrum of compound **4**

In the case of *Z* isomer, the distance of 3.9 Å between the olefinic proton and the oxymethylene protons preclude any correlation whereas the short distance (2.3 Å) of the methyl at δ 1.87 with methine at 5.74 ppm should be enough to give a cross-peak in the ROESY spectrum.

Thus, compound **4** has been identified as *E*-trichoclin (Figure 27)

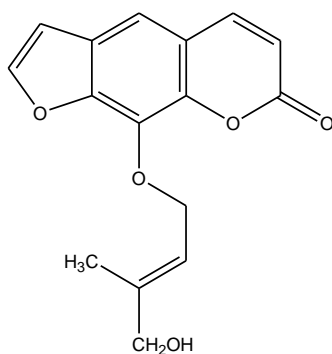


Figure 27. Structure of *E*-trichoclin

Compound 5

Compound **5** has been identified as 5-methoxy-trichoclin by comparison with analytical and spectroscopic data reported in the literature⁹² With respect to *trichoclin*, compound **5** contained the same chain and an additional methoxyl at position 5.

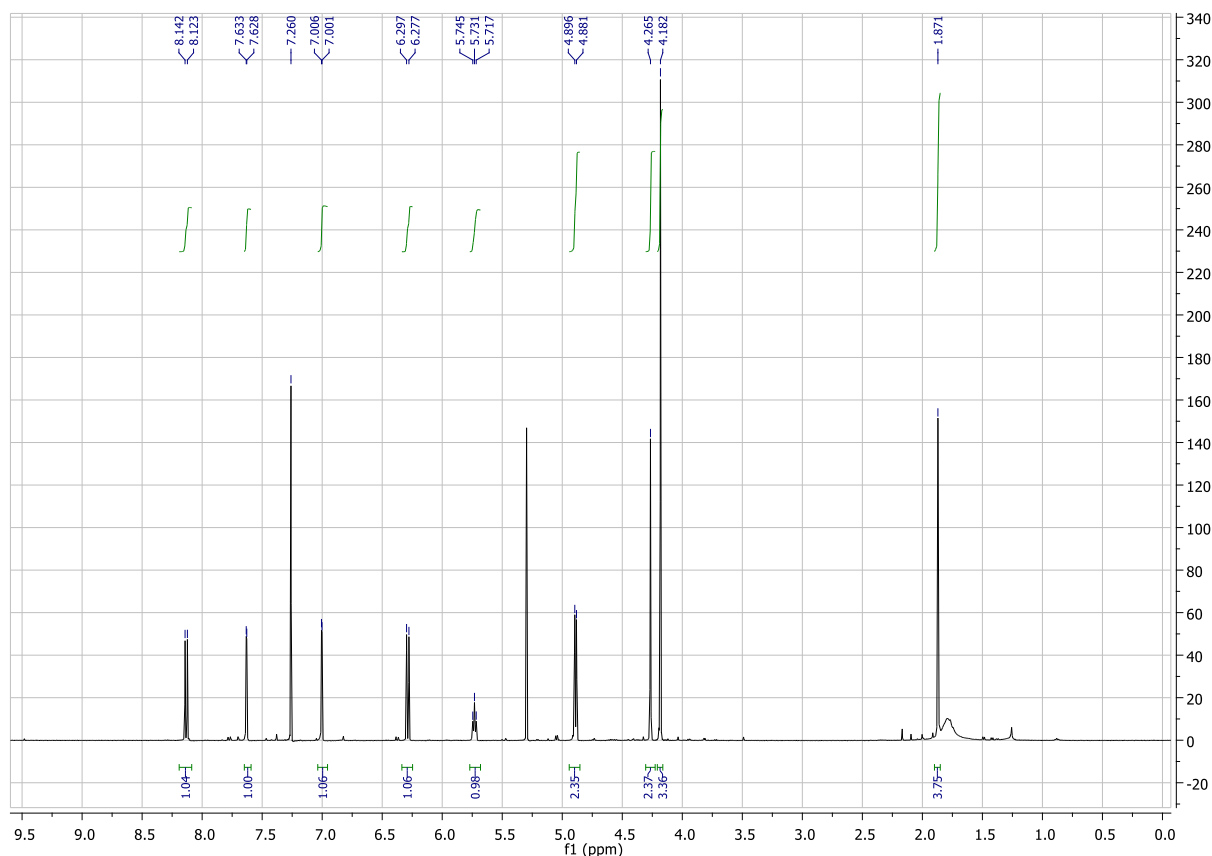


Figure 28. ¹H NMR Spectrum of compound **5** measured in CDCl₃, 500 MHz

As for *E*-trichoclin, the geometry of 5-methoxy-trichoclin double bond was determined by ROESY experiments. In the ROESY spectrum the cross peak between the olefinic proton at δ 5.73 (1H, t, $J = 7$ Hz) and the methylene protons at δ 4.89 (2H, d, $J = 7.5$ Hz), but not the methyl group at δ 1.87 (3H, s) could be observed (Figure 29). Therefore, compound **5** has been identified as *E*-5-methoxy-trichoclin (Figure 30):

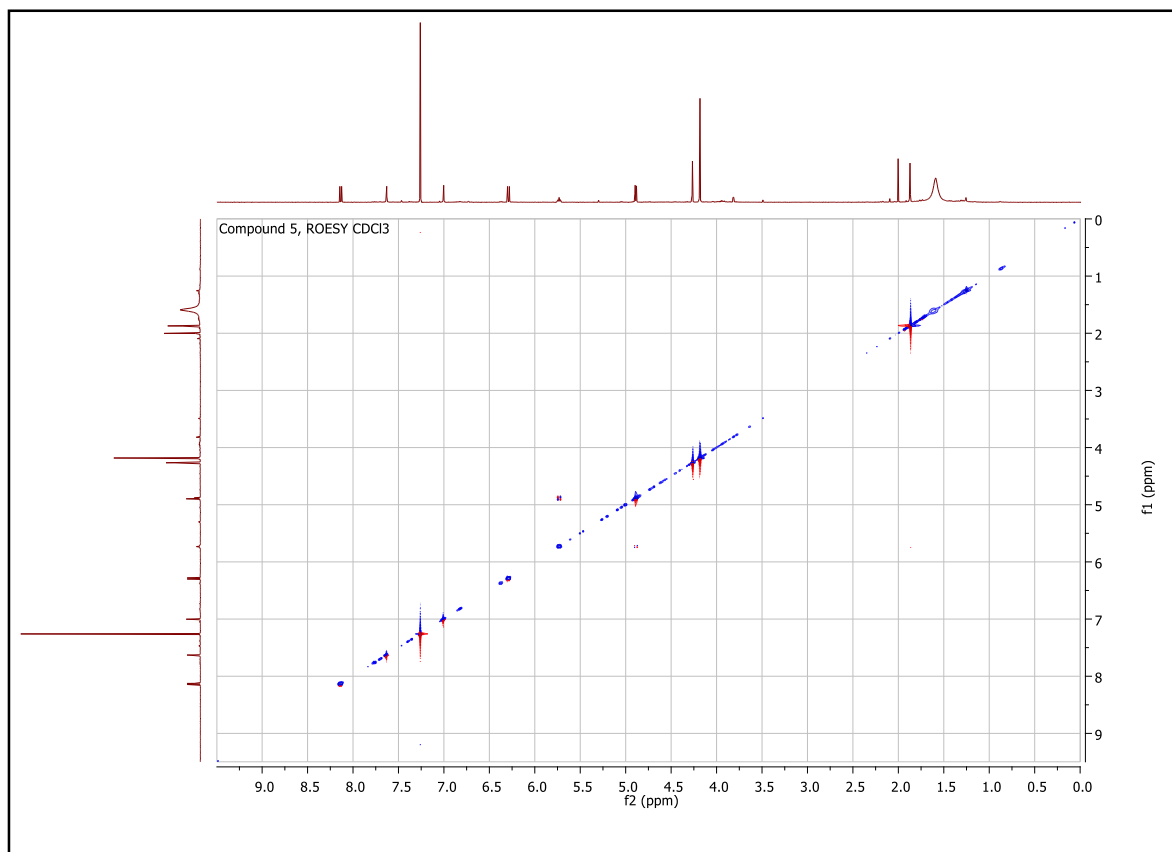


Figure 29. ROESY spectrum of compound **5**

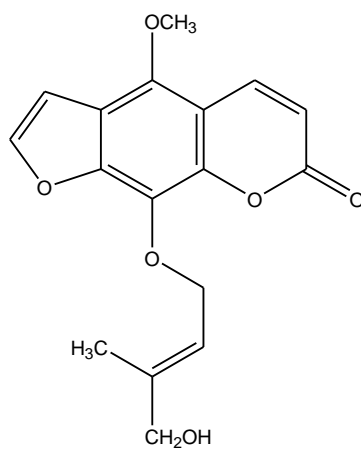


Figure 30. Structure of compound **5**

Compounds 1-3, 6-10 and 12-15

The structures of bergapten (**1**), xanthotoxin (**2**), isopimpinellin (**3**), imperatorin (**6**), phellopterin (**7**), heraclenin (**8**), (-)-heraclenol (**9**), osthol (**12**), meranzin (**13**), 2'-acetoxy-3'-hydroxy-osthol (**14**) and umbelliprenin (**15**) were deduced from the 1D and 2D NMR spectra and confirmed by comparison of ^1H - and ^{13}C NMR data with those reported in the literature.^{7,92,93-98} (See experimental part).

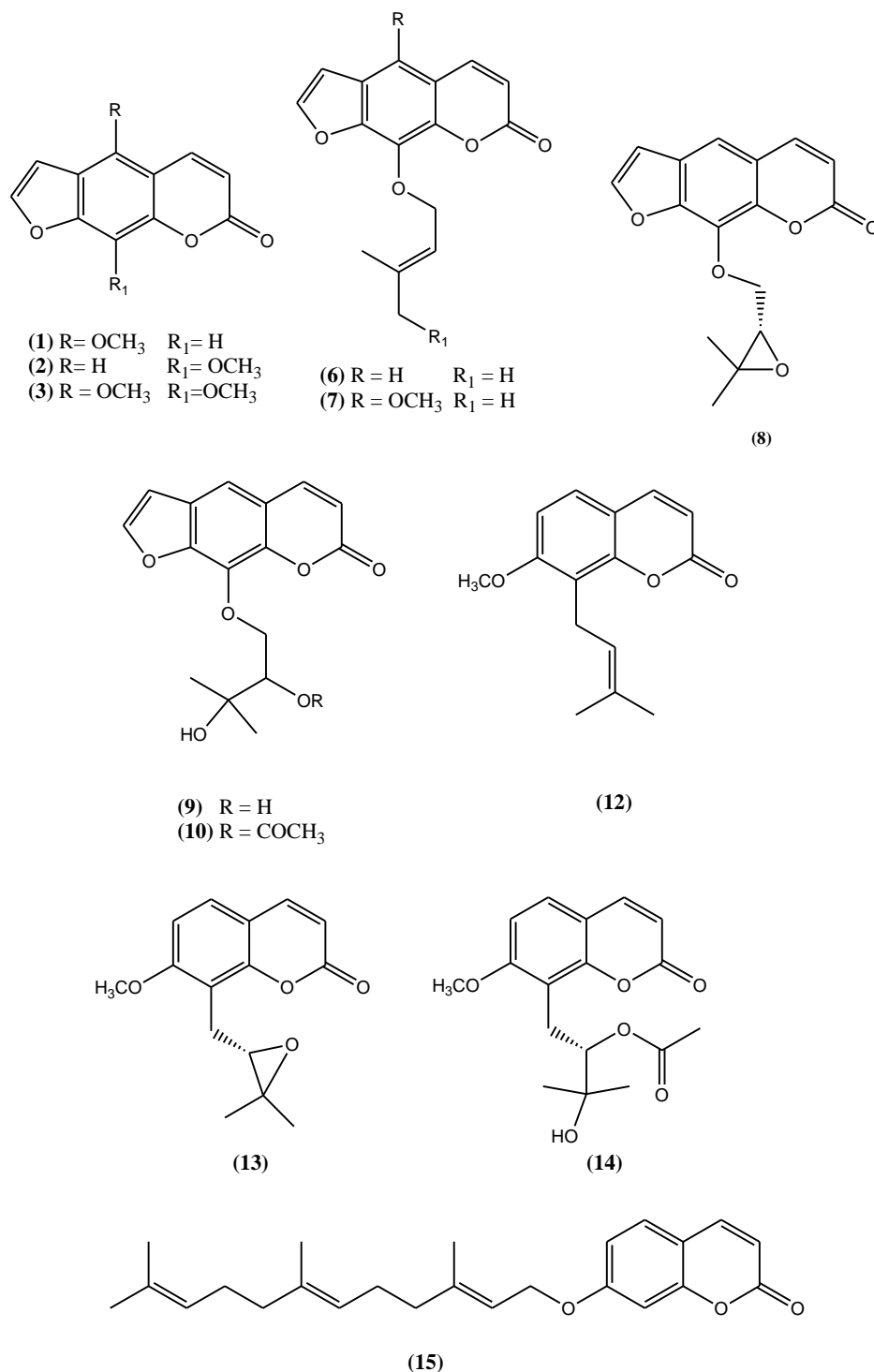


Figure 31. Structures of the known compounds isolated from the two extracts of *M. pastinacea*

4.5.3 Inhibitory effects of compounds 1-15 toward human carbonic anhydrase

The petroleum ether and ethyl acetate extracts together with all the isolated coumarins were tested against four hCA isoenzymes (I, II, IX and XII) (Table 2). The results showed that both extracts were selective towards the tumor-associated CA IX and CA XII since none was active against CA I and CA II up the concentration of 100 ng/ml, whereas they were highly potent especially against CA XII. The ethyl acetate extract was more potent respect to the ether extract either against CA IX ($K_i = 1.74$ ng/ml) either against CA XII ($K_i = 0.5$ ng/ml).

The furocoumarins **1-9**, **11** and coumarins **12**, **15** inhibited both hCA IX and hCA XII in a nanomolar range and they were completely inactive (K_i values > 10.000 nM) against hCA I and II, thus showing high selectivity over these isoforms that are considered responsible of side-effects of CAIs. Interestingly, meranzin (**13**) and especially the furocoumarin **10**, inhibited exclusively the IX isoform of CA with K_i ratios XII/IX > 5 and > 52 , respectively. On the contrary, compound **14** was a selective inhibitor of the XII isoform with a K_i ratio IX/XII > 34 .

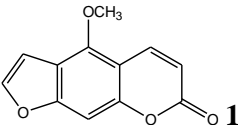
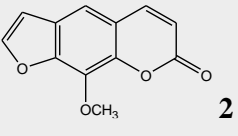
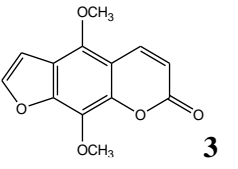
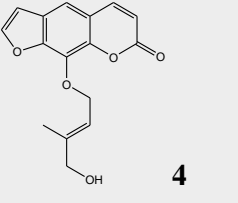
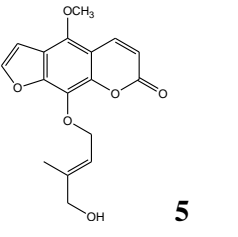
The most potent compound was umbelliprenin (**15**), with a K_i value against CA XII of 5.8 nM, comparable to that of acetazolamide (AAZ) and demonstrated high selectivity over the off-target CA I/II isoforms (K_i ratios I/XII > 1724). Also *S*-heraclenol (**9**) ($K_i = 27.5$ nM), osthol (**12**) ($K_i = 75$ nM) and the furocoumarin **5** ($K_i = 63.5$ nM) revealed a strong inhibitory effect toward CA IX (heraclenol) and CA XII (osthol and *E*-5-methoxy-trichoclin).

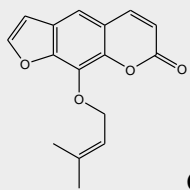
The SAR study pointed out that, in the 8-*O*-monosubstituted furocoumarins (**2**, **4**, **6**, **8-10**), the 2,3-dihydroxy-3-methylbutyl moiety present in *S*-heraclenol (**9**), elicited the better inhibitory profile towards hCA IX ($K_i = 27.5$ nM). (+)-*S*-heraclenol acetate (**10**) compared to *S*-heraclenol, showed a reduction of inhibitory effects toward hCA IX and hCA XII and most interestingly, a high selectivity towards the poorly expressed in healthy tissues hCA IX over hCAXII with a selectivity index > 52 . Among furocoumarins **2**, **4**, **6**, **8-10**, we found that, in compounds **2**, **4**, **6**, the introduction of a methoxy group at C-5, giving compounds **3**, **5**, **7**, furnished enhanced inhibitory activity against hCA IX and hCA XII. In particular, when the methoxy derivative **5** was compared with *E*-tricholin (**4**), a 23-fold gain in potency toward the isoform CAXII was observed.

As regards 7-methoxy-8-alkyl coumarins (**12-14**), osthol (**12**) was the most potent of the hCAXII inhibitors ($K_i = 75$ nM), highlighting the importance of a prenyl chain at C-8.

The new angular dihydrofurocoumarin, magydarin (**11**), had submicromolar inhibition of the validated cancer-associated isozymes hCA IX and XII with K_i s of 150.9 and 623 nM, respectively.

Table 2. Effect of the isolated compounds against hCA I, II, IX and XII

Extract/Compound	K_i (nM)*			
	hCA I	hCAII	hCA IX	hCA XII
Petroleum ether	>100 ^a	>100 ^a	20 ^a	0.8 ^a
Ethyl acetate	>100 ^a	>100 ^a	1.74 ^a	0.5 ^a
 1	>10000	>10000	1953	855.1
 2	>10000	>10000	194.8	876.3
 3	>10000	>10000	159.8	590.1
 4	>10000	>10000	2339	550.0
 5	>10000	>10000	1501	63.5

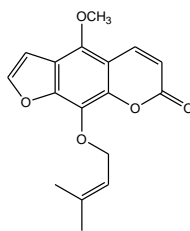


>10000

>10000

221.4

832.9

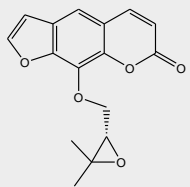


>10000

>10000

201.9

786.9

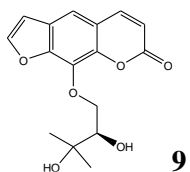


>10000

>10000

162.5

835.6

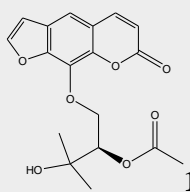


>10000

>10000

27.5

813.8

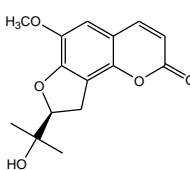


>10000

>10000

192.5

>10000

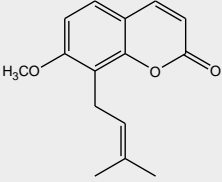
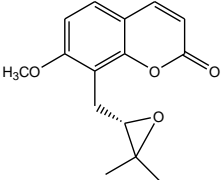
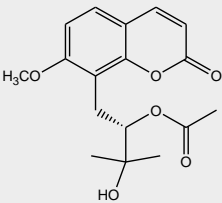
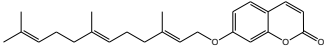


>10000

>10000

150.9

623.0

 12	>10000	>10000	2471	74.5
 13	>10000	>10000	1888	>10000
 14	>10000	>10000	>10000	290.9
 15	>10000	>10000	266.4	5.8
AAZ	250.0	12.1	25.8	5.7

^aData expressed in ng/ml

* Mean from 3 different assays, by a stopped flow technique (errors were in the range of \pm 5-10 % of the reported values).

4.5.4 In silico modelling of the interaction of compounds **9**, **11**, **15** with CAs

Compounds **9**, **11** and **15** are characterized by an interesting activity toward the CA-XII isoform, therefore, their mechanism of action was investigated in more detail by means of computational methods. The protocol consisted in docking experiments followed by energy minimization of obtained complexes.

In particular, recently an interesting CA inhibition mechanism was reported for coumarin derivatives.^{61,77} This was also found as plausible mechanism of action of previous synthesized compounds.⁹⁹

Hence, the coumarin derivatives **15**, **11** and **9** were docked to understand if coumarin moiety could be hydrolyzed by the Zn²⁺ activated water molecule of the enzyme cavity, which acts as a very potent nucleophile.

These experiments showed that only compound **15** was able to dock the coumarin portion close enough to the Zn²⁺ (Figure 32a). Therefore, only this compound could be hydrolyzed. Instead, the compounds **11** and **9** binding did not show the right orientation, probably because of steric hindrance of furocoumarin moiety (Figure 32b, 32c).

Then, the **15** open compound conformations (E/Z) were subjected to docking experiments in order to predict the binding mode of hydrolyzed forms.

It is possible to see in figure 33 as both conformations diastereoisomers are stabilized by several hydrogen bonds and π - π interactions in the catalytic site. The hydrophobic portion fold up and is stabilized by internal contacts and interactions with hydrophobic residues in the cavity. The predicted affinity of open compounds was estimated to be better than the closed one.

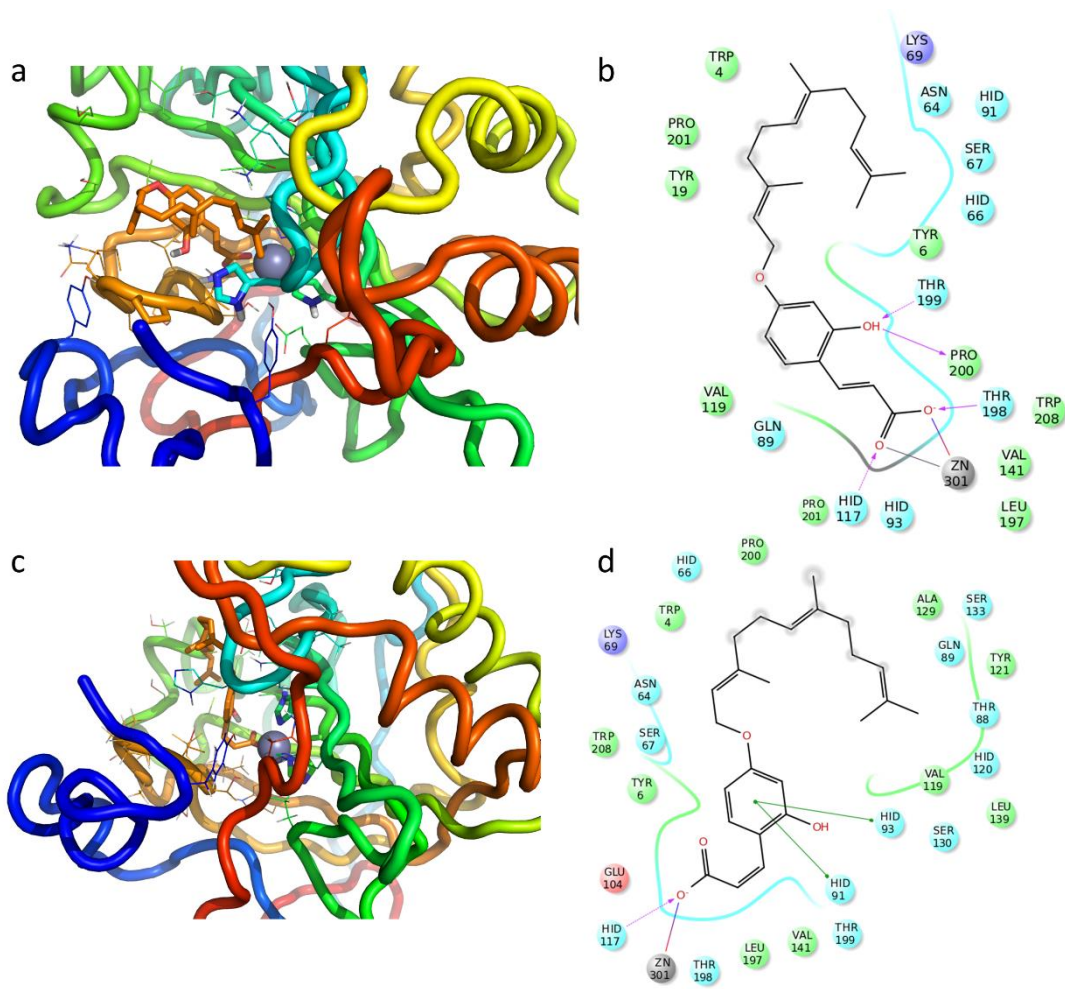


Figure 33. 3D representation of the putative binding mode obtained by docking experiments. a) CA -XII-15-openE c) CA -XII-15-openZ and the relative 2D representation of the complexes stabilizing interactions with the binding site residues.

4.5.5 Cytotoxicity of compounds 1-15 toward cancer cells

On basis of the CA inhibition results, the growth inhibitory effect of the most the most active/interesting coumarins (**5**, **9**, **10**, **12**, **15**) against HeLa tumor cell line have been carried out (Table 3). Umbelliprenin showed moderate cytotoxicity against HeLa cells ($IC_{50}=75\mu M$) and this result is in accord with other studies reporting low cytotoxicity of the compound toward the breast cancer cell lines MCF and 4T1.^{100,101} However, umbelliprenin was effective to inhibit tumor growth, angiogenesis and metastasis in mammary-tumor-bearing mice when intraperitoneally administrated.¹⁰² This date were confirmed by Zhang *et al.*¹⁰³, which provided evidence that umbelliprenin may inhibit the growth, invasion and migration of gastric cancer cells by targeting the Wnt signaling pathway, with little to no harm in the lung, heart and kidney.

The low cytotoxicity of umbelliprenin may be related to its very high liposolubility. This hypothesis was confirmed by the fact that when umbelliprenin was encapsulated in nanoliposomes its antiproliferative effect against 4T1 cells increased by 5 folds.¹⁰⁰ Also osthol (**12**) showed only a moderate cytotoxicity with an IC_{50} of 98 μM but, as reported in previous works,^{104, 105} its cytotoxicity greatly depends on the cancer cell line.

Most importantly, CA IX and CA XII are overexpressed in cancer cells under hypoxic condition. Thus, the moderate antiproliferative action showed by the isolated compounds is not surprising since the assay has been carried out under normoxic conditions.

Table 3. Cytotoxic effect of compounds **5**, **9-12** and **15** evaluated toward cancer HeLa cells

Compound	IC_{50}^a (μM)
5	>100
9	>100
11	>100
10	>100
12	98
15	75

^aConcentration of compound that reduces the cell viability to 50% measured at 48h.

4.5.6 Conclusion

Fifteen coumarins were isolated from the seeds of *M. pastinacea*. Magydarin (**11**) is new to the literature, while meranzine (**13**), xanthotoxin (**2**), *E*-trichoclin (**4**), *E*-5-methoxy-trichoclin (**5**), fellopterin (**7**), (+)-*S*-heraclenol acetate (**10**) and meranzine acetate hydrate (**14**) were isolated for the first time from this plant. None of the fifteen isolated coumarins have ever been evaluated for its inhibitory activity on carbonic anhydrases. All isolated compounds were inactive towards the ubiquitous cytosolic isoform hCA I and II ($K_i > 10000$ nM) that are considered responsible for the side-effects of CAIs. On the contrary, they were significantly active against the tumor-associated isoforms hCA IX and XII. CA XII was inhibited with single-digit K_i by umbelliprenin (**15**) (5.7 nM) and with K_i s spanning in the nanomolar range (63.5-74.5 nM) by compounds **5** and **12**. As regards the other tumor-associated isoform hCA IX, it was potently inhibited by *S*-heraclenol (**9**) ($K_i = 27.5$ nM) and, to a lesser extent, by the new furocoumarin magydarin (**11**). Particularly noteworthy is the selectivity of heraclenol acetate (**10**) towards hCA IX over hCAI, hCAII and hCAXII (SI>52). As far as we know, umbelliprenin is the most potent natural coumarin CA inhibitor.

Molecular docking experiments suggested that the most potent coumarin **15** could be hydrolyzed in the enzyme catalytic pocket. Furthermore, docking experiments estimated that the predicted affinity of open compounds was better than that of the closed ones. Overall the computational methods helped to rationalize the strong activity of compound **15** toward the CA-XII isoform and to suggest a plausible mechanism of action that would be further investigated to confirm it.

Future work on these compounds will attempt to synthesize analogues with lower lipophilicity to achieve a better drug-like profile.

4.6 EXPERIMENTAL PART

4.6.1 Materials and Methods

4.6.1.1 General procedures

Optical rotations were measured in CHCl_3 or MeOH at 25 °C using a Perkin-Elmer 241 polarimeter. Circular dichroism spectra were recorded on a JASCO J-810 spectropolarimeter equipped with a Peltier temperature controller using a 10 mm path-length cell. All measurements were performed in methanol at compound concentration of 300 μM . Each reported spectrum represents the average of 3 scans recorded with 1-nm step resolution. Observed ECD signals were converted to molar ellipticity $[\Theta] = \text{deg} \times \text{cm}^2 \times \text{dmol}^{-1}$. UV spectra were recorded on a GBC Cintra 5 spectrophotometer. NMR spectra of all isolated compounds were recorded at 25 °C on Unity Inova 500NB high-resolution spectrometer (Agilent Technologies, CA, USA) operating at 500 MHz for ^1H and 100 MHz for ^{13}C , respectively. Spectra were measured in CDCl_3 and CD_3OD and referenced against residual non-deuterated solvents. HRESIMS were measured on an Agilent 6520 Time of Flight (TOF) MS instrument. Column chromatography was carried out under TLC monitoring using silica gel (40-63 μm , Merck), and Sephadex LH-20 (25-100 μm , Pharmacia). For vacuum-liquid chromatography (VLC), silica gel (40-63 μm) (Merck) was used. TLC was performed on silica gel 60 F₂₅₄ or RP-18 F₂₅₄ (Merck). LiChrolut RP-18 (40–63 μm) 500 mg, 3 mL (Merck) solid phase extraction (SPE) cartridges were also used. Semi-preparative HPLC was conducted by means of a Varian 920 LH instrument fitted with an autosampler module with a 1000 μL loop. The peak purities were monitored using a dual-wavelength UV detector settled at 254 and 360 nm. The columns were a 250 x 10 mm Spherisorb silica, particle size 5 μm (Waters) and a 300 x 7.5 mm Polymeric Reversed Phase (PLRP-S 100 Å), particle size 8 μm (Varian).

4.6.1.3 Plant material

The seeds of *M. pastinacea* were collected in July 2017 at Siniscola (Nuoro), Sardinia, Italy. The plant material was identified by Prof. Marco Leonti (University of Cagliari, Department of Biomedical Sciences). A voucher specimen (No. 0485) was deposited in the Herbarium of the Department of Life and Environmental Science, Drug Sciences Section, University of Cagliari.

4.6.1.3 Petroleum ether extract

Air-dried and powdered seeds of *M. pastinacea* (720 g) were ground and extracted with petroleum ether (3.5 L) by percolation at room temperature to give 77.6 g dried extract. The remaining plant material was then extracted with EtOAc (3 L), giving 42 g dried extract.

An aliquot (20 g) of the petroleum ether extract was subjected to Vacuum Liquid Chromatography (VLC) (silica gel, 90 g, 40-63 μm) using a step gradient of *n*-hexane/ethyl acetate (9 : 1 to 0 : 10, 500 mL each) to yield 24 fractions. Based on the TLC similarities, identical fractions were combined to give a total of eight fractions (F1-F8). Fraction F3 (0.98 g) was separated by column chromatography (CC) over silica gel using toluene/ CH_2Cl_2 (7 : 3) as eluent to isolate compound **15** (96 mg). Fraction F4 (1.55 g) was chromatographed by CC over silica gel using hexane-EtOAc (1 : 9) as eluent giving compound **12** (330 mg). Fraction F7 (1.04 g) was purified by CC over silica gel, using CH_2Cl_2 -EtOAc (9.5 : 0.5) as eluent to give eight subfractions (F7.1 - F7.8). F7.2 (11 mg) was subjected to chromatography by Sephadex LH (MeOH) yielding compound **1** (3 mg). Subfraction F7.3 (110 mg) was further subjected to CC over silica gel using CH_2Cl_2 as eluent to give compound **2** (2.5 mg) and a white solid (90 mg). The obtained solid was purified further by PLRP HPLC using acetonitrile : H_2O (6 : 4, flow 2.5 mL/min) as eluent to give compound **2** (1.5 mg, t_R 11.2 min) and compound **3** (1.2 mg, t_R 13 min). Subfractions F7.6 and F7.8 were purified by Sephadex LH-20 (MeOH) yielding compounds **8** (38.9 mg) and **13** (170 mg), respectively. Fraction F8 (800 mg), after purification by CC over Sephadex LH-20 (MeOH), furnished compound **13** (670 mg).

4.6.1.4 Ethyl acetate extract

An aliquot (16.6 g) of the EtOAc extract was subjected to Vacuum Liquid Chromatography (VLC) (silica gel, 80 g, 40-63 μm) using a step gradient of *n*-hexane/ethyl acetate/MeOH (9 : 0 : 0 to 0 : 1 : 9, 500 mL each) to yield 38 fractions. Based on the TLC similarities, identical fractions were combined to give a total of ten fractions (F1-F10). An aliquot (0.5 g) of F3 (3.74 g) was chromatographed over silica gel using CH_2Cl_2 as eluent, giving compound **6** (61.2 mg) and compound **7** (4.7 mg). An aliquot (50 mg) of F4 (1.56 g) was purified and an impure compound (12 mg) that was purified by PLRP HPLC using acetonitrile : H_2O (7 : 3, flow 2 mL/min) as eluent to give compound **2** (3.9 mg, t_R 8.5 min) and compound **1** (2.1 mg, t_R 14.2 min). Fraction F6 (0.18 g) was subjected to CC over silica gel using CH_2Cl_2 : EtOAc (7.5 : 2.5) as eluent, giving eight subfractions (F6.1 – F6.8). Fraction F6.3 (41 mg) was further chromatographed by PLRP HPLC, using acetonitrile : H_2O (5 : 5, flow of 2 mL/min) as eluent, to give compounds **4** (1 mg, t_R 13.2 min) and **5** (1.3 mg, t_R

15.2 min). Fraction F6.5 (6.5 mg) was separated by PLRP HPLC, using acetonitrile : H₂O (5 : 5, flow of 2 mL/min) as eluent, to give compounds **10** (0.9 mg, t_R 8.5 min) and **11** (2.8 mg, t_R 7.5 min). An aliquot (40 mg) of F7 (70 mg) was chromatographed on CC over Sephadex LH-20 (MeOH) to furnish an impure compound (16 mg) that was further purified by PLRP HPLC using acetonitrile : H₂O (5:5, flow 2 ml/min) as eluent, to give compound **11** (1.3 mg, t_R 11.0 min), compound **10** (1 mg, t_R 13 min), compound **4** (1.2 mg, , t_R 14.5 min) and compound **5** (3.6 mg, , t_R 15.5 min). Fraction F8 (165 mg) was subjected to CC over Sephadex LH (MeOH), yielding four subfraction (F8.1 – F8.4). Subfraction F8.2 (34.8 mg) was purified by CC over Sephadex LH-20, followed by PLRP HPLC using acetonitrile : H₂O (4 : 6, flow 2.0 ml/min) as eluent, to give compound **14** (3.8 mg, t_R 13.5 min). Subfraction F8.3 (42.2 mg) was purified by PLRP HPLC using acetonitrile : H₂O (4 : 6, flow 2.0 ml/min) as eluent, to give compound **9** (5.1 mg, t_R 9.5 min). Subfraction F8.4 (30 mg), was further subjected to CC over Sephadex LH-20 (MeOH) to yield compound **9** (2.7 mg).

4.6.1.5 Semi-Synthesis of (+)-heraclenol acetate (**10**)

To a solution of (-)-heraclenol (**9**) (38.9 mg, 0.13 mmol) in pyridine (2 mL) acetic anhydride (0.012 ml, 0.13 mmol) was added dropwise and left at room temperature for 48 h. The crude product was dried and purified by CC (Sephadex LH-20), using MeOH as eluent to provide 24.9 mg of (+)-heraclenol acetate (**10**).¹⁰⁶

4.6.2 Structural Elucidation of the known compounds

Compound 1

Compound **1** was identified as *bergapten* through the study of the spectra 1D (^1H and ^{13}C NMR), and 2D NMR (DQF-COSY, HSQC, HMBC) and for comparison with the data reported in the literature.⁹⁸

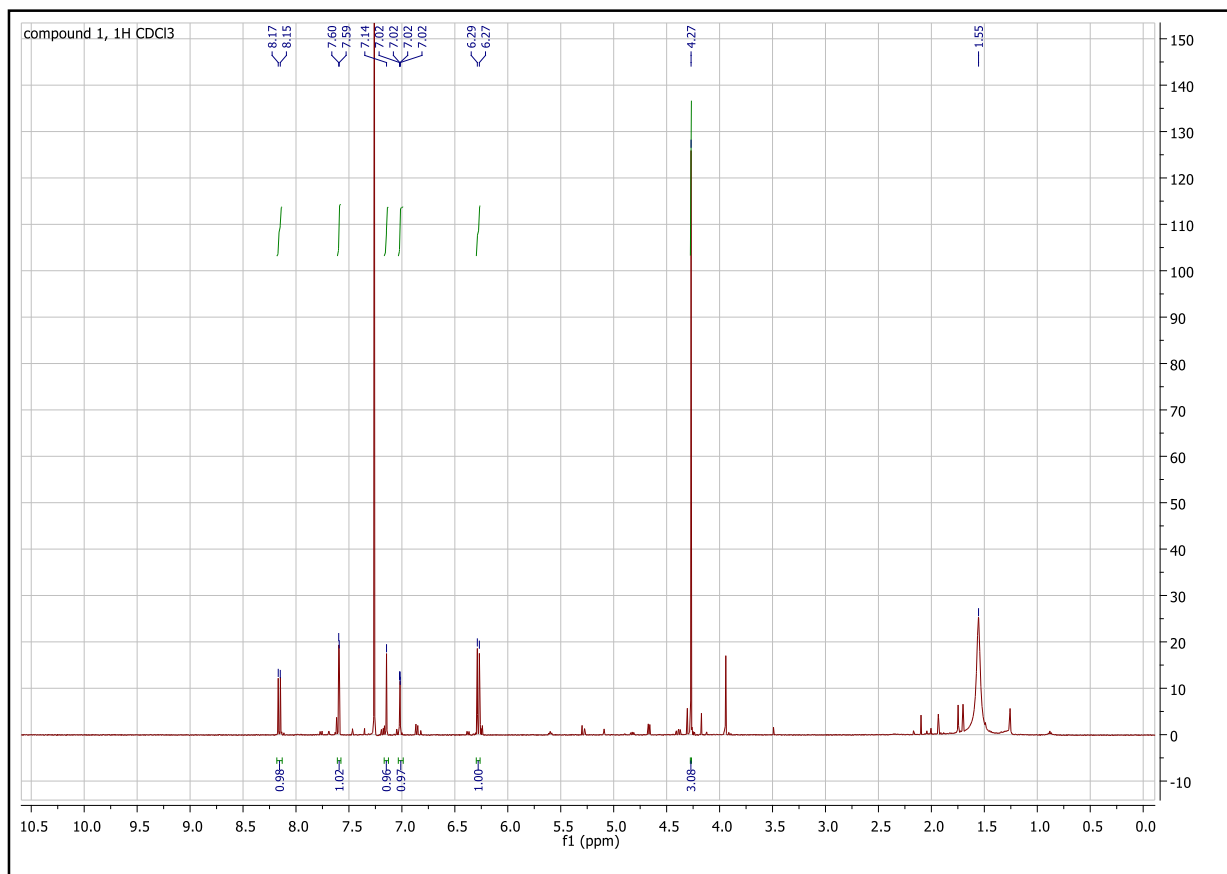


Figure 34. ^1H NMR Spectrum of compound **1** measured in CDCl_3 , 500 MHz

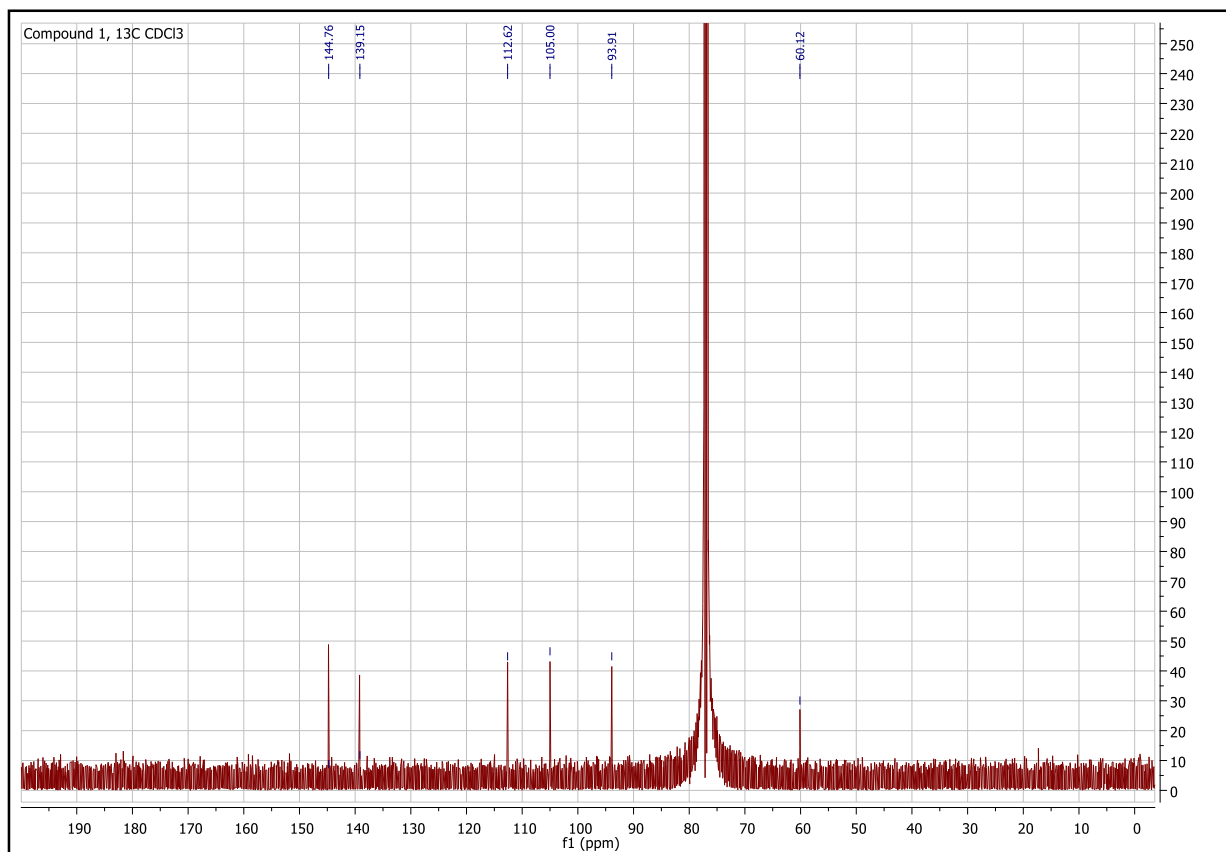


Figure 35. ^{13}C NMR Spectrum of compound **1** measured in CDCl_3 , 100 MHz

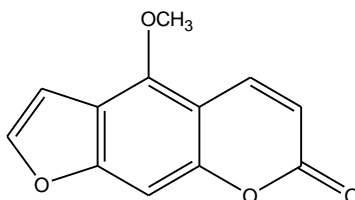


Figure 36. ^1H NMR (500 MHz, CDCl_3) δH 4.27 (s, 3H, OCH_3), 6.28 (d, 1H, $^3\text{J} = 9.5$, H-3), 7.02 (d, 1H, $^4\text{J} = 1.5$ H-3'), 7.14 (d, 1H, $^4\text{J} = 0.5$ H-8'), 7.59 (d, 1H, $^4\text{J} = 2.5$ H-2'), 8.16 (d, 1H, $^3\text{J} = 9.5$, H-4); ^{13}C NMR (100 MHz, CDCl_3) δC 60.12 (OCH_3), 93.91 (C-8), 105.00 (C-3'), 112.62 (C-6, C-3), 139.15 (C-4), 144.76 (C-2') ppm.

Compound 2

Compound 2 was identified as *xanthotoxin* through the study of the spectra 1D (^1H and ^{13}C NMR), and 2D NMR (DQF-COSY, HSQC, HMBC) and for comparison with the data reported in the literature.⁹⁸

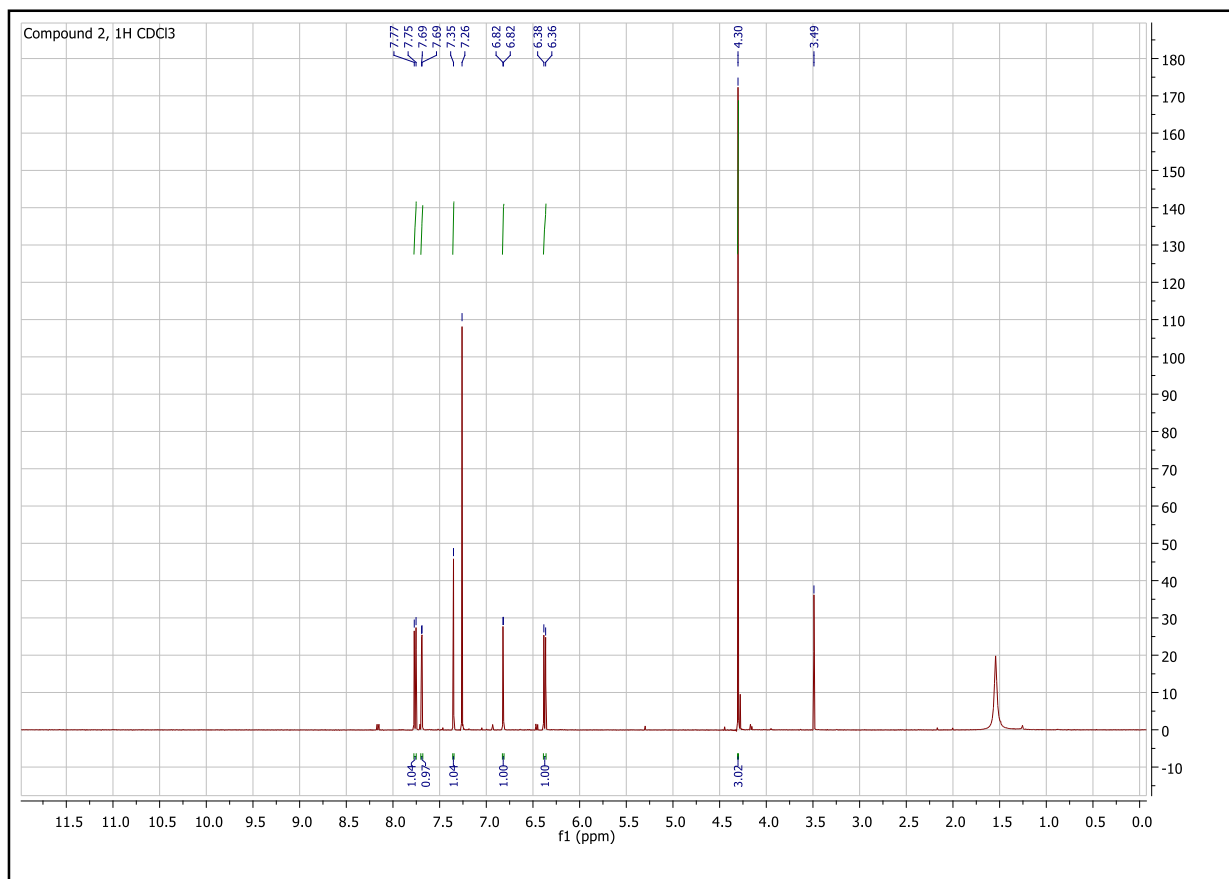


Figure 37. ^1H NMR Spectrum of compound 2 measured in CDCl_3 , 500 MHz

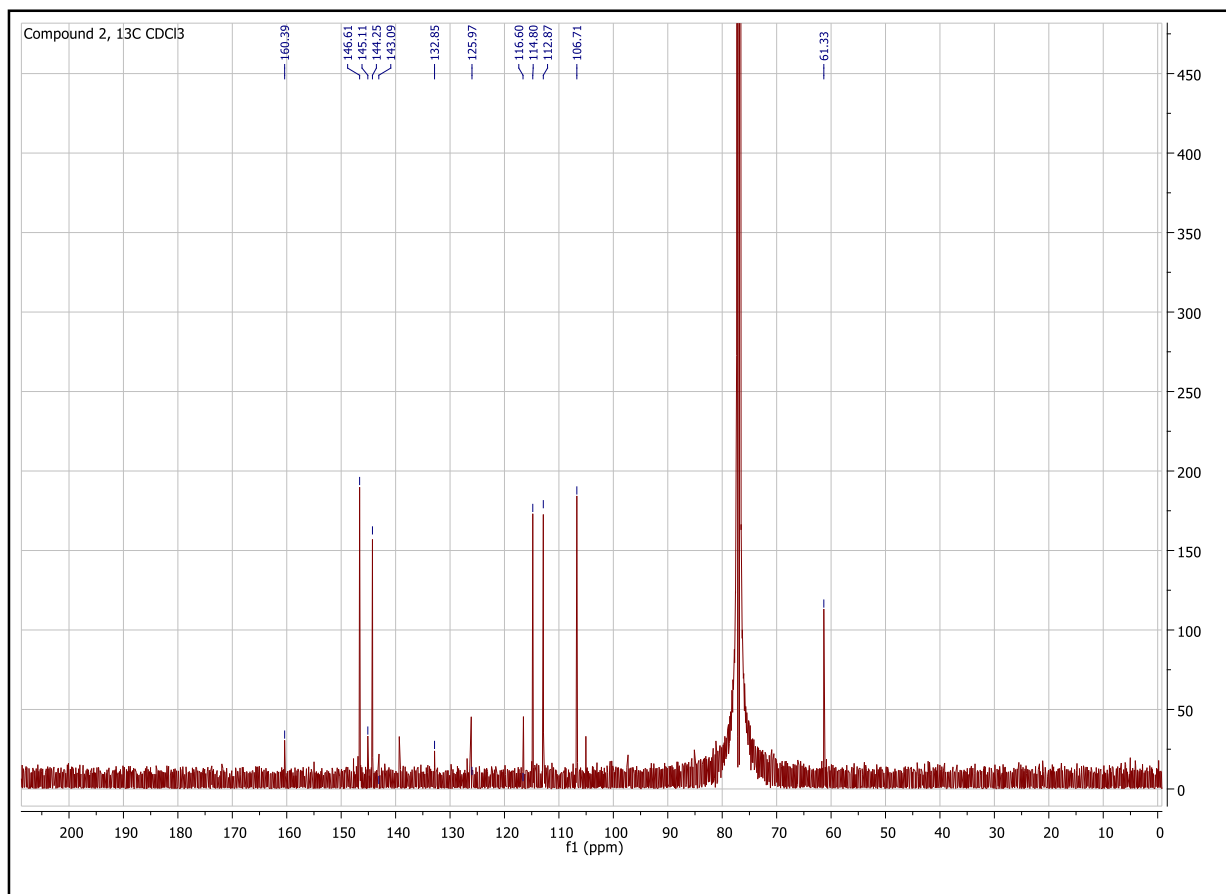


Figure 38. ^{13}C NMR Spectrum of compound **2** measured in CDCl_3 , 100 MHz

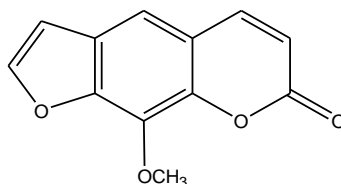


Figure 39. ^1H NMR (500 MHz, CDCl_3) δ_{H} 3.92 (d, 3H, $^4J = 0.5$, OCH_3), 6.37 (d, 1H, $^3J = 9.5$, H-3), 6.82 (s, 1H, H-3'), 7.35 (s, 1H, H-5), 7.69 (s, 1H, H-2'), 7.76 (d, 1H, $^3J = 9.5$, H-4); ^{13}C NMR (100 MHz, CDCl_3) δ_{C} 61.3 (OCH_3), 106.7 (C-3), 112.9 (C-5), 114.8 (C-3), 116.5 (C-4a), 126.1 (C-6), 132.9 (C-8), 143.09 (C-4), 144.3 (C-8a), 145.1 (C-2'), 146.6 (C-7), 160.4 (C-2) ppm.

Compound 3

Compound **3** has been identified as *isopimpinellin* through the study of the spectra 1D (^1H and ^{13}C NMR), and 2D NMR (DQF-COSY, HSQC, HMBC) and for comparison with the data reported in the literature.⁹⁸

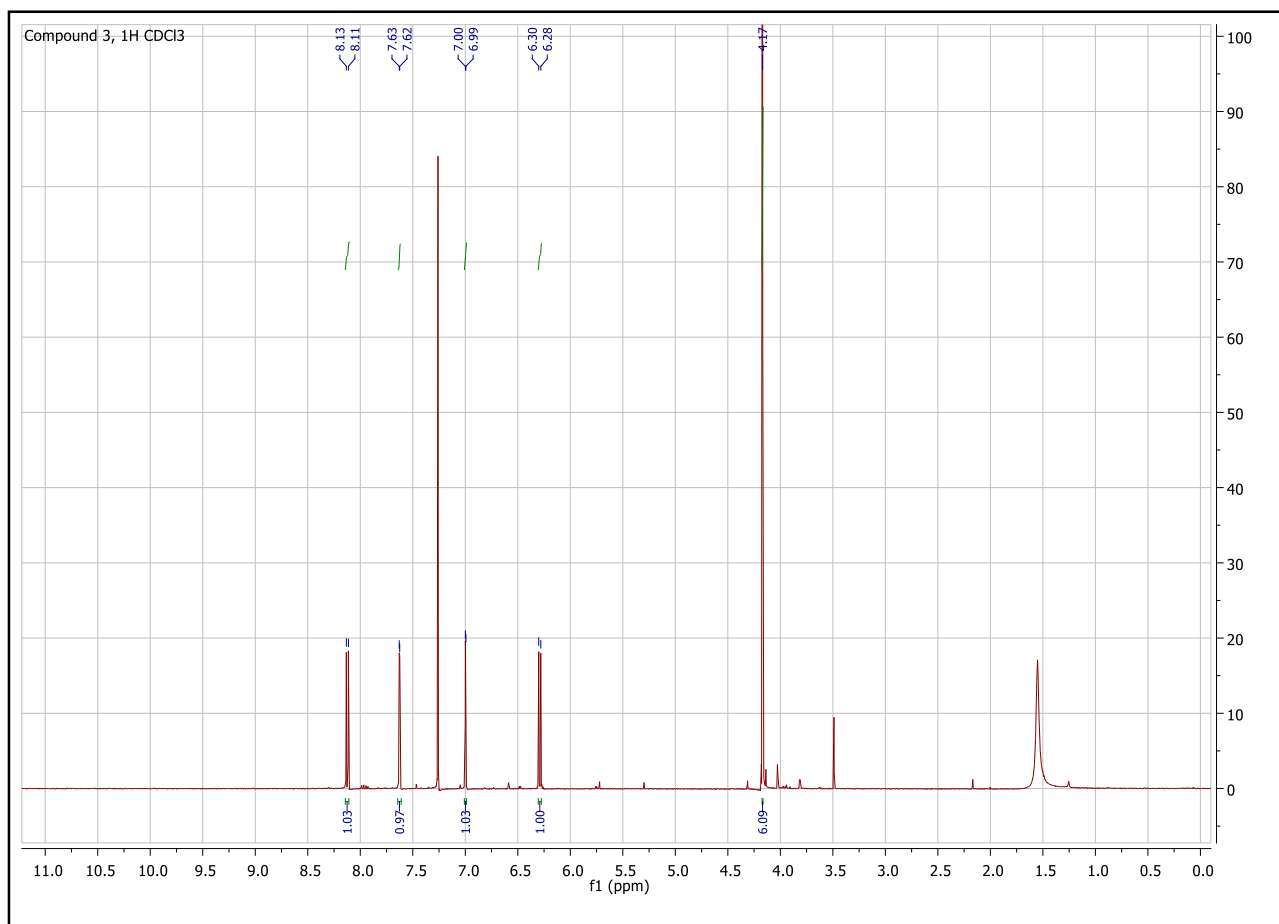


Figure 40. ^1H NMR Spectrum of compound **3** measured in CDCl_3 , 500 MHz

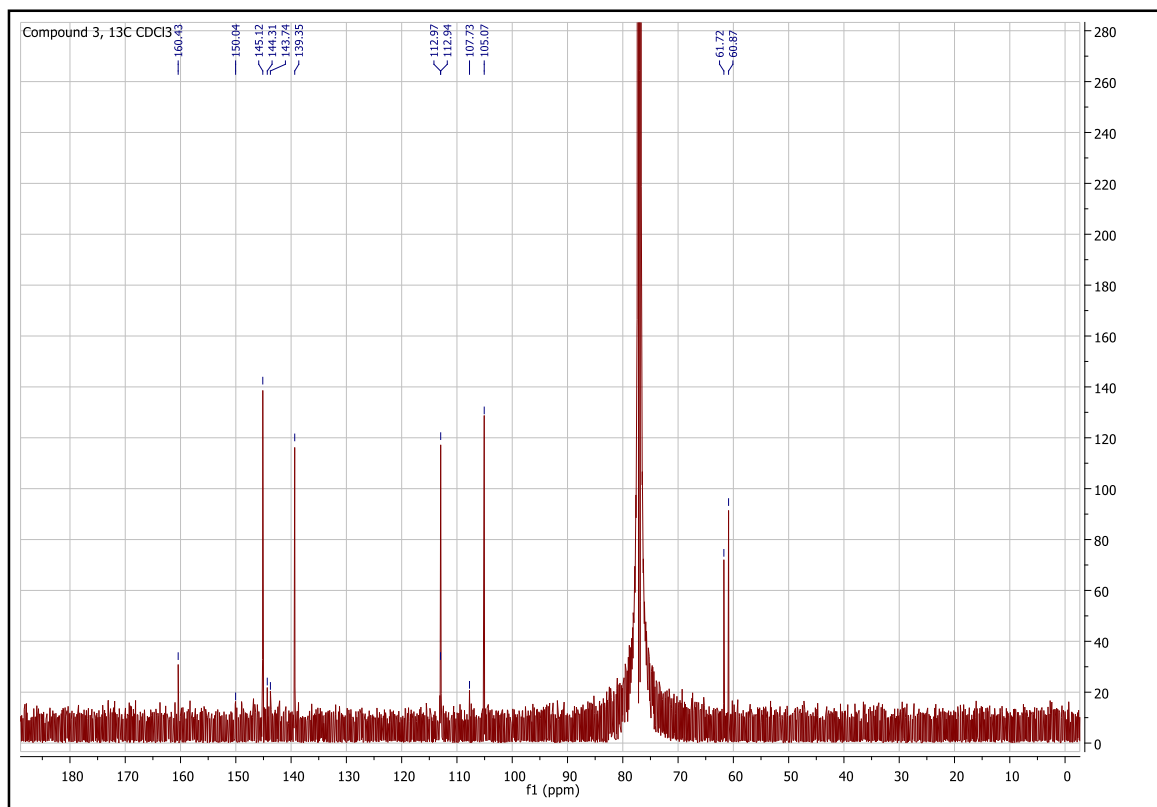


Figure 41. ^{13}C NMR Spectrum of compound **3** measured in CDCl_3 , 100 MHz

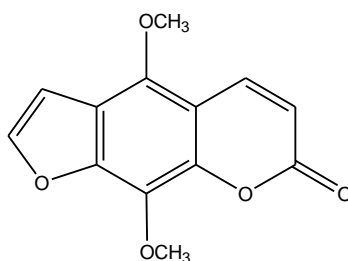


Figure 42. ^1H NMR (500 MHz, CDCl_3) δ_{H} 4.17 (s, 6H, OCH_3), 6.29 (d, 1H, $^3J = 10$, H-3), 6.99 (d, 1H, $^4J = 2$ H-3'), 7.63 (d, 1H, $^4J = 2.5$ H-2'), 8.12 (d, 1H, $^3J = 10$, H-4); ^{13}C NMR (100 MHz, CDCl_3) δ_{C} 60.87 (OCH_3), 61.72 (OCH_3), 105.07 (C-3'), 107.73 (C-4a), 112.94 (C-3), 112.97 (C-6), 139.35 (C-4, C-8), 143.74 (C-8a), 144.31 (C-5), 145.12 (C-2'), 150.04 (C-7), 160.43 (C-2) ppm.

Compound 4

Compound 4 has been identified as *E*-trichoclin (for the ^1H NMR and ROESY spectra see Results and Discussion)

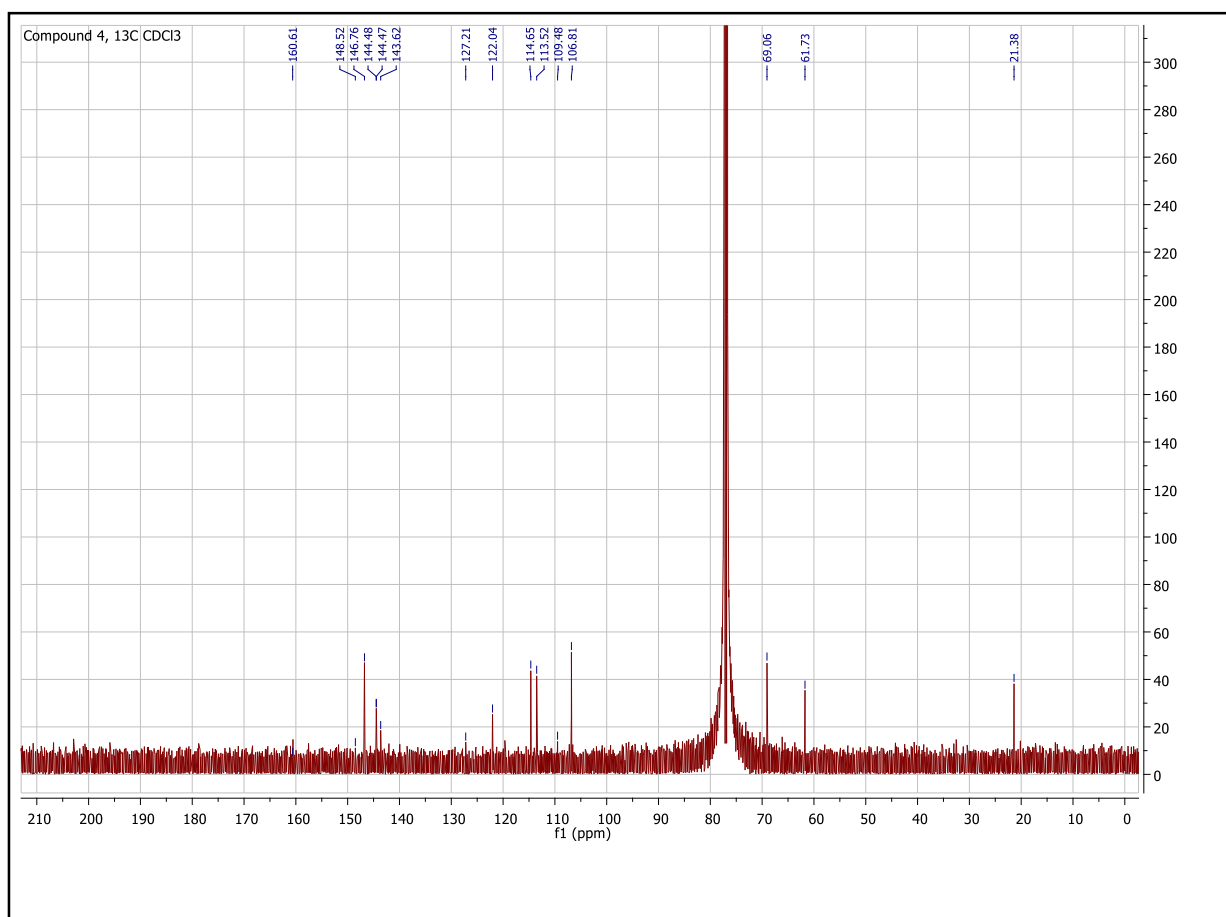


Figure 43. ^{13}C NMR Spectrum of compound 4 measured in CDCl_3 , 100 MHz

Compound 5

Compound 5 has been identified as 5-methoxy-trichoclin (for the ^1H NMR and ROESY spectra see Results and Discussion)

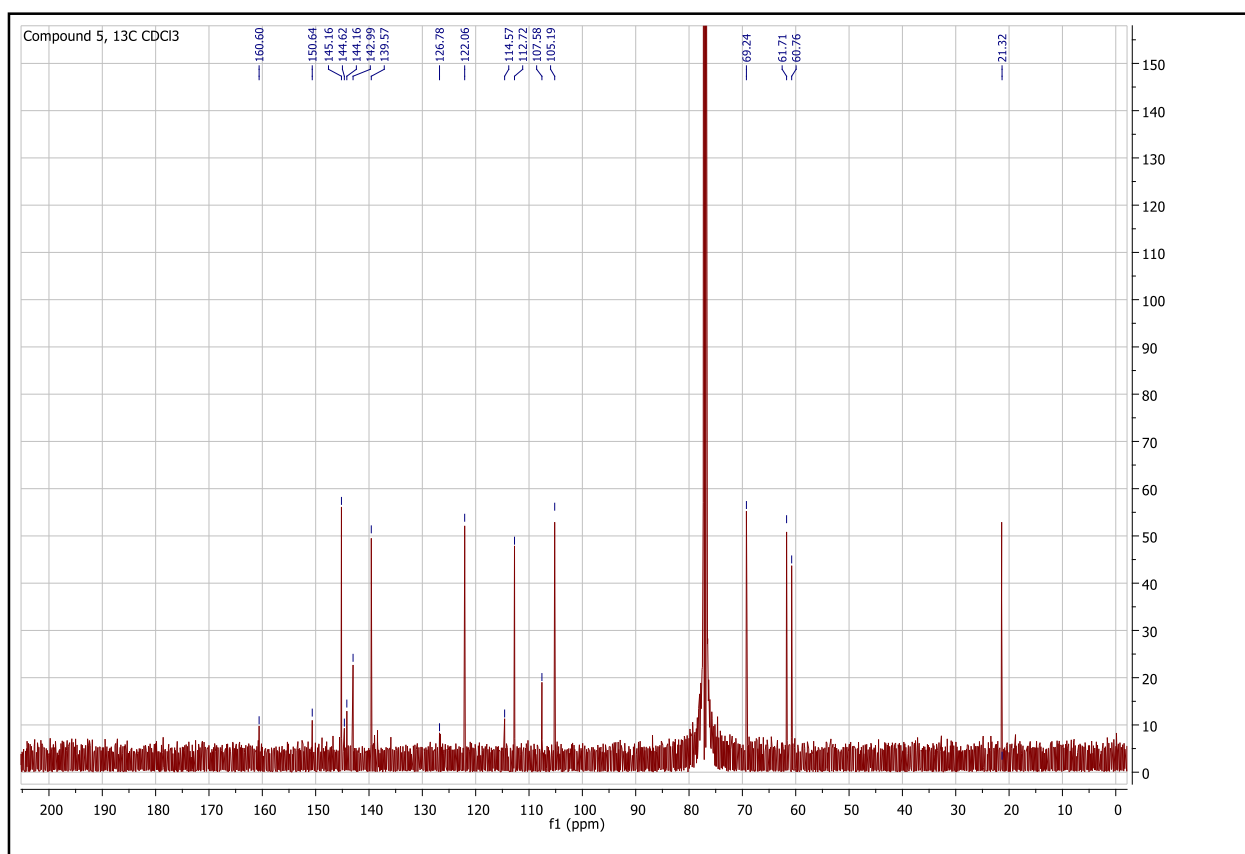


Figure 44. ^{13}C NMR Spectrum of compound 5 measured in CDCl_3 , 100 MHz

Compound 6

Compound **6** was identified as *imperatorin* through the study of the spectra 1D (^1H and ^{13}C NMR), and 2D NMR (DQF-COSY, HSQC, HMBC) and for comparison with data reported in the literature.⁹⁴

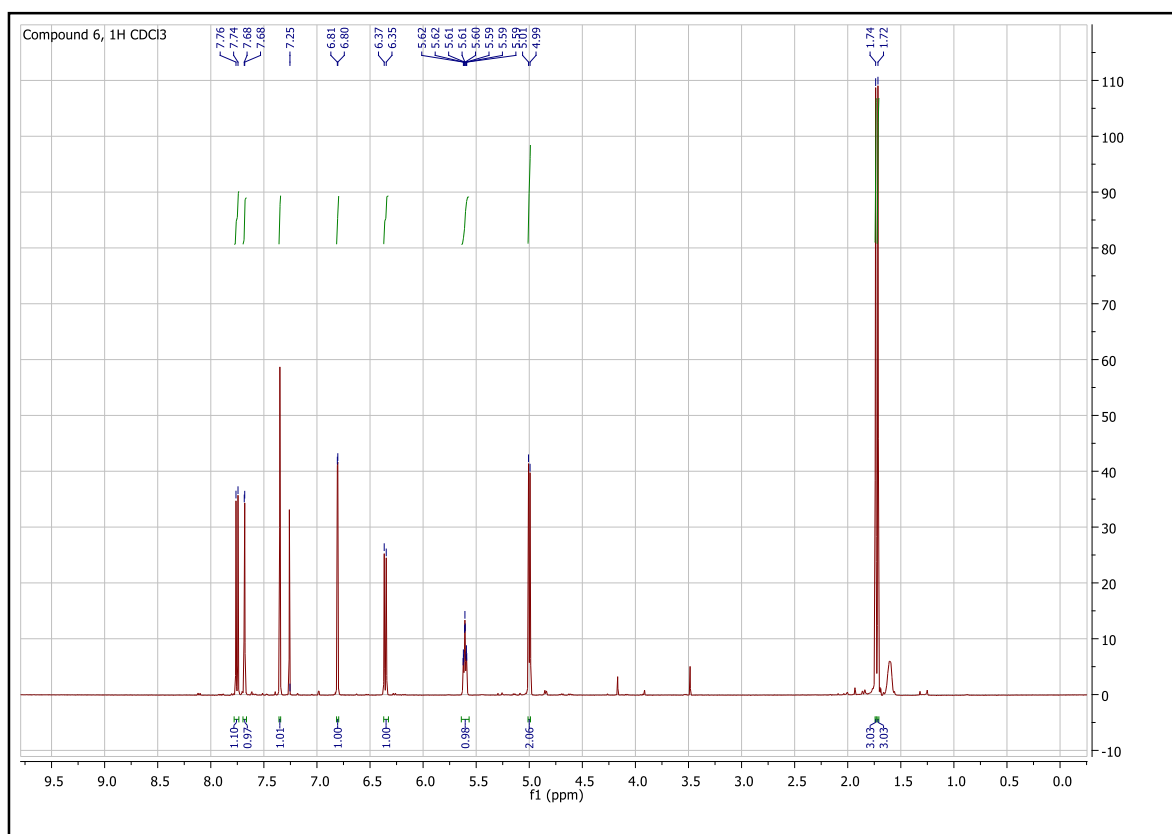


Figure 45. ^1H NMR Spectrum of compound **6** measured in CDCl_3 , 500 MHz

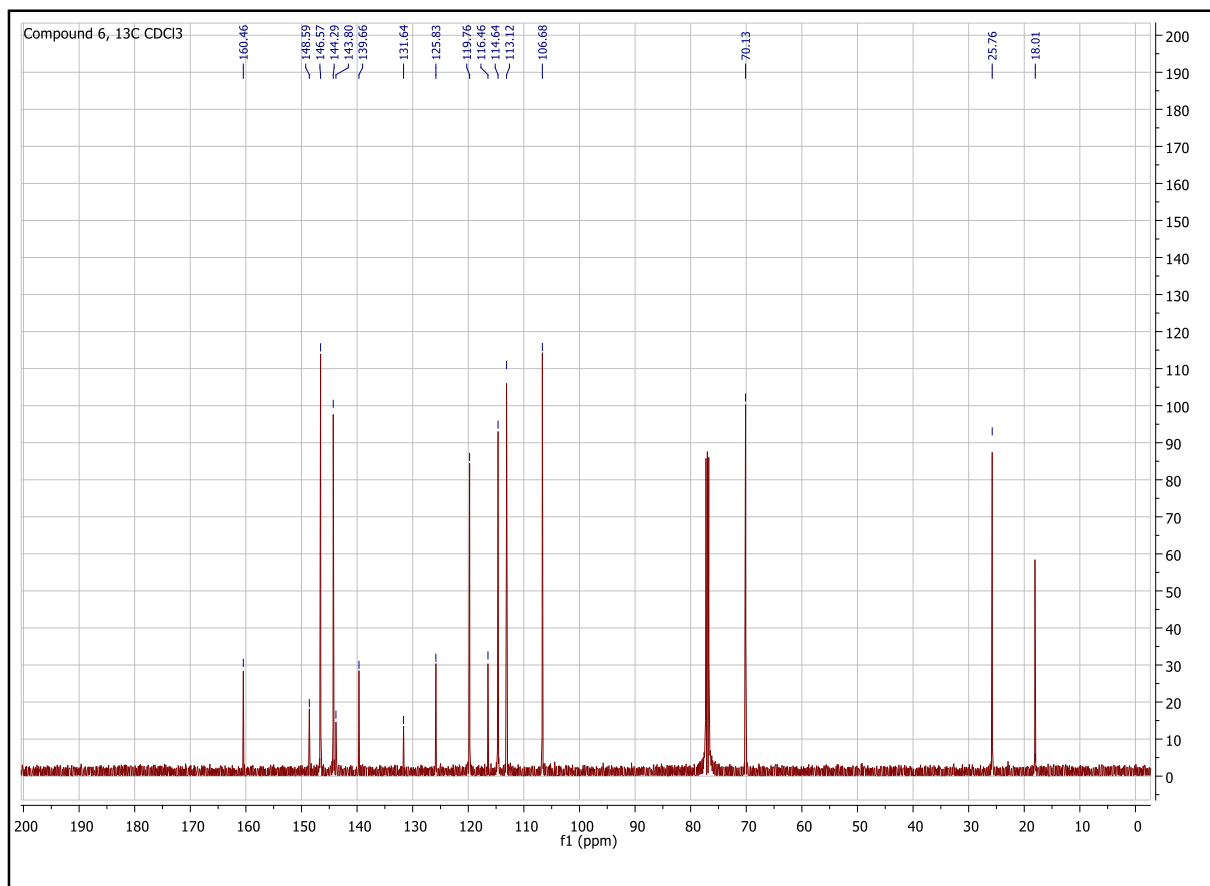


Figure 46. ^{13}C NMR Spectrum of compound **6** measured in CDCl_3 , 100 MHz

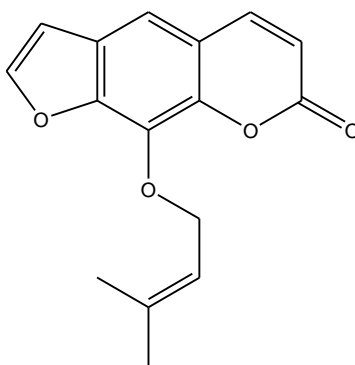


Figure 47. ^1H NMR (500 MHz, CDCl_3) δ_{H} 1.72 (s, 3H, H-5''), 1.74 (s, 3H, H-4''), 5.0 (d, 2H, $^3J = 7.5$, H-1''), 5.61 (m, 1H, H-2''), 6.36 (d, 1H, $^3J = 9.5$, H-3), 6.81 (d, 1H, $^3J = 2.5$, H-3'), 7.35 (s, 1H, H-5), 7.68 (d, 1H, $^3J = 2.5$, H-2'), 7.75 (d, 1H, $^3J = 9.5$, H-4); ^{13}C NMR (100 MHz, CDCl_3) δ_{C} 18.01 (C-5''), 25.76 (C-4''), 70.13 (C-1''), 106.68 (C-3'), 113.12 (C-5), 114.64 (C-3), 116.45 (C-4a), 119.76 (C-2''), 125.83 (C-6), 131.64 (C-8), 139.66 (C-3''), 143.80 (C-8a), 144.29 (C-4), 146.57 (C-2'), 148.59 (C-7), 160.46 (C-2) ppm.

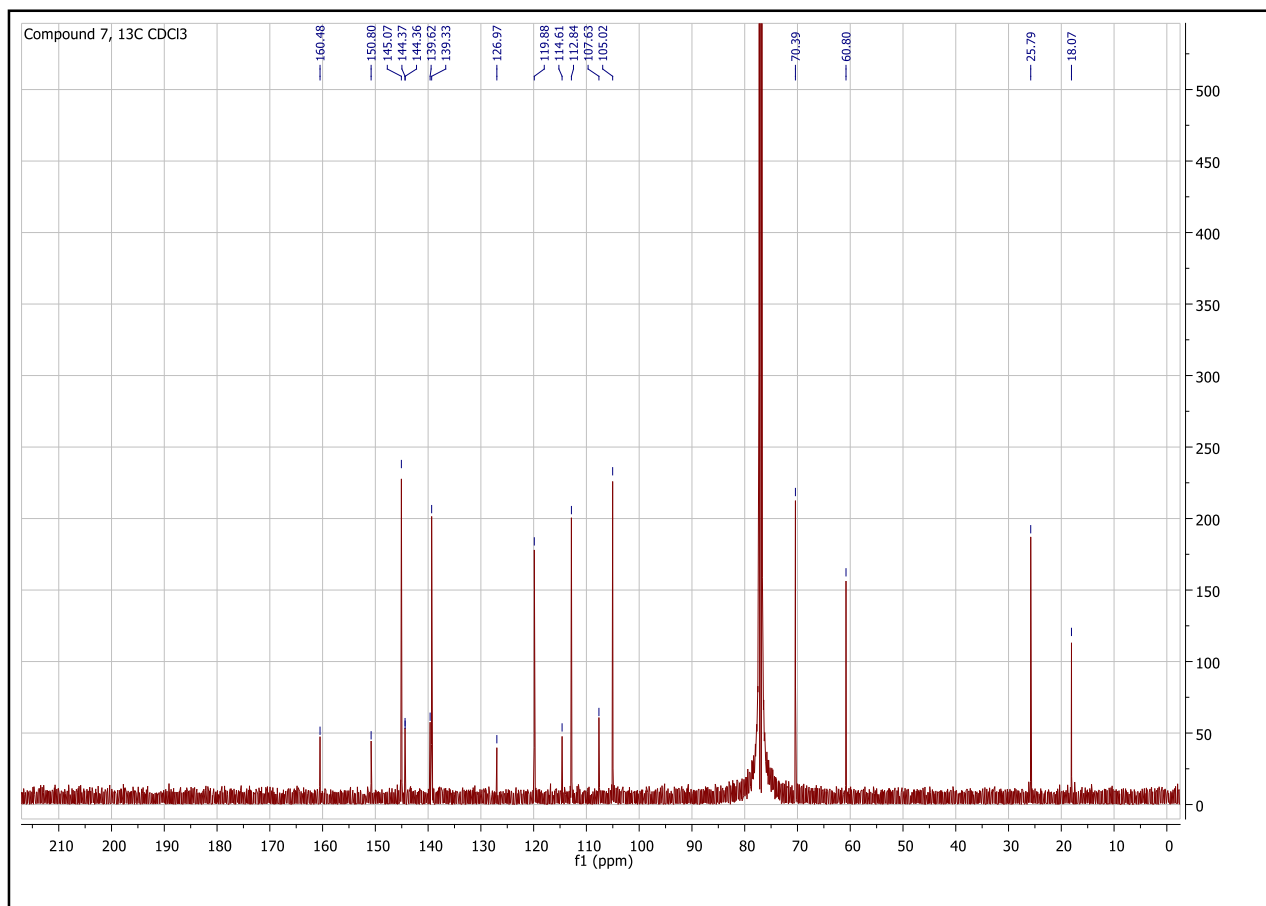


Figure 49. ^{13}C NMR Spectrum of compound **7** measured in CDCl_3 , 100 MHz

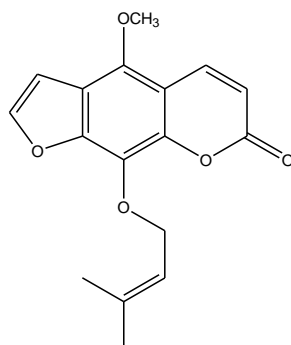


Figure 50. ^1H NMR (500 MHz, CDCl_3) δ_{H} 1.70 (s, 3H, H-5''), 1.74 (s, 3H, H-4''), 4.17 (s, 3H, OCH_3), 4.85 (d, 2H, $^3J = 7.0$, H-1''), 5.60 (m, 1H, H-2''), 6.28 (d, 1H, $^3J = 10$, H-3), 6.99 (d, 1H, $^3J = 2.5$, H-3'), 7.62 (d, 1H, $^3J = 2.0$, H-2'), 8.12 (d, 1H, $^3J = 9.5$, H-4); ^{13}C NMR (100 MHz, CDCl_3) δ_{C} 18.07 (C-5''), 25.80 (C-4''), 60.80 (OCH_3), 70.39 (C-1''), 105.03 (C-3'), 107.63 (C-4a), 112.84, 114.61 (C-6), 119.88 (C-2''), 126.97 (C-8), 139.33 (C-4), 139.62 (C-3''), 144.36 (C-8a), 144.37 (C-5), 145.07 (C-2'), 150.80 (C-7), 160.48 (C-2) ppm.

Compound 8

Compound **8** was identified as *heraclenin* through the study of the 1D spectra (^1H and ^{13}C NMR), and 2D NMR (DQF-COSY, HSQC, HMBC) and for comparison with the data reported in the literature.⁹³

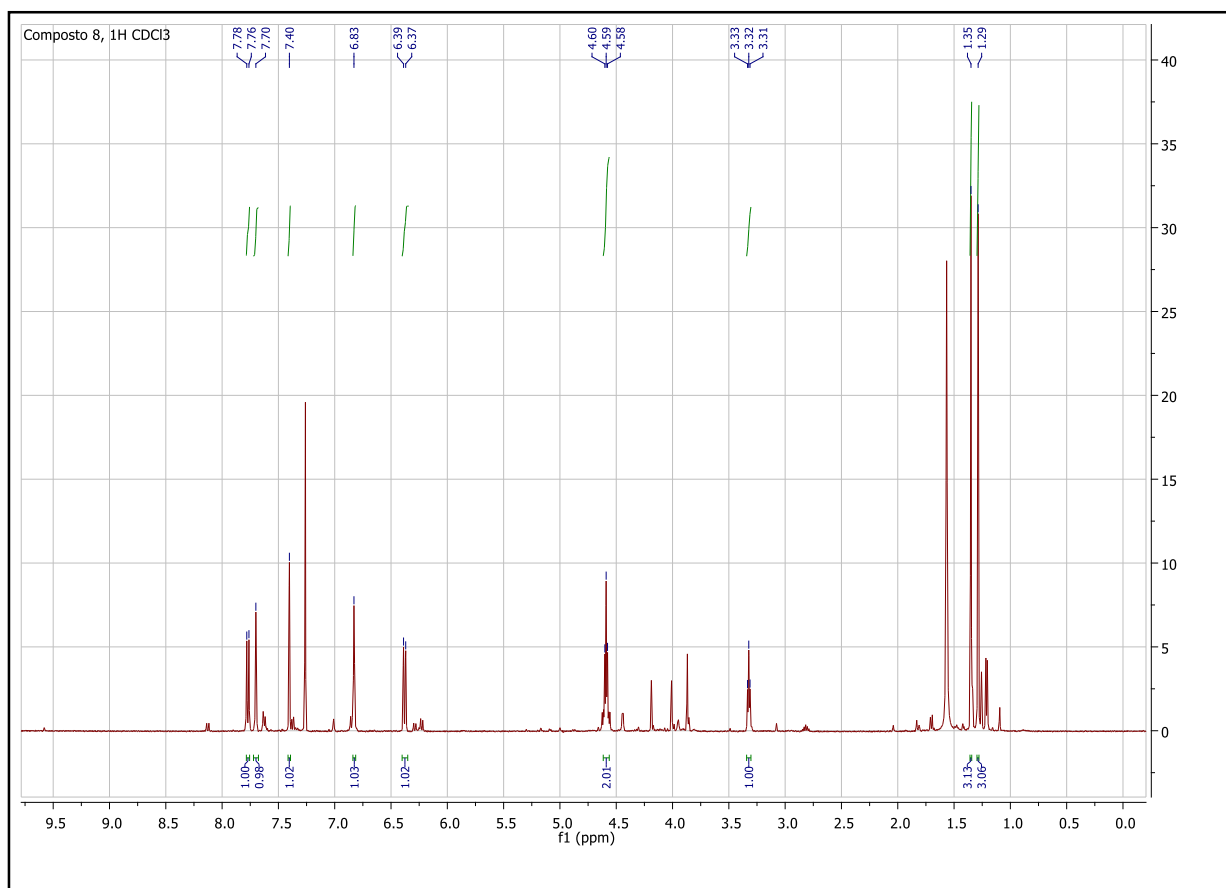


Figure 51. ^1H NMR Spectrum of compound **8** measured in CDCl_3 , 500 MHz

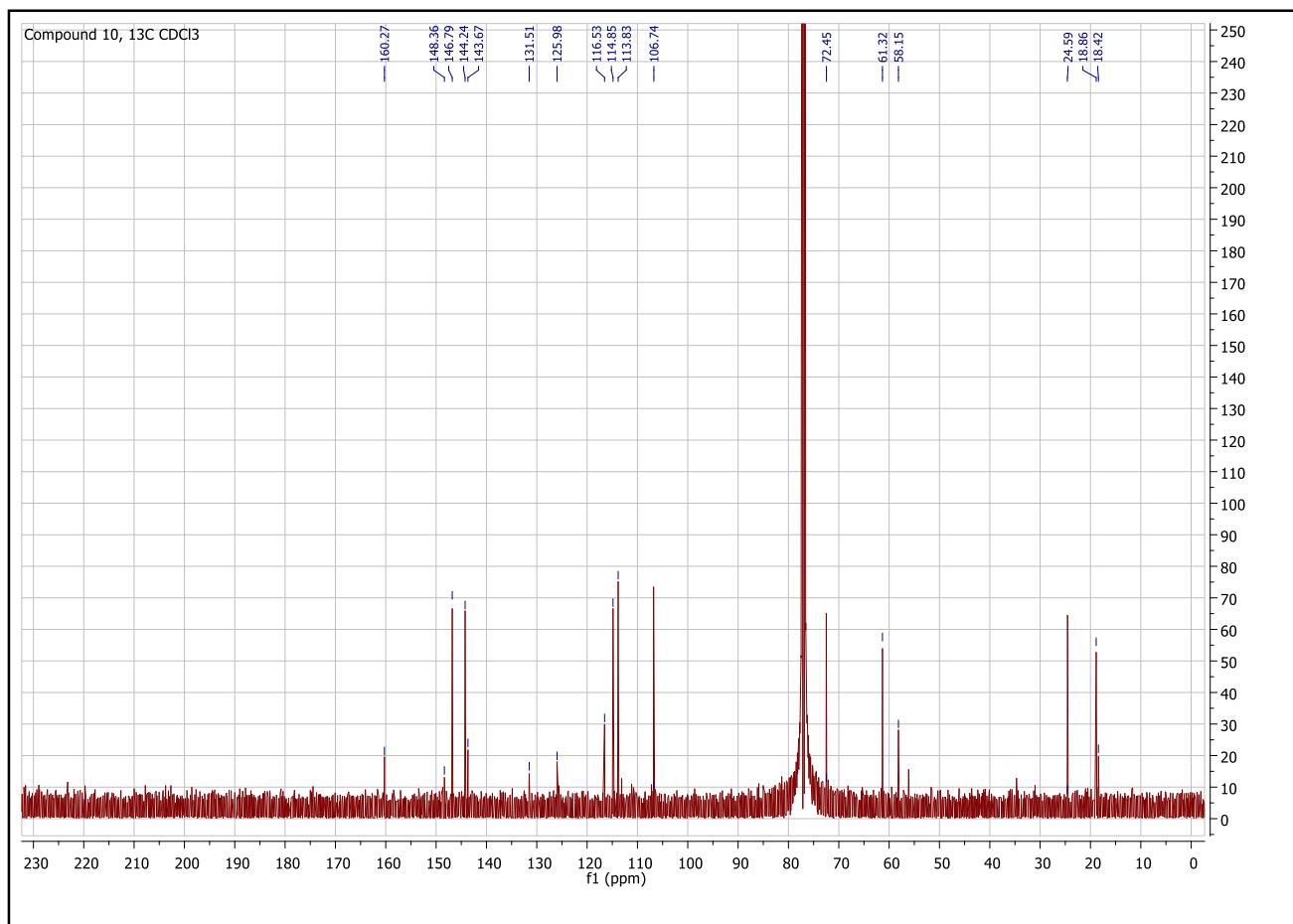


Figure 52. ^{13}C NMR Spectrum of compound **8** measured in CDCl₃, 100 MHz

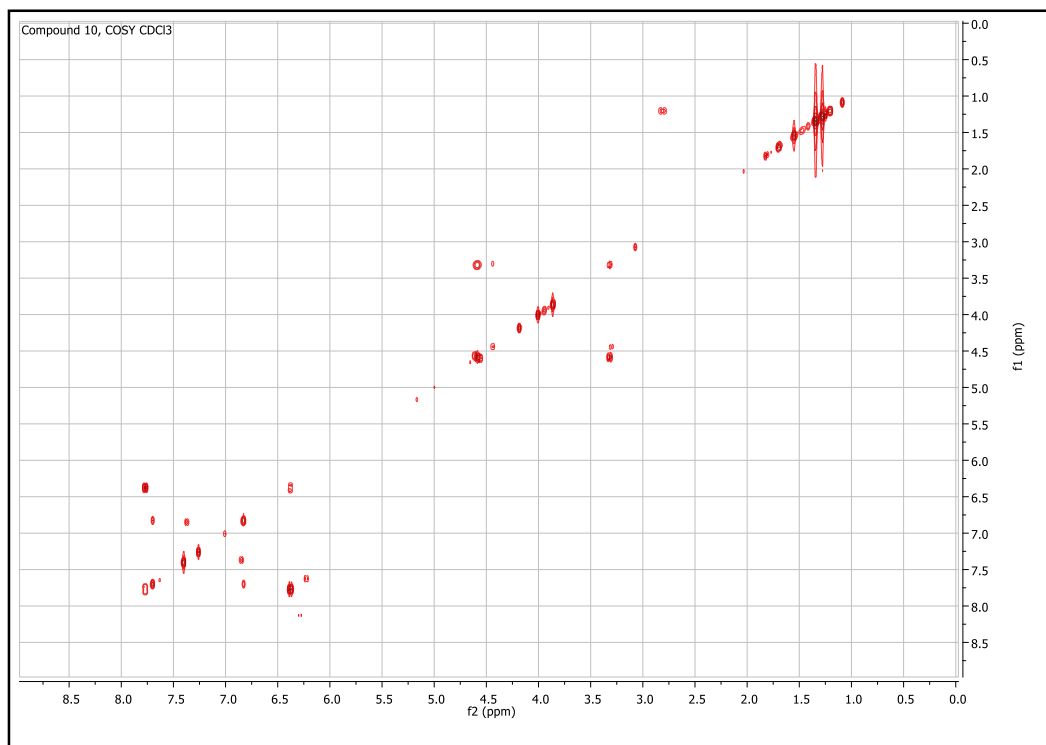


Figure 53. COSY Spectrum of compound **8** measured in CDCl₃, 500 MHz

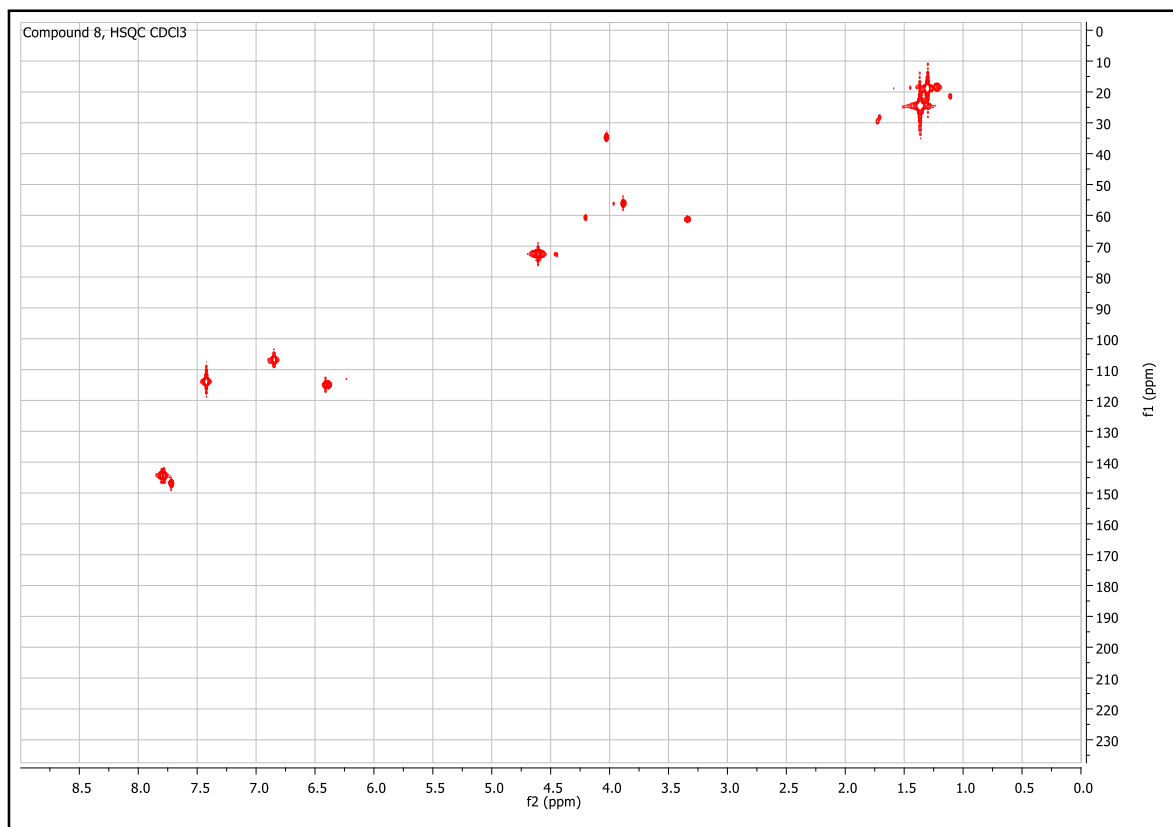


Figure 54. HSQC Spectrum of compound **8** measured in CDCl₃, 500 MHz

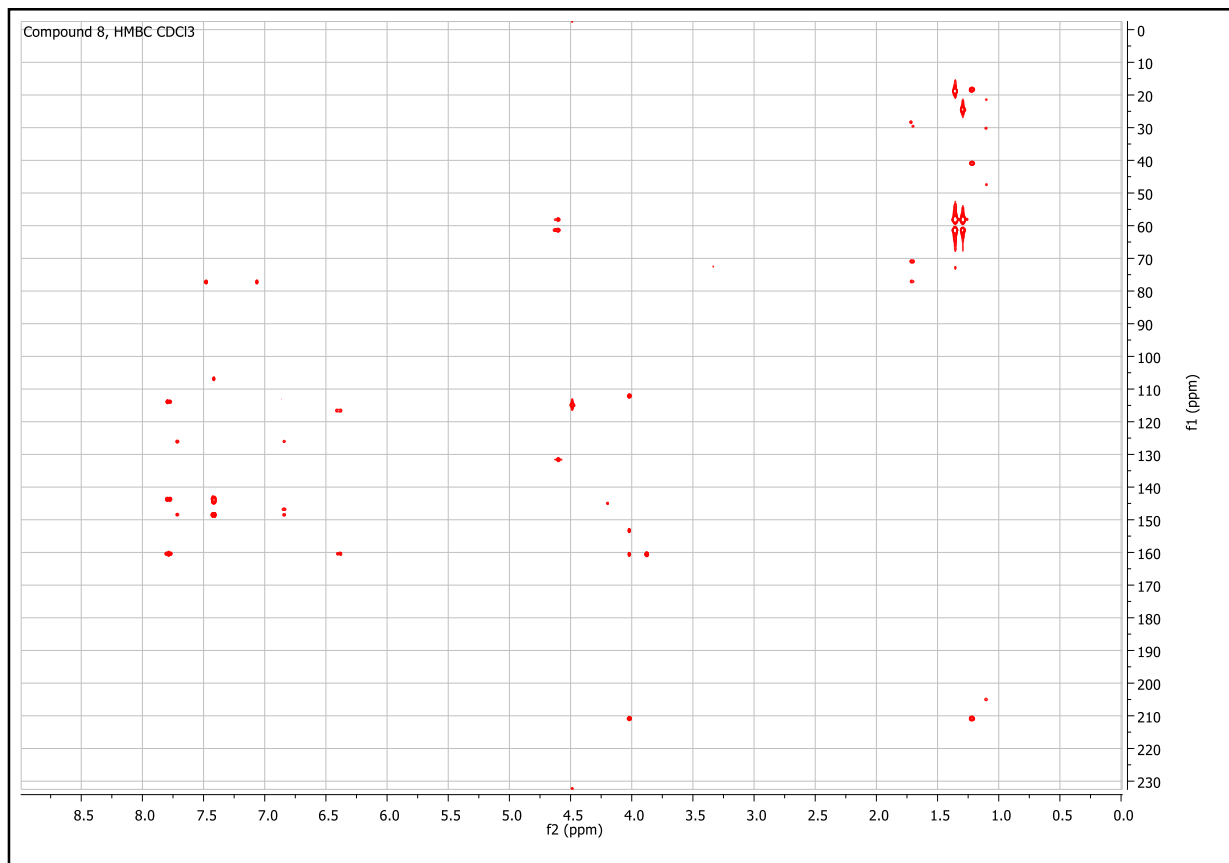


Figure 55. HMBC Spectrum of compound **8** measured in CDCl₃, 500 MHz

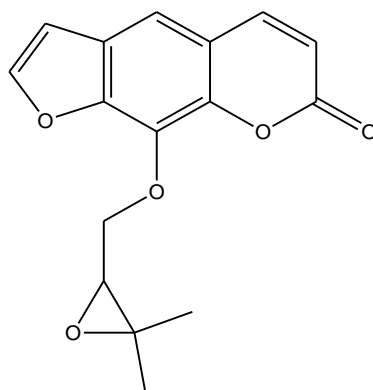


Figure 56. ^1H NMR (500 MHz, CDCl_3) δ_{H} 1.29 (s, 3H, CH_3), 1.35 (s, 3H, CH_3), 3.32 (t, 1H, $^3J = 5.5$, H-2''), 4.59 (t, 2H, $^3J = 6.0$, H-1''), 6.38, (d, 2H, $^3J = 6.0$, H-3), 6.83 (s, 1H, H-3'), 7.40 (s, 1H, H-5), 7.70 (s, 1H, H-2'), 7.77 (d, 1H, $^3J = 9.5$, H-4); ^{13}C NMR (100 MHz, CDCl_3) δ_{C} 18.86 (C-5''), 24.55 (C-4''), 58.15 (C-3''), 61.32 (C-2''), 72.48 (C-1''), 106.79 (C-4), 113.13 (C-3', C-3), 113.83 (C-3', C-3), 114.85 (C-4a), 116.53 (C-6), 125.98 (C-8), 143.64 (C-8a), 144.24 (C-4), 146.79 (C-2'), 148.36 (C-7), 160.27 (C-2) ppm.

Compound 9

Compound **9** was identified as (-)-*heraclenol*, through the study of the spectra 1D (^1H and ^{13}C NMR), and 2D NMR (DQF-COSY, HSQC, HMBC) and for comparison with the data reported in the literature.⁹¹

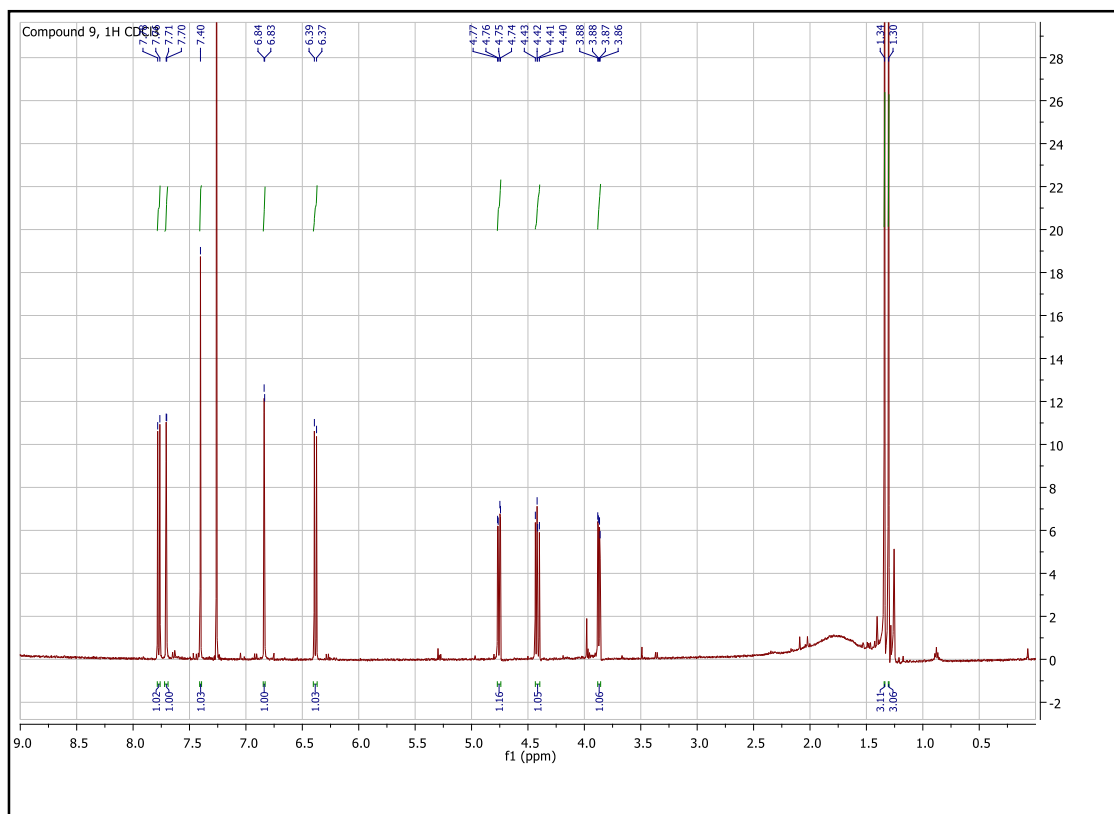


Figure 57. ^1H NMR Spectrum of compound **9** measured in CDCl_3 , 500 MHz

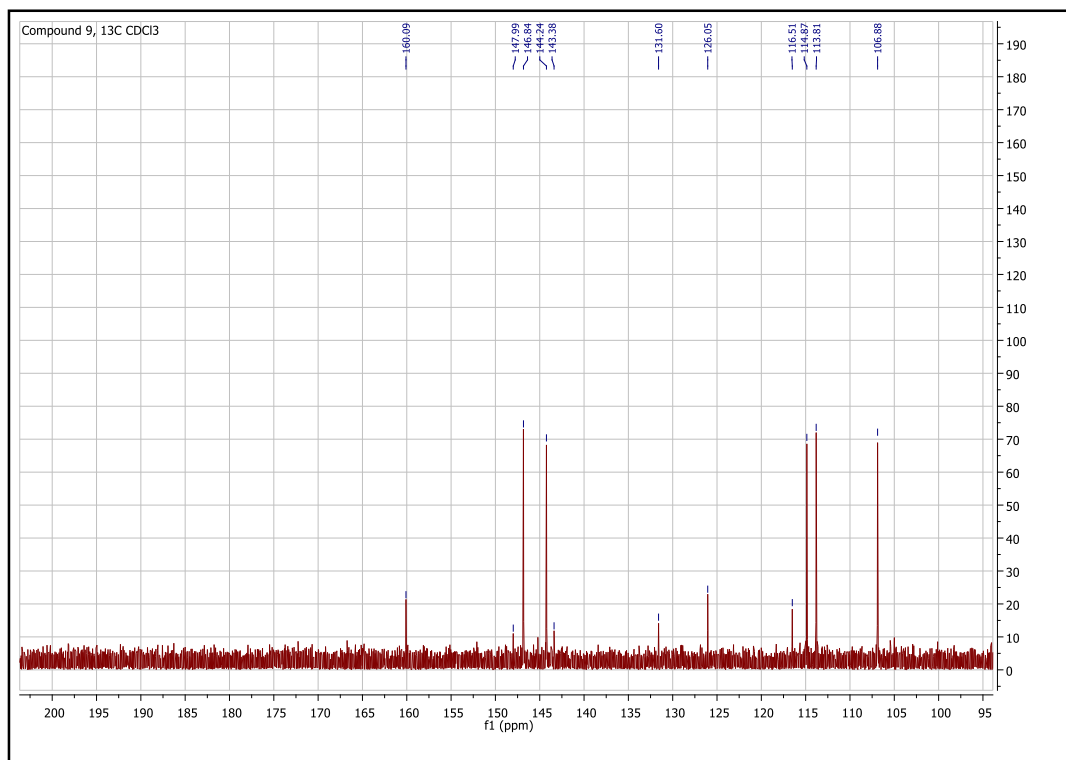


Figure 58. ^{13}C NMR Spectrum of compound **9** measured in CDCl_3 , 100 MHz

$[\alpha]_{\text{D}}^{20} = -7.14$

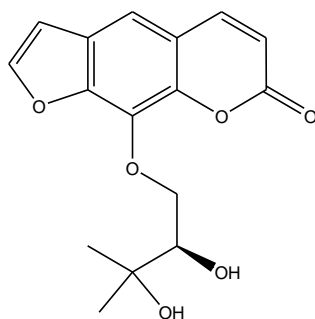


Figure 59. ^1H NMR (500 MHz, CD_4O) δ_{H} 1.30 (s, 3H, H-4''), 1.34 (s, 3H, H-5''), 3.87 (dd, 1H, $^3J = 7.5$, $^4J = 2.5$, H-2''), 4.42 (dd, 1H, $^3J = 10.0$, $^4J = 7.5$, H-1''), 4.76 (dd, 1H, $^3J = 10.0$, $^4J = 2.5$, H-1''), 6.38 (d, 1H, $^3J = 9.5$, H-3), 6.84 (d, 1H, $^3J = 2.0$, H-3'), 7.40 (s, 1H, H-5), 7.71 (d, 1H, $^3J = 1.5$, H-2'), 7.77 (d, 1H, $^3J = 9.5$, H-4); ^{13}C NMR (100 MHz, CDCl_3) δ_{C} 25.09 (C-5''), 26.69 (C-4''), 71.53 (C-3''), 75.75 (C-1''), 76.04 (C-2''), 106.88 (C-3'), 113.81 (C-5), 114.87 (C-3), 116.51 (C-4a), 126.05 (C-6), 131.60 (C-8), 143.38 (C-8a), 144.24 (C-4), 146.84 (C-2'), 147.99 (C-7), 160.09 (C-2) ppm.

Compound 10

Compound **10** was identified as (*S*)-heraclenol acetate through the study of the spectra 1D (^1H and ^{13}C NMR), and 2D NMR (DQF-COSY, HSQC, HMBC), by synthesis and for comparison with the data reported in the literature.⁸⁸

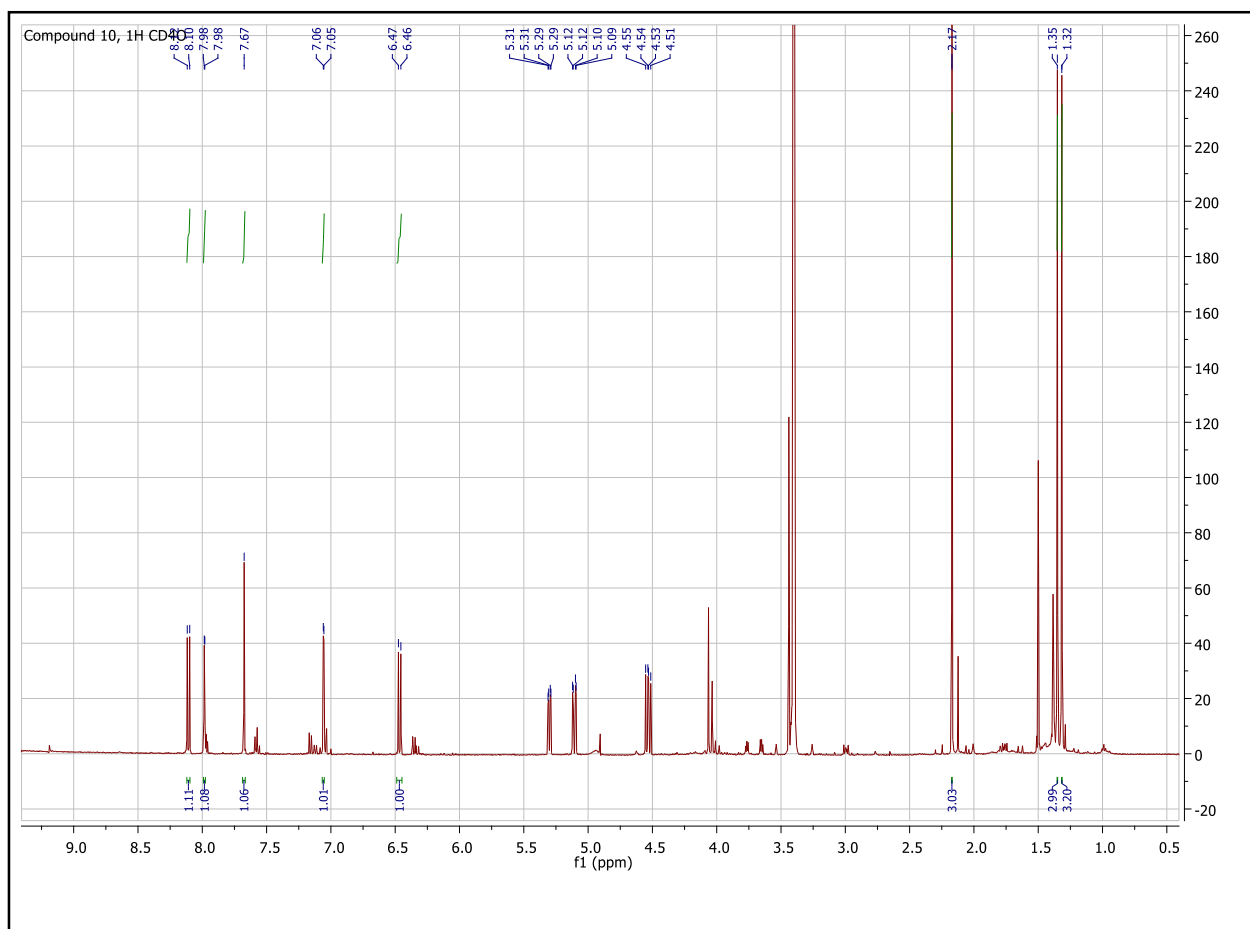


Figure 60. ^1H NMR Spectrum of compound **10** measured in CD_4O , 500 MHz

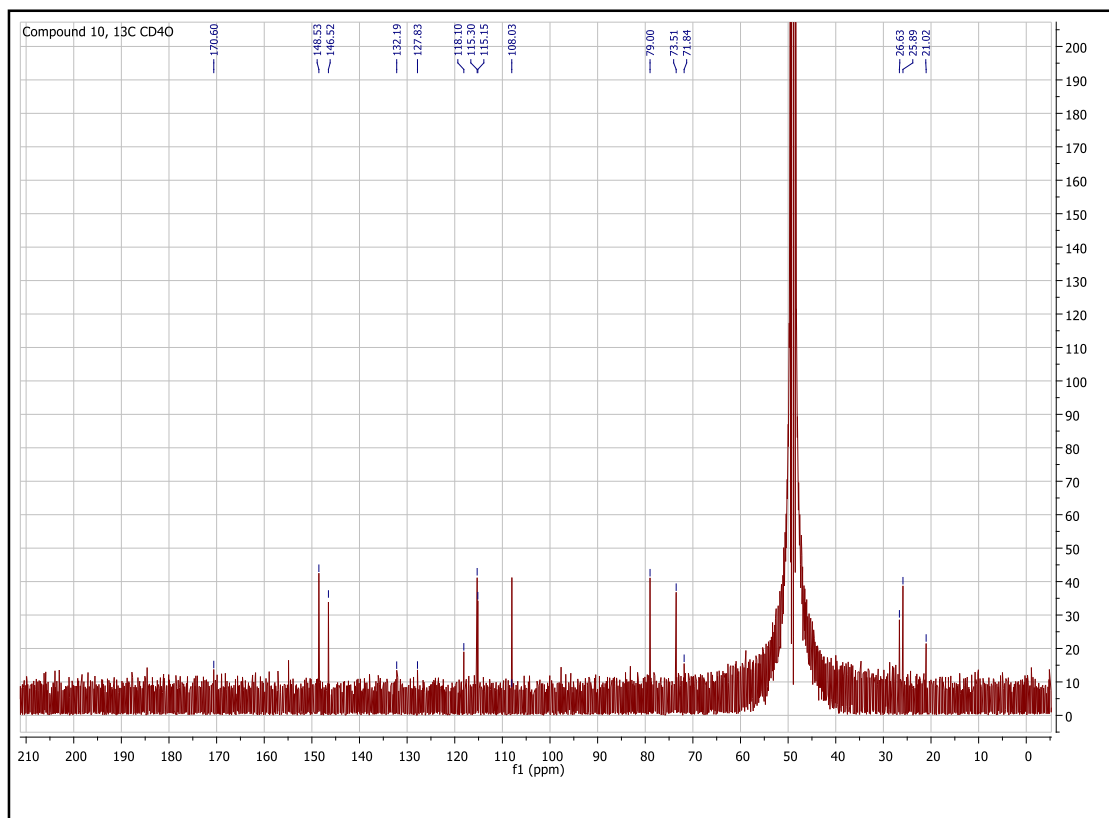


Figure 61. ^{13}C NMR Spectrum of compound **10** measured in CD_4O , 100 MHz

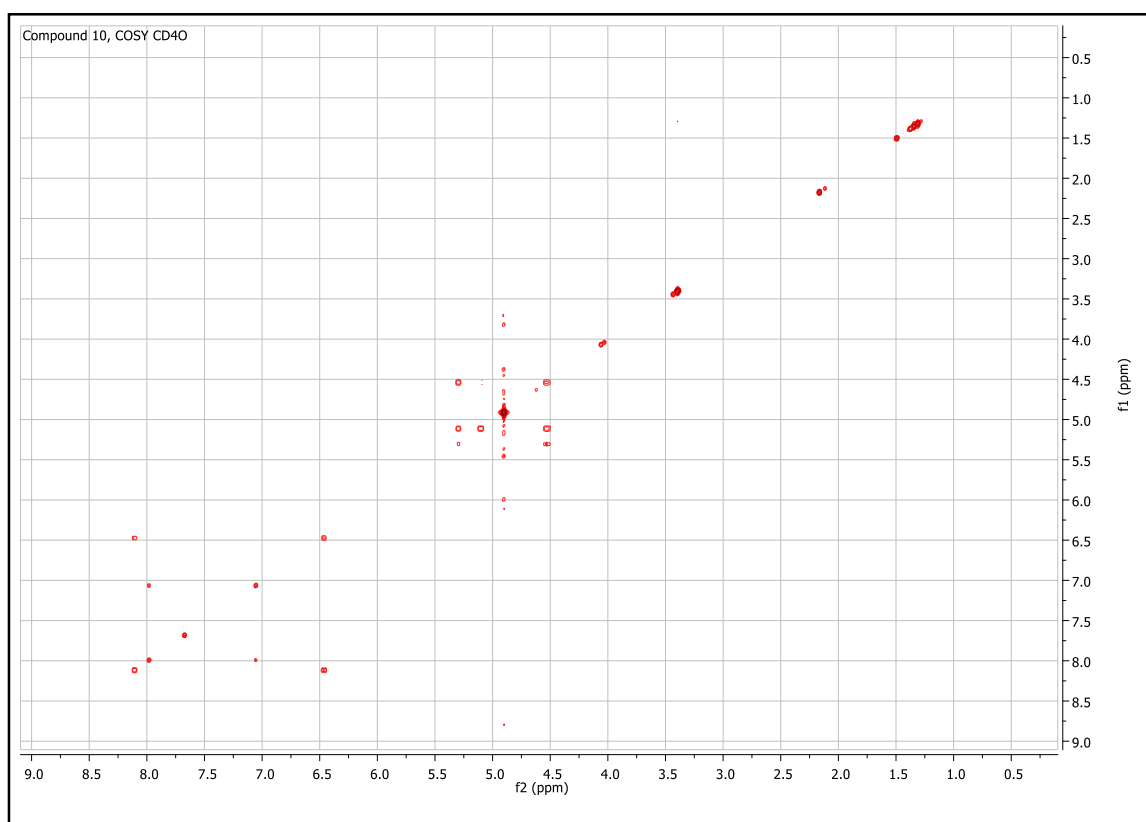


Figure 62. COSY Spectrum of compound **10** measured in CD_4O , 500 MHz

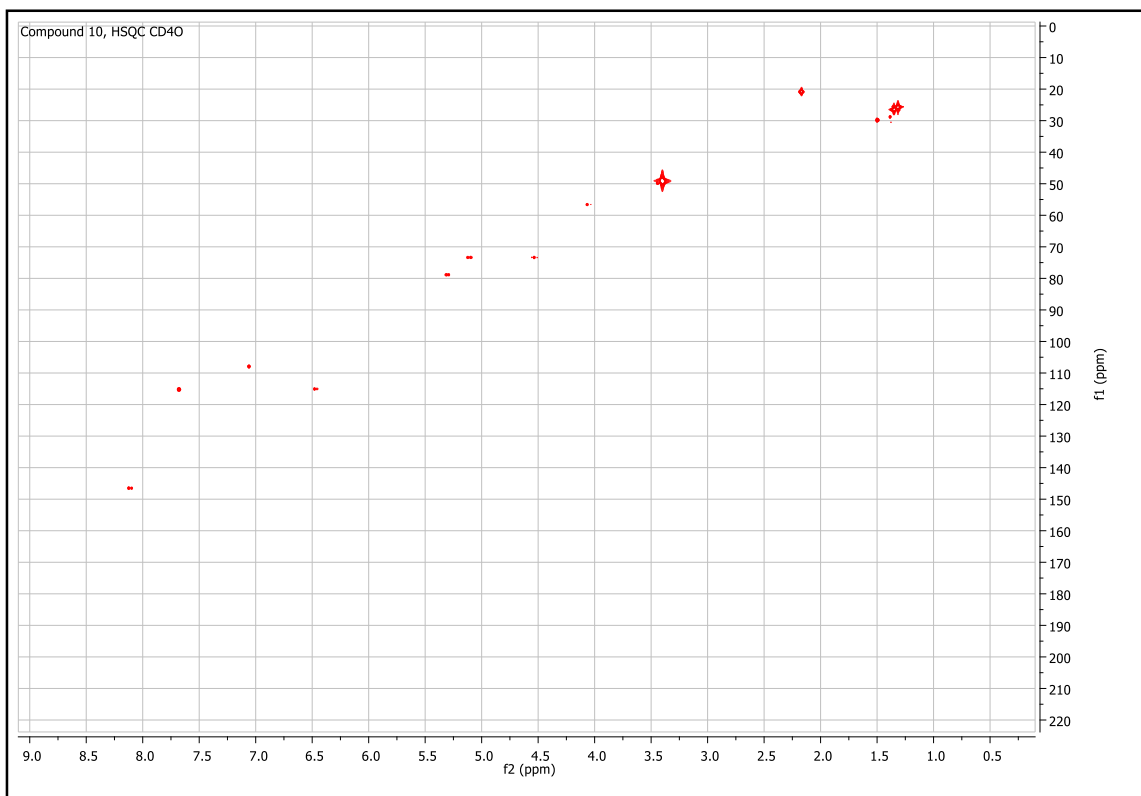


Figure 63. HSQC Spectrum of compound **10** measured in CD₄O, 500 MHz

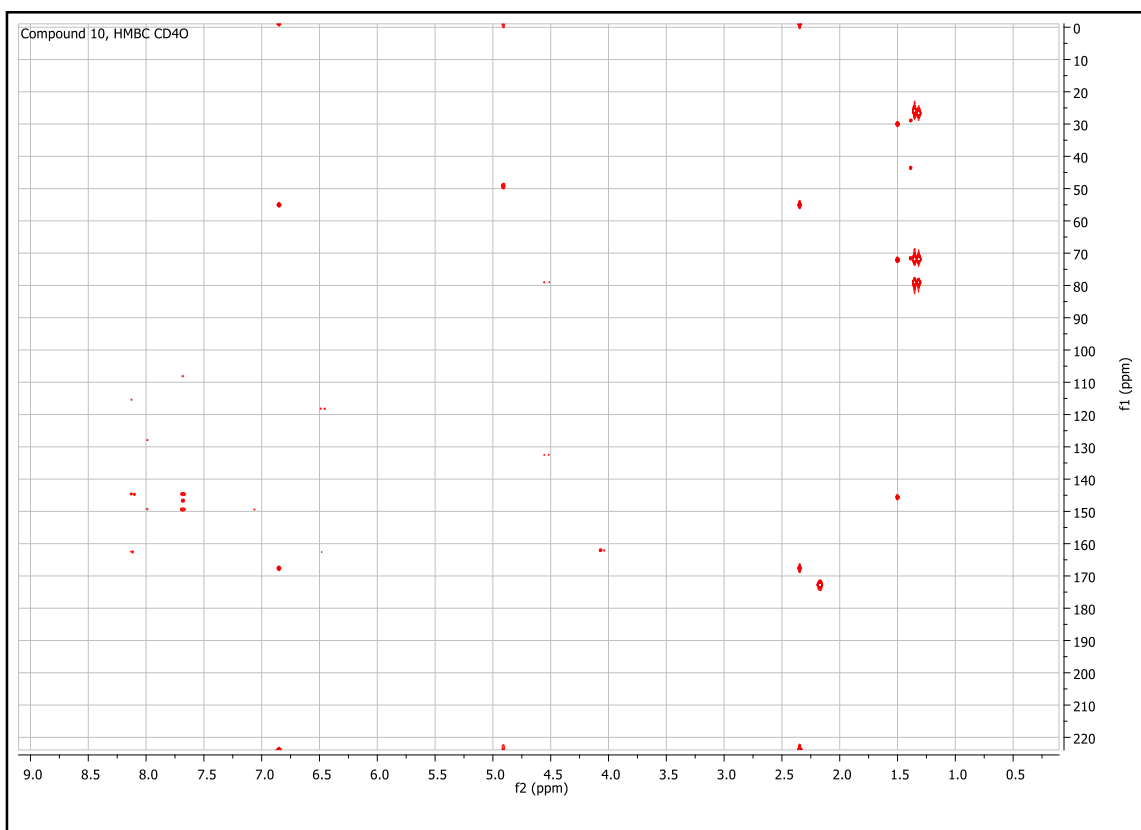


Figure 64. HMBC Spectrum of compound **10** measured in CD₄O, 500 MHz

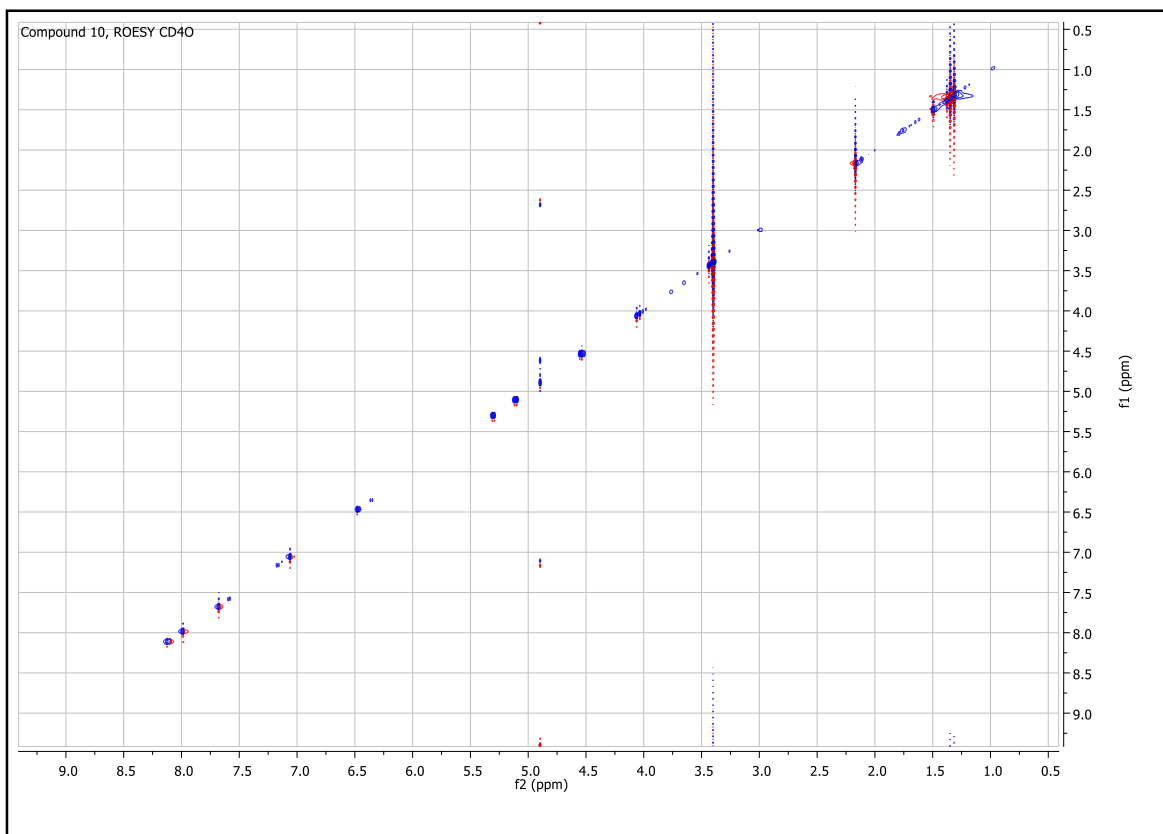


Figure 65. ROESY Spectrum of compound **10** measured in CD₄O, 500 MHz

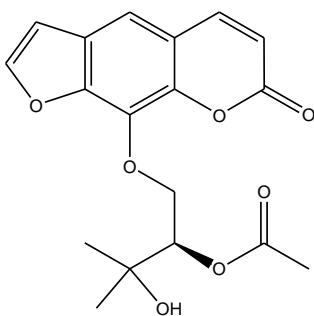


Figure 66. ¹H NMR (500 MHz, CD₄O) δ_H 1.32 (s, 3H, H-4''), 1.35 (s, 3H, H-5''), 2.17 (s, 3H, COCH₃), 4.54 (dd, 1H, ³J = 11.5, ⁴J = 9.0, H-1''), 5.11 (dd, 1H, ³J = 11.5, ⁴J = 2.5, H-1''), 5.30 (dd, 1H, ³J = 9.0, ⁴J = 2.5, H-2''), 6.47 (d, 1H, ³J = 9.5, H-3), 7.06 (d, 1H, ³J = 2.5, H-3'), 7.68 (s, 1H, H-5), 7.99 (d, 1H, ³J = 2.5, H-2'), 8.11 (d, 1H, ³J = 9.5, H-4); ¹³C NMR (100 MHz, CDCl₃) δ_C 21.02 (COCH₃), 25.89 (C-5''), 26.63 (C-4''), 71.84 (C-3''), 73.51 (C-1''), 78.90 (C-2''), 108.00 (C-3'), 115.15 (C-3), 115.30 (C-5), 118.10 (C-4a), 127.83 (C-6), 132.19 (C-8), 146.52 (C-4), 148.53 (C-2'), 170.60 (COCH₃) ppm.

Compound 11

Magydarin (**11**): white powder; $[\alpha]_D^{25} + 96.3$ (c 0.05, CH_2Cl_2); UV (MeOH) λ_{max} ($\log \epsilon$) 348 (8.5) nm; ECD (300 μM , MeOH) λ ($\Delta\epsilon$) 348 (+2950) nm; ^1H (CDCl_3 , 500 MHz) and ^{13}C (CDCl_3 , 100 MHz) NMR, see Table 1; HRTOFESIMS m/z 277.1078 $[\text{M} + \text{H}]^+$ (calcd for $\text{C}_{15}\text{H}_{16}\text{O}_5$, 277.1076).

Compound 12

Compound **12** was identified as *osthol*, through the study of 1D spectra (^1H and ^{13}C NMR), and 2D NMR spectra (DQF-COSY, HSQC, HMBC) and for comparison with data reported in the literature.⁹⁶

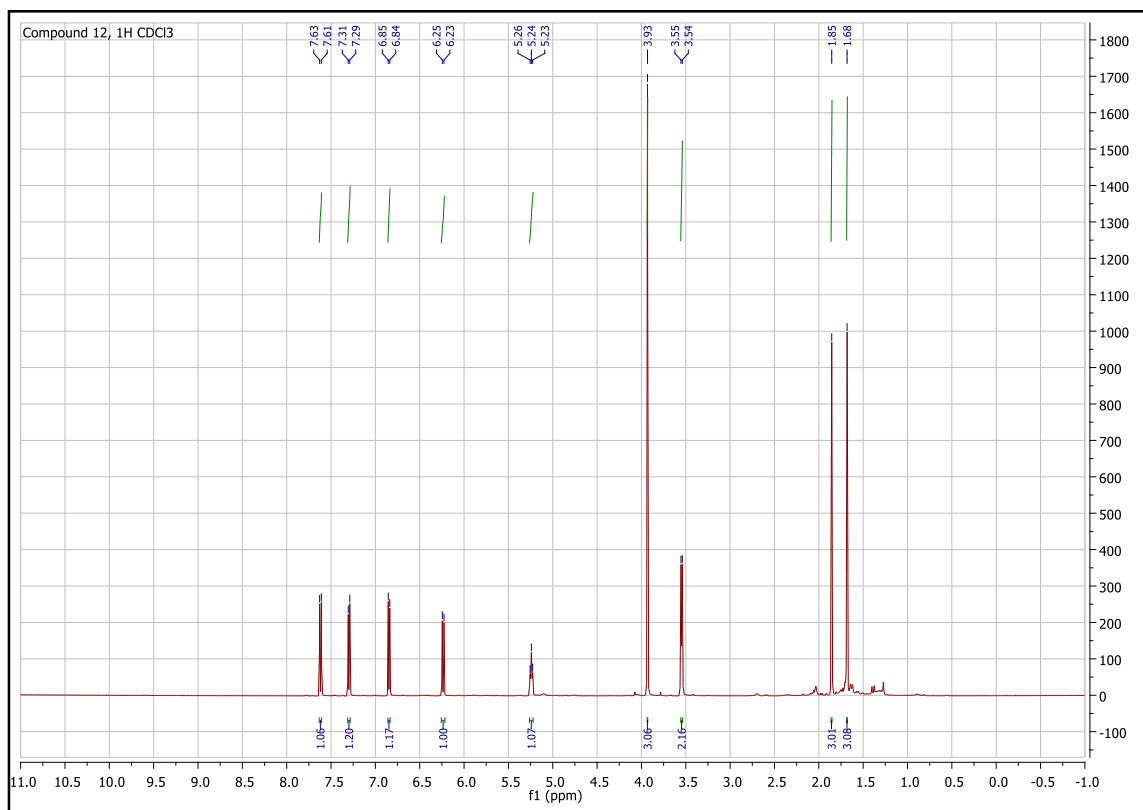


Figure 67. ^1H NMR Spectrum of compound **12** measured in CD_3Cl , 500 MHz

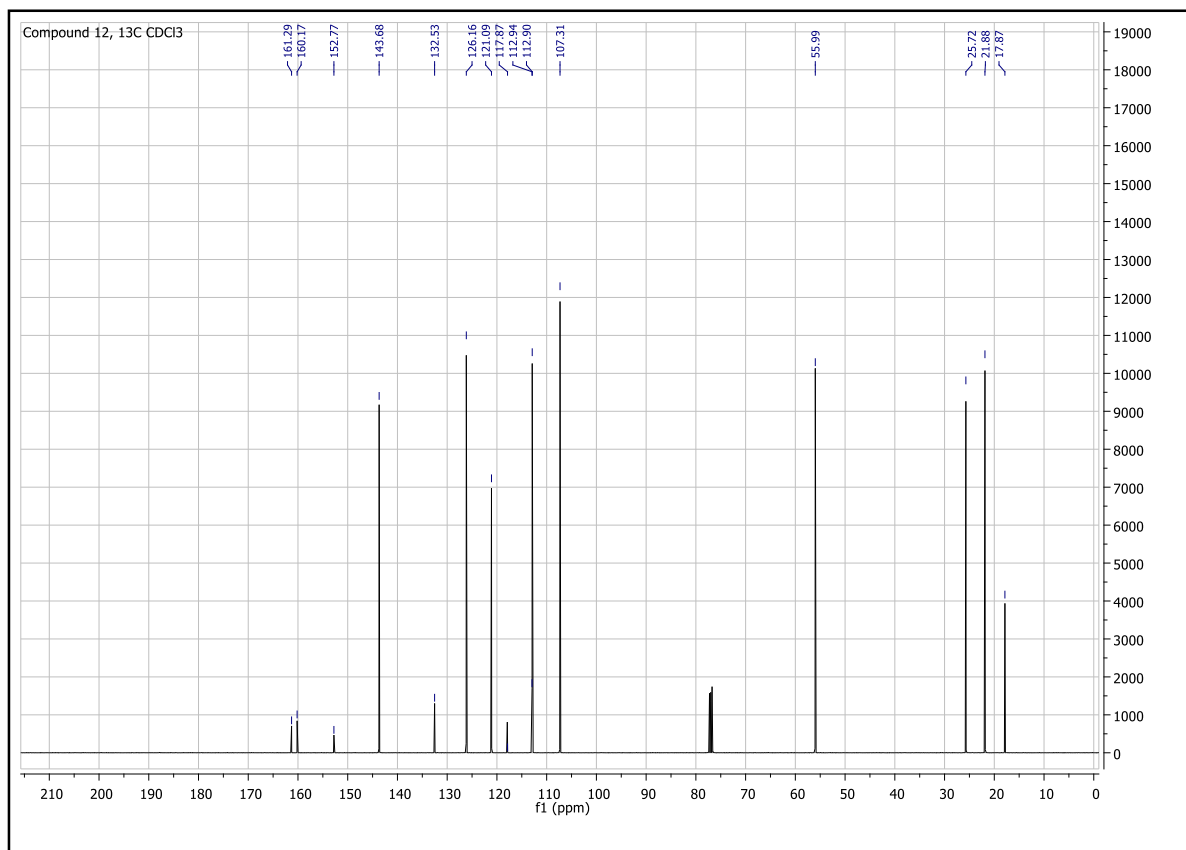


Figure 68. ^{13}C NMR Spectrum of compound **12** measured in CD_3Cl , 100 MHz

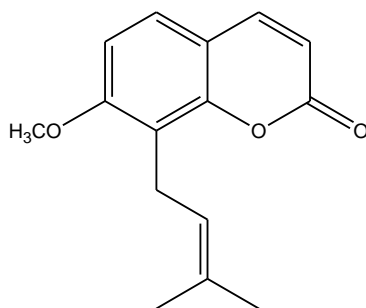


Figure 69. ^1H NMR (500 MHz, CDCl_3) δ_{H} 1.68 (s, 3H, H-4'), 1.85 (s, 3H, H-5'), 3.55 (d, 2H, $^3J = 7.5$, H-1'), 3.93 (s, 3H, OCH_3), 5.24 (t, 1H, H-2'), 6.24 (d, 2H, $^3J = 9.5$, H-3), 6.85 (d, 1H, $^3J = 8.5$ H-6), 7.30 (d, 1H, $^3J = 8.5$ H-5), 7.62 (d, 1H, $^3J = 9.5$, H-4) ppm; ^{13}C NMR (100 MHz, CDCl_3) δ_{C} 17.87 (C-5'), 21.88 (C-1'), 25.72 (C-4'), 55.99 (OCH_3), 107.31 (C-6), 112.90 (C-3), 112.94 (C-4a), 117.9 (C-8), 121.10 (C-2'), 126.16 (C-5), 132.53 (C-3'), 143.68 (C-4), 152.77 (C-8a), 160.17 (C-7), 161.29 (C-2) ppm.

Compound 13

Compound **13** was identified as *meranzin* through the study of the 1D spectra (^1H and ^{13}C NMR), and 2D NMR (DQF-COSY, HSQC, HMBC) and for comparison with data reported in the literature.⁹⁷

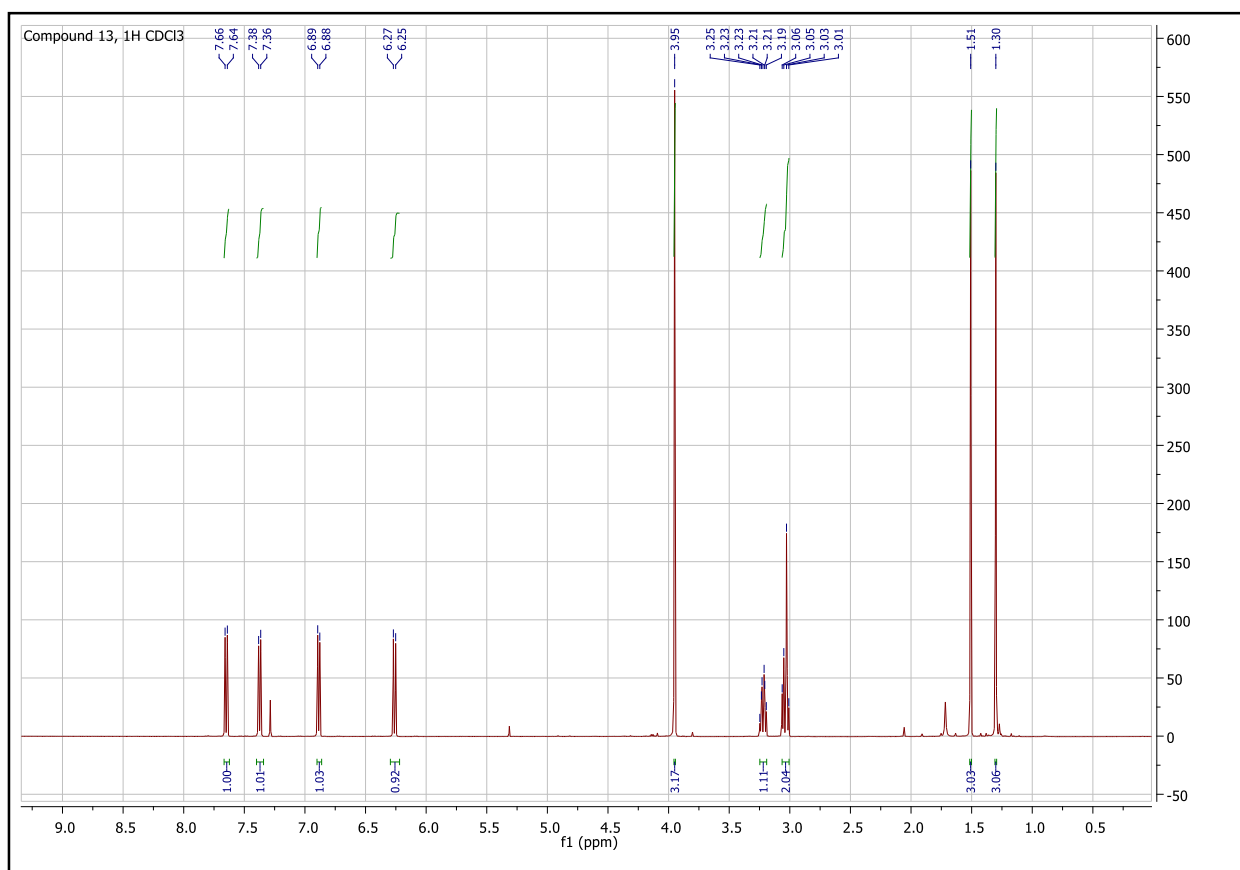


Figure 70. ^1H NMR Spectrum of compound **13** measured in CD_3Cl , 500 MHz

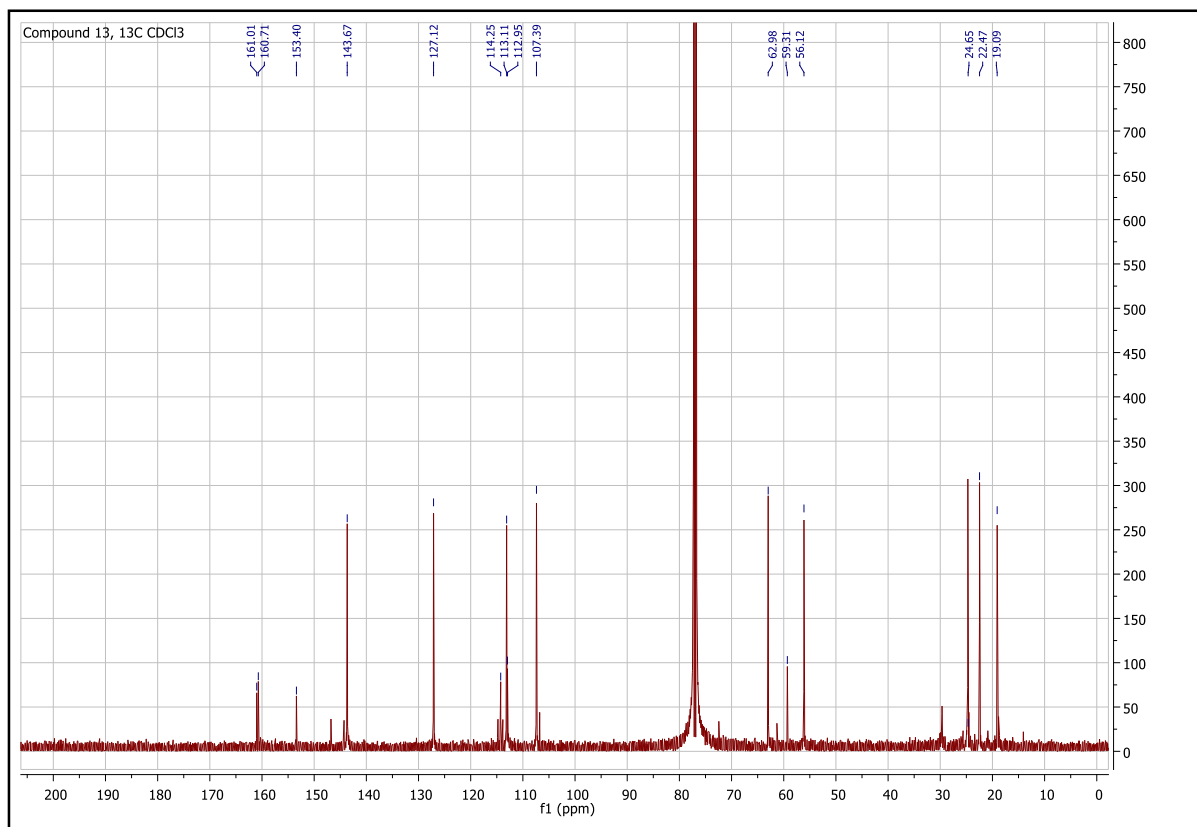


Figure 71. ^{13}C NMR Spectrum of compound **13** measured in CD_3Cl , 100 MHz

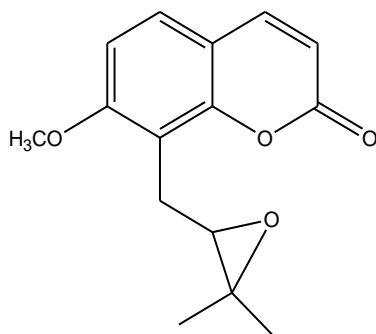


Figure 72. ^1H NMR (500 MHz, CDCl_3) δ_{H} 1.27 (s, 3H, H-5'), 1.48 (s, 3H, H-4'), 3.01 (m, 2H, H-1'), 3.19 (m, 1H, H-2'), 3.92 (s, 3H, OCH_3), 6.23 (d, 1H, $^3J = 9.5$, H-3), 6.86 (d, 1H, $^3J = 9.0$, H-6), 7.35 (d, 1H, $^3J = 8.5$, H-5), 7.62 (d, 1H, $^3J = 9.5$, H-4), ^{13}C NMR (100 MHz, CDCl_3) δ_{C} 19.09 (C-5'), 22.47 (C-4'), 24.52 (C-1), 56.12 (OCH_3), 59.31 (C-3'), 62.98 (C-2'), 107.40 (C-6), 112.95 (C-4a), 113.12 (C-3), 114.25 (C-8), 127.12 (C-5), 143.67 (C-4), 153.40 (C-8a), 160.71 (C-7), 161.01 (C-2) ppm.

Compound 14

Compound **14** was identified as *2'-acetoxy-3'-hydroxy-osthol* through the study of the spectra 1D (^1H and ^{13}C NMR), and 2D NMR (DQF-COSY, HSQC, HMBC) and for comparison with the data reported in the literature.^{92,95}

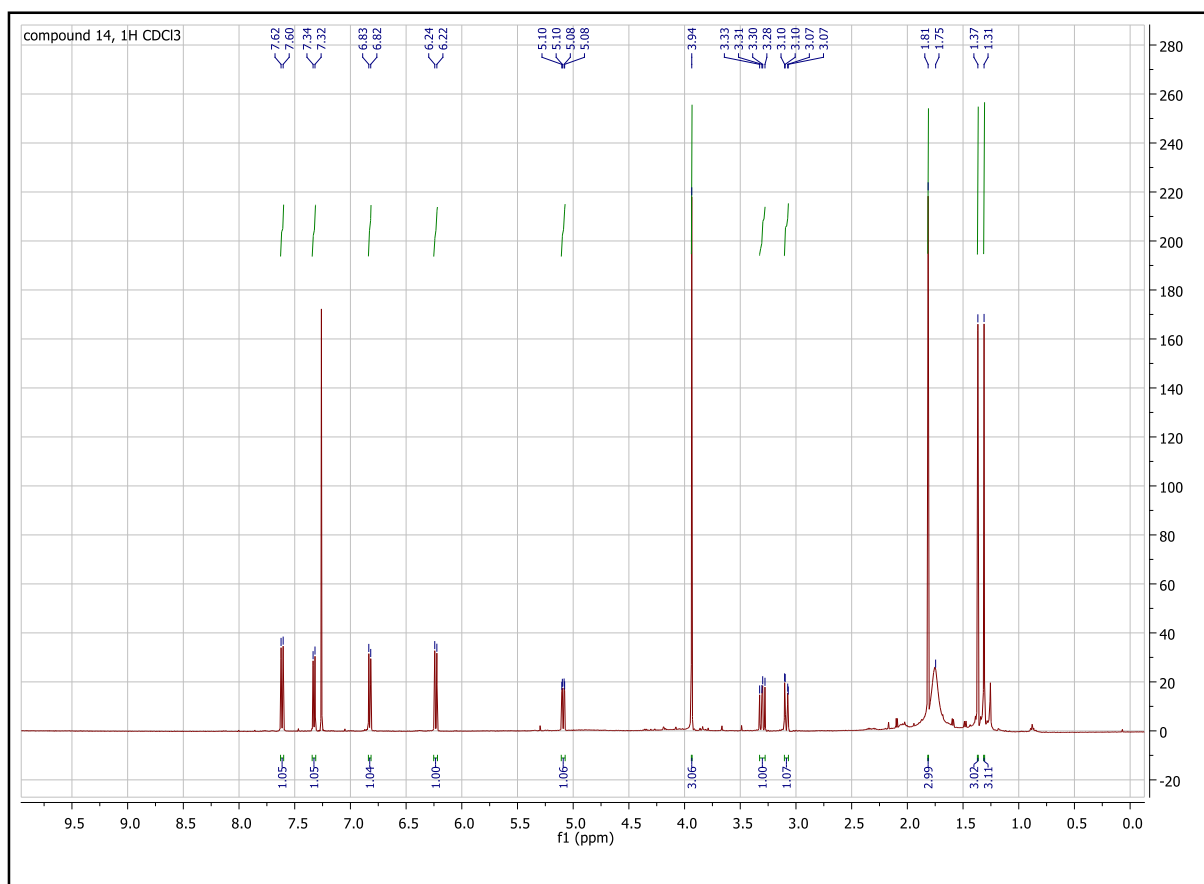


Figure 73. ^1H NMR Spectrum of compound **14** measured in CD_3Cl , 500 MHz

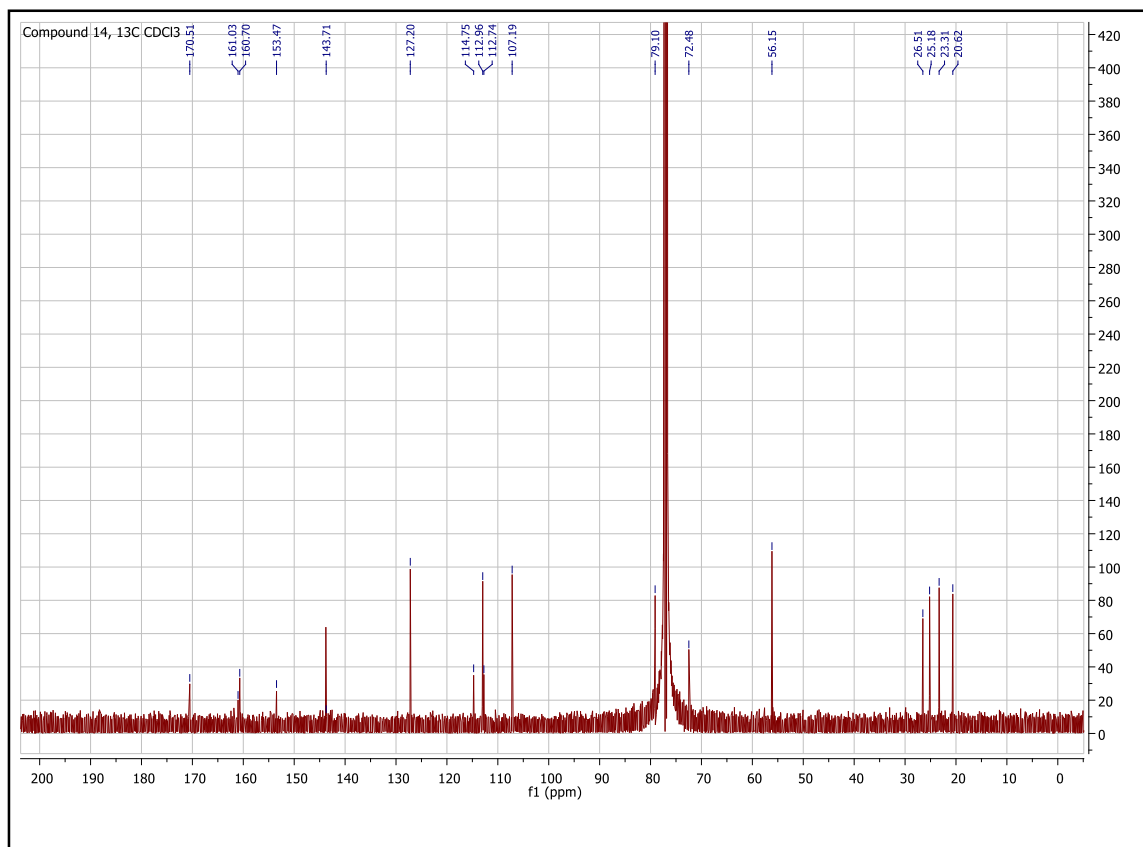


Figure 74. ^{13}C NMR Spectrum of compound **14** measured in CD_3Cl , 100 MHz

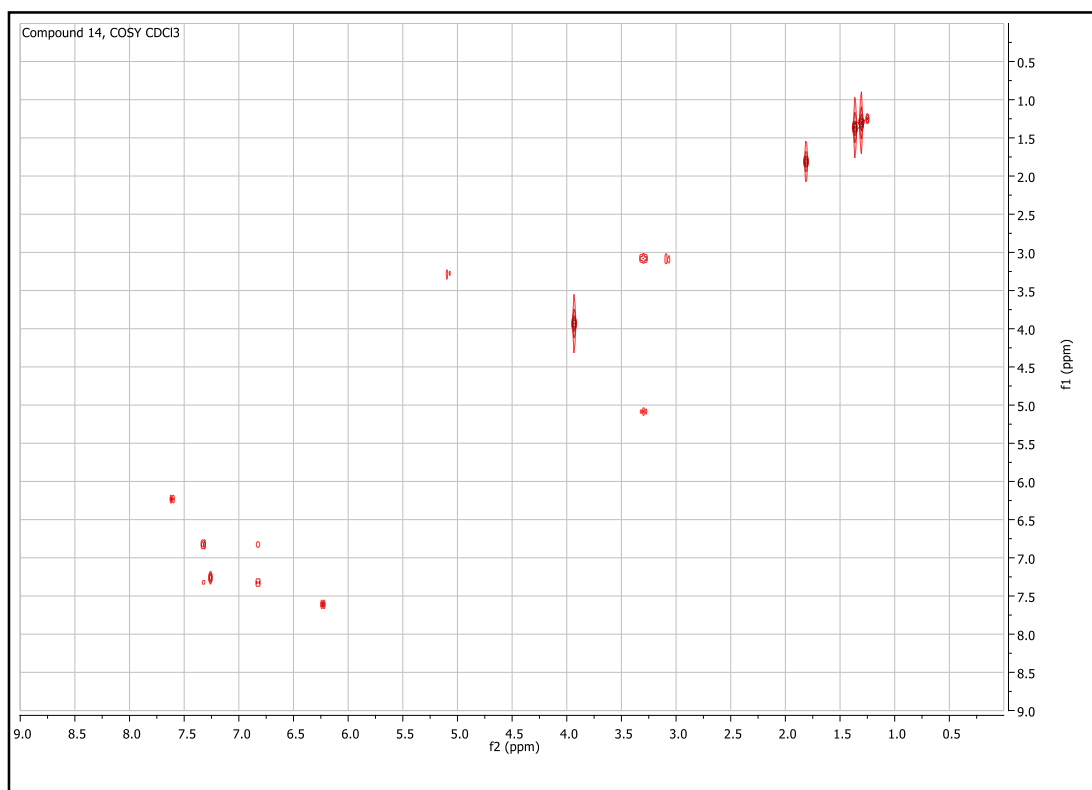


Figure 75. COSY Spectrum of compound **14** measured in CD_3Cl , 500 MHz

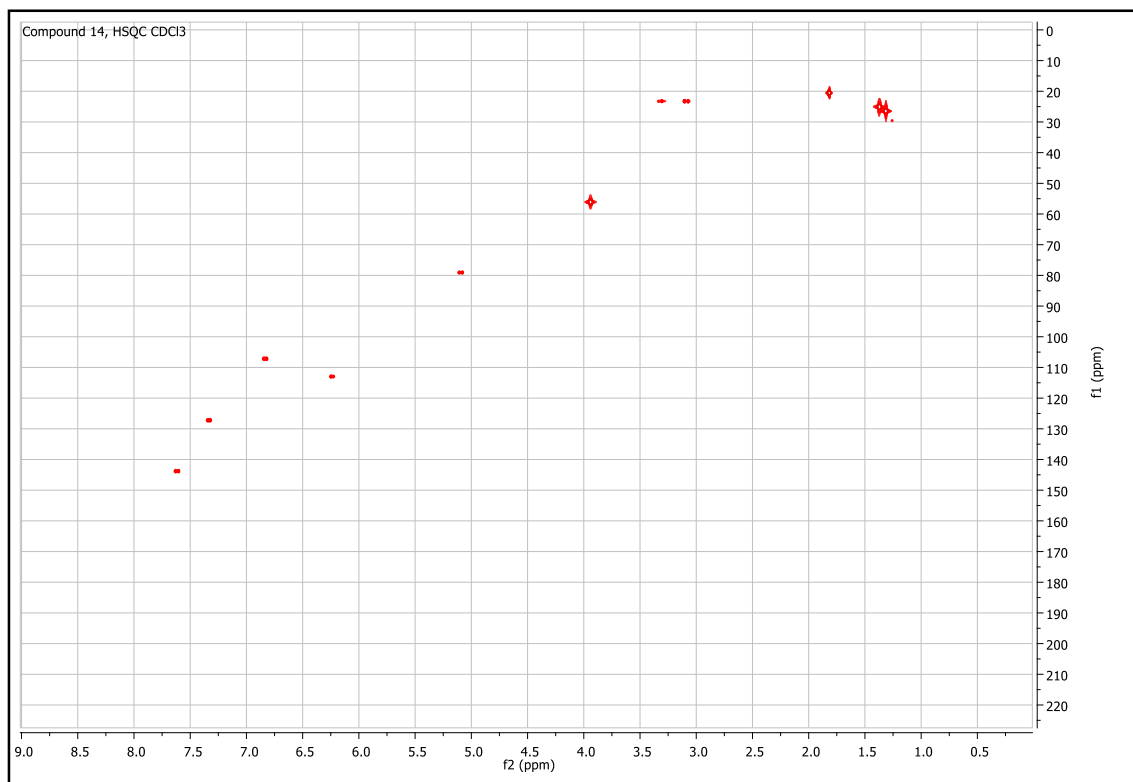


Figure 76. HSQC Spectrum of compound **14** measured in CD₃Cl, 500 MHz

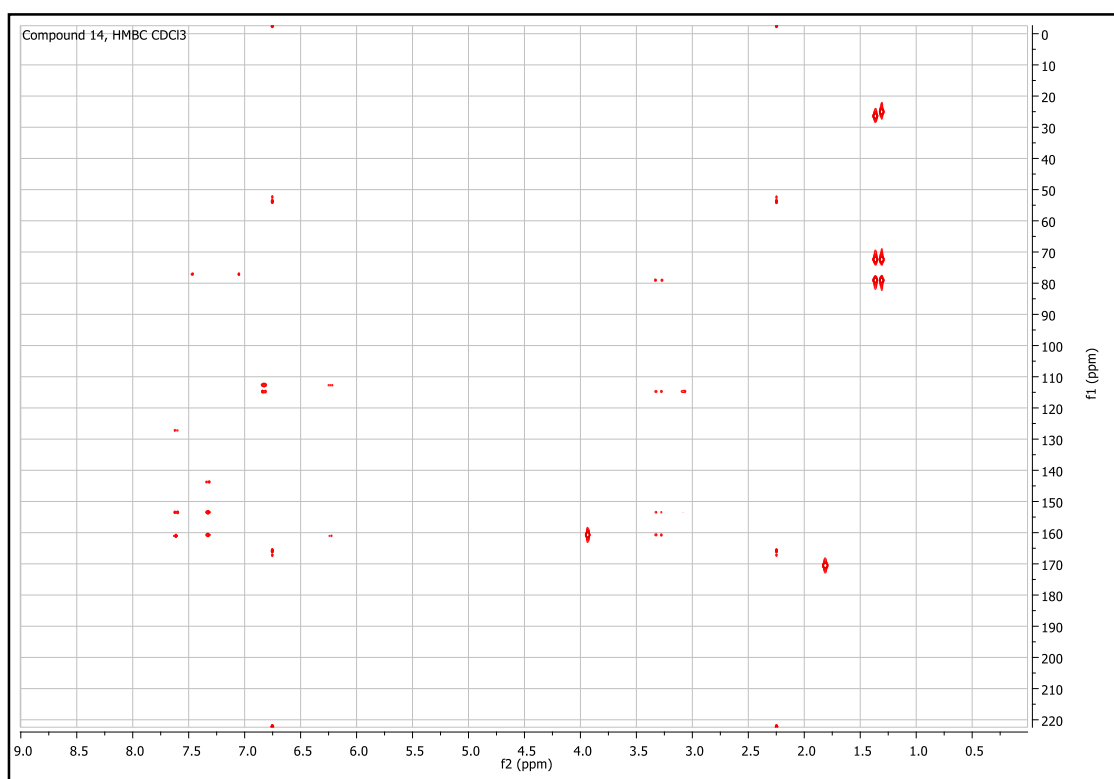


Figure 77. HMBC Spectrum of compound **14** measured in CD₃Cl, 500 MHz

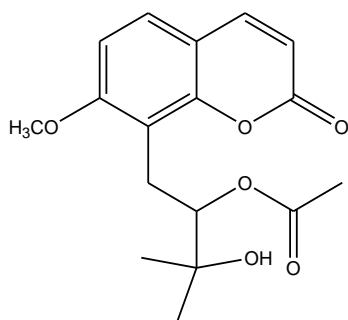


Figure 78. ^1H NMR (500 MHz, CD_4O) δ_{H} 1.31 (s, 3H, H-5'), 1.37 (s, 3H, H-4'), 1.75 (s br, 1H, OH), 1.81 (s, 3H, COCH_3), 3.09 (dd, 1H, $^3J = 14.0$, $^4J = 2.5$, H-1'), 3.30 (dd, 1H, $^3J = 13.5$, $^4J = 3.5$, H-1'), 3.94 (s, 3H, OCH_3), 5.09 (dd, 1H, $^3J = 10.0$, $^4J = 2.5$, H-2'), 6.23 (d, 1H, $^3J = 9.5$, H-3), 6.83 (d, 1H, $^3J = 8.5$, H-6), 7.33 (d, 1H, $^3J = 8.5$, H-5), 7.61 (d, 1H, $^3J = 9.5$, H-4); ^{13}C NMR (100 MHz, CDCl_3) δ_{C} 20.62 (COCH_3), 23.31 (C-1'), 25.18 (C-4'), 26.50 (C-5'), 56.15 (OCH_3), 72.48 (C-3'), 79.10 (C-2'), 107.19 (C-6), 112.74 (C-4a), 112.96 (C-3), 114.75 (C-8), 127.20 (C-5), 143.71 (C-4), 153.47 (C-8a), 160.70 (C-7), 161.03 (C-2), 170.51 (C-1').

Compound 15

Compound **15** was identified as *umbelliprenin* through the study of the 1D spectra (^1H and ^{13}C NMR), and 2D NMR (DQF-COSY, HSQC, HMBC) and for comparison with data reported in the literature.¹⁰⁷

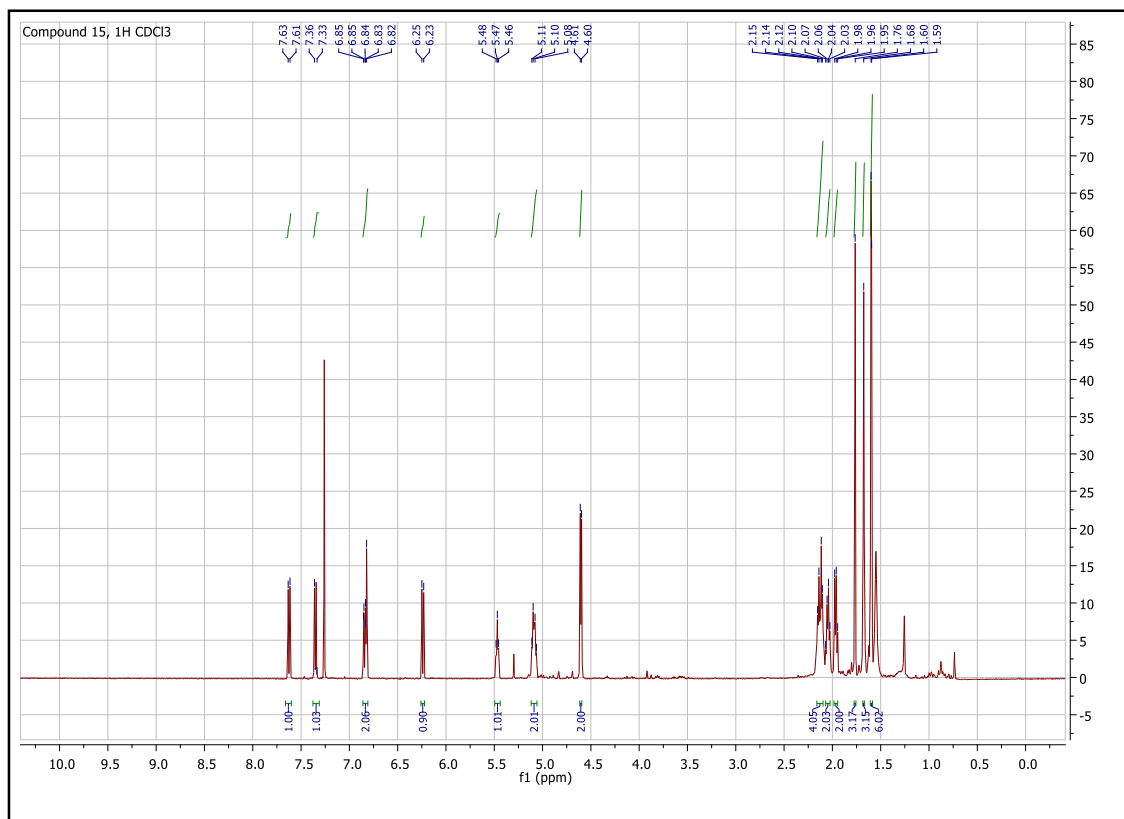


Figure 79. ^1H NMR Spectrum of compound **15** measured in CD_3Cl , 500 MHz

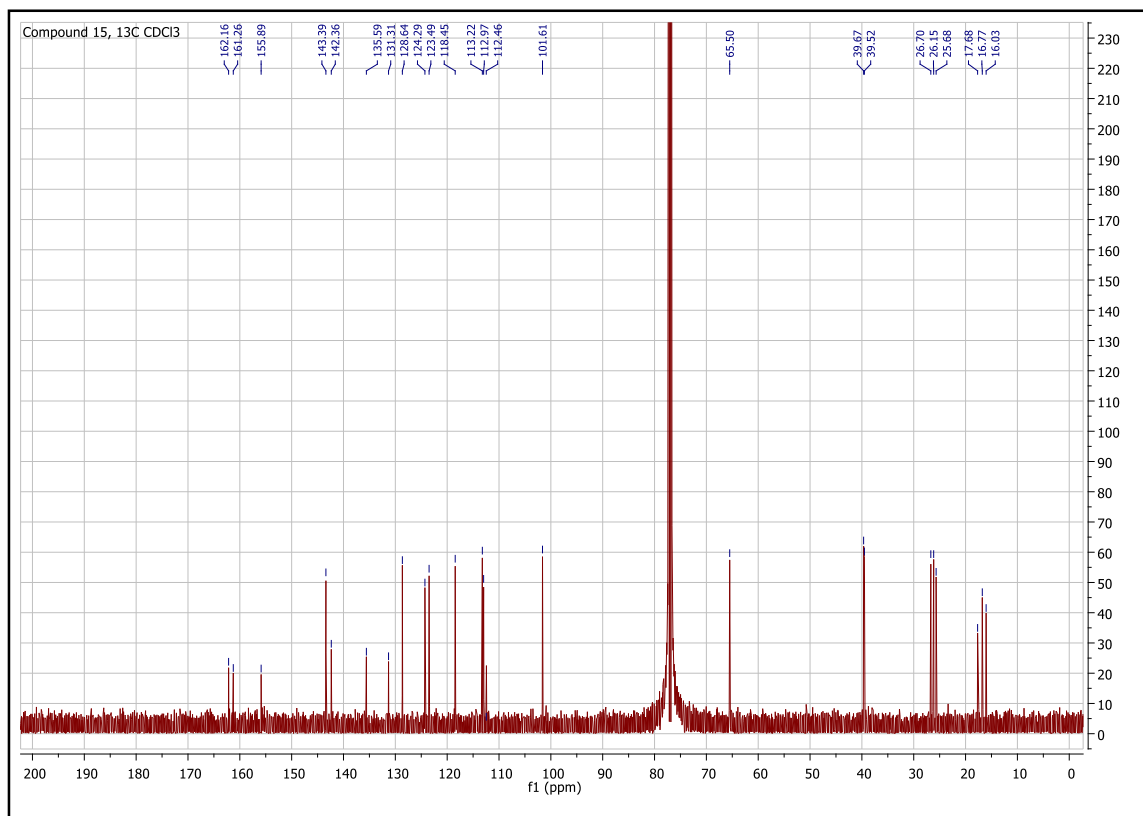


Figure 80. ^{13}C NMR Spectrum of compound **15** measured in CD_3Cl , 100 MHz

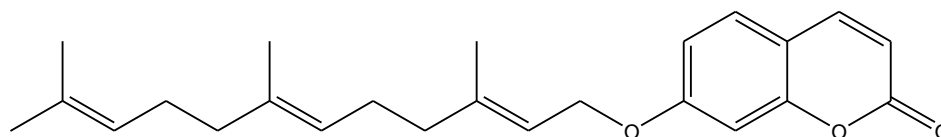


Figure 81. ^1H NMR (500 MHz, CDCl_3) δ_{H} 1.59 (d, 6H, H-14', H-15'), 1.68 (s, 3H, H-13'), 1.76 (s, 3H, H-12'), 1.97 (t, 2H, H-7', H-9'), 2.05 (m, 2H, H-8'), 2.13 (m, 4H, H-4', H-5') 4.60 (d, 2H, $^3J = 7.0$, H-1') 5.09 (m, 2H, H-6', H-10'), 5.47 (t, 1H, H-2'), 6.24 (d, 1H, $^3J = 5.5$, H-3), 6.83 (t, 1H, H-8), 6.85 (d, 1H, $^4J = 2.0$, H-6), 7.35 (d, 1H, $^3J = 8.5$, H-5), 7.62 (d, 1H, $^3J = 9.0$, H-4); ^{13}C NMR (100 MHz, CDCl_3) δ_{C} 16.04 (C-13'), 16.77 (C-12'), 17.68 (C-15'), 25.68 (C-14'), 26.15 (C-5'), 26.70 (C-9'), 39.52 (C-4'), 39.67 (C-8'), 65.50 (C-1'), 101.61 (C-8), 112.43 (C-4a), 112.97 (C-3), 113.22 (C-2'), 118.45 (C-6), 123.49 (C-10'), 124.29 (C-6'), 128.64 (C-5), 131.31 (C-11'), 135.59 (C-7'), 142.36 (C-3'), 143.39 (C-4), 155.89 (C-8a), 161.26 (C-2), 162.17 (C-7) ppm.

4.6.3 Molecular modelling

4.6.3.1 Ligand preparation

The ligands were built within the Maestro platform. The most stable conformation has been determined by molecular mechanics conformational analysis performed with MacroModel software version 9.2.¹⁰⁶ using the Merck Molecular Force Fields (MMFFs)¹⁰⁸ and GB/SA water implicit solvation model,¹⁰⁹ Polak-Ribier Conjugate Gradient (PRCG) method, 5000 iterations and a convergence criterion of 0.05 kcal/(mol Å). All the other parameters were left as default.

4.6.3.2 Protein preparation

The coordinates for CA enzyme was taken from the RCSB Protein Data Bank¹¹⁰ (PDB codes 4ww8).¹¹¹ The protein was prepared by using the Maestro Protein Preparation Wizard. Original water molecules were removed.

4.6.3.3 Docking protocol

Molecular docking studies were performed using QMPL workflow protocol. Grids were defined around the refined structure by centering on crystallized ligand. The other settings were left as default.

4.6.3.4 Post docking protocol

In order to better take into account, the induced fit phenomena, the most energy favored generated complexes were fully optimized with the OPLS2005 force field in GB/SA implicit water.¹¹² The optimization process was performed setting 10000 steps interactions up to the derivative convergence criterion equal to 0.05 kJ/(mol*Å). The resulting complexes were considered for the binding modes graphical analysis with Pymol and Maestro.

4.6.4 Biological evaluation

4.6.4.1 Carbonic anhydrase inhibition assay

An Applied Photophysics stopped-flow instrument has been used for assaying the CA catalyzed CO₂ hydration activity.¹¹³ Phenol red (at a concentration of 0.2 mM) was used as indicator, working at the absorbance maximum of 557 nm, with 20 mM Hepes (pH 7.5) as buffer and 20 mM Na₂SO₄ (for maintaining constant the ionic strength), following the initial rates of the CA-catalyzed CO₂ hydration reaction for a period of 10–100 s. The CO₂ concentrations ranged from 1.7 to 17 mM for the determination of the kinetic parameters and inhibition constants. For each inhibitor, at least six traces of the initial 5–10% of the reaction have been used for determining the initial velocity. The uncatalyzed rates were determined in the same manner and subtracted from the total observed rates. Stock solutions of inhibitor (0.1 mM) were prepared in distilled–deionized water, and dilutions up to 0.01 nM were done thereafter with the assay buffer. Inhibitor and enzyme solutions were preincubated together for 6 hours at room temperature prior to assay in order to allow for the formation of the E–I complex. The inhibition constants were obtained by nonlinear least-squares methods using PRISM 3 and the Cheng–Prusoff equation, as reported earlier,^{114–120} and represent the mean from at least three different determinations. All CA isoforms were recombinant ones obtained in-house as reported earlier.^{121–124}

4.6.4.2 Cytotoxic activity

4.6.4.2.1 Cell culture

Human carcinoma HeLa cell line was obtained from the American Type Culture Collection (ATCC, Rockville, MD). Cells were grown in Dulbecco's modified Eagle's medium (DMEM) with high glucose, supplemented with 10% foetal calf serum (FCS), penicillin (100 units/mL)–streptomycin (100 µg/mL), and 2 mM L-glutamine in a 5% CO₂ incubator at 37 °C. Subcultures of the HeLa cells were grown in T-75 culture flasks and passaged with a trypsin-EDTA solution. Cell culture materials were purchased from Invitrogen (Milan, Italy).

4.6.4.2.2 MTT assay

The *in vitro* cytotoxic effect of coumarins **5**, **9-12**, **15** was evaluated in cancer HeLa cells by the MTT (3-(4,5-dimethylthiazol-2-yl)-2,5-diphenyltetrazolium bromide) reduction assay.¹²⁵ Cancer cells were seeded in 96-well plates (density of 3×10^4 cells/mL) in 100 μ L of medium and cultured for 48 h (80% of cell confluence). Cells were subsequently incubated for 48 h with various concentrations (0.1-100 μ M, dissolved in DMSO) of coumarins in culture medium (treated cells). Treated cells were compared for viability to untreated cells (control cells) and vehicle-treated cells (incubated for 48 h with an equivalent volume of DMSO; the maximal final concentration was 1%). After the cell medium removing and washing, cells were subjected to the MTT test (Rosa et al., 2017). After incubation (3 h), colour development was measured at 570 nm with an Infinite 200 auto microplate reader (Infinite 200, Tecan, Austria); the absorbance is proportional to the number of viable cells. Two independent experiments were performed. The results were calculated as the percentage of cell viability in comparison with non-treated control cells and expressed as IC₅₀ value (the concentration of compound that reduces the cell viability to 50%).

4.7 REFERENCES

1. Pignatti, S. *Flora d'Italia*. 1982; Vol. 2.
2. Euro + Med Plantbase. <http://ww2.bgbm.org/EuroPlusMed/query.asp>
3. Fiori, A. *Nuova Flora Analitica d'Italia vol. II*. 1969.
4. Cerri, R. P., G.; Dessi, G.; Asproni, B.; Piseddu, G.; Sini, S.; Isolation, characterization and pharmacological activity of magydaris pastinacea (lam) paol. Glucosides. *IL FARMACO* **1995**, 50, 841-848.
5. Cerri, R. D., G.; Manconi, P.M.; Serra, D.; Pau, A.; Glycosides of the magydaris pastinacea l. *Pharmacological Research Communication* **1988**, 20, 109-112.
6. Camarda, L. D. S., V.; Lentini, F.; Mazzola, P.; Coumarins from the fruits of Magydaris pastinacea. *Fitoterapia* **1996**, 67, 282.
7. Rosselli, S. M., A.; Bellone, G.; Formisano, C.; Basile, A.; Cicala, C.; Alfieri, A.; Mascolo, N.; Bruno, M.; Antibacterial and anticoagulant activities of coumarins isolated from the flowers of Magydaris tomentosa. *Planta medica* **2007**, 73, 116-120.
8. Rosselli, S. M., AM.; Bellone, G.; Formisano, C.; Senatore, F.; Bruno, M.; A new irregular diterpenoid of biogenetic interest from the flowers of Magydaris tomentosa (Desf.) DC. (Apiaceae). *Nat Prod Commun* **2007**, 2, 5-8.
9. Khaoukha, G.; Ben Jemia, M.; Amira, S.; Laouer, H.; Bruno, M.; Scandolera, E.; Senatore, F. Characterisation and antimicrobial activity of the volatile components of the flowers of Magydaris tomentosa (Desf.) DC. collected in Sicily and Algeria. *Natural product research* **2014**, 28, 1152-1158.
10. Autore, G.; Marzocco, S.; Formisano, C.; Bruno, M.; Rosselli, S.; Jemia, M. B.; Senatore, F. Cytotoxic activity and composition of petroleum ether extract from Magydaris tomentosa (Desf.) W. D. J. Koch (Apiaceae). *Molecules* **2015**, 20, 1571-1578.
11. Abdel Hafez, O. M.; Amin, K. M.; Abdel-Latif, N. A.; Mohamed, T. K.; Ahmed, E. Y.; Maher, T. Synthesis and antitumor activity of some new xanthotoxin derivatives. *European journal of medicinal chemistry* **2009**, 44, 2967-74.
12. Maneerat, W. P., U.; Saewan, N.; Laphookhieo, S.; New coumarins from Clausena lansium twigs. *J. Braz. Chem. Soc.* **2010**, 2.
13. Conforti, F. M., M.; Menichini, F.; Bonesi, M.; Statti, G.; Provenzano, E.; Menichini, F.; Natural and synthetic furanocoumarins as treatment for vitiligo and psoriasis. *Curr. Drug Ther.* **2009**, 4, 38-58.
14. Lindskog, S.; Silverman, D. N. The catalytic mechanism of mammalian carbonic anhydrases. *Exs* **2000**, 175-195.
15. Hewett-Emmett, D. Evolution and distribution of the carbonic anhydrase gene families. *Exs* **2000**, 29-76.
16. Sly, W. S.; Hu, P. Y. Human carbonic anhydrases and carbonic anhydrase deficiencies. *Annual review of biochemistry* **1995**, 64, 375-401.
17. Supuran, C. T.; Scozzafava, A.; Casini, A. Carbonic anhydrase inhibitors. *Medicinal research reviews* **2003**, 23, 146-189.
18. Supuran, C. T. a. S., A.; Carbonic anhydrase inhibitors and their therapeutic potential. *Expert Opinion on Therapeutic Patents* **2000**, 10, 575-600.
19. Supuran, C. T. a. S., A.; Applications of carbonic anhydrase inhibitors and activators in therapy. *Expert Opinion on Therapeutic Patents* **2002**, 12, 217-242.
20. Capasso, C.; Supuran, C. T. An overview of the alpha-, beta- and gamma-carbonic anhydrases from Bacteria: can bacterial carbonic anhydrases shed new light on evolution of bacteria? *Journal of enzyme inhibition and medicinal chemistry* **2015**, 30, 325-332.
21. Del Prete, S.; De Luca, V.; De Simone, G.; Supuran, C. T.; Capasso, C. Cloning, expression and purification of the complete domain of the eta-carbonic anhydrase from Plasmodium falciparum. *Journal of enzyme inhibition and medicinal chemistry* **2016**, 31, 54-59.
22. Supuran, C. T. Structure and function of carbonic anhydrases. *The Biochemical journal* **2016**, 473, 2023-2032.
23. Supuran, C. T.; Capasso, C. New light on bacterial carbonic anhydrases phylogeny based on the analysis of signal peptide sequences. *Journal of enzyme inhibition and medicinal chemistry* **2016**, 31, 1254-1260.
24. Supuran, C. T. Carbonic anhydrases: novel therapeutic applications for inhibitors and activators. *Nature reviews. Drug discovery* **2008**, 7, 168-181.
25. Supuran, C. T. Carbonic anhydrase inhibitors. *Bioorganic & medicinal chemistry letters* **2010**, 20, 3467-3474.
26. Vullo, D.; De Luca, V.; Del Prete, S.; Carginale, V.; Scozzafava, A.; Capasso, C.; Supuran, C. T. Sulfonamide inhibition studies of the gamma-carbonic anhydrase from the Antarctic cyanobacterium Nostoc commune. *Bioorganic & medicinal chemistry* **2015**, 23, 1728-1734.
27. Del Prete, S.; Vullo, D.; De Luca, V.; Supuran, C. T.; Capasso, C. Biochemical characterization of the delta-carbonic anhydrase from the marine diatom Thalassiosira weissflogii, TweCA. *Journal of enzyme inhibition and medicinal chemistry* **2014**, 29, 906-911.
28. Elleuche, S.; Poggeler, S. Carbonic anhydrases in fungi. *Microbiology (Reading, England)* **2010**, 156, 23-29.
29. Supuran, C. T. Carbonic Anhydrases and Metabolism. *Metabolites* **2018**, 8, 1-5.
30. Xu, Y.; Feng, L.; Jeffrey, P. D.; Shi, Y.; Morel, F. M. Structure and metal exchange in the cadmium carbonic anhydrase of marine diatoms. *Nature* **2008**, 452, 56-61.

31. Zimmerman, S. A.; Ferry, J. G.; Supuran, C. T. Inhibition of the archaeal beta-class (Cab) and gamma-class (Cam) carbonic anhydrases. *Current topics in medicinal chemistry* **2007**, *7*, 901-908.
32. Supuran, C. T.; Capasso, C. The eta-class carbonic anhydrases as drug targets for antimalarial agents. *Expert opinion on therapeutic targets* **2015**, *19*, 551-63.
33. Masini, E.; Carta, F.; Scozzafava, A.; Supuran, C. T. Antiglaucoma carbonic anhydrase inhibitors: a patent review. *Expert Opin Ther Pat* **2013**, *23*, 705-716.
34. Aggarwal, M.; Kondeti, B.; McKenna, R. Anticonvulsant/antiepileptic carbonic anhydrase inhibitors: a patent review. *Expert Opin Ther Pat* **2013**, *23*, 717-724.
35. Buzas, G. M.; Supuran, C. T. The history and rationale of using carbonic anhydrase inhibitors in the treatment of peptic ulcers. In memoriam Ioan Puscas (1932-2015). *Journal of enzyme inhibition and medicinal chemistry* **2016**, *31*, 527-533.
36. Carradori, S.; Mollica, A.; De Monte, C.; Ganese, A.; Supuran, C. T. Nitric oxide donors and selective carbonic anhydrase inhibitors: a dual pharmacological approach for the treatment of glaucoma, cancer and osteoporosis. *Molecules* **2015**, *20*, 5667-5679.
37. Supuran, C. T.; Di Fiore, A.; De Simone, G. Carbonic anhydrase inhibitors as emerging drugs for the treatment of obesity. *Expert opinion on emerging drugs* **2008**, *13*, 383-392.
38. Supuran, C. T. Carbonic Anhydrase Inhibition and the Management of Hypoxic Tumors. *Metabolites* **2017**, *7*.
39. Kumar, R.; Sharma, V.; Bua, S.; Supuran, C. T.; Sharma, P. K. Synthesis and biological evaluation of benzenesulphonamide-bearing 1,4,5-trisubstituted-1,2,3-triazoles possessing human carbonic anhydrase I, II, IV, and IX inhibitory activity. *Journal of enzyme inhibition and medicinal chemistry* **2017**, *32*, 1187-1194.
40. Karali, N.; Akdemir, A.; Goktas, F.; Eraslan Elma, P.; Angeli, A.; Kizilirmak, M.; Supuran, C. T. Novel sulfonamide-containing 2-indolinones that selectively inhibit tumor-associated alpha carbonic anhydrases. *Bioorganic & medicinal chemistry* **2017**, *25*, 3714-3718.
41. D'Ascenzio, M.; Guglielmi, P.; Carradori, S.; Secci, D.; Florio, R.; Mollica, A.; Ceruso, M.; Akdemir, A.; Sobolev, A. P.; Supuran, C. T. Open saccharin-based secondary sulfonamides as potent and selective inhibitors of cancer-related carbonic anhydrase IX and XII isoforms. *Journal of enzyme inhibition and medicinal chemistry* **2017**, *32*, 51-59.
42. Queen, A.; Khan, P.; Azam, A.; Hassan, M. I. Understanding the Role and Mechanism of Carbonic Anhydrase V in Obesity and its Therapeutic Implications. *Current protein & peptide science* **2018**, *19*, 909-923.
43. Lomelino, C. L.; Supuran, C. T.; McKenna, R. Non-Classical Inhibition of Carbonic Anhydrase. *International journal of molecular sciences* **2016**, *17*.
44. Supuran, C. T. Carbonic anhydrase inhibition and the management of neuropathic pain. *Expert review of neurotherapeutics* **2016**, *16*, 961-8.
45. Saad, A. E.; Ashour, D. S.; Abou Rayia, D. M.; Bedeer, A. E. Carbonic anhydrase enzyme as a potential therapeutic target for experimental trichinellosis. *Parasitology research* **2016**, *115*, 2331-2339.
46. Carta, F.; Maresca, A.; Covarrubias, A. S.; Mowbray, S. L.; Jones, T. A.; Supuran, C. T. Carbonic anhydrase inhibitors. Characterization and inhibition studies of the most active beta-carbonic anhydrase from Mycobacterium tuberculosis, Rv3588c. *Bioorganic & medicinal chemistry letters* **2009**, *19*, 6649-6654.
47. Cox, E. H.; McLendon, G. L.; Morel, F. M.; Lane, T. W.; Prince, R. C.; Pickering, I. J.; George, G. N. The active site structure of Thalassiosira weissflogii carbonic anhydrase 1. *Biochemistry* **2000**, *39*, 12128-30.
48. Ozensoy Guler, O.; Capasso, C.; Supuran, C. T. A magnificent enzyme superfamily: carbonic anhydrases, their purification and characterization. *Journal of enzyme inhibition and medicinal chemistry* **2016**, *31*, 689-694.
49. Briganti, F.; Mangani, S.; Orioli, P.; Scozzafava, A.; Vernaglion, G.; Supuran, C. T. Carbonic anhydrase activators: X-ray crystallographic and spectroscopic investigations for the interaction of isozymes I and II with histamine. *Biochemistry* **1997**, *36*, 10384-10392.
50. Carta, F.; Supuran, C. T. Diuretics with carbonic anhydrase inhibitory action: a patent and literature review (2005 - 2013). *Expert Opin Ther Pat* **2013**, *23*, 681-691.
51. Supuran, C. T. Structure-based drug discovery of carbonic anhydrase inhibitors. *Journal of enzyme inhibition and medicinal chemistry* **2012**, *27*, 759-772.
52. Scozzafava, A.; Supuran, C. T.; Carta, F. Antiobesity carbonic anhydrase inhibitors: a literature and patent review. *Expert Opin Ther Pat* **2013**, *23*, 725-735.
53. Supuran, C. T. Advances in structure-based drug discovery of carbonic anhydrase inhibitors. *Expert opinion on drug discovery* **2017**, *12*, 61-88.
54. Capasso, C.; Supuran, C. T. Sulfa and trimethoprim-like drugs - antimetabolites acting as carbonic anhydrase, dihydropteroate synthase and dihydrofolate reductase inhibitors. *Journal of enzyme inhibition and medicinal chemistry* **2014**, *29*, 379-387.
55. Scozzafava, A.; Carta, F.; Supuran, C. T. Secondary and tertiary sulfonamides: a patent review (2008 - 2012). *Expert Opin Ther Pat* **2013**, *23*, 203-213.
56. Carta, F.; Di Cesare Mannelli, L.; Pinard, M.; Ghelardini, C.; Scozzafava, A.; McKenna, R.; Supuran, C. T. A class of sulfonamide carbonic anhydrase inhibitors with neuropathic pain modulating effects. *Bioorganic & medicinal chemistry* **2015**, *23*, 1828-1840.

57. Di Cesare Mannelli, L.; Micheli, L.; Carta, F.; Cozzi, A.; Ghelardini, C.; Supuran, C. T. Carbonic anhydrase inhibition for the management of cerebral ischemia: in vivo evaluation of sulfonamide and coumarin inhibitors. *Journal of enzyme inhibition and medicinal chemistry* **2016**, *31*, 894-899.
58. Lou, Y.; McDonald, P. C.; Oloumi, A.; Chia, S.; Ostlund, C.; Ahmadi, A.; Kyle, A.; Auf dem Keller, U.; Leung, S.; Huntsman, D.; Clarke, B.; Sutherland, B. W.; Waterhouse, D.; Bally, M.; Roskelley, C.; Overall, C. M.; Minchinton, A.; Pacchiano, F.; Carta, F.; Scozzafava, A.; Touisni, N.; Winum, J. Y.; Supuran, C. T.; Dedhar, S. Targeting tumor hypoxia: suppression of breast tumor growth and metastasis by novel carbonic anhydrase IX inhibitors. *Cancer research* **2011**, *71*, 3364-3376.
59. Neri, D.; Supuran, C. T. Interfering with pH regulation in tumours as a therapeutic strategy. *Nature reviews. Drug discovery* **2011**, *10*, 767-777.
60. Supuran, C. T.; Scozzafava, A. Carbonic anhydrases as targets for medicinal chemistry. *Bioorganic & medicinal chemistry* **2007**, *15*, 4336-4350.
61. Supuran, C. T. How many carbonic anhydrase inhibition mechanisms exist? *Journal of enzyme inhibition and medicinal chemistry* **2016**, *31*, 345-360.
62. Supuran, C. T. Drug interaction considerations in the therapeutic use of carbonic anhydrase inhibitors. *Expert opinion on drug metabolism & toxicology* **2016**, *12*, 423-431.
63. De Simone, G.; Scozzafava, A.; Supuran, C. T. Which carbonic anhydrases are targeted by the antiepileptic sulfonamides and sulfamates? *Chemical biology & drug design* **2009**, *74*, 317-321.
64. Klonoff, D. C.; Greenway, F. Drugs in the pipeline for the obesity market. *Journal of diabetes science and technology* **2008**, *2*, 913-918.
65. Colinas, P. A.; Bravo, R. D.; Vullo, D.; Scozzafava, A.; Supuran, C. T. Carbonic anhydrase inhibitors. Inhibition of cytosolic isoforms I and II, and extracellular isoforms IV, IX, and XII with sulfamides incorporating sugar moieties. *Bioorganic & medicinal chemistry letters* **2007**, *17*, 5086-5090.
66. Stiti, M.; Cecchi, A.; Rami, M.; Abdaoui, M.; Barragan-Montero, V.; Scozzafava, A.; Guari, Y.; Winum, J. Y.; Supuran, C. T. Carbonic anhydrase inhibitor coated gold nanoparticles selectively inhibit the tumor-associated isoform IX over the cytosolic isozymes I and II. *Journal of the American Chemical Society* **2008**, *130*, 16130-16131.
67. Ciani, L.; Cecchi, A.; Temperini, C.; Supuran, C. T.; Ristori, S. Dissecting the inhibition mechanism of cytosolic versus transmembrane carbonic anhydrases by ESR. *The journal of physical chemistry. B* **2009**, *113*, 13998-4005.
68. Carta, F.; Temperini, C.; Innocenti, A.; Scozzafava, A.; Kaila, K.; Supuran, C. T. Polyamines inhibit carbonic anhydrases by anchoring to the zinc-coordinated water molecule. *Journal of medicinal chemistry* **2010**, *53*, 5511-5522.
69. Innocenti, A. V. D.; Scozzafava, A.; Supuran, C. T. Carbonic anhydrase inhibitors. Interactions of phenols with the 12 catalytically active mammalian isoforms (CA I–XIV). *Bioorg Med Chem Lett* **2008**, *18*, 1583-1587.
70. Martin, D. P.; Cohen, S. M. Nucleophile recognition as an alternative inhibition mode for benzoic acid based carbonic anhydrase inhibitors. *Chemical communications (Cambridge, England)* **2012**, *48*, 5259-5261.
71. Davis, R. A.; Hofmann, A.; Osman, A.; Hall, R. A.; Muhlschlegel, F. A.; Vullo, D.; Innocenti, A.; Supuran, C. T.; Poulsen, S. A. Natural product-based phenols as novel probes for mycobacterial and fungal carbonic anhydrases. *Journal of medicinal chemistry* **2011**, *54*, 1682-1692.
72. Tars, K.; Vullo, D.; Kazaks, A.; Leitans, J.; Lends, A.; Grandane, A.; Zalubovskis, R.; Scozzafava, A.; Supuran, C. T. Sulfocoumarins (1,2-benzoxathiine-2,2-dioxides): a class of potent and isoform-selective inhibitors of tumor-associated carbonic anhydrases. *Journal of medicinal chemistry* **2013**, *56*, 293-300.
73. Ekinci, D.; Karagoz, L.; Ekinci, D.; Senturk, M.; Supuran, C. T. Carbonic anhydrase inhibitors: in vitro inhibition of alpha isoforms (hCA I, hCA II, bCA III, hCA IV) by flavonoids. *Journal of enzyme inhibition and medicinal chemistry* **2013**, *28*, 283-288.
74. Maresca, A.; Temperini, C.; Pochet, L.; Masereel, B.; Scozzafava, A.; Supuran, C. T. Deciphering the mechanism of carbonic anhydrase inhibition with coumarins and thiocoumarins. *Journal of medicinal chemistry* **2010**, *53*, 335-344.
75. Murray, R. M., J.; Brown, S.A. The Natural Coumarins: Occurrence, Chemistry and Biochemistry. *Wiley* **1982**.
76. Borges, F.; Roleira, F.; Milhazes, N.; Santana, L.; Uriarte, E. Simple coumarins and analogues in medicinal chemistry: occurrence, synthesis and biological activity. *Curr Med Chem* **2005**, *12*, 887-916.
77. Maresca, A.; Temperini, C.; Vu, H.; Pham, N. B.; Poulsen, S. A.; Scozzafava, A.; Quinn, R. J.; Supuran, C. T. Non-zinc mediated inhibition of carbonic anhydrases: coumarins are a new class of suicide inhibitors. *Journal of the American Chemical Society* **2009**, *131*, 3057-3062.
78. Thiry, A.; Dogne, J. M.; Masereel, B.; Supuran, C. T. Targeting tumor-associated carbonic anhydrase IX in cancer therapy. *Trends in pharmacological sciences* **2006**, *27*, 566-573.
79. Davis, R. A. V., D.; Maresca, A.; Supuran, C. T.; Poulsen, S. A. Natural product coumarins that inhibit human carbonic anhydrases. *Bioorganic & medicinal chemistry* **2013**, *21*, 1539-1543.
80. Winum, J. Y.; Colinas, P. A.; Supuran, C. T. Glycosidic carbonic anhydrase IX inhibitors: a sweet approach against cancer. *Bioorganic & medicinal chemistry* **2013**, *21*, 1419-1426.
81. Touisni, N.; Maresca, A.; McDonald, P. C.; Lou, Y.; Scozzafava, A.; Dedhar, S.; Winum, J. Y.; Supuran, C. T. Glycosyl coumarin carbonic anhydrase IX and XII inhibitors strongly attenuate the growth of primary breast tumors. *Journal of medicinal chemistry* **2011**, *54*, 8271-8277.

82. Maresca, A.; Supuran, C. T. Coumarins incorporating hydroxy- and chloro-moieties selectively inhibit the transmembrane, tumor-associated carbonic anhydrase isoforms IX and XII over the cytosolic ones I and II. *Bioorganic & medicinal chemistry letters* **2010**, *20*, 4511-4514.
83. De Luca, L.; Mancuso, F.; Ferro, S.; Buemi, M. R.; Angeli, A.; Del Prete, S.; Capasso, C.; Supuran, C. T.; Gitto, R. Inhibitory effects and structural insights for a novel series of coumarin-based compounds that selectively target human CA IX and CA XII carbonic anhydrases. *European journal of medicinal chemistry* **2018**, *143*, 276-282.
84. Nocentini, A.; Carta, F.; Ceruso, M.; Bartolucci, G.; Supuran, C. T. Click-tailed coumarins with potent and selective inhibitory action against the tumor-associated carbonic anhydrases IX and XII. *Bioorganic & medicinal chemistry* **2015**, *23*, 6955-6966.
85. Melis, C.; Distinto, S.; Bianco, G.; Meleddu, R.; Cottiglia, F.; Fois, B.; Taverna, D.; Angius, R.; Alcaro, S.; Ortuso, F.; Gaspari, M.; Angeli, A.; Del Prete, S.; Capasso, C.; Supuran, C. T.; Maccioni, E. Targeting Tumor Associated Carbonic Anhydrases IX and XII: Highly Isozyme Selective Coumarin and Psoralen Inhibitors. *ACS medicinal chemistry letters* **2018**, *9*, 725-729.
86. Snatzke, G. Circulardichroismus—X : Modifizierung der octantenregel für α,β -ungesättigte ketone: cisoide enone, dienone und arylketone. *Tetrahedron* **1965**, *21*, 439-448.
87. Lin, S.; Zhang, Y.; Liu, M.; Yang, S.; Gan, M.; Zi, J.; Song, W.; Fan, X.; Wang, S.; Liu, Y.; Yang, Y.; Chen, X.; Guo, Y.; Wang, W.; Shi, J.; Abietane and C20-Norabietane Diterpenes from the Stem Bark of *Fraxinus sieboldiana* and Their Biological Activities. *J.Nat. Prod.* **2010**, *73*, 1914-1921.
88. Elgamal, M. H. A. S.; N.M.M.; Duddeck, H.; Hiegemann, M.; Coumarins and coumarin glucosides from the fruits of *Ammi majus*. *Phytochemistry* **1993**, *34*, 813-823.
89. Atta Ur, R.; Sultana, N.; Khan, M. R.; Choudhary, M. I. Triterpene and coumarins from *Skimmia laureola*. *Natural product letters* **2002**, *16*, 305-313.
90. Boyd, D. R.; Sharma, N. D.; Loke, P. L.; Malone, J. F.; McRoberts, W. C.; Hamilton, J. T. Absolute configuration assignment and enantiopurity determination of chiral alkaloids and coumarins derived from O- and C-prenyl epoxides. *Chemical communications (Cambridge, England)* **2002**, 3070-3071.
91. Trani, M. C., A.; Delle Monache, G.; Delle Monache, F.; Dihydrochalcones and coumarins of *Esenbeckia grandiflora* subsp. *brevipetiolata*. *Fitoterapia* **2004**, *75*, 99-102.
92. Kikuchi, T. Y., T.; Umemoto, K.; Shingu, T.; Constituents of *Scaevola frutescens* (Miller) Krause. *Yakugaku Zasshi* **1974**, *94*, 1616-1619.
93. Abou-Elzahab, M. M. A., W.; Saha-Moller, C.R.; Synthesis of Furocoumarin-Type Potential Intercalative Alkylating and Oxidizing Agents of DNA Through Dimethyldioxirane Epoxidation of Imperatorin and Its Derivatives. *Liebigs Ann. Chem* **1992**, 731-733.
94. Bergendorff, O. D., K.; Nielsen, M.; Shan, R.; Witt, R.; Ai, J.; Sterner, O.; Furanocoumarins with affinity to brain benzodiazepine receptors in vitro. *Phytochemistry* **1997**, *44*, 1121-1124.
95. Lv, X.; Xin, X.-L.; Deng, S.; Zhang, B.-J.; Hou, J.; Ma, X.-C.; Wang, C.-y.; Wang, Z.-B.; Kuang, H.-X. Biotransformation of osthole by *Mucor spinosus*. *Process Biochemistry* **2012**, *47*, 2542-2546.
96. Thongthoom, T.; Songsiang, U.; Phaosiri, C.; Yenjai, C. Biological activity of chemical constituents from *Clausena harmandiana*. *Archives of pharmacal research* **2010**, *33*, 675-680.
97. Yan, R.; Shen, J.; Liu, X.; Zou, Y.; Xu, X. Preparative isolation and purification of hainanmurpanin, meranzin, and phebalosin from leaves of *Murraya exotica* L. using supercritical fluid extraction combined with consecutive high-speed countercurrent chromatography. *Journal of separation science* **2018**, *41*, 2092-2101.
98. Yoo SW, K. J., Kang SS, Son KH, Chang HW, Kim HP, Bae K, Lee CO. Constituents of the Fruits and Leaves of *Euodia daniellii*. *Archives of pharmacal research* **2002**, *25*, 824-830.
99. Melis, C.; Distinto, S.; Bianco, G.; Meleddu, R.; Cottiglia, F.; Fois, B.; Taverna, D.; Angius, R.; Alcaro, S.; Ortuso, F.; Gaspari, M.; Angeli, A.; Del Prete, S.; Capasso, C.; Supuran, C. T.; Maccioni, E. Targeting Tumor Associated Carbonic Anhydrases IX and XII: Highly Isozyme Selective Coumarin and Psoralen Inhibitors. *ACS Medicinal Chemistry Letters* **2018**, *9*, 725-729.
100. Rashidi, M.; Ahmadzadeh, A.; Ziai, S. A.; Narenji, M.; Jamshidi, H. Evaluating cytotoxic effect of nanoliposomes encapsulated with umbelliprenin on 4T1 cell line. *In vitro cellular & developmental biology. Animal* **2017**, *53*, 7-11.
101. Hasan, M.; Genovese, S.; Fiorito, S.; Epifano, F.; Witt-Enderby, P. A. Oxyprenylated Phenylpropanoids Bind to MT1 Melatonin Receptors and Inhibit Breast Cancer Cell Proliferation and Migration. *J Nat Prod* **2017**, *80*, 3324-3329.
102. Rashidi, M.; Khalilnezhad, A.; Amani, D.; Jamshidi, H.; Muhammadnejad, A.; Bazi, A.; Ziai, S. A. Umbelliprenin shows antitumor, antiangiogenesis, antimetastatic, anti-inflammatory, and immunostimulatory activities in 4T1 tumor-bearing Balb/c mice. *Journal of cellular physiology* **2018**, *233*, 8908-8918.
103. Zhang, L.; Sun, X.; Si, J.; Li, G.; Cao, L. Umbelliprenin isolated from *Ferula sinkiangensis* inhibits tumor growth and migration through the disturbance of Wnt signaling pathway in gastric cancer. *PLoS one* **2019**, *14*, e0207169.
104. Farooq, S.; Shakeel u, R.; Dangroo, N. A.; Priya, D.; Banday, J. A.; Sangwan, P. L.; Qurishi, M. A.; Koul, S.; Saxena, A. K. Isolation, cytotoxicity evaluation and HPLC-quantification of the chemical constituents from *Prangos pabularia*. *PLoS one* **2014**, *9*.

105. Hitotsuyanagi, Y. K., H. Ikuta Yukio, H. et al. Identification and structure-activity relationship studies of osthol, a cytotoxic principle from *Cnidium monnieri*. *Bioorganic & medicinal chemistry letters* **1996**, 6, 1791-1794.
106. Mohamadi, F.; Richards, N. G.; Guida, W. C.; Liskamp, R.; Lipton, M.; Caufield, C.; Chang, G.; Hendrickson, T.; Still, W. C. MacroModel—an integrated software system for modeling organic and bioorganic molecules using molecular mechanics. *Journal of Computational Chemistry* **1990**, 11, 440-467.
107. Mehrdad Iranshahi, A. R. S., Roohollah Mirjani, Gholamreza Amin, and Abbas Shafiee. Umbelliprenin from *Ferula persica* Roots Inhibits the Red Pigment Production in *Serratia marcescens*. *Z Naturforsch C* **2004**, 69, 506-508.
108. Halgren, T. A. Merck molecular force field. II. MMFF94 van der Waals and electrostatic parameters for intermolecular interactions. *Journal of Computational Chemistry* **1996**, 17, 520-552.
109. Kollman, P. A.; Massova, I.; Reyes, C.; Kuhn, B.; Huo, S.; Chong, L.; Lee, M.; Lee, T.; Duan, Y.; Wang, W.; Donini, O.; Cieplak, P.; Srinivasan, J.; Case, D. A.; Cheatham, T. E. Calculating structures and free energies of complex molecules: combining molecular mechanics and continuum models. *Accounts of Chemical Research* **2000**, 33, 889-897.
110. Berman, H. M.; Westbrook, J.; Feng, Z.; Gilliland, G.; Bhat, T. N.; Weissig, H.; Shindyalov, I. N.; Bourne, P. E. The Protein Data Bank. *Nucleic Acids Research* **2000**, 28, 235-242.
111. Zubrienė, A.; Smirnovienė, J.; Smirnov, A.; Morkūnaitė, V.; Michailovienė, V.; Jachno, J.; Juozapaitienė, V.; Norvaiša, P.; Manakova, E.; Gražulis, S.; Matulis, D. Intrinsic thermodynamics of 4-substituted-2,3,5,6-tetrafluorobenzenesulfonamide binding to carbonic anhydrases by isothermal titration calorimetry. *Biophysical Chemistry* **2015**, 205, 51-65.
112. Jorgensen, W. L. OPLS force fields. In chemistry, E. o. c., Ed. 1998.
113. Khalifah, R. G. The carbon dioxide hydration activity of carbonic anhydrase. I. Stop-flow kinetic studies on the native human isoenzymes B and C. *The Journal of biological chemistry* **1971**, 246, 2561-2573.
114. Akocak, S.; Lolak, N.; Bua, S.; Supuran, C. T. Discovery of novel 1,3-diaryltriazene sulfonamides as carbonic anhydrase I, II, VII, and IX inhibitors. *Journal of enzyme inhibition and medicinal chemistry* **2018**, 33, 1575-1580.
115. Bua, S.; Bozdog, M.; Del Prete, S.; Carta, F.; Donald, W. A.; Capasso, C.; Supuran, C. T. Mono- and dithiocarbamate inhibition studies of the delta-carbonic anhydrase TweCAdelta from the marine diatom *Thalassiosira weissflogii*. *Journal of enzyme inhibition and medicinal chemistry* **2018**, 33, 707-713.
116. El-Gazzar, M. G.; Nafie, N. H.; Nocentini, A.; Ghorab, M. M.; Heiba, H. I.; Supuran, C. T. Carbonic anhydrase inhibition with a series of novel benzenesulfonamide-triazole conjugates. *Journal of enzyme inhibition and medicinal chemistry* **2018**, 33, 1565-1574.
117. Ferraroni, M.; Gaspari, R.; Scozzafava, A.; Cavalli, A.; Supuran, C. T. Dioxygen, an unexpected carbonic anhydrase ligand. *Journal of enzyme inhibition and medicinal chemistry* **2018**, 33, 999-1005.
118. Nocentini, A.; Bonardi, A.; Gratteri, P.; Cerra, B.; Gioiello, A.; Supuran, C. T. Steroids interfere with human carbonic anhydrase activity by using alternative binding mechanisms. *Journal of enzyme inhibition and medicinal chemistry* **2018**, 33, 1453-1459.
119. Nocentini, A.; Trallori, E.; Singh, S.; Lomelino, C. L.; Bartolucci, G.; Di Cesare Mannelli, L.; Ghelardini, C.; McKenna, R.; Gratteri, P.; Supuran, C. T. 4-Hydroxy-3-nitro-5-ureido-benzenesulfonamides Selectively Target the Tumor-Associated Carbonic Anhydrase Isoforms IX and XII Showing Hypoxia-Enhanced Antiproliferative Profiles. *Journal of medicinal chemistry* **2018**, 61, 10860-10874.
120. Ozturk Sarikaya, S. B.; Topal, F.; Senturk, M.; Gulcin, I.; Supuran, C. T. In vitro inhibition of alpha-carbonic anhydrase isozymes by some phenolic compounds. *Bioorganic & medicinal chemistry letters* **2011**, 21, 4259-4262.
121. Awadallah, F. M.; Bua, S.; Mahmoud, W. R.; Nada, H. H.; Nocentini, A.; Supuran, C. T. Inhibition studies on a panel of human carbonic anhydrases with N1-substituted secondary sulfonamides incorporating thiazolinone or imidazolone-indole tails. *Journal of enzyme inhibition and medicinal chemistry* **2018**, 33, 629-638.
122. Sentürk, M. G., I; Daştan, A. et al. . Carbonic anhydrase inhibitors. Inhibition of human erythrocyte isozymes I and II with a series of antioxidant phenols. *Bioorg Med Chem.* **2009**, 17, 3207-3211.
123. Supuran, C. T., Clare, B.W., Carbonic anhydrase inhibitors – Part 57: Quantum chemical QSAR of a group of 1,3,4-thiadiazole- and 1,3,4-thiadiazoline disulfonamides with carbonic anhydrase inhibitory properties. *European journal of medicinal chemistry* **1999**, 34, 41-50.
124. Supuran, C. T. I., M.A., Scozzafava, A.; Carbonic anhydrase inhibitors. Part 29. Interaction of isozymes I, II and IV with benzolamide-like derivatives. . *European journal of medicinal chemistry* **1998**, 33, 739-752.
125. Rosa, A. A., A.; Nieddu, M. et al. New insights into the antioxidant activity and cytotoxicity of arzanol and effect of methylation on its biological properties. . *Chemistry and Physics of Lipids* **2017**, 205, 55-64.

LIST OF PUBLICATIONS

- Vijay P. Sonar, Angela Corona, Simona Distinto, Elias Maccioni, Rita Meleddu, **Benedetta Fois**, Costantino Floris, Nilesh V. Malpure, Stefano Alcaro, Enzo Tramontano, Filippo Cottiglia, “Natural product-inspired esters and amides of ferulic and caffeic acid as dual inhibitors of HIV-1 reverse transcriptase”, *European Journal of Medicinal Chemistry*, Vol 130, Pages 248–260, **2017**, DOI:10.1016/j.ejmech.2017.02.054.
- **Benedetta Fois**, Giulia Bianco, Vijay P. Sonar, Simona Distinto, Elias Maccioni, Rita Meleddu, Claudia Melis, Luisa Marras, Raffaello Pompei, Costantino Floris, Pierluigi Caboni, and Filippo Cottiglia, “Phenylpropenoids from *Bupleurum fruticosum* as Anti-Human Rhinovirus Species A Selective Capsid Binders”, *Journal of Natural Products*, Vol 80(10), Pages 2799–2806, **2017**, DOI: 10.1021/acs.jnatprod.7b00648.
- Claudia Melis, Simona Distinto, Giulia Bianco, Rita Meleddu, Filippo Cottiglia, **Benedetta Fois**, Domenico Taverna, Rossella Angius, Stefano Alcaro, Francesco Ortuso, Marco Gaspari, Andrea Angeli, Sonia Del Prete, Clemente Capasso, Claudiu T. Supuran, and Elias Maccioni, “Targeting Tumor Associated Carbonic Anhydrases IX and XII: Highly Isozyme Selective Coumarin and Psoralen Inhibitors”, *ACS Medical Chemistry Letters*, Vol 9(7), Pages 725–729, **2018**, DOI: 10.1021/acsmchemlett.8b00170.
- Rita Meleddu, Simona Distinto, Filippo Cottiglia, Rossella Angius, Marco Gaspari, Domenico Taverna, Claudia Melis, Andrea Angeli, Giulia Bianco, Serenella Deplano, **Benedetta Fois**, Sonia Del Prete, Clemente Capasso, Stefano Alcaro, Francesco Ortuso, Matilde Yanez, Claudiu T. Supuran, and Elias Maccioni “Tuning the Dual Inhibition of Carbonic Anhydrase and Cyclooxygenase by Dihydrothiazole Benzensulfonamides”, *ACS Medical Chemistry Letters*, Vol 9(10), Pages 1045–1050, **2018**, DOI: 10.1021/acsmchemlett.8b00352.
- Rita Meleddu, Vilma Petrikaite, Simona Distinto, Antonella Arridu, Rossella Angius, Lorenzo Serusi, Laura Skarnulyte, Ugnė Endriulaityte, Miglė Paskeviciute, Filippo Cottiglia, Marco Gaspari, Domenico Taverna, Serenella Deplano, **Benedetta Fois**, and Elias Maccioni “Investigating the Anticancer Activity of Isatin/Dihydropyrazole Hybrids”, *ACS Medical Chemistry Letters*, Article Vol 10(4), Pages 571-576, **2019**, DOI: 10.1021/acsmchemlett.8b00596.
- Vijay Sonar; **Benedetta Fois**; Simona Distinto; Elias Maccioni; Rita Meleddu; Filippo Cottiglia; Elio Acquas; Sanjay Kasture; Costantino Floris; Daniele Colombo; Enrico; Sanna Giuseppe Talani, “Ferulic acid esters and withanolides: in search of *Withania somnifera* GABAA receptor modulators”, *Journal of Natural Products*, Vol 82(5), Pages 1250-1257, **2019**, DOI: 10.1021/acs.jnatprod.8b01023
- Simona Distinto; Rita Meleddu; Francesco Ortuso; Filippo Cottiglia; Serenella Deplano; Lisa Sequeira; Claudia Melis; **Benedetta Fois**; Andrea Angeli; Clemente Capasso; Rossella Angius; Stefano Alcaro; Claudiu Supuran; Elias Maccioni, “Exploring new structural features of the

4-[(3-methyl-4-aryl-2,3-dihydro-1,3-thiazol-2-ylidene)amino]benzenesulphonamide scaffold for the inhibition of human carbonic anhydrases”, *Journal of Enzyme Inhibition and Medicinal Chemistry*, Vol 34(1), Pages 1526-1533, **2019**, DOI: 10.1080/14756366.2019.1654470

- **Benedetta Fois**, Žiga Skok, Tihomir Tomašič, Janez Ilaš, Nace Zidar, Anamarija Zega, Lucija Peterlin Mašič, Petra Szili, Gábor Draskovits, Ákos Nyerges, Csaba Pal, Danijel Kikelj, “Dual Escherichia coli DNA Gyrase A and B Inhibitors with Antibacterial Activity” *ChemMedChem*, accepted for publication. DOI: 10.1002/cmdc.201900607
- **Benedetta Fois**, Simona Distinto, Rita Meleddu, Serenella Deplano, Elias Maccioni, Costantino Floris, Antonella Rosa, Mariella Nieddu, Pierluigi Caboni, Claudia Sissi, Andrea Angeli, Claudiu T. Supuran, Filippo Cottiglia, “Coumarins from *Magydaris pastinacea* as inhibitors of the tumor-associated carbonic anhydrases IX and XII: isolation, biological studies and in silico evaluation”, *Journal of Enzyme Inhibition and Medicinal Chemistry*, DOI: 10.1080/14756366.2020.1713114

ORAL AND POSTER COMMUNICATIONS

- VII Meeting of the Paul Ehrlich Euro-PhD Network, Vienna (Austria),
Poster Communication: “Phenylpropenoids and polyacetylenes isolated from *Bupleurum fruticosum* targeting the capsid of rhinoviruses”
B. Fois, G. Bianco, S. Distinto, E. Macciona, R. Meleddu, C. Melis, P. Caboni, R. Pompei, V. Sonar, C. Floris, F. Cottiglia, August 2016
- VIII Meeting of the Paul Ehrlich Euro-PhD Network, Porto (Portugal)
Oral Communication: “Design, Synthesis and Evaluation of Potential Dual Gyrase A/Gyrase B Inhibitors”
B. Fois, Ž. Skok, T. Tomašič, Á. Nyerges, J. Ilaš and D. Kikelj, July 2018
- VIII Meeting of the Paul Ehrlich Euro-PhD Network, Catanzaro (Italy),
Poster Communication: “Heterocyclic amides as selective inhibitors of HRV-B replication”
B. Fois, D. Jochmans, J. Neyts, C. Floris, R. Meleddu, S. Distinto, E. Maccioni, F. Cottiglia, June 2019
- SardiniaChem 2019, Sassari (Italy)
Oral Communication: “Natural and Hydrolyzed Compounds from *Teucrium flavum* subsp. *glaucum* as Inhibitors of HIV-1 RT RNase H Function”
B. Fois, A. Corona, C. Floris, R. Meleddu, S. Distinto, E. Maccioni, E. Tramontano, F. Cottiglia, June 2019